

1 gallon of gasoline was formed from 100 tons (200,000 lbs) of plant matter (40 acres of wheat including roots and stalk) over millions of years

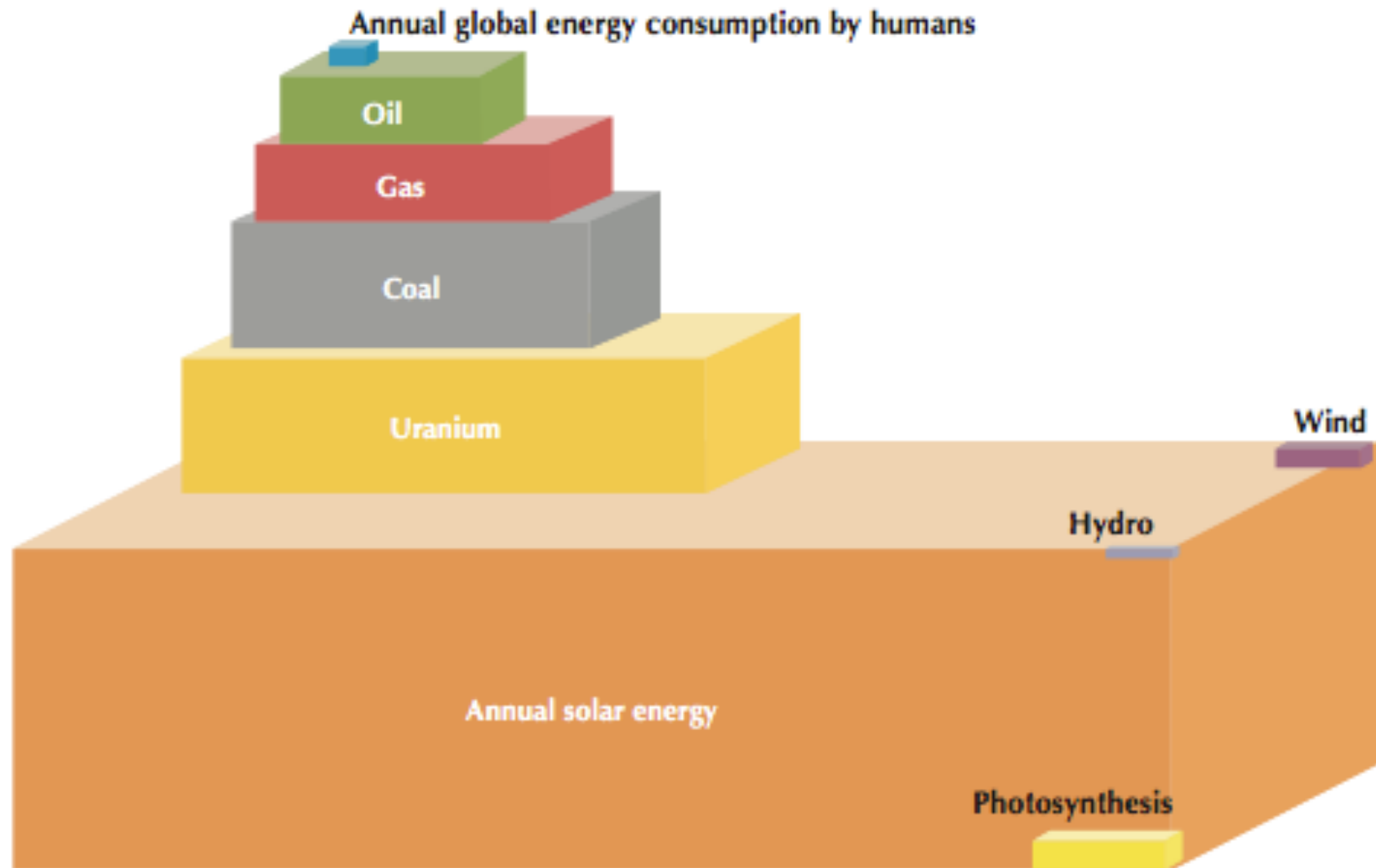
In 1-year humans consume in fossil fuels 500 to 1,000 years of total plant matter from the earth.

The total amount of fossil fuels is effectively fixed for these reasons.

Using modern conversion technology, we would need to burn about half of all the land plant matter on earth each year to meet current energy consumption

<https://www.eurekalert.org/news-releases/654287>

Figure 2.1 Total energy resources



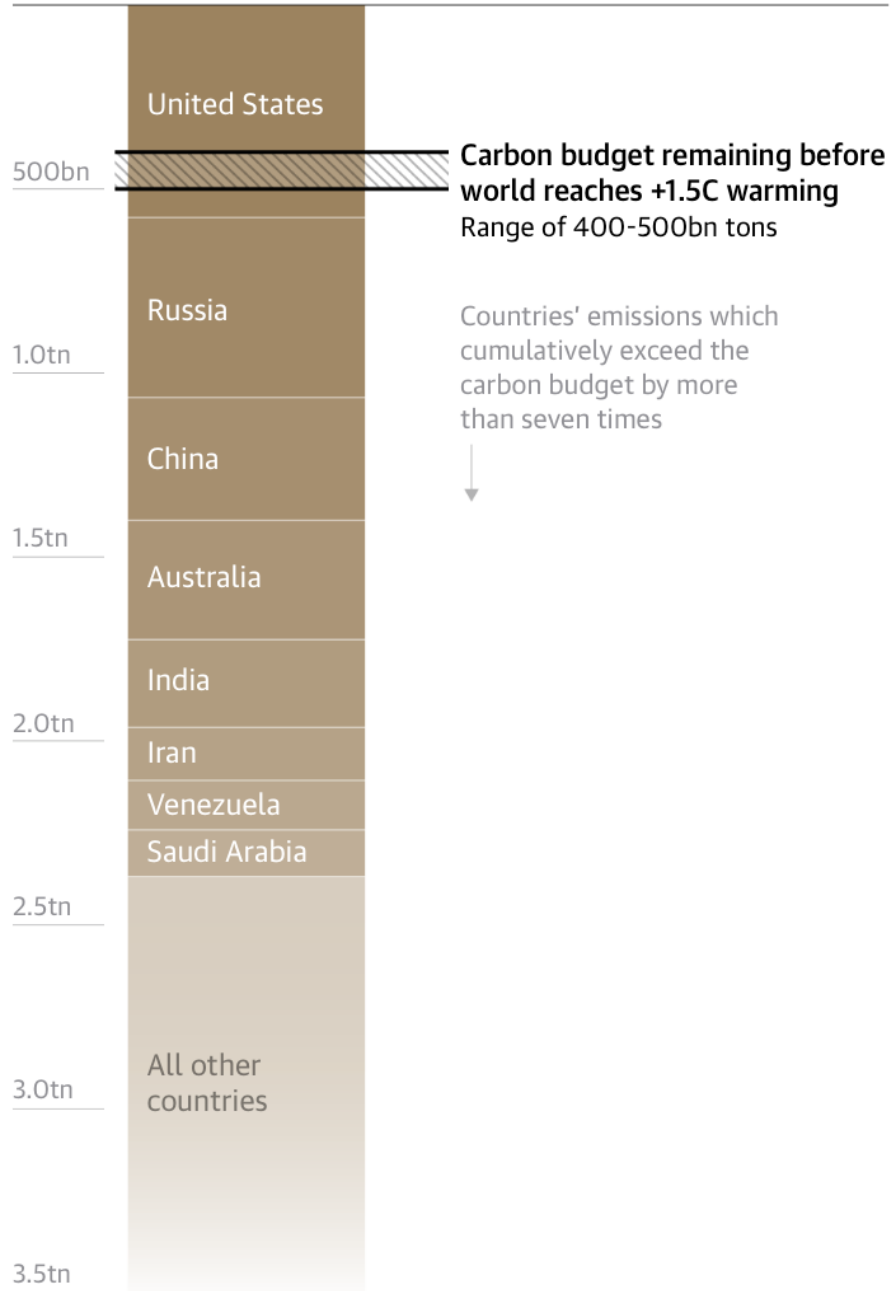
Source: National Petroleum Council, 2007, after Craig, Cunningham and Saigo (republished from IEA, 2008b).

Key point

Solar energy is the largest energy resource on Earth – and is inexhaustible.

Global emissions from fossil fuel reserves would exceed carbon budget by more than seven times

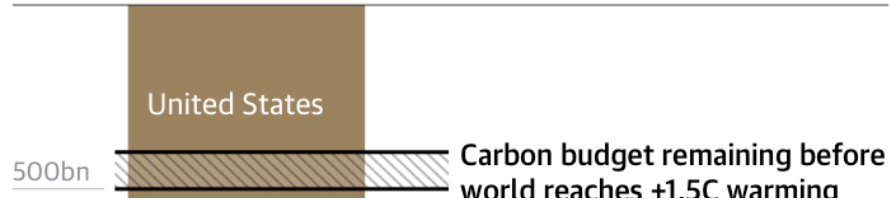
0 tons of CO2e emissions embedded in fossil fuel reserves



Guardian graphic. Source: The Global Registry of Fossil Fuels. Note: Carbon budget to reach +1.5C warming from pre-industrial levels based on IPCC 50% probability scenario.

Global emissions from fossil fuel reserves would exceed carbon budget by more than seven times

0 tons of CO₂e emissions embedded in fossil fuel reserves



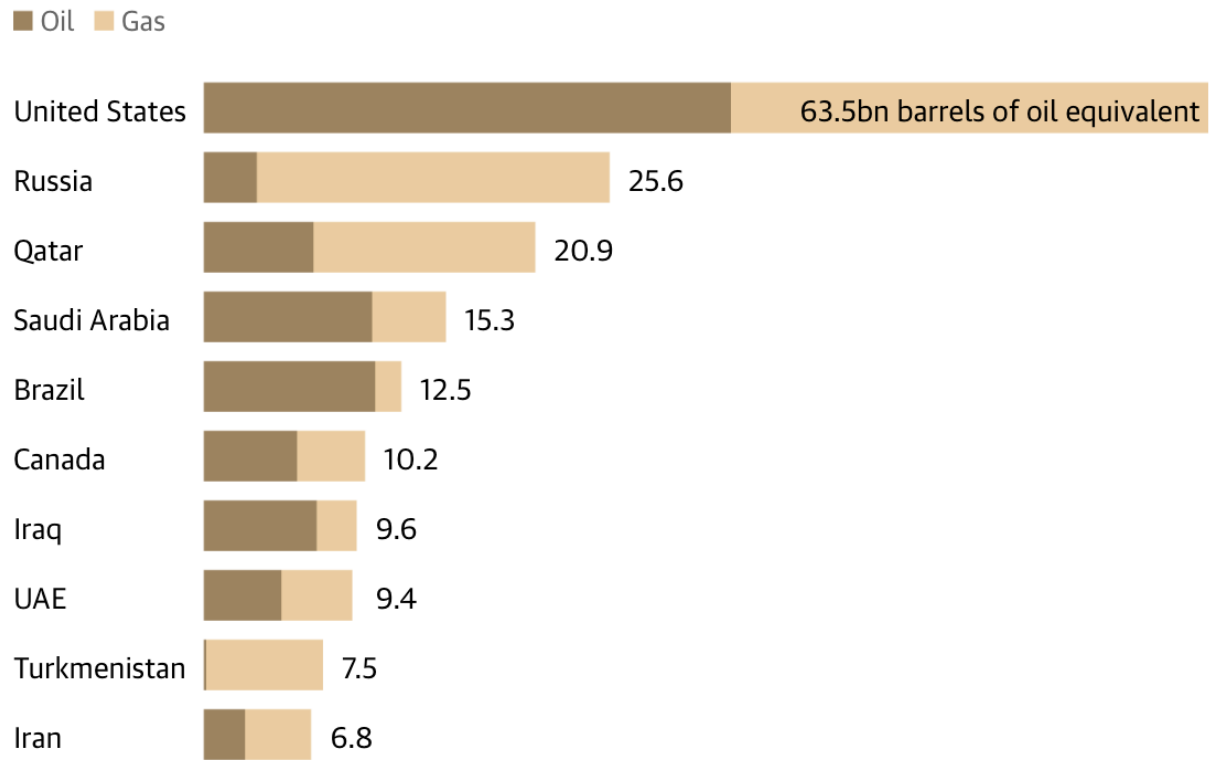
📷 The Bruce Mansfield power station, a coal-fired power station on the Ohio River near Shippingport, Pennsylvania. Photograph: Clarence Holmes Photography/Alamy



Guardian graphic. Source: The Global Registry of Fossil Fuels. Note: Carbon budget to reach +1.5C warming from pre-industrial levels based on IPCC 50% probability scenario.

Non-Photovoltaic Solar Energy Harvesting

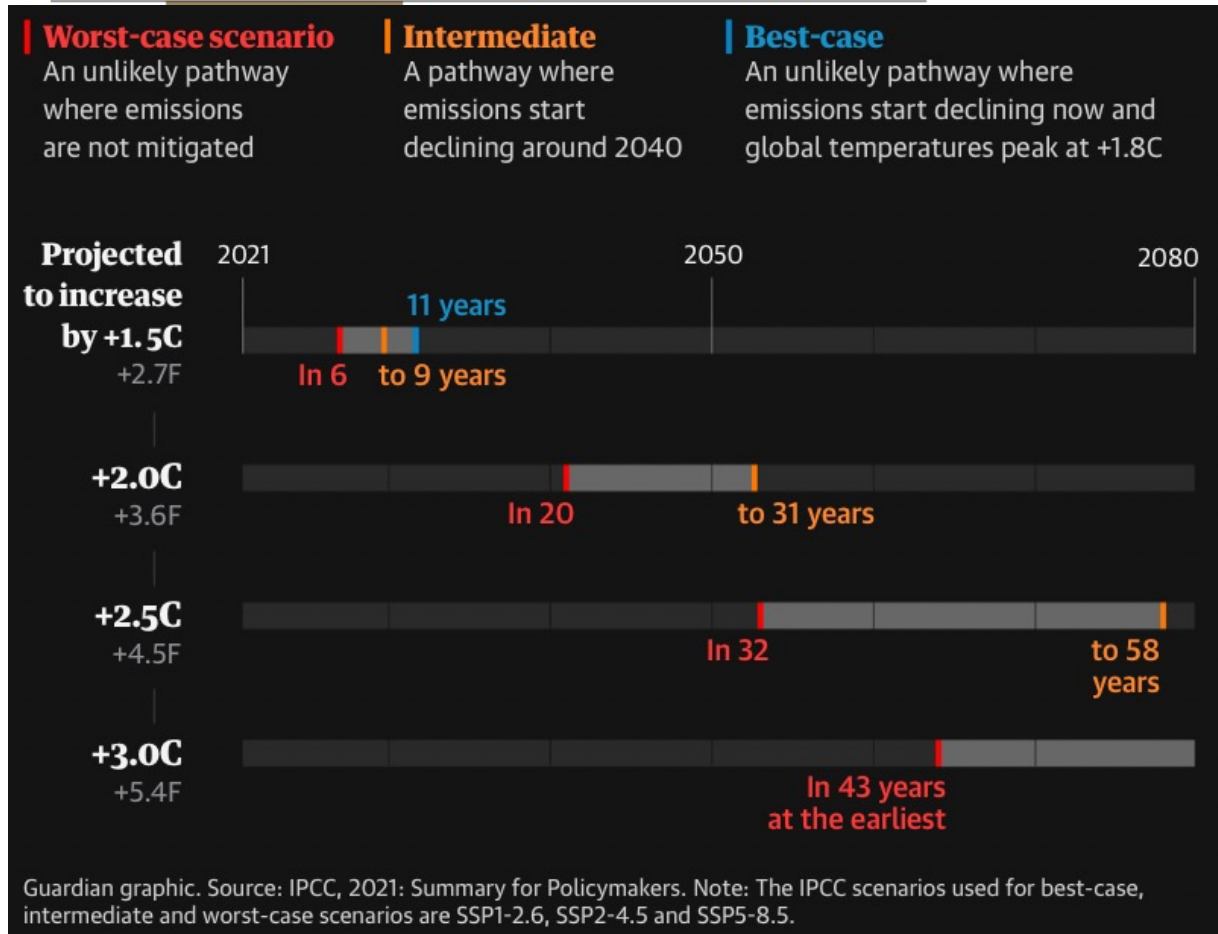
Countries with the most fossil fuel reserves in development



Guardian graphic. Source: The Global Registry of Fossil Fuels.

Global emissions from fossil fuel reserves would exceed carbon budget by more than seven times

0 tons of CO2e emissions embedded in fossil fuel reserves



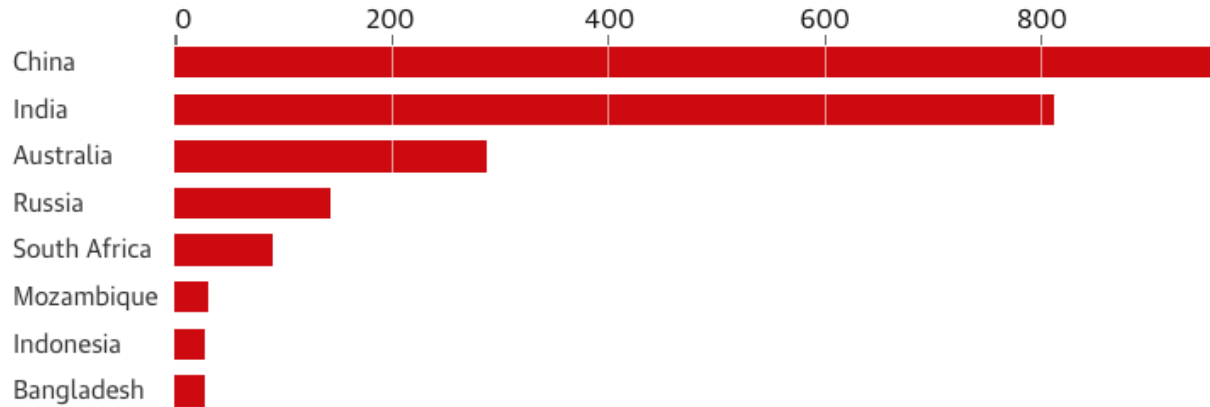
📍 The Bruce Mansfield power station, a coal-fired power station on the Ohio River near Shippingport, Pennsylvania. Photograph: Clarence Holmes Photography/Alamy

The world has already heated up by around 1.2C, on average, since the preindustrial era, pushing humanity beyond almost all historical boundaries. Cranking up the temperature of the entire globe this much within little more than a century is, in fact, extraordinary, with the oceans alone absorbing the heat equivalent of five Hiroshima atomic bombs dropping into the water every second.

Guardian graphic. Source: The Global Registry of Fossil Fuels. Note: Carbon budget to reach +1.5C warming from pre-industrial levels based on IPCC 50% probability scenario.

Australian companies are planning the most new coal mining after China and India

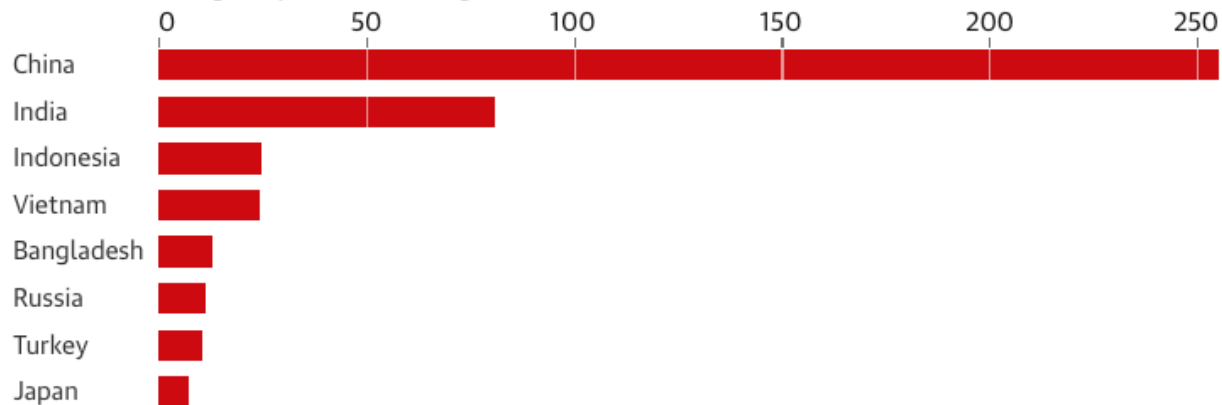
New coal mining capacity (millions of tonnes per year)



Guardian graphic | Source: Urgewald Global Coal Exit List - top eight countries

China and India are planning the most new coal-fired power

Planned new capacity of coal-fired power (GW)



Guardian graphic | Source: Urgewald Global Coal Exit List - top eight countries

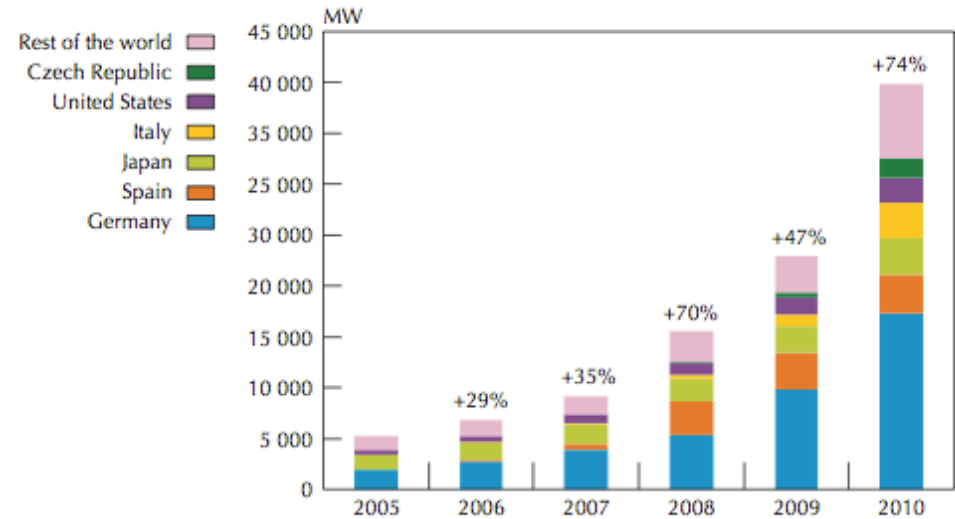
Solar Energy Perspectives

Solar Energy Engineering

Solar Energy Projects for the Evil Genius

http://app.knovel.com/web/toc.v/cid:kpSEEPS001/viwerType:toc/root_slug:solar-energy-engineering/url_slug:solar-energy-engineering/

Figure 3.1 Global cumulative PV capacities by 2010



Sources: IEA PVPS, BP Statistical Report, BNEF.

Key point

Installed PV capacities show a steep growth curve.

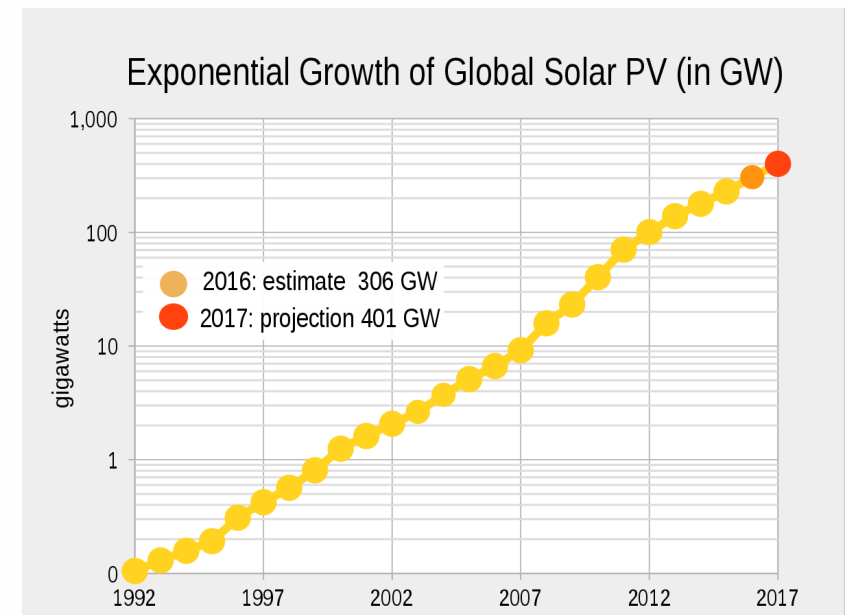
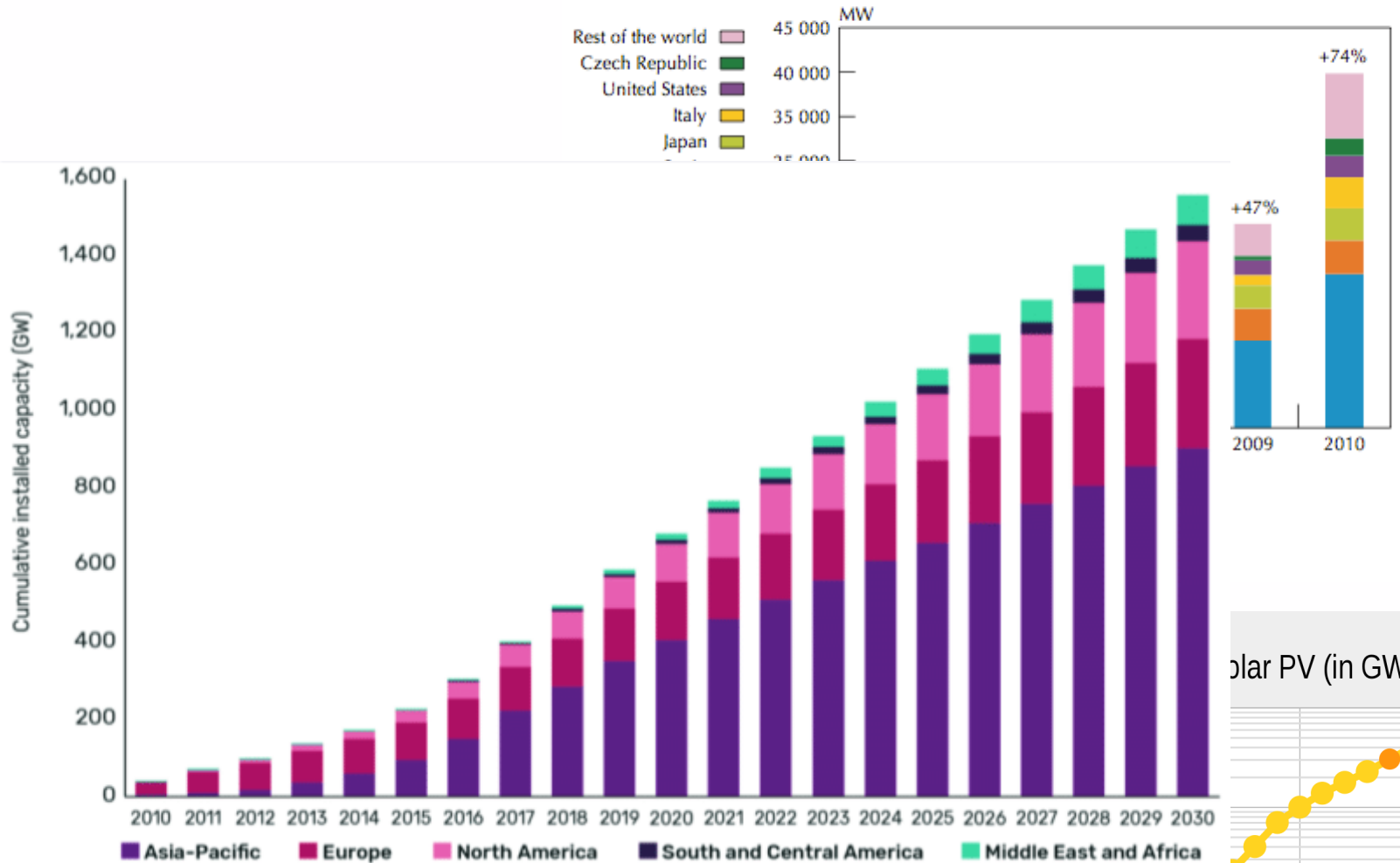
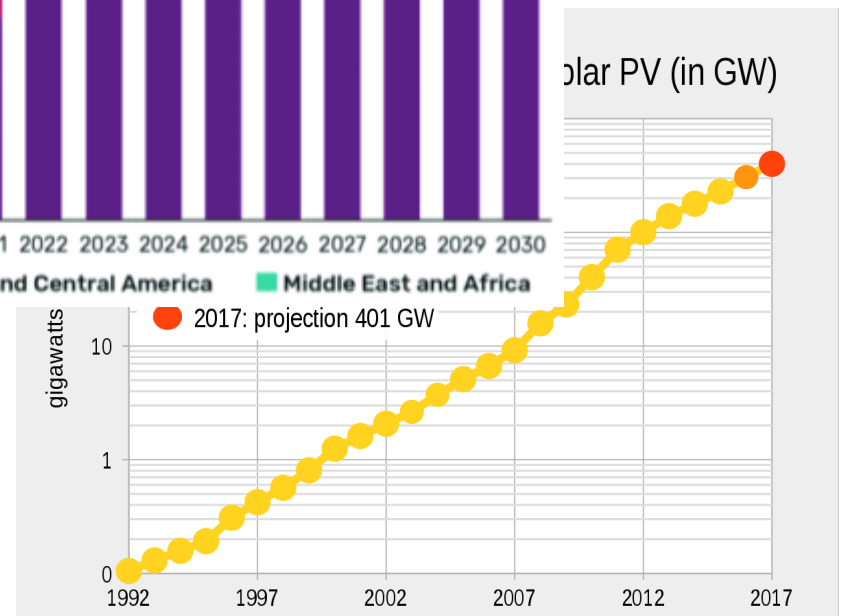


Figure 3.1 Global cumulative PV capacities by 2010



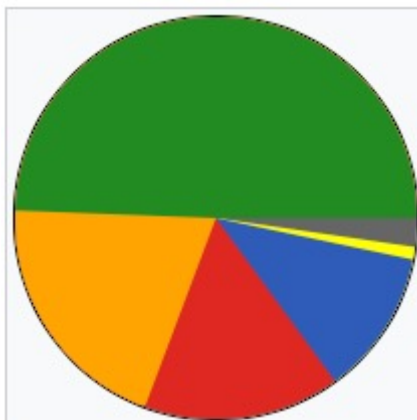
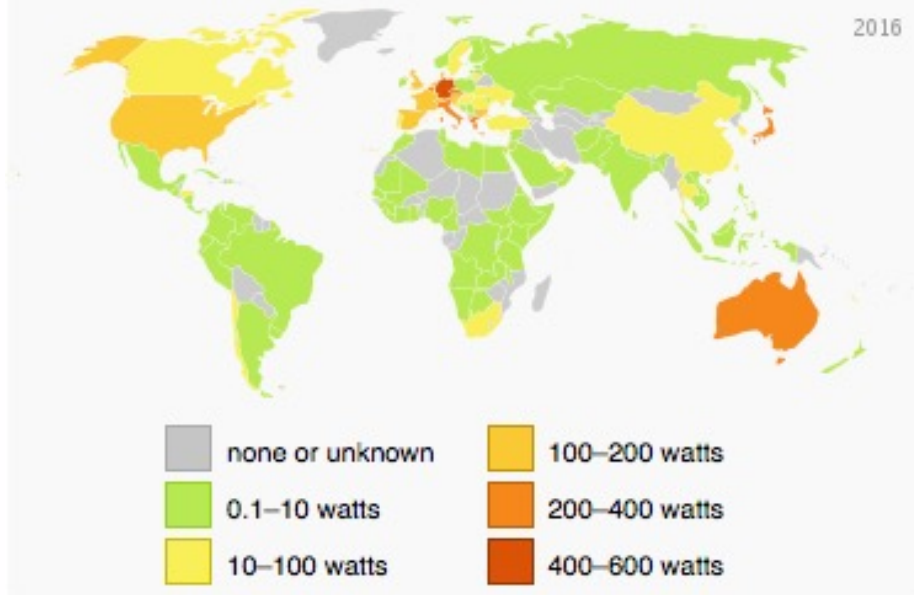
Solar Energy
Solar Energy
Solar Energy

Solar PV (in GW)

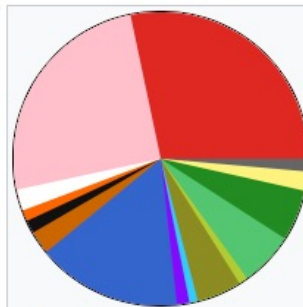
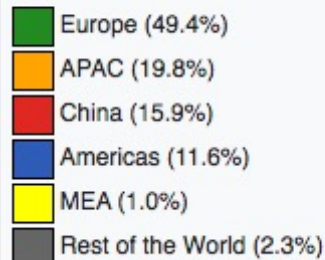


http://app.knovel.com/web/toc.v/cid:kpSEEPS001/viwerType:toc/root_slug:solar-energy-engineering/url_slug:solar-energy-engineering/

Installed PV in watts per capita



Cumulative PV capacity by region as of the end of 2014.^[4]

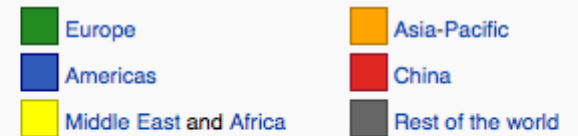
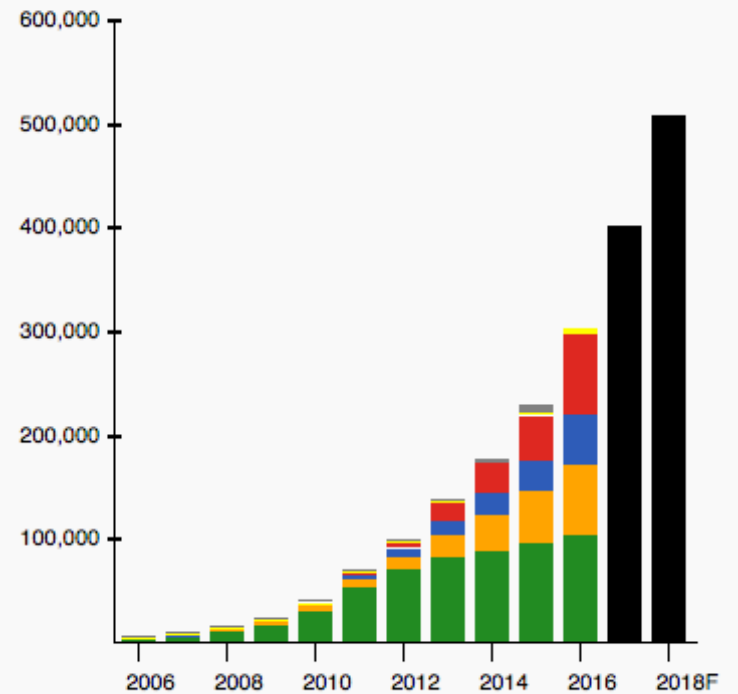


Added PV capacity by country in 2014 (clustered by region)^[4]



Worldwide growth of photovoltaics

Cumulative capacity in megawatts [MW_p] grouped by region^{[1][2][3][4][5]}
 Split-up for 2016 estimated from IEA.^[6]



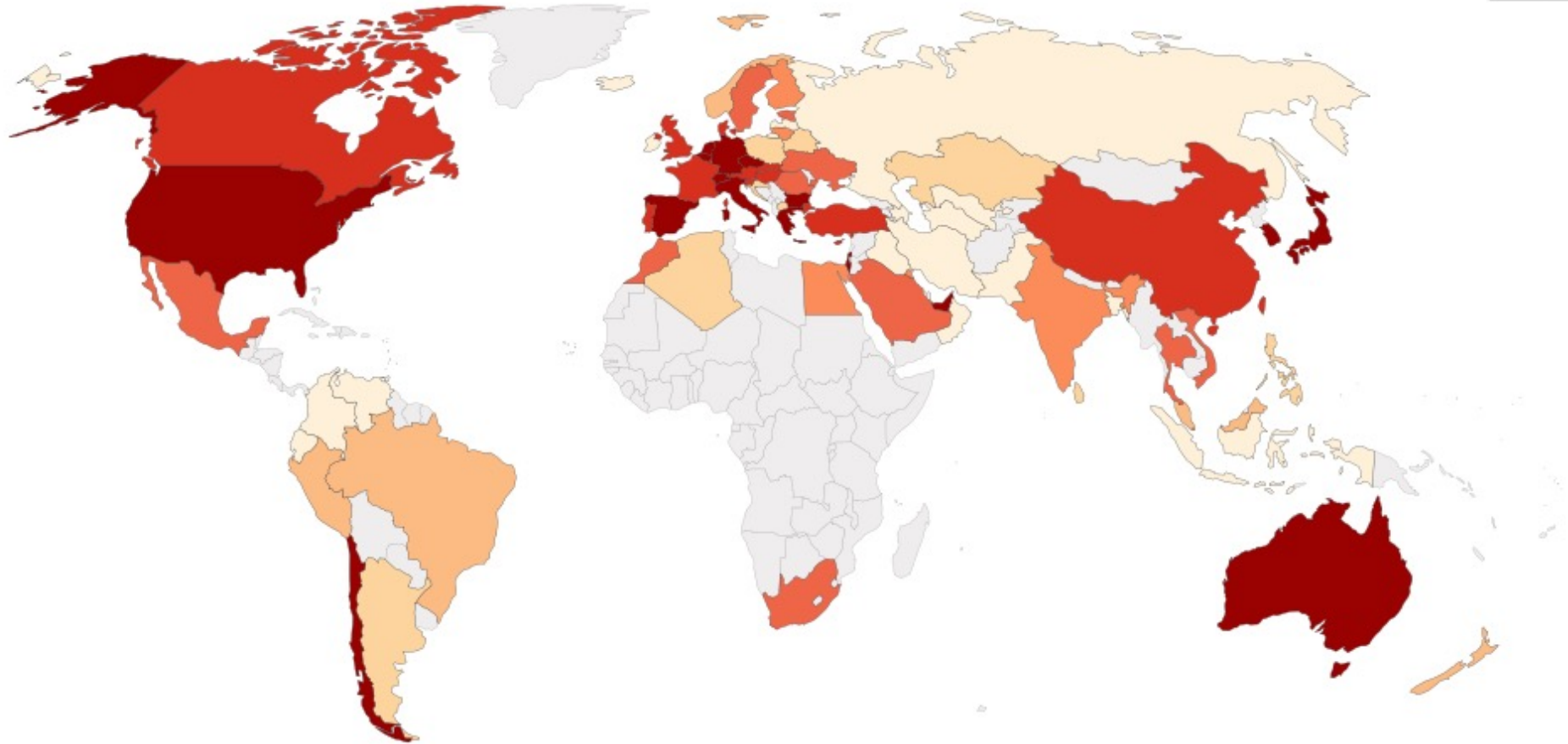
Global total: no split-up by region available yet.

Forecast for 2018

Per capita energy consumption from solar, 2019

Energy consumption is based on primary energy equivalents, rather than final electricity use.

World

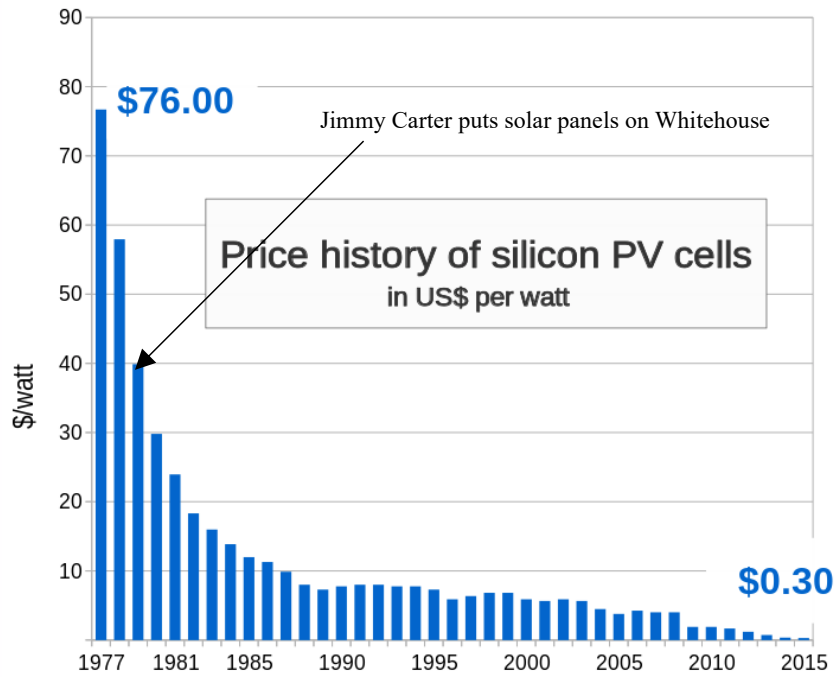


Source: Our World in Data based on BP Statistical Review of World Energy & UN Population Division

OurWorldInData.org/energy • CC BY

Note: 'Primary energy' refers to energy in its raw form, before conversion into electricity, heat or transport fuels. It is here measured in terms of 'input equivalents' via the substitution method: the amount of primary energy that would be required from fossil fuels to generate the same amount of electricity from solar.

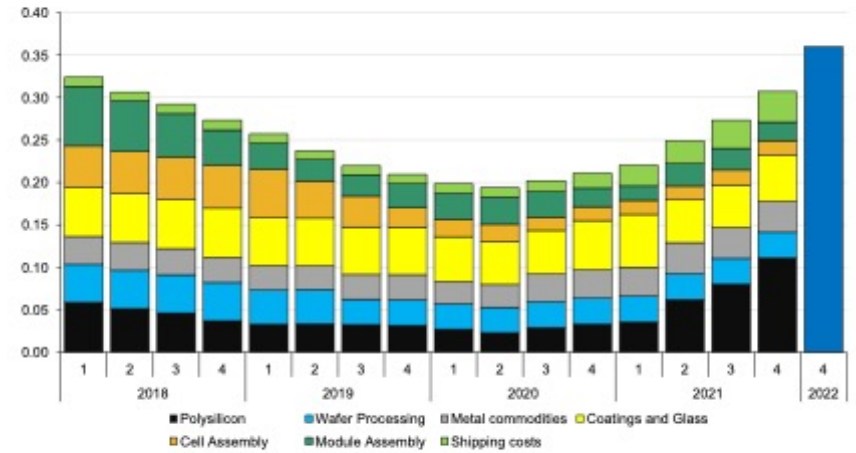
[Time-line interactive map](#)



Source: Bloomberg New Energy Finance & pv.energytrend.com

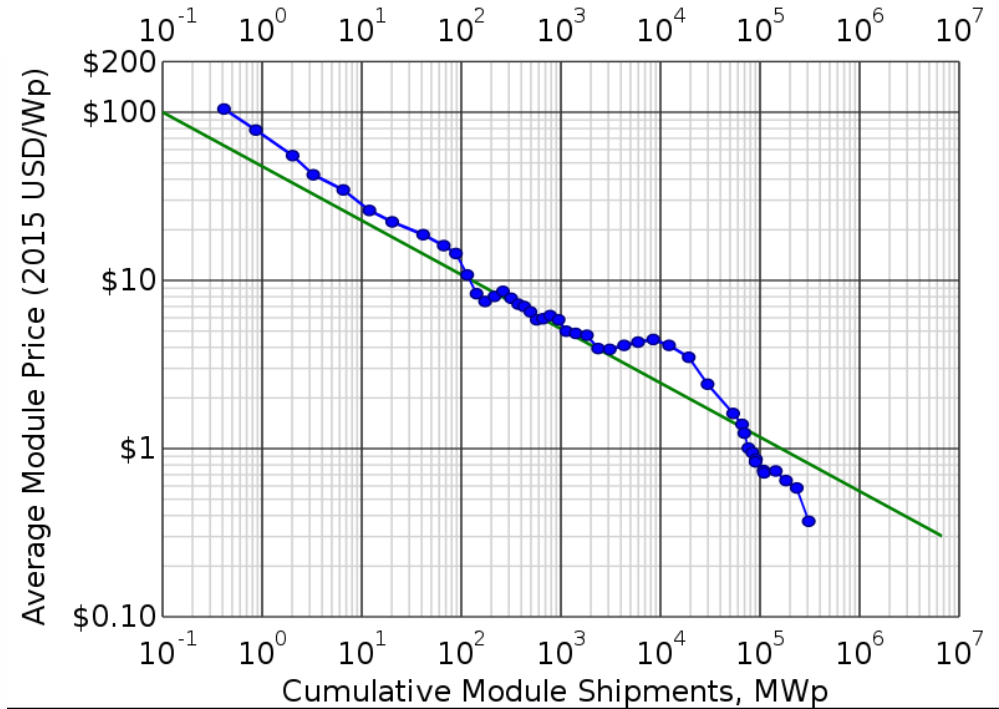


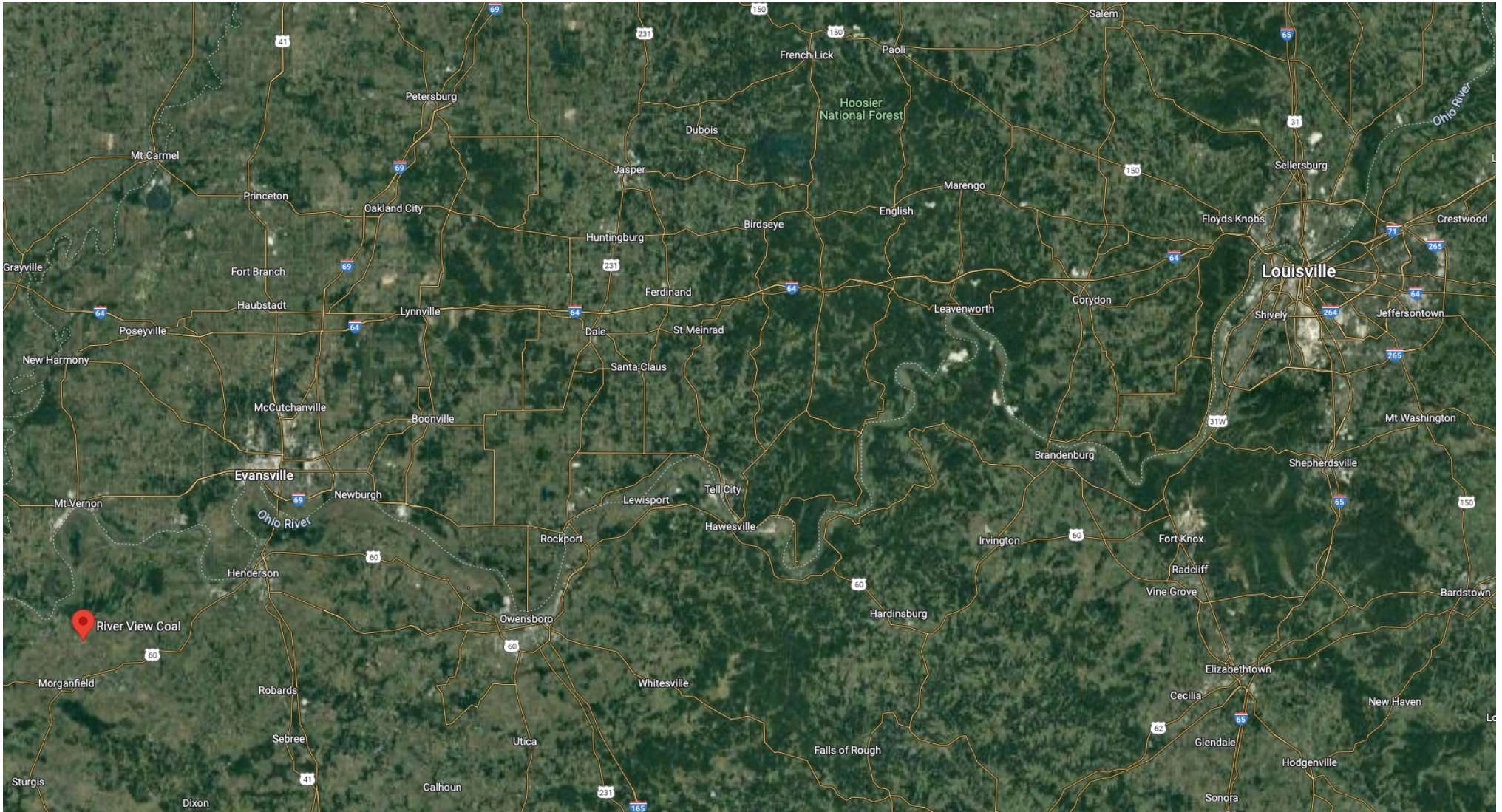
PV module quarterly costs split for 2018-22*
USD/Wp



*The 2022 Q4 values have been provided
Source: PVEL Energy research and analysis

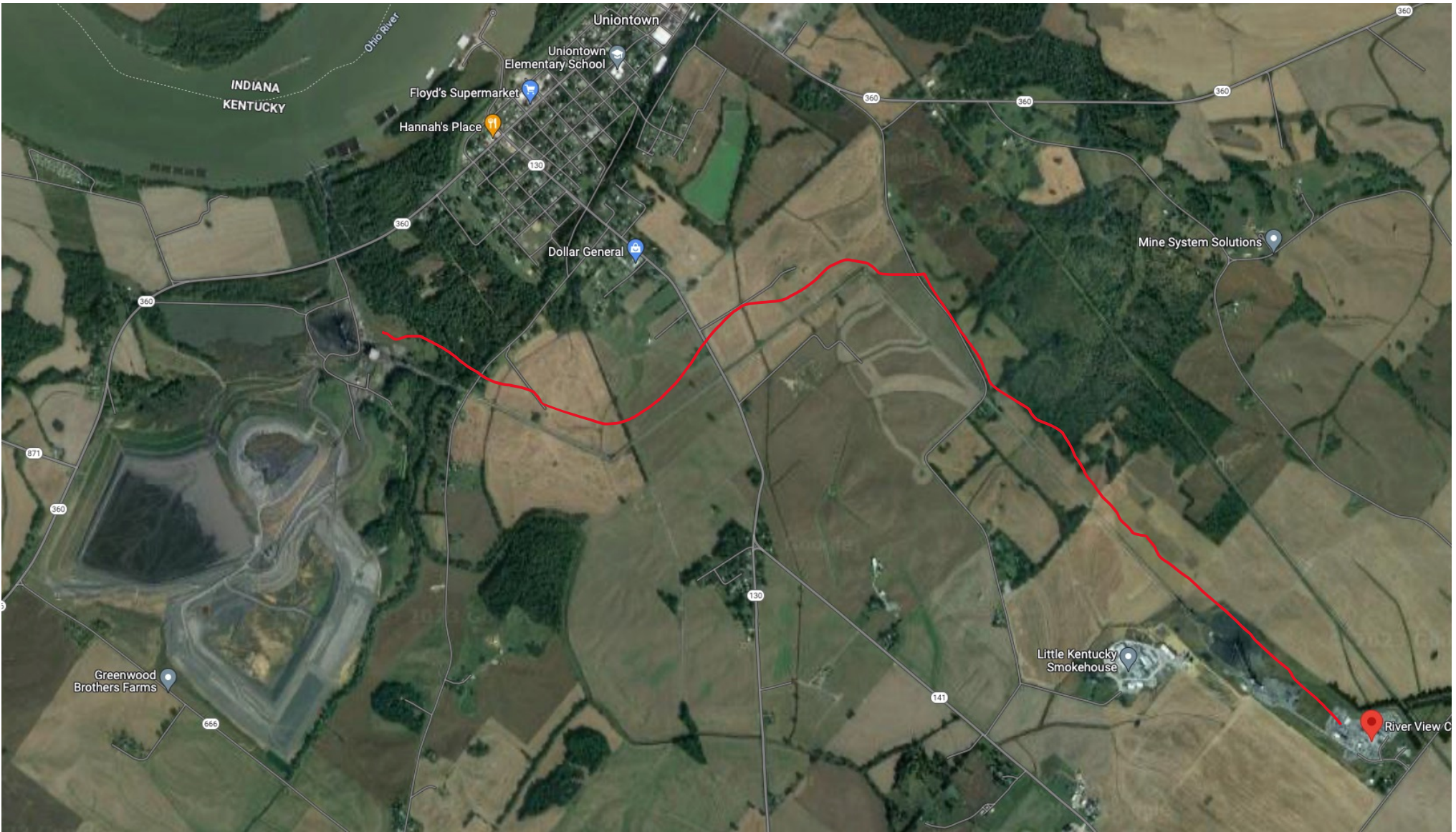
Swanson's Law





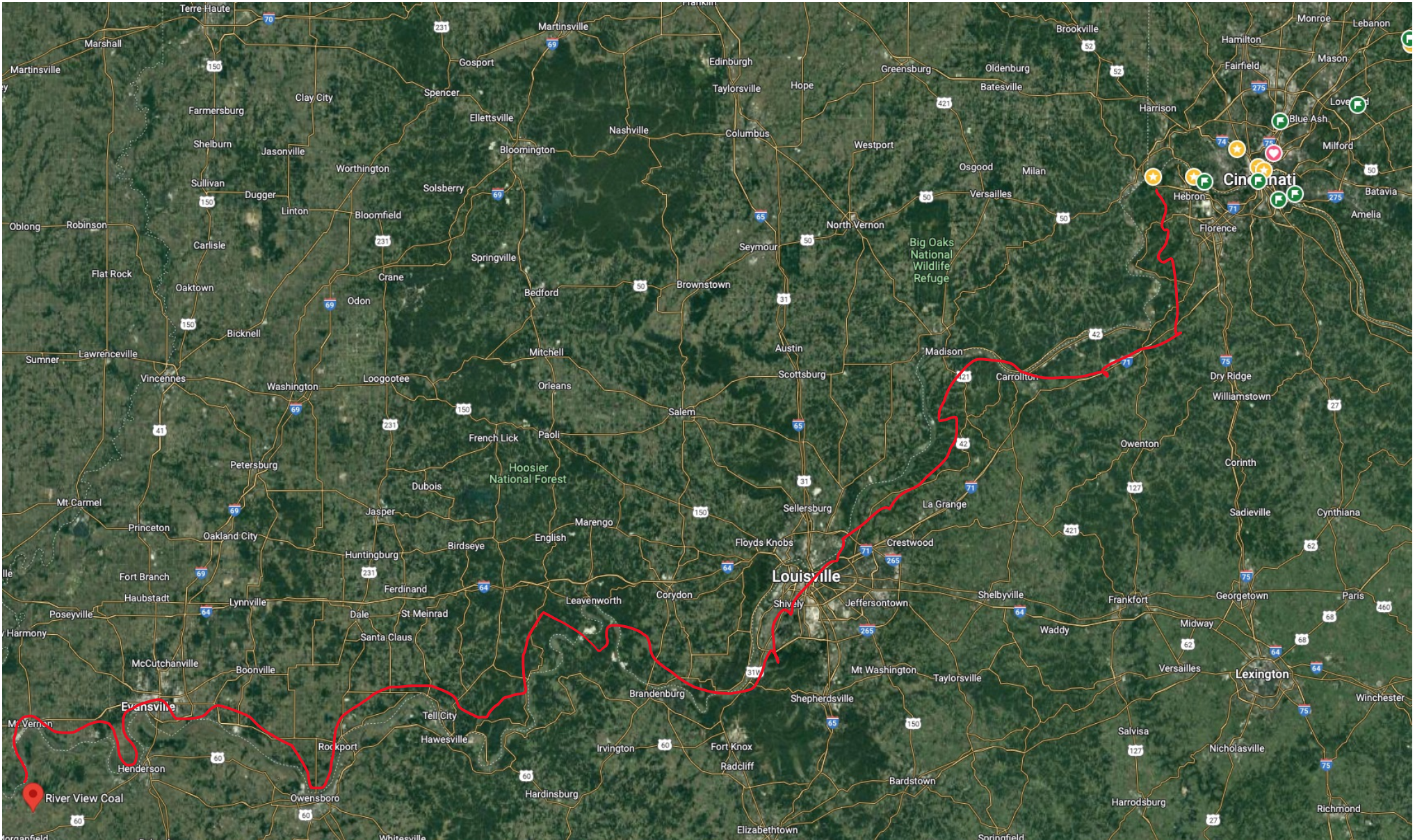
















19 Closed Coal Power Plants In Ohio (13,515 MW)

Closed plants [\[edit \]](#)

Name	Location	Capacity (MW)	Owner	Type	Notes and Links
Ashtabula Power Plant	Ashtabula	244	FirstEnergy	Coal	Closed in 2015. ^[29]
W.C. Beckjord Power Station	New Richmond	1304	Duke Energy , DPL Inc. , AEP	Coal (6 units)	Closed in 2014. ^{[30][31]}
R.E. Burger Power Station	Shadyside	568	FirstEnergy	Coal	Closed in 2011
Conesville Power Plant	Conesville	2005	AEP , AES/DPL Inc.	6 units: coal & oil	Units 5-6 shut down in 2019 and Unit 4 closed in 2020. ^[3]
Eastlake Power Plant	Eastlake	1257	FirstEnergy	Coal (units 1-5) / Natural Gas (unit 6)	Units 4-5 closed 2012, Units 1-3 closed in 2015, Unit 6 closed 2021. ^[29]
O.H. Hutchings Station	Miamisburg	414	DPL Inc.	Coal	Closed in 2013. ^[32]
Richard H. Gorsuch Station	Marietta	200	American Municipal Power	Coal	Built by Union Carbide in 1951 as Marietta Steam Plant, sold to American Municipal Power in 1988 and renamed to Richard H. Gorsuch, closed in 2012.
Killen Station	Wrightsville	618	AES/DPL Inc. , Dynegy	Coal (1 unit)	Sold to AES 2012. ^[3] Closed in 2018.
Lake Shore Power Plant	Cleveland	245	FirstEnergy	Coal	Closed in 2015. ^[29] and demolished in 2017. ^[33]
Muskingum River Power Plant	Beverly	1375	American Electric Power	Coal (5 units)	Closed in 2015. ^[34]
Philo Power Plant	Philo	510	Ohio Power	Coal	Closed in 1975; Philo Unit 6 was the first commercial supercritical steam-electric generating unit in the world, ^[35] and it could operate short-term at ultra-supercritical levels. ^[36]
Picway Power Plant	Lockbourne	220	AEP	Coal	Closed in 2015
E.M. Poston Power Plant	Nelsonville		AEP	Coal	Closed in 1987
Shelby Municipal Light Plant	Shelby	37	City of Shelby	Coal (4 units)	Closed in 2013, power monitoring remains ^[37]
Sidney Waterworks and Electric Light Building	Sidney		City of Sidney	Hydroelectric (1 unit)	Began generation in 1900 ^[38]
J.M. Stuart Station	Aberdeen	2318	AES/DPL Inc. , Dynegy , and AEP	Coal (4 units)	Sold to AES 2012. ^[3] Closed in 2018.
Tait Power Station	Dayton	586	DPL Inc.	Natural Gas/Oil	Closed 2013
Tidd Plant	Brilliant	220	Ohio Power	Coal	Retired in 1976. Was used as a demonstration for pressurized fluidized bed combustion (PFBC) for four years from 1991–1995.
Toronto Power Plant	Toronto		Ohio Edison	Coal	Closed in 1993
Trash Burning Power Plant	Columbus		SWACO	Waste-to-energy	Closed in 1994
Avon Lake Power Station	Avon Lake	680	NRG Energy	Coal	Closed in 2022. ^[39]
William H. Zimmer Power Station	Moscow	1300	Vistra Corp	Coal	Closed in May 2022. ^[13]

15 Operating Natural Gas Power Plants In Ohio (10,743 MW)

Natural gas [\[edit \]](#)

Name	Location	Capacity (MW)	Owner	Type	Notes and Links
Hanging Rock Energy Facility	Hanging Rock	1430	Dynegy	Natural Gas Combined Cycle	^[3]
Lordstown Energy Center	Lordstown	940	Clean Energy Future, LLC	Natural Gas Combined Cycle	Opened in 2018, Second Unit Planned ^[4]
Oregon Clean Energy Center	Oregon	908	Ares Management	Natural Gas Combined Cycle	Opened in 2017
Rolling Hills Generating Station	Wilkesville	865	Rolling Hills Generating LLC	Natural Gas Simple Cycle (5 units)	
Waterford Energy Center	Waterford	821	Waterford Power, LLC	Natural Gas Combined Cycle	
Carroll County Energy	Carrollton	700	Advanced Power	Natural Gas Combined Cycle	Opened in 2018 ^[5]
Washington Energy Facility	Beverly	620	Dynegy	Natural Gas Combined Cycle	
Darby Generating Station	Mount Sterling	480	Darby Power, LLC	Natural Gas Simple Cycle	
Middletown Energy Center	Middletown	475	NTE Energy	Natural Gas Combined Cycle	Opened in 2018
West Lorain Plant	Lorain	545	Starwood Energy	Natural Gas Simple Cycle	
Robert P Mone Plant	Convoy	510	Buckeye Power	Natural Gas Simple Cycle	
Fremont Energy Center	Fremont	707	American Municipal Power	Natural Gas Combined Cycle	
Dresden Plant	Dresden	580	American Electric Power	Natural Gas Combined Cycle	Opened in 2012
Madison Peaking Station	Trenton	677	Duke Energy	Natural Gas Simple Cycle	
Long Ridge Energy Terminal	Hannibal	485	Long Ridge Energy	Hydrogen - Natural Gas Blend	Opened in 2021 ^[6]

4 Operating Coal Power Plants In Ohio (6,546 MW)

Coal [\[edit \]](#)

Name ↕	Location ↕	Capacity (MW) ↕	Owner ↕	Type ↕	Notes and Links ↕
Bay Shore	Oregon	150	Walleye Energy LLC	Petroleum Coke (1 unit)	Opened in 1955. ^[7]
Cardinal Power Plant	Brilliant	1800	American Electric Power (AEP)/Buckeye Power	Coal (3 units)	To be converted to natural gas by 2030. ^[8]
Gavin Power Plant	Cheshire	2640	Gavin Power, LLC	Coal (2 units)	^[9] Only runs 60% of the time. Up to 50% of Gavin's cash flow comes from being on standby for emergency power ^[10]
Kyger Creek Power Plant	Cheshire	1086	Ohio Valley Electric Corporation	Coal (5 units)	^[11] Subsidized by the controversial HB6 Bill until 2030 ^[12]
Miami Fort Power Station	North Bend	1020	Vistra Corp	Coal (2 units)	Older units shut down in 2015. Planned retirement by year-end 2027 or earlier. ^{[13][14]}
Toledo Refining Power Recovery	Oregon	6.0	Toledo Refining Co.	Petroleum Coke (1 unit)	Opened in 1986. ^[15]

2 Operating Nuclear Power Plants In Ohio (2,191 MW)

Nuclear [\[edit \]](#)

Name	Location	Capacity (MW)	Owner	Type	Notes and Links
Perry Nuclear Generating Station	North Perry	1231	Energy Harbor	Nuclear boiling water reactor (1 unit)	
Davis-Besse Nuclear Power Station	Oak Harbor	960	Energy Harbor	Nuclear Pressurized water reactor (1 unit)	

8 Operating Wind Power Plants In Ohio (1,090 MW)

Wind [edit]

See also: *Wind power in Ohio*

Name	Location	Capacity (MW)	Turbines	Owner	Notes and Links
AMP Wind Farm	Wood County	7.2		American Municipal Power ^[16]	
Blue Creek Wind Farm	Paulding and Van Wert Counties	304	160	Iberdrola Renewables	Operational. ^[17]
Timber Road Wind Farm	Paulding County	362.7	158	EDP Renewables	Operational. ^[17]
Hog Creek	Hardin County	66	30		Operational. ^[17]
Northwest Ohio	Paulding County	100	42		Operational. ^[17]
Scioto Ridge	Hardin County & Logan County	249.8	75	Innogy	Operational. ^[17]
Icebreaker	Cuyahoga County	20.7	6		Approved for Construction. ^[17]
Emerson Creek	Hardin County & Erie County	297.7	71		Approved for Construction. ^[17]

18 Operating Solar Power Plants In Ohio (2,398 MW)

27 Planned Solar Power Plants In Ohio (4,141 MW)

Solar [\[edit \]](#)

See also: *Solar power in Ohio*

Name	Location	Capacity (MW)	Owner	Notes and Links
Bowling Green Solar Facility	Bowling Green	20	NextEra	^[18]
Napoleon Solar Facility	Napoleon	3.54	American Municipal Power	^[18]
Wadsworth Rittman Rd. Facility	Wadsworth	2.625	American Municipal Power	^[18]
Wadsworth Seville Rd. Facility	Wadsworth	6.25	American Municipal Power	^[18]
Wyandot Solar Facility	Upper Sandusky	12	Public Service Enterprise Group	Opened in 2010.
Hardin I	Hardin County	150		Operational. ^[19]
Hillcrest	Brown County	200		Operational. ^[19]
New Market	Highland County	100		Operational. ^[19]
Hardin II	Hardin County	170		Under Construction. ^[19] Operational in Q2 2023. ^[20]
Yellowbud	Pickaway & Ross County	274		Operational. ^[19]
Willowbrook I	Brown County	150		Under Construction. ^[19] Operational Dec 2022. ^[21]
Nestlewood	Brown County	80		Under Construction. ^[19]
Big Plain	Madison County	196		Under Construction. ^[19] Operational June 2023. ^[22]
Arche	Fulton County	107		Under Construction. ^[19] Operational in early 2023. ^[23]
Hardin III	Hardin County	300		Under Construction. ^[19] Operational in 2023. ^[24]
AEUG Union	Union County	325		Under Construction. ^[19] Operational in 2023. ^[25]
Highland	Highland County	300		Under Construction. ^[19]
Fox Squirrel	Madison County	577		Under Construction. ^[19] Operational in Q4 2024. ^[26]
Atlanta Farms	Pickaway County	200		Approved for Construction. ^[19]
Vinton	Vinton County	125		Approved for Construction. ^[19]
Madison Fields	Madison County	180		Under Construction. ^[19]
Alamo	Preble County	69.9		Approved for Construction. ^[19]
Angelina	Preble County	80		Approved for Construction. ^[19]
Powell Creek	Putnam County	150		Approved for Construction. ^[19]
Wheatsborough	Erie County	125		Under Construction. ^[19]
Mark Center	Defiance County	110		Approved for Construction. ^[19]
Clearview	Champaign County	144		Approved for Construction. ^[19]
Ross County	Ross County	120		Under Construction. ^[19]
Cadence	Union County	275		Approved for Construction. ^[19]
Juliet	Wood County	101		Approved for Construction. ^[19]

Sycamore Creek	Crawford County	117		Approved for Construction. ^[19]
Marion County	Marion County	100		Approved for Construction. ^[19]
Union Ridge	Licking County	107.7		Approved for Construction. ^[19]
Tymochee	Wyandot County	120		Approved for Construction. ^[19]
Nottingham	Harrison County	100		Approved for Construction. ^[19]
Wild Grains	Van Wert County	150		Approved for Construction. ^[19]
Dodson Creek	Highland County	117		Approved for Construction. ^[19]
Pleasant Prairie	Franklin County	250		Approved for Construction. ^[19]
Harvey	Licking County	350		Approved for Construction. ^[19]
Springwater	Franklin and Madison County	155		Approved for Construction. ^[19]
Border Basin	Hancock County	120		Approved for Construction. ^[19]
South Branch	Hancock County	130		Approved for Construction. ^[19]
Palomino	Hancock County	200		Approved for Construction. ^[19]
Blossom	Morrow and Marion County	144		Approved for Construction. ^[19]
Yellow Wood	Clinton County	300		Approved for Construction. ^[19]

9 Operating Hydro Power Plants In Ohio (312 MW)

Hydroelectricity [edit]

See also: *List of dams and reservoirs in Ohio*

Name	Location	Capacity (MW)	Owner	Notes and Links
O'Shaughnessy Dam	Dublin	5.2	City of Columbus	^[27] Offline as of August 2018. It is unknown when or if it will be fixed.
Hamilton Hydro	Hamilton	2	City of Hamilton	^[27]
Auglaize Hydroelectric Plant	Bryan	4.5	City of Bryan	^[27]
Captain Anthony Meldahl Locks and Dam	Felicity	105	American Municipal Power	^[27] Largest hydroelectric plant on the Ohio river and is located on Kentucky side of the Ohio River. The City of Hamilton retains 51.4% of the power generation ^[28]
Greenup Lock and Dam	Franklin Furnace	70.2	American Municipal Power	^[27]
Racine Lock and Dam	Racine	20	AEP	^[27]
Belleville Lock and Dam	Reedsville	42	American Municipal Power	^[27] Hydroelectric plant is located on West Virginia side of the Ohio River.
Willow Island Lock and Dam	Newport	44	American Municipal Power	^[27] Hydroelectric plant is located on West Virginia side of the Ohio River.
Hannibal Locks and Dam	Hannibal	19	New Martinsville Hannibal Hydro	^[27] Hydroelectric plant is located on West Virginia side of the Ohio River.

9 Operating Battery Power Plants In Ohio (33 MW)

Battery storage [\[edit \]](#)

Name	Location	Capacity (MW)	Owner	Notes and Links
Battery Utility of Ohio	Sunbury	4	Battery Utility of Ohio	[27]
AEP Bluffton NaS	Bluffton	2	Ohio Power Co	[27]
HMV Minster Energy Storage System	Minster	7	Half Moon Ventures LLC	[27]
Willey Battery Utility	Hamilton	6	Willey Battery Utility	[27]
Clinton Battery	Blanchester	10	Clinton Battery Utility	[27]
Beckjord Power Station	New Richmond	4	Duke Energy	[27]

The Moss Landing battery storage project is a massive battery energy storage facility built at the retired Moss Landing power plant site in California, US. At 400MW/1,600MWh capacity, it is currently the world's biggest battery storage facility.

Vistra Energy, an integrated retail electricity and power generation company based in Texas, US, developed the project in two phases under two separate resource adequacy agreements with Pacific Gas and Electric Company (PG&E).

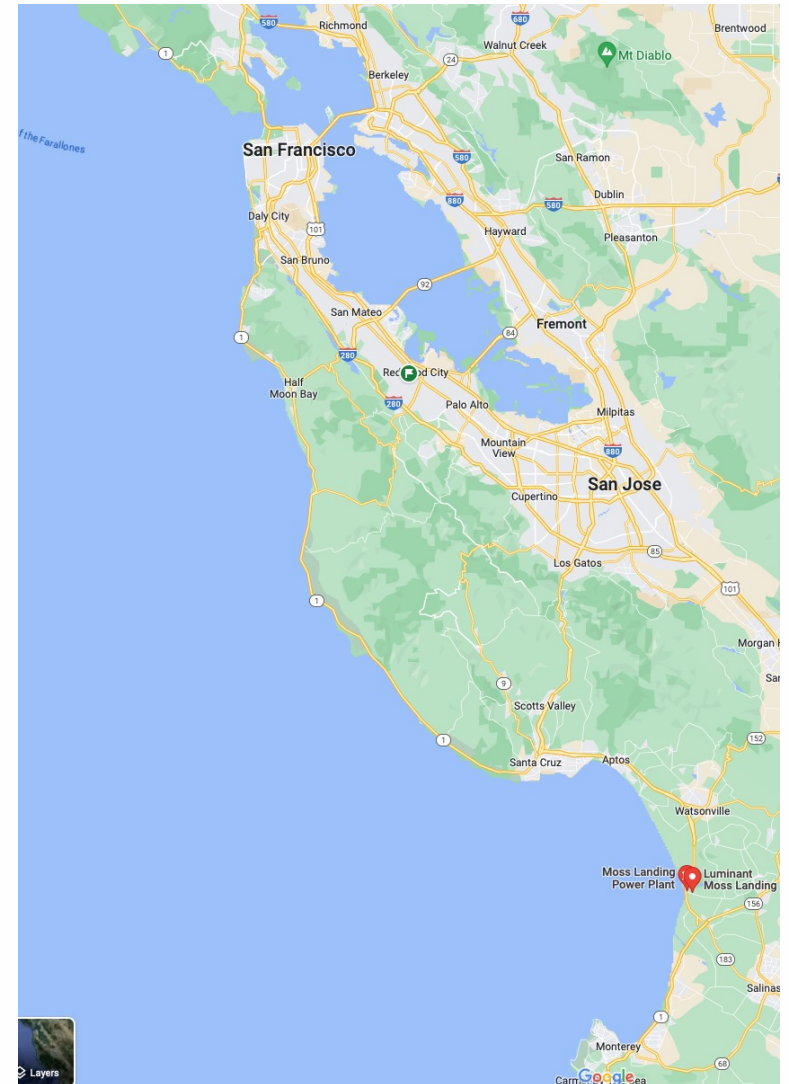
The 300MW/1,200MWh phase one of the Moss Landing [battery energy storage system](#) (BESS) was connected to California's power grid and began operating in December 2020. Construction on the 100MW/400MWh phase two expansion was started in September 2020, while its commissioning took place in July 2021.

An overheating incident, however, affected a few battery modules of the phase one storage facility in the first week of September 2021. Vistra has since then kept the entire facility offline as it investigates the cause of the incident.

PROJECT GALLERY

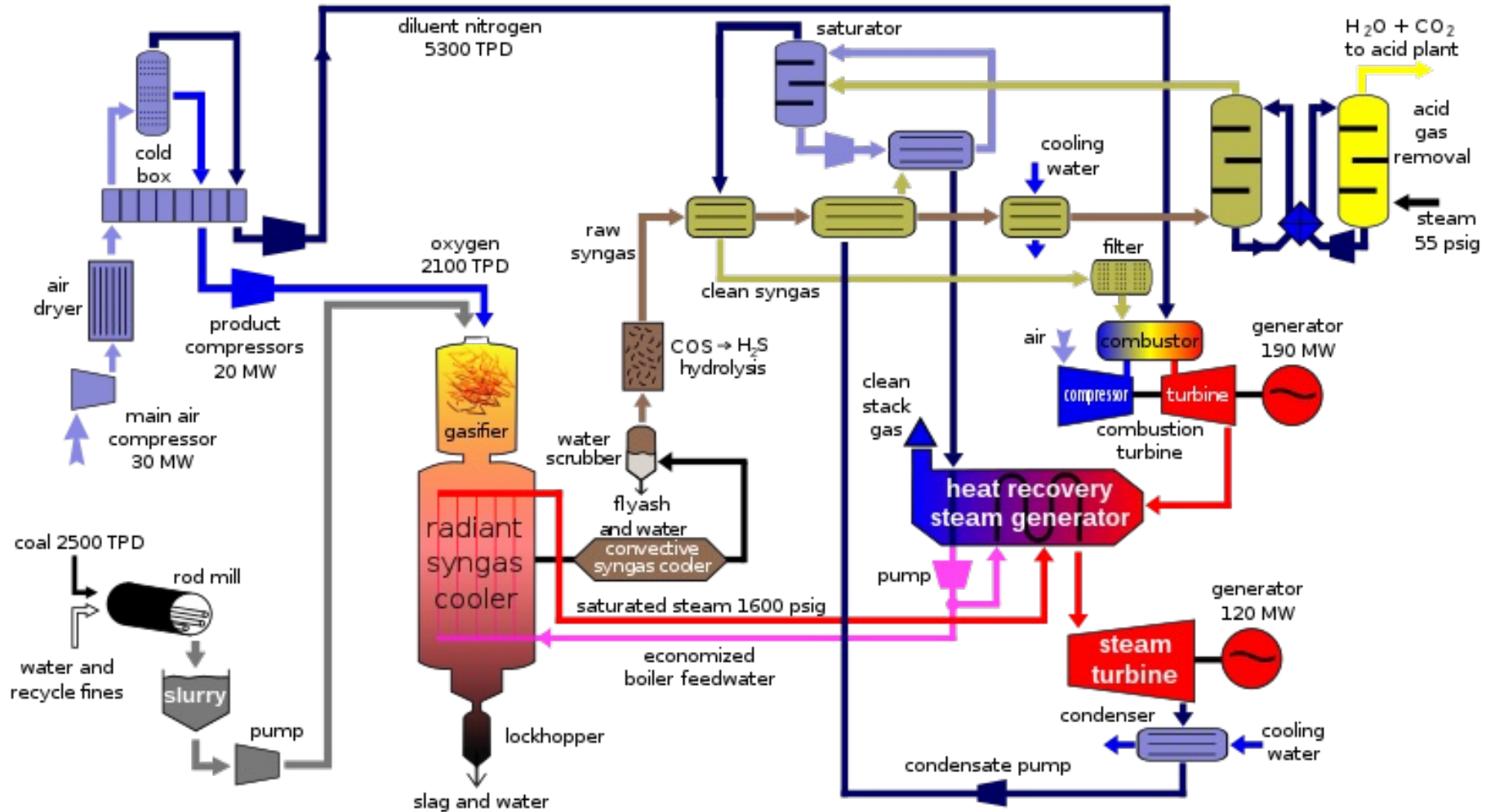


The Moss Landing battery energy storage project began operations in December 2020. Image courtesy of David Monniaux.



<https://www.carbonbrief.org/mapped-worlds-coal-power-plants/>

Integrated gasification combined cycle (IGCC)



- The solid coal is gasified to produce syngas, or synthetic gas. Syngas is synthesized by gasifying coal in a closed pressurized reactor with a shortage of oxygen. The shortage of oxygen ensures that coal is broken down by the heat and pressure as opposed to burning completely. The chemical reaction between coal and oxygen produces a product that is a mixture of carbon and hydrogen, or syngas. $C_xH_y + (x/2)O_2 \rightarrow (x)CO_2 + (y/2)H_2$

- The heat from the production of syngas is used to produce steam from cooling water which is then used for [steam turbine](#) electricity production.

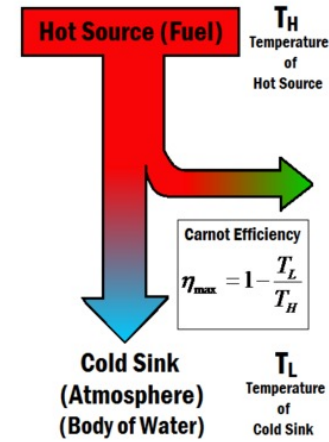
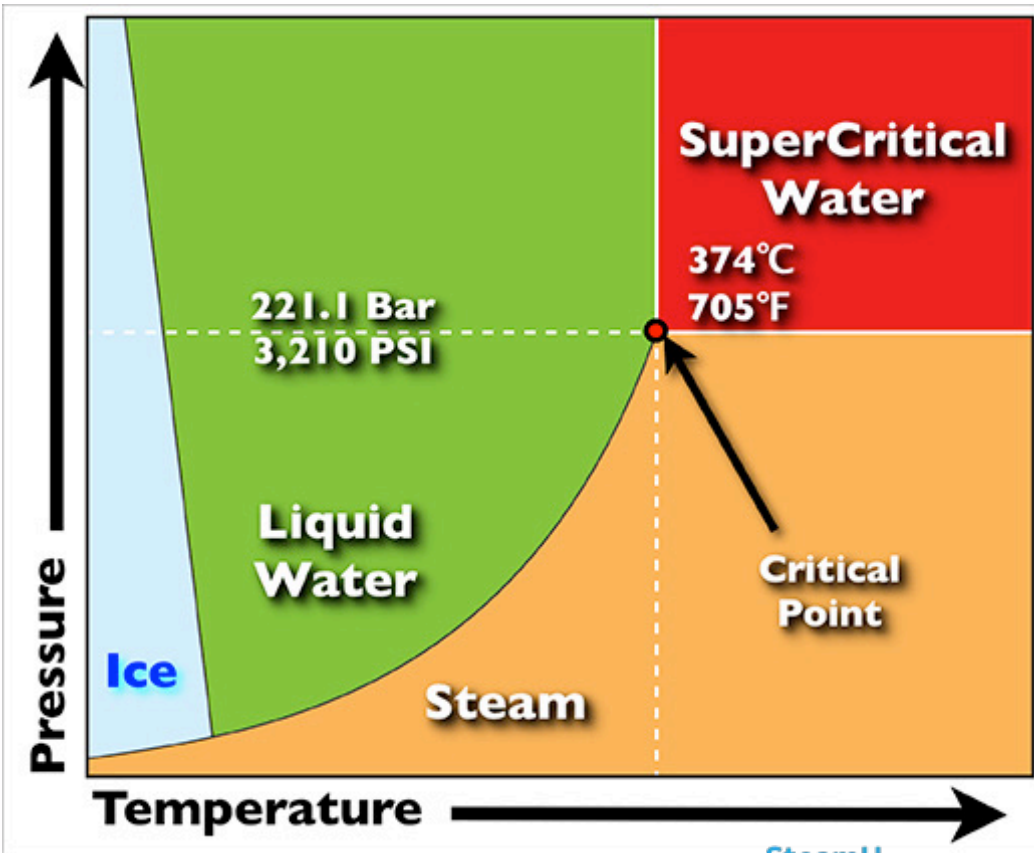
- The syngas must go through a pre-combustion separation process to remove CO₂ and other impurities to produce a more purified fuel. Three steps are necessary for the separation of impurities:

1. [Water-gas-shift reaction](#). The reaction that occurs in a water-gas-shift reactor is $CO + H_2O \rightarrow CO_2 + H_2$. This produces a syngas with a higher composition of hydrogen fuel which is more efficient for burning later in combustion.

2. Physical separation process. This can be done through various mechanisms such as absorption, adsorption or membrane separation.

3. Drying, compression and storage/shipping.

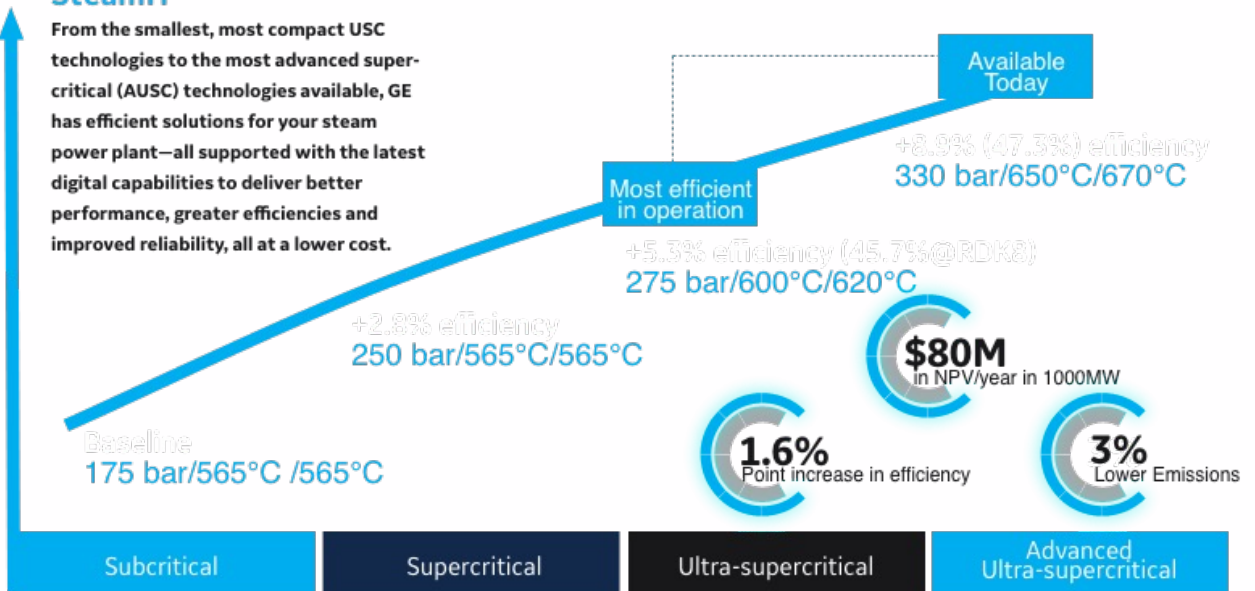
- The resulting syngas fuels a [combustion turbine](#) that produces electricity. At this stage the syngas is fairly pure H₂.



Hotter is better

SteamH

From the smallest, most compact USC technologies to the most advanced supercritical (AUSC) technologies available, GE has efficient solutions for your steam power plant—all supported with the latest digital capabilities to deliver better performance, greater efficiencies and improved reliability, all at a lower cost.



* For a 1000MW base plant in Asia, this is an economic benefit of \$80M in additional value for our customers.

Table 1.1 Coal ranks*.

Rank	Description
Lignite	The largest portion of the coal reserves of the world. A soft, brownish-black coal which is the lowest level of the coal family. The texture of the original wood can even be seen in some pieces primarily found west of the Mississippi River.
Subbituminous coal	A dull black coal which, when burned, releases more energy (heat) than lignite when burned; mined mostly in Montana, Wyoming, and a few other western states.
Bituminous coal	Sometimes called <i>soft coal</i> ; found primarily east of the Mississippi River in midwestern states such as Ohio and Illinois and in the Appalachian mountain range from Kentucky to Pennsylvania.
Anthracite	The hardest coal and gives off the greatest amount of heat when burned; the reserves of anthracite in the United States are located primarily in Pennsylvania.

*As mined in the United States.

To develop combustion technology for efficient production of electricity,

- (i) the elemental composition of the coal,
- (ii) rank of the coal, the mineral matter content of the coal, (peat to anthracite)
- (iii) the size of the pulverized coal particles, and
- (iv) the tendency of the combustion system to produce fly ash and bottom slag.

Table 1.1 Coal ranks*.

Rank	Description
Lignite	The largest portion of the coal reserves of the world. A soft, brownish-black coal which is the lowest level of the coal family. The texture of the original wood can even be seen in some pieces primarily found west of the Mississippi River.
Subbituminous coal	A dull black coal which, when burned, releases more energy (heat) than lignite when burned; mined mostly in Montana, Wyoming, and a few other western states.
Bituminous coal	Sometimes called <i>soft coal</i> ; found primarily east of the Mississippi River in midwestern states such as Ohio and Illinois and in the Appalachian mountain range from Kentucky to Pennsylvania.
Anthracite	The hardest coal and gives off the greatest amount of heat when burned; the reserves of anthracite in the United States are located primarily in Pennsylvania.

*As mined in the United States.

- (i) handling and storage characteristics,
- (ii) pulverizing behavior,
- (iii) combustion behavior,
- (iv) mineral matter and ash chemistry interactions in addition to the characteristics of the coal and its ash in terms of environmental factors such as dust, self-heating and emissions components.

Table 1.1 Coal ranks*.

Rank	Description
Lignite	The largest portion of the coal reserves of the world. A soft, brownish-black coal which is the lowest level of the coal family. The texture of the original wood can even be seen in some pieces primarily found west of the Mississippi River.
Subbituminous coal	A dull black coal which, when burned, releases more energy (heat) than lignite when burned; mined mostly in Montana, Wyoming, and a few other western states.
Bituminous coal	Sometimes called <i>soft coal</i> ; found primarily east of the Mississippi River in midwestern states such as Ohio and Illinois and in the Appalachian mountain range from Kentucky to Pennsylvania.
Anthracite	The hardest coal and gives off the greatest amount of heat when burned; the reserves of anthracite in the United States are located primarily in Pennsylvania.

*As mined in the United States.

- (i) handling and storage characteristics,
- (ii) pulverizing behavior,
- (iii) combustion behavior,
- (iv) mineral matter and ash chemistry interactions in addition to the characteristics of the coal and its ash in terms of environmental factors such as dust, self-heating and emissions components.

Table 1.2 Illustration of the effects that can contribute to the coalification process.*

Coal rank	DoB	MT	C	VM	CV	M
Lignite	650-4,900	25-45	60	49-53	23,000	30-50
Subbituminous	4,900-8,200	45-75	71-77	42-49	29,300	10-30
Bituminous	8,200-19,500	75-180	77-87	29-42	36,250	5-10
Anthracite	>19,500	>180	87-92	8-29	>38,000	<5

Key:

DoB: approximate depth of burial, feet.

MT: approximate maximum temperature during burial, °C.

C: approximate carbon content, % w/w dry ash-free basis.

VM: approximate volatile matter, % w/w dry, ash-free basis.

CV: approximate calorific value (heat content), ash-free basis.

M: approximate moisture content, % w/w (*in situ*).

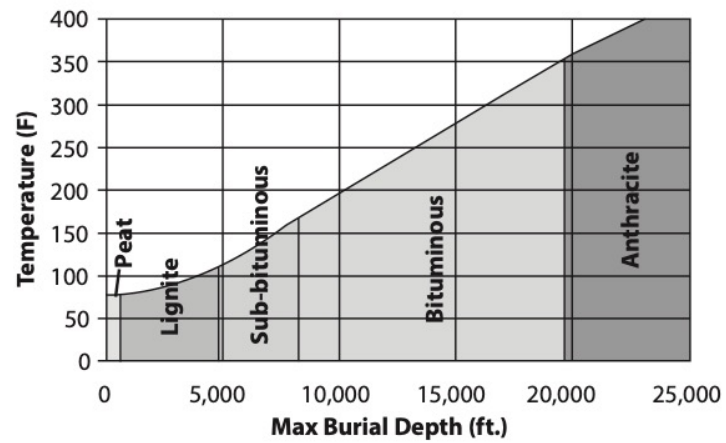


Figure 1.1 Schematic showing tendency of coal rank to increase with depth of burial*.

*Numbers are approximate and used for illustration only; peat is included only for comparison and it should not be construed for this diagram that peat is a type of coal.

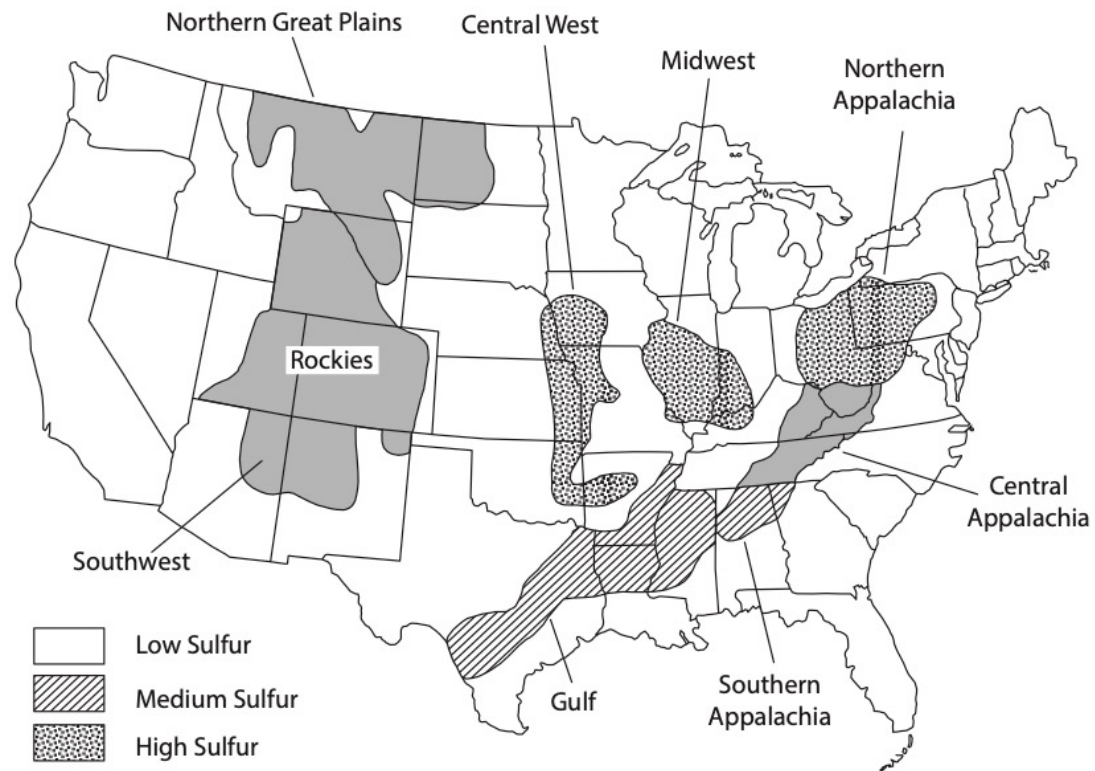


Figure 1.3 Distribution of Sulfur content of US Coals (Energy information Administration, 2011).

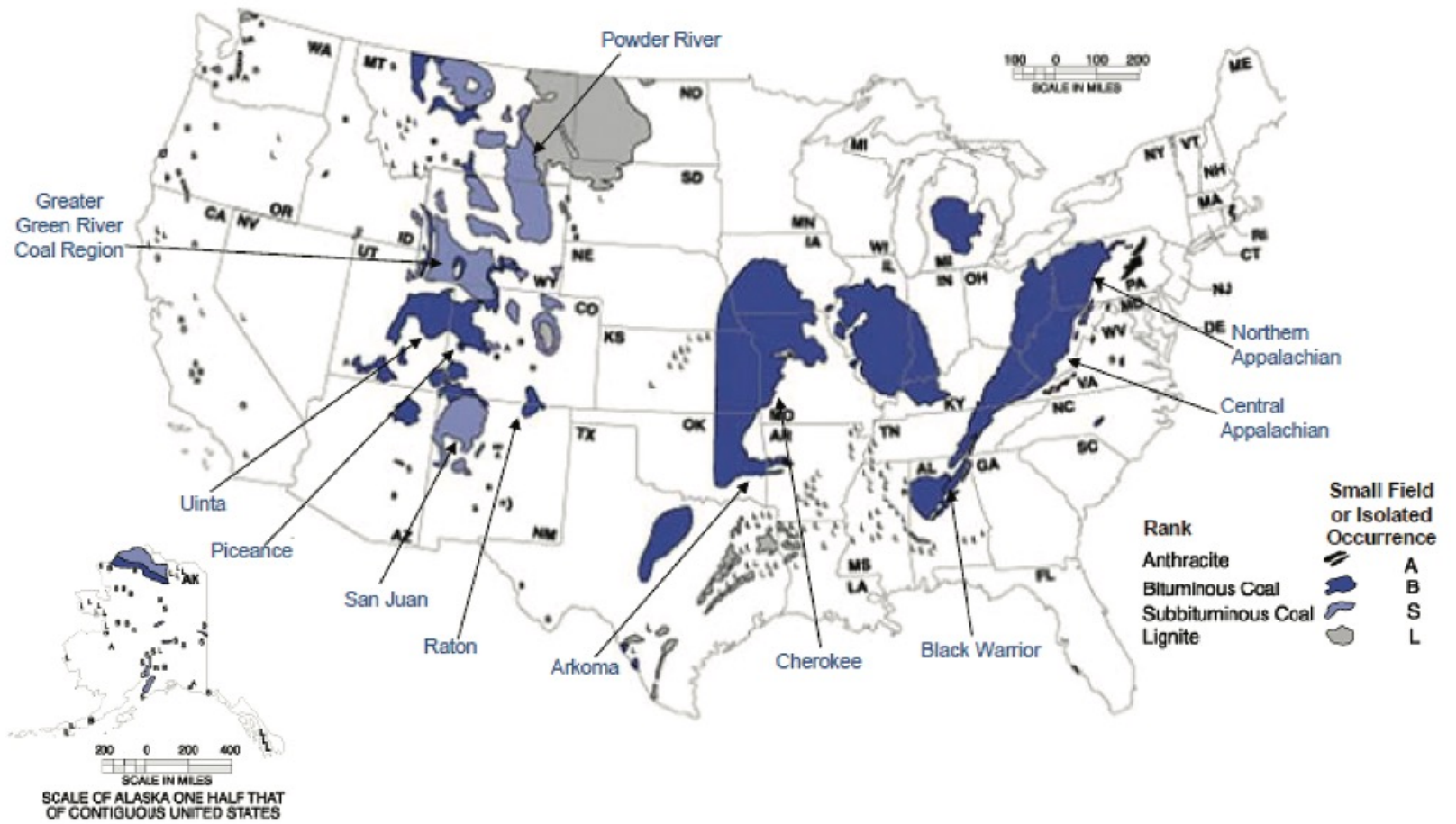


Figure 2.1 Coal reserves and distribution in the United States (DOE/EIA, 1995).

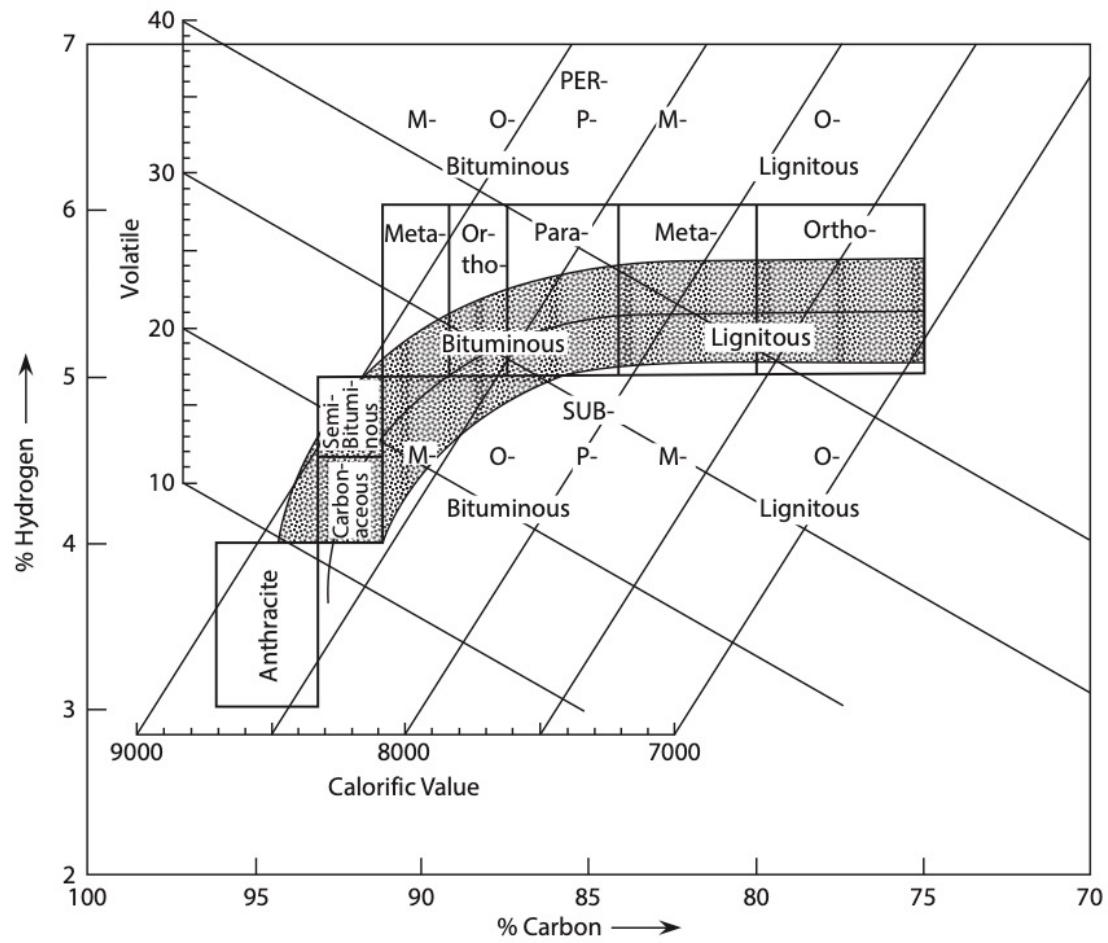
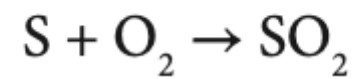
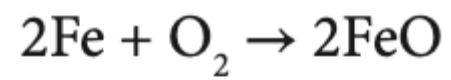
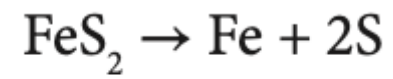


Figure 2.2 Classification by the Seyler System.

Pyrite



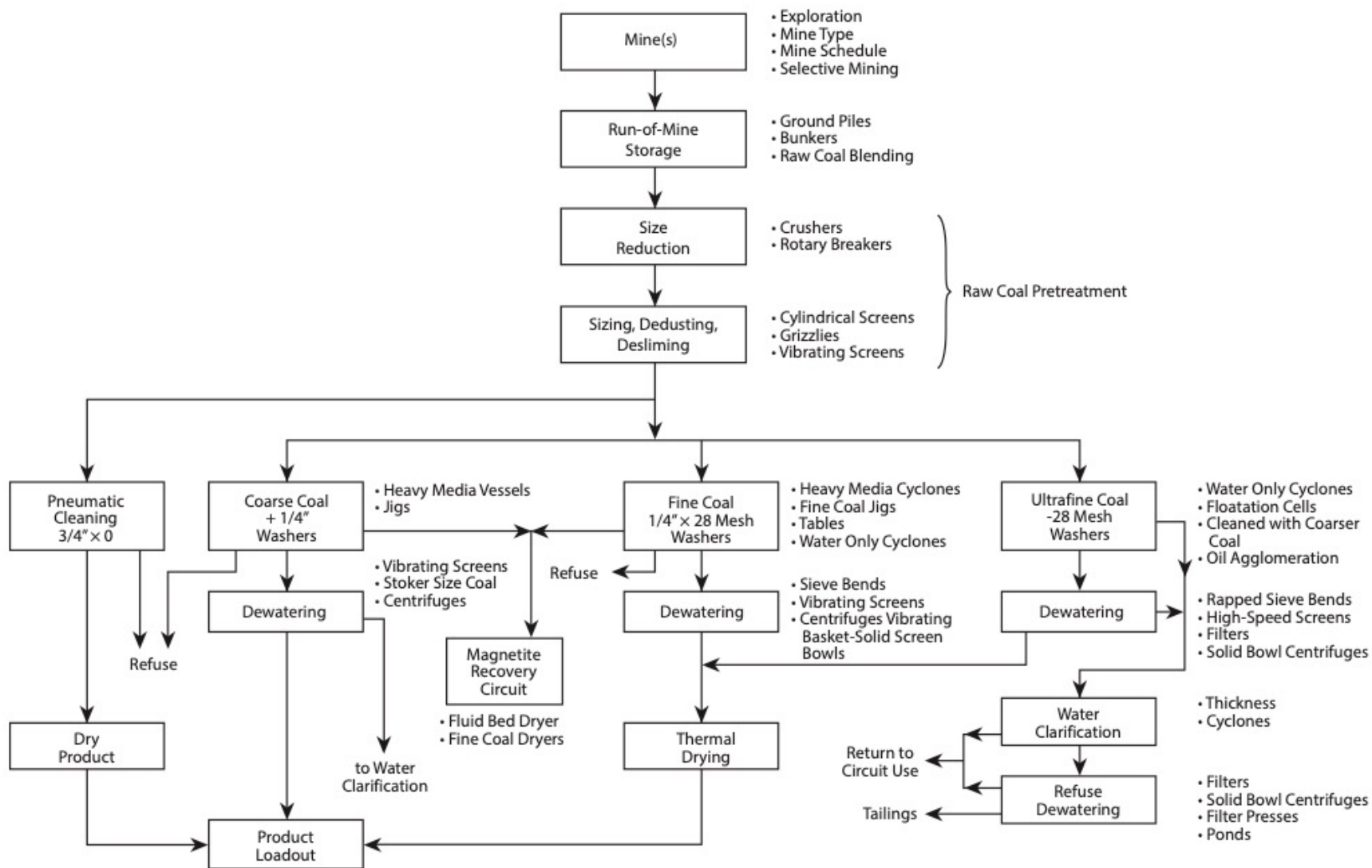


Figure 3.1 General layout of a coal preparation/coal cleaning plant (Speight, 2013).

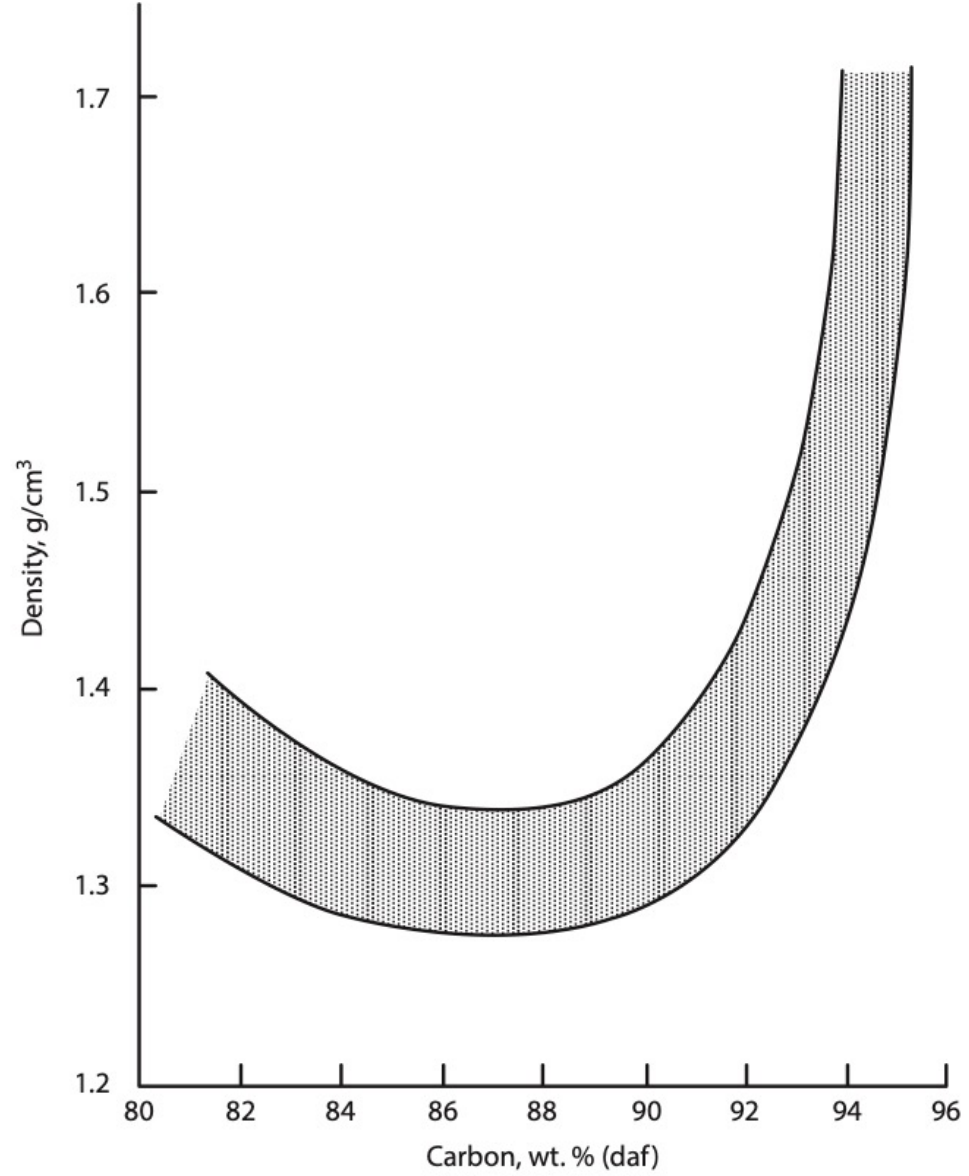


Figure 6.2 Variation of coal density with carbon content (Berkowitz, 1979).

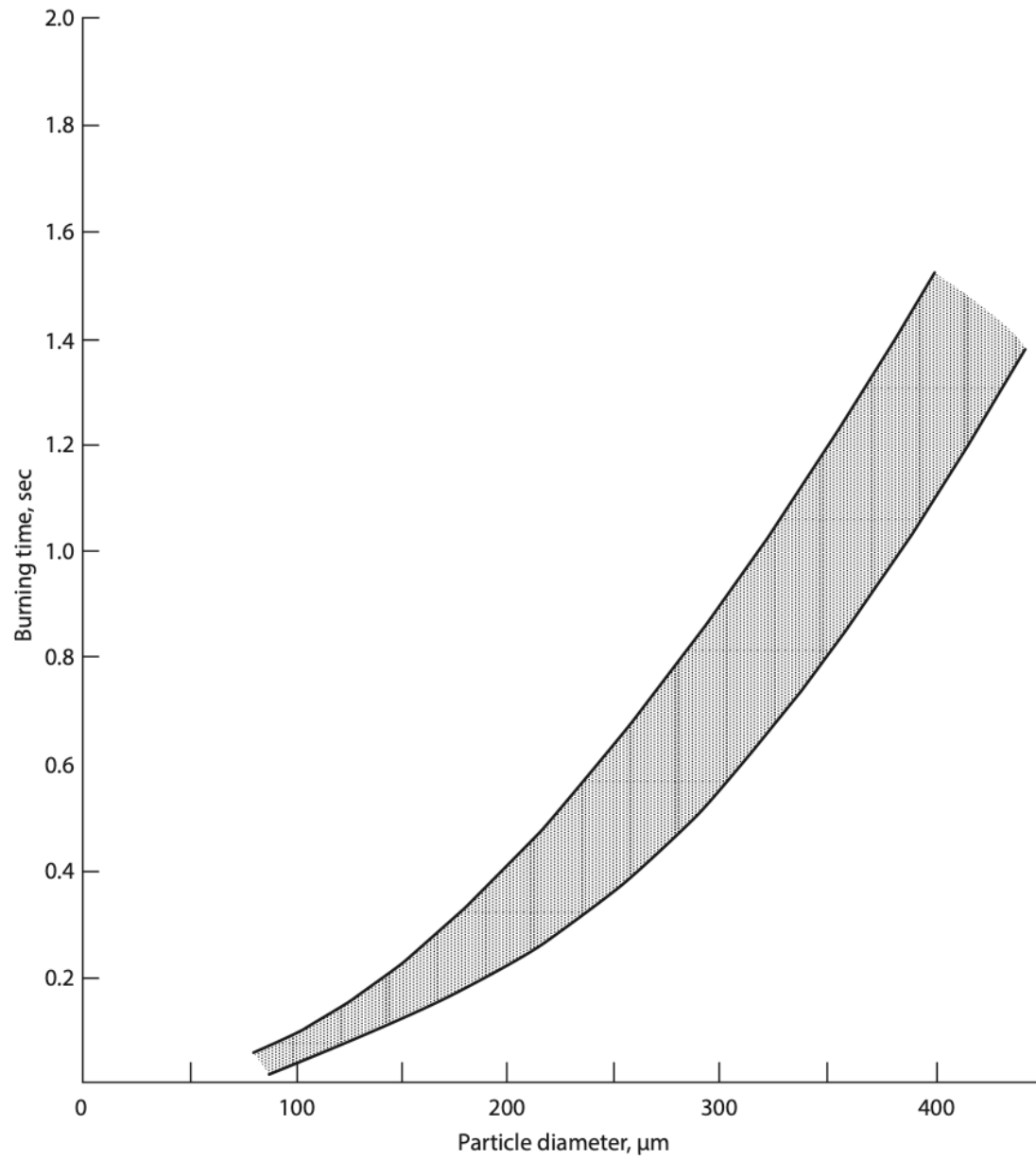


Figure 7.2 Relationship of burning time to particle size (Speight, 2013).

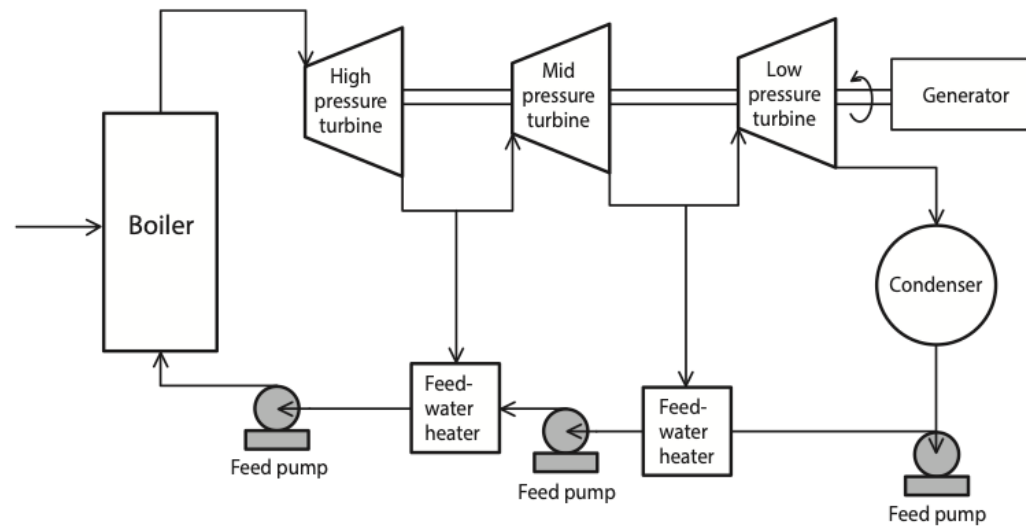


Figure 6.1 Schematic representation of a coal-fired power plant.

Pulverized Coal Boiler and Steam Turbine

<https://youtu.be/IdPTuwKEfmA>

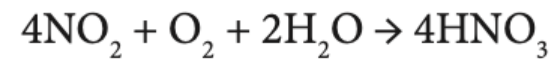
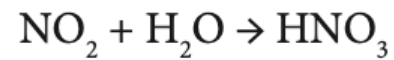
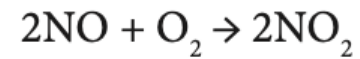
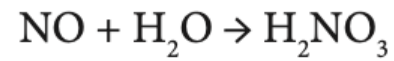
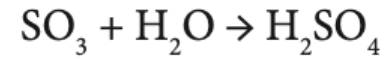
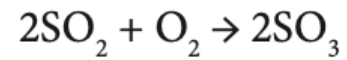
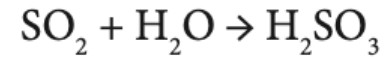
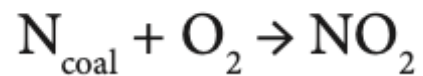
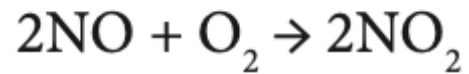
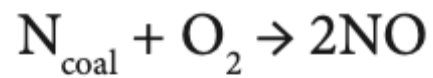
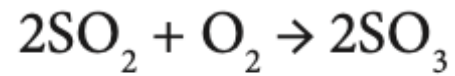
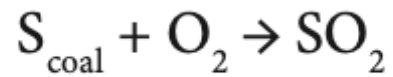
Table 7.2 Thermodynamics of coal combustion.

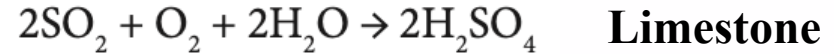
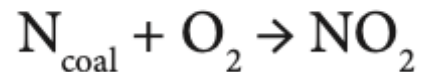
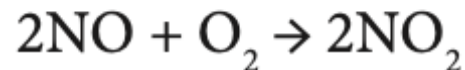
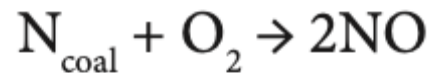
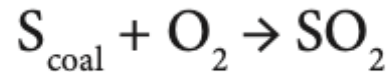
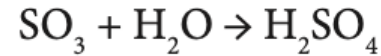
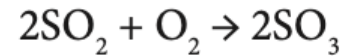
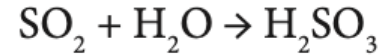
$C(s) + O_2(g) \rightarrow CO_2(g)$	-169,290 Btu/lb	-94.4 kcal/kg
$2 C(s) + O_2(g) \rightarrow 2 CO (g)$	-95,100 Btu/lb	-52.8 kcal/kg
$C(s) + CO_2(g) \rightarrow 2 CO (g)$	-74,200 Btu/lb	-41.2 kcal/kg
$2 CO(g) + O_2(g) \rightarrow 2 CO (g)$	-243,490 Btu/lb	-135.3 kcal/kg
$2 H_2(g) + O_2(g) \rightarrow 2 H_2O (g)$	-208,070 Btu/lb	-115.6 kcal/kg
$C(s) + H_2O(g) \rightarrow CO(g) + H_2 (g)$	+56,490 Btu/lb	+31.4 kcal/kg
$C(s) + 2 H_2O(g) \rightarrow CO_2 + 2 H_2 (g)$	+38,780 Btu/lb	+21.5 kcal/kg
$CO(g) + H_2O(g) \rightarrow CO_2(g) + H_2 (g)$	-17,710 Btu/lb	-9.8 kcal/kg

(g): gaseous state; (s): solid state.

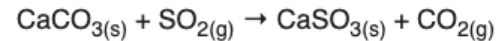
Exothermic reaction: illustrated by a negative heat of reaction.

Endothermic reaction: illustrated by a positive heat of reaction.

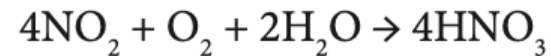
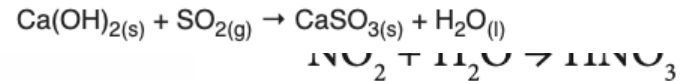


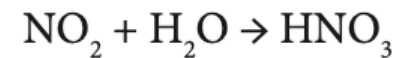
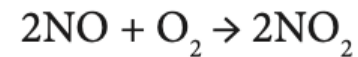
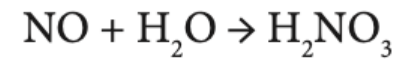
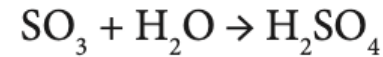
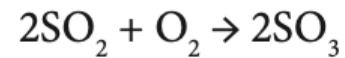
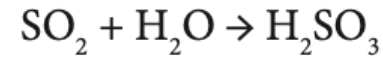
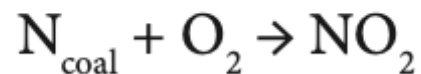
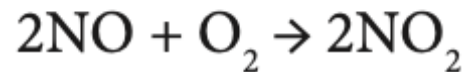
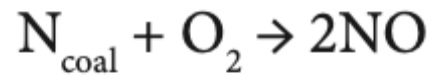
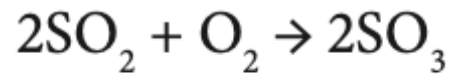
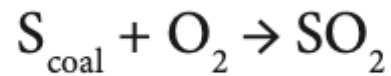


SO₂ is an **acid gas**, and, therefore, the typical sorbent slurries or other materials used to remove the SO₂ from the flue gases are alkaline. The reaction taking place in wet scrubbing using a CaCO₃ (**limestone**) slurry produces **calcium sulfite** (CaSO₃) and may be expressed in the simplified dry form as:

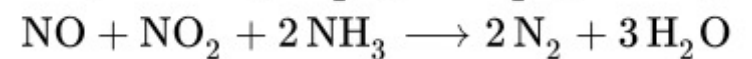
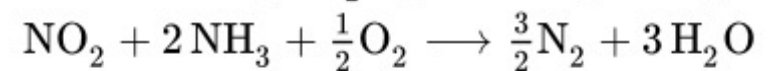
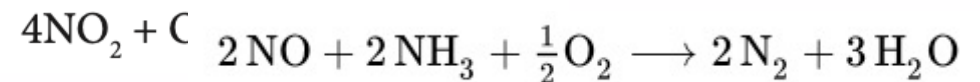


When wet scrubbing with a Ca(OH)₂ (**hydrated lime**) slurry, the reaction also produces CaSO₃ (**calcium sulfite**) and may be expressed in the simplified dry form as:





Ammonia



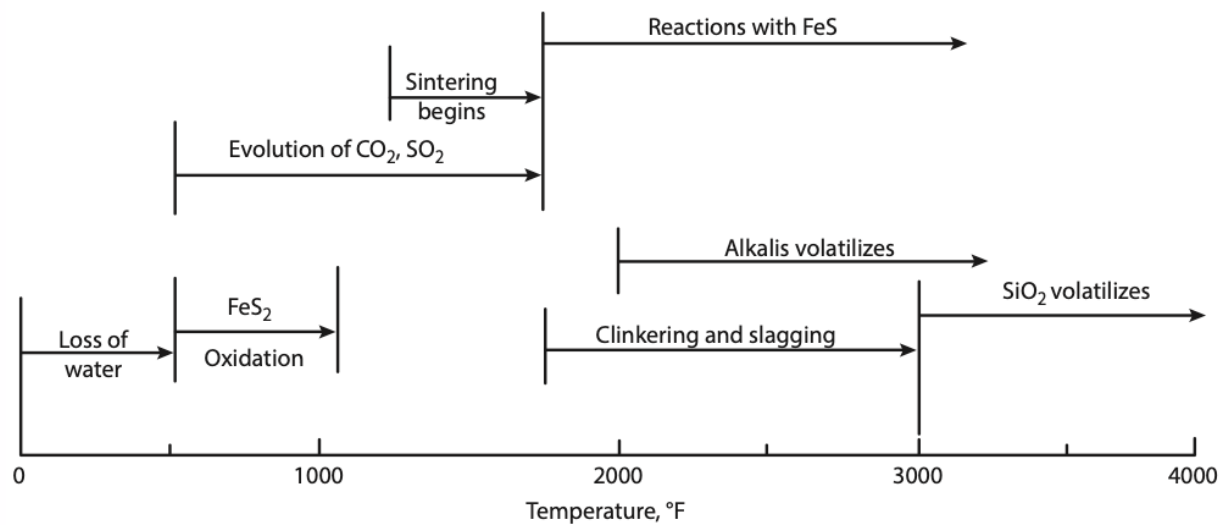


Figure 7.1 Changes occurring to the mineral matter during coal combustion (Reid, 1971).

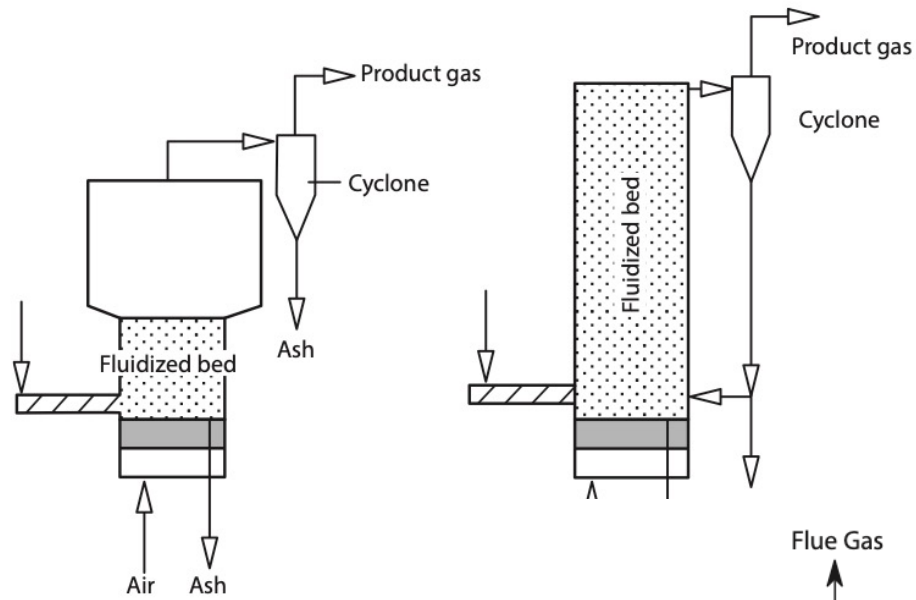


Figure 8.4 Schematic comparison of (a) a bubbling reactor.

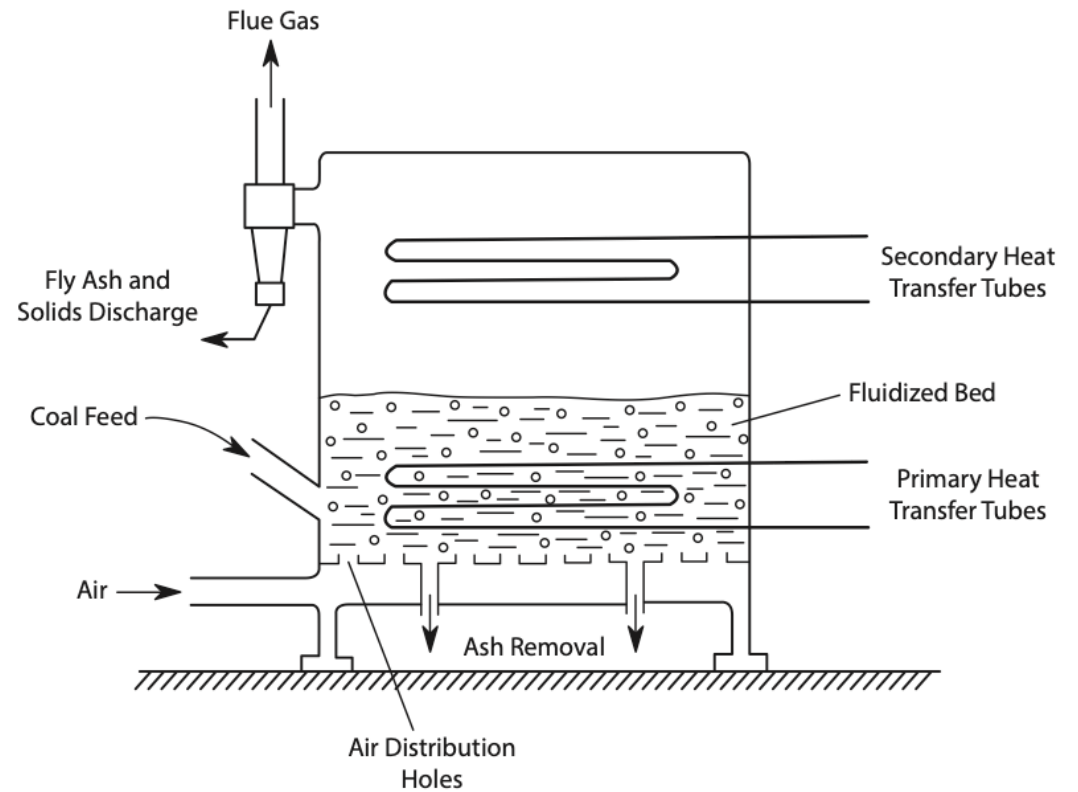


Figure 8.5 A Fluidized-Bed Combustor (Speight, 2013).

The main features of circulating fluidized-bed combustors (CFBC) are

- (i) compatibility with wide range of fuels – conventional boilers for power generation can use only fossil fuels, such as high-grade coal, oil, and gas where the circulating fluidized-bed combustor is also capable of using low-grade coal, biomass, sludge, waste plastics, and waste tires as fuel,
- (ii) low polluting NO_x and SO_x emissions are significantly decreased without special environmental modifications. The operation of circulating fluidized-bed boilers involves a two-stage combustion process: the reducing combustion at the fluidized-bed section, and the oxidizing combustion at the freeboard section. Next, the unburned carbon is collected by a high-temperature cyclone located at the boiler exit to recycle to the boiler, thus increasing the efficiency of denitrogenation, and
- (iii) high combustion efficiency. Improved combustion efficiency is attained through the use of a circulating fluidization-mode combustion mechanism.

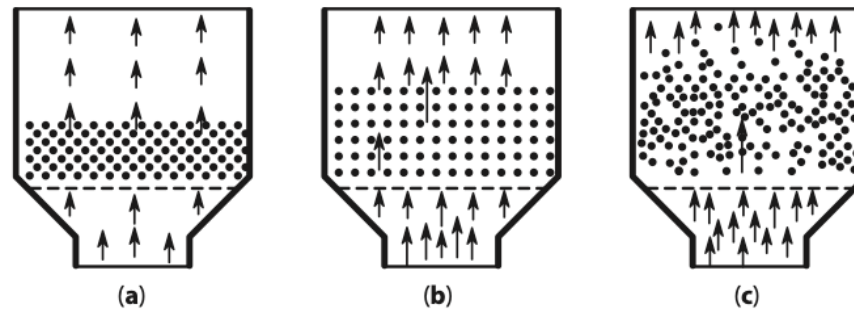


Figure 8.6 Illustration of the fluidized-bed concept: (a) Gas velocity less than the fluidizing velocity, (b) Gas velocity at the minimum fluidizing velocity, (c) Gas velocity greater than the fluidizing velocity (Speight, 2013).

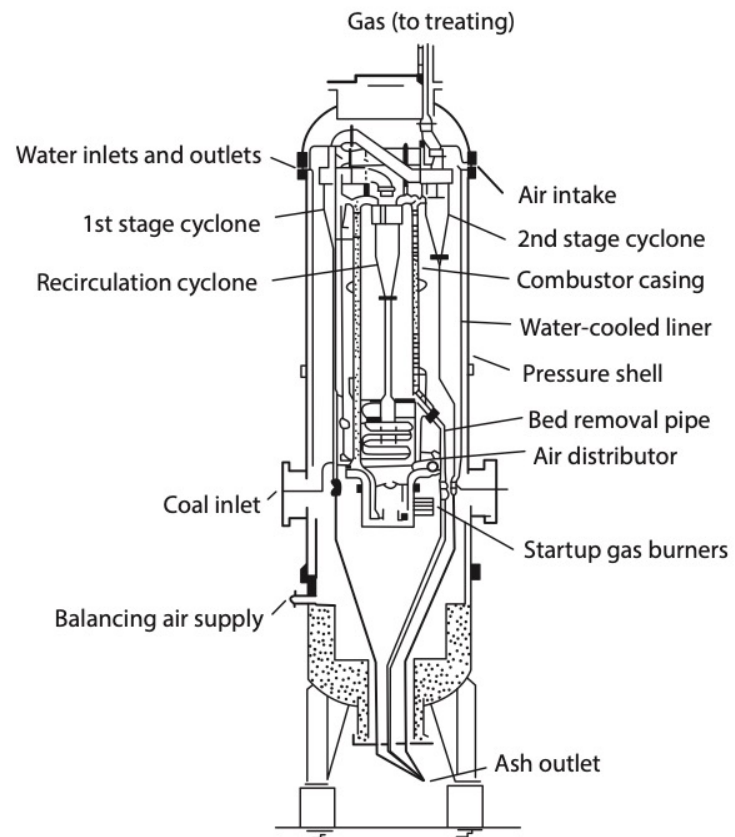
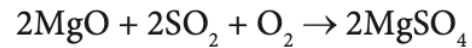
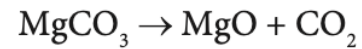
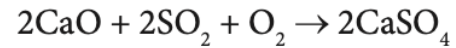
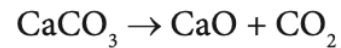


Figure 8.7 A pressurized fluidized-bed combustor (Speight, 2013).

Combustion in a fluidized bed has some particular benefits including suitability for use with low-grade, high-ash coals and the lower bed temperatures compared to those in a conventional furnace. As a result of this lower temperature the nitrogen oxide levels in the flue gas are reduced considerably. In addition, a reduction in sulfur dioxide emissions can also be achieved by mixing the coal with limestone (or dolomite). At the temperature of the bed the carbonate is converted to the oxide which reacts with any sulfur dioxide to give calcium (or magnesium) sulfate.



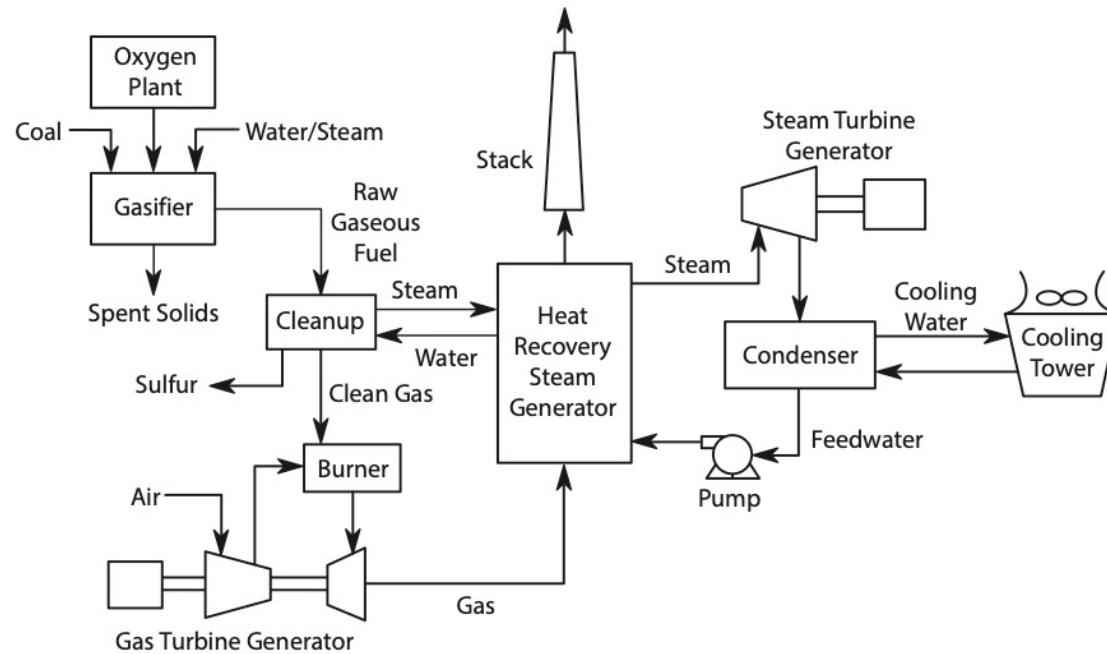
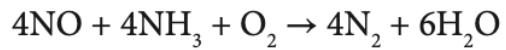


Figure 8.8 The Integrated Gasification Combined Cycle (IGCC) process (Speight, 2013).

Briefly, in the utility industry, combined cycle technology refers to the combined use of **hot combustion gas turbines** and **steam turbines** to generate electricity. This process can raise, quite significantly, the overall thermal efficiency of power plants above the thermal efficiency of conventional fossil fuel power plants using either type of turbine alone. Combined cycle plants that incorporate a gasification technology are called integrated gasification combined cycle (IGCC) plants (Figure 8.8)

Indeed, many coal-fired boilers are being built with burners designed to reduce nitrogen oxide formation by delaying fuel/air mixing, or distributed fuel addition, thereby establishing fuel-rich combustion zones within the burner whereby the reduced oxygen level maintains a low level of nitrogen oxides production (Slack, 1981; Wendt and Mereb, 1990). Other procedures employ ammonia to reduce the nitrogen oxides by injection of ammonia and oxygen into the post combustion zone.



Circulating Fluidized Bed Boiler

<https://youtu.be/4MQVJ6qbRuE>

[**https://youtu.be/Vjda91aVbYI**](https://youtu.be/Vjda91aVbYI)

<https://youtu.be/T6IcdLfV3G4>

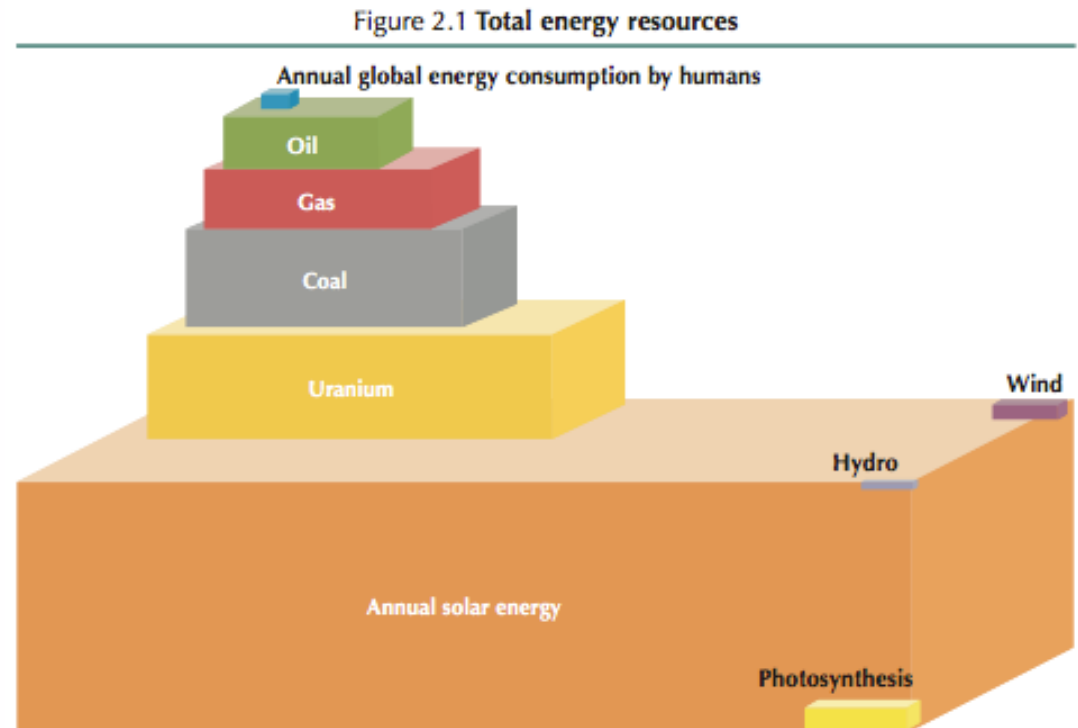
Pulverized Coal Boiler

<https://www.facebook.com/psmecpm/videos/a-pulverized-coal-fired-boiler-is-an-industrial-or-utility-boiler-that-generates/1346739345739888/>

<https://youtu.be/eqn0VBVWS50>

Non-Photovoltaic Solar Energy Harvesting

Solar Chimney
Solar Greenhouse
Biomass
Solar Heat
Passive Solar
Solar Water Heater
Solar Oven
Desalination
Solar Towers
ZnO Redox Reaction
Biomass/syngas
Solar Thermolysis
Solar Electricity & Electrolysis
Algae Tower



Source: National Petroleum Council, 2007, after Craig, Cunningham and Saigo (republished from IEA, 2008b).

Key point

Solar energy is the largest energy resource on Earth – and is inexhaustible.

Solar Green Houses in India

(<http://www.youtube.com/watch?feature=endscreen&v=8xFe91IMRH0&NR=1>)



Tomato Green House in Kenya (<http://www.youtube.com/watch?v=obsLwew-NT0>)

Roses Greenhouse in Ethiopia



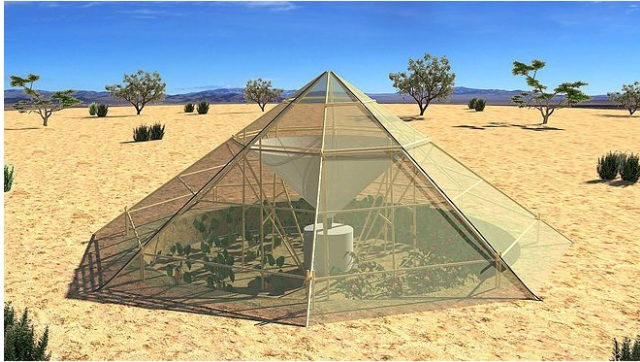
Lake Ziway Greenhouse



[Moorehead, KY AppHarvest](#)

Dew Collector /Greenhouse

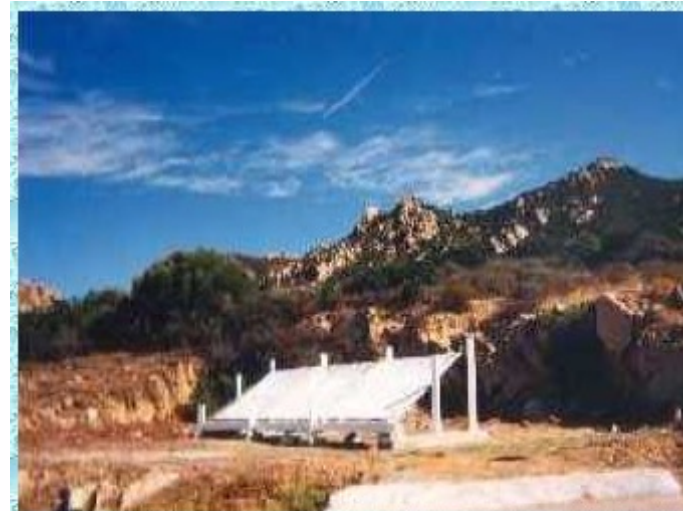
https://www.google.com/url?sa=t&rct=j&q=&esrc=s&source=video&cd=&cad=rja&uact=8&ved=2ahUKEwiq_pu00t2BAxV4j4kEHXzbAKAQtwj6BAgPEAI&url=https%3A%2F%2Fwww.youtube.com%2Fwatch%3Fv%3D1-dpSZIt_jw&usg=AOvVaw05SLURVmQ3CUbjTI7weiY&opi=89978449



International Organization for Dew Utilization



project in Morocco



**Experimental dew condenser in Vignola
(Corsica island, France)**

<https://www.opur.cloud>

Solar Desalination/Water Purification

[Solar Still Video](http://www.youtube.com/watch?v=GrPRnaS449w) (http://www.youtube.com/watch?v=GrPRnaS449w)



[Sea water still for survival](#)

Solar Desalination/Water Purification

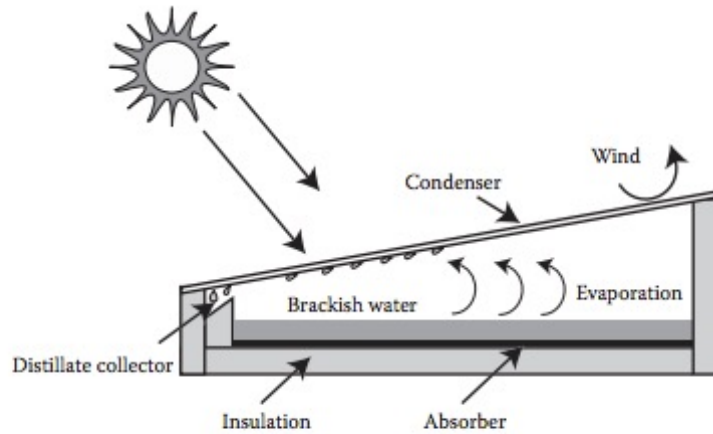


FIGURE 4.26 Basic operation of a solar still.

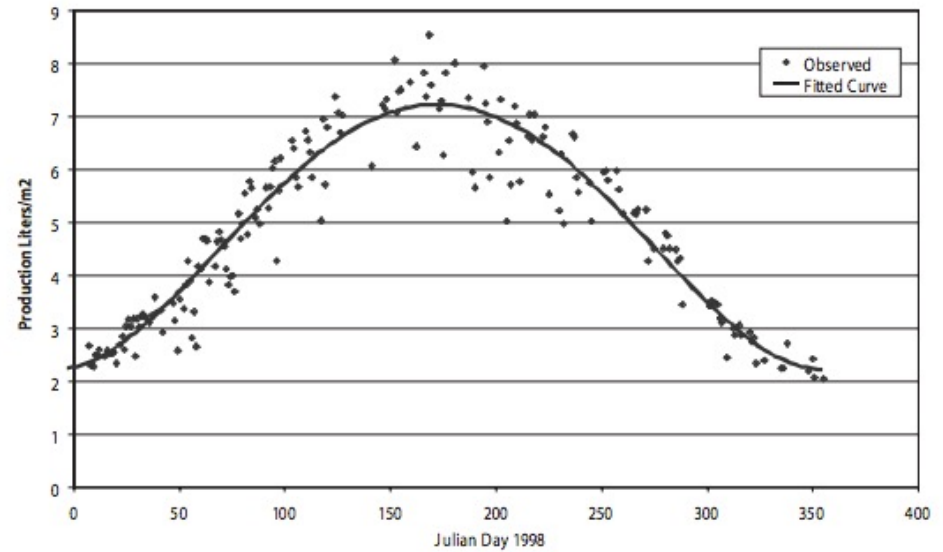


FIGURE 4.27 Measured basin solar still annual performance in Las Cruces, New Mexico, on a square-meter basis (Zachritz, 2000).

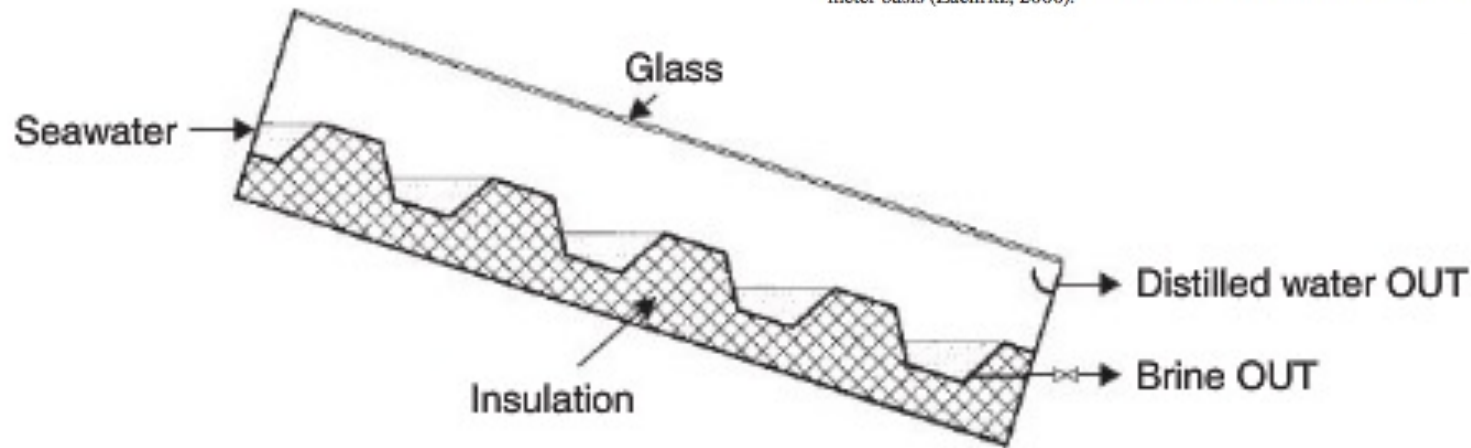


FIGURE 8.3 Schematic of a cascaded solar still.

Solar Desalination/Water Purification

TABLE 4.7
Sandia National Laboratories Still-Water Quality Test Results (Zirzow, SAND92-0100)

Sample type	13% Salinity feedwater	Distilled water (13% case)	16% Salinity feedwater	Distilled water (16% case)
Calcium (total)	340	1.5	371	<0.10
Iron (total)	0.27	<0.05	0.48	<0.06
Magnesium (total)	2.1	2.1	<0.005	<0.005
Manganese (total)	0.04	<0.02	0.07	<0.02
Ammonia as N	<0.1	0.1	<0.1	<0.1
Chloride	19,000	<1.0	25,000	2.6
Fixed solids	32,000	<1.0	41,000	31
Nitrate as NO ₃	34	0.1	26	<0.1
Nitrate as NO ₂	0.013	<0.01	0.02	<0.01
TDS	36,000	<1.0	48,000	<1.0
Volatiles and organics	4,200	<1.0	6,000	13

TABLE 4.6
Microbial Test Results for Solar Stills

Sample	Volume tested ml	Total organisms per liter
Supply	50	16,000
Distillate	1,000	4
<i>E. coli</i> seed		2,900,000,000
Distillate	750	11 (No <i>E. coli</i>)
<i>E. coli</i> seed	—	7,500,000,000
Distillate	1,000	18 (No <i>E. coli</i>)
Supply	10	24,000
Distillate	1,000	13
Supply	1	12,000
Distillate	1,000	6

Source: New Mexico State University, 1992.



FIGURE 4.28 SolAqua solar still village array under test at Sandia National Laboratories.

Solar Desalination/Water Purification



Figure 7-2 *Demonstration solar still.*

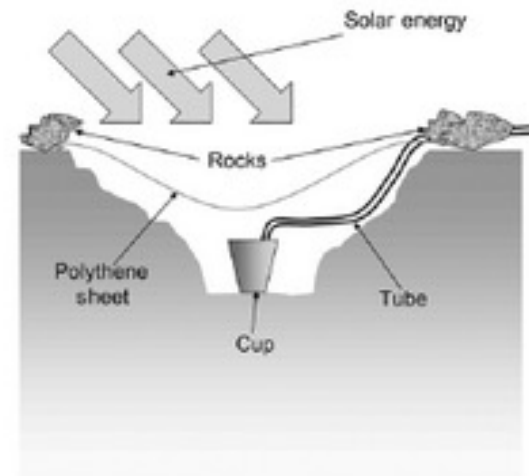


Figure 7-4 *Diagram of a pit solar still.*



Figure 7-5 *A solar still in operation.* Image courtesy © U.S. Department of Agriculture—Agricultural Research Service.

Solar Desalination/Water Purification

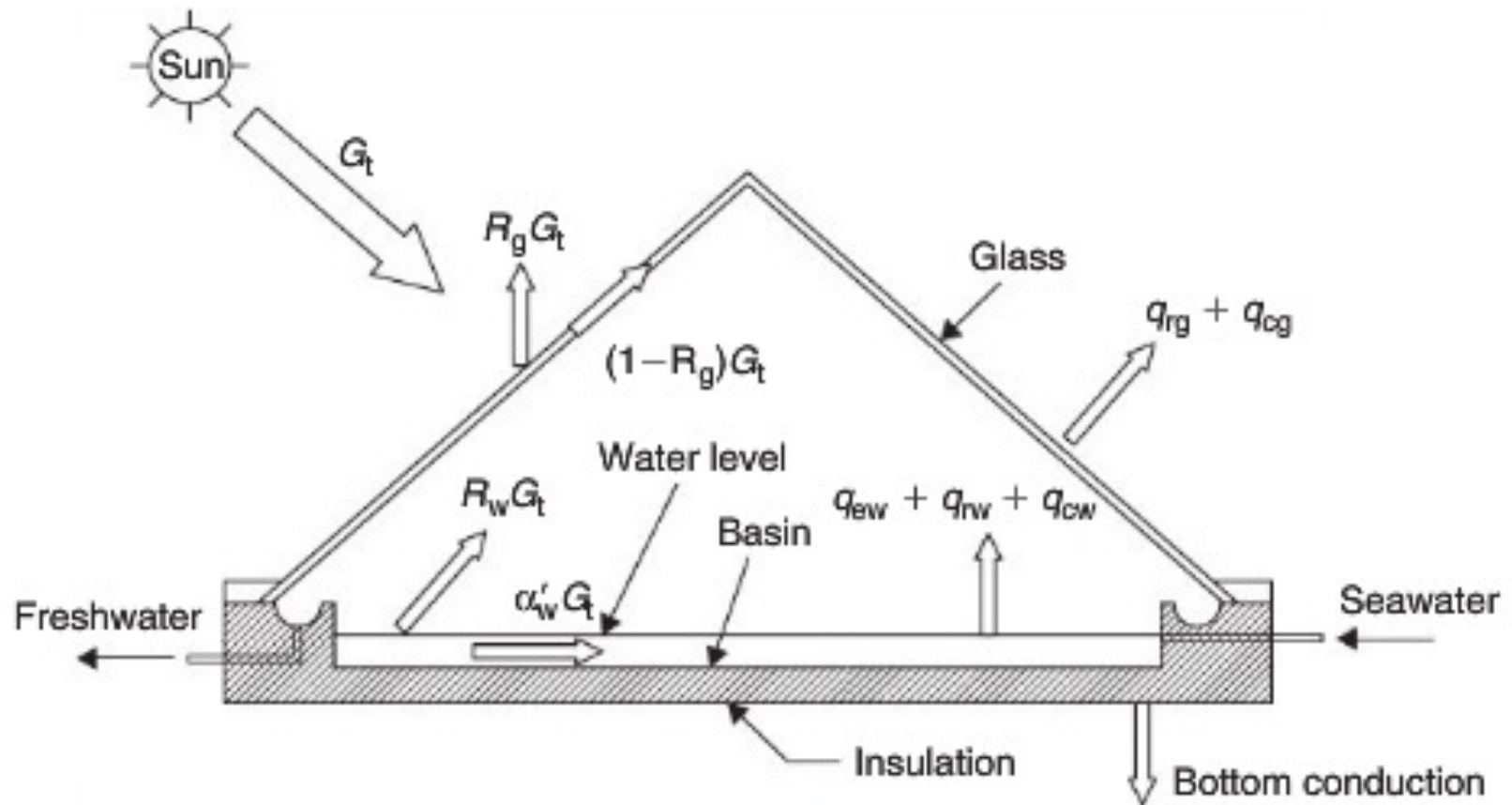


FIGURE 8.1 Schematic of a solar still.

Solar Desalination/Water Purification

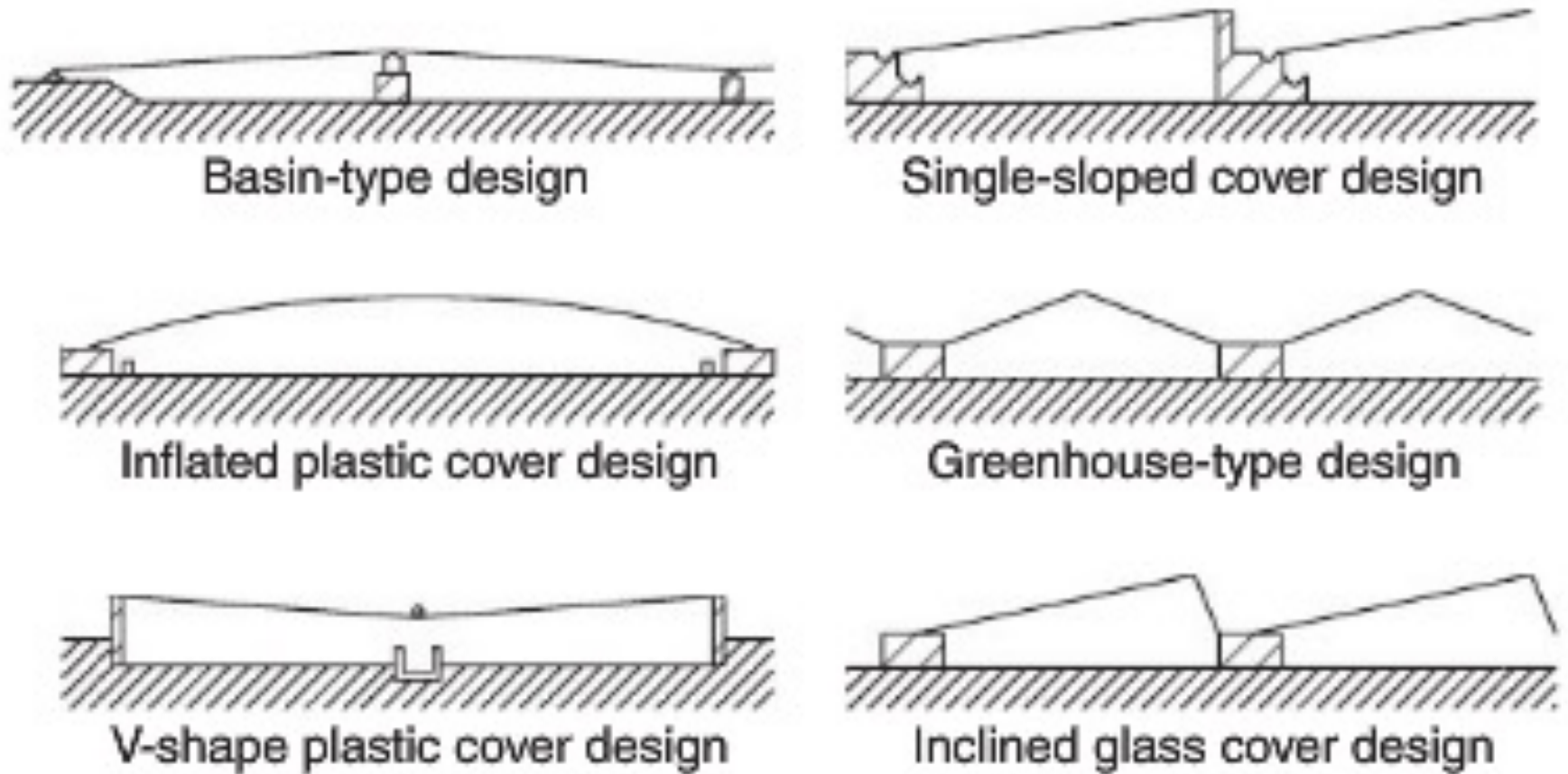


FIGURE 8.2 Common designs of solar stills.

Solar Desalination/Water Purification

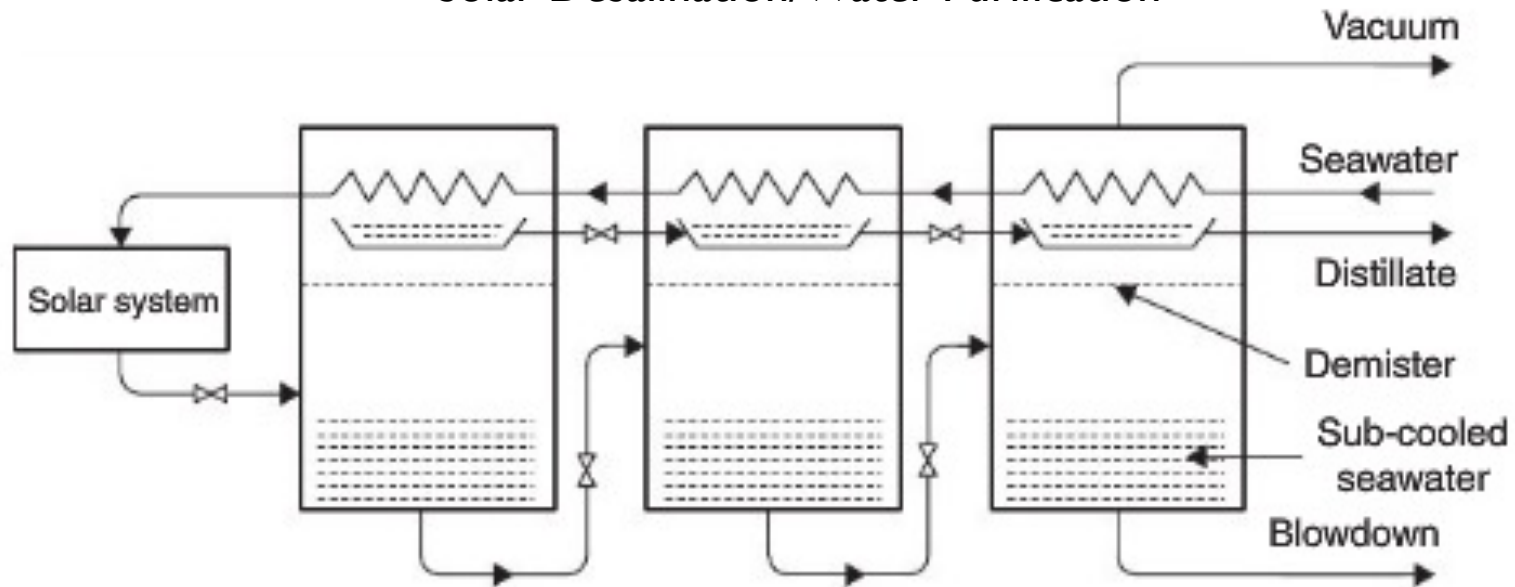


FIGURE 8.4 Principle of operation of the multi-stage flash (MSF) system.

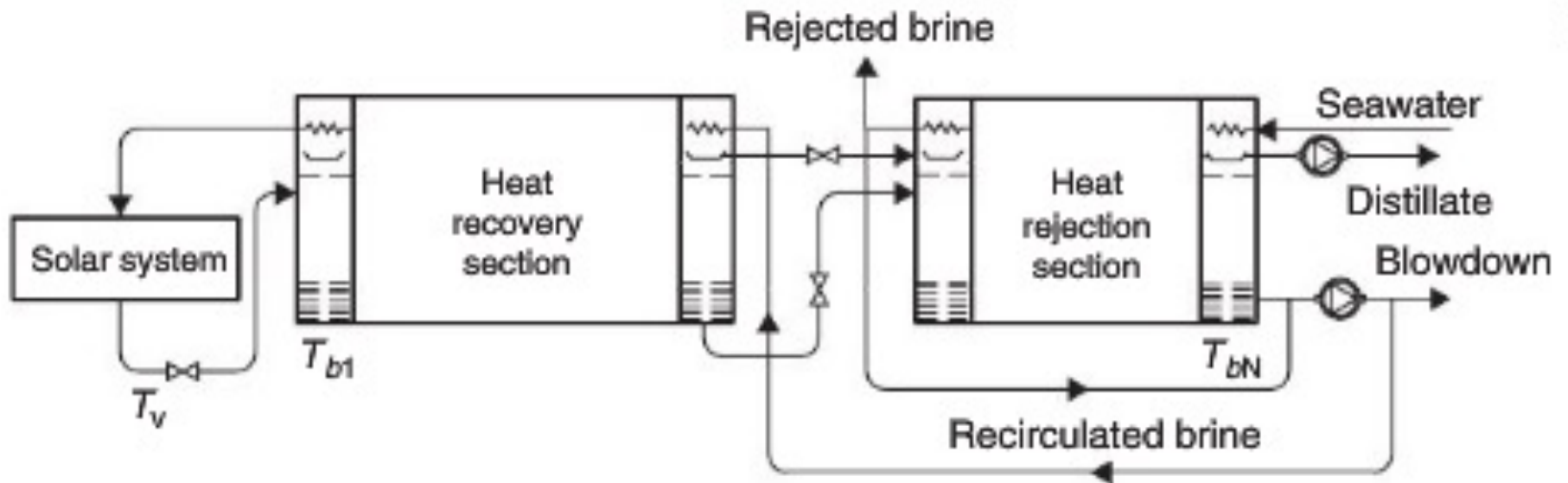


FIGURE 8.5 A multi-stage flash (MSF) process plant.

Solar Desalination/Water Purification

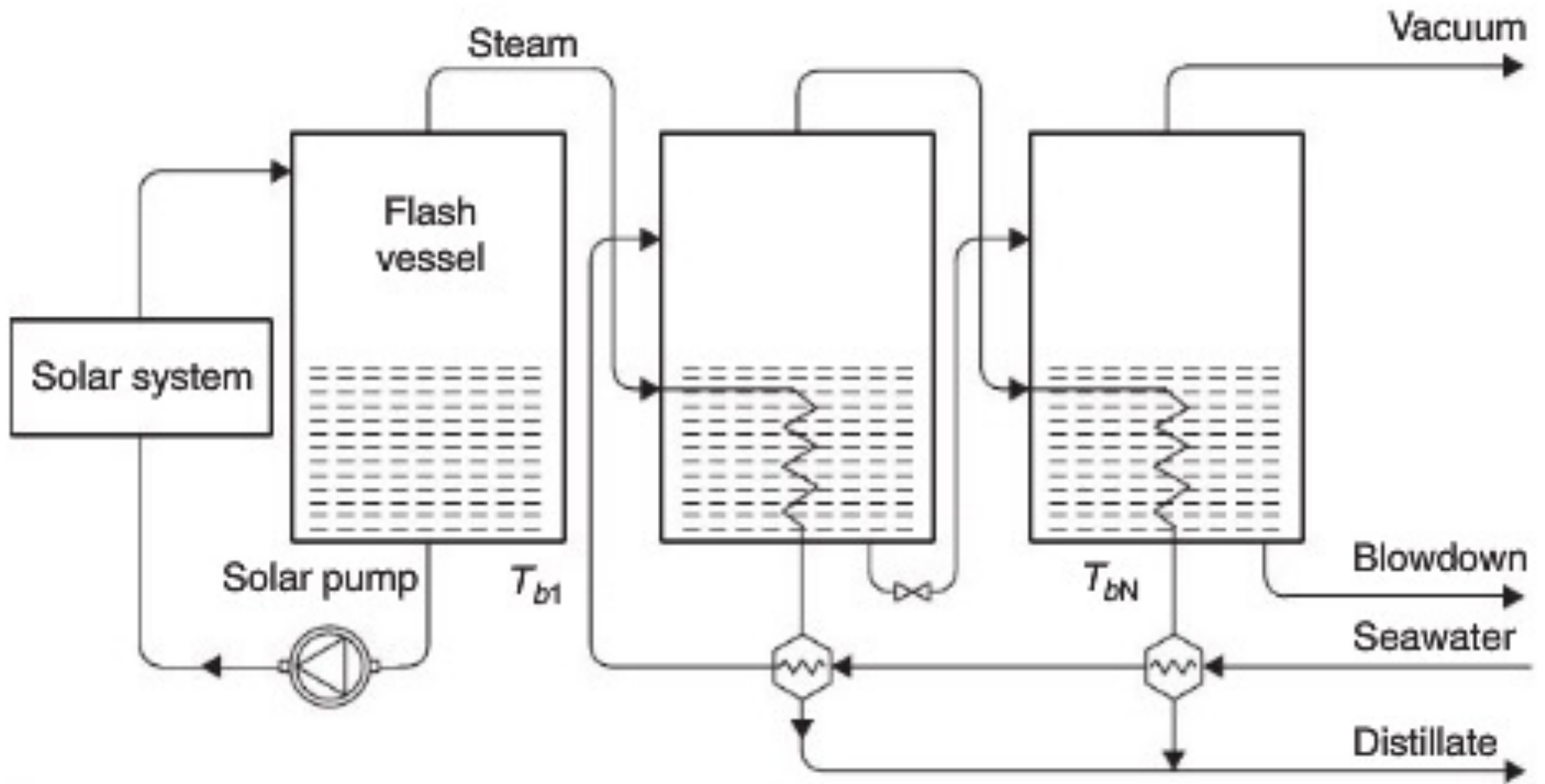


FIGURE 8.6 Principle of operation of a multiple-effect boiling (MEB) system.

Solar Desalination/Water Purification

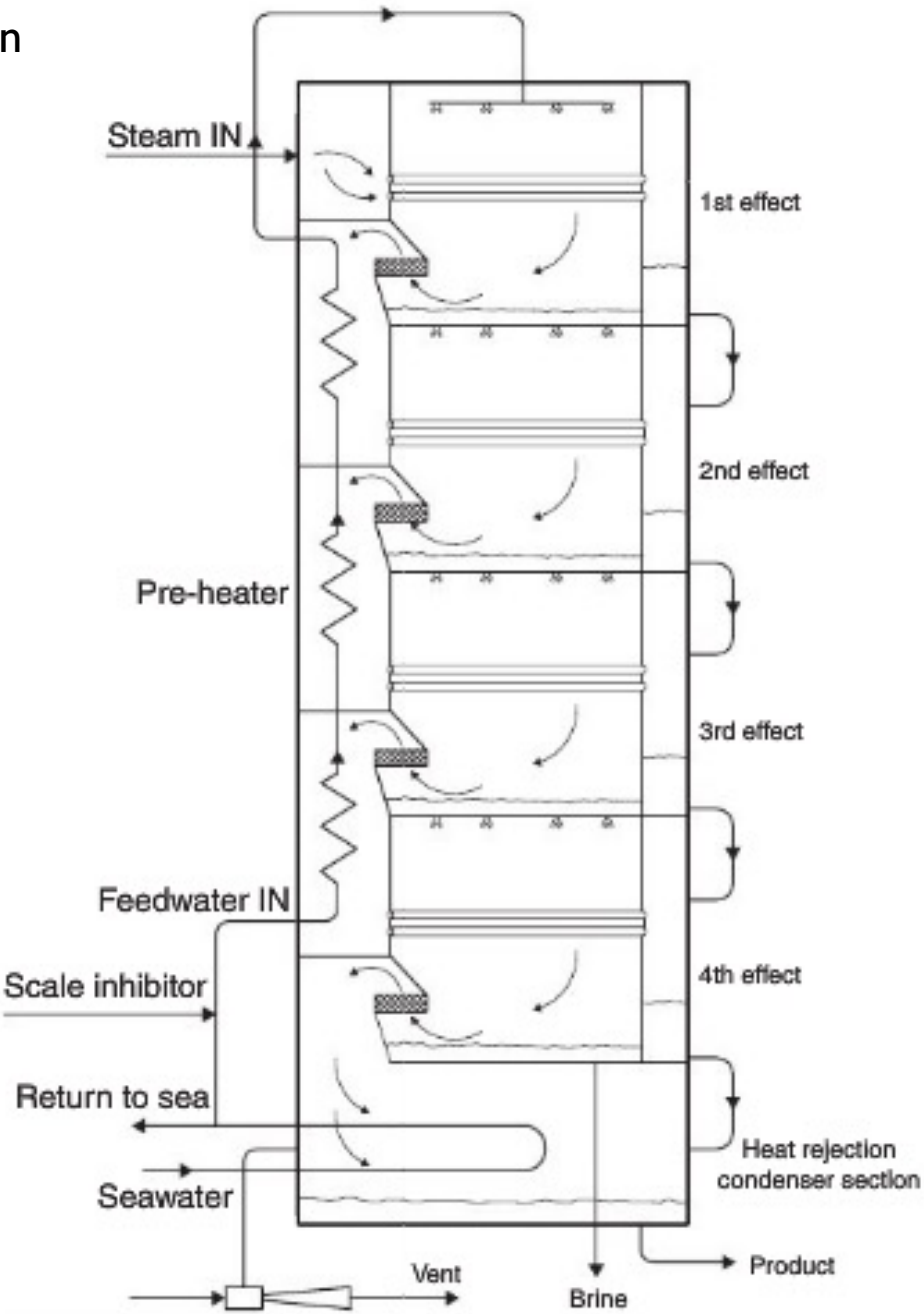
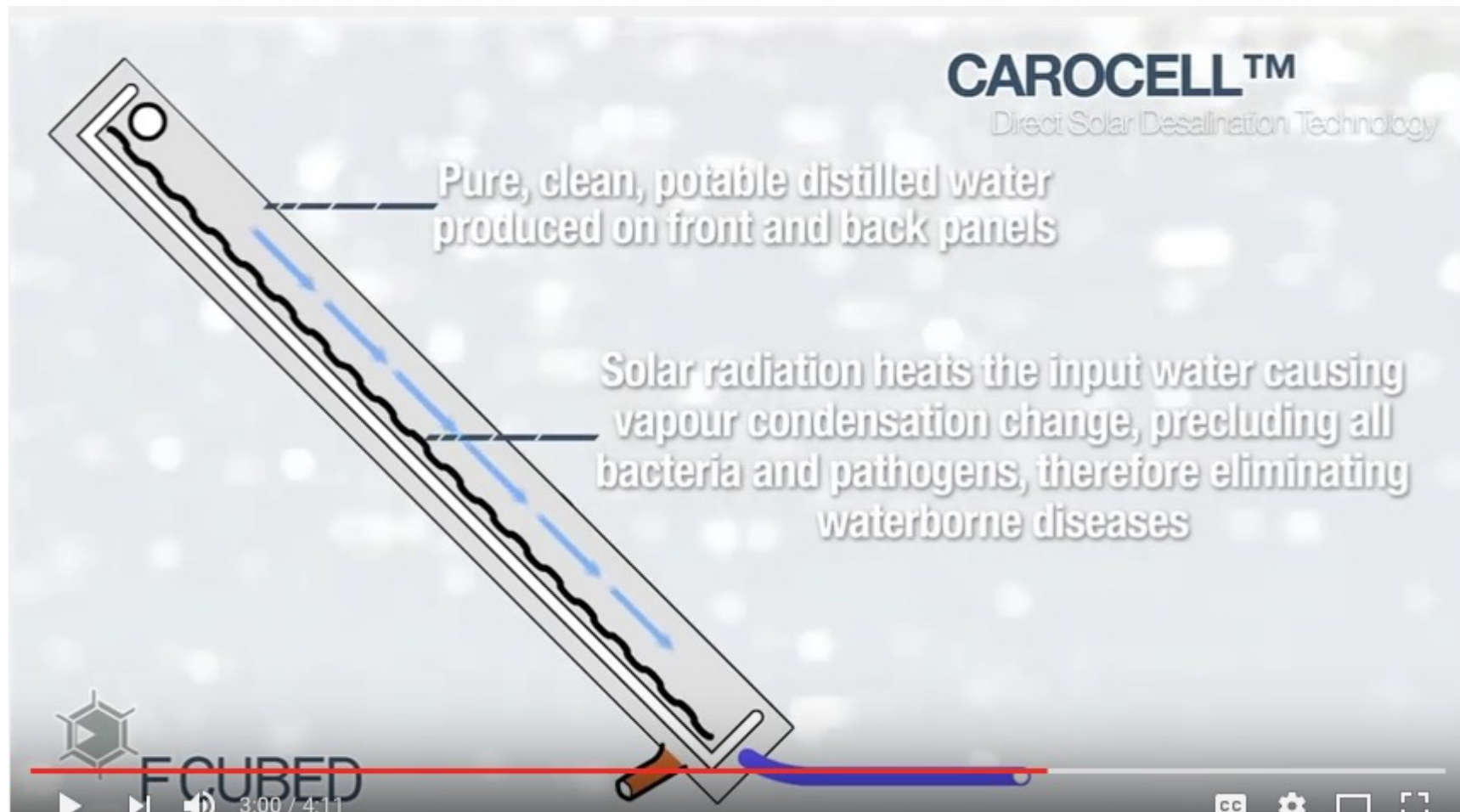


FIGURE 8.8 Schematic of the MES evaporator.

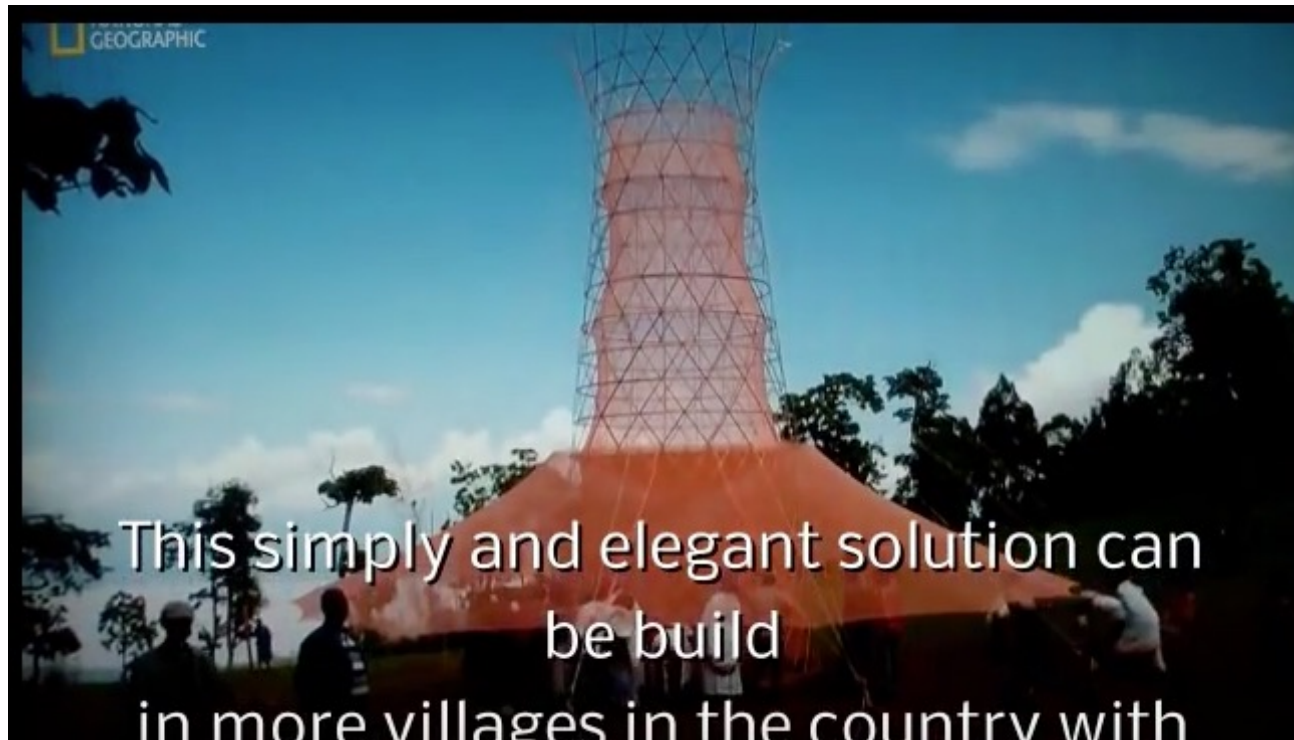
Carocell Australia



King Abdullah's Desalinization Plant



Clean Water from Air



Seawater Greenhouse

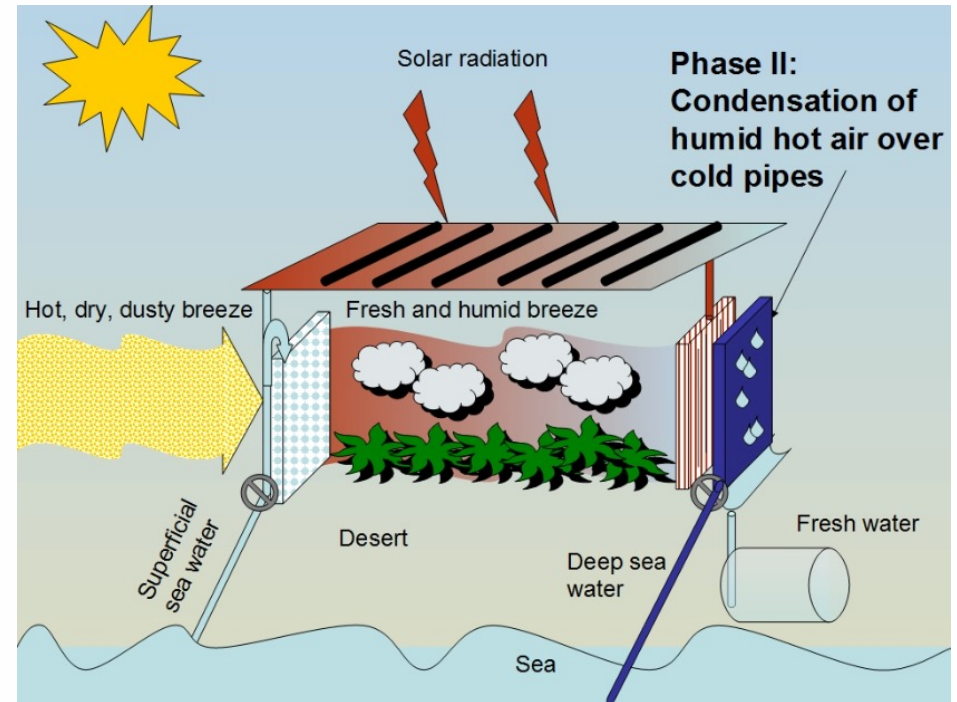
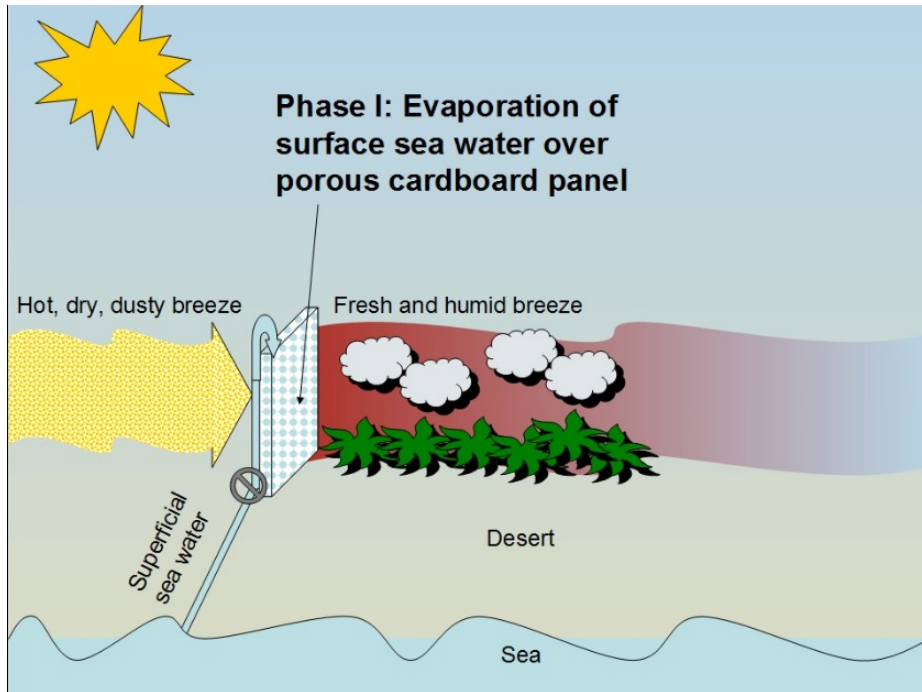


Figure 3. The surrounding area from the front of the greenhouse



Figure 4. Two years into operation from the back of the greenhouse

Seawatergreenhouse.com

A restorative approach to agriculture



Solar Heat Collectors

[Do it yourself webpage](http://www.n3fjp.com/solar/construction101/construction101.htm)

<http://www.n3fjp.com/solar/construction101/construction101.htm>



- Direct or open loop systems, in which potable water is heated directly in the collector.
 - Indirect or closed loop systems, in which potable water is heated indirectly by a heat transfer fluid that is heated in the collector and passes through a heat exchanger to transfer its heat to the domestic or service water.
-
- Natural (or passive) systems.
 - Forced circulation (or active) systems.

Table 5.1 Solar Water Heating Systems

Passive systems	Active systems
Thermosiphon (direct and indirect)	Direct circulation (or open loop active) systems
Integrated collector storage	Indirect circulation (or closed loop active) systems, internal and external heat exchanger
	Air systems
	Heat pump systems
	Pool heating systems

Passive Systems

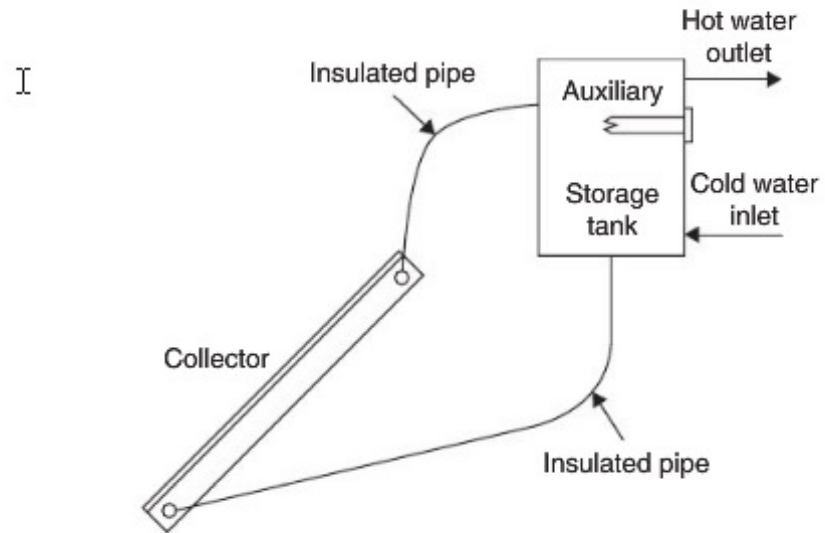
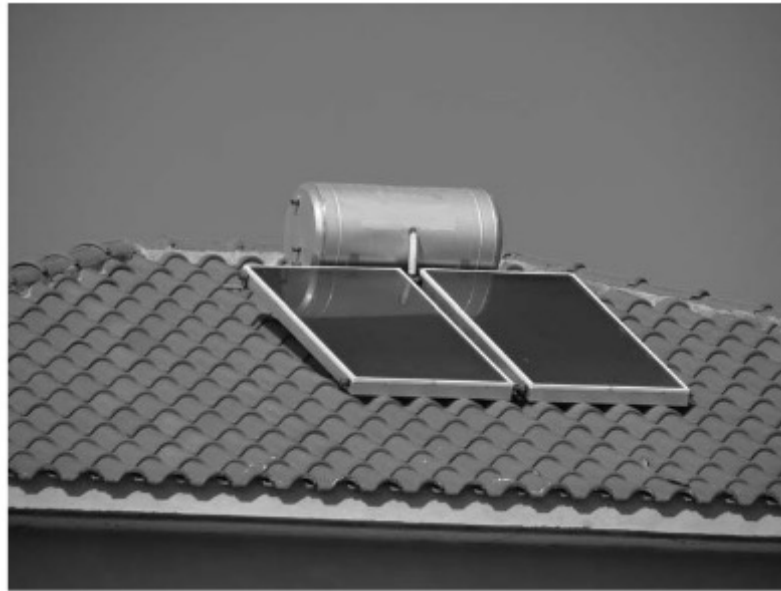


FIGURE 5.1 Schematic diagram of a thermosiphon solar water heater.



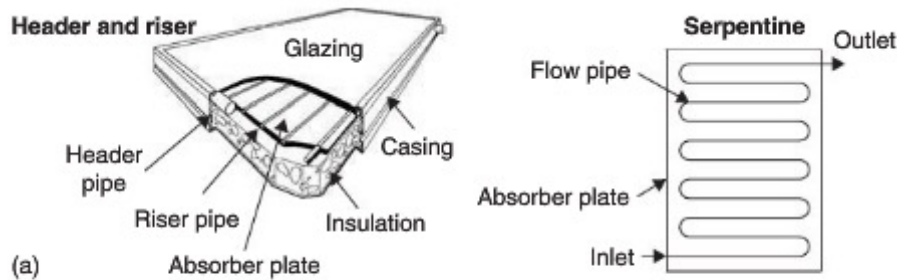
(a)



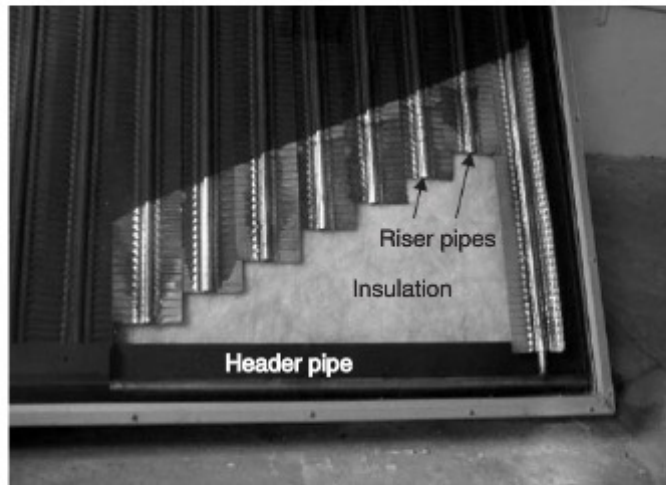
(b)

FIGURE 5.2 Thermosiphon system configurations. (a) Flat-plate collector configuration. (b) Evacuated tube collector configuration.

Solar Heat Collectors



(a)



(b)

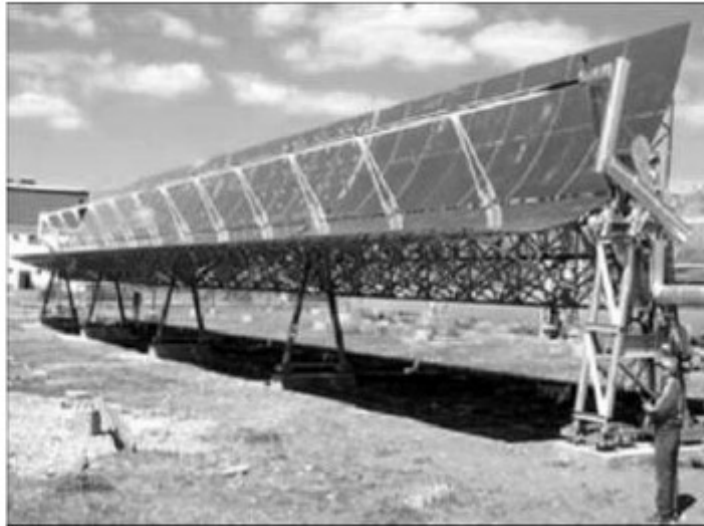
FIGURE 3.1 Typical flat-plate collector. (a) Pictorial view of a flat-plate collector. (b) Photograph of a cut header and riser flat-plate collector.

Table 3.1 Solar Energy Collectors

Motion	Collector type	Absorber type	Concentration ratio	Indicative temperature range (°C)
Stationary	Flat-plate collector (FPC)	Flat	1	30–80
	Evacuated tube collector (ETC)	Flat	1	50–200
	Compound parabolic collector (CPC)	Tubular	1–5	60–240
5–15			60–300	
Single-axis tracking	Linear Fresnel reflector (LFR)	Tubular	10–40	60–250
	Cylindrical trough collector (CTC)	Tubular	15–50	60–300
	Parabolic trough collector (PTC)	Tubular	10–85	60–400
Two-axis tracking	Parabolic dish reflector (PDR)	Point	600–2000	100–1500
	Heliostat field collector (HFC)	Point	300–1500	150–2000

Note: Concentration ratio is defined as the aperture area divided by the receiver/absorber area of the collector.

Solar Heat Collectors



(a)



(b)

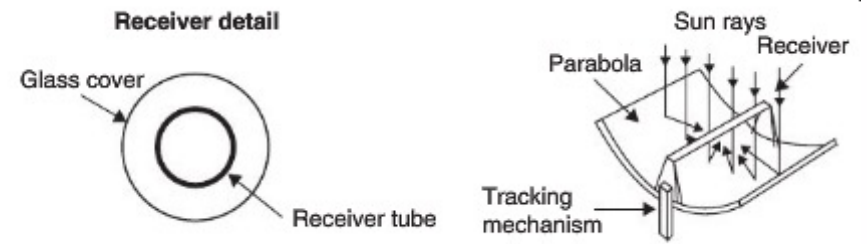


FIGURE 3.13 Schematic of a parabolic trough collector.

FIGURE 3.14 Photos of actual parabolic trough collectors. (a) The EuroTrough (from www.sbp.de/en/html/projects/detail.html?id=1043). (b) An Industrial Solar Technology collector.

Solar Heat Collectors

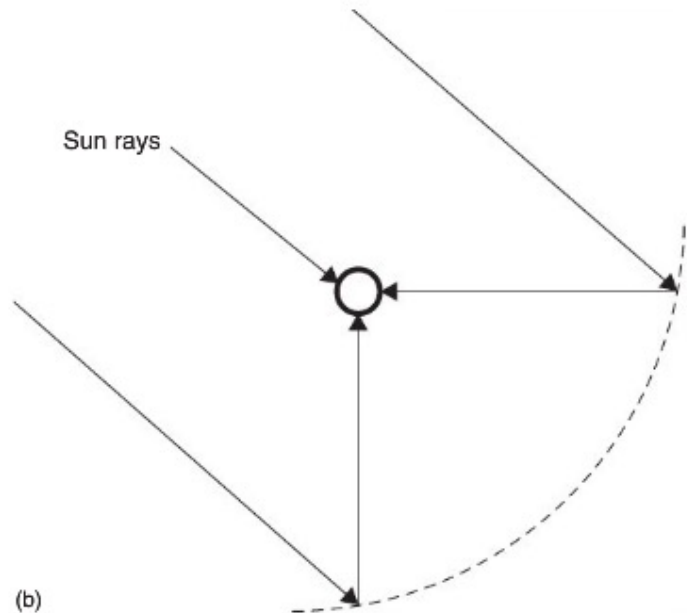
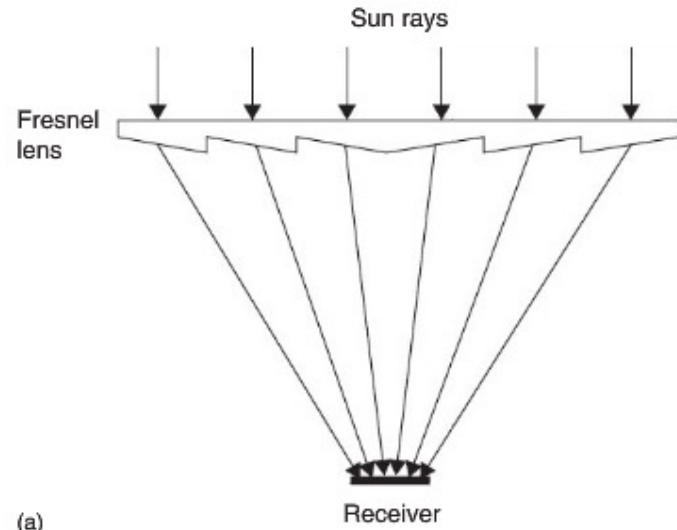
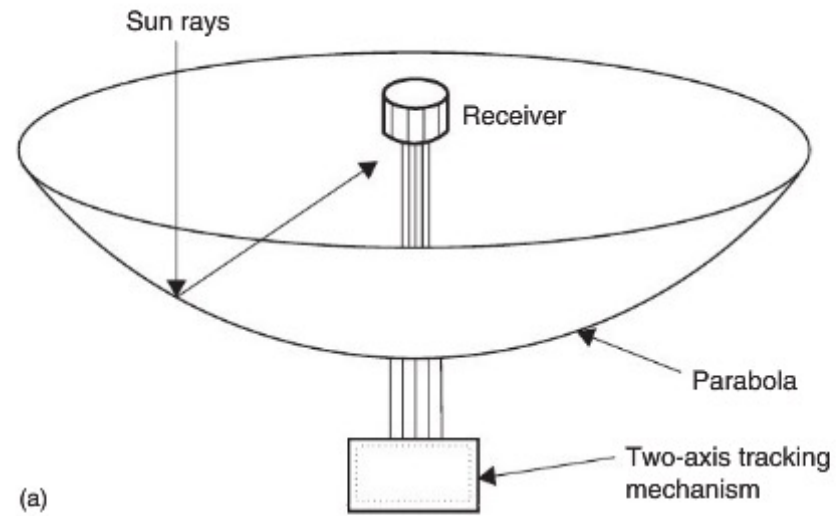


FIGURE 3.17 Fresnel collectors. (a) Fresnel lens collector (FLC). (b) Linear Fresnel-type parabolic trough collector.

Solar Heat Collectors



(a)



(b)

FIGURE 3.20 Parabolic dish collector. (a) Schematic diagram. (b) Photo of a Eurodish collector (from www.psa.es/webeng/instalaciones/discos.html).

Solar Heat Collectors



FIGURE 10.8 Photograph of a dish concentrator with Stirling engine (source: www.energylan.sandia.gov/sunlab/pdfs/dishen.pdf).



FIGURE 10.7 Heliostat detail of the Solar Two plant (source: www.energylan.sandia.gov/sunlab/overview.htm).

[Eurodish Solar Stirling Engine](https://www.youtube.com/watch?v=wfDWDqyToBg) (https://www.youtube.com/watch?v=wfDWDqyToBg)

[Stirling Engine Wiki](http://en.wikipedia.org/wiki/Stirling_engine) (http://en.wikipedia.org/wiki/Stirling_engine)

[Stirling Engine Water Pump \(Large\)](http://www.youtube.com/watch?v=CEBuzq5ilqk)
(http://www.youtube.com/watch?v=CEBuzq5ilqk)

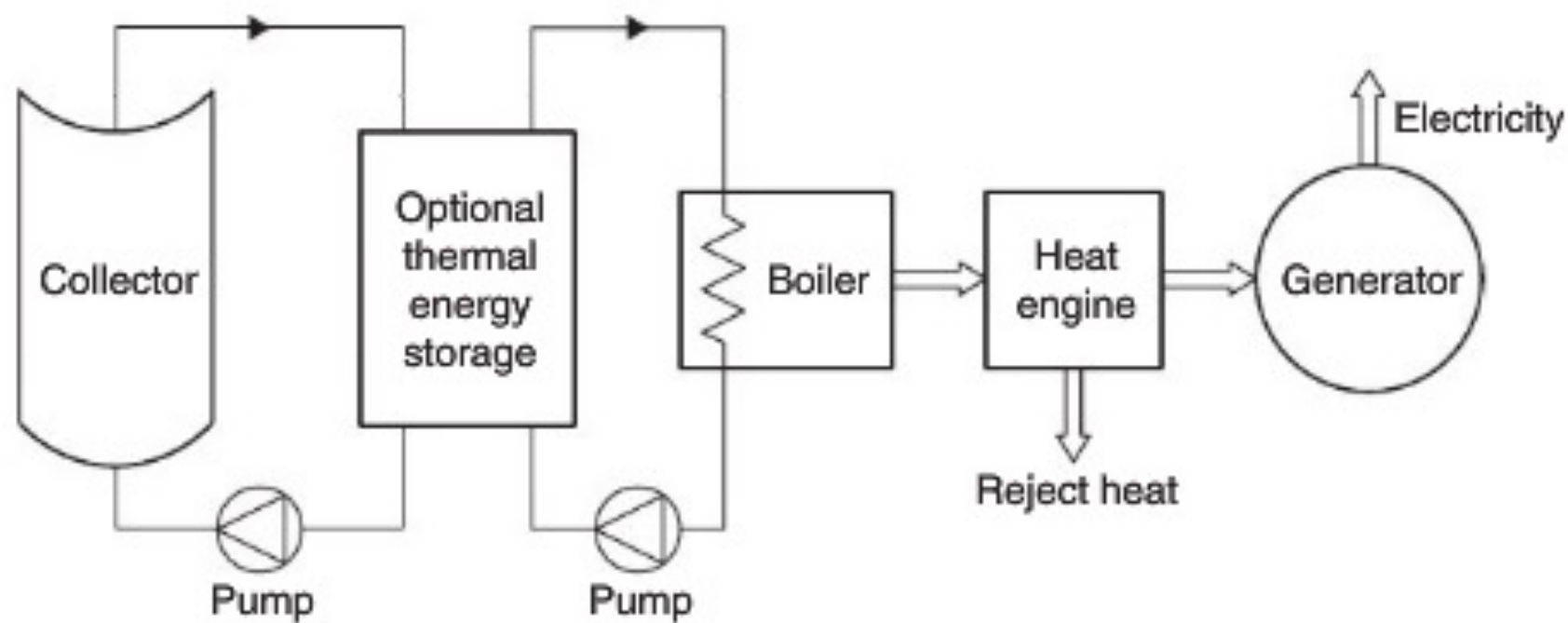


FIGURE 10.1 Schematic diagram of a solar-thermal energy conversion system.

Solar Heat Collectors



FIGURE 3.22 Detail of a heliostat.

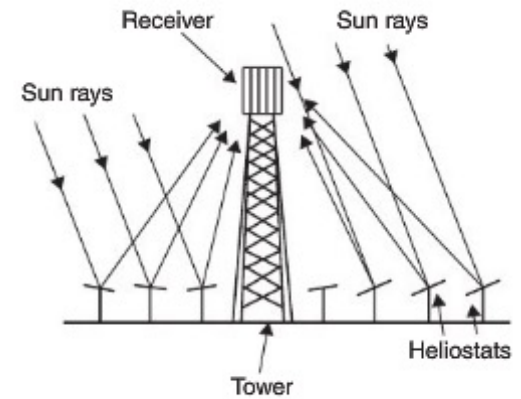


FIGURE 3.21 Schematic of central receiver system.

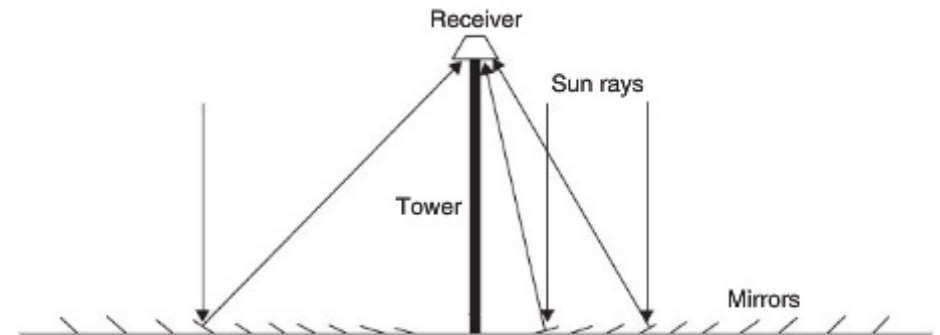


FIGURE 3.18 Schematic diagram of a downward-facing receiver illuminated from an LFR field.

Solar Heat Collectors

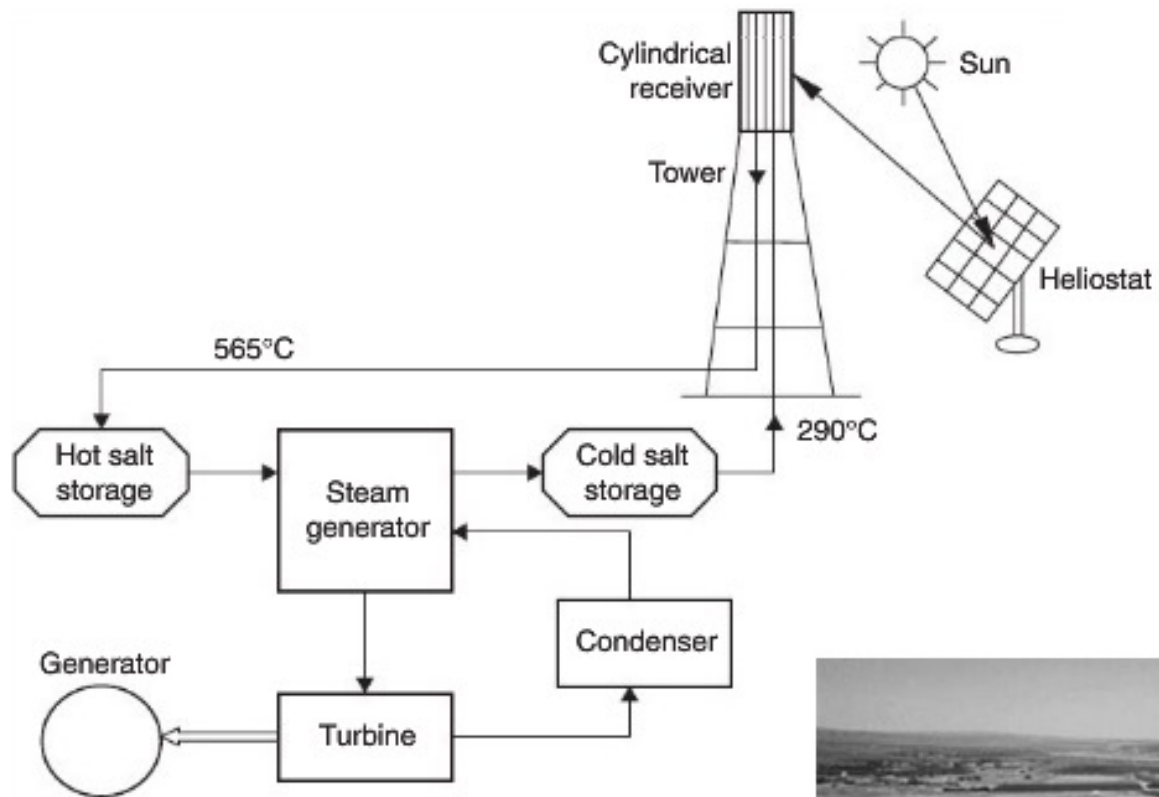


FIGURE 10.5 Schematic of the Solar Two plant.



FIGURE 10.6 Photograph of the Solar Two central receiver plant (source: www.energylan.sandia.gov/sunlab/Snapshot/STFUTURE.HTM).

Solar Heat Collectors

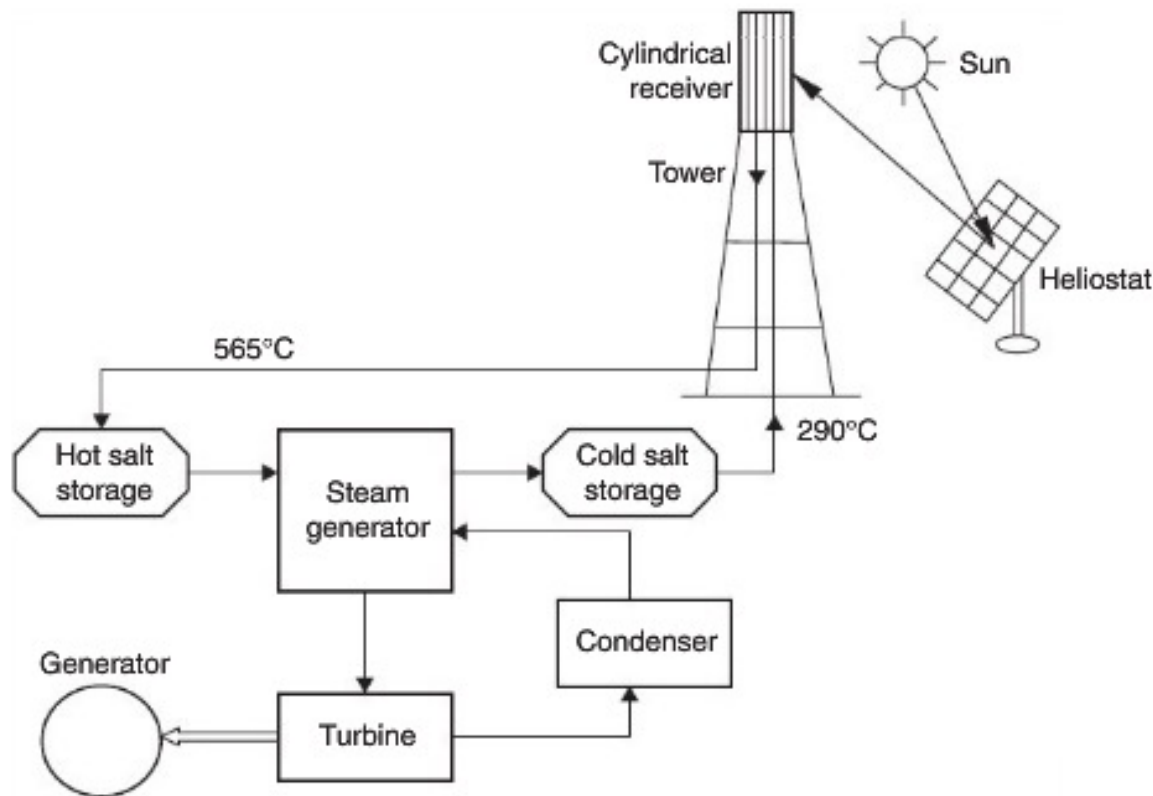


FIGURE 10.5 Schematic of the Solar Two plant.

Solar Tres (Gemasolar)

How it works

<http://www.youtube.com/watch?v=GhV2LT8KVgA>

<https://www.youtube.com/watch?v=5nd7fGMXciA>

Gemasolar



Gemasolar



Location of Gemasolar

Country	Spain
Location	Fuentes de Andalucía, Sevilla
Coordinates	37°33'29.11"N 5°19'44.6"W
Status	Operational
Commission date	May 2011
Owner(s)	Torresol Energy

Solar farm

Type	CSP
CSP technology	Solar power tower
Heliostats	2,650

Power generation

Installed capacity	19.9 MW
Annual generation	110 GW-h

Photo 3.1 **The Gemasolar power tower near Sevilla (Spain)**



Source: Torresol Energy.

Key point

Molten-salts solar towers can generate electricity round the clock.

[Aroa Solar Ethiopia](#)

<http://www.alternative-energy-news.info/tulip-solar-ethiopia/>



[Aroa Solar .com](http://AroaSolar.com)

<https://sustainability.asu.edu/research/project/aora-solar-tulip/>

Table 10.1 Performance Characteristics of Various CSP Technologies

Technology	Capacity range (MW)	Concentration	Peak solar efficiency (%)	Solar-electric efficiency (%)	Land use (m ² /MWh-a)
Parabolic trough	10–200	70–80	21	10–15	6–8
Fresnel reflector	10–200	25–100	20	9–11	4–6
Power tower	10–150	300–1000	20	8–10	8–12
Dish-Stirling	0.01–0.4	1000–3000	29	16–18	8–12

[Images for dish stirling](#) - Report images



Solar Chimney's

Enviromission (Australia)

http://www.enviromission.com.au/EVM/content/about_companyprofile.html

Solar Chimney Spain (Madrid)

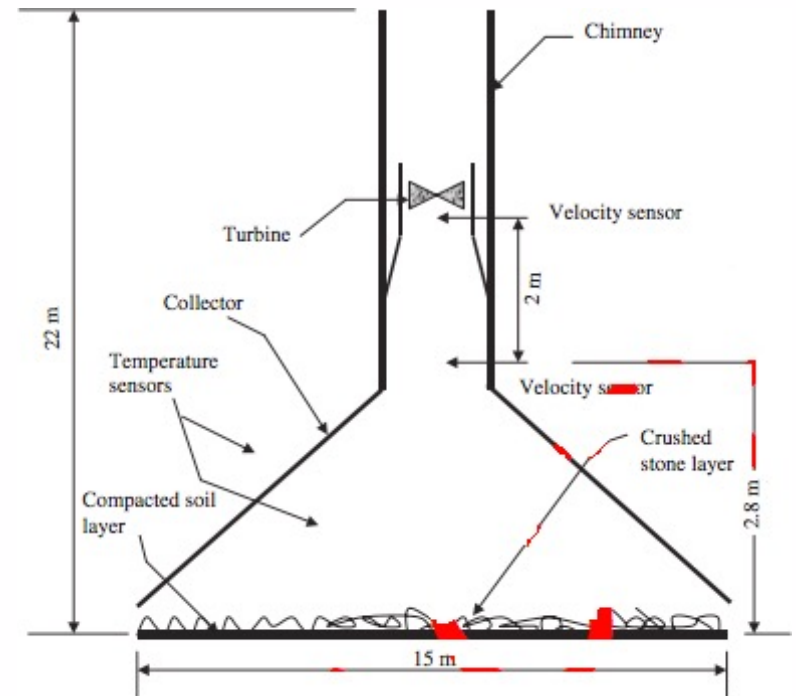
<http://www.youtube.com/watch?v=XCGVTYtjEFk>



Solar Chimney's



Gaborone, Botswana



Hot Water Systems

This webpage goes through types of solar water heaters

<http://www.alternative-energy-tutorials.com/solar-hot-water/evacuated-tube-collector.html>

Hot Water Systems

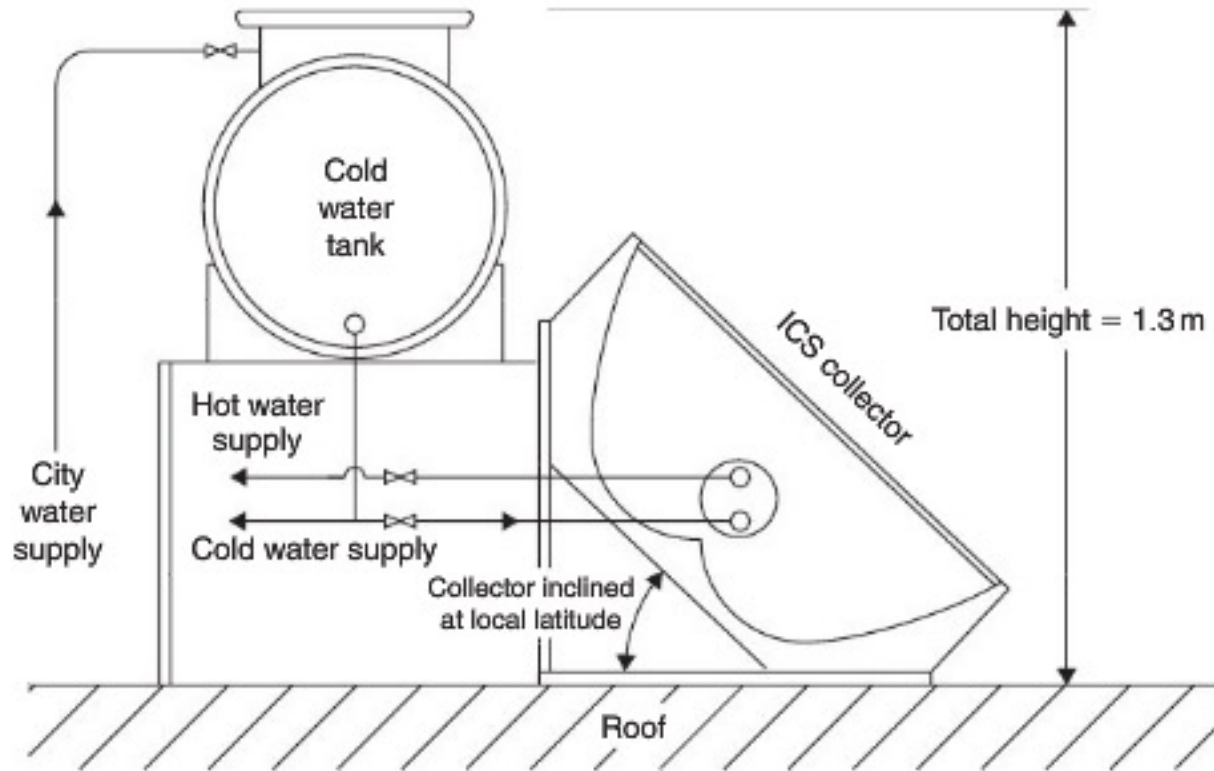
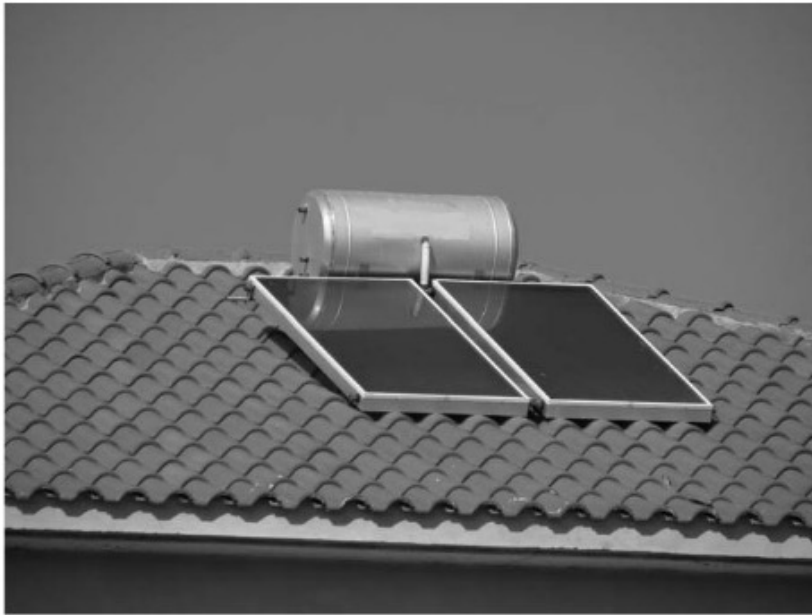


FIGURE 5.8 The complete solar ICS hot water system.

Hot Water Systems



(a)



(b)

FIGURE 5.2 Thermosiphon system configurations. (a) Flat-plate collector configuration. (b) Evacuated tube collector configuration.

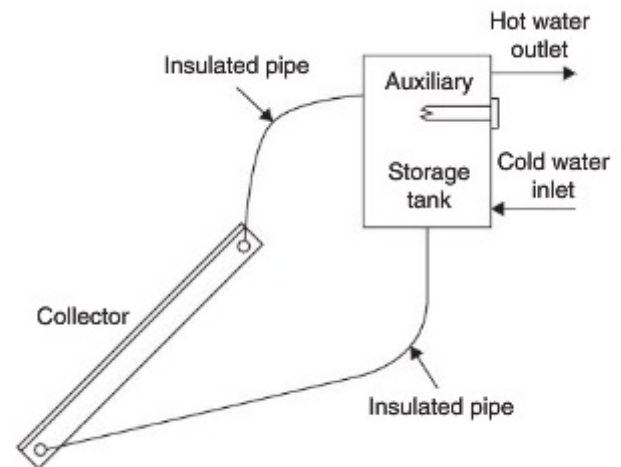


FIGURE 5.1 Schematic diagram of a thermosiphon solar water heater.

Hot Water Systems

Direct vs Indirect Systems

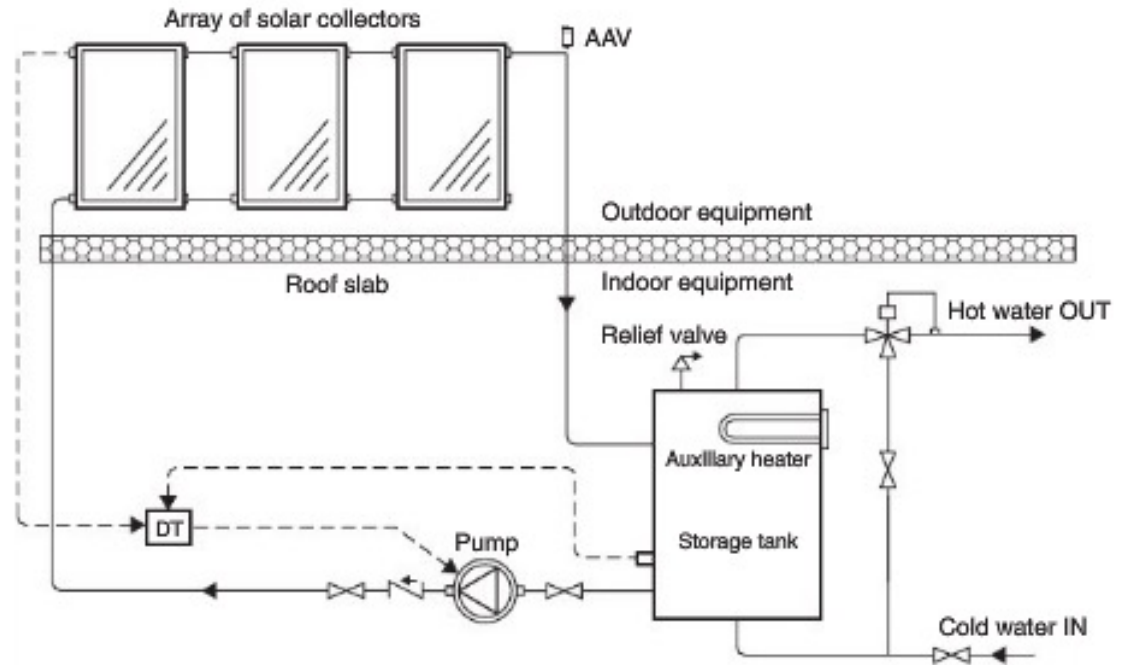


FIGURE 5.9 Direct circulation system.

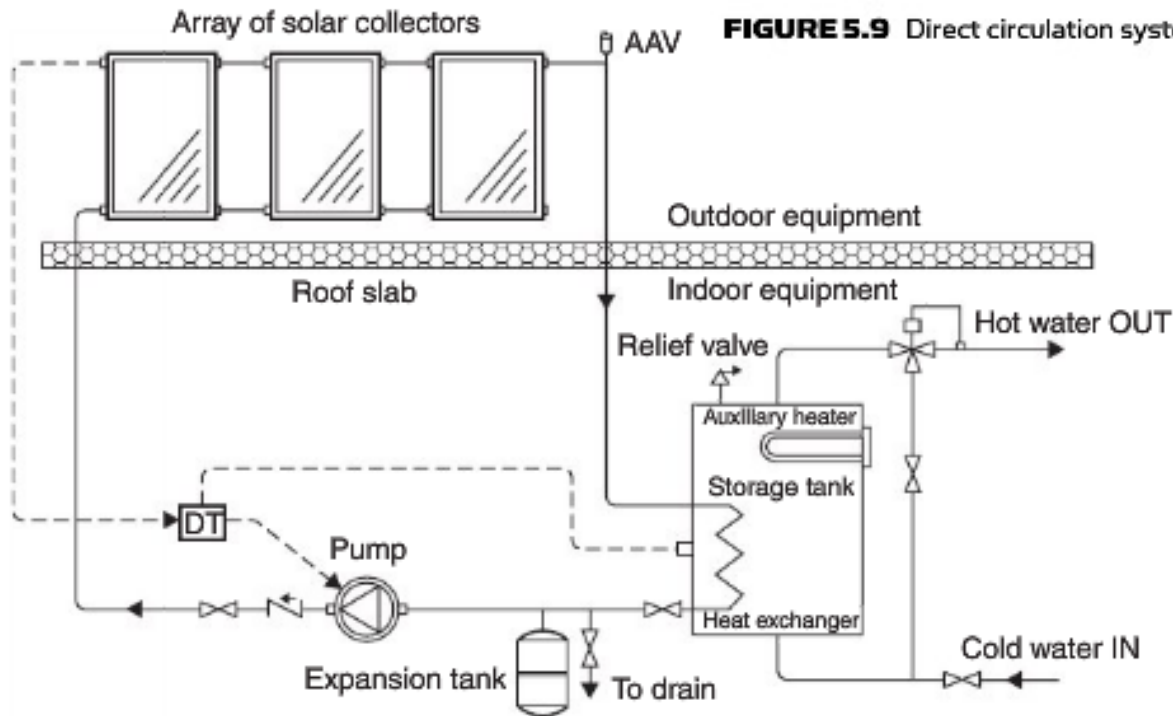


FIGURE 5.11 Indirect water heating system.

Hot Water Systems



Figure 4-7 A home-made clip fin collector.

that faces away from the sun. We need to try to eliminate thermal bridges as far as we possibly can.

Aluminum clip fins are one of the easiest ways of assembling a solar collector quickly, as they essentially clip onto a matrix of copper pipe.

Another way of constructing a solar collector is to use an old radiator painted black inside an insulated box—crude but effective! (Figure 4-9). This system contains more water, and as a result has a slower response time. This is because it takes more time to heat up the thermal mass of the radiator.

Warning

One of the problems that solar collectors suffer from is freezing in the winter. When temperatures drop too low, the water in the pipes of the collectors expands—this runs the risk of severely damaging the collectors.



Figure 4-8 Aluminum clip fins.



Figure 4-9 A recycled radiator collector.

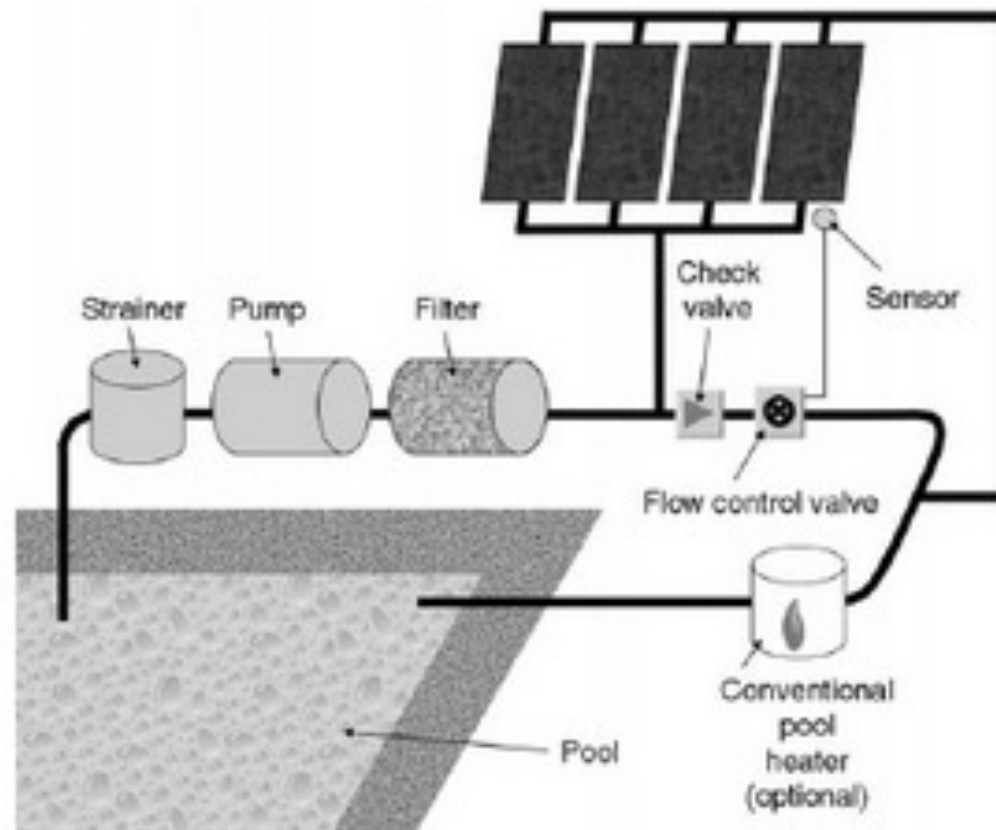


Figure 4-10 *Solar pool heating.*

Tip

Enerpool is a free program that can be used to simulate your swimming pool being heated with solar collectors. By inputting information such as your location, and how the pool is covered. The program can predict what temperature your pool will be at, at any given time!

www.powermat.com/enerpool.html

Hot Air Heating Systems

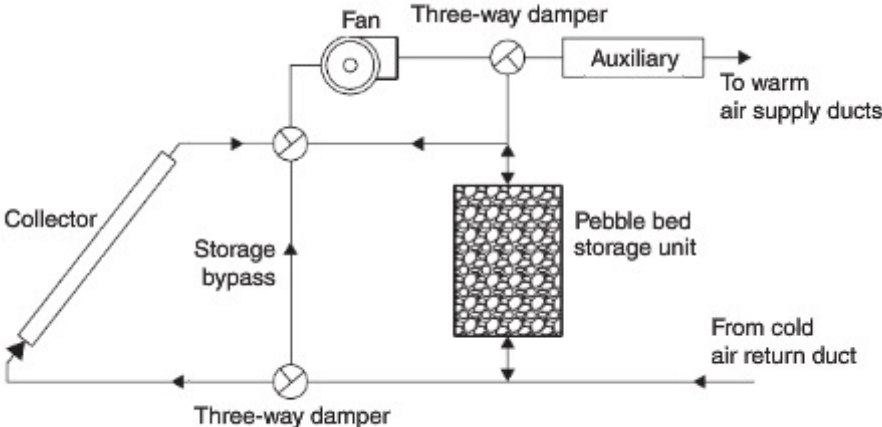


FIGURE 6.11 Schematic of basic hot air system.

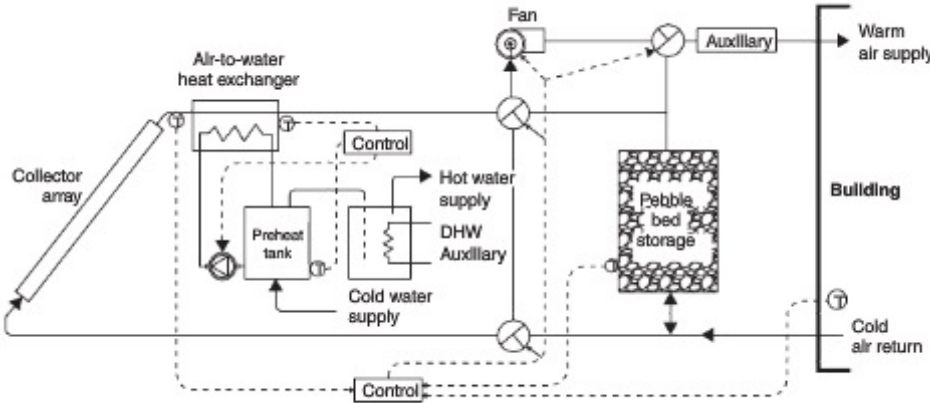


FIGURE 6.12 Detailed schematic of a solar air heating system.

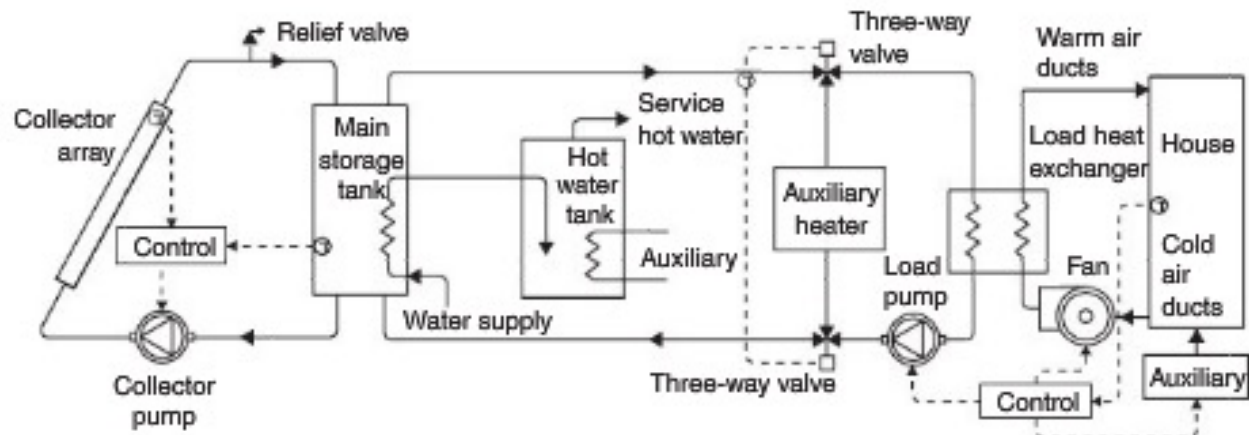


FIGURE 6.13 Schematic diagram of a solar space heating and hot water system.

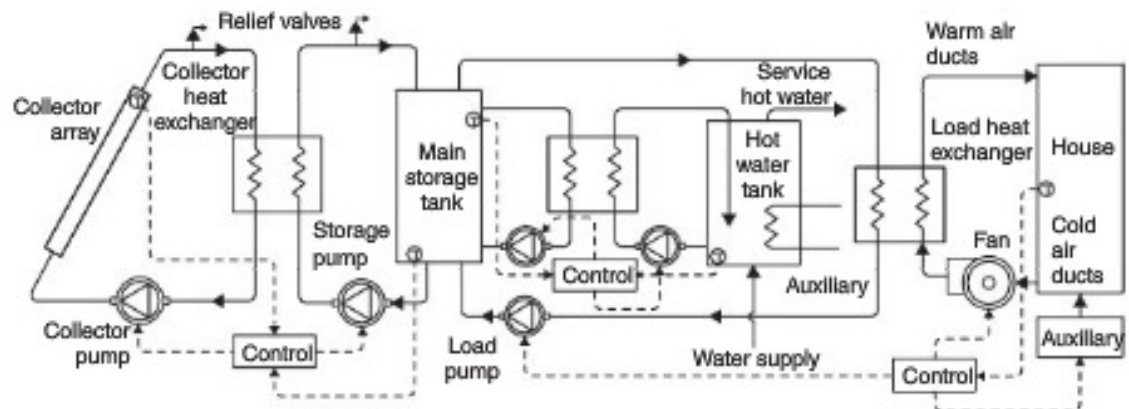


FIGURE 6.14 Detailed schematic diagram of a solar space heating and hot water system with antifreeze solution.

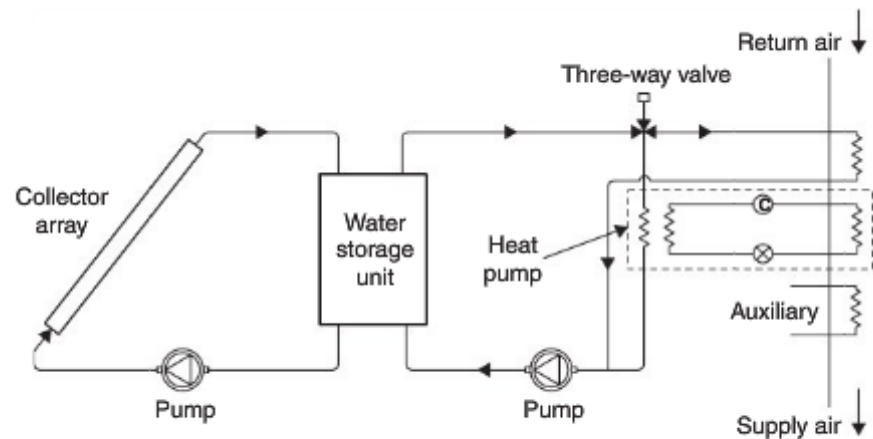


FIGURE 6.16 Schematic diagram of a domestic water-to-air heat pump system (series arrangement).

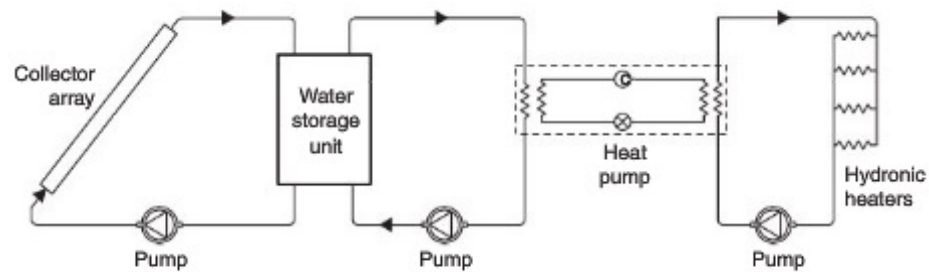


FIGURE 6.17 Schematic diagram of a domestic water-to-water heat pump system (parallel arrangement).

Industrial Solar Water Heating Mek'elle Ethiopia

http://www.solarthermalworld.org/sites/gstec/files/Kahsay_ISES%20Kassel.pdf

No.	Factory	Process	Working Temperature (°C)	Consumption (m ³ /day)	Current Source of Energy
1.	Sheba Tannery	Skin Tanning	35	18.4	Furnace oil for a steam boiler
		Skin Re-tanning	50	66.6	
		Hide Tanning	40	29.3	
		Hide Re-tanning	65	27.0	
2.	Maichew Particleboard	Glue preparation	40	6.0	Furnace oil, fire wood
		Impregnation	55	1.2	
3.	Bahirdar Textile	Pre-heater	60	36.0	Furnace oil for a steam boiler
		Washing	70	7.8	
		Chemical Preparation	80	5.2	
4.	Ashraf Edible Oil	Conditioning	85	6.0	Furnace oil for a steam boiler
		Degumming	90	5.0	
		Neutralization	90	5.0	
		Washing	70	7.7	

Passive Solar

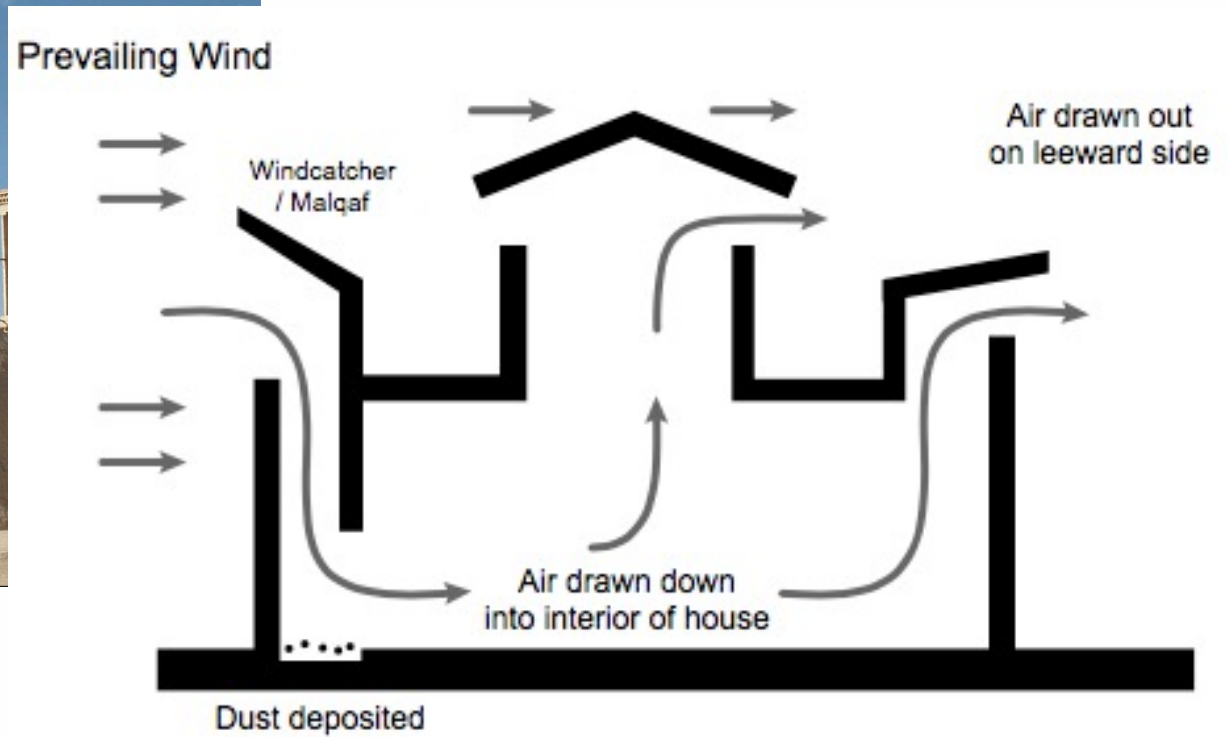
<https://en.wikipedia.org/wiki/Windcatcher>

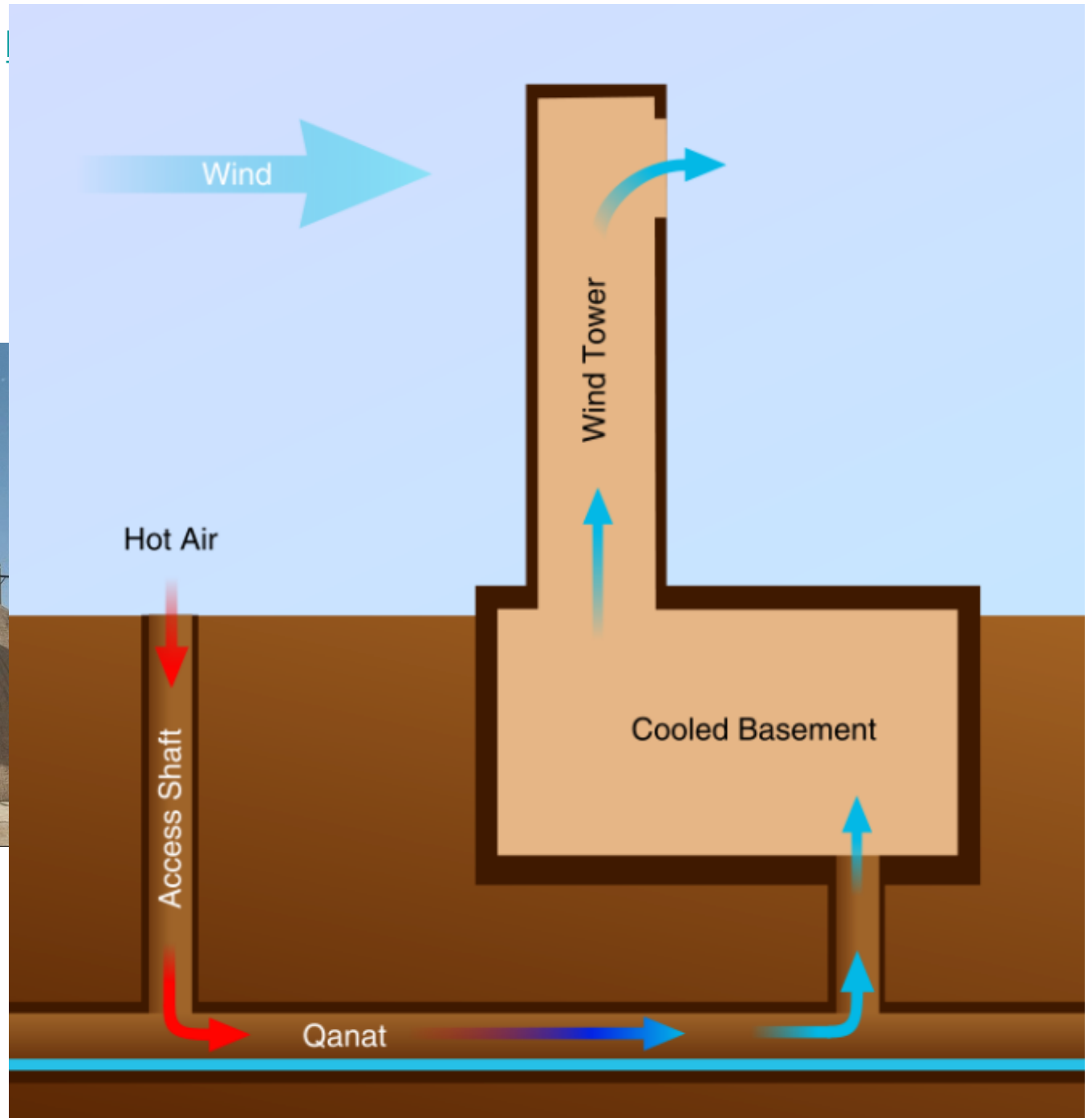
Iranian Wind Catchers



<https://en.wikipedia.org/wiki/Windcatcher>

Iranian Wind Catchers





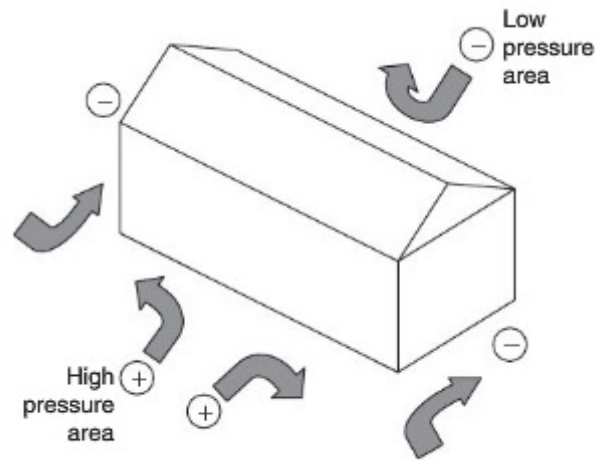


FIGURE 6.8 Pressure created because of the wind flow around a building.

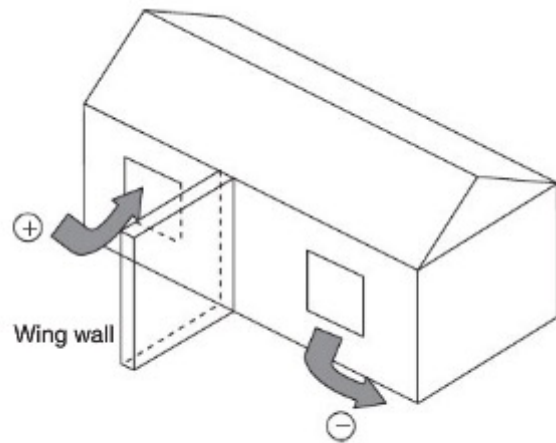


FIGURE 6.9 Use of a wing wall to help natural ventilation of windows located on the same side of the wall.

Ethiopian Institute of Architecture, Building, and Construction, EIABC

<http://www.hebel.arch.ethz.ch/wp-content/uploads/2012/10/Building-Future-Hebel.pdf>

Sustainable Rural Dwelling Unit (SRDU)

[PHASE 1] Background Research

PROCESS

Location and Project Site

The research area is in Gusha, Gusha zone located 170km from Addis Ababa. Gusha is 170km from Addis, the main town of Gusha zone, and is accessible by car on a gravel road. The size of the project site is about 70m² and will include renewable energy such as solar energy and bio gas. To develop renewable energy for one housing unit only is very expensive. Therefore, despite the construction of only one dwelling unit, the renewable energy will be developed considering for dwelling units.

Local people

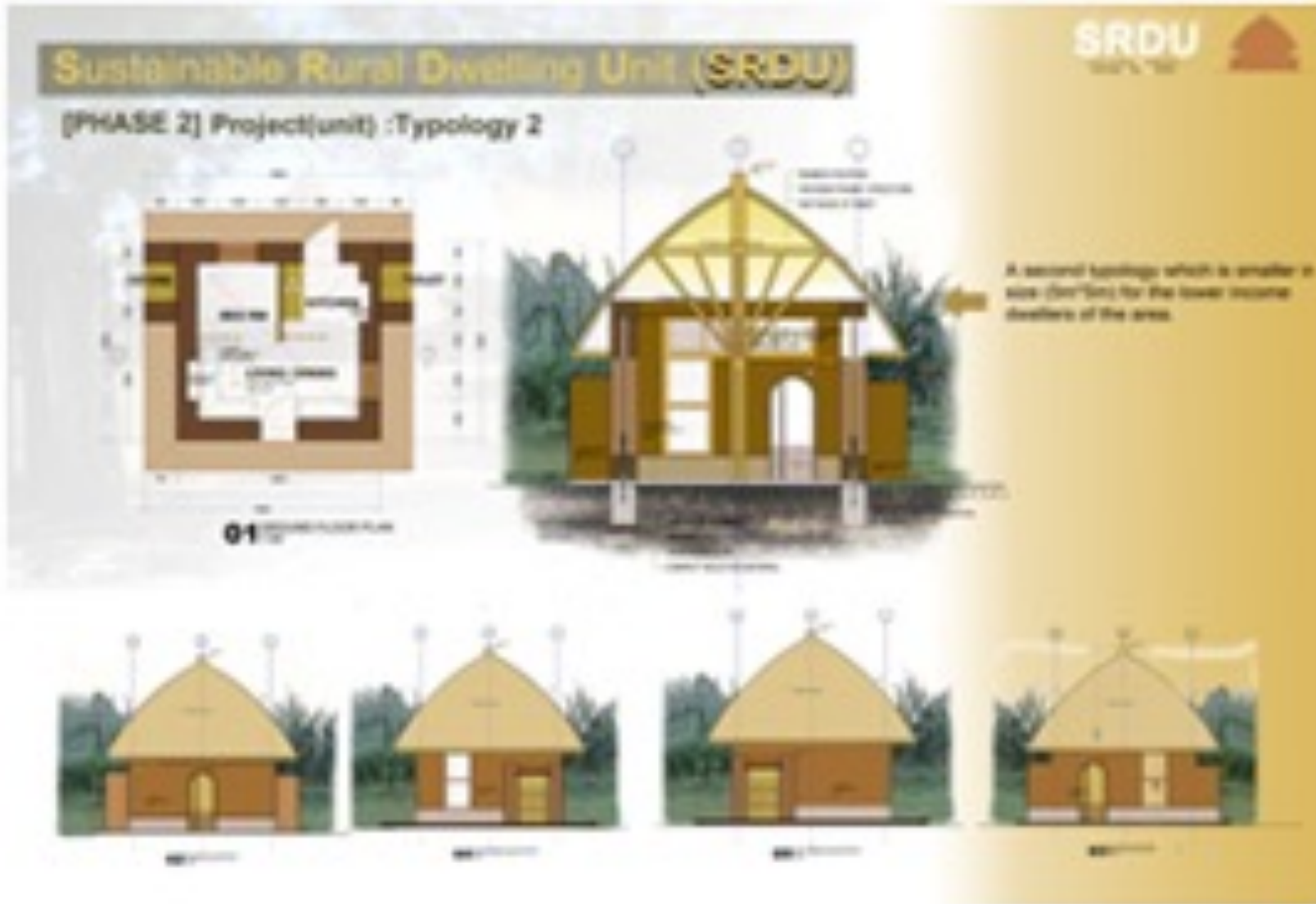
EIABC students research team

Government

Construction Unit Cluster

SRDU

EIABC



Tanzanian Hotel for Trip (Possible)



<http://hikersbay.com/africa/tanzania/hotel/tz/lifelights-and-apartments.html?lang=en>



Tanzanian Hotel for Trip (Possible)



Passive Solar: Trombe Walls

Trombe walls

As with many of the themes in this book, this idea is not a new one, in fact it was patented in 1881 (U.S. Patent 246626). However, the idea never really gained much of a following until 1964, when the engineer Felix Trombe and architect Jacques Michel began to adopt the idea in their buildings. As such, this type of design is largely referred to as a “Trombe wall.”

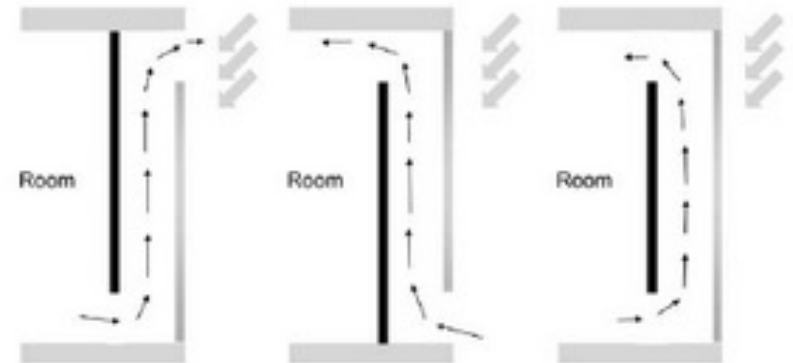


Figure 5-2 *Trombe wall modes of operation.*

Passive Solar: Trombe Walls

[Ice Fishing Shack](#)



[http://www.builditsolar.com/Projects/SpaceHeating/
SolarIceShack/SolarIceShack.htm](http://www.builditsolar.com/Projects/SpaceHeating/SolarIceShack/SolarIceShack.htm)

Passive Solar: Trombe Walls

<http://www.choiceenergy.org/Solar.Air.htm>

[Choice Energy .org](http://www.choiceenergy.org)



<https://youtu.be/N6QOZGbj-g>

<http://www.choiceenergy.org/Solar.Air.Eagle.Mount.htm>

[http://www.choiceenergy.org/Solar.Air.Eagle.Mount.
htm](http://www.choiceenergy.org/Solar.Air.Eagle.Mount.htm)

Passive Solar: Trombe Walls



<http://www.choiceenergy.org/Solar.Air.Eagle.Mount.htm>

<http://www.choiceenergy.org/Solar.Air.Eagle.Mount.htm>

Thrombe Walls in Peru



https://www.theguardian.com/global-development/2020/may/25/now-we-sleep-peacefully-life-in-peru-transformed-by-warm-houses?CMP=Share_iOSApp_Other

Thrombe Walls in Peru



https://www.theguardian.com/global-development/2020/may/25/now-we-sleep-peacefully-life-in-peru-transformed-by-warm-houses?CMP=Share_iOSApp_Other

Thrombe Walls in Peru



https://www.theguardian.com/global-development/2020/may/25/now-we-sleep-peacefully-life-in-peru-transformed-by-warm-houses?CMP=Share_iOSApp_Other

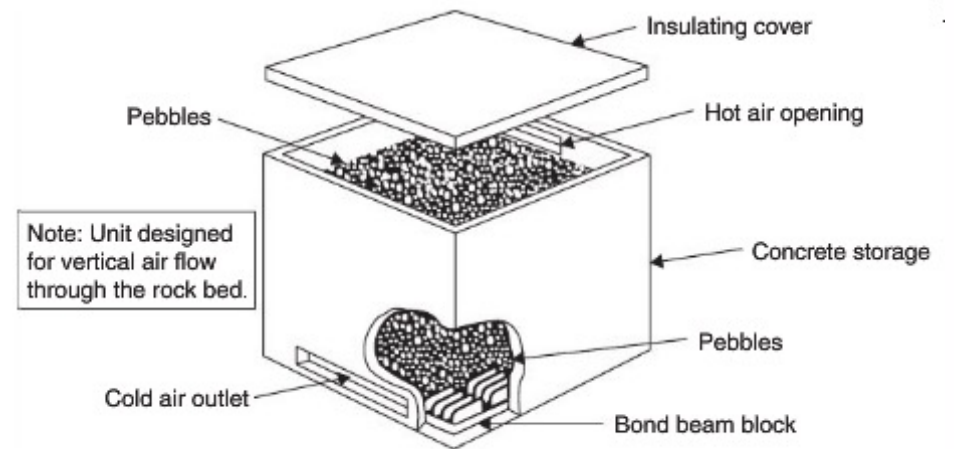


FIGURE 5.15 Vertical flow packed rock bed.

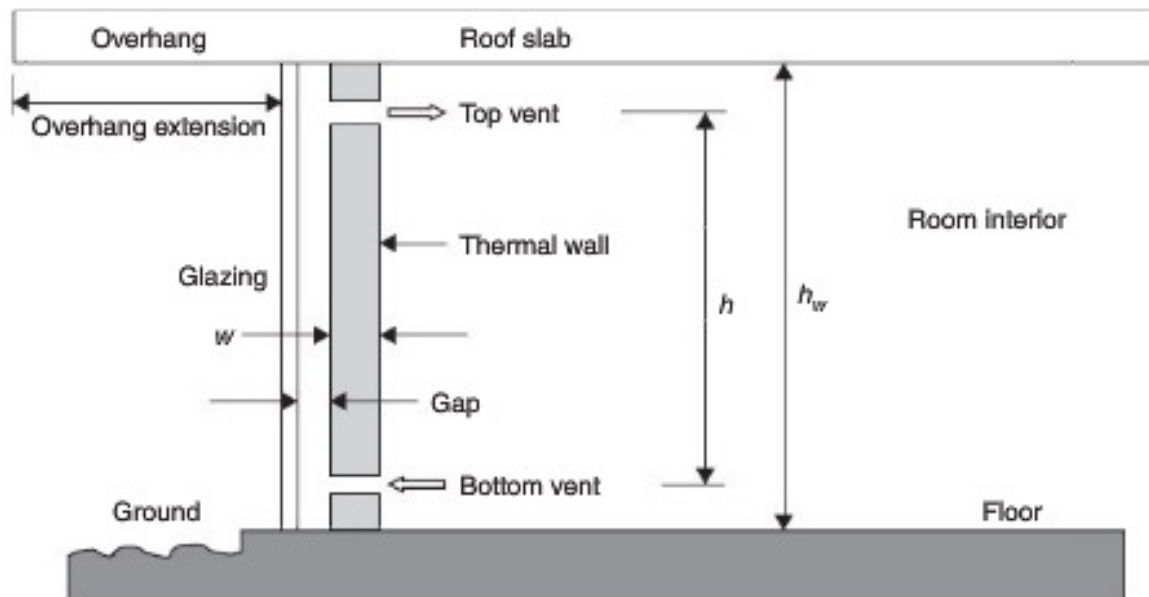


FIGURE 6.4 Schematic of the thermal storage wall.

Passive Solar Cooling in India

<https://www.bbc.com/news/av/world-asia-58820950>

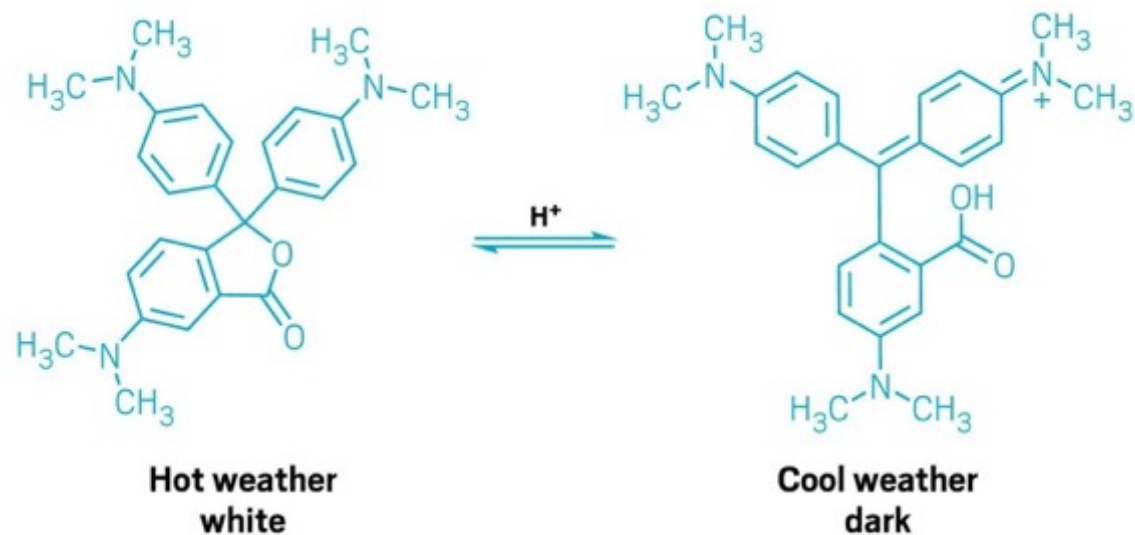
50° C = 120° F



Passive Solar Cooling in US

https://cendigitalmagazine.acs.org/2023/10/22/can-cool-coatings-combat-climate-change-2/content.html?utm_email+=64779482E4856401E565D4536D

Can cool coatings combat climate change?



Formulated with bisphenol A as a hydrogen donor or acceptor, crystal violet lactone changes from white at high temperatures to dark violet in the cold. Paint researchers are looking to exploit the effect to make color-changing roof coatings.

Passive Solar Cooling in US

https://cendigitalmagazine.acs.org/2023/10/22/can-cool-coatings-combat-climate-change-2/content.html?utm_email+=64779482E485640IE565D4536D



Craig Bettenhausen/C&EN

Microscopic aluminum flakes are used as an infrared-reflective and other coatings. These flakes from Eckart are encapsulated in glass to prevent oxidation.

Roofs coated in reflective paint can be as much as 13 °C cooler than dark-colored roofs, the default for many flat roofing systems.

Solar Power Cooling

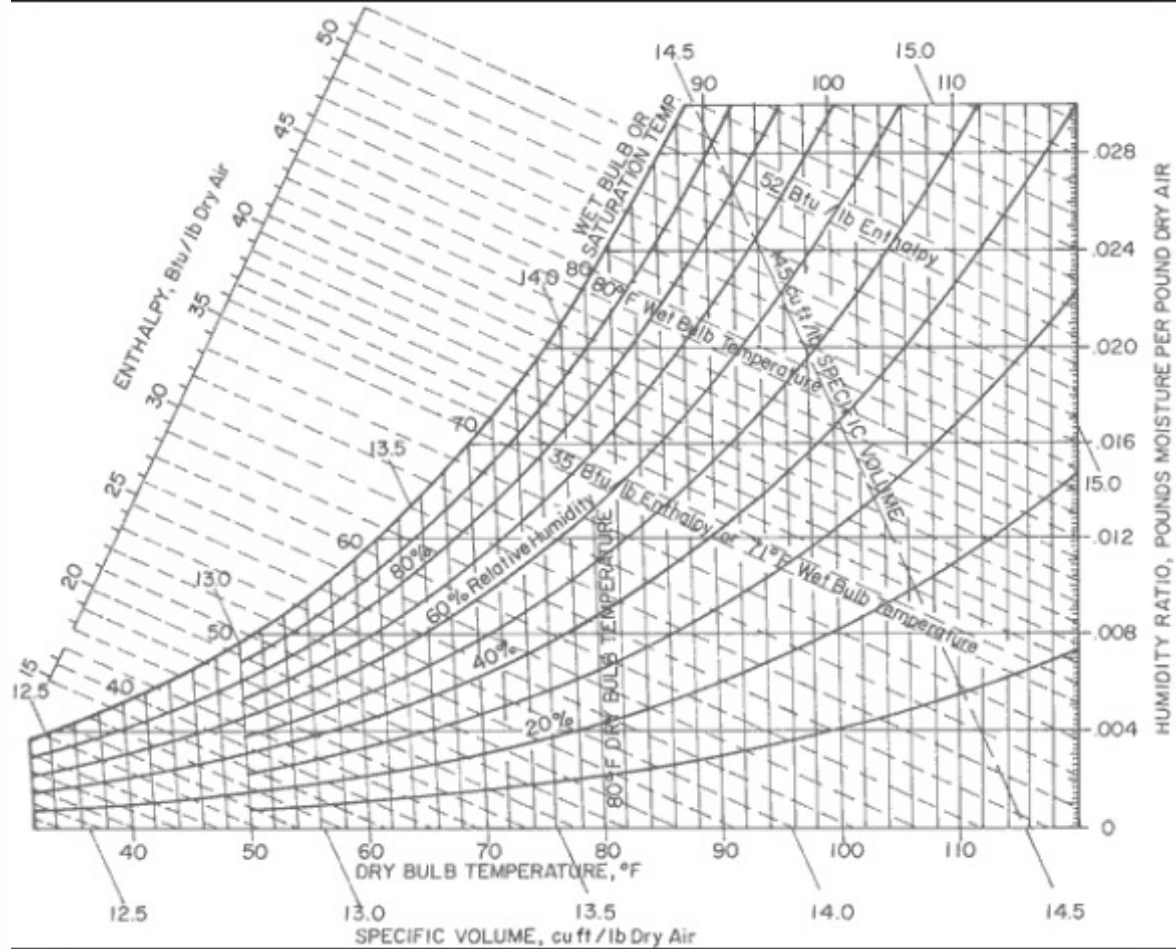
Swamp Cooler (http://www.youtube.com/watch?v=6ooAAcsbf_0)



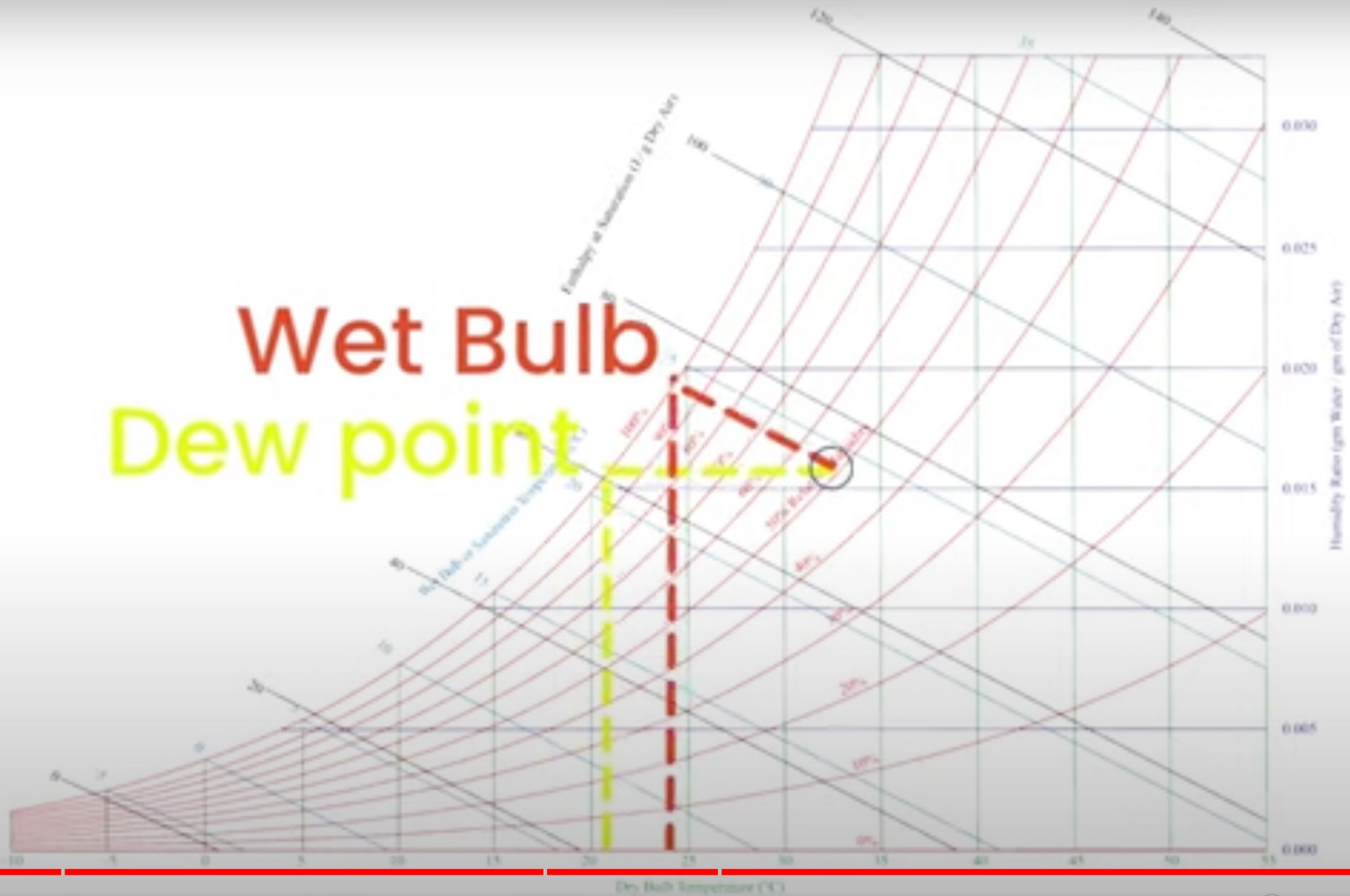
Figure 2. In areas of the United States where humidity tends to run high in the summertime, evaporative cooling is not the best way to stay cool; in the West, it's a very good choice.



Psychrometric Chart



Wet Bulb Dew point



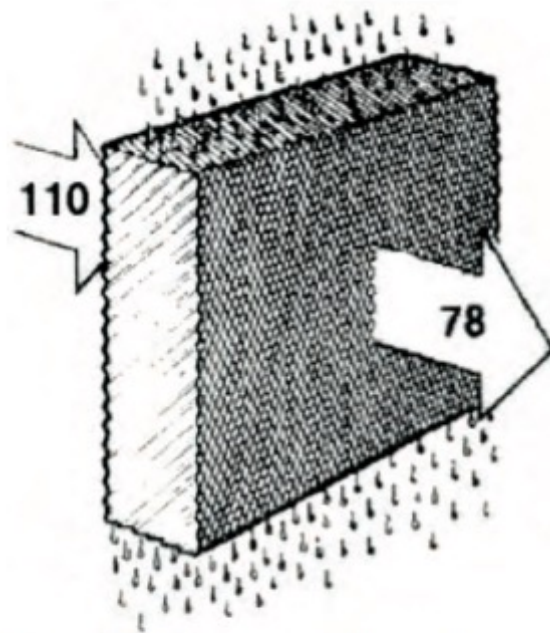


Figure 1. Direct evaporative cooling through a wetted medium. *Source: www.energy.ca.gov/appliances/2003rulemaking/documents/case_studies/CASE_Evaporative_Cooler.pdf*

Up to 38°F (21.1°C) of cooling can theoretically be achieved (110°F (43.3°C) – 72°F (22.2°C)) by simply

PSYCHROMETRIC CHART Sea Level

Direct evaporative cooling process

A: Entering air properties

$T_{DB} = 110^{\circ}\text{F}$ (43.3°C)

$T_{WB} = 72^{\circ}\text{F}$ (22.2°C)

RH = 15%

B: Leaving air properties

$T_{DB} = 78^{\circ}\text{F}$ (25.6°C)

$T_{WB} = 72^{\circ}\text{F}$ (22.2°C)

RH = 75%

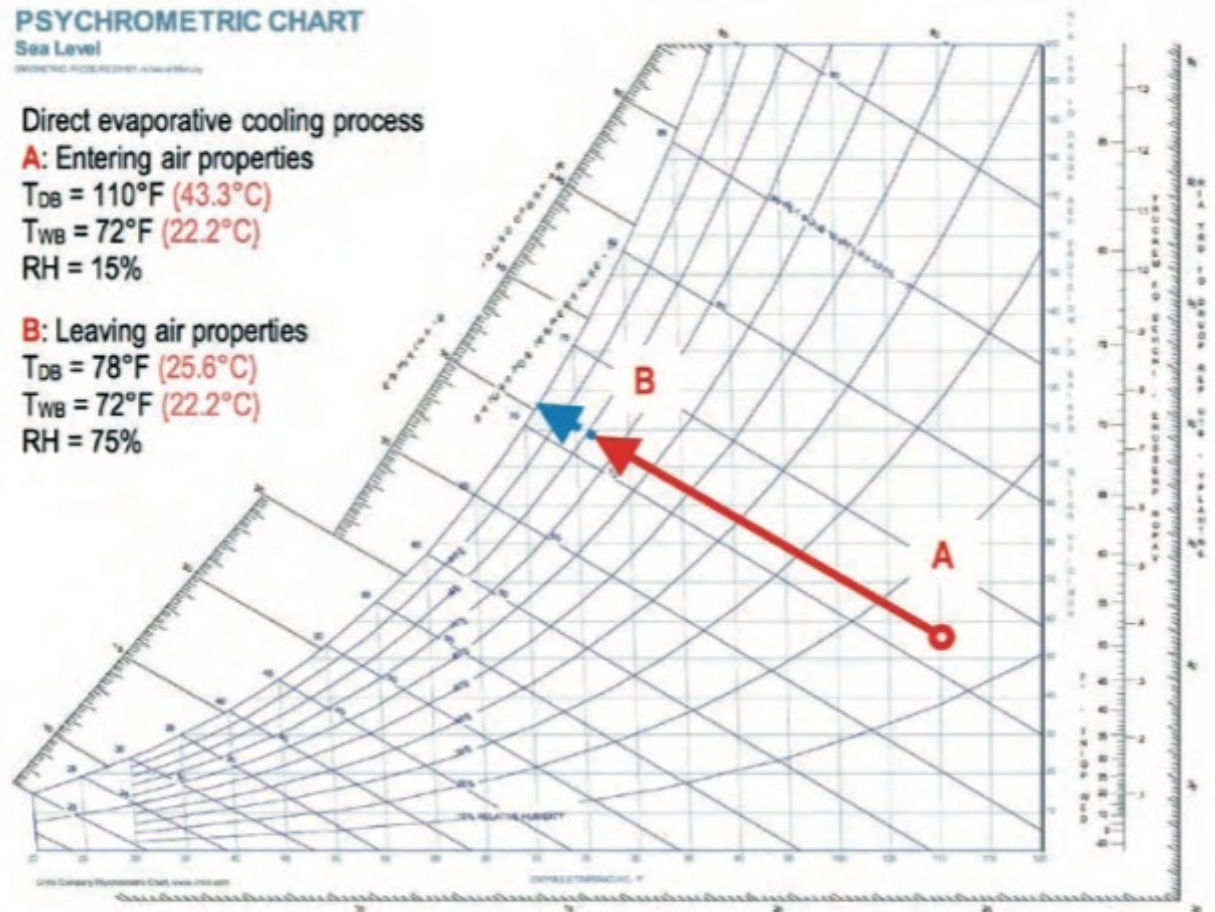


Figure 2. Direct evaporative cooling process shown psychrometrically. *Source: PsycPro software at www.Linric.com*

PSYCHROMETRIC CHART

Sea Level

Potential cooling from direct evaporative cooling

A: 95°F (35°C) - 86°F (30°C) = 9°F (5°C) of cooling possible

B: 95°F (35°C) - 60°F (15.6°C) = 35°F (19.4°C) of cooling possible

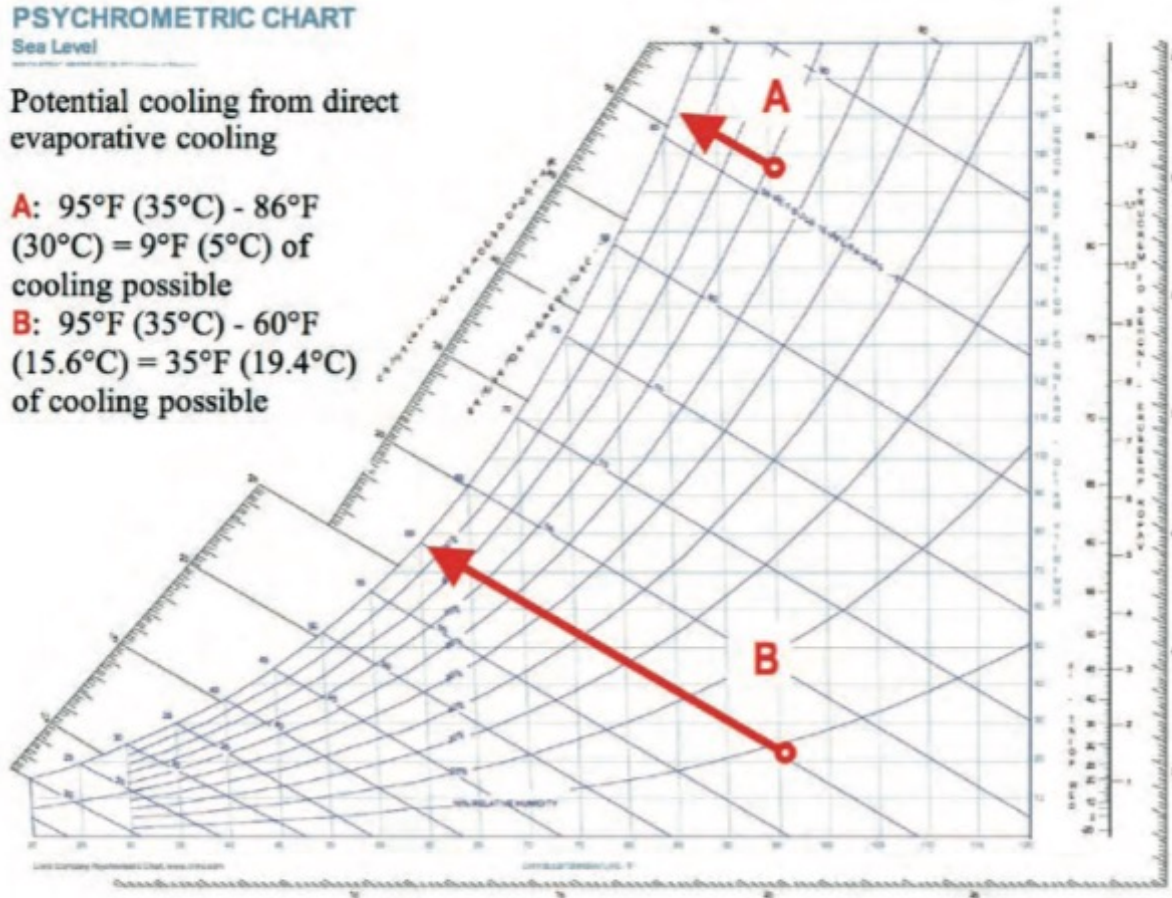


Figure 3. Comparison of the direct evaporative cooling possible when starting with T_{DB} of 95°F (35°C) at 70% RH vs. at 10% RH. Source: *PsycPro* software at www.Linric.com

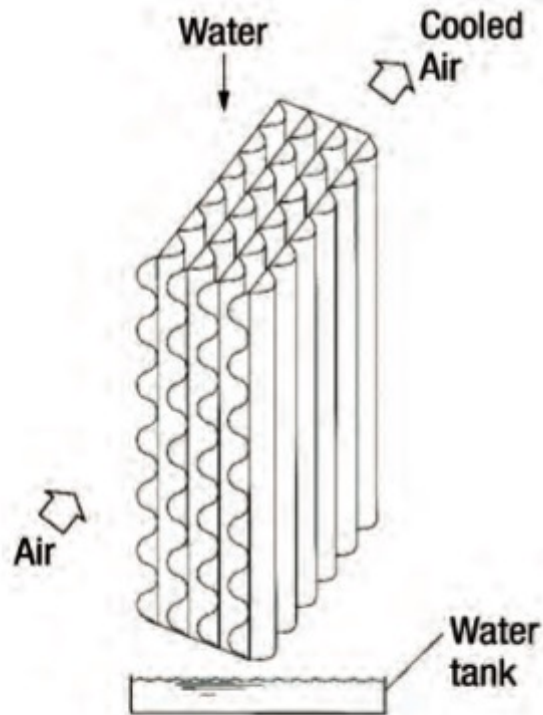


Figure 4. In an indirect evaporative cooling process, the primary airstream flows in a different channel than the secondary airstream. *Source: Wang, Shan K., Handbook of Air Conditioning and Refrigeration (2nd Edition), McGraw-Hill, p. 5, 2001; www.knovel.com/knovel2/Toc.jsp?BookID=568&VerticalID=0*

PSYCHROMETRIC CHART

Sea Level

Indirect evaporative cooling process

A: Entering air properties

$T_{DB} = 100^{\circ}\text{F}$ (37.8°C) $T_{WB} = 65^{\circ}\text{F}$
 (18.3°C) RH = 12.8% W = 36.7

B: Leaving air properties

$T_{DB} = 78^{\circ}\text{F}$ (25.6°C) $T_{WB} = 56^{\circ}\text{F}$
 (13.3°C) RH = 28.4% W = 36.7

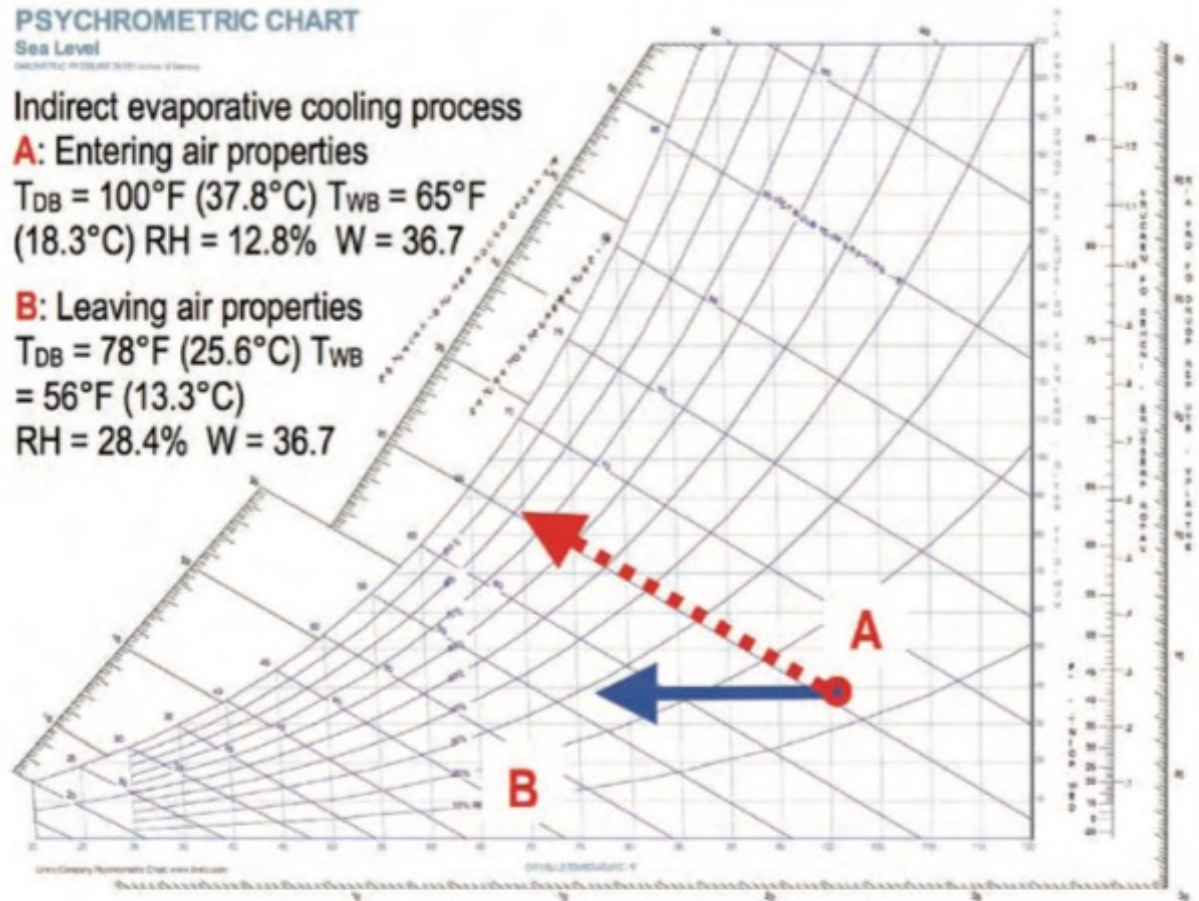


Figure 5. In the indirect evaporative cooling process, no water is shown being added to the primary airstream as it cools from A to B. *Source: PycPro software, www.Linric.com*

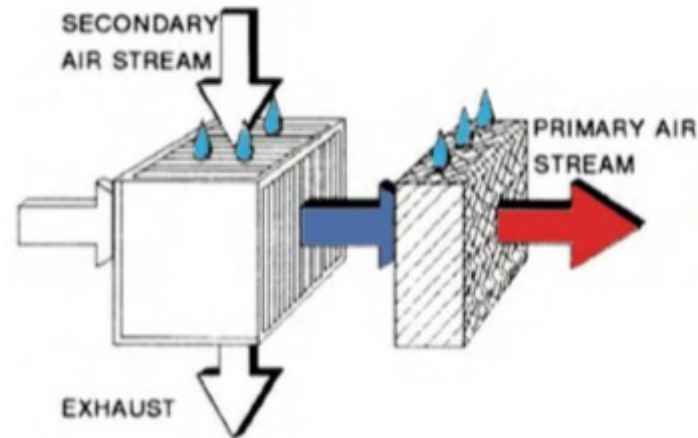


Figure 6. Two-stage indirect/direct evaporative cooling. *Source: www.energy.ca.gov/appliances/2003rulemaking/documents/case_studies/CASE_Evaporative_Cooler.pdf*

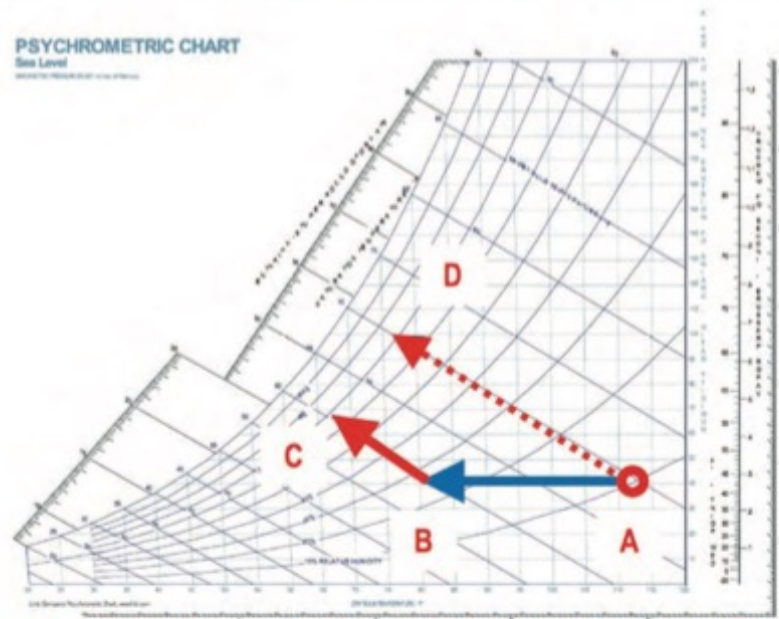


Figure 7. Two-stage indirect/direct evaporative cooling (indirect from A to B and then direct from B to C) yields a lower T_{DB} than does direct-only from A to D. *Source: PsycPro software at www.Linric.com*

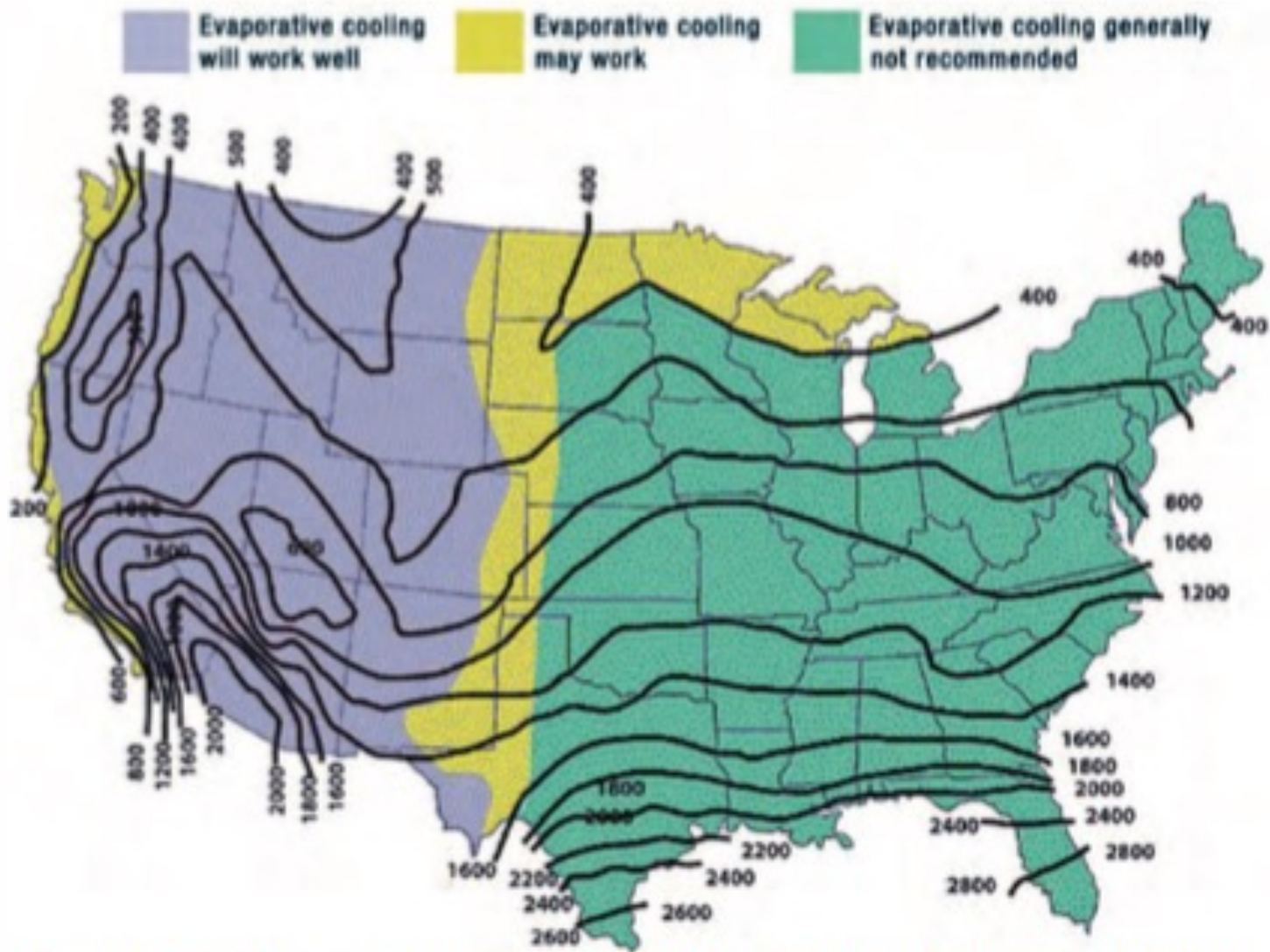
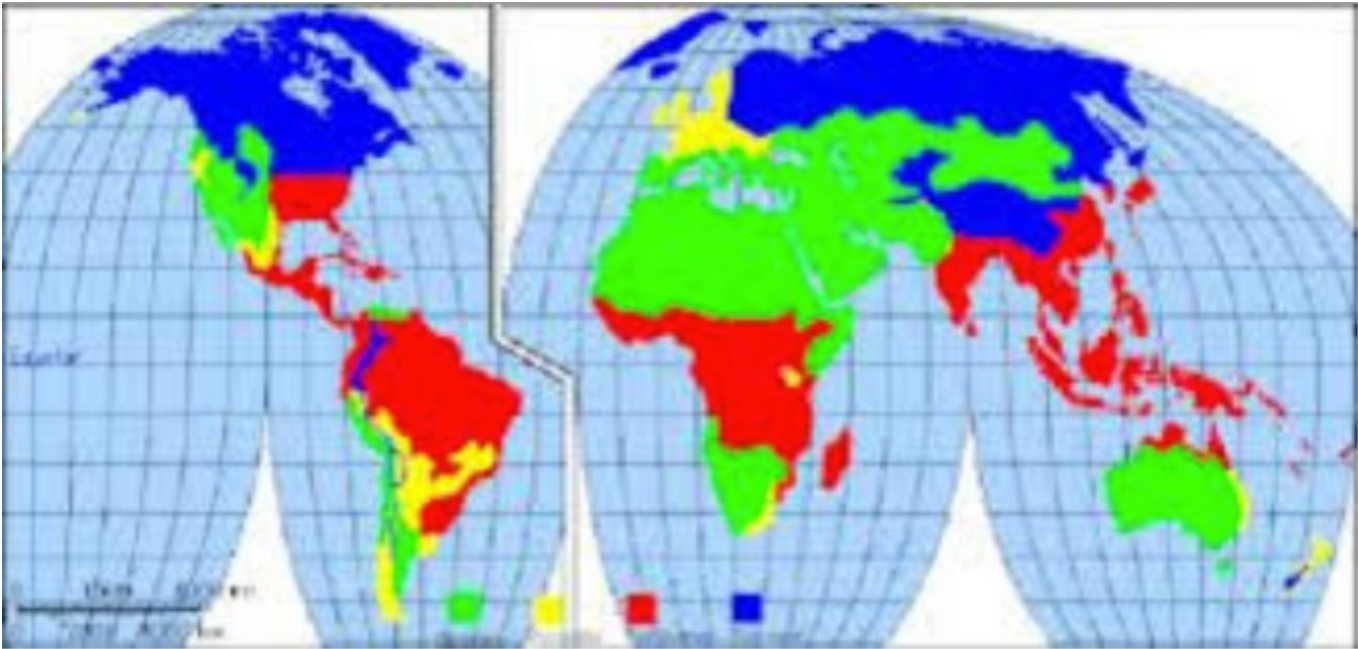
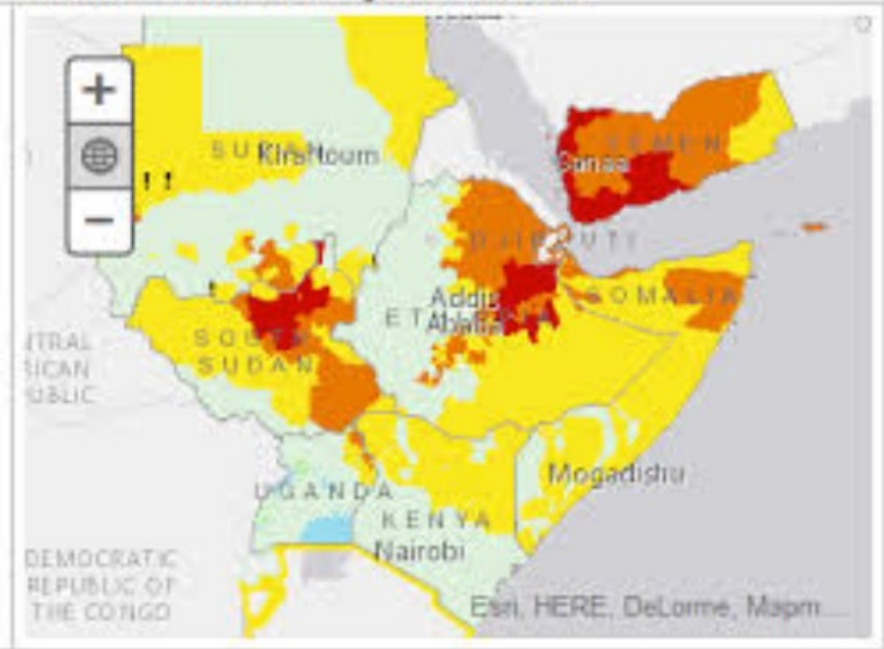


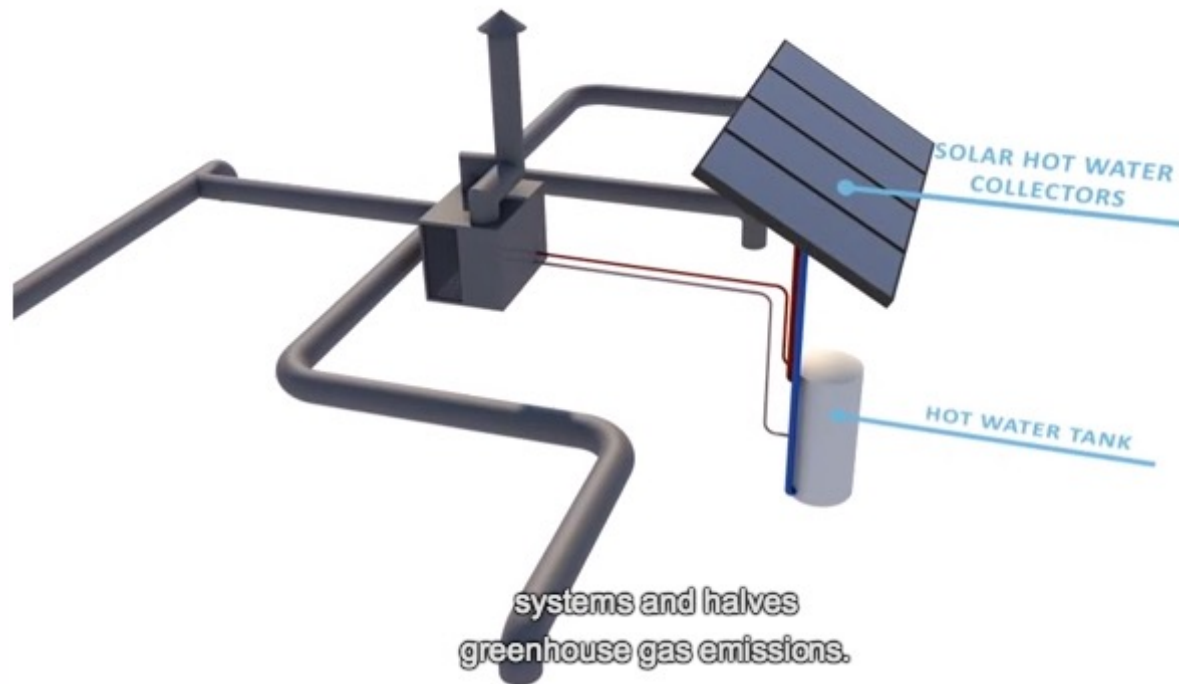
Figure 15. Map of summer cooling load hours. *Source: ARI Unitary Directory, August 1, 1992, to January 31, 1993, pp. 16-17; Air-Conditioning and Refrigeration Institute, www.energyexperts.org/ac_calc/default.asp.*



Medium Term: January-March 2016



[A simple system](http://www.youtube.com/watch?v=cz-kquRmvqk) (<http://www.youtube.com/watch?v=cz-kquRmvqk>)



Industrial Scale Evaporative Cooling

https://www.cambridge-eng.com/commercial-industrial-evaporative-cooling?gclid=Cj0KCQjwoqDtBRD-ARIsAL4pviA8l-oC4dtLQxM_TaqN6CsLLvu98orey6-zXgx90RIIOxOIUM4E6YaAkn6EALw_wcB



PROJECT ROLE

PROJECT TYPES

MARKETS SERVED

PRODUCTS

PARTS & SERVICE

RESOURCES



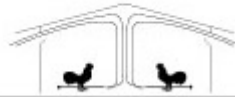
INDUSTRIAL & COMMERCIAL EVAPORATIVE COOLING SYSTEMS

Cambridge Engineering's evaporative cooling systems provide industry-leading cooling solutions for commercial and industrial facilities. Improving indoor air quality is the driving force behind our evaporative cooling systems and does so while also reducing energy consumption and operational costs. The Cambridge Engineering **ESC-Series indirect evaporative cooling units** are best suited for industrial or commercial facilities in need of higher quality air without inflating operational costs. Similarly, our **E-Series direct evaporative cooling units** are best suited for facilities in hot, dry and arid climates in need of fresh and cool conditioned air.

<http://www.dairyreporter.com/Processing-Packaging/Sub-Saharan-milk-cooler-project-awarded-Im-grant>

Evaporative cooler to cool milk





Poultry Housing Tips

Evaporative Cooling Pad Quality Makes a Difference

Volume 20 Number 7

June, 2008



Six-inch evaporative cooling pad systems are a vital part of a tunnel-ventilated poultry house's cooling system. When properly installed and maintained, a six-inch pad system can reduce the incoming air temperature on a hot summer day 20°F or more, dramatically reducing heat-stress-related problems. Furthermore, six-inch pad systems have virtually eliminated the need for interior fogging nozzles which has resulted in cleaner houses, increased equipment life, and reduced risk of electrical shocks due to wet thermostats. Last but not least, six-inch pad systems have eliminated the wasteful run-off associated with traditional two-inch fogging pad systems. Most people would agree that the transition of the poultry industry from fogging and fogging pad systems to six-inch evaporative cooling pad systems has proven to be very beneficial to the birds we grow as well as to growers.

Though on the surface the construction of an evaporative cooling pad looks fairly simple, there is in fact a fair amount of science and engineering that goes into their design. The paper used to construct the pads has to have just the right type and amount of resins that will not only enable the pad to last seven years or more when exposed to the elements, but also allow water to easily "wick" throughout the pad to maximize water evaporation. The "flutes" need to be just the right size and angle to produce maximum cooling of the incoming air while at the same time not causing excessive static pressure that would adversely affect the air moving capacity of the exhaust fans. Last but not least, pad surface coatings need to be formulated and applied in a way that surface rigidity is maximized, while at the same time not adversely affecting pad cooling or air flow through the pad.

The good news for poultry producers is that the vast majority of pads sold in the U.S. are of superior design and quality. The bad news is that because all pads look very similar, producers may unknowingly purchase a pad from a new manufacturer that is not of the same quality as those traditionally sold in the U.S. The following are a few things to look for when considering installing new evaporative cooling pads, that though not always conclusive, can provide some indication as to pad quality.

[BBC Article](#)

<http://www.bbc.com/future/story/20120727-when-good-milk-turns-bad>

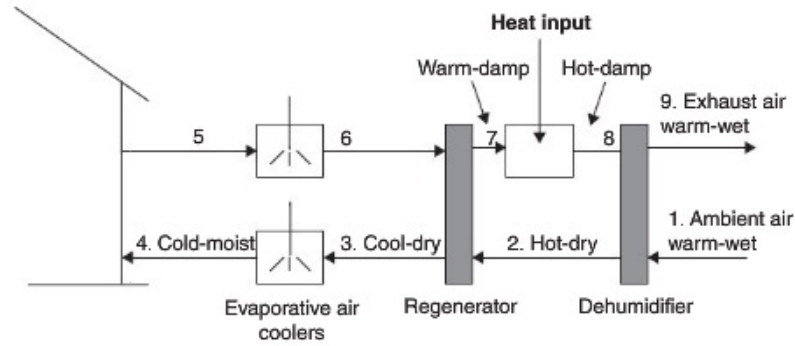


FIGURE 6.19 Schematic of a solar adsorption system.

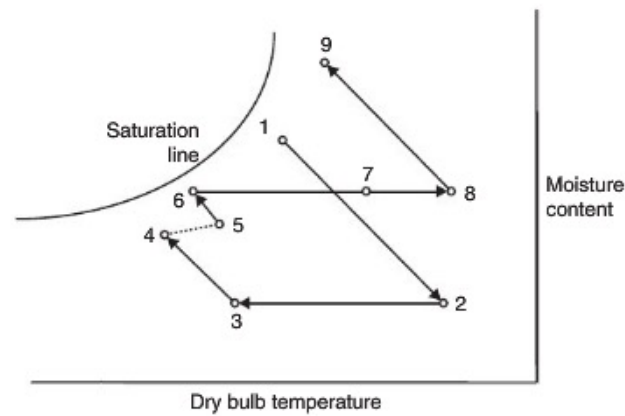


FIGURE 6.20 Psychrometric diagram of a solar adsorption process.

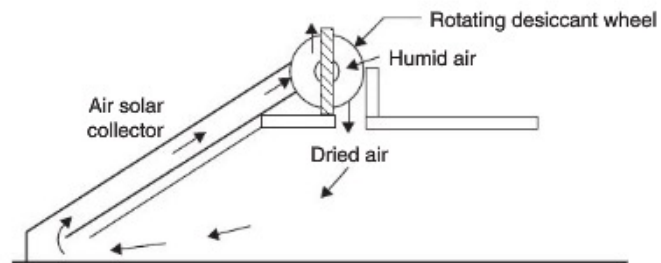


FIGURE 6.21 Solar adsorption cooling system.

Ohio Avenue in Clifton

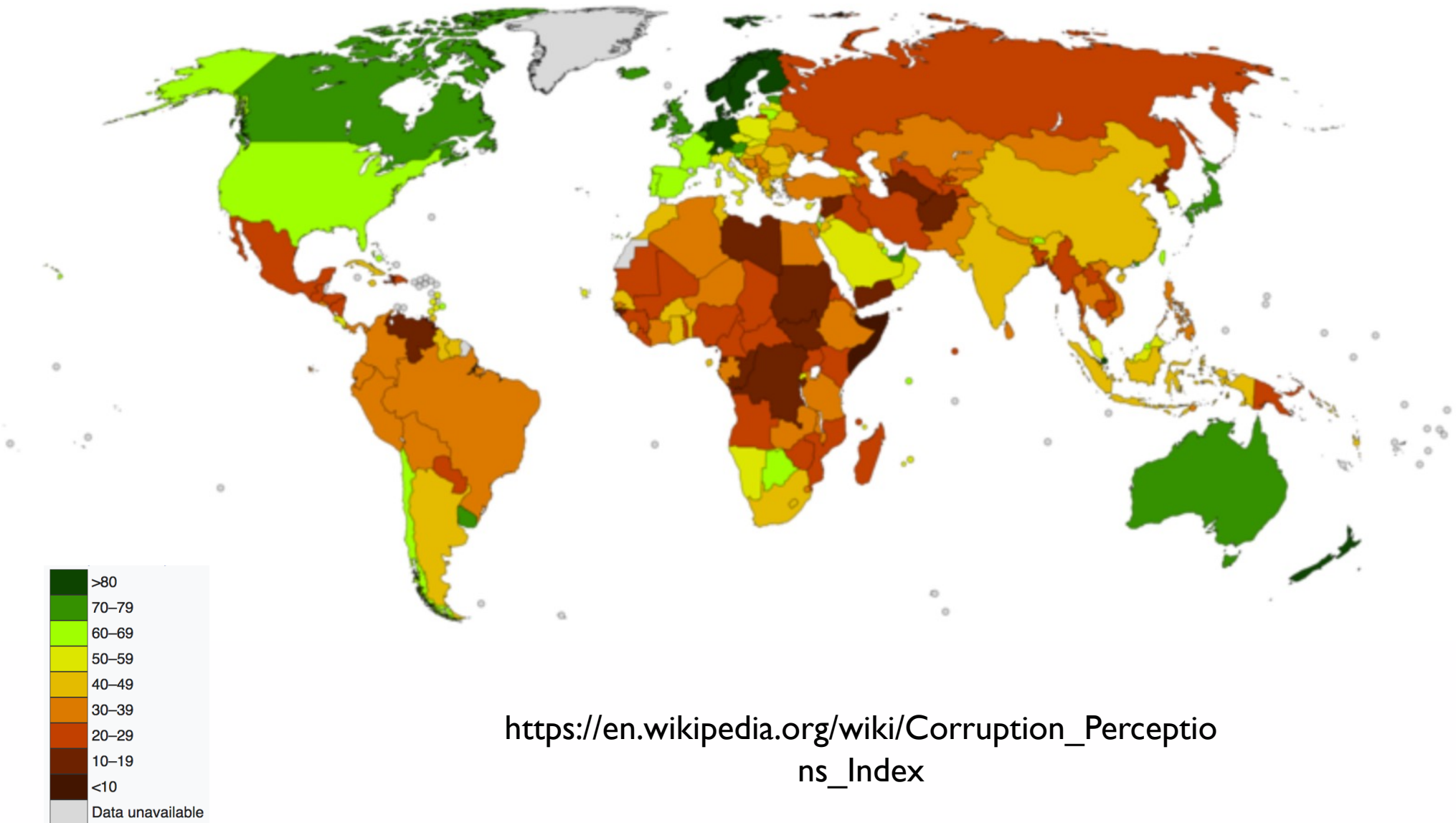




WARNING
ELECTRIC FENCE
ENCLOSURE

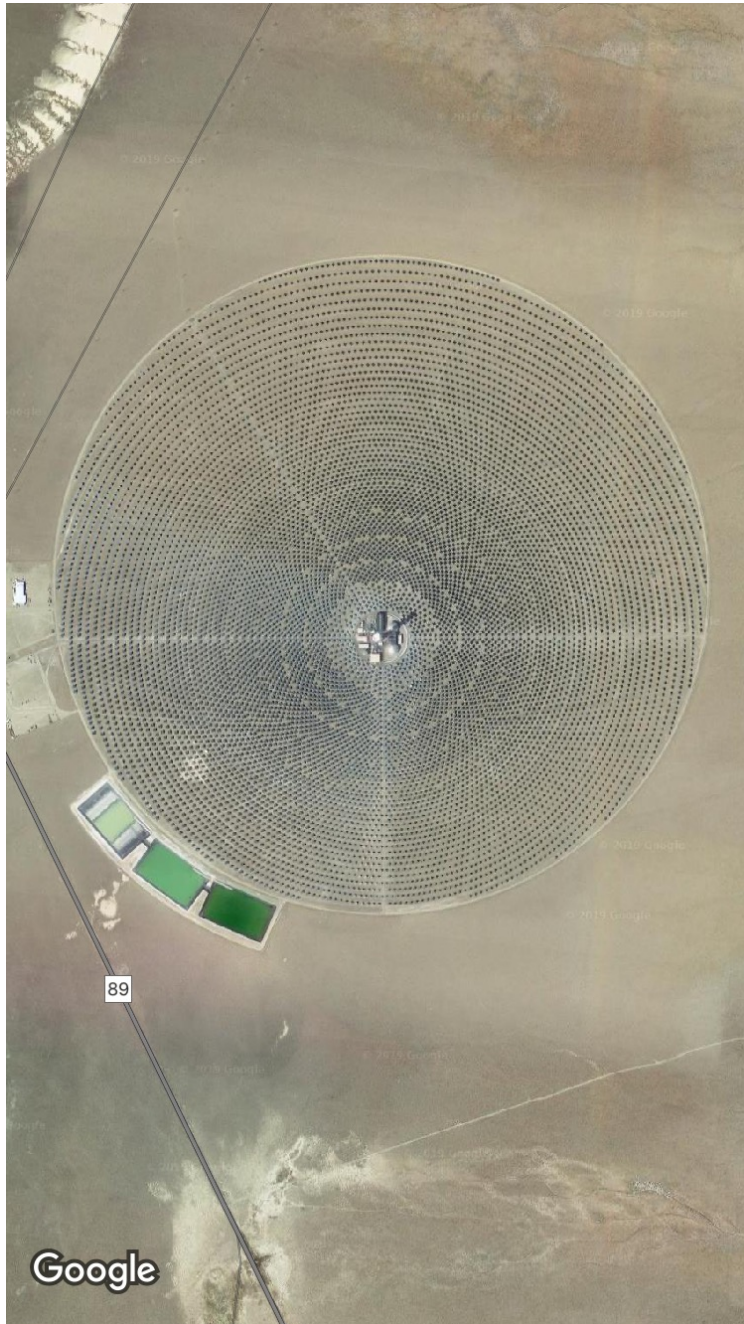
Corruption Index

"the misuse of public power for private benefit"



https://en.wikipedia.org/wiki/Corruption_Perceptions_Index

Crescent Dunes Nevada



Solar Refrigeration Using Absorption/Desorption/Evaporation

Carbon/Solvent Systems

A Simple Solar Ice Maker

K.Sumathy
 Department of Mechanical Engineering, University of Hong Kong, Hong Kong.
 Fax: 852-2858-5415; e-mail: ksumathy@hkucc.hku.hk

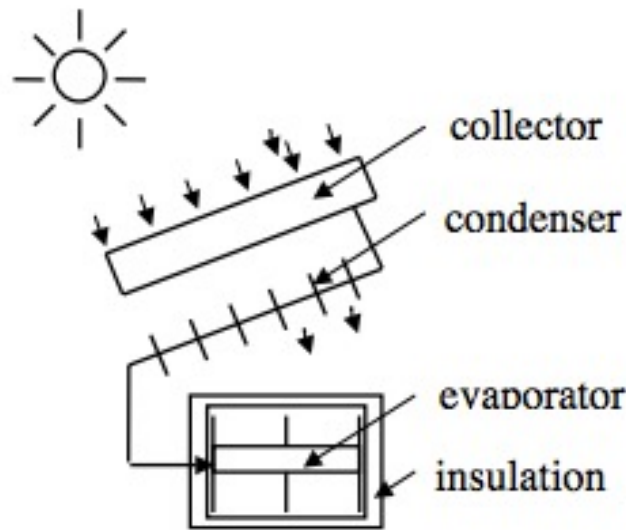


Fig.1 Schematic of a prototype adsorption refrigerator

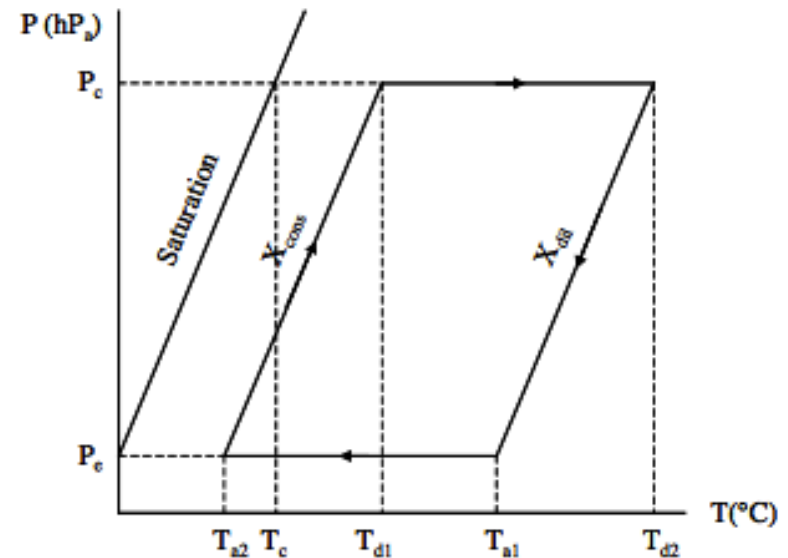


Fig. 2 Thermodynamic cycle for adsorption

The principle of the solid-adsorption ice-maker is explained using a P-T-X diagram as shown in Fig.2. To begin with, the adsorption bed along with the refrigerant gets heated up, and when it reaches the required desorption temperature (T_{d1}), the methanol gets desorbed. In the evening, the flat-plate collector (adsorption bed) loses its heat to the surroundings and hence the temperature of the adsorbent bed is reduced rapidly ($T_{d2} \rightarrow T_{a1}$), and the pressure in the adsorber drops to a value below evaporation pressure (P_e). Evaporation could happen if the connecting valve is open, and ice will be made in the refrigeration box.

A laboratory prototype system built is capable of producing 4 to 5 kg of ice a day and could achieve a COP of about 0.12. The total size of the ice-maker is about 1 cu m, and weighs about 50 kg. The experimental tests were carried out at various working conditions ($-10^{\circ}\text{C} < T_E < -5^{\circ}\text{C}$ – evaporation; $30^{\circ}\text{C} < T_C < 45^{\circ}\text{C}$ – condensation; $100^{\circ}\text{C} < T_G < 105^{\circ}\text{C}$ – generation). The refrigerator performance (Specific cooling power, SCP, and the amount of ice made per day) at the evaporating temperature limits ($T_E = -10^{\circ}\text{C}$ and $T_E = 15^{\circ}\text{C}$) are shown in Table 1. The performance is relatively low mainly because of the high cycle time (only one cycle a day).

A Simple Solar Ice Maker (Anthony Tong/Amanda)



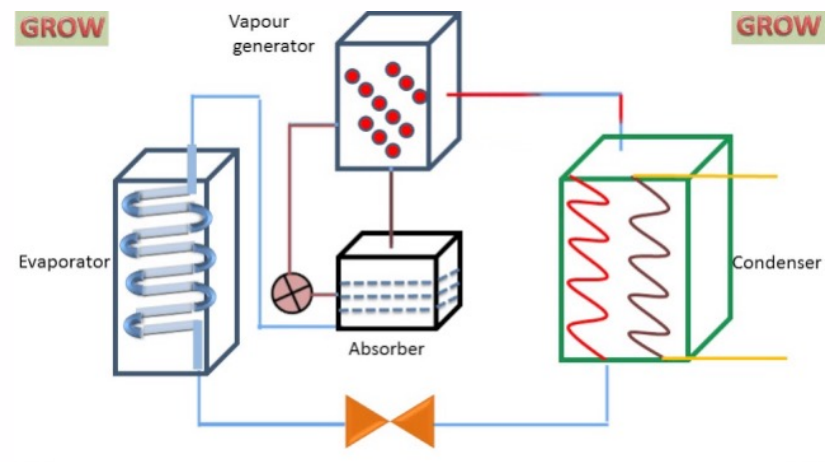
Methanol/Carbon
Based Absorption
Refrigerator/Ice Maker



Amy Ciric University of Dayton (aciric1@udayton.edu)



Ethanol/Carbon Based
Absorption
Refrigerator



A Simple Solar Ice Maker

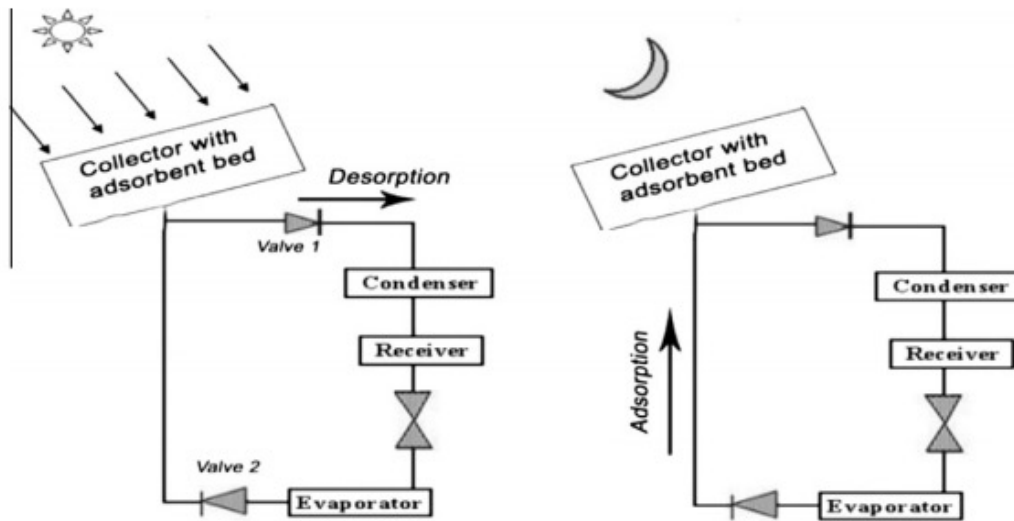


Fig. 1a. Schematic of the solar adsorption cooling system.

There is a single adsorbent bed in the intermittent solar adsorption cooling cycle. The adsorption system consists of three main parts: solar collector with adsorbent bed where activated carbon is placed, condenser and evaporator as show in Fig. 1a. The operating cycle of the system has four processes as shown in the Clapeyron diagram in Fig. 1b. The heating process (1–2) and the desorbing process (2–3) represent half the cycle while the cooling (3–4) and adsorption (4–1) processes represent the other half. During the heating period, the adsorbent bed receives heat from solar energy that raises the temperature of the pair of

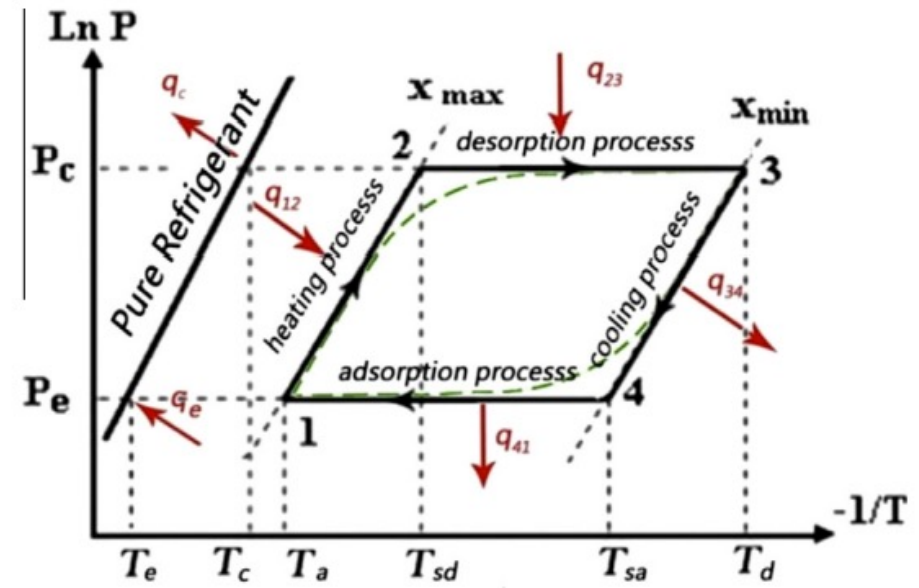


Fig. 1b. Schematic view of the adsorption process on Clapeyron diagram.

adsorbent and adsorbate as shown in Fig. 1b by line 1–2 (isosteric heating process, at constant concentration of the adsorbate = x_{max}). When the adsorbent bed pressure reaches the condenser pressure, the adsorbate vapor diffuses from the collector to the condenser and condensed there (line 2–3, desorption process at condenser pressure). So the concentration of the adsorbate in the reactor reaches the minimum value (x_{min}) at the end of this desorption process. This process is followed by cooling the generator (line 3–4, isosteric cooling process). Then, the liquid adsorbate flows from the condenser to the evaporator where it vaporizes by absorbing heat from the water to be cooled. As a result, the liquid water in evaporator becomes cold or may be converted totally or partially into ice. After that, the adsorbent adsorbs the refrigerant vapor that is coming from the evaporator (line 4–1, adsorption process at evaporator pressure). Thus, the heating and cooling processes are run at constant concentration of adsorbate while the concentration of refrigerant varies through adsorption and desorption processes.

A Simple Solar Ice Maker

N.A.A. Qasem, M.A.I. El-Shaarawi / Solar Energy 98 (2013) 523–542

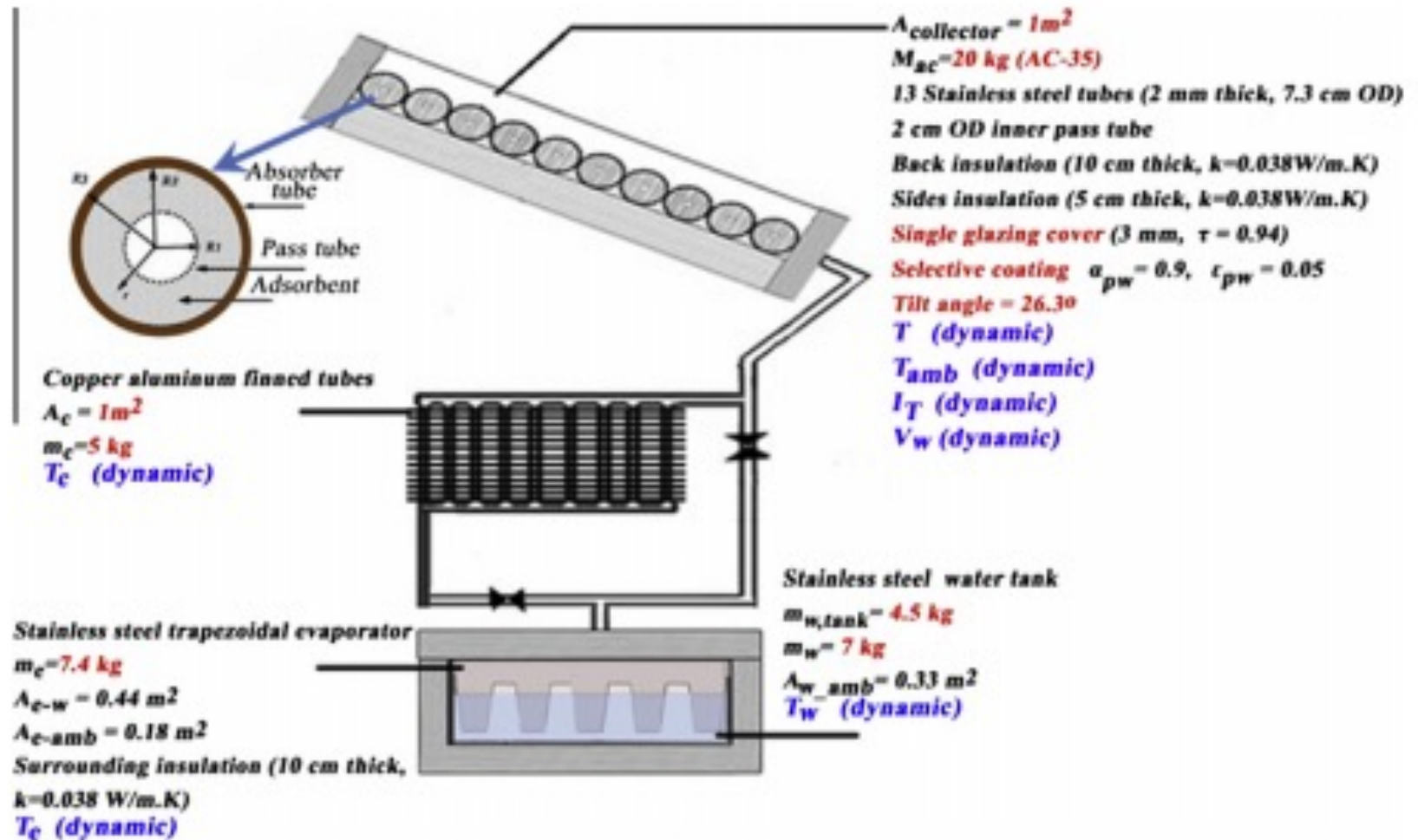


Fig. 2. Schematic details of the system.

Ammonia/Water Systems

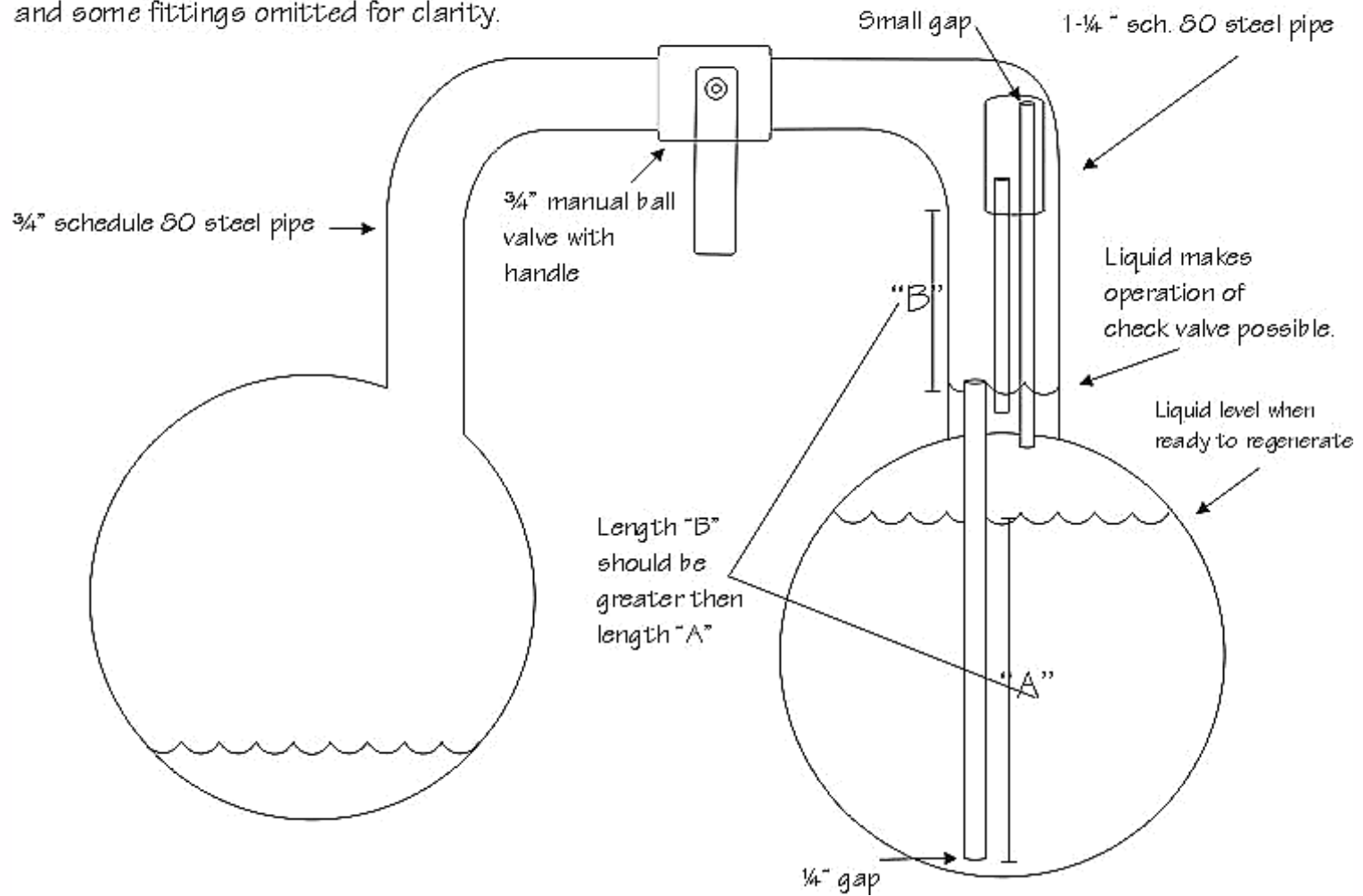
THE
~~CROSLEY~~
ICYBALL



The Crosley Radio Corporation
Cincinnati, Ohio, U. S. A.



Sketch of Larry D. Hall's homemade icyball.
Pressure gauges, service valves, sight glasses
and some fittings omitted for clarity.



Rural Milk Preservation with the ISAAC Solar Icemaker

Carl Erickson
Solar Ice Company
627 Ridgely Avenue
Annapolis, Maryland 21401



Figure 2. Local people helped install the solar icemakers.



Figure 3. Three units were installed in Kilifi District at Sovimwamri Dairy.



Figure 4. Three more units installed in Kwale District at Kidzo Farmer's Dairy Co-operative.

[ISAAC write-up](#)

Rural Milk Preservation with the ISAAC Solar Icemaker

Carl Erickson
Solar Ice Company
627 Ridgely Avenue
Annapolis, Maryland 21401



Figure 5. On a good solar day, the icemaker makes six blocks. Each block is 2 by 9.5 by 26 inches, weighing 8.3 kg each.



Figure 6. Milk is chilled in an ice-bath milk chiller. Each ISAAC produces enough ice to chill 100 liters per day.

Rural Milk Preservation with the ISAAC Solar Icemaker

Carl Erickson
Solar Ice Company
627 Ridgely Avenue
Annapolis, Maryland 21401



Figure 7. Farmers average 3 liters per day. Mostly they bring milk by bicycle or by foot. The two dairies are serving a total 138 farmers.



Figure 8. Milk, yogurt, and mala are sold from the dairy or distributed to the local community via bicycle.

Carl Erickson
Solar Ice Company
627 Ridgely Avenue
Annapolis, Maryland 21401

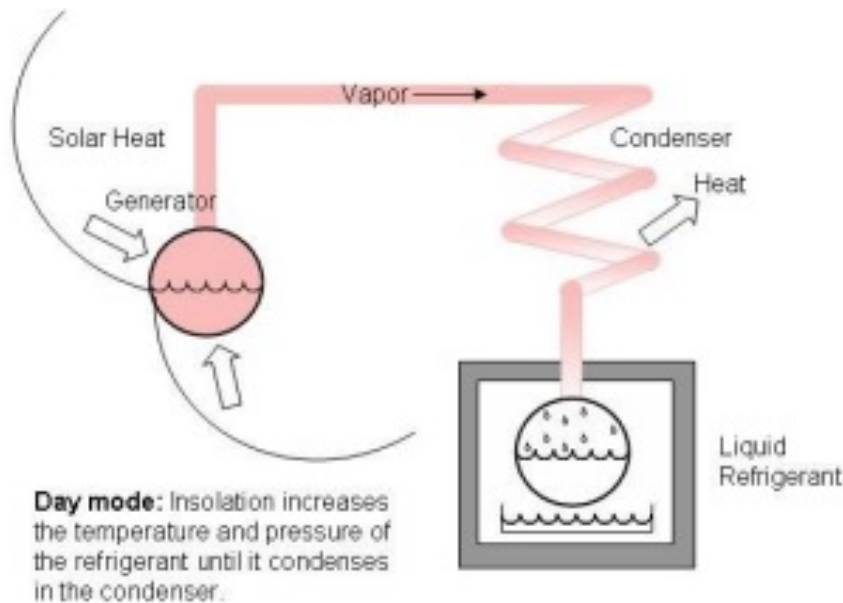


Figure 9. Day Mode Diagram

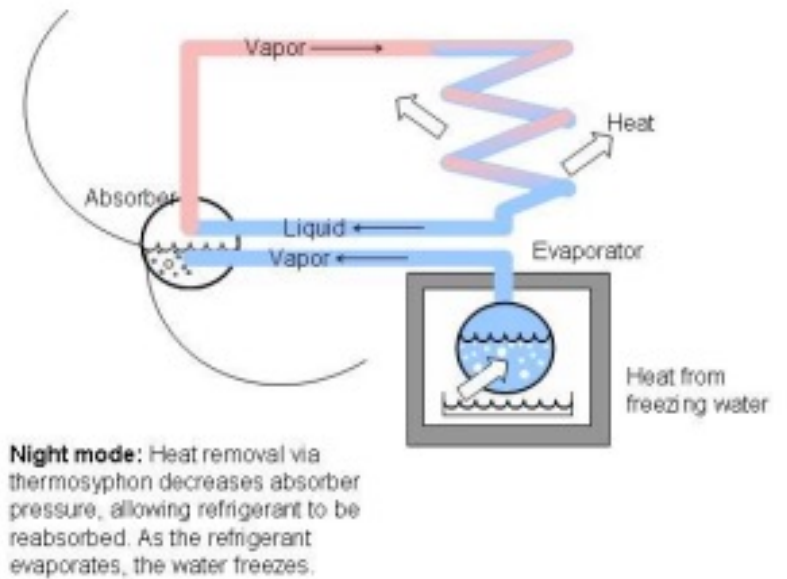


Figure 10. Night Mode Diagram.

Rural Milk Preservation with the ISAAC Solar Icemaker

Carl Erickson
Solar Ice Company
627 Ridgely Avenue
Annapolis, Maryland 21401

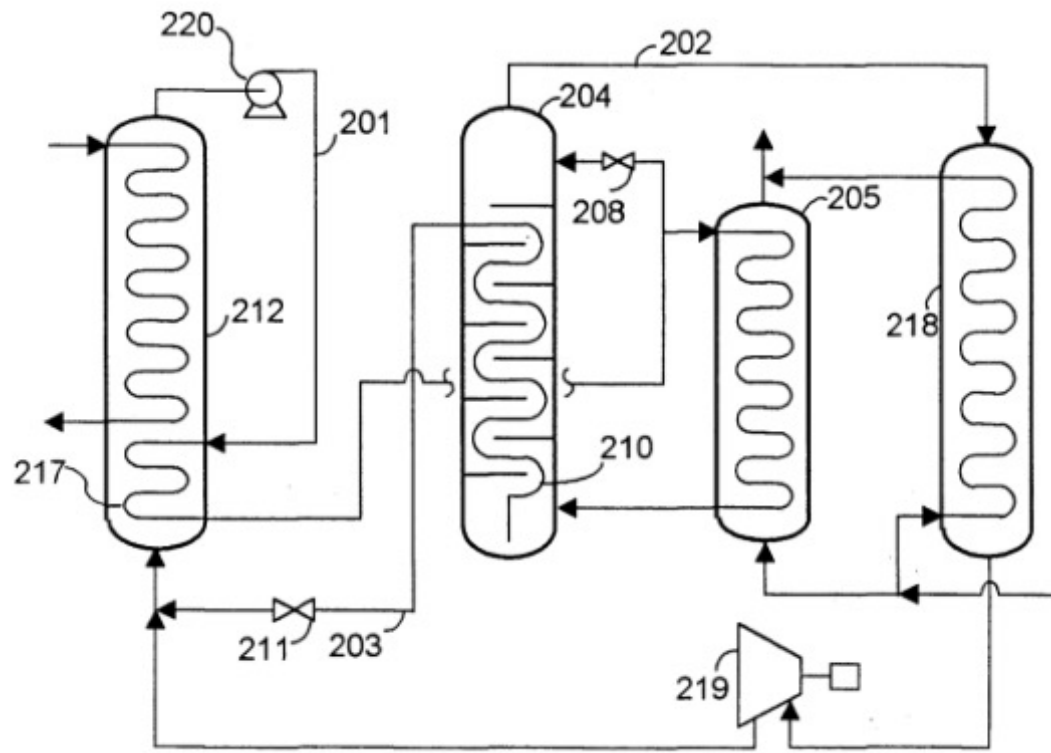


Figure 11. The system is operated by manual valves. Operation is routine and easy to do. The valves are operated in the morning and late afternoon. Water to be frozen is put into the evaporator in the afternoon; it is ready to be removed as ice early the next morning.

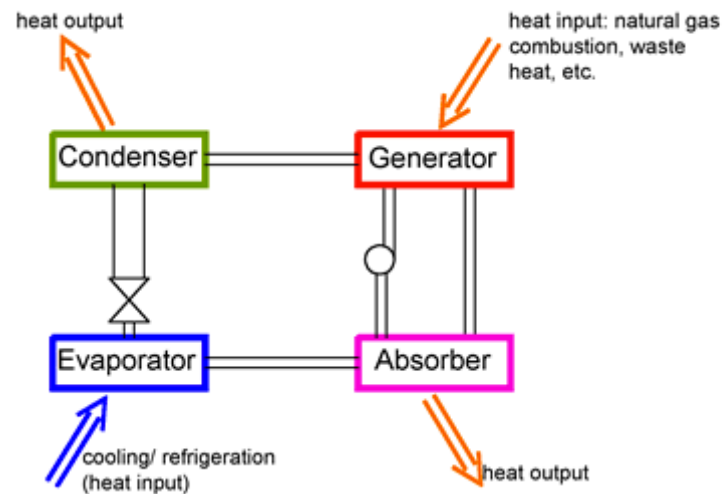
Issac Ice Maker (<http://www.energy-concepts.com>)



Fig.2



Referring to FIG. 2, weak absorbent solution in conduit **201** is separated into volatile component vapor of at least 95% purity in conduit **202** and strong absorbent liquid in conduit **203** by fractionating apparatus comprised of fractionating column **204** and co-current desorber **205**. Preheater **217** (an "absorption heat exchanger" (AHX) in this example) heats the solution to near saturation temperature before it is divided by divider **208** into a reflux stream for column **204** and a feed stream for desorber **205**. Desorbed mixture from desorber **205** is separated and fractionated in column **204** to bottom liquid and overhead vapor, and the bottom liquid causes additional reboil via heat exchange from GHX **210**. Distilled vapor in conduit **202** is superheated in superheater **218** and work-expanded in expander **219**. The superheating is done over the same approximate temperature range as desorption, i.e., desorber **205** and superheater **218** are heated in parallel, thus maximizing the temperature glide linearity. The expanded vapor is absorbed into the strong absorbent after pressure letdown by valve **211**, in absorber **212**, cooled both by external fluid in the colder section, and by absorbent in AHX **217**. Pump **220** completes the absorbent cycle. The low temperature glide heat can be geothermal liquid, solar heated liquid, combustion exhaust gases, etc. Thus, a simple, economical, and highly efficient absorption power cycle is realized.



The basic operation of an ammonia-water absorption cycle is as follows. Heat is applied to the generator, which contains a solution of ammonia water, rich in ammonia. The heat causes high pressure ammonia vapor to desorb the solution. Heat can either be from combustion of a fuel such as clean-burning natural gas, or waste heat from engine exhaust, other industrial processes, solar heat, or any other heat source. The high pressure ammonia vapor flows to a condenser, typically cooled by outdoor air. The ammonia vapor condenses into a high pressure liquid, releasing heat which can be used for product heat, such as space heating.

The high pressure ammonia liquid goes through a restriction, to the low pressure side of the cycle. This liquid, at low pressures, boils or evaporates in the evaporator. This provides the cooling or refrigeration product. The low pressure vapor flows to the absorber, which contains a water-rich solution obtained from the generator. This solution absorbs the ammonia while releasing the heat of absorption. This heat can be used as product heat, or for internal heat recovery in other parts of the cycle, thus unloading the burner and increasing cycle efficiency. The solution in the absorber, now once again rich in ammonia, is pumped to the generator, where it is ready to repeat the cycle.

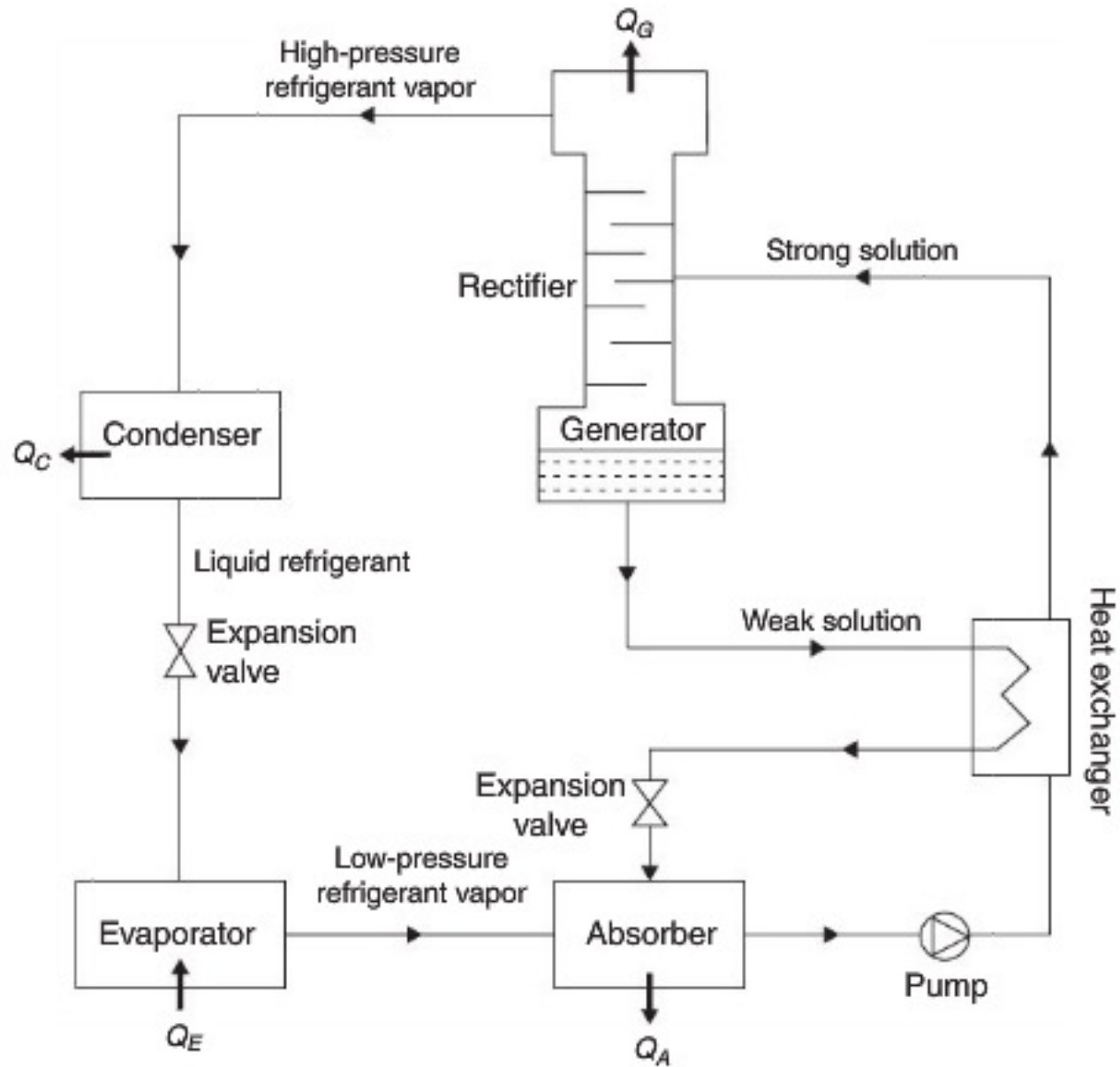


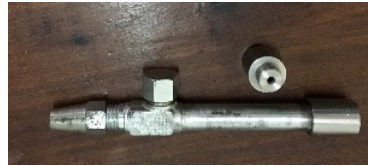
FIGURE 6.27 Schematic of the ammonia-water refrigeration system cycle.

Michael John UDSM



Cuthbert Kimambo, Provost UDSM





LiBr/Water Systems

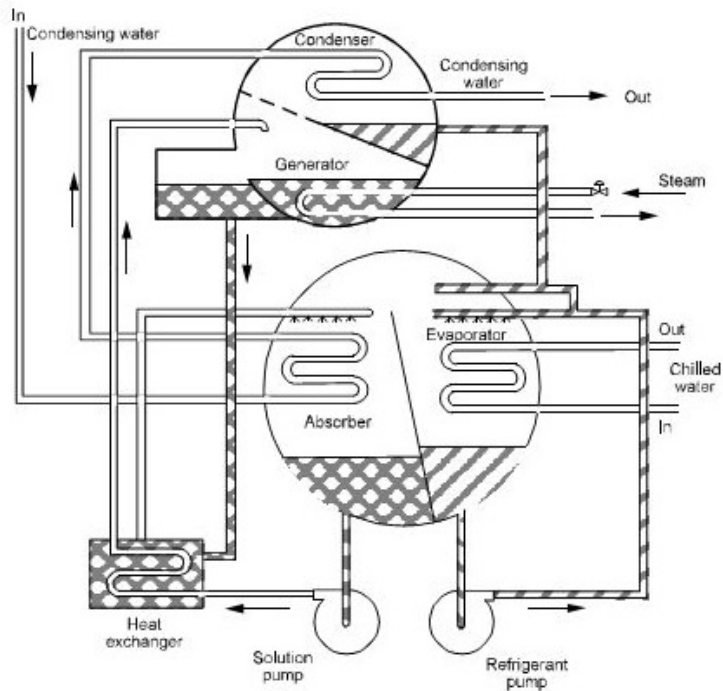


Figure 13.1 Diagram of two-shell lithium bromide cycle water chiller (ASHRAE, 1983).

LiBr/Water Refrigerator

1) Evaporator: Water as the refrigerant enters the evaporator at a very low pressure and temperature. Since very low pressure is maintained inside the evaporator the water exists in a partial liquid state and partial vapor state. This water refrigerant absorbs the heat from the substance to be chilled and gets fully evaporated. It then enters the absorber.

2) Absorber: A concentrated solution of lithium bromide is available in the absorber. Since water is highly soluble in lithium bromide, solution of water-lithium bromide is formed. This solution is pumped to the generator.

3) Generator: Heat is supplied to the refrigerant water and absorbent lithium bromide solution in the generator from the steam or hot water. The water becomes vaporized and moves to the condenser, where it gets cooled. As water refrigerant moves further in the refrigeration piping and through nozzles, its pressure is reduced along with the temperature. This water refrigerant then enters the evaporator where it produces the cooling effect. This cycle is repeated continuously. Lithium bromide on the other hand, leaves the generator and re-enters the absorber for absorbing water refrigerant.

As seen in the image above, the condenser water is used to cool the water refrigerant in the condenser and the water-Li Br solution in the absorber. Steam is used for heating water-Li Br solution in the generator. To change the capacity of this water-Li Br absorption refrigeration system the concentration of Li Br can be changed.

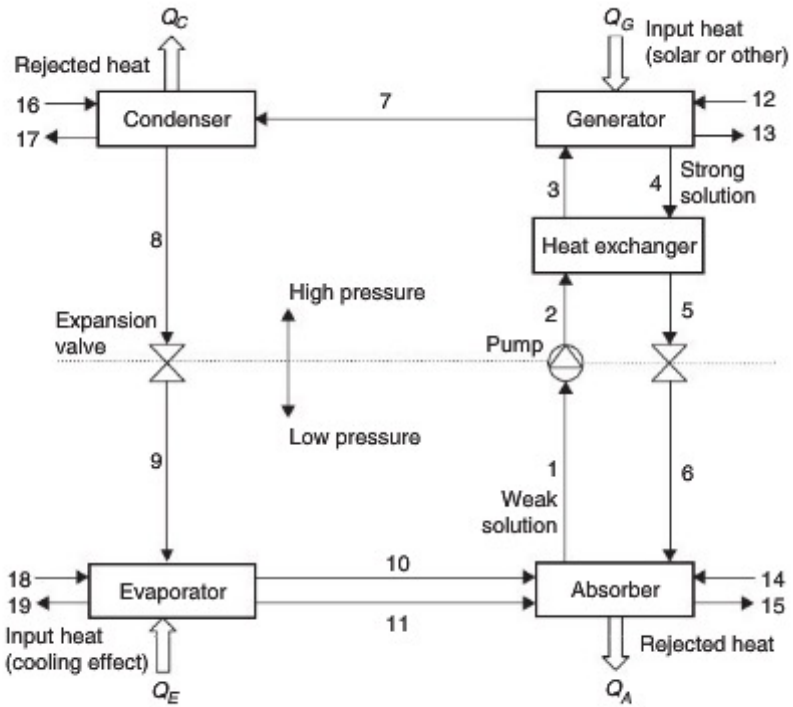


FIGURE 6.23 Schematic diagram of an absorption refrigeration system.

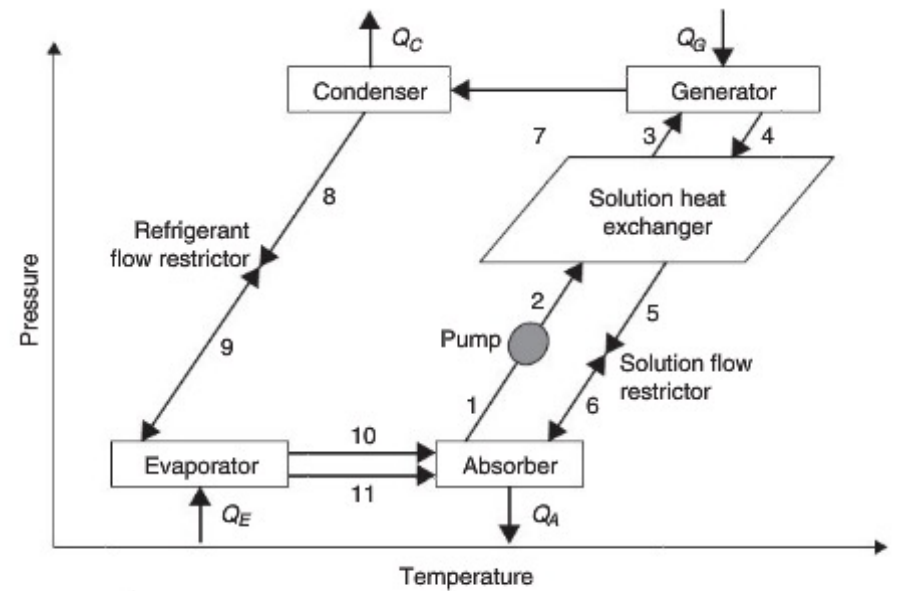


FIGURE 6.24 Pressure-temperature diagram of a single effect, LiBr-water absorption cycle.

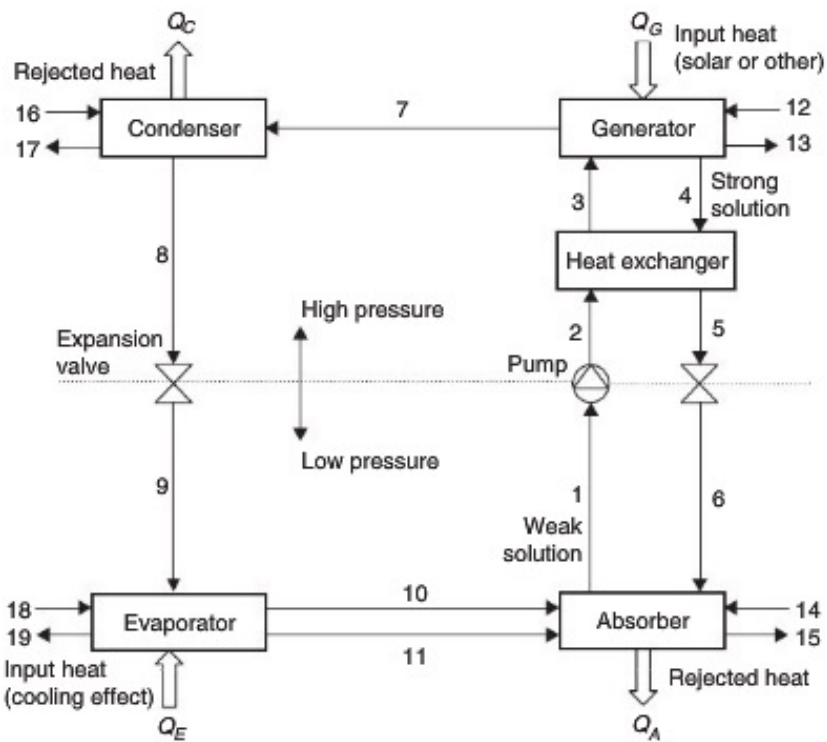


FIGURE 6.23 Schematic diagram of an absorption refrigeration system.

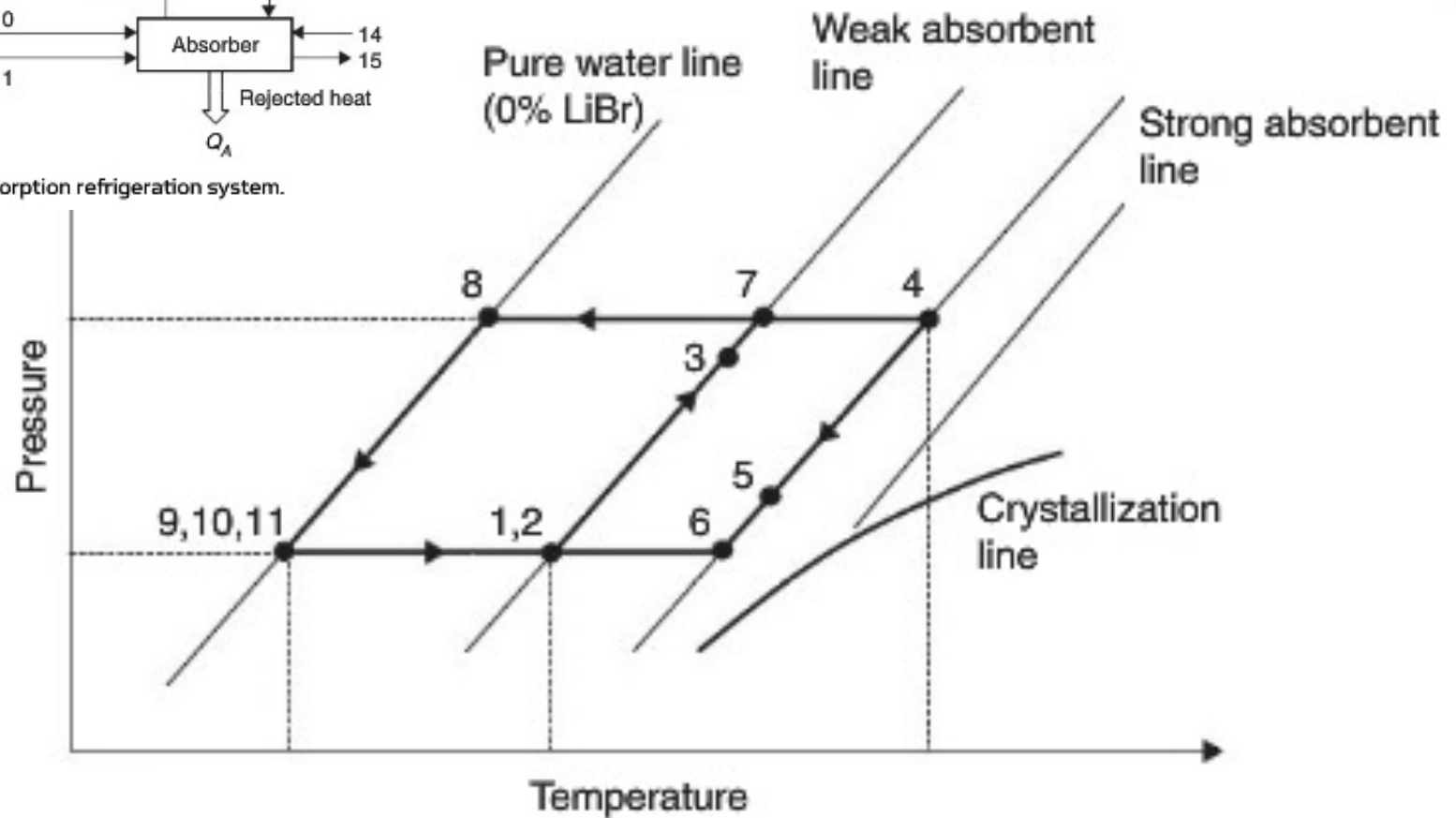
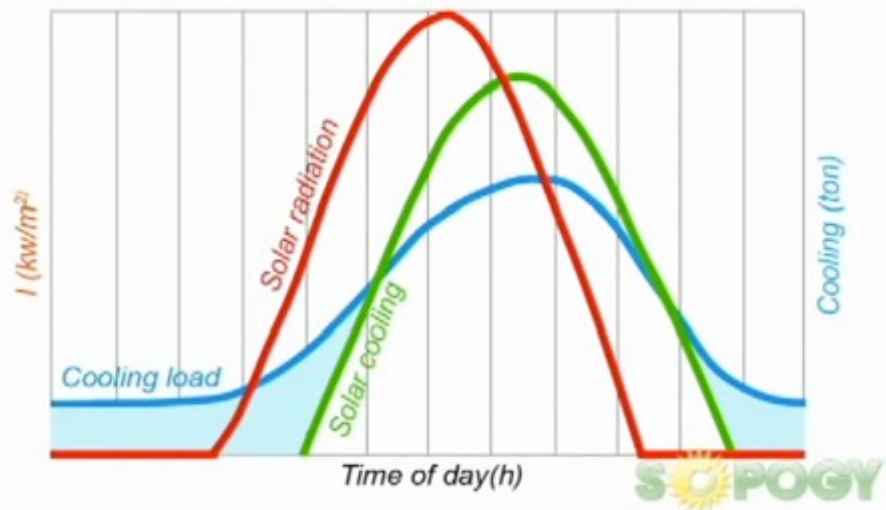
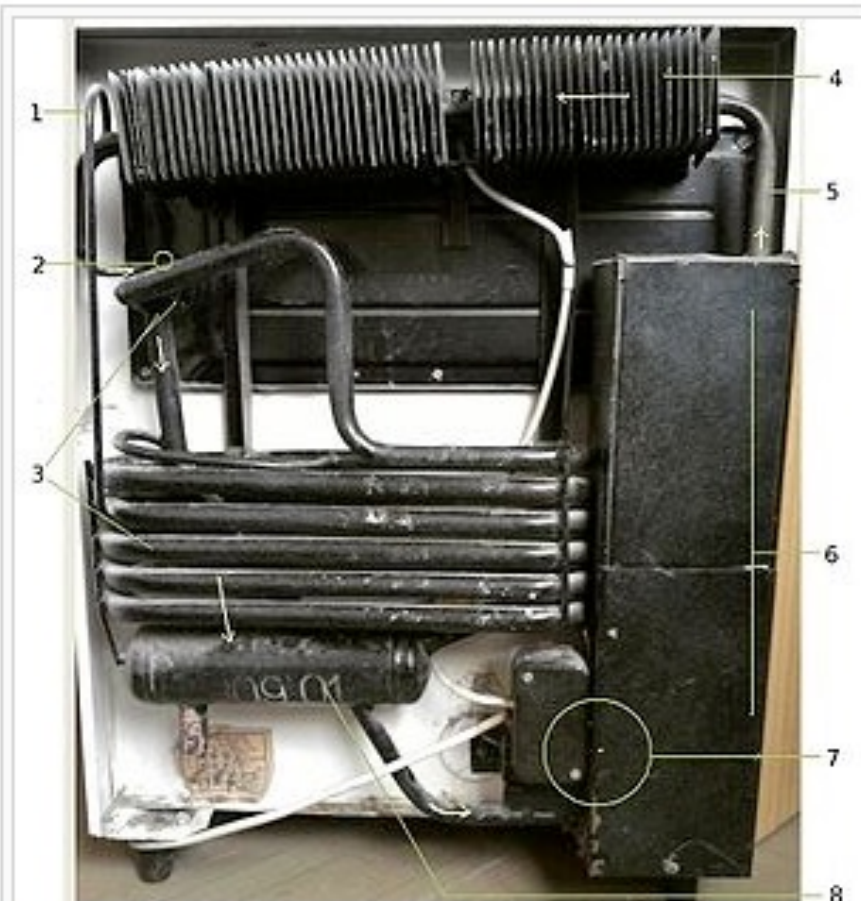



FIGURE 6.25 Duhring chart of the water–lithium bromide absorption cycle.

SOPOGY Solar Air Conditioning LiBr

http://www.youtube.com/watch?v=2usC_BbILSw





Labeled photo of a domestic absorption refrigerator. 

1. Hydrogen enters the pipe with liquid ammonia
2. Ammonia+hydrogen enter the inner compartment of the refrigerator. Change in partial pressure causes ammonia to evaporate. Energy is being drawn from the surroundings - this causes the cooling effect. Ammonia+hydrogen return from the inner part, ammonia returns back to absorber and dissolves in water. Hydrogen is free to rise upwards
3. Ammonia gas condensation (passive cooling)
4. Hot ammonia (gas)
5. Heat insulation and separation of water from ammonia gas
6. Heat source (electric)
7. Absorber vessel (water + ammonia solution)

[How it works: Absorption Refrigerator](https://youtu.be/udeSVyx6_9A)

https://youtu.be/udeSVyx6_9A

[Industrial Solar Refrigerator in Tunisia](http://www.youtube.com/watch?v=EPbjwv-7fWI)

<http://www.youtube.com/watch?v=EPbjwv-7fWI>



[Example of one of these large scale systems](http://www.youtube.com/watch?v=AtMC2MXc_n8) (http://www.youtube.com/watch?v=AtMC2MXc_n8)

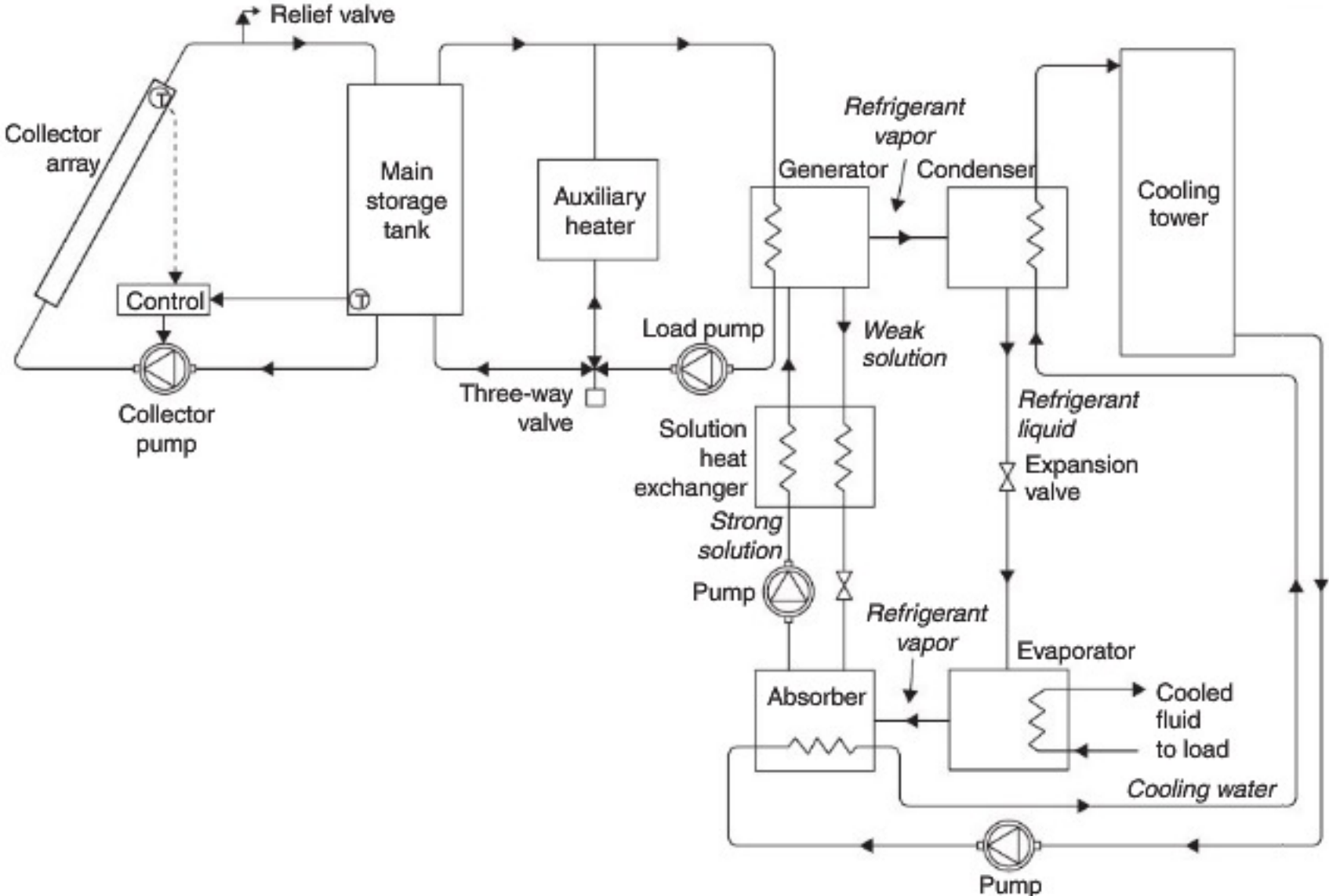
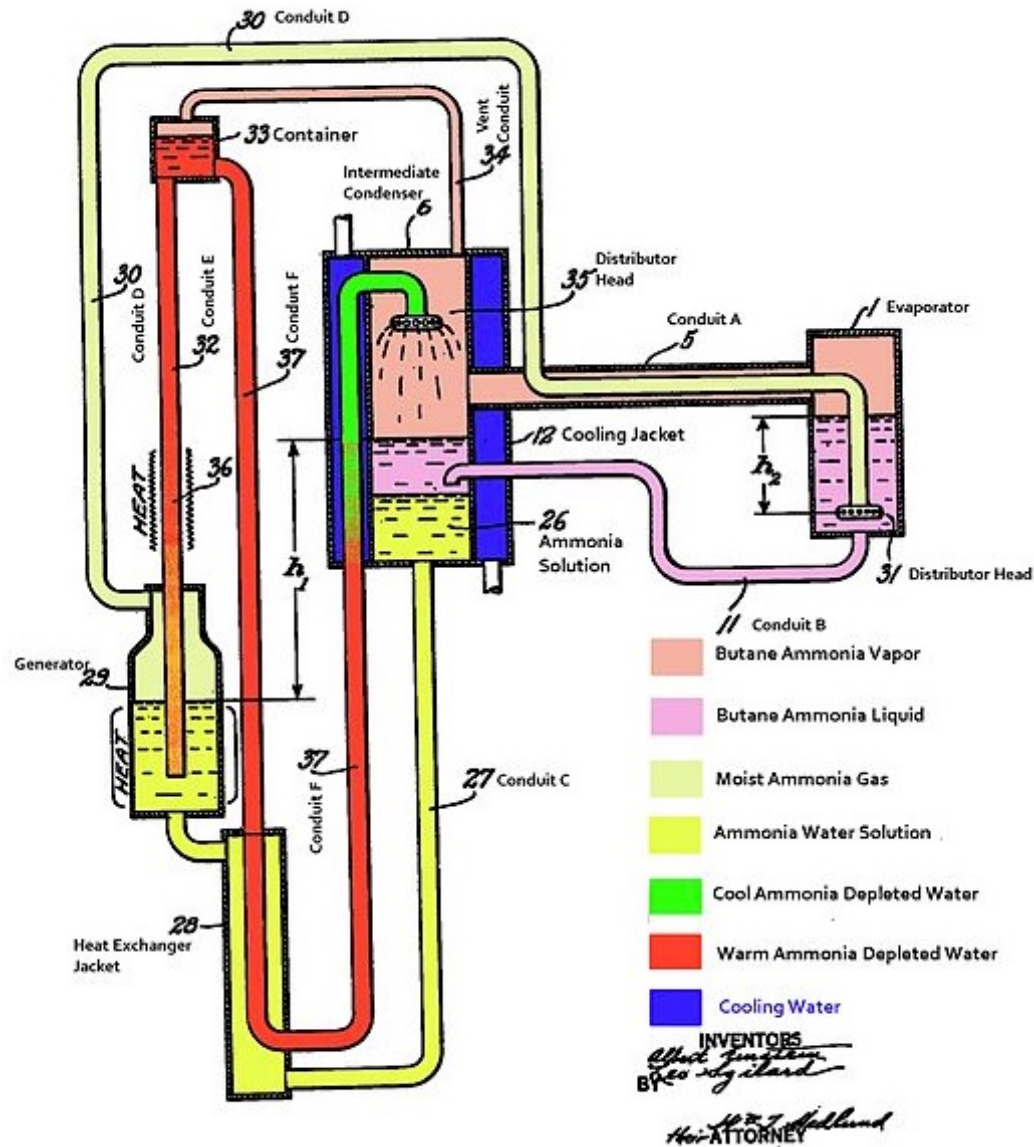


FIGURE 6.28 Schematic diagram of a solar-operated absorption refrigeration system.

Einstein Refrigerator



Project 7: Solar-Powered Ice-Maker

You will need

- Four sheets galvanized metal, 26 ga.
- 3 in. black iron pipe, 21 ft length
- 120 sq ft mirror plastic
- 2½ in. stainless steel valves
- Evaporator/tank (4 in. pipe)
- Freezer box (free if scavenged)
- 4 ft × 8 ft sheet ¾ in. plywood
- six 2 × 4 timbers, 10 ft long
- Miscellaneous ¼ in. plumbing
- Two 3 in. caps
- 1½ in. black iron pipe, 21 ft length
- Four 78 in. long 1½ in. angle iron supports
- 15 lb ammonia
- 10 lb calcium chloride

This design is for an ice-maker which will produce about 10 lb of ice in a single cycle. It uses the evaporation and condensation of ammonia as a refrigerant. If you remember in the explanation above, I mentioned that we needed a refrigerant and an absorber for this type of cooler to work. Well, the ammonia is our refrigerant, and we use a salt—calcium chloride—as the absorber. You might have seen small gas fridges often used in caravans and RVs which can be powered by propane—these also generally use ammonia as a

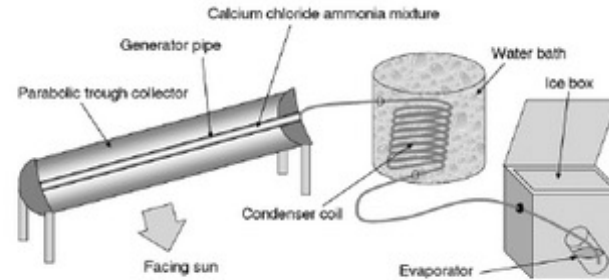


Figure 5-3 Solar cooler layout.

Warning

For the system to operate for long periods of time, the materials used should be resistant to corrosion by ammonia. Steel and stainless steel are ideal in this respect as both are immune to corrosion by ammonia. Another consideration is the pressure under which the system will have to operate.

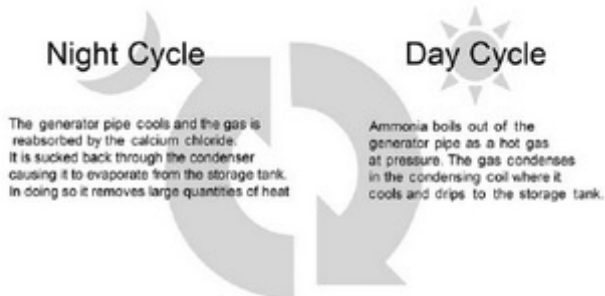


Figure 5-5 The solar cooler cycle.

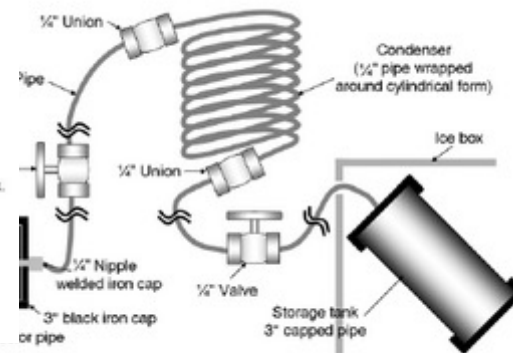


Figure 5-4 Solar cooler plumbing details.

How does the ice-maker work?

The ice-maker works on a cycle—during the daytime ammonia is evaporated from the pipe at the focal point of the parabolic mirrors. This is because the sun shines on the collector which is painted black to absorb the solar energy—this collector heats up, driving the ammonia from the salt inside.

At night, the salt cools and absorbs the ammonia, as it does this, it sucks it back through the collector. As it evaporates from the storage vessel, it takes heat with it.

http://www.ted.com/talks/adam_grosser_and_his_sustainable_fridge.html

[Ted Talk on Developing World Refrigerator](#)





Roll over image to zoom in

BestFire

BestFire Car Mini Fridge Portable Thermoelectric Cooler and Warmer Travel Refrigerator for Home ,Office, Car or Boat AC & DC, White - 12L Capacity

★★★★☆ 6 customer reviews

Price: **\$91.88** ✓prime

Your cost could be \$81.88: Qualified customers get a \$10 bonus on their first reload of \$100 or more.

In Stock.

Want it Saturday, Oct. 14? Order within **8 hrs 21 mins** and choose **Two-Day Shipping** at checkout. [Details](#)

Sold by [BestFire](#) and [Fulfilled by Amazon](#). Gift-wrap available.

- **【BestFire Advantage】** -- A built-in removable shelf for different capacity and demand, which makes this 12L fridge holds up to 4



COWIN

DC12V 68W Solar Refrigerator Freezer 7.4 Cubic. ft, Cowin Solar Powered Fridge, 150 W Solar Pannel, Double Doors, Low Voltage

[Be the first to review this item](#) | [15 answered questions](#)

Price: ~~\$2,198.80~~

Sale: **\$1,998.80** & **FREE Shipping**

You Save: **\$200.00 (9%)**

Item is eligible: No interest if paid in full within 12 months with the [Amazon.com Store Card](#).

Note: Not eligible for Amazon Prime.

In stock.

Get it as soon as Nov. 6 - 29 when you choose **Standard Shipping** at checkout.

<https://sundanzer.com/product/bfrv15/>

3-5% propylene glycol in water

Solar Powered Medical Refrigerator, 15 liters

Category: [Medical](#)



Pre-Qualified by the World Health Organization (WHO) the SunDanzer BFRV15 provides vaccine storage using solar direct-drive battery-free technology. Designed in conjunction with DIVAF and PATH, the BFRV55 solves a very important problem in the vaccine cold chain by eliminating the need for batteries.

Features

- Meets WHO/PQS/E003/RF05-VP.2 standard
- Rated for Hot Zone + 43° C
- Requires no battery or charge controller
- User Independent Freeze Protection
- Complete kit in crate includes PV array, mount, wiring and grounding, user and installation manual, external digital temperature display, lock and key



\$2,495.00

1   **Add to cart**

Amazon's Choice

2



100 Watts 100W Solar Panel 12V Poly Off Grid Battery Charger for RV - Mighty Max Battery brand product

by Mighty Max Battery

\$99⁹⁵

Get it by **Saturday, Oct 14**

More Buying Choices
\$79.96 (3 used & new offers)

★★★★★ 41

Product Features

MLS-100WP is 12v 100 watt polycryst solar panel

4



SunDanzer

Sundanzer Solar-Powered Refrigerator - 8 Cubic Ft., 30in.L x 50in.W x 37in.H

★★★★☆ 7 customer reviews

Price: **\$1,870.00** + \$159.99 shipping

Get \$40 off instantly: Pay \$1,830.00 upon approval for the Amazon.com Store Card.

Note: Not eligible for Amazon Prime.

Get it as soon as Nov. 17 - Dec. 7 if you choose Standard Shipping at checkout.

Ships from and sold by Savana Solar Industries, Ltd

FlexMax 60-Amp Solar Charge Controller OutBack Power 150V 60A FM6C by Outback

\$453.00 (6 used & new offers)

★★★★★ 7



Sponsored ⓘ

NPP 6V 200 Amp NP6 200Ah AGM Deep Cycle Camper Golf Cart RV Boat Solar Wind Battery

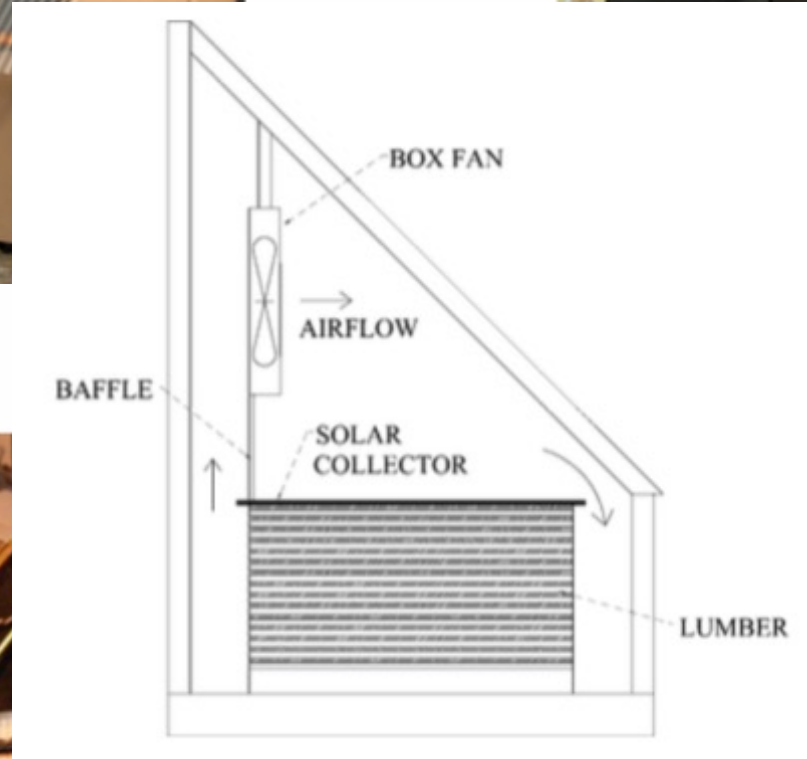
\$219⁹⁹

★★★★★ 2

Total = \$3500

Solar Drying, Solar Kiln
Solar Baking
Solar Charcoal





https://pubs.ext.vt.edu/content/dam/pubs_ext_vt_edu/420/420-030/420-030_pdf.pdf



Solar Charcoal



2.5 The stages in charcoal formation

As the wood is heated in the retort it passes through definite stages on its way to conversion into charcoal. The formation of charcoal under laboratory conditions has been studied and the following stages in the conversion process have been recognised.

- at 20 to 110°C

The wood absorbs heat as it is dried giving off its moisture as water vapour (steam). The temperature remains at or slightly above 100°C until the wood is bone dry.

- at 110 to 270°C

Final traces of water are given off and the wood starts to decompose giving off some carbon monoxide, carbon dioxide, acetic acid and methanol. Heat is absorbed.

- at 270 to 290°C

This is the point at which exothermic decomposition of the wood starts. Heat is evolved and breakdown continues spontaneously providing the wood is not cooled below this decomposition temperature. Mixed gases and vapours continue to be given off together with some tar.

- at 290 to 400°C

As breakdown of the wood structure continues, the vapours given off comprise the combustible gases carbon monoxide, hydrogen and methane together with carbon dioxide gas and the condensable vapours: water, acetic acid, methanol, acetone, etc. and tars which begin to predominate as the temperature rises.

- at 400 to 500°C

At 400°C the transformation of the wood to charcoal is practically complete. The charcoal at this temperature still contains appreciable amounts of tar, perhaps 30% by weight trapped in the structure. This soft burned charcoal needs further heating to drive off more of the tar and thus raise the fixed carbon content of the charcoal to about 75% which is normal for good quality commercial charcoal.

To drive off this tar the charcoal is subject to further heat inputs to raise its temperature to about 500°C, thus completing the carbonisation stage.

<http://www.fao.org/docrep/x5555e/x5555e03.htm>

about 0.50 USD/kg in Tanzania

Design of semi-static solar concentrator for charcoal production

G. Ramos^{a*} and David Pérez-Márquez^a

a Instituto Politécnico Nacional, CICATA-IPN, Cerro Blanco 141, Col. Colinas del Cimatario, 76090 Querétaro, QRO, México

https://ac.els-cdn.com/S1876610214015501/1-s2.0-S1876610214015501-main.pdf?_tid=2825d798-b4f4-11e7-b1ff-00000aab0f26&acdnat=1508434819_32b09327f2c7717ac422cf07c1e471ce

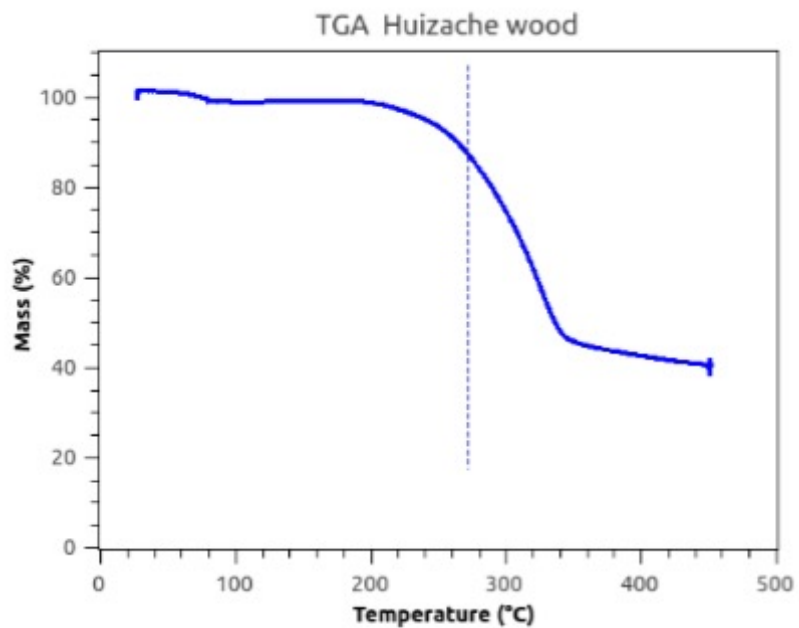


Figure 1. Thermogravimetric analysis of saw dust of *Vachellia farnesiana*.

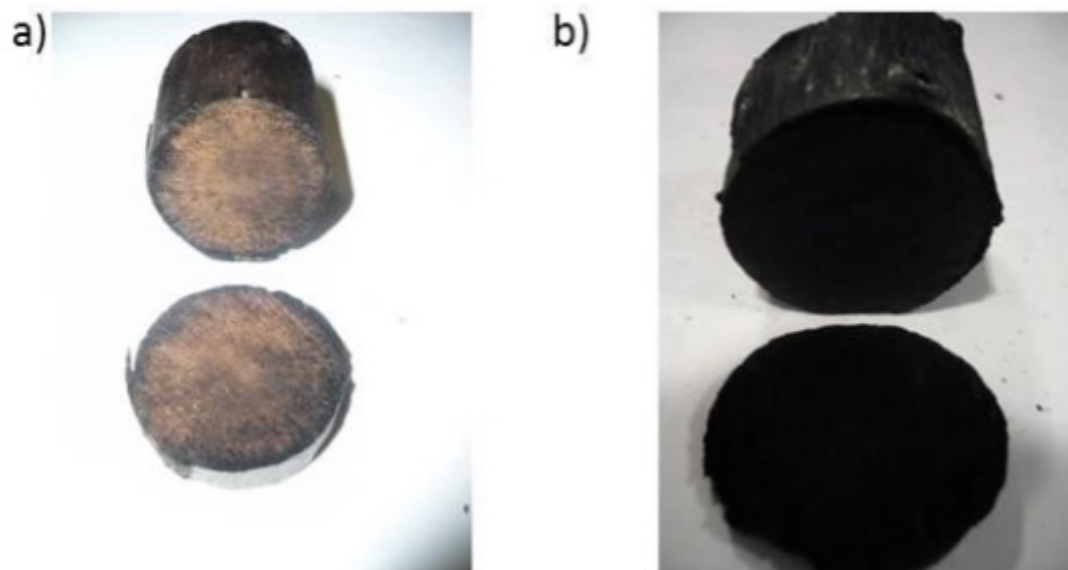


Figure 2. Pictures of Samples a) after 2 hours and b) 6 hours of carbonization at 275°C.



Figure 8 Picture of the prototype in its final version with the evacuated tube receiver.



Figure 9 Picture of the prototype in its final version with the evacuated tube receiver.

http://solarcooking.wikia.com/wiki/Solar_charcoal

The information below was provided by [Helen Dawson](#):

- Pack dry sticks in a metal tin as tightly as possible.
- Heat wood in the closed tin to approximately 300 °C (572 °F) in a solar cooker.
- (Somewhere between 200 °C (392 °F) for a couple of hours and 400 °C (752 °F) for half an hour will do). There is a good explanation of the overall benefits of turning woodchips or other biomass such as corn cobs to charcoal on the Solar Fire open source web page:

<http://www.solarfire.org/Solar-Charcoal>

- The wood will give off smoke and water vapour below 200 °C (392 °F) unless the lid is very tight..
- Wipe the pyrex bowl lid to remove moisture and soot if its building up on the inside, before it gets too hot to handle.
- Over 200 °C (392 °F) approx. the wood is **carbonizing**.
- The time and temperature needed to turn the entire contents to charcoal depend on the wood used, the size of the sticks and the solar variables like cloud cover.
- Over 400 °C (752 °F) approx. the wood which is now charcoal ignites and burns to ash.
- Best to leave one set up for a whole day first time, with enough mirror capacity to get over 200 °C (392 °F) for a couple of hours, but less than what it would take to set it alight. Same as with cooking food, you're cooking the wood.
- This is the solar pyrolysis process.
- The wood doesn't create embers, when there is no air flow in the tin, there isn't enough oxygen for it to burn, and under 400 °C (752 °F) it is less likely to ignite.
- Sit an oven thermometer on top of the tin under the pyrex, so you can see the temp climb.
- Remove tin from pyrex bowls in the evening or next morning, when cooled.
- When you open the cooled tin the heat from the sun has turned the sticks to charcoal.
- You can do a drawing with them, and/or the following project.
- Solar cooked charcoal retains the tar in the tin and on the charcoal, making it a bit sticky to handle. As the temperature increases the stickiness decreases. Many Australian seed pods such as gumnuts and banksias, are germinated by fire, so putting them in the solar cooker will result in seedlings in the PET moss garden.
- Charcoal improves the soils ability to grow plants AND captures carbon dioxide, it is carbon sequestration.
- You can help cool the planet by putting charcoal in the soil.
- **Terra preta** owes its name to its very high charcoal content, and was made by adding a mixture of charcoal, bone, and manure to the otherwise relatively infertile Amazonian soil. It is very stable and remains in the soil for thousands of years. Its called Biochar in English speaking countries.



Pyrex bowls trap heat stop wind loss



Solar Cooker two mirrors and aluminium reflector base

200° C water vapor
Above 200 below 400 wood gas
Charcoal in about 2 hours from sticks

Small solar charcoal kiln for cloth


<https://www.youtube.com/watch?v=8Makaciz3Xc>

Fresnel Lens

<https://www.bladesmithsforum.com/index.php?/topic/32781-charcoal-through-solar-power/>

Home Solar Charcoal Distiller

Pollution free charcoal
generation - at home!

 [vote
for,
against]
(+12)

Charcoal has been used for fuel for millenia. Produced by heating wood in the absence of oxygen, it is nearly pure carbon, without the water or volatiles that cause smoky,uneven combustion in wood. As currently done, charcoal production is wasteful, burning some charcoal to produce more. Many operations also pollute heavily, discharging the tar and turpentine distilled from the wood into the air.

The Solar Charcoal Distiller allows you to make your own charcoal at home, without bathing your neighbors in clouds of turpentine. The SCD kit (from BUNGCO!) comes with a large plastic Fresnel lens and a special top designed to fit on a standard Weber Kettle. Simply load your Weber with branches and sticks from your neighborhood, put on the special lid, close those air intakes at the bottom, and set up the Fresnel to bathe your grill in concentrated rays (you will want to remove the wooden handles first). Already painted black with heat resistant paint, it will only be a few moments before your kettle glows cheery red and your wood begins to cook. Cook it all day, and then when the sun gets low you will have a kettle full of warm charcoal, ready for grilling dinner!

The special lid is fitted with a metal hose on the top. Place the end of this hose in a bucket of water. Operating on the same principle as a hookah, the steam and volatiles cooked off the wood are cooled and left in the water, for you to use later as you see fit. In our test runs here at BUNGCO we used a lot of eucalyptus and pine - the distilled products proved excellent for treating the bottom of the BUNGCO yacht!

—[bungston](#), Nov 20 2005

Homemade solar charcoal

<http://www.youtube...watch?v=8Makaciz3Xc>

Giant lens - check. Backyard - check. [[bungston](#), Jul 01 2013]

http://www.halfbakery.com/idea/Home_20Solar_20Charcoal_20Distiller

Design and Testing of a Solar Torrefaction Unit to Produce Charcoal

Rajaram Swaminathan*, Frans Nelongo Pandeni Nandjembo

Department of Mechanical and marine Engineering, Namibia University of Science and Technology, Windhoek, Namibia

https://file.scirp.org/pdf/JSBS_2016081016170057.pdf

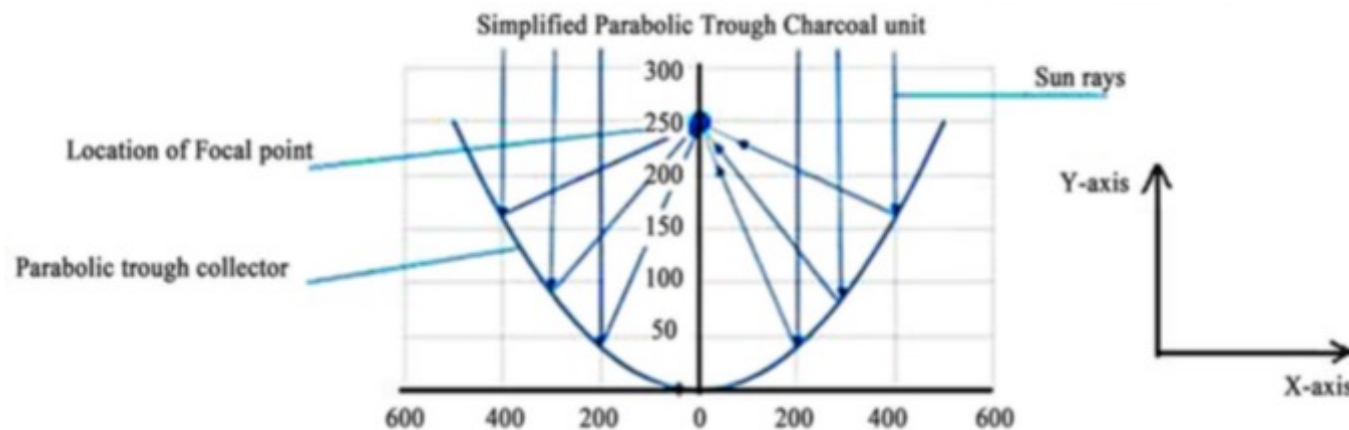


Figure 1. Indicates the focal point in the parabolic trough collector.

Design and Testing of a Solar Torrefaction Unit to Produce Charcoal

Rajaram Swaminathan*, Frans Nelongo Pandeni Nandjembo

Department of Mechanical and marine Engineering, Namibia University of Science and Technology, Windhoek, Namibia

<https://www.researchgate.net/publication/353111111>

.p



Figure 3. The unit.

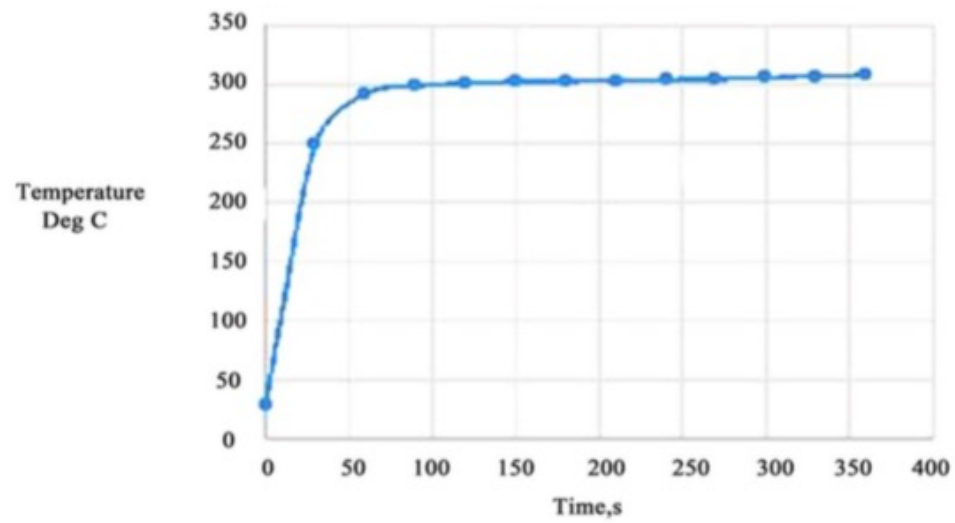


Figure 4. The tube inside temperature recorded at regular interval starting at 9AM.



Acacia



Berchemia



White oak



Charcoal



Figure 5. Shows the different woods tested and the charcoal obtained.

Type of wood	Time for charcoal production (h)	Charcoal yield %
White Oak Charcoal	01; 30	21
Berchemia discolor	01; 30	35
Acacia	01; 30	28

The time taken for these types of wood is the same [Figure 5](#). The yield ranges from 21% - 35% depending on the wood. It is observed that the charcoal of white oak is lighter than those of Acacia and Berchemia.

http://www.scienceforums.com/topic/6307-solar-parabolic-trough-charcoal-oven/page-18



Like 0

Solar Parabolic Trough Charcoal Oven

Started By Turtle, May 04 2006 02:16 PM

« PREV Page 18 of 19 16 17 18 19 NEXT »

Please log in to reply

306 replies to this topic

Nitack

#290 <

Understanding



Members
447 posts

Posted 12 March 2009 - 01:14 PM

So this may be the most lowtech idea of making my frasnell lens actually make charcoal, but I actually think it might work. This came to me as I was testing out a traditional burner and retort (which did not work because I used unseasoned, large pieces of wood). I never got the retort to fire, but I came up with an idea. I am going to take apple sauce jars, the big mothers, punch a few holes in the top, pack them with mulch, and then sit them in the fire to char and eventually give off wood gas to help fuel the burn for my 55 gallon drum.

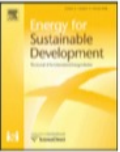
But I was thinking, why wouldn't that also work with a Fresnel directly on the mulch in the jar? As long as I pack the much there should be relatively low oxygen. Additionally, as long as I don't completely focus the beam, it should get hot enough to char everything. The stuff towards the inside may not get hot enough for long enough, but the stuff around the outside should all char right? 💡

I think the biggest mistake I was making with the Fresnel was to just try to make one point supper hot and then have conduction/convection heat the material. Too damn much heat was being lost to the air around me. Thoughts?

Edit: finding the most long and skinny jar I can should probably help as well.

Turtle

#291 <



Review

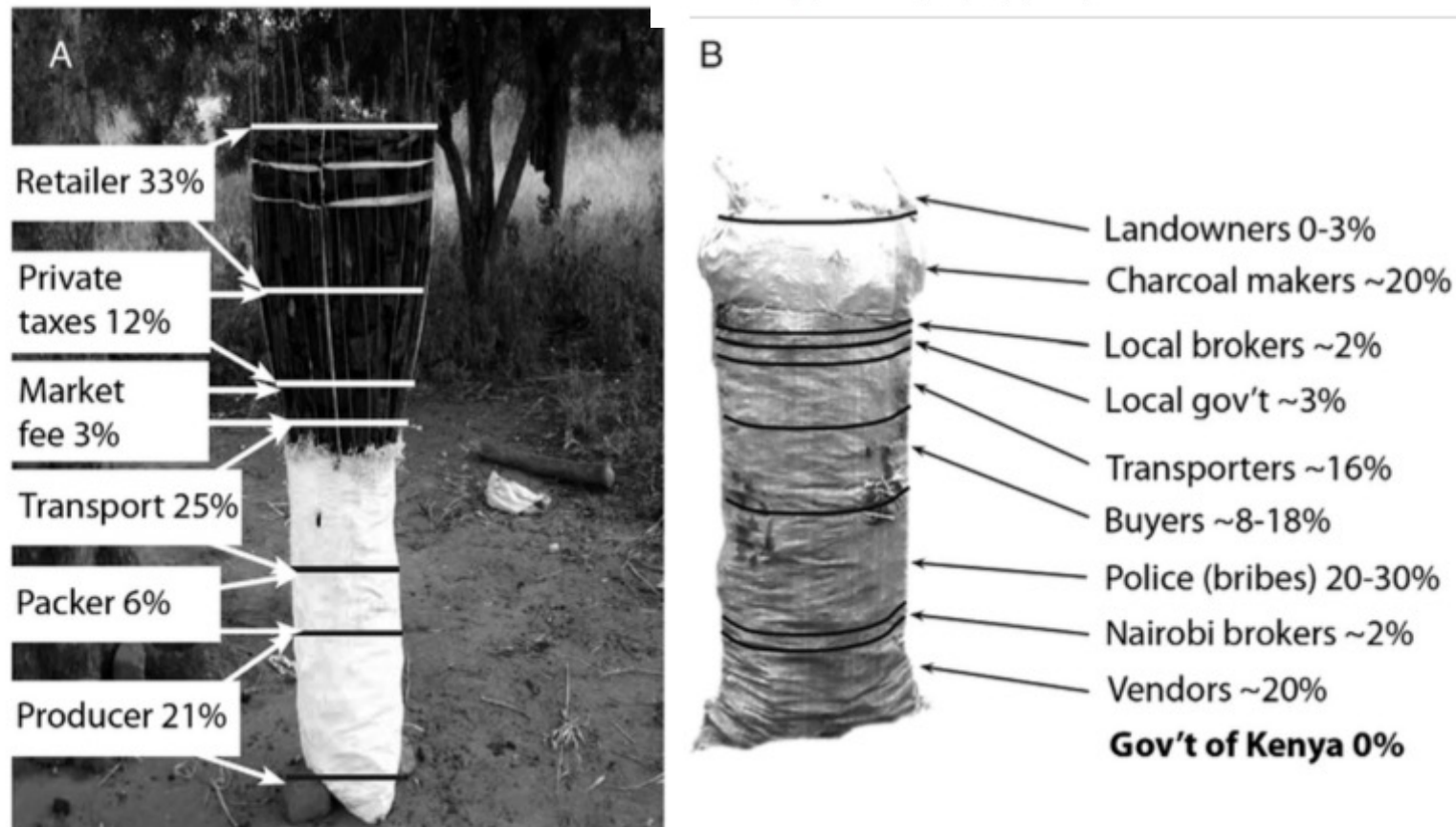
Dispelling common misconceptions to improve attitudes and policy outlook on charcoal in developing countries[☆]Tuyeni H. Mwampamba^{a,*}, Adrián Ghilardi^{b,c}, Klas Sander^d, Kim Jean Chaix^e^a Centro de Investigaciones en Ecosistemas (CIEco), Universidad Nacional Autónoma de México, antigua carretera a Pátzcuaro 8701, Morelia, Michoacán 58190, Mexico^b Centro de Investigaciones en Geografía Ambiental (CIGA), Universidad Nacional Autónoma de México, antigua carretera a Pátzcuaro 8701, Morelia, Michoacán 58190, Mexico^c School of Forestry & Environmental Studies, Yale University, 195 Prospect Street, New Haven, CT 06511, USA^d World Bank 1818 H Street, N.W.10 Washington, DC 20433, USA^e The Charcoal Project, 378 Clinton Street, Ste. #1, Brooklyn, NY 11231, USA

Fig. 3. The proportion of revenue captured by different stakeholders along the charcoal commodity chain in Malawi (A) and Kenya (B). Note how in both cases, the government captures none of the charcoal revenue, yet 12% to 30% is captured by ‘private taxes’ otherwise known as bribes. Legalizing and regulating the charcoal sector could divert revenue from bribes to government coffers without affecting charcoal prices for consumers [Rights to reprint from original sources pending].



Opportunities, challenges and way forward for the charcoal briquette industry in Sub-Saharan Africa

Tuyeni H. Mwampamba ^{a,*}, Matthew Owen ^b, Maurice Pigaht ^c

^a Centro de Investigaciones en Ecosistemas, Universidad Nacional Autónoma de México, Campus Morelia, Antigua Carretera a Pátzcuaro No. 870, Col. Ex-Hacienda de San José de La Huerta, C.P. 58190, Morelia Michoacán, México

^b Chardust Ltd., P.O. Box 24371, Karen 00502, Nairobi, Kenya

^c MARGE Consulting, Franz-Henle Strasse 9, 65929 Frankfurt, Germany

166

T.H. Mwampamba et al. / Energy for Sustainable Development 17 (2013) 158–170

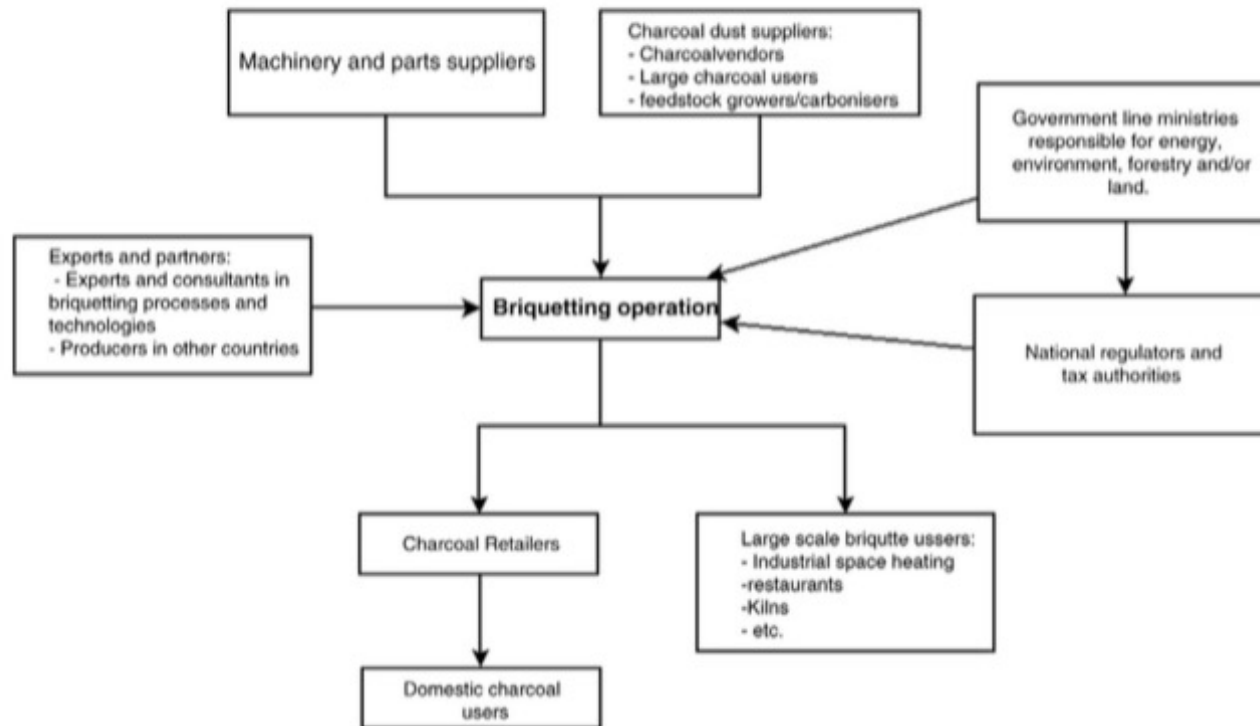
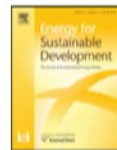


Fig. 3. Stakeholder analysis revealing the central role of the briquetting operation along the briquette value chain. A briquetting operation is influenced by several actors. Through sale of briquettes, however, the briquetting operation ultimately influences briquette retailers and consumers and is highly dependent on the willingness of end-users to accept and incorporate charcoal briquettes into their energy portfolios. Balancing the pressures and requirements of different stakeholders has made briquetting in East Africa a constant juggling of different stakeholder interests.



Cogenerating electricity from charcoaling: A promising new advanced technology[☆]

Rogério Carneiro de Miranda^{a,*}, Rob Bailis^b, Adriana de Oliveira Vilela^c

^a Prolenha, Brazil

^b School of Forestry and Environment, Yale University, USA

^c Rima Industrial, SA, Brazil

172

R.C. de Miranda et al. / Energy for Sustain

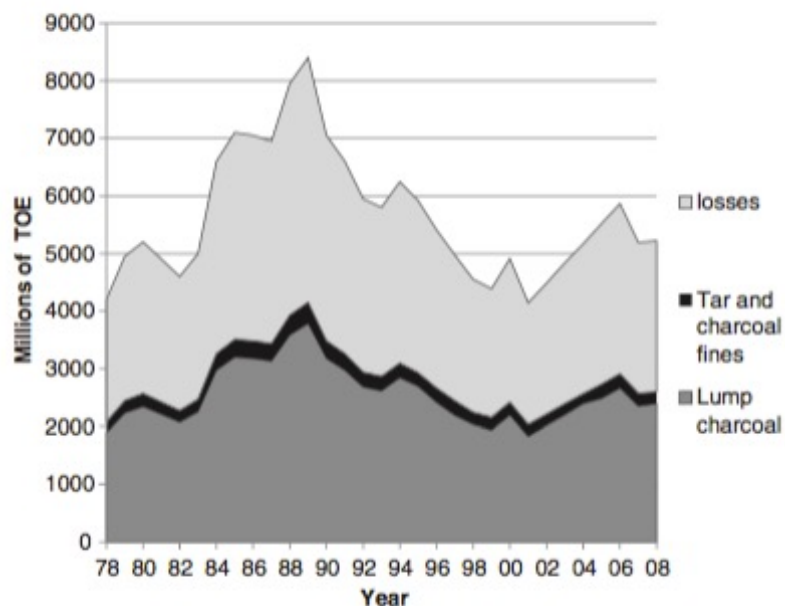


Fig. 1. Total energy breakdown from charcoal production in Minas Gerais, Brazil from 1978 to 2008, as lump charcoal, other sub-products (charcoal fines and tar), and losses (smoke). (Source: BEEMG, 2009).

Table 1

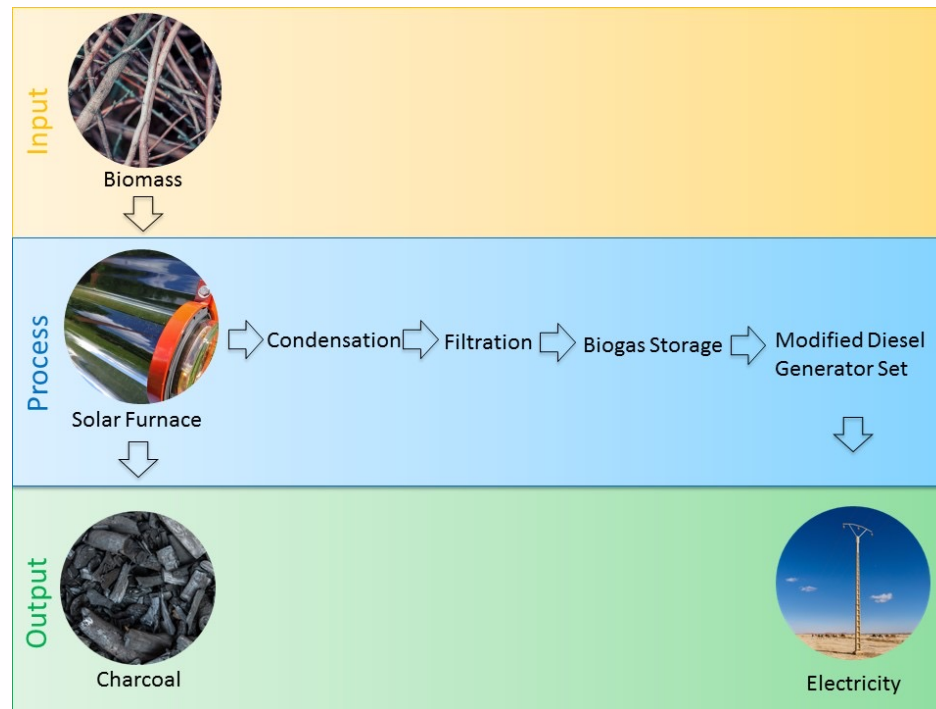
Characteristic temperatures, carbonization and gas content in each phase of wood pyrolysis.

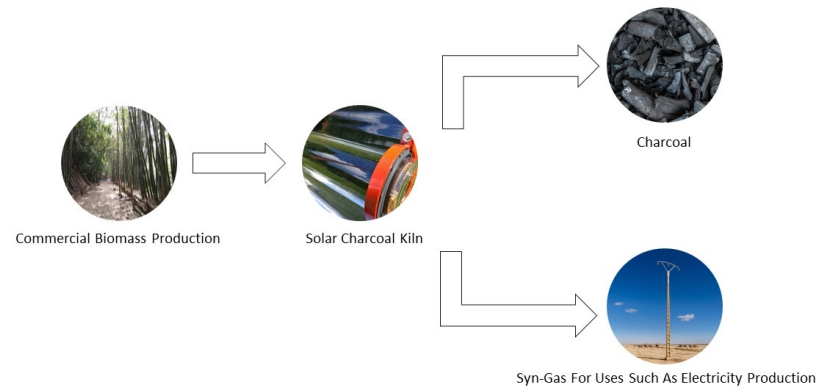
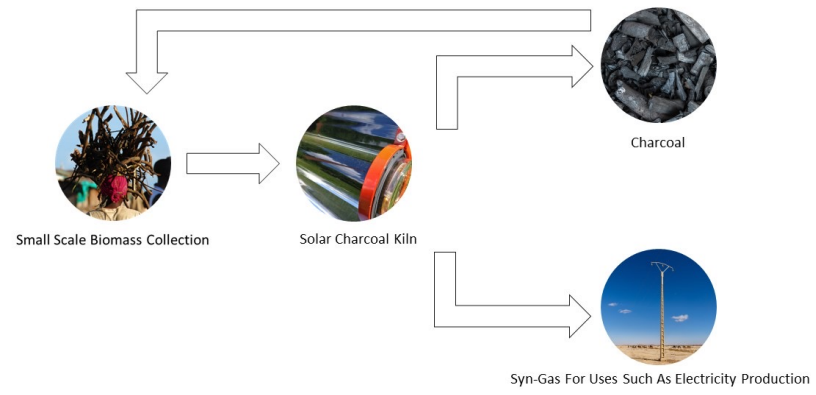
Parameters	Drying	Pre-carbonization	Beginning of tars phase	Tars phase
Process temperature (°C)	150–200	200–280	280–380	380–500
Carbon content of charcoal (%) ^a	60	68	78	84
NCG (%) ^b				
CO ₂	68	66.5	35.5	31.5
CO	30	30	20.5	12.3
H ₂	–	0.2	6.5	7.5
Hydrocarbons (mainly CH ₄)	2	3.3	37.5	48.7
NCG heat value (kcal/Nm ³) ^c	1100	1210	3920	4780

^a (%) percentage based on dry mass of charcoal.

^b (%) percentage based on dry mass of non-condensable gases (NCG).

^c Based on NCG mass balance (Brito and Barrichelo, 1981).





Kinetic Study on Bamboo Pyrolysis

Edward L. K. Mui, W. H. Cheung, Vinci K. C. Lee, and Gordon McKay*

Department of Chemical Engineering, Hong Kong University of Science and Technology, Clear Water Bay, Hong Kong SAR

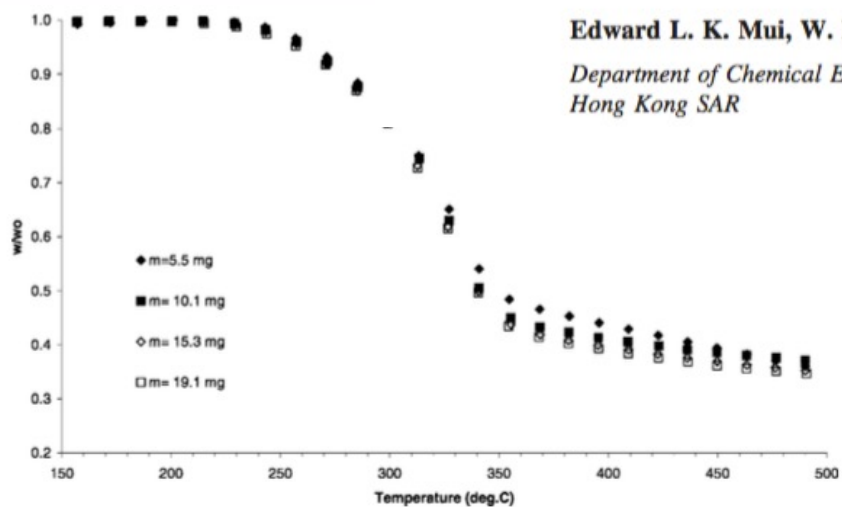


Figure 2. Thermograms of raw bamboo (710–500 μm) with different initial mass pyrolyzed under flowing nitrogen at 5 °C/min.

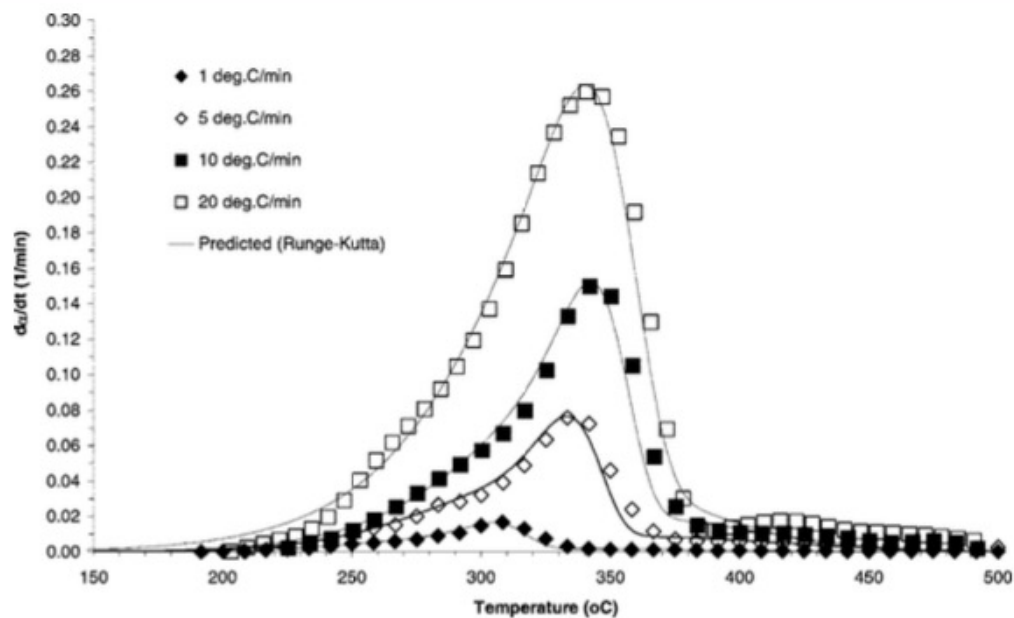


Figure 8. Comparison between experimental data and predicted values (three-component model).

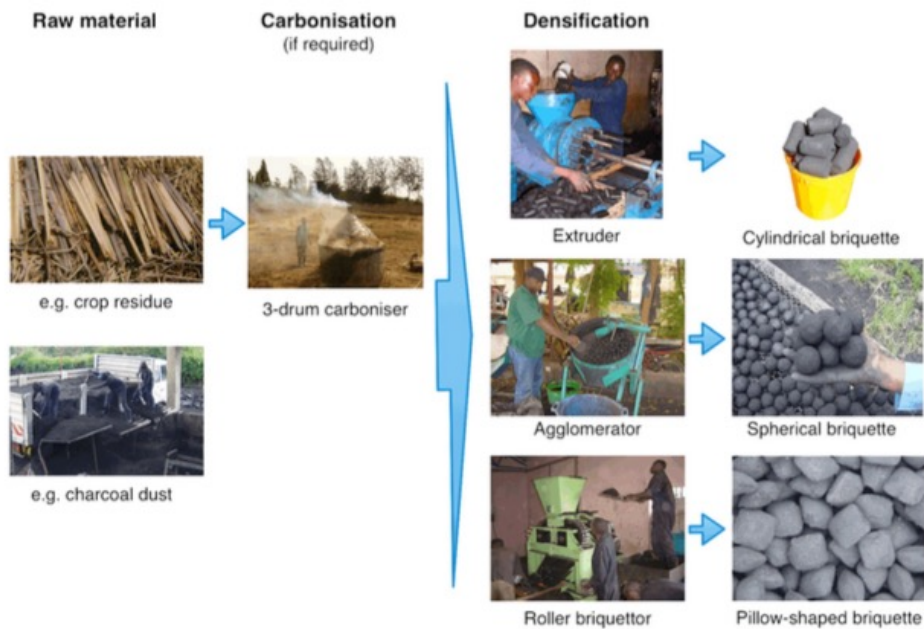


Fig. 2. Schematic diagram of “carbonize-first” briquetting method, in which raw biomass is carbonized (or salvaged in carbonized form) before it undergoes the densification process to form uniformly shaped briquettes.

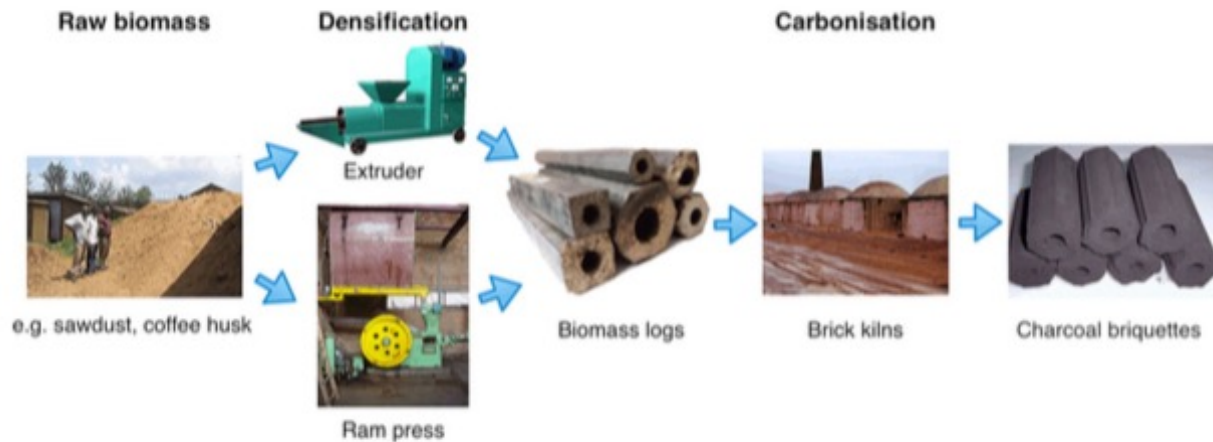


Fig. 1. Schematic diagram of “densify-first” briquetting method, in which raw biomass is densified into uniformly shaped masses before it is carbonized to form charcoal briquettes.

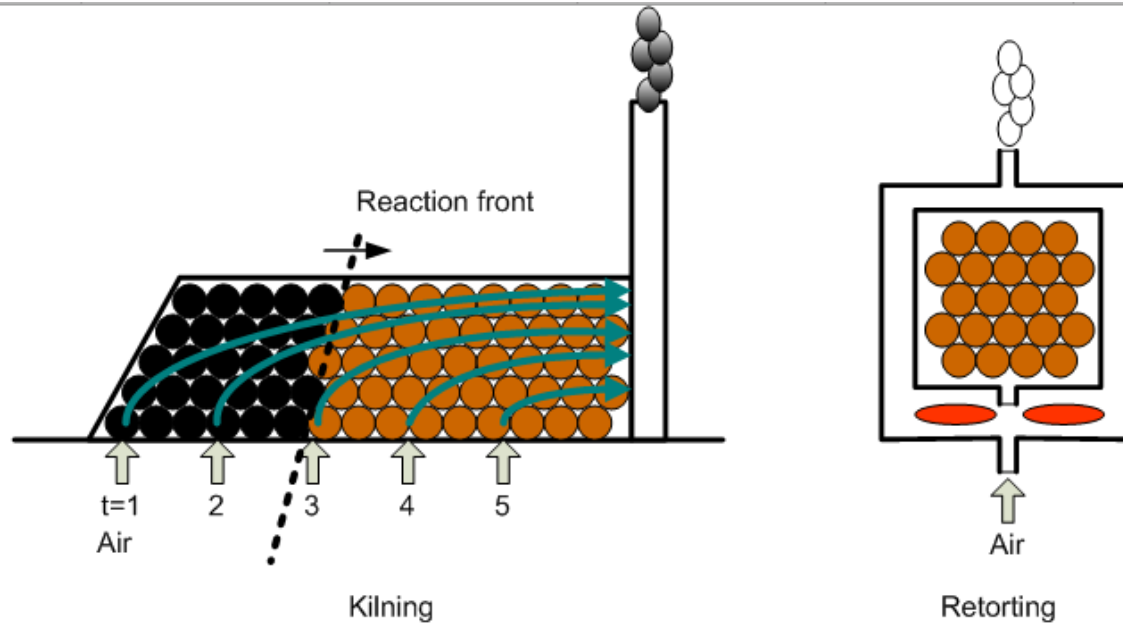
UDSM Charcoal briquette production Dr. Hassan M. Rajabu



Dr Hassan M. Rajabu's briquette equipment UDSM







Kilning: The reaction front moves gradually from one side to the other during interval $1 < t < 5$. Air valves are controlled to provide combustion air at the required place and time. Uncombusted vapour cools down on the heating load. The cooled vapour cannot ignite and gives dirty emissions.

Retorting: Released vapour is combusted to 1/ indirectly provide heat to the load, and 2/ to prevent dirty emissions.

Illustration: © Clean Fuels B.V. www.cleanfuels.nl

<http://www.cleanfuels.nl/Sitepics/Kilning-principle.png>

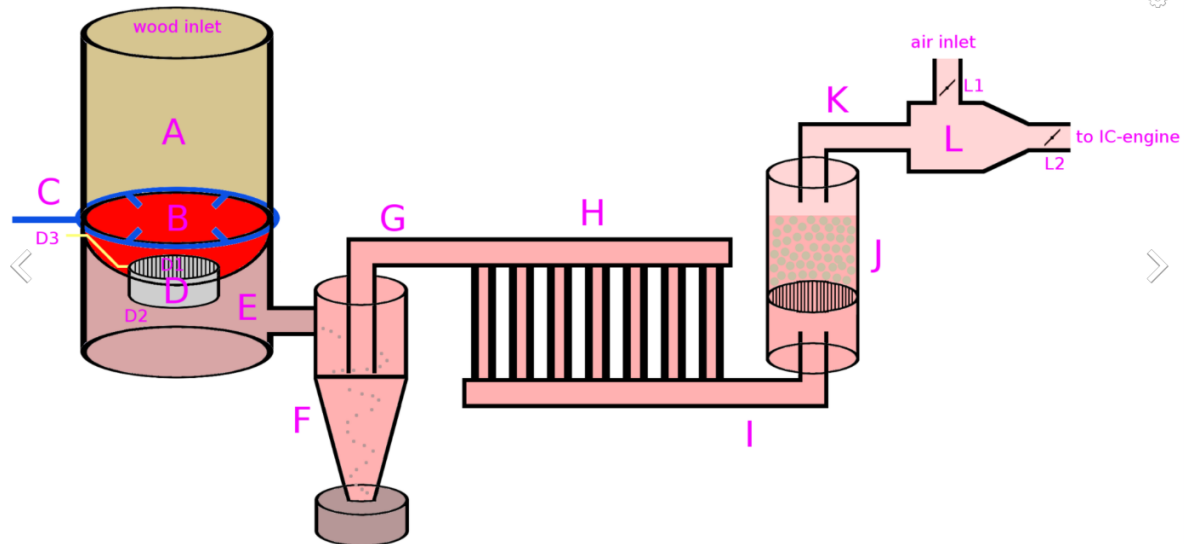
Wood Gas Byproduct

<https://www.youtube.com/watch?v=fBYaP5K0AkE>

A retort kiln using wood gas



Wood gasifier system

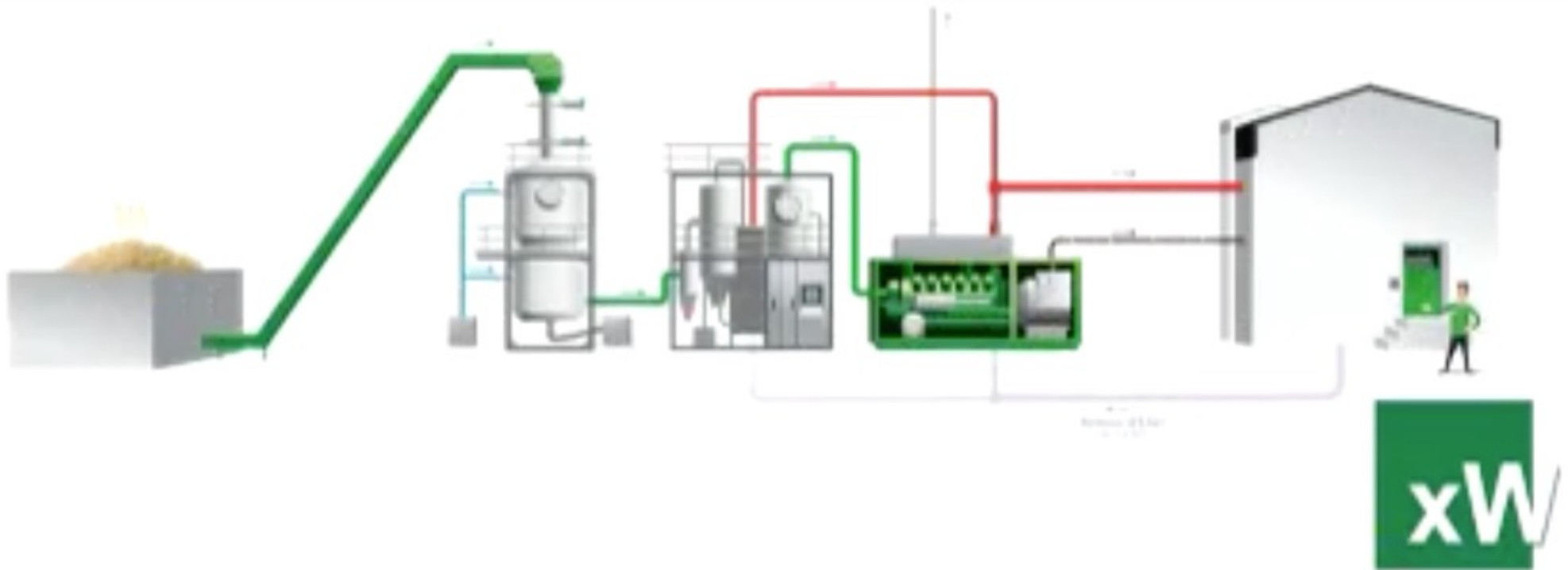


A schematic showing the wood gasifier built by Dick Strawbridge and Jem Stansfield for the show "Planet Mechanics". Parts: A: wood B: fire C: air inlet (air going to 4 nozzles) D: reduction zone; contains charcoal; smoke goes through the accumulated charcoal and reacts with it. H₂O and CO₂ becomes H₂ and CO D1: top grating (movable) D2: lower grating (not movable) D3: handle: used to stir up the wood to provide evenly high temperature over top grating E: smoke F: single-cyclone separator (coarse filter) G: partially filtered smoke H: radiator (reduces heat of gas and hence condenses the gas, making it more flammable/potent) I: cooled, partially filtered smoke J: fine filter (consisting of clay balls on top of a grating) K: wood gas (= fully filtered, cooled smoke) L: air/gas mixer (replaces IC engine carburetor) L1: air inlet valve (operated via handle mounted to gear stick) L2: choke valve

https://en.wikipedia.org/wiki/Wood_gas#/media/File:Planet_Mechanics_wood_gasifier.png

Biomass/Syngas/Wood Gas

Moderate Scale Plant (http://www.dailymotion.com/video/xit4aj_xyLOWatt-biomass-gasification-renewable-syngas_tech)



Home > A charcoal production plant that also generates heat and electricity from the by-product gas

A charcoal production plant that also generates heat and electricity from the by-product gas

Author: Heggie

Post date: Saturday, November 8, 2008 - 8:02am

Tom Miles

[Log in to post comments](#)

[A charcoal production plant that also generates heat and electricity from the by-product gas](#)

Biofuel Energy Susters, Sustainable Energy Ltd., UK, 2004



In 2004 Biofuel Energy Systems Ltd. developed a plant for charcoal production, which uses the gases given off during production to drive a gas turbine, generating heat and electricity. The electricity generated can be used on site (especially useful in remote areas with no electrical grid connection) or sold back to the grid for additional profit.

Conventional charcoal production is very inefficient and wastes half of the energy within the wood. Biofuel Energy Systems' unique plant, however, uses 90% of the wood's energy and uses a totally clean, emission-free process. See the diagram on the Biofuel Energy Systems website that shows the steps involved in simplified terms. This represents a huge advancement in the efficiency and cleanliness of charcoal production.

<https://terrapreta.bioenergylists.org/biofuelenergysystems>

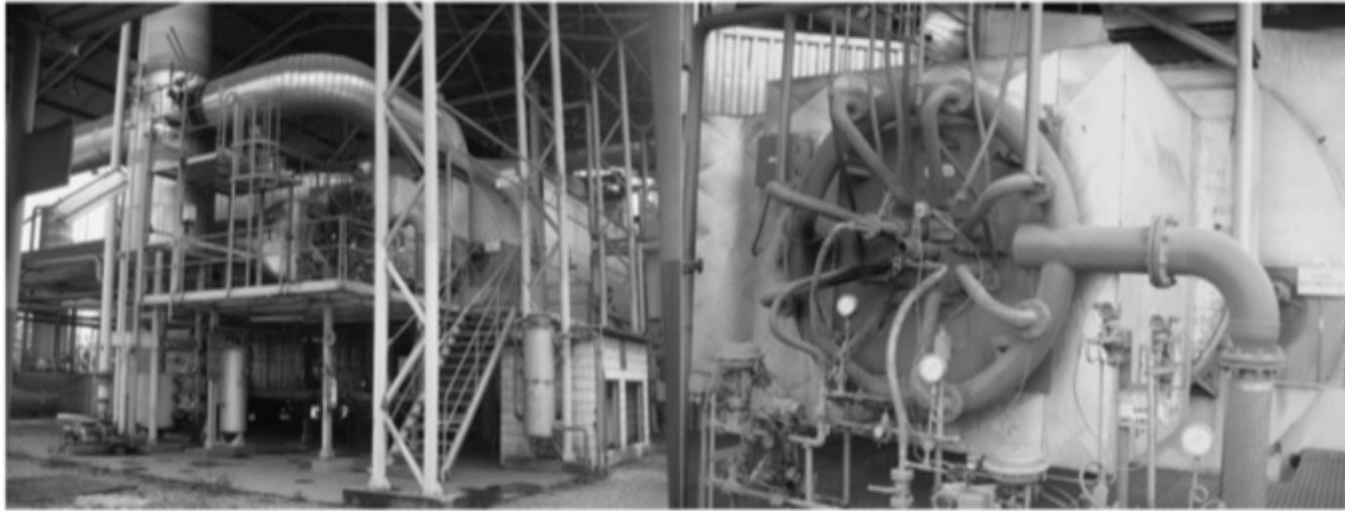


Fig. 2. View of the Barreiro power plant boiler (left photo) and detail view of the fuel feeding system in the boiler (right photo), with the central hole (open tube) used for wood tar injection, and the main round tube used for steel furnace gas injection.

2009 the Minas Gerais state power utility (CEMIG)² operated a 15 MW power plant designed to use tar as complementary fuel to hot exhaust gases from steel furnaces (Fig. 2). The plant used tar at the rate of 500 kg per hour. It required a tar filter and a heater to reduce the viscosity of the tar before it was injected under pressure inside the boiler. However after 2009 CEMIG stopped using tar because the supplier found a more lucrative market (Miranda, 2012).

Brazil

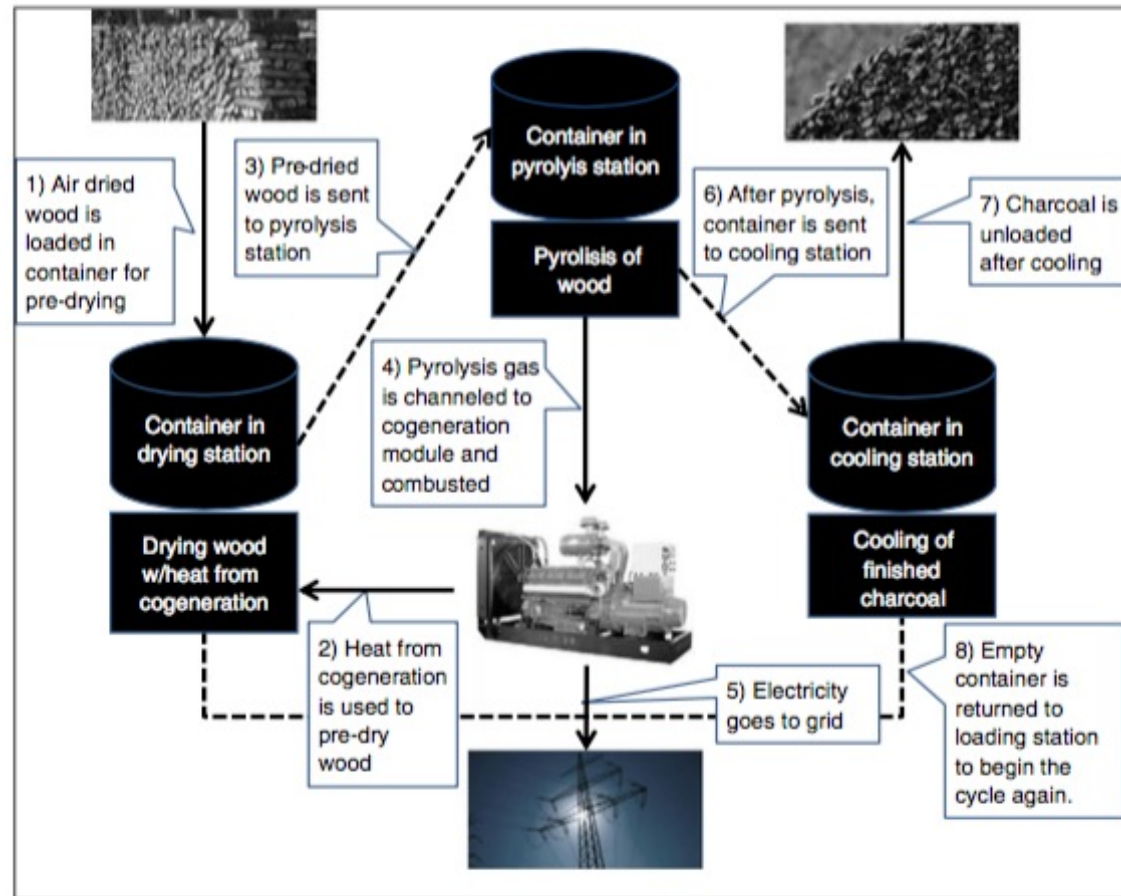


Fig. 3. An example of a charcoal cogeneration cycle utilizing waste heat for pre-drying.

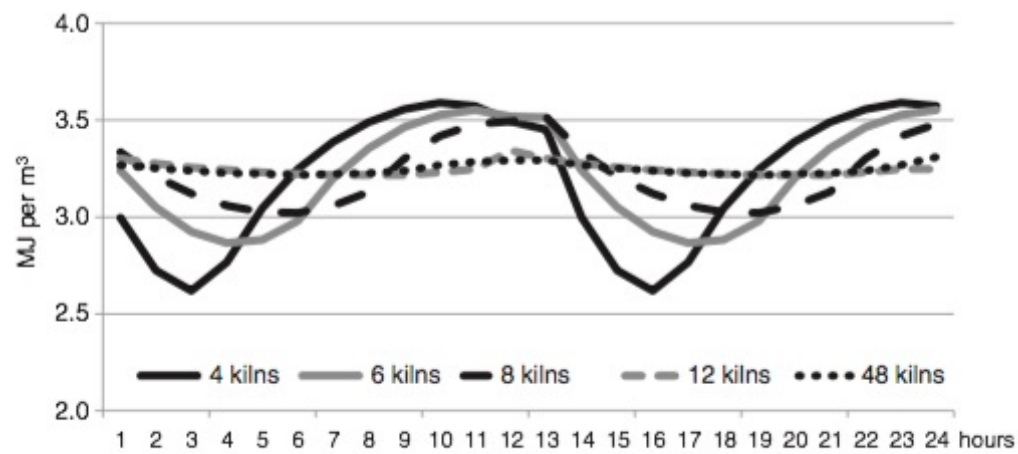


Fig. 4. Variation in calorific value of pyrolysis gas with variation of number of kilns in series (Vilela, 2010).



Fig. 5. Biochar plant in Denmark, with 35 KWe cogeneration capacity, powered by Stirling engine.

Solar Cooking

<http://solarfire.org/GoSol>

Bakers and Peanut Butter Producers Using our Tech in Kenya

In partnership with the NGO World Vision Finland and World Vision Kenya, GoSol has started a pilot project in the Western part of Kenya during Spring 2016. Through World Vision's Weconomy collaboration, GoSol has initiated and supported building of solar concentrators by local artisans using only available materials in Kisumu region, near lake Victoria. A local bakery has been able to reduce operating costs and can now produce and sell more baked goods to local schools and students. A peanut butter workshop in Karemo produces organic peanut butter with renewable energy. They have replaced the use of charcoal with solar thermal energy, which reduces cost and improves the taste of the end product.





Figure 6-1 A solar cooker being used in the developing world. Image courtesy Tom Sponheim.

Project 11: Build a Solar Cooker

You will need

- Sheet of thin MDF
- Sheet of flexible mirror plastic
- Sheet of thin polystyrene
- Veneer panel pins

Tools

- Bandsaw
- Pin hammer
- Sharp knife/scalpel
- Angle marking gauge

This solar cooker is a very simple project to construct—we will be harnessing the sun's energy from a relatively wide area and concentrating it to a smaller area using mirrors (read more in Chapter 8 about this). The area which we will concentrate it into will be lined with polystyrene to keep in the heat.

Construct a box for your cooker out of MDF. I find small veneer pins to be very useful as they can be hammered neatly into the end grain of thin MDF without splitting the wood. For this application they are perfectly strong enough. When you have finished the box it should look something like Figure 6-6.

Now you need to line the box with polystyrene, this will prevent the heat from escaping. The lined box will look like Figure 6-7.

Now measure the size of the cube inside the lined polystyrene box. You should cut the mirror plastic to this size, and further line the box with it. Duck Tape is more than ideal for making good all of the joints and securing things into place.

We now need to cut the mirrored reflectors. Cut a strip of mirror plastic about two feet wide on the bandsaw. Now, using an angle marking gauge, mark from the long side of the mirror to the very corner of the mirror, a line which makes an angle of 67° , forming a right-angled triangle in the scrap piece of plastic. You now need to mark out a series of trapeziums along this length of mirror, where

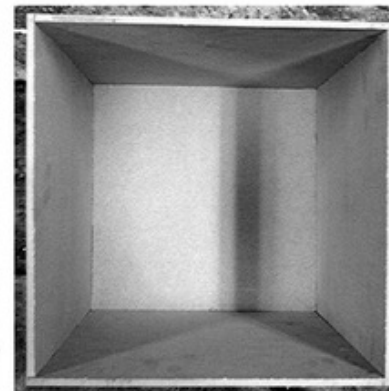


Figure 6-6 The box constructed from MDF.



Figure 6-7 The box lined with polystyrene.

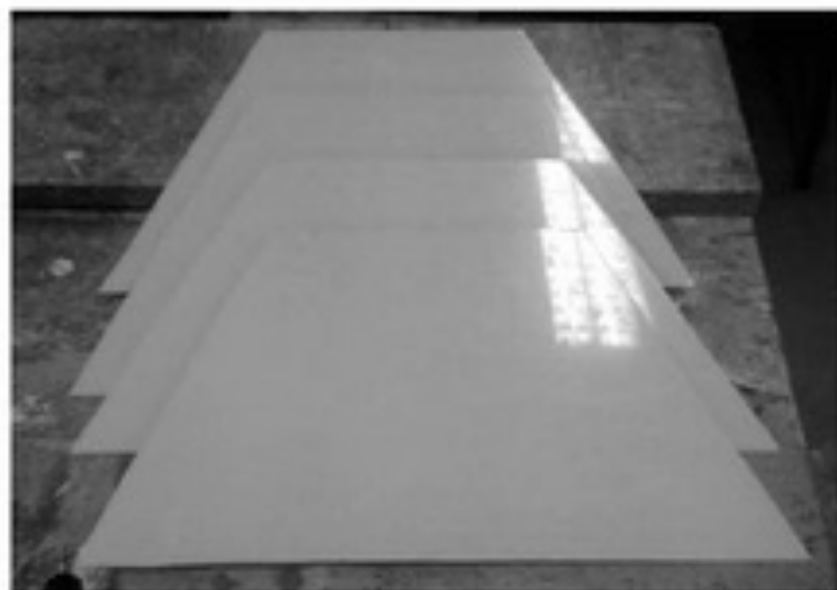


Figure 6-8 *The mirrored reflectors cut ready.*

the shortest side is equal to the length of the inside of the box cooker (Figure 6-8).

Now take the mirrored reflectors, and on the nonreflective side, use Duck Tape to join them together to form the reflector which will sit on the top. Using Duck Tape allows you to make flexible hinges, which allow the reflector to be folded and stored out of the way.



Figure 6-9 *The solar cooker ready and complete.*

When the cooker is finished it will look like Figure 6-9. It is now ready for cooking!

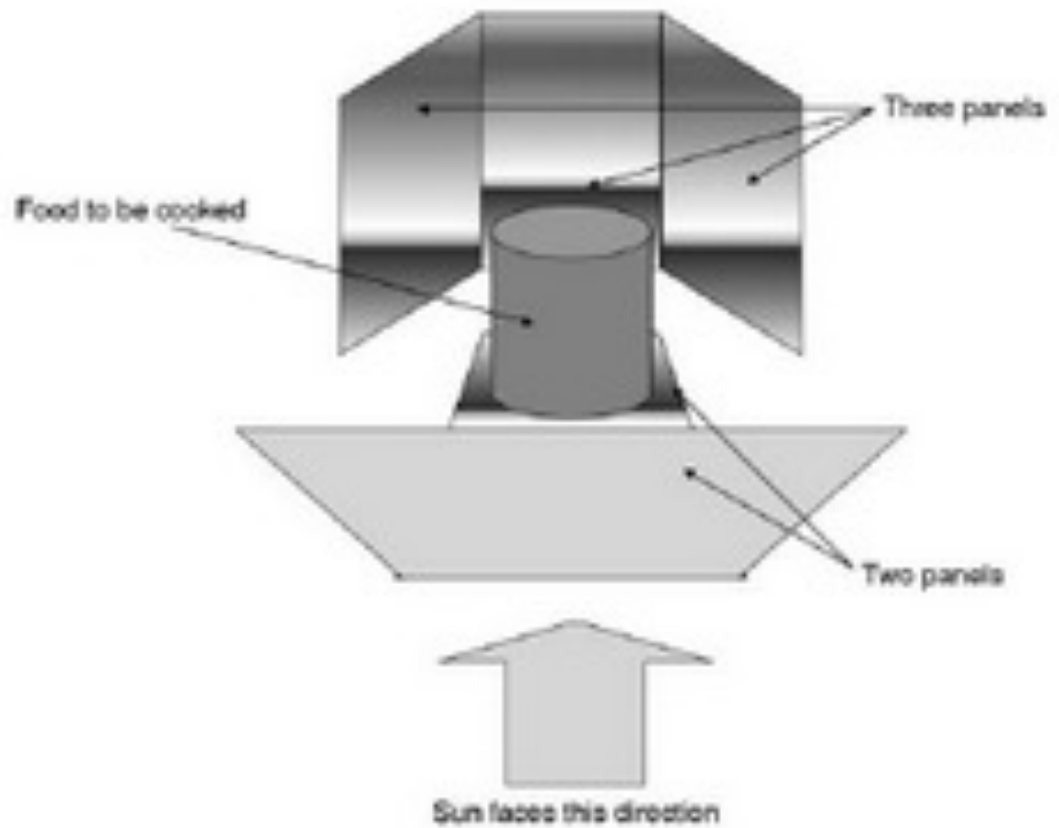


Figure 6-10 *The set-up solar stove.*


Indian Solar Cooker
<https://www.youtube.com/watch?v=AI8Dab6BluY>

Solar Cookers International (<http://video.nationalgeographic.com/video/environment/energy-environment/solar-cooking/>)



Advanced Energy Systems

ADVANCED ENERGY SYSTEMS L.L.C. Home Hybrid Solar Ovens Accessories Why The Soelov? More ▾



WE HAVE EVOLVED - JOIN THE EVOLUTION
PORTABLE COOKER

AES Has Eliminated The Limitations of Traditional Solar Cooking

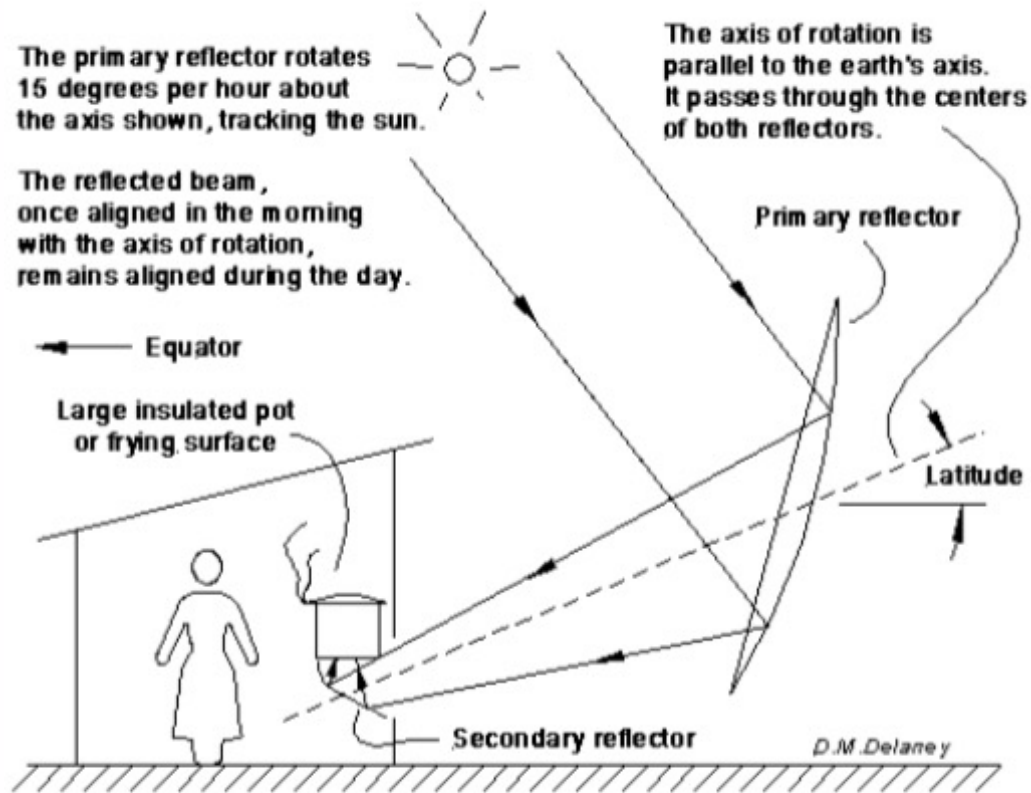
Designing and building a simple solar oven is easy.
But when the goal is to cook 24-7-365 anytime, anywhere, turn to AES for the answer!

BIG TIME COOKING IN A SMALL PACKAGE - SOELOV 100



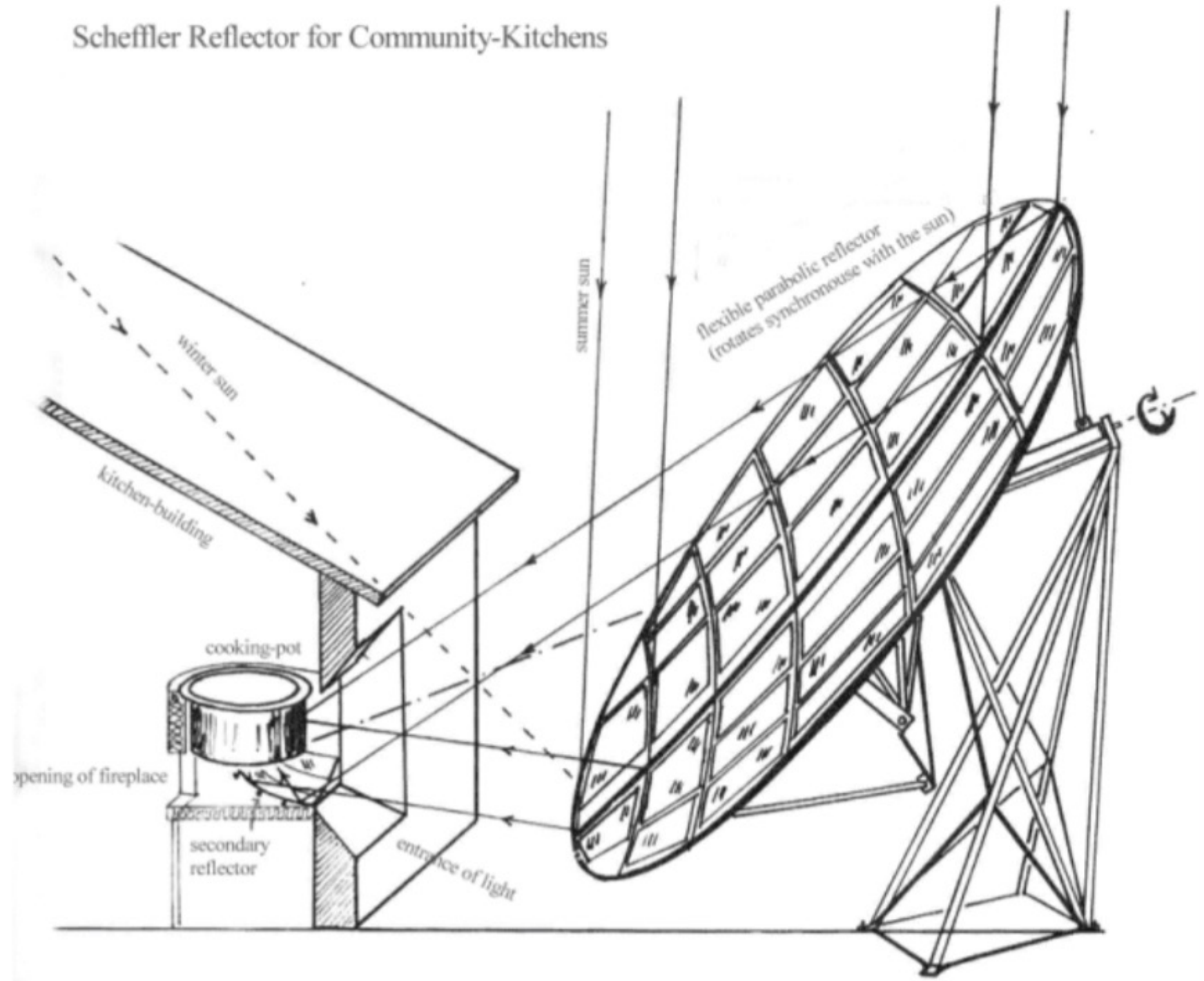


Figure 4: "Rose Bud" Solar Cooker



How a Scheffler reflector used for cooking keeps its focus on the cooking place as the sun moves.

Scheffler Reflector for Community-Kitchens





for [18]

Figure V.i.4 Scheffeler solar
community collector [19]

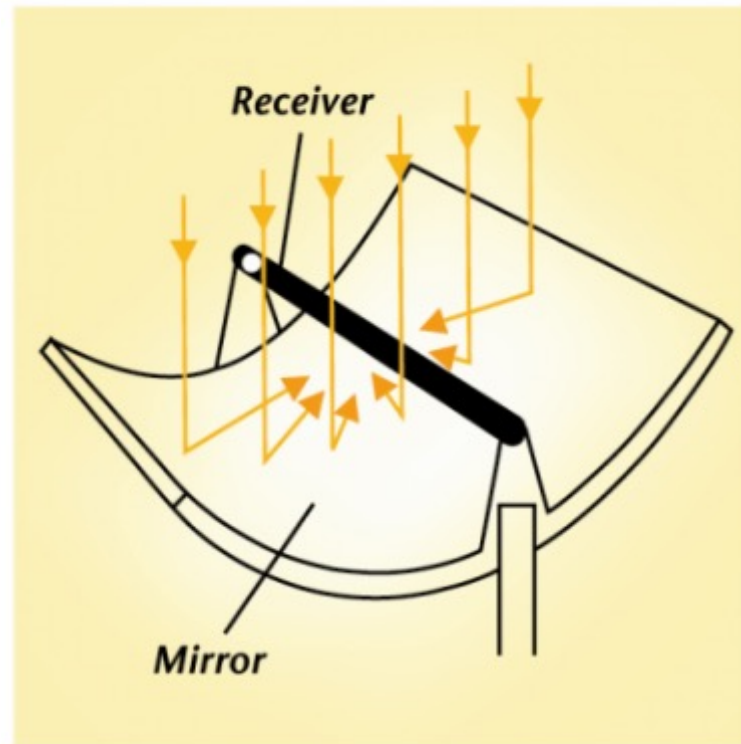


Figure 5: Parabolic Trough Design Overview



Figure V.iv.2: Berkley's Blazing Tube solar collector

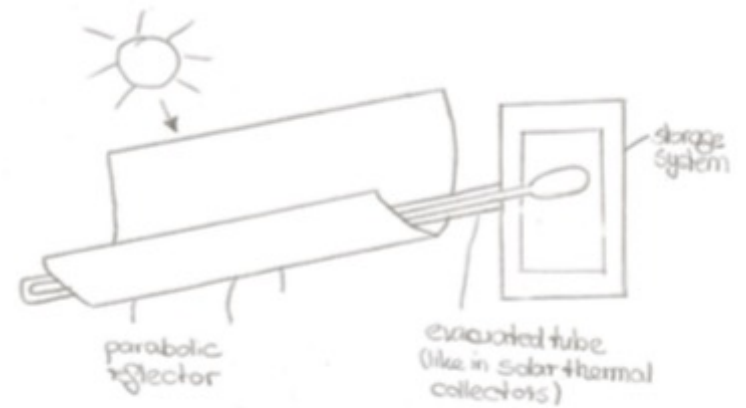


Fig. 2.1: Heat pipe collection system.

To Cook at Night

- Large collection area focused to an insulated heat storage material
1500 W-hr/day delivered to food

- Heat storage materials: NaCl; Bricks; Ceramic tiles; Silicon oil; Water; Sand;
Combinations of heat storage and heat transfer materials

- Insulation

- Ideally you would cook indoors, collect heat outdoors

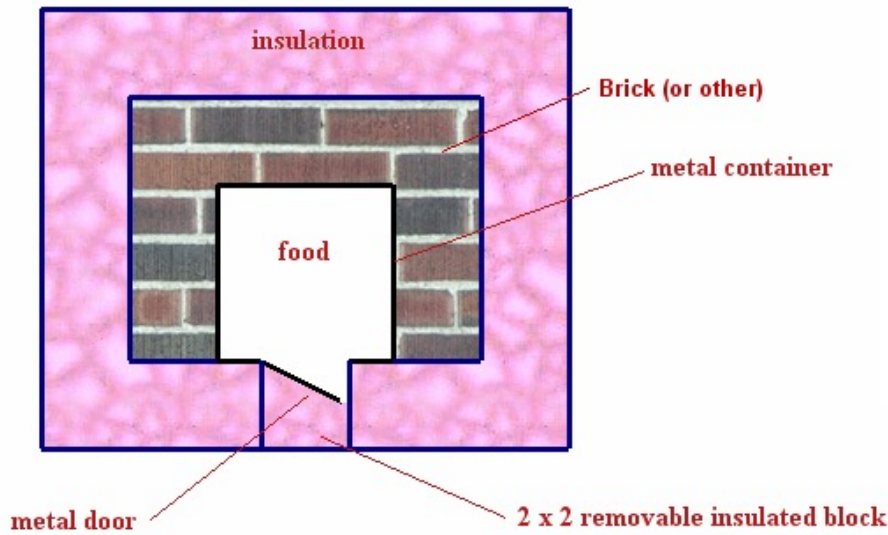
- Ideally the heat supplied to food would be adjustable

<http://www.webplaces.org/solaroven/design.htm>

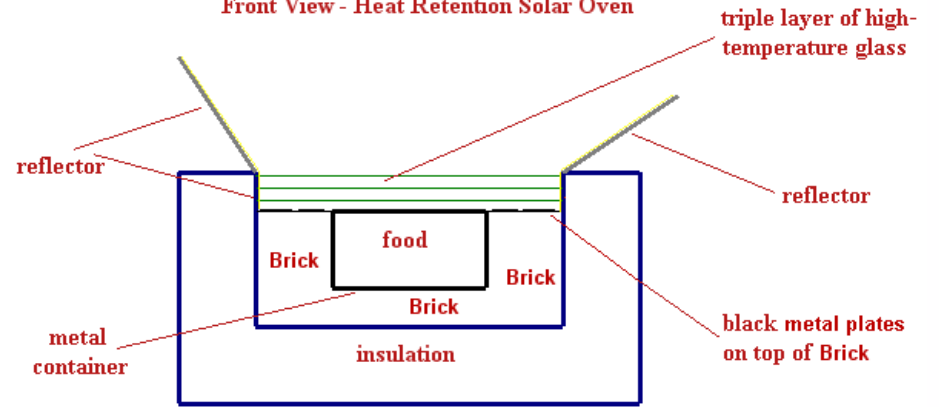
To Cook at Night

<http://www.webplaces.org/solaroven/design.htm>

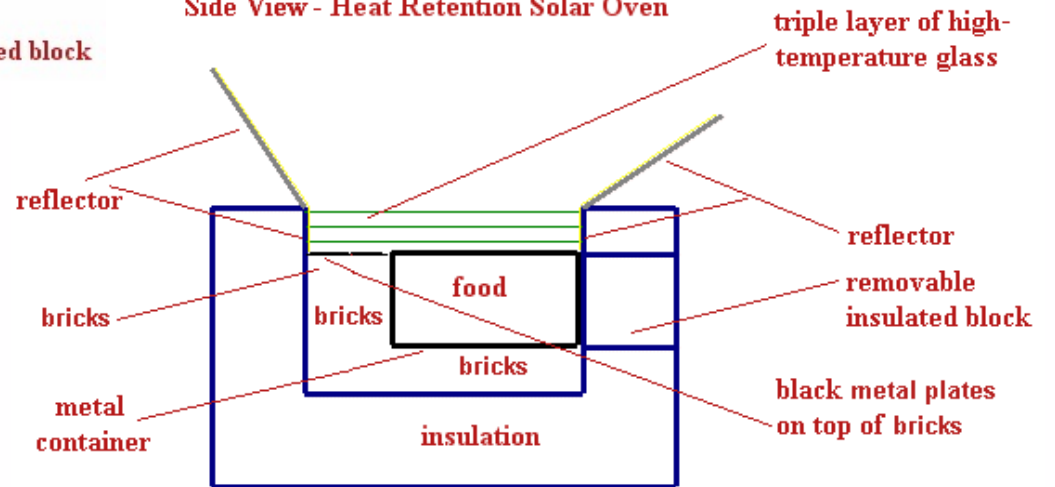
Top View - Heat Retention Solar Oven



Front View - Heat Retention Solar Oven



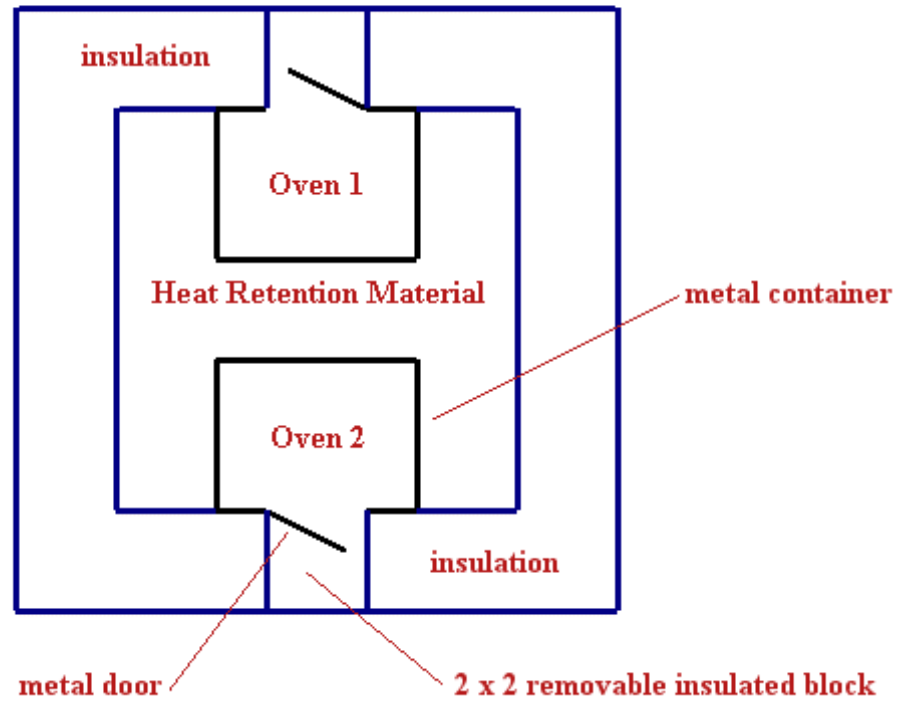
Side View - Heat Retention Solar Oven



To Cook at Night

<http://www.webplaces.org/solaroven/design.htm>

Top View - Heat Retention Solar Oven



To Cook at Night

<http://www.webplaces.org/solaroven/design.htm>

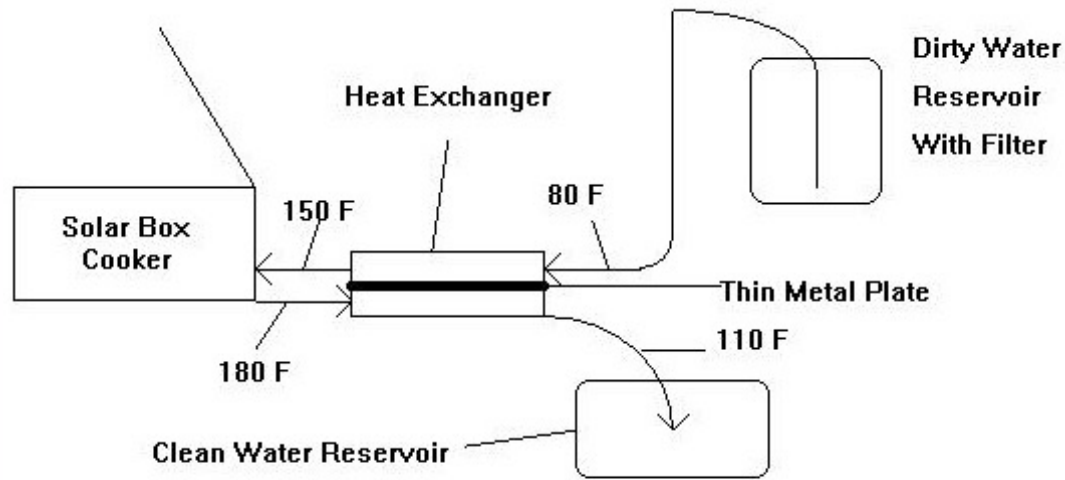


Figure 3: PAX -style water pasteurizer with heat exchanger. Typical temperatures are shown in degrees Fahrenheit.

To Cook at Night

<http://www.webplaces.org/solaroven/design.htm>

New Solar Stove Is Capable of Cooking at Night

Joshua Krause
Ready Nutrition
0 Comments



If there's one technology preppers love, it's solar panels. They're an essential piece of equipment if you're planning on living off the grid, and they're getting cheaper and more efficient every year. But while they're an excellent choice for running lights and electronics, they tend to fall short when it comes to heating (especially cooking).

That's because solar panels only convert roughly 15% of the sun's energy into electricity, and there are additional losses when that electricity is converted back into heat. Heating

always requires way more energy than electronics, so that means you're either going to need more solar panels, or find an additional source of energy.

<https://www.engineeringforchange.org/10-solar-cookers-that-work-at-night/>

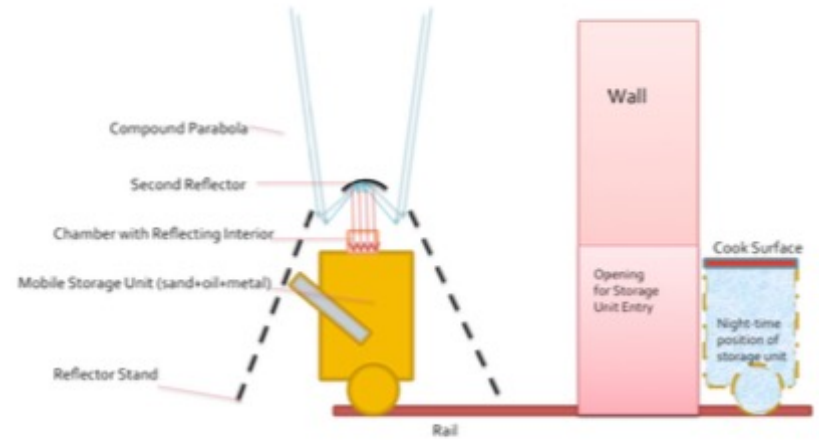
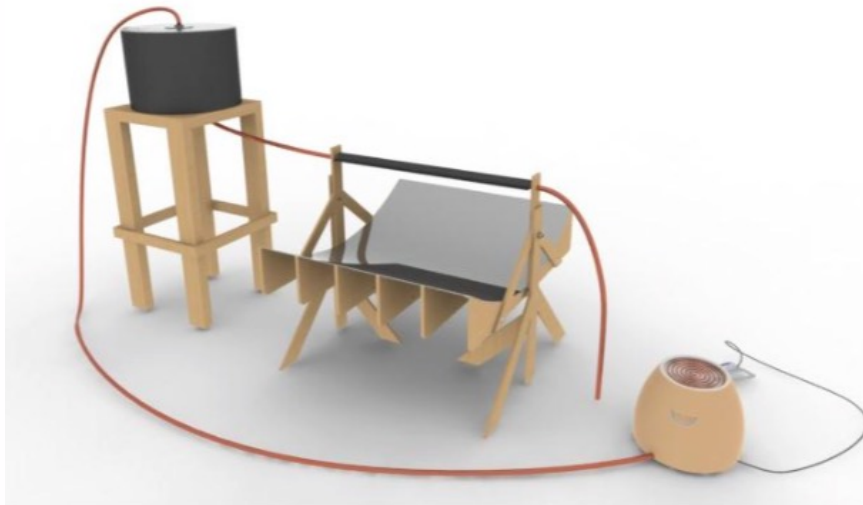


Figure V.iv.3: Iowa Design Side View

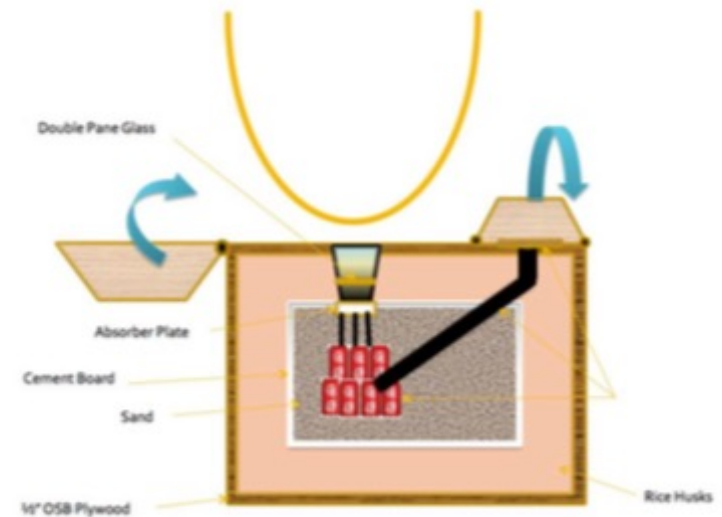
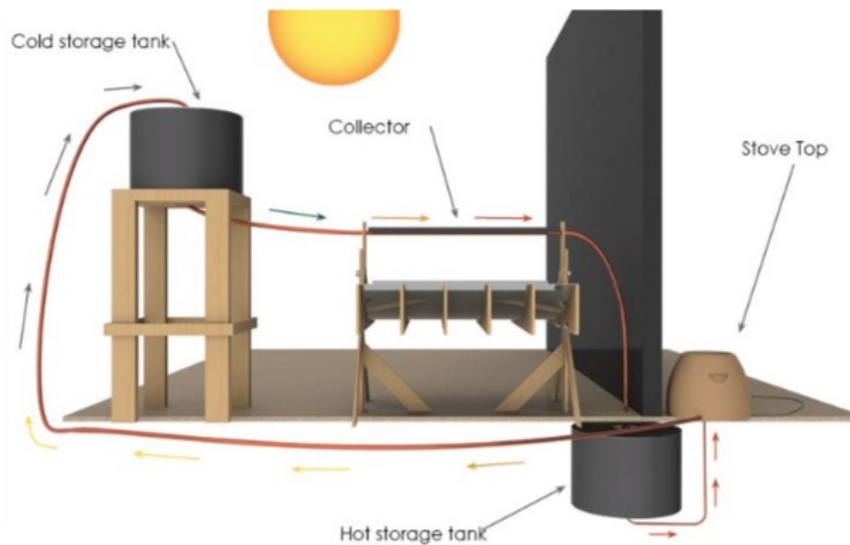


Figure V.iv.4: Iowa Design Interior View[31]

https://www.engineeringforchange.org/wp-content/uploads/2015/10/sol_r_final_report.pdf

https://www.engineeringforchange.org/wp-content/uploads/2015/10/medp_final_report_2011.pdf



The iHawk Cooker prototype. Photo courtesy of H. S. Udaykumar

Heat transfer fluid is air
Heat storage material is Sand
Large parabolic collector
Also uses metal heat transfer plate

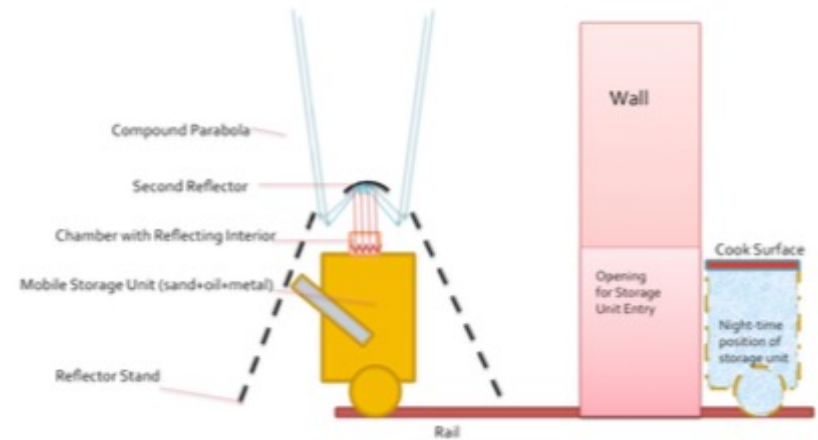


Figure V.iv.3: Iowa Design Side View

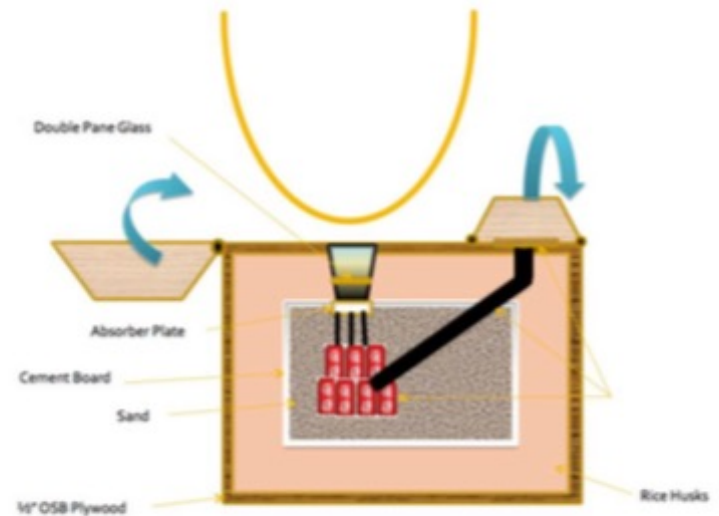


Figure V.iv.4: Iowa Design Interior View[31]

https://www.engineeringforchange.org/wp-content/uploads/2015/10/medp_final_report_2011.pdf

Transfer to cook indoors by wheels



The iHawk Cooker prototype. Photo courtesy of H. S. Udaykumar

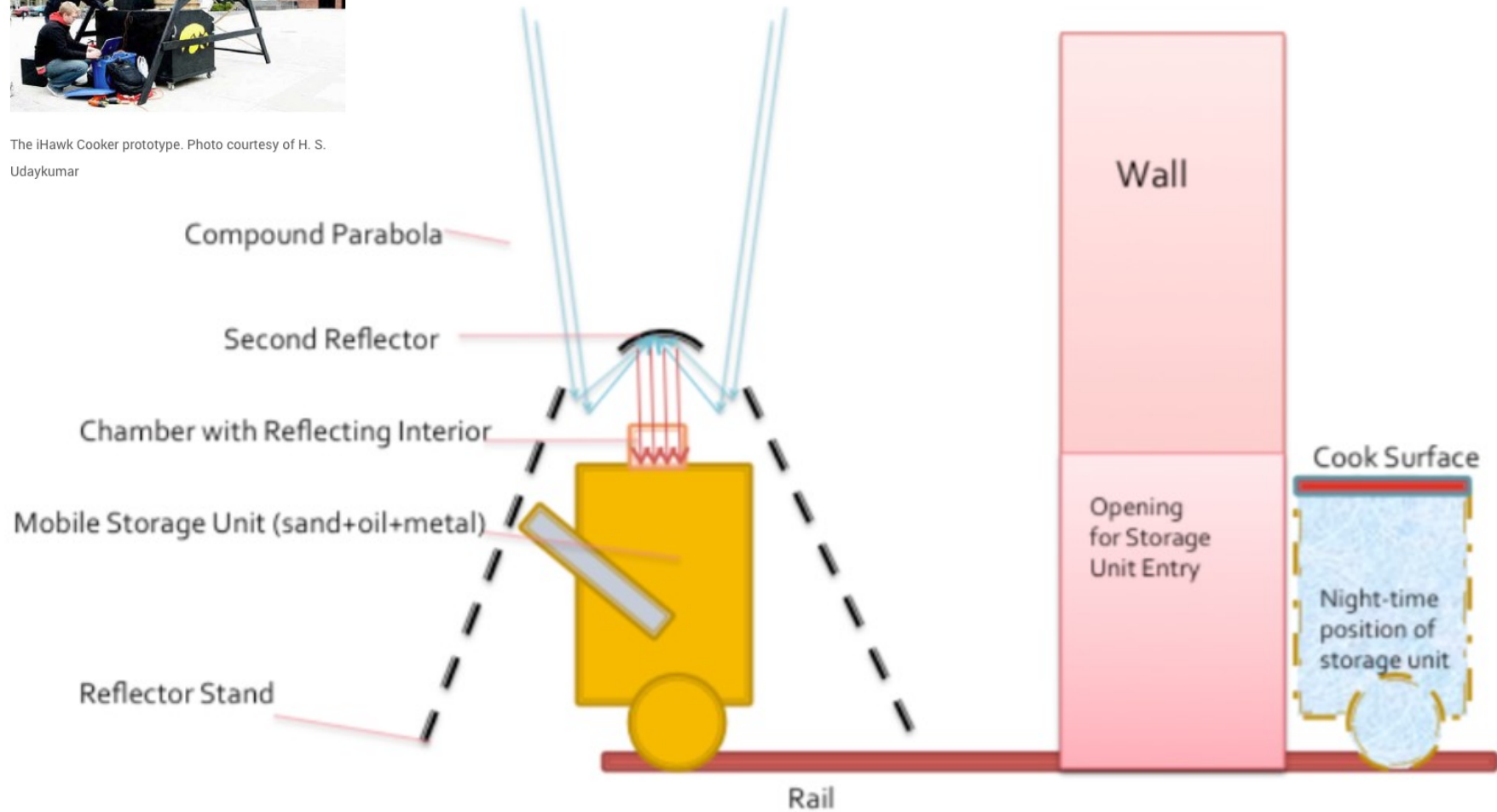


Figure 7: Side View Preliminary Design Overview

https://www.engineeringforchange.org/wp-content/uploads/2015/10/medp_final_report_2011.pdf



The iHawk Cooker prototype. Photo courtesy of H. S. Udaykumar

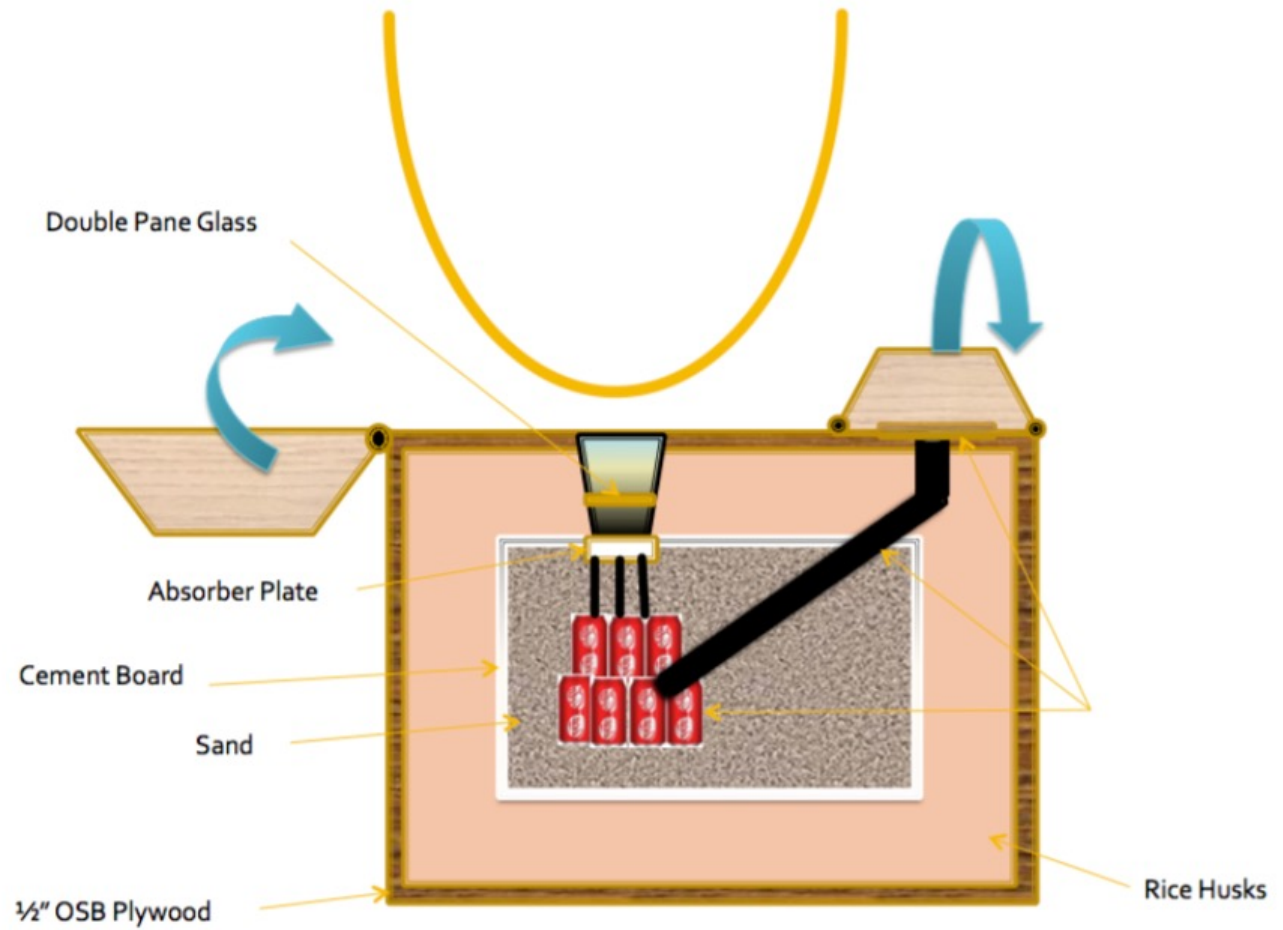


Figure 8: Preliminary Design Interior Overview

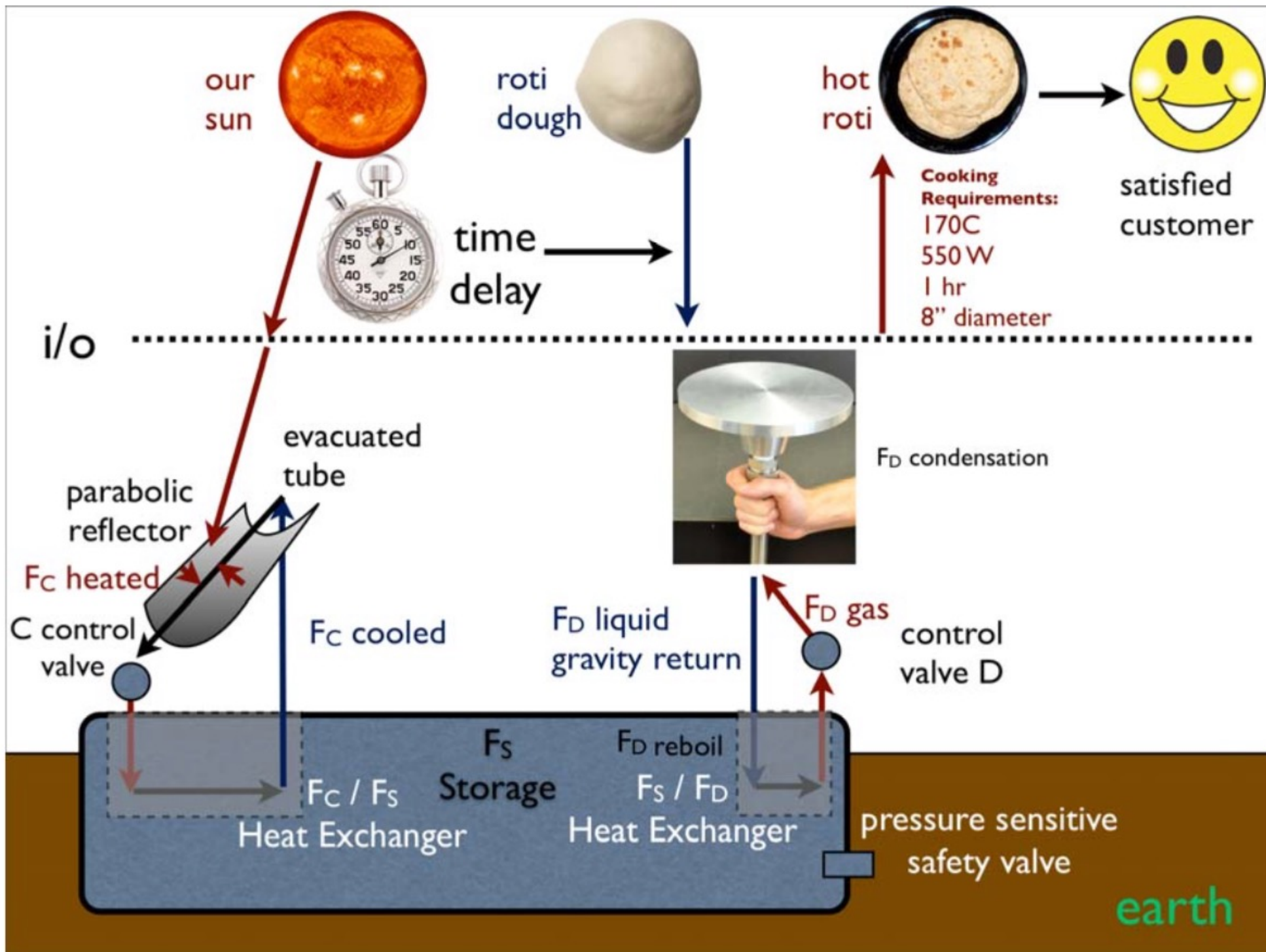
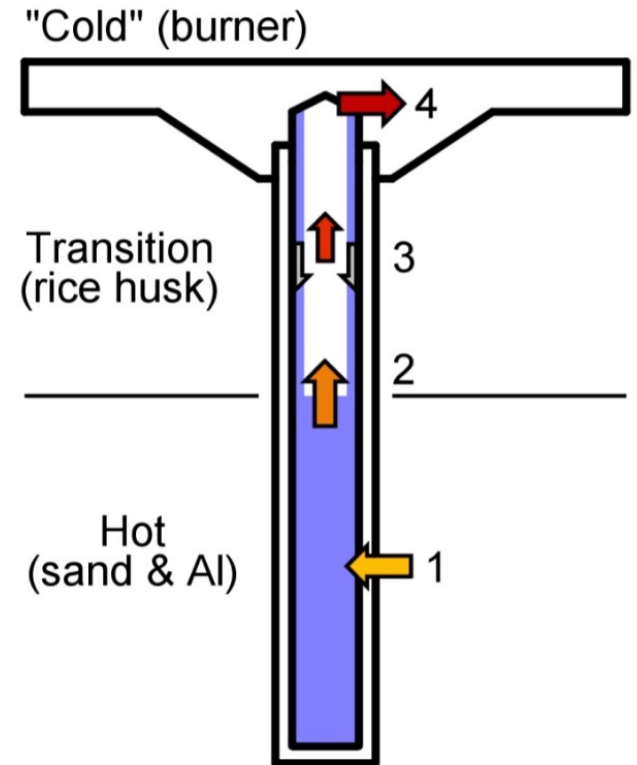
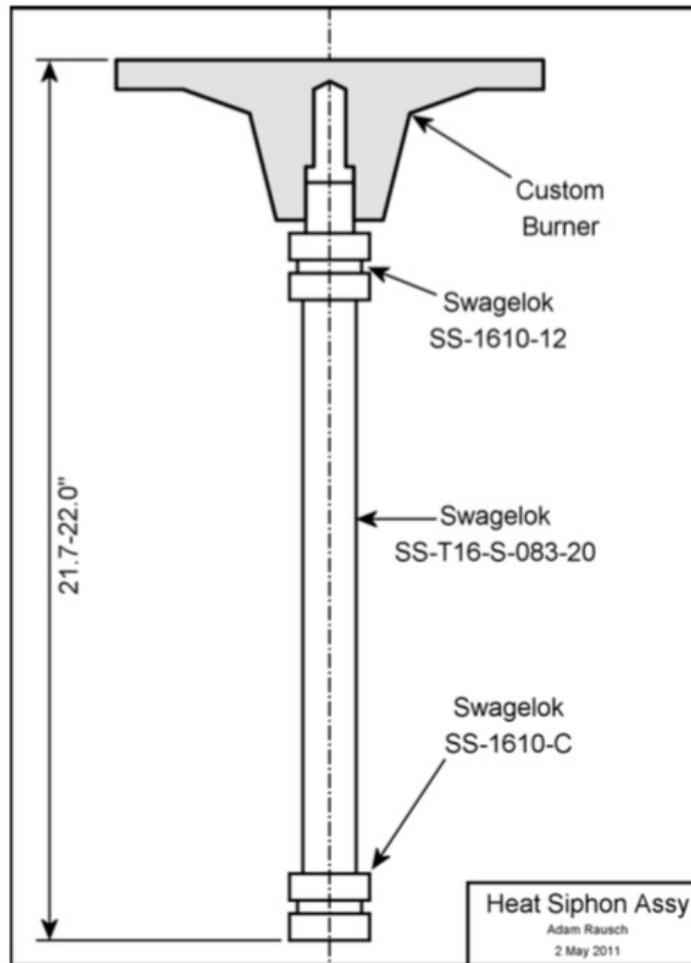


Figure 6.3. All-Fluid Design.

Appendix D: Design drawings and prototype images



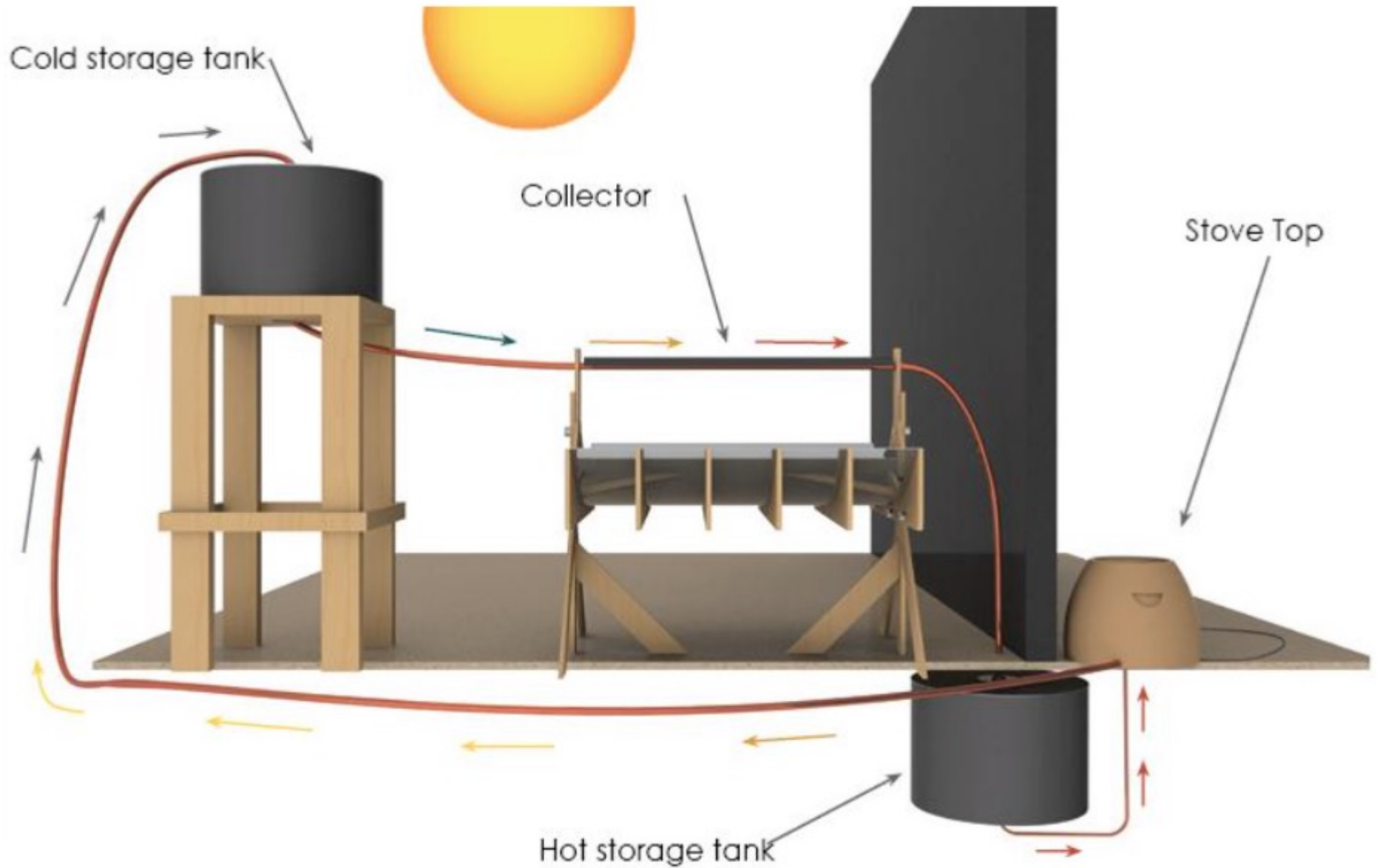


Figure VII.1. Depiction of the entire system

User Interface



Figure VII.iii.1 Schematic of heat output subsystem

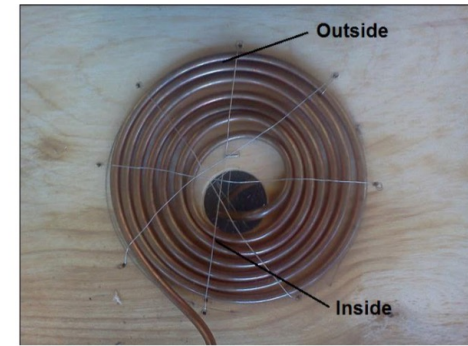


Figure VII.iii.4 Thermometer placement inside and outside of the coil.

Figure VII.iii.3 Heat dissipation coil experiment setup.

Table VII.iii.1 Heat dissipation experimental results

Fluid	Flow Rate (cm ³ /s)	Fluid Inlet Temperature (°C)	Coil Steady State Maximum Temperature (°C)	Coil Steady State Minimum Temperature (°C)
Water	11.6	99.3	93.3	92.8
Olive Oil	6.9	204	187	158
Olive Oil	8.85	204	186	163
Olive Oil	10.4	204	195.6	156

Table IX.I.1: Reflective Material Comparison

Material	Reflectivity [55], [56]	Price	Advantages	Disadvantages
Polished Anodized Aluminum	95.00%	\$75/m ²	Highly reflective for the price, lightweight. Durable and easily shaped.	Easily scratched.
Mylar	>98%	\$1.66/m ² [57]	Highly reflective, light, cheap	Not good at standing up to the elements, forms 'bubbles' if glue starts to give, requires a rigid backing
Aluminum Foil	88%	\$0.34/m ² [58]	Cheap and widely available	Not so reflective, corrodes when mixed with acidic juices, structurally weak
Can lids	70-80% (estimate)	Price of canned food	Common material and very cheap	Not very reflective, non-uniform shape is labor intensive to shape and use
Acrylic Mirror	99%	\$67.81/m ² [59]	Very reflective (nearly 100%), nearly unbreakable	Comes in plane, very difficult to fit to parabola as a sheet. More expensive than most but long lifespan
Glass Mirror	99%	\$122.0/m ² [60]	Very reflective	Expensive and comes in rigid plane, breakable and heavy
Astro-foil	76%	\$6.63/m ² [61]	Strong and Reliable	Not reflective Enough

Table IX.I.2: Piping Material Comparison

Piping	Material	Thermal Conductivity, k (W/mK) [63, 64]	Melting Point
Steel	Carbon Steel	54	1425-1540°C [65]
Copper	Copper	401	1084°C [65]
PEX	Cross-linked High-Density polyethylene	0.51	130°C [66]
CPVC	Chlorinated Polyvinyl Chloride	0.14	175°C[67]
PE	Polyethylene	0.38	110°C [66]
PVC	Polyvinyl Chloride	0.19	180°C [66]

Table IX.iii.1: Breakdown of origin of materials of the Solar system.

Material/Component	Here/There?	Tools Needed (In Rajasthan)
Cold and Hot storage Tanks With Fittings	Built and sent from India	Shovel and wood for cold storage tank stand
Collector Shape	Cut and sent from India	None
Reflector: Mylar and Acrylic	Cut and sent from India	For application: Need polystyrene for collector surface, epoxy for application of Mylar and Acrylic panels
Solar collector stand	There	Saw & nails/screws
Piping for system	Piping in India	Expected to be Cut and soldered there. Portable Soldering iron will be sent.
Stovetop and Oven	Piping in India. Clay found there	Clay stoves can be built there individually, copper tubing to be installed by someone else.
Installation and Maintenance	There	Tools and Education provided for team of villagers on an Installation and maintenance crew.

Table IX.iii.2: Material cost breakdown of the entire system

Item	Description	Unit Cost (\$)	Qty.	Total Cost (\$)	Here/There	References
UN-Compliant Steel Pail (Open Pail + Lid)	Cold and Hot storage tanks	\$13.69	2	\$27.38	Here	[68]
Copper 90° Tube Fitting	Tube fitting for installation	\$1.12	5	\$5.60	Here	[22]
Anderson Fittings 4213591 5/16Comp X1/4 Comp Union	Compression Fittings on Tanks	\$3.00	2	\$6.00	Here	[69]
World 27-3/4G 3/4 Galv Malibl Floor Flange	Pipe fitting (Flange) on Tanks	\$2.00	2	\$4.00	Here	[70]
Owens Corning R-6.7 Unfaced 2 in. x 16 in. x 48 in. Multi Purpose Continuous Roll Insulation	Insulation for collector olive oil heating pipe	\$3.94	2	\$7.88	Here	[71]
Plywood				\$0.00	There	
Olive Oil (13 gallons)	Energy Storage Material	\$20.40	13	\$265.20	There	[72]
Cooper Tools Cordless Soldering Iron, Battery-Powered	Soldering Iron for tube fittings	\$19.99	1	\$19.99	There	[73]
Solder-Joint Copper Tube Fitting for Water, Union, Socket (Female) X Socket (Female) for 3/4" Tube Size	Unions for ease of installation and maintenance	\$5.52	3.00	\$16.56	There	[70]
Mylar Sheeting (1.2m ²)	Reflective backing of solar collector	\$1.66	1.2	\$1.99	Here	[74]
Mirrored Acrylic (1.2m ²)	Reflective Strips for solar collector	\$67.81	1.2	\$81.37	Here	[75]
Copper Pipe (Est)	Piping system for olive oil	\$1.70	12	\$20.40	There	[70]
Permatex High-Temperature RTV Silicone Gasket Maker, 3-Ounce Tube	Sealant Silicone used on Storage Tanks (high temp)	\$6.41	2	\$12.82	Here	[76]
Heavy Duty Metal Drum Pump Zinc-Plated STL, 22 oz/Stroke, 35-1/4" L Intake Tube	Stovetop and storage tank pump	\$29.51	1	\$29.51	Here	[77]
020" Thick High Impact Styrene Sheet 40" X 72"	Styrene Sheet	\$3.39	1	\$3.39	Here	[78]
Clay	Stove Base Material	0		\$0.00	There	
Total				\$502.09		

[Go Sun Stove](http://www.kickstarter.com/projects/707808908/gosun-stove-portable-high-efficiency-solar-cooker) (<http://www.kickstarter.com/projects/707808908/gosun-stove-portable-high-efficiency-solar-cooker>)



[Go Sun Fusion](#)

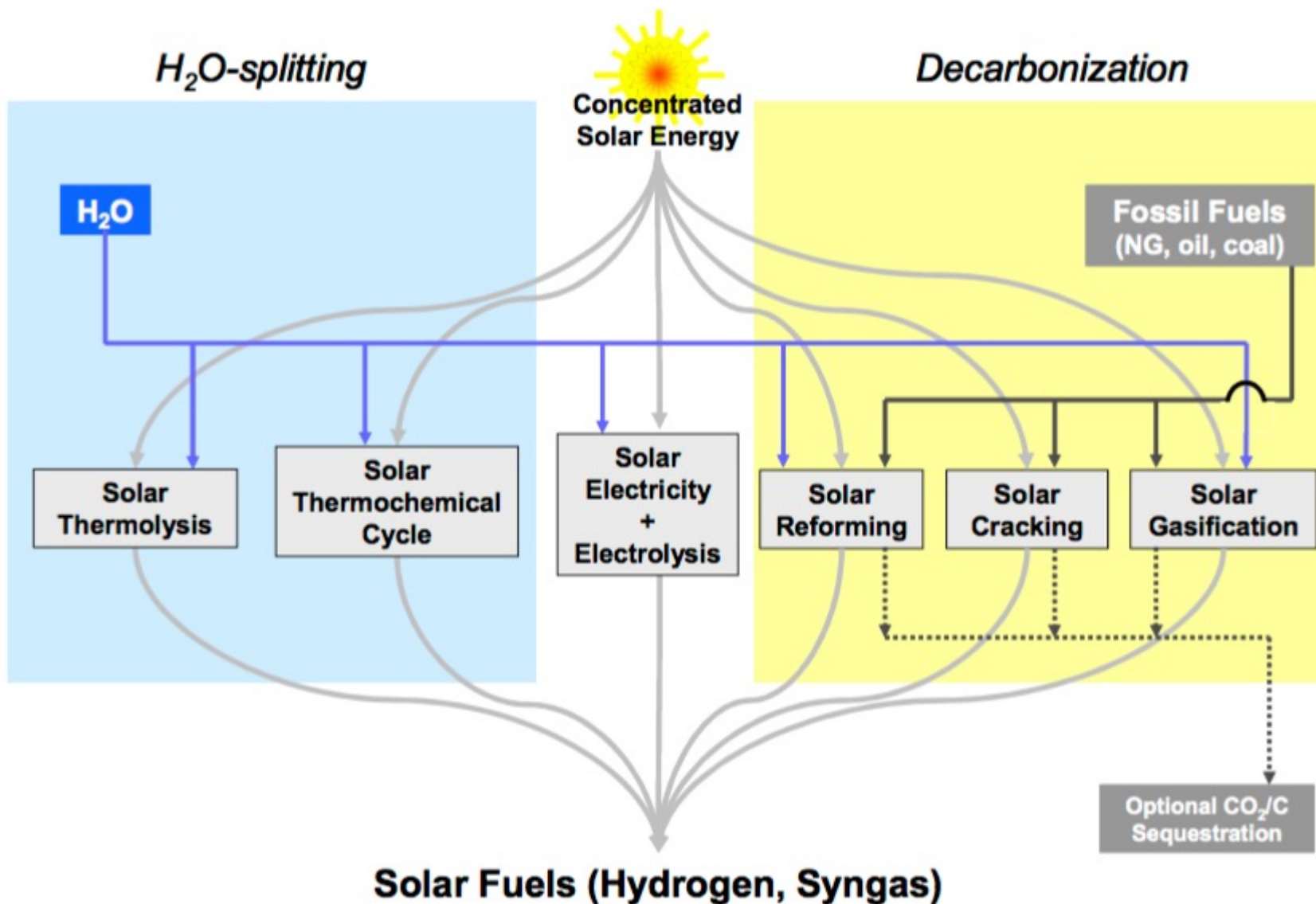
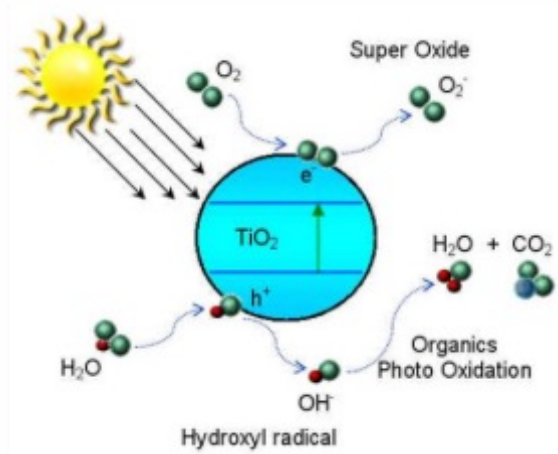


Fig. 2: Thermochemical routes for solar hydrogen production – Indicated is the chemical source of H₂: H₂O for the solar thermolysis and the solar thermochemical cycles; fossil fuels for the solar cracking, and a combination of fossil fuels and H₂O for the solar reforming and gasification. For the solar decarbonization processes, optional CO₂/C sequestration is considered. All of those routes involve energy consuming (endothermic) reactions that make use of concentrated solar radiation as the energy source of high-temperature process heat. Adapted from [1,2].²⁵⁴

Photocatalysis



Titania as a photocatalyst

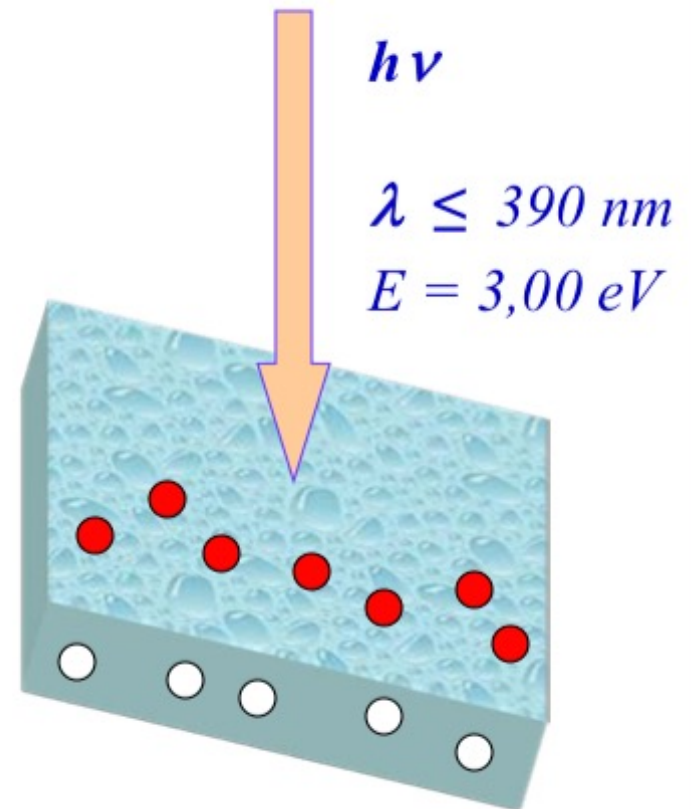
- Irradiation of semiconductors having a band gap (2 - 4 eV) with UV light energy \geq energy of the band gap E_g*
- Generation of charge carriers*



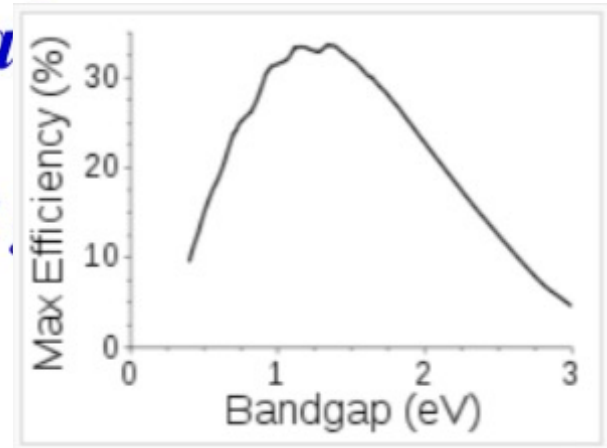
- Formation of active radicals (OH^* , O_2^*)*



- Recombination process*



Titania as a photocatalyst



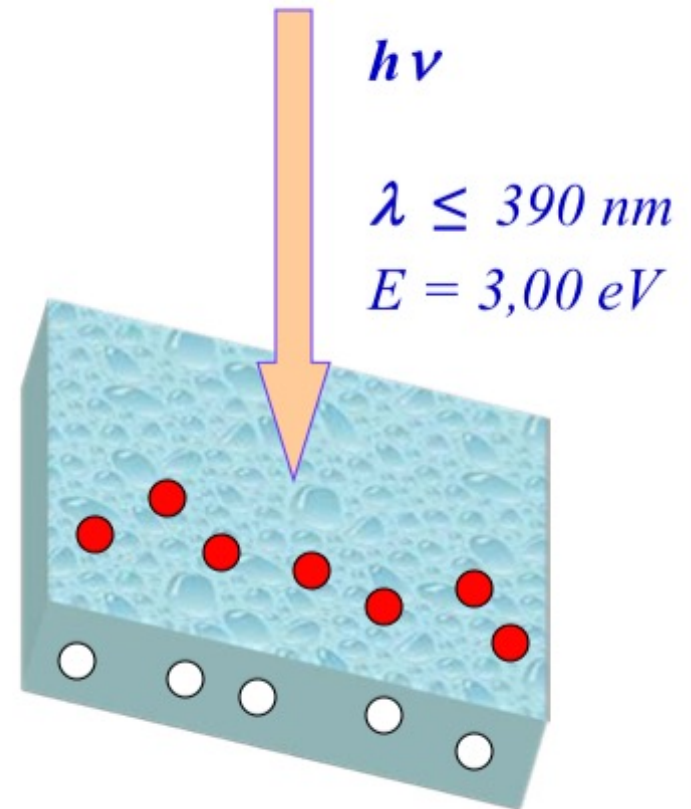
- Irradiation of semiconductors having a band light energy \geq energy of the band gap E_g*
- Generation of charge carriers*



- Formation of active radicals (OH^* , O_2^*)*



- Recombination process*



Water is decomposed using only light

≠

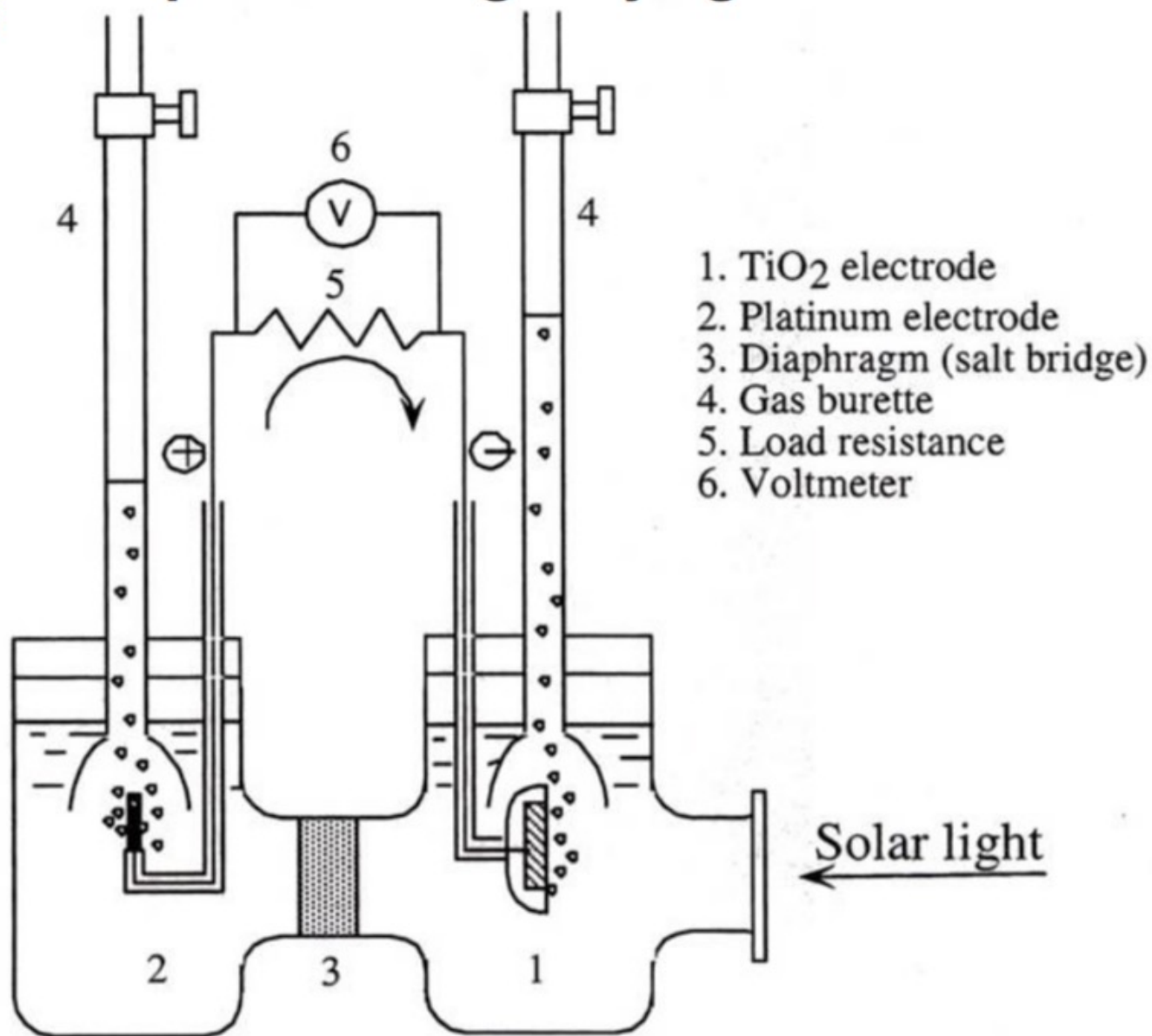
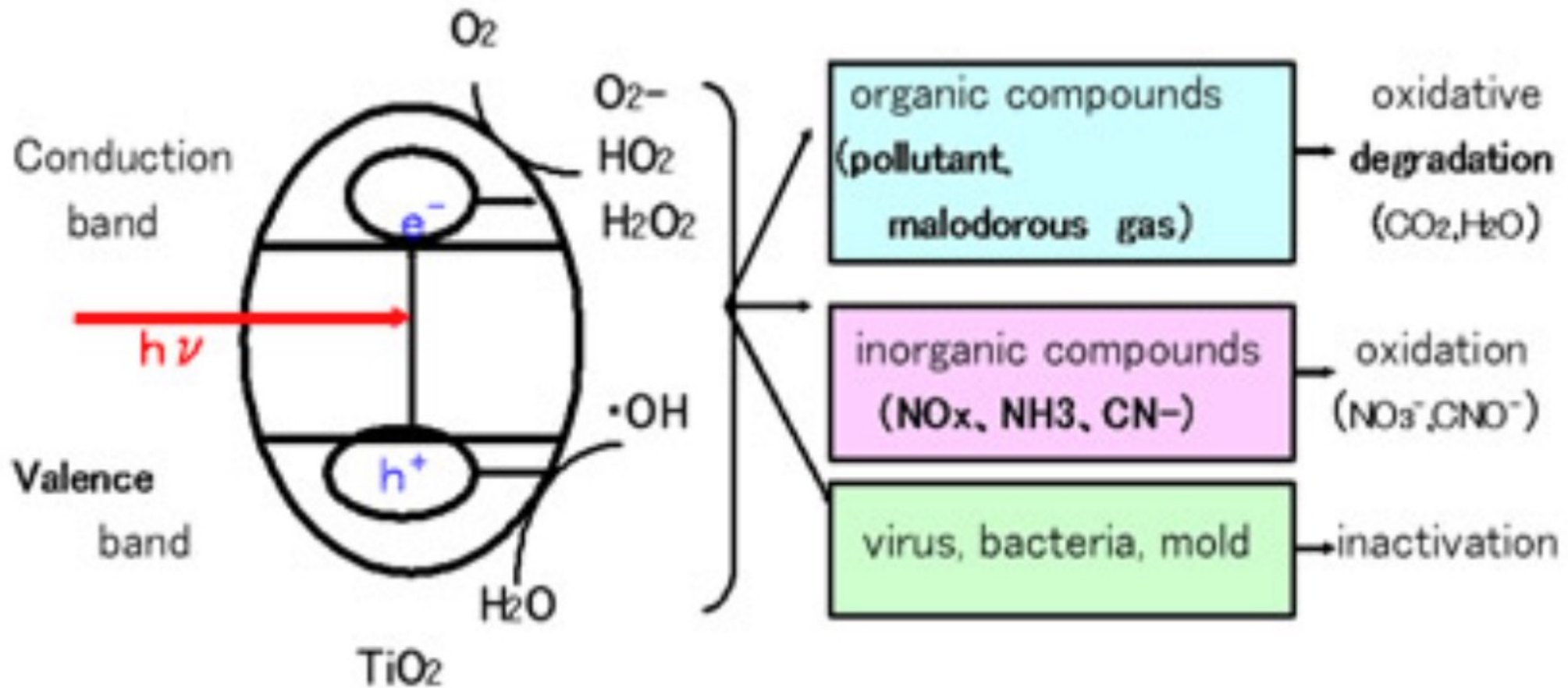


Figure reprinted from;

AKIRA FUJISHIMA, KENICHI HONDA "Electrochemical Photolysis of Water at a Semiconductor Electrode"
Nature 238, 37-38 (1972)

Reaction mechanism of TiO₂ photocatalysis





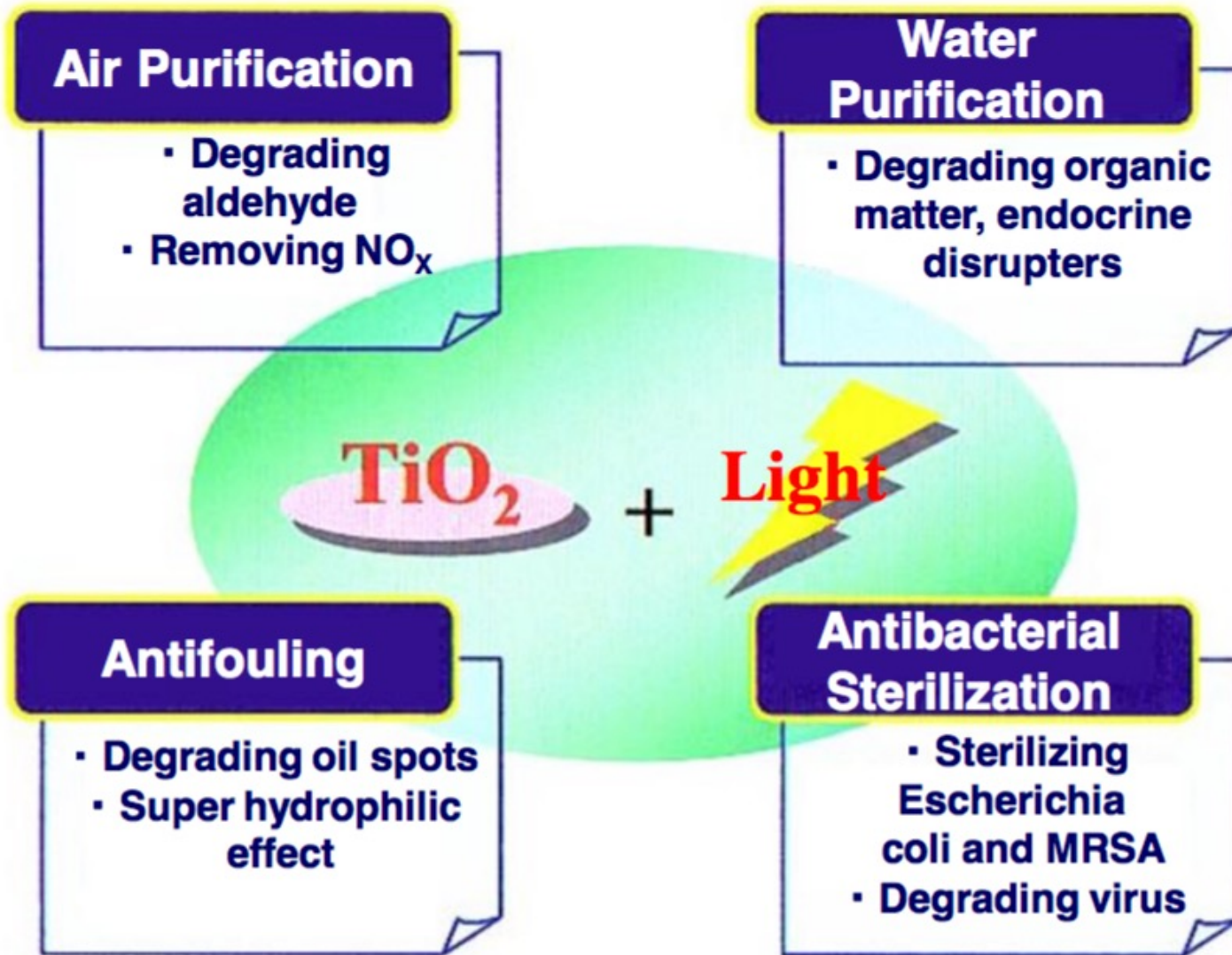
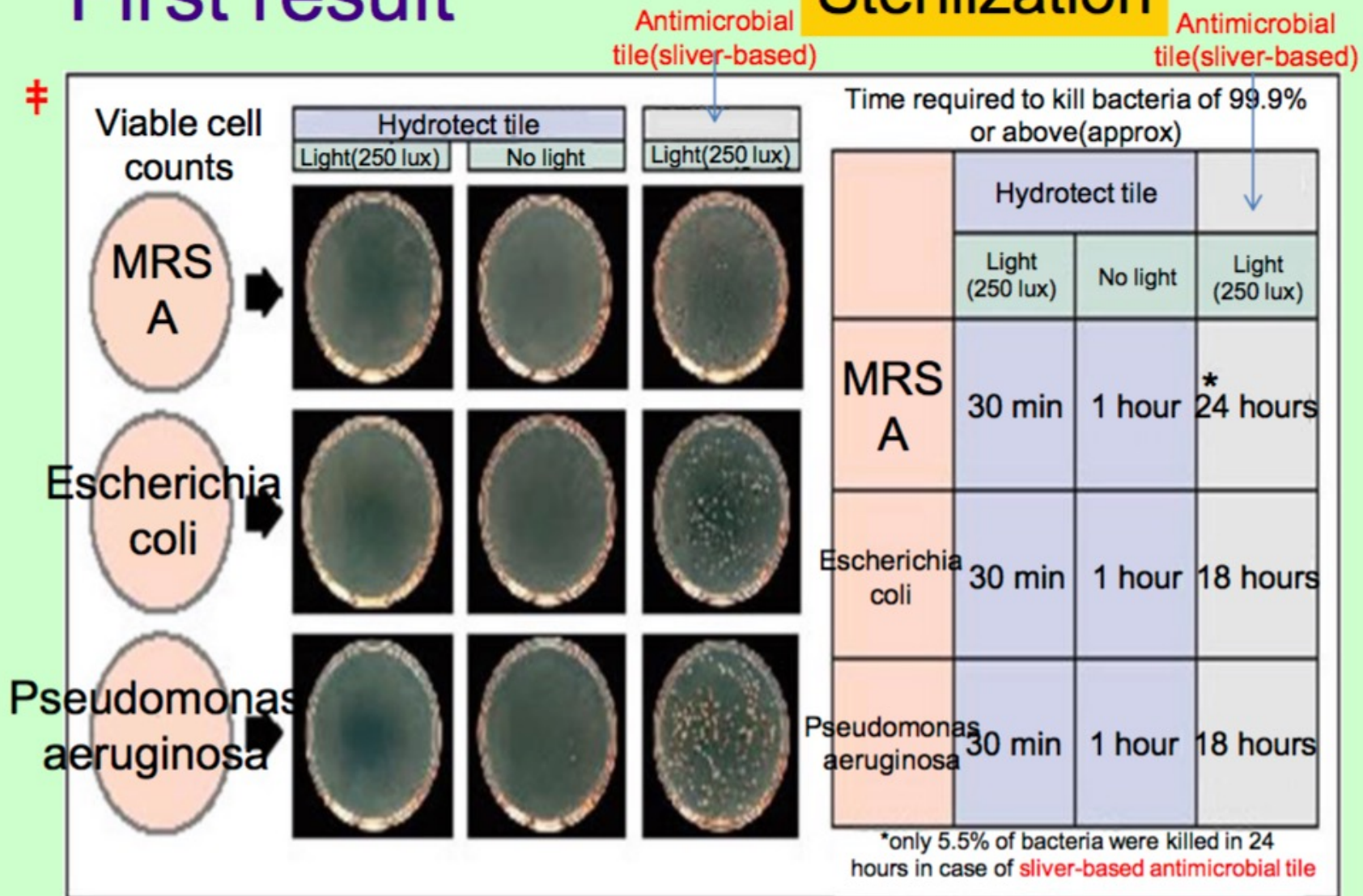


Fig.1 Area of Photocatalyst

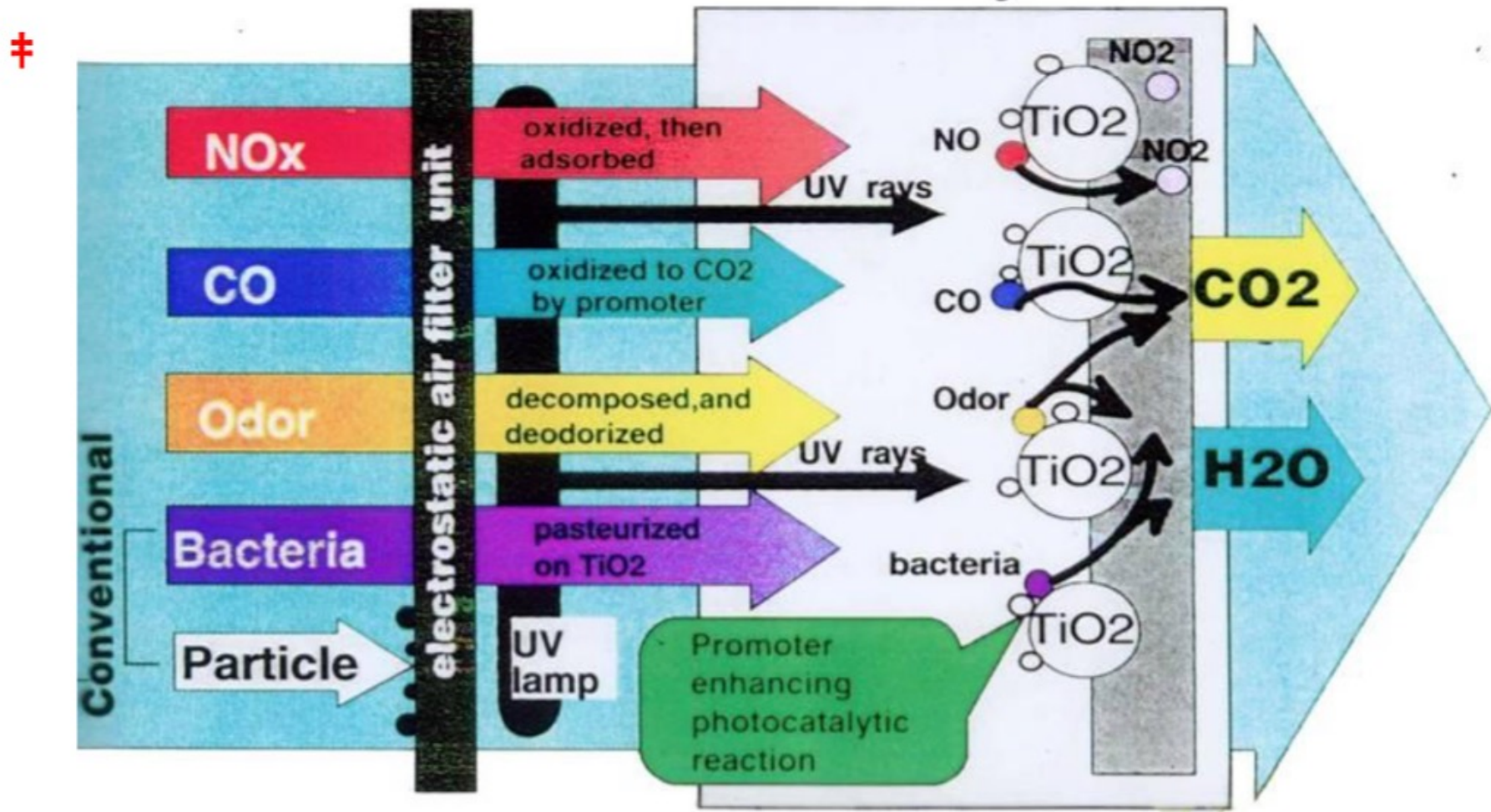
Degradation of Bacteria

First result

Sterilization



Photocatalyst Filter



Deodorizing, Sterilization, Degradation

Nano-Catalyst Synthesized by Flame Spray Pyrolysis (FSP) for visible light Photocatalysis

A dissertation submitted to the Division of Research and
Advanced Studies of the University of Cincinnati

In partial fulfillment of the
requirement for the degree of

DOCTOR OF PHILOSOPHY

In the Chemical Engineering Program of School of Energy, Environmental,
Biological and Medical Engineering

by

Siva Nagi Reddy Inturi

Committee:

Professor Panagiotis (Peter) G. Smirniotis (Chair)

Professor Makram Suidan

Professor Vesselin Shanov

Professor Gregory Beaucage

Assoc. Professor Anastasios Angelopoulos

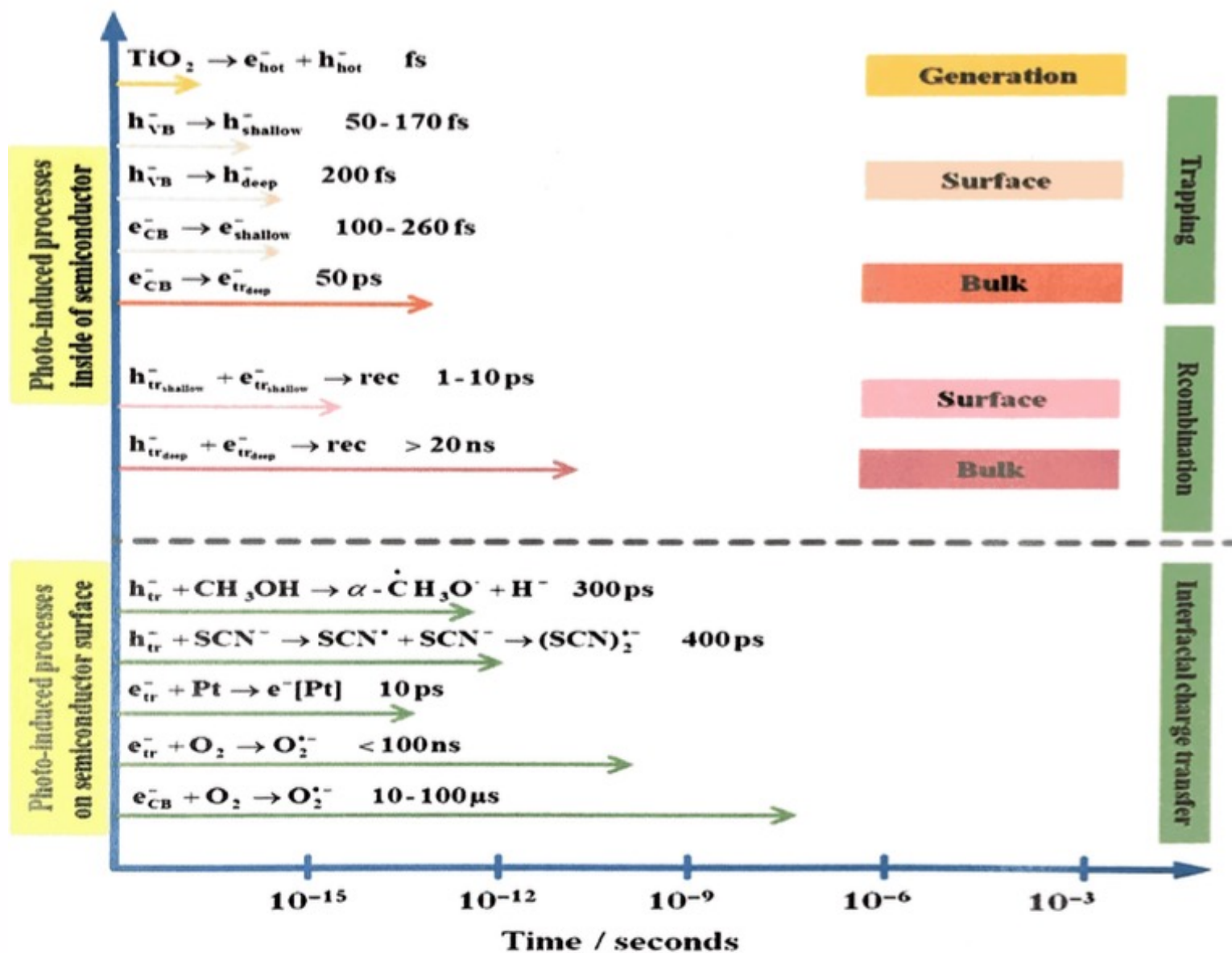


Figure 1.2: The general mechanism for heterogeneous photocatalysis on TiO₂.

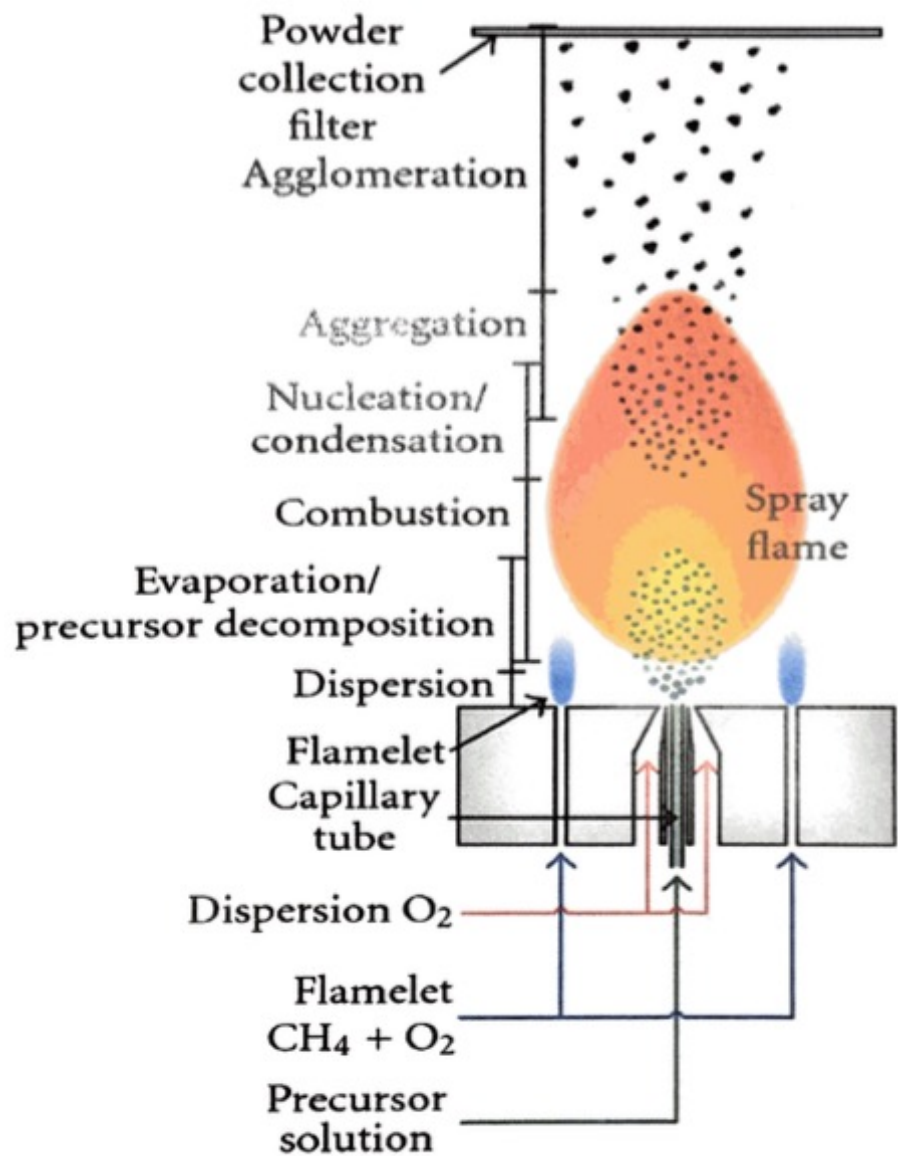


Table 2-5: Photocatalytic activity of the catalyst used in the present study

Catalyst	Absorption region	Band gap (eV)	K_A ($\text{m}^3\text{g}^{-1}\text{s}^{-1}$)
P25	UV	3.11	0.051
FSP TiO_2	UV	3.08	0.098
Ce/TiO_2	UV	3.13	0.014
Co/TiO_2	Visible	2.54	0.021
Cr/TiO_2	Visible	2.82	0.616
Cu/TiO_2	Visible	2.86	0.010
Fe/TiO_2	Visible	2.69	0.152
Mn/TiO_2	Visible	2.86	0.006
Mo/TiO_2	UV	3.19	0.004
Ni/TiO_2	Visible	2.37	0.019
V/TiO_2	Visible	2.63	0.165
Y/TiO_2	UV	3.20	0.004
Zr/TiO_2	UV	3.21	0.008

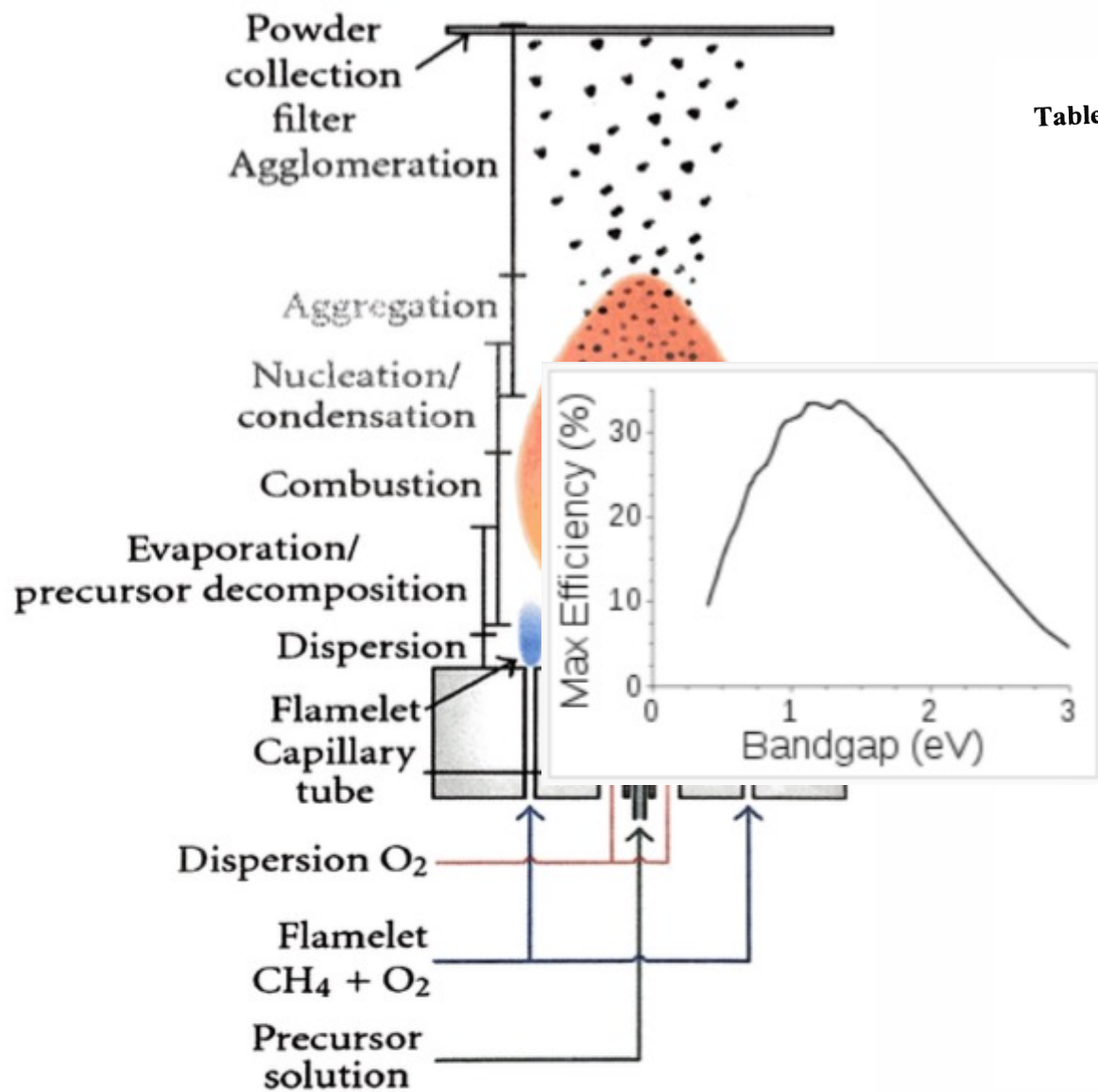
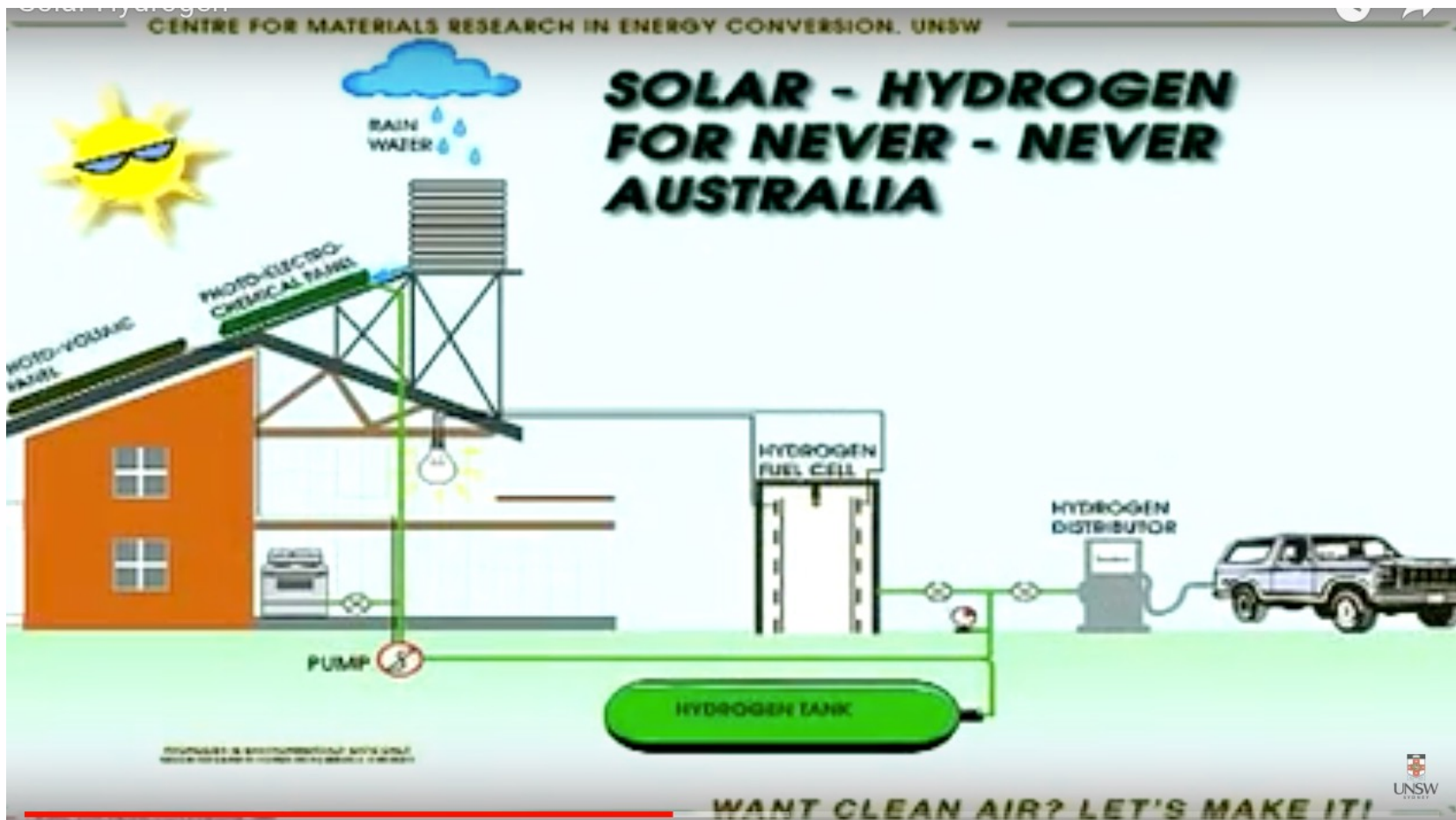


Table 2-5: Photocatalytic activity of the catalyst used in the present study

Catalyst	Absorption region	Band gap (eV)	K_A ($m^3 g^{-1} s^{-1}$)
P25	UV	3.11	0.051
FSP TiO ₂	UV	3.08	0.098
Ce/TiO ₂	UV	3.13	0.014
Co/TiO ₂	Visible	2.54	0.021
Cr/TiO ₂	Visible	2.82	0.616
Cu/TiO ₂	Visible	2.86	0.010
Fe/TiO ₂	Visible	2.69	0.152
Mn/TiO ₂	Visible	2.86	0.006
Mo/TiO ₂	UV	3.19	0.004
Ni/TiO ₂	Visible	2.37	0.019
V/TiO ₂	Visible	2.63	0.165
Y/TiO ₂	UV	3.20	0.004
Zr/TiO ₂	UV	3.21	0.008

Solar Thermolysis

[Titania Catalyst](http://www.youtube.com/watch?v=8kjqsDh8cs0) (<http://www.youtube.com/watch?v=8kjqsDh8cs0>)

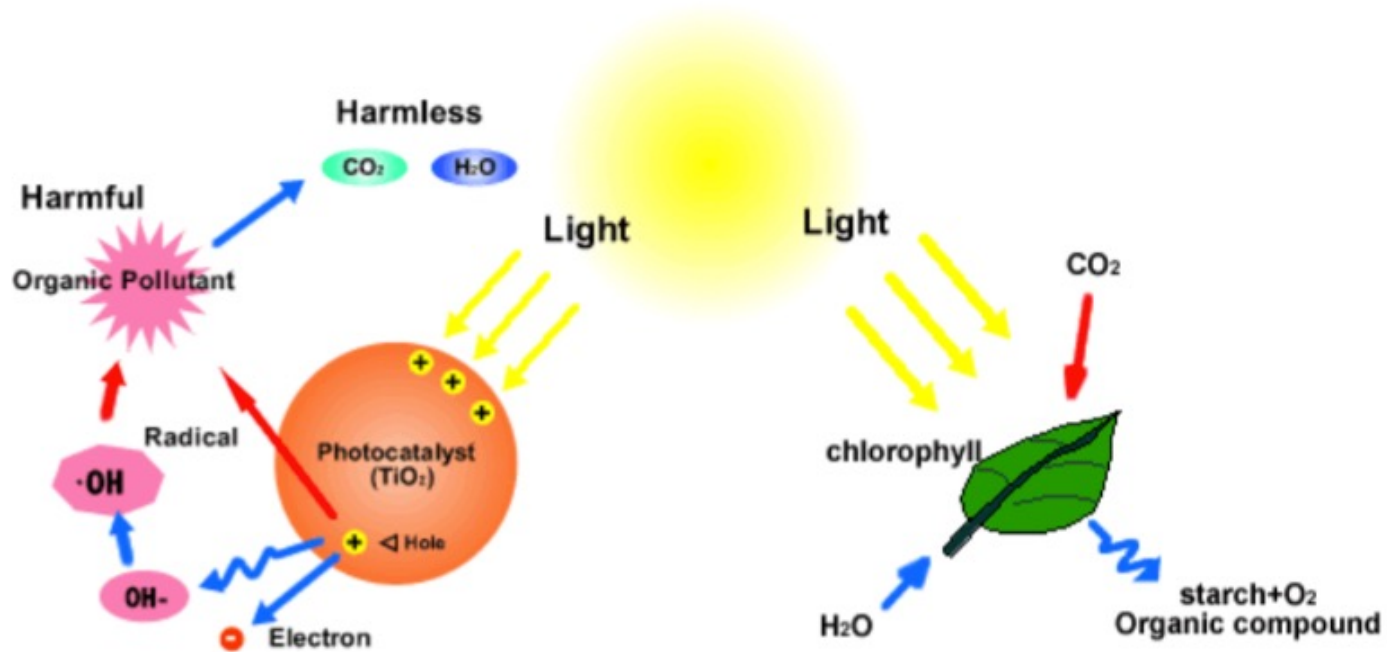


Solar Thermolysis

Titania as a photocatalyst

http://www.mvt.ovgu.de/mvt_media/Vorlesungen/VO_ENAP/Folien_ENAP_10.pdf

Titania - photocatalyst for waste water decontamination



Solar Thermolysis

Titania as a photocatalyst

<https://cdn.intechopen.com/pdfs-wm/51861.pdf>

Chapter 7

Concretes with Photocatalytic Activity

Magdalena Janus and Kamila Zajęc

Additional information is available at the end of the chapter

<http://dx.doi.org/10.5772/64779>

Solar Thermolysis

Titania as a photocatalyst

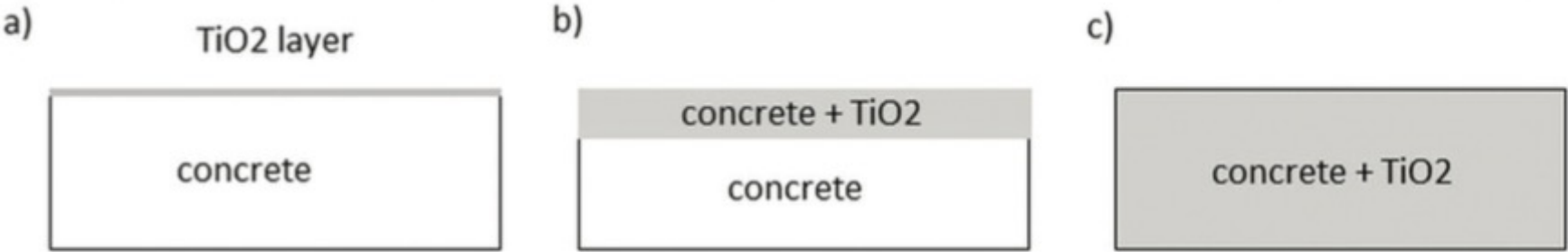


Figure 2. Scheme of possible ways for concrete modification by photocatalysts.

Solar Thermolysis

Titania as a photocatalyst

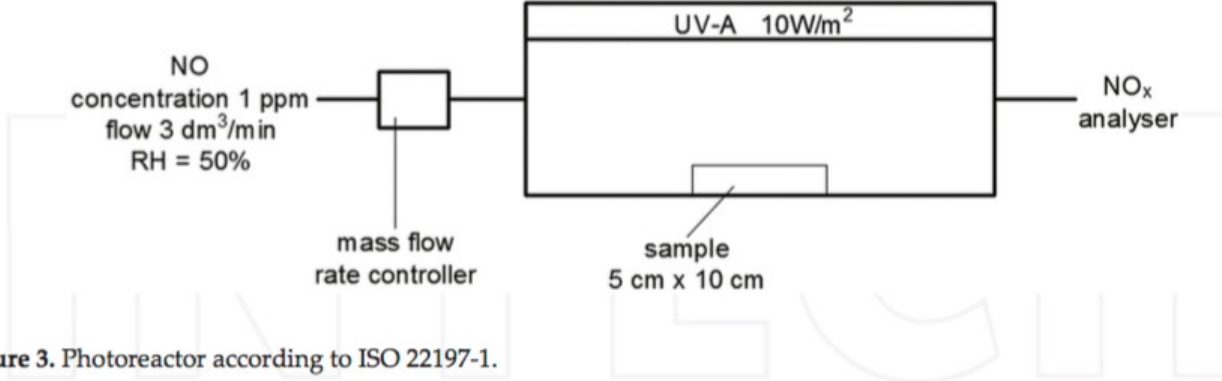


Figure 3. Photoreactor according to ISO 22197-1.



Figure 4. Separate parking lanes at the Leien of Antwerp with photocatalytic pavement blocks [15].

Solar Thermolysis

Titania as a photocatalyst

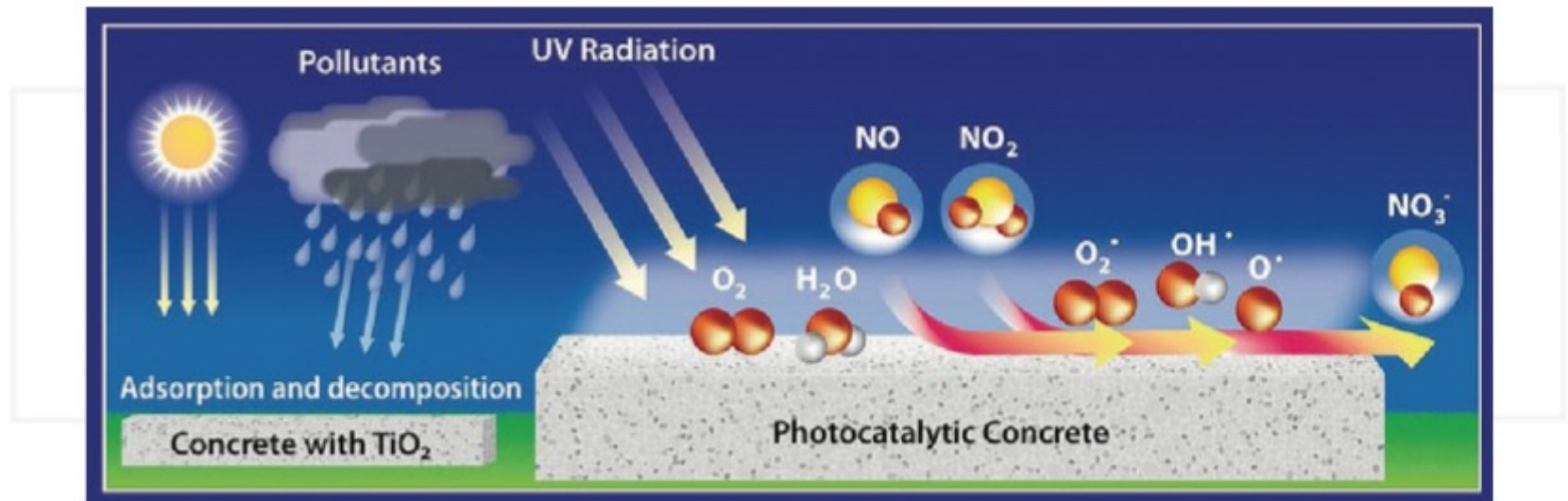


Figure 6. Scheme of photocatalytic air purifying pavement [15].

Solar Thermolysis

Titania as a photocatalyst

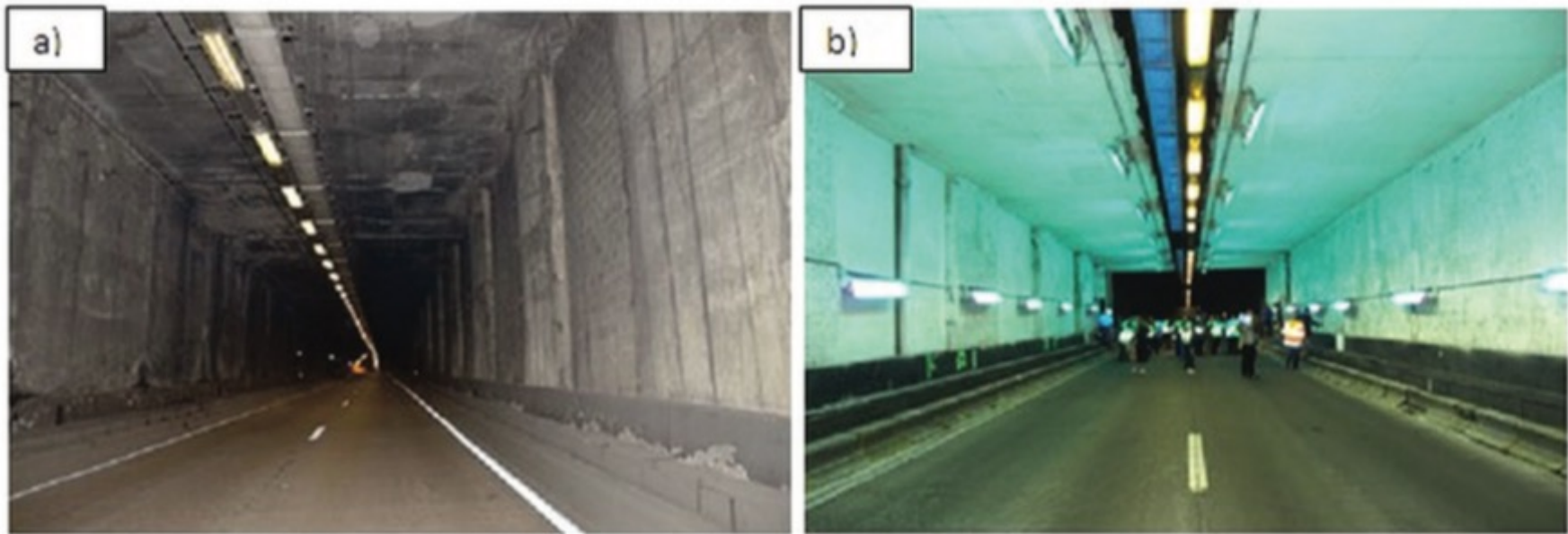


Figure 7. Inside view of test site within Leopold II tunnel in Brussels (a) before renovation, (b) after renovation with using photocatalytic walls [15].

Solar Thermolysis

Titania as a photocatalyst

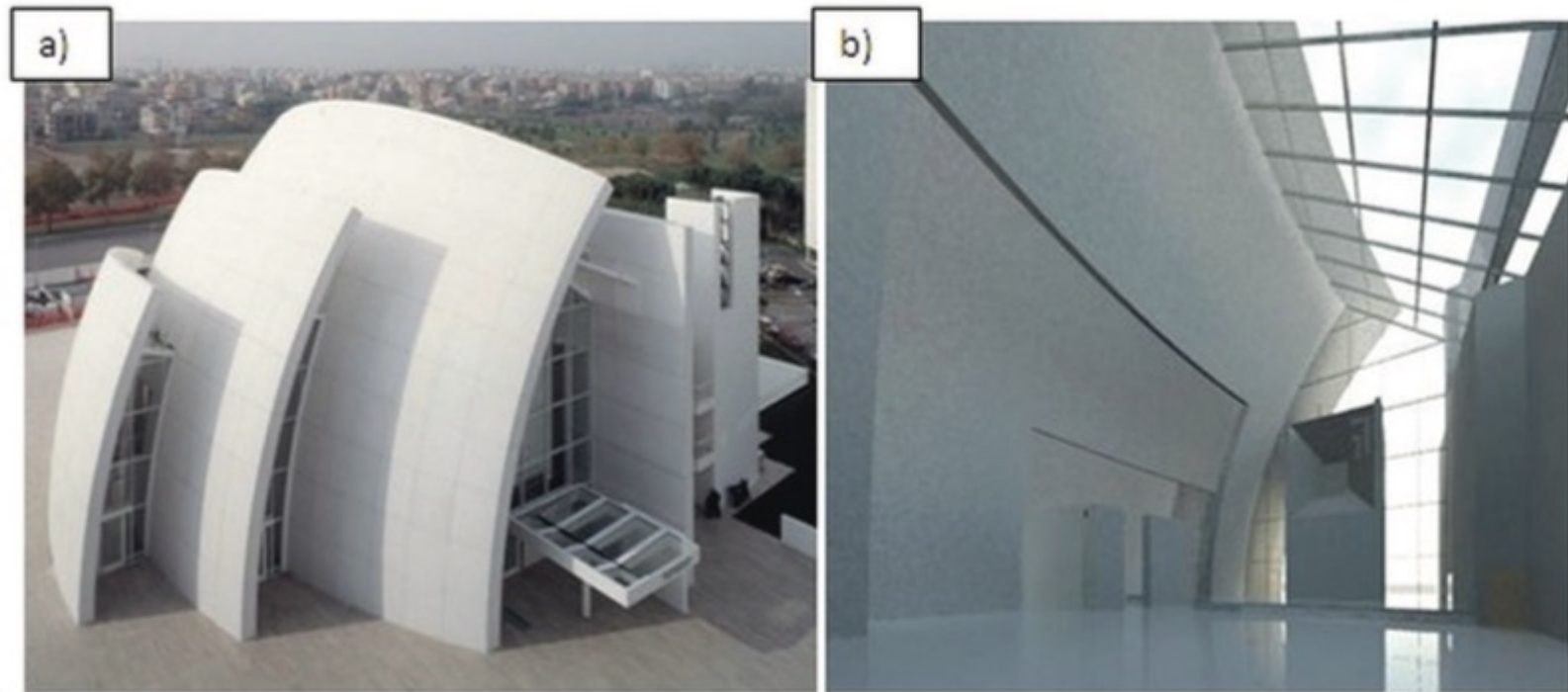


Figure 8. Dives in Misericordia Church in Rome (a), zoom insight (b) [41].

Solar Thermolysis

Titania as a photocatalyst

[42, 43]. It is impressive that according to Fujishima and Zhang [44] by 2003, self-cleaning TiO_2 -based tiles had been used in over 5000 buildings in Japan. Among them the most famous is the Maru Building, located in Tokyo's main business district.

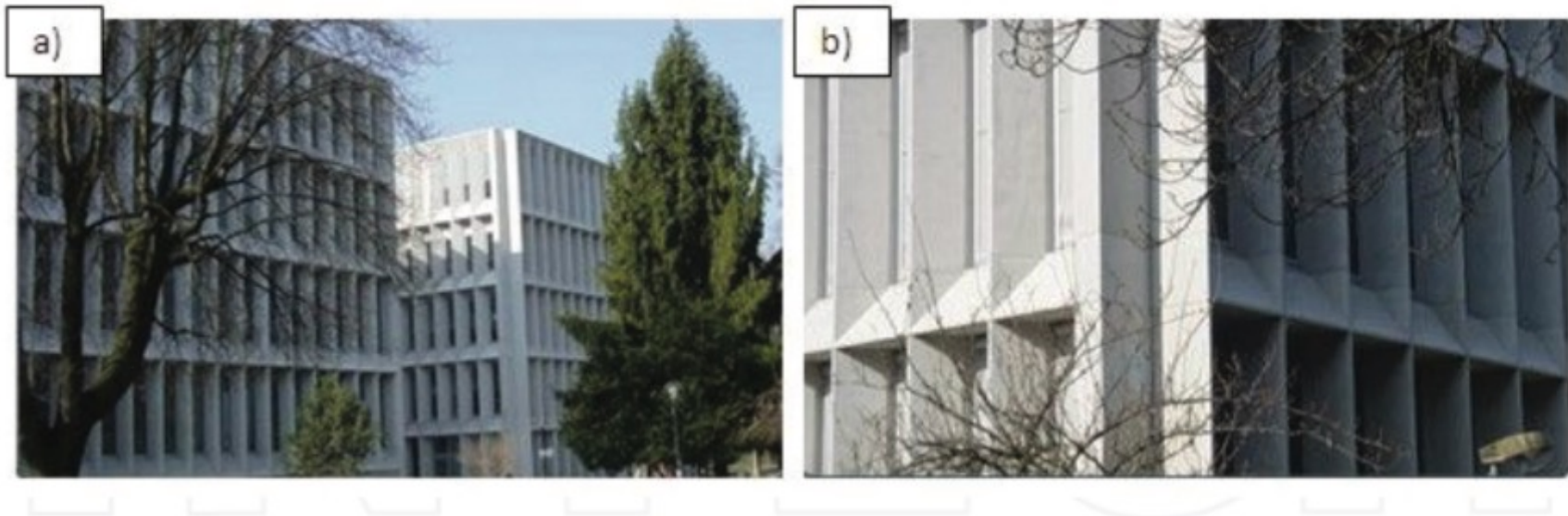


Figure 9. Cité de la Musique et des Beaux- Arts in Chambéry [45].

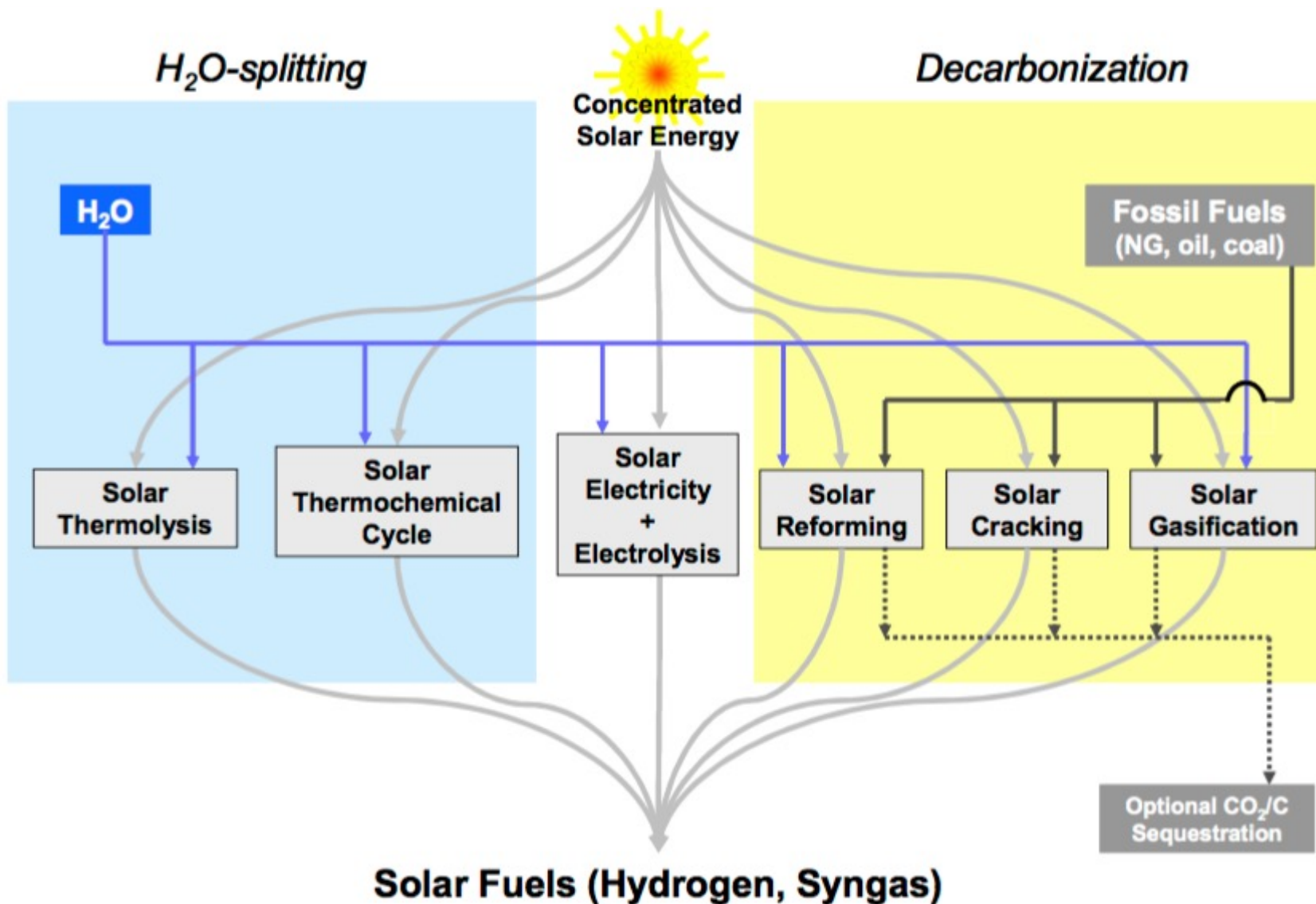
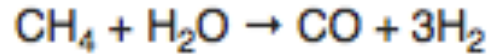


Fig. 2: Thermochemical routes for solar hydrogen production – Indicated is the chemical source of H_2 : H_2O for the solar thermolysis and the solar thermochemical cycles; fossil fuels for the solar cracking, and a combination of fossil fuels and H_2O for the solar reforming and gasification. For the solar decarbonization processes, optional CO_2/C sequestration is considered. All of those routes involve energy consuming (endothermic) reactions that make use of concentrated solar radiation as the energy source of high-temperature process heat. Adapted from [1,2].²⁷⁷

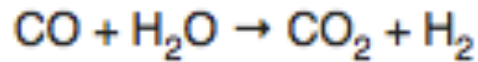
Biomass/Syngas

Steam Reforming Reaction: CH₄ to H₂ and CO



At high temperatures (700 – 1100 °C) and in the presence of a metal-based catalyst (nickel), **steam** reacts with methane to yield carbon monoxide and hydrogen. ...

Water Shift Gas Reaction: CO to H₂



The shift reaction will operate with a variety of catalysts between 400°F and 900

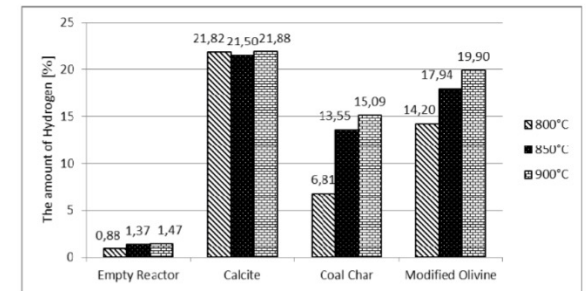
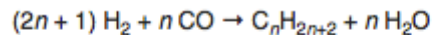


Fig. 3. Average percentage representation of hydrogen for the studied catalysts at t=800, 850 and 900°C

Fischer-Tropsch Reaction: H₂ and CO to Liquid Fuel

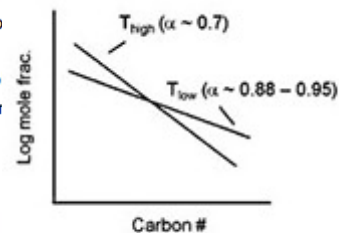
Reaction mechanism [\[edit \]](#)

The Fischer–Tropsch process involves a series of chemical reactions that produce a variety of hydrocarbons, ideally having the formula (C_nH_{2n+2}). The more useful reactions produce **alkanes** as follows:

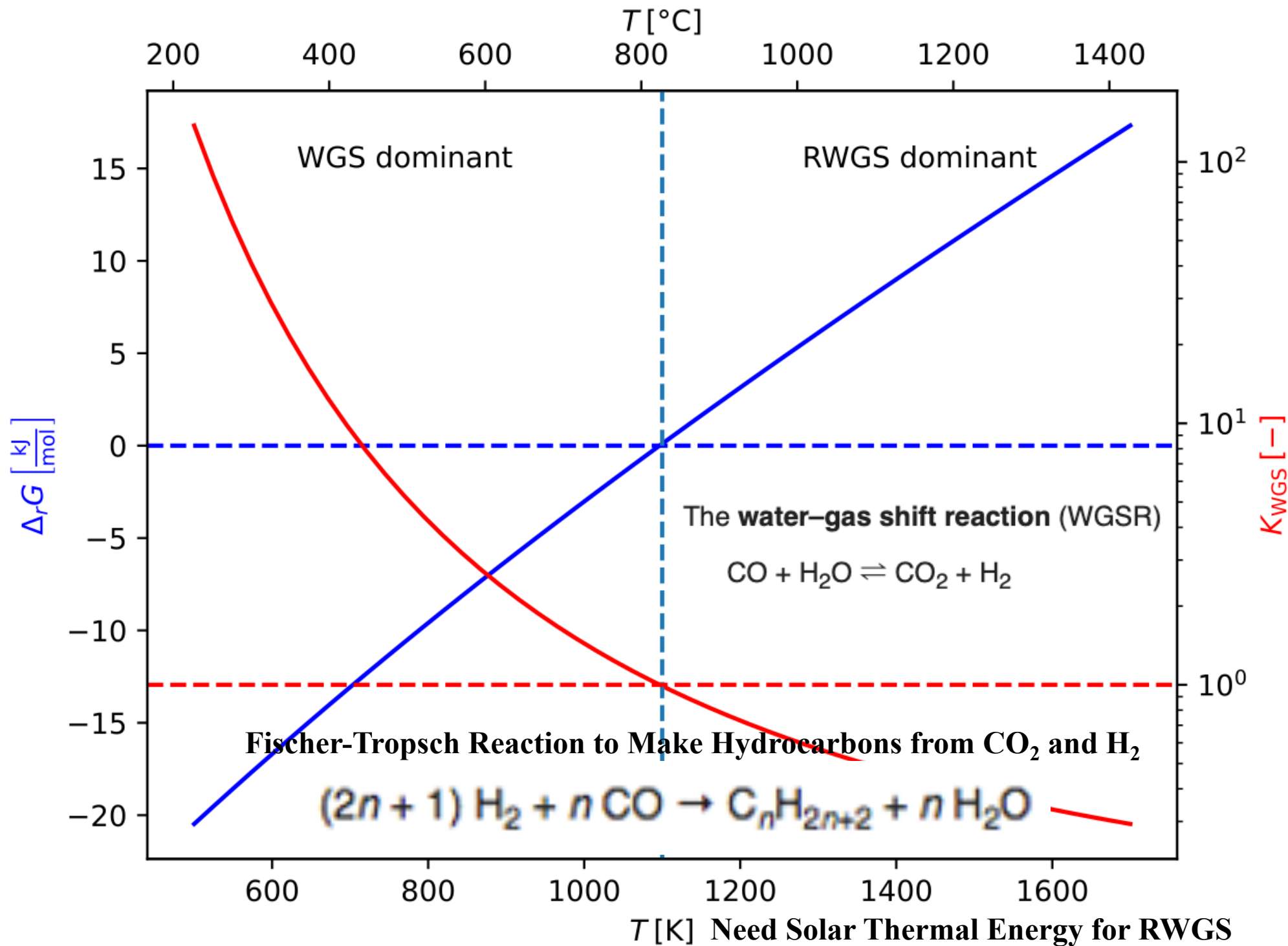


where *n* is typically 10–20. The formation of methane (*n* = 1) is unwanted. Most of the alkanes produced tend to be straight-chain, suitable as **diesel fuel**. In addition to alkane formation, competing reactions give small amounts of **alkenes**, as well as **alcohols** and other oxygenated hydrocarbons.^[4]

- Nickel (Ni) tends to promote methane formation, as in a [methanation process](#); thus generally it is not desirable
- Iron (Fe) is relatively low cost and has a higher water-gas-shift activity, and is therefore more suitable for a lower hydrogen/carbon monoxide ratio (H₂/CO) syngas such as those derived from coal gasification
- Cobalt (Co) is more active, and generally preferred over ruthenium (Ru) because of the prohibitively high cost of Ru
- In comparison to iron, Co has much less water-gas-shift activity, and is much more costly.



	Low T	Sasol Arge	High T	Sasol Synthol
• low C ₁ – C ₄		13.3	• higher C ₁ – C ₄	43.0
• low C ₅ – C ₁₁		17.9	• higher C ₅ – C ₁₁	40.0
• low C ₁₂ –C ₁₉		13.9	• less C ₁₂ –C ₁₉	7.0
• 50-70% wax		51.7	• low wax	4.0
• 220-270°C			• 325 – 350°C	
• α: 0.87+			• α: ~0.7	
• gasoline/diesel: 1:2			• gasoline/diesel: 2:1	
• 80° Cetane #			• 50-60 Cetane #	
• 0-20 Octane #			• 0-60 Octane #	



One Scenario that is being considered by German National Science Foundation (DFG), Saudi Arabia, Australia and Japan

- Wind turbines far offshore (or solar in the desert),**
- on turbine electrolysis reactors using reverse osmosis of seawater for pure water feed,**
- on turbine conversion of H₂ to ammonia for transport (like propane so 1 MPa for liquid)**
- Ammonia can be used as a fuel (replace bunker fuel for ships),**
- converted to urea for fertilizer,**
- converted back to H₂ for fuel**
- converted back to H₂ for RWSG and Fischer-Tropsch to make plastics, rubber, and other hydrocarbons to feed a green petrochemical industry**
- Direct Air Capture (DAC) of CO₂ using membranes or separation technology or solar splitter (slide 296) for RWSG conversion of H₂ to hydrocarbons or use commercial CO₂**

This is a renewable petrochemical economy with no fossil fuels

The technical elements of this exist. Much research is being conducted around the world to improve conversion and catalytic technologies

This involves a major makeover of the petrochemical industry (jobs and \$) that will require government investment. This is being led by the EU (Germany), Japan, Australia, Saudi Arabia. China, Russia and the US are not funding much of this work.

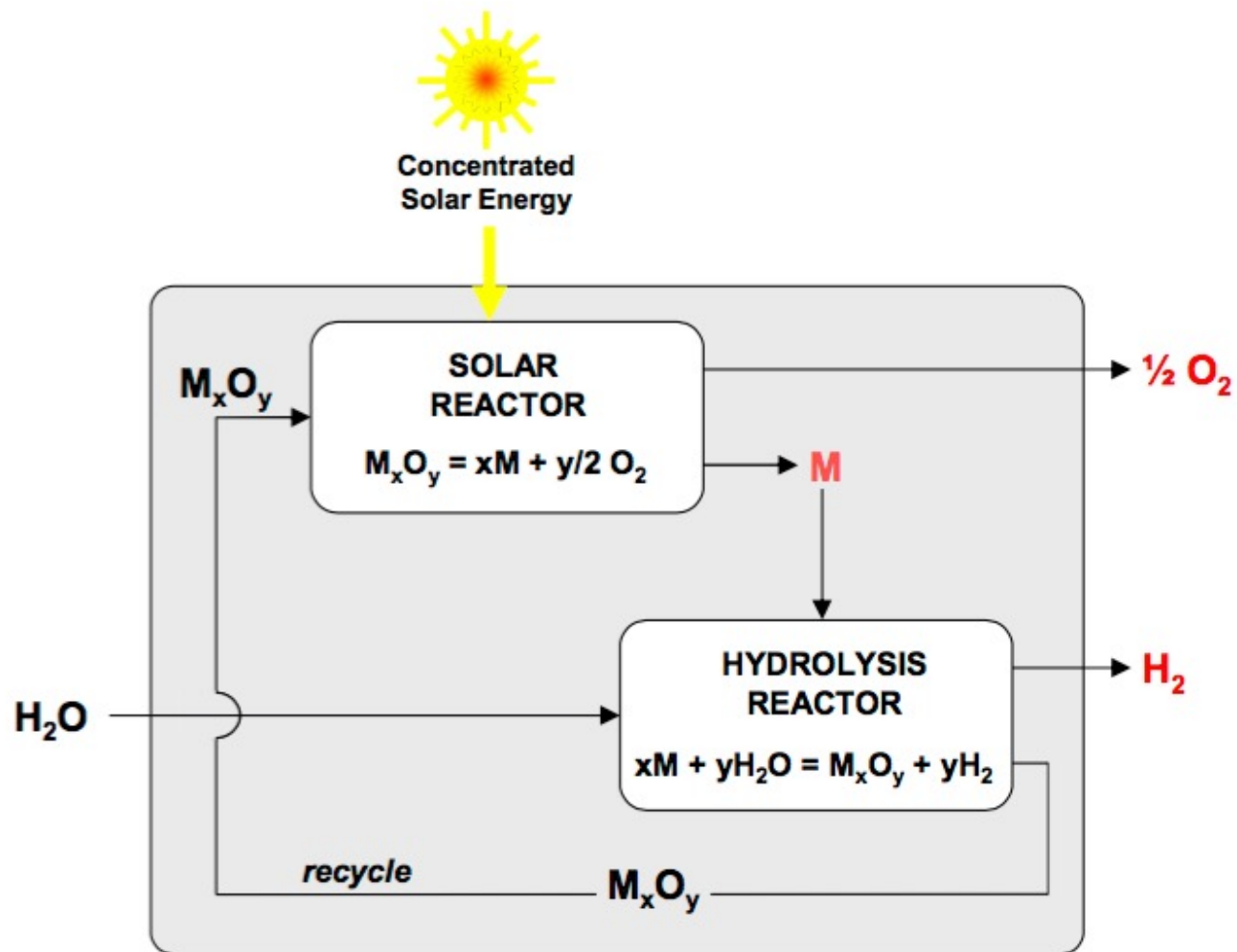


Fig. 3: Thermochemical route based on metal oxide redox reactions – The first step of the cycle is the solar thermal release of O_2 from the metal oxide (M_xO_y). This step requires very high temperatures. The second step is the reaction of the metal (M) with H_2O to form H_2 and the corresponding M_xO_y . This step proceeds at lower temperatures and does not require additional heating in some cases. Since H_2 and O_2 are formed in different steps, the need for high-temperature gas separation is thereby eliminated. This cycle was originally proposed for an iron oxide FeO/Fe_3O_4 redox system. Adapted from [1].

Solar Reduction/Oxidation Reactions

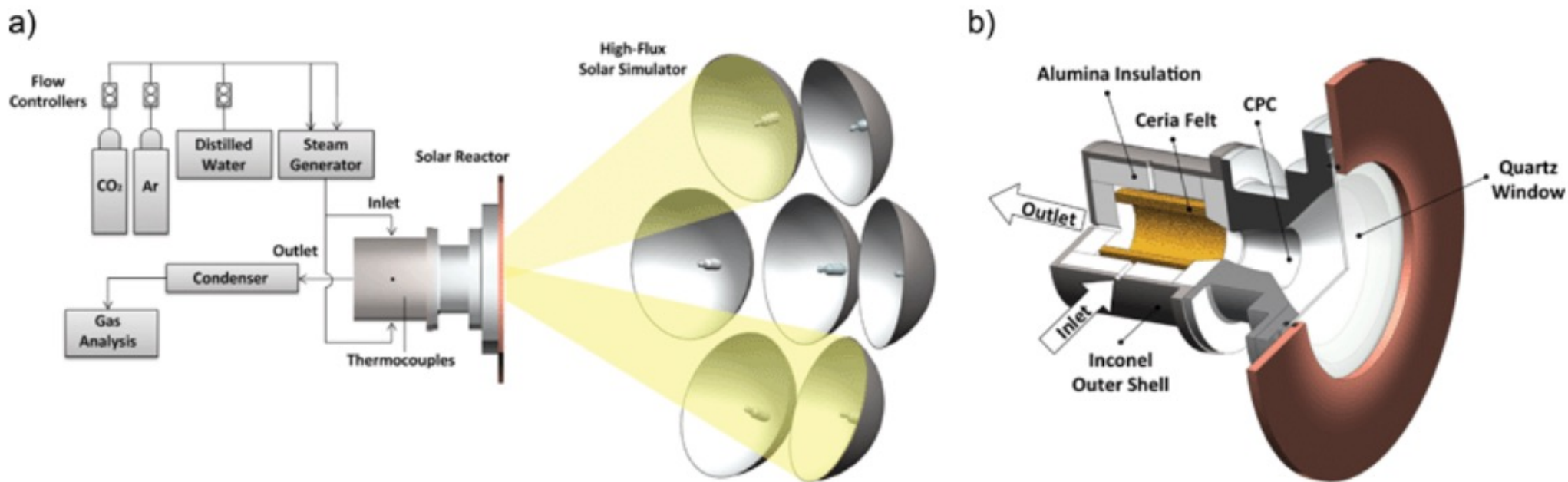


Fig. 1 (a) Experimental setup of ETH's High-Flux Solar Simulator and (b) schematic of the solar reactor configuration.

[Paper on ETHZ's program in solar redox](#)

Solar Reduction/Oxidation Reactions

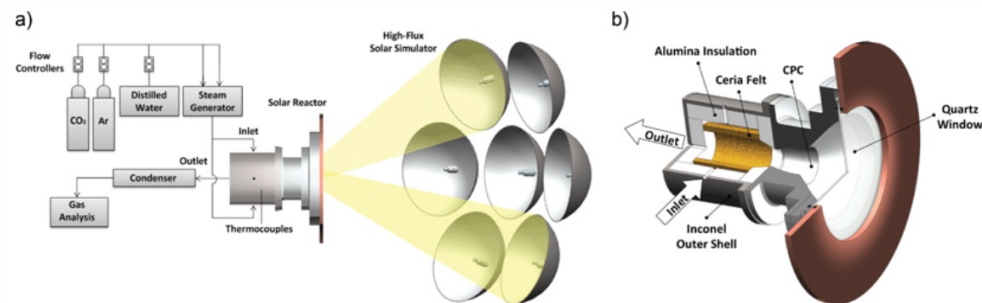


Fig. 1 (a) Experimental setup of ETH's High-Flux Solar Simulator and (b) schematic of the solar reactor configuration.

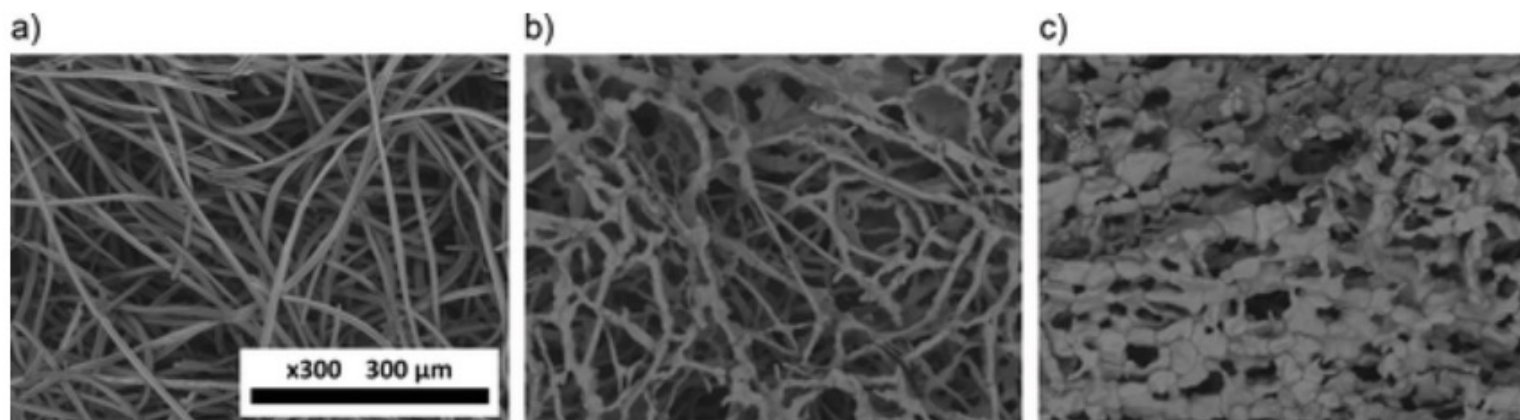


Fig. 6 (a) SEM micrographs of unreacted ceria felt, (b) the outermost surface of the ceria felt, and (c) the innermost ceria felt after the experimental campaign.

Solar Reduction/Oxidation Reactions

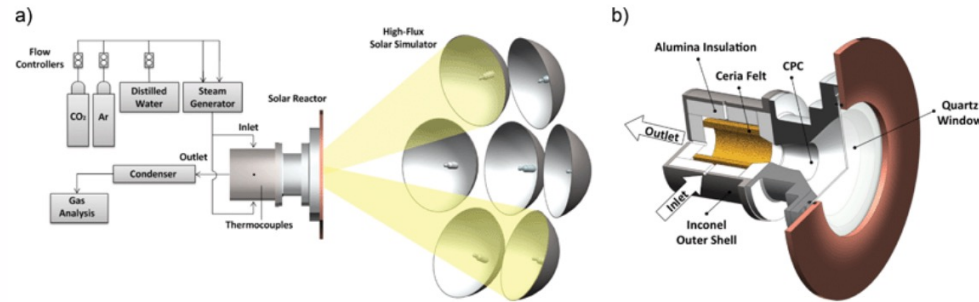
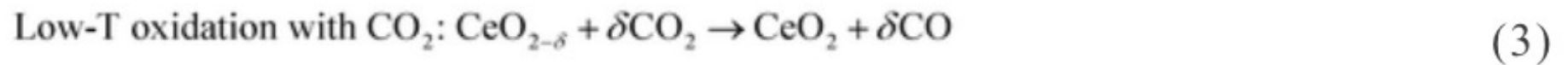
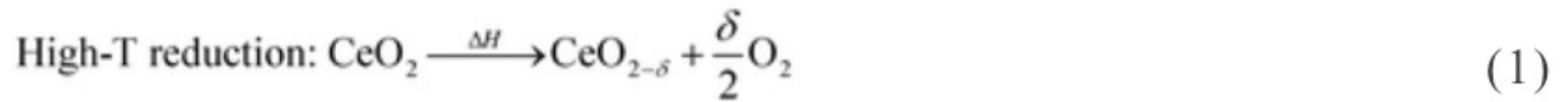


Fig. 1 (a) Experimental setup of ETH's High-Flux Solar Simulator and (b) schematic of the solar reactor configuration.



Solar Reduction/Oxidation Reactions

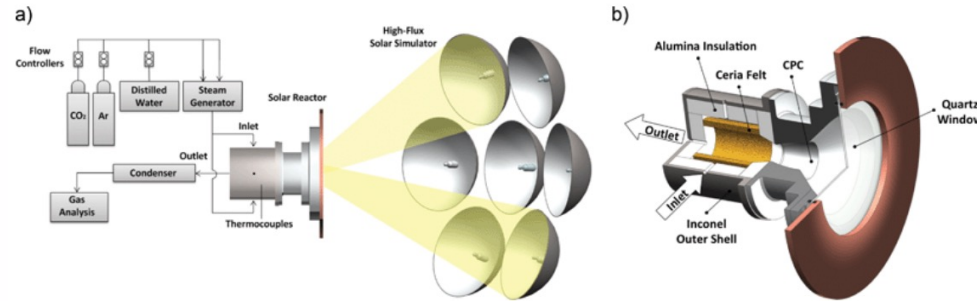
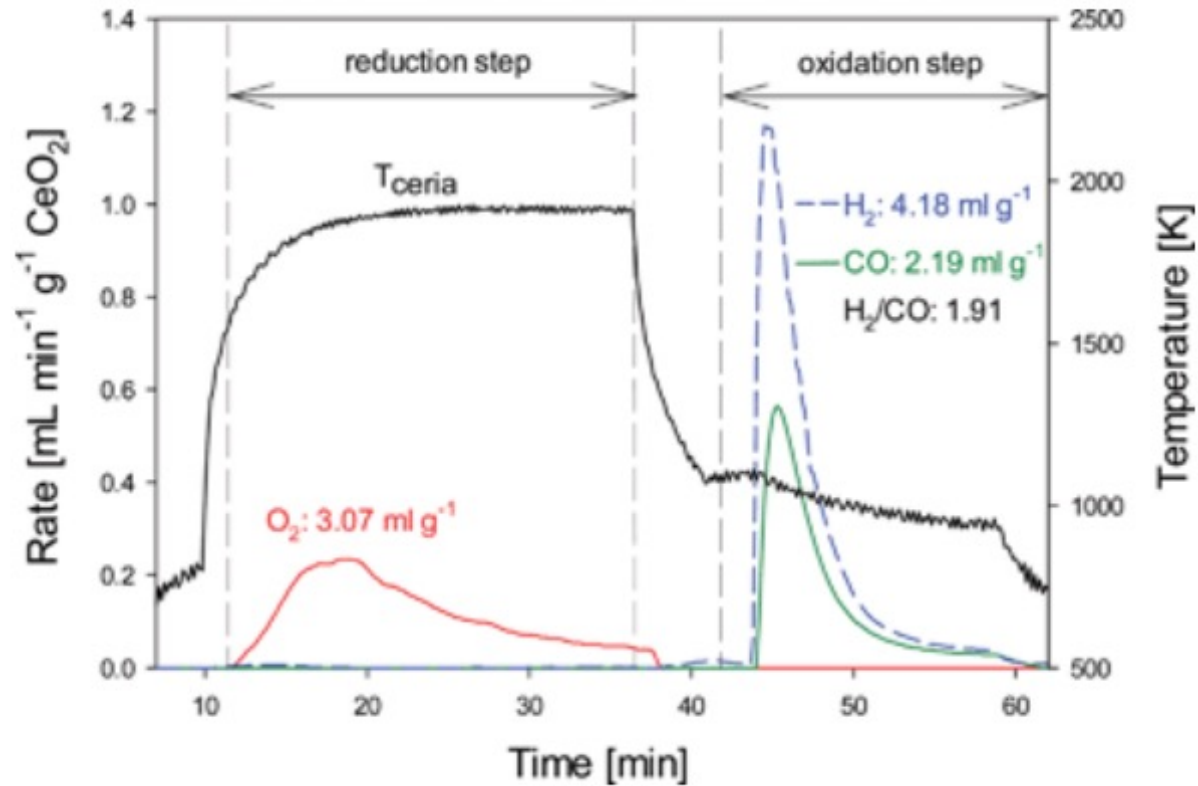
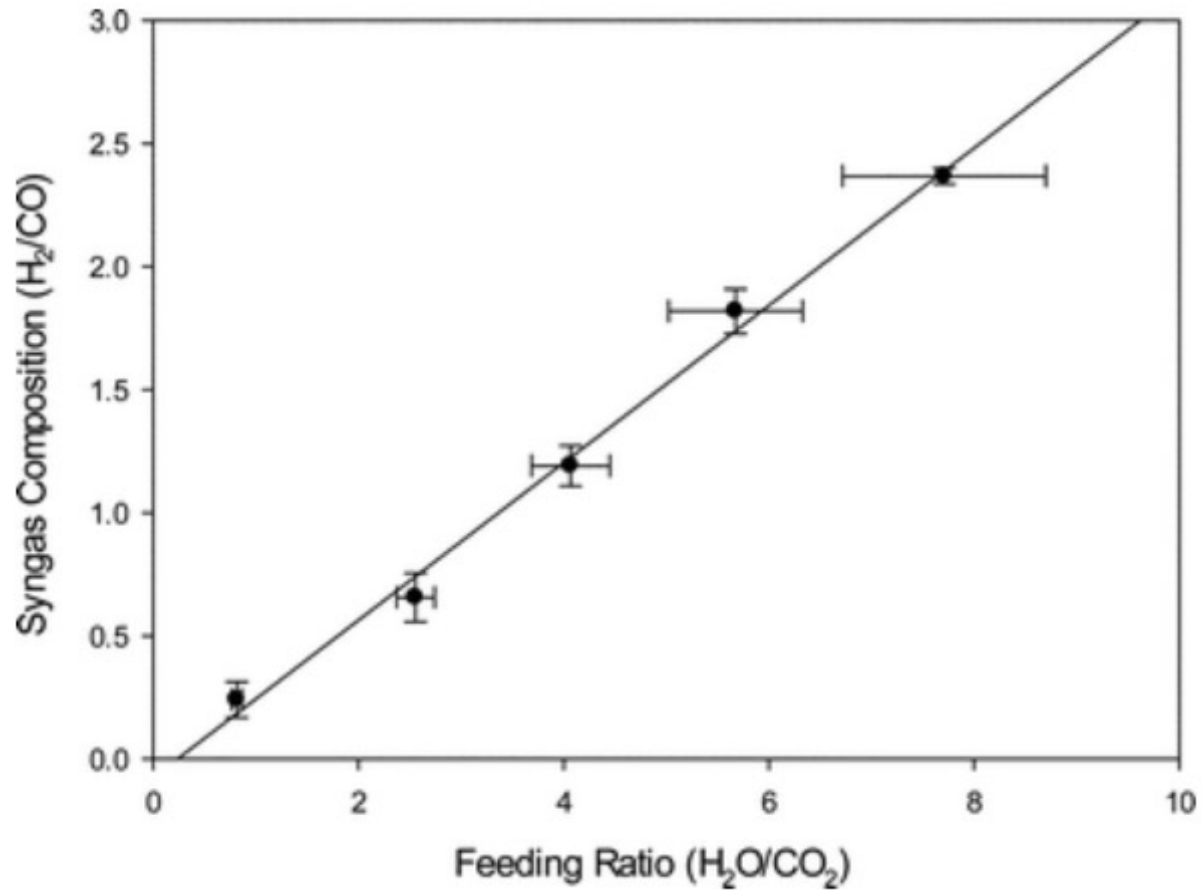
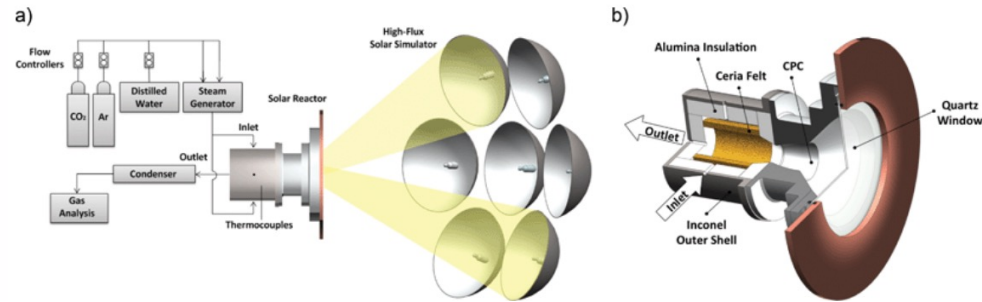


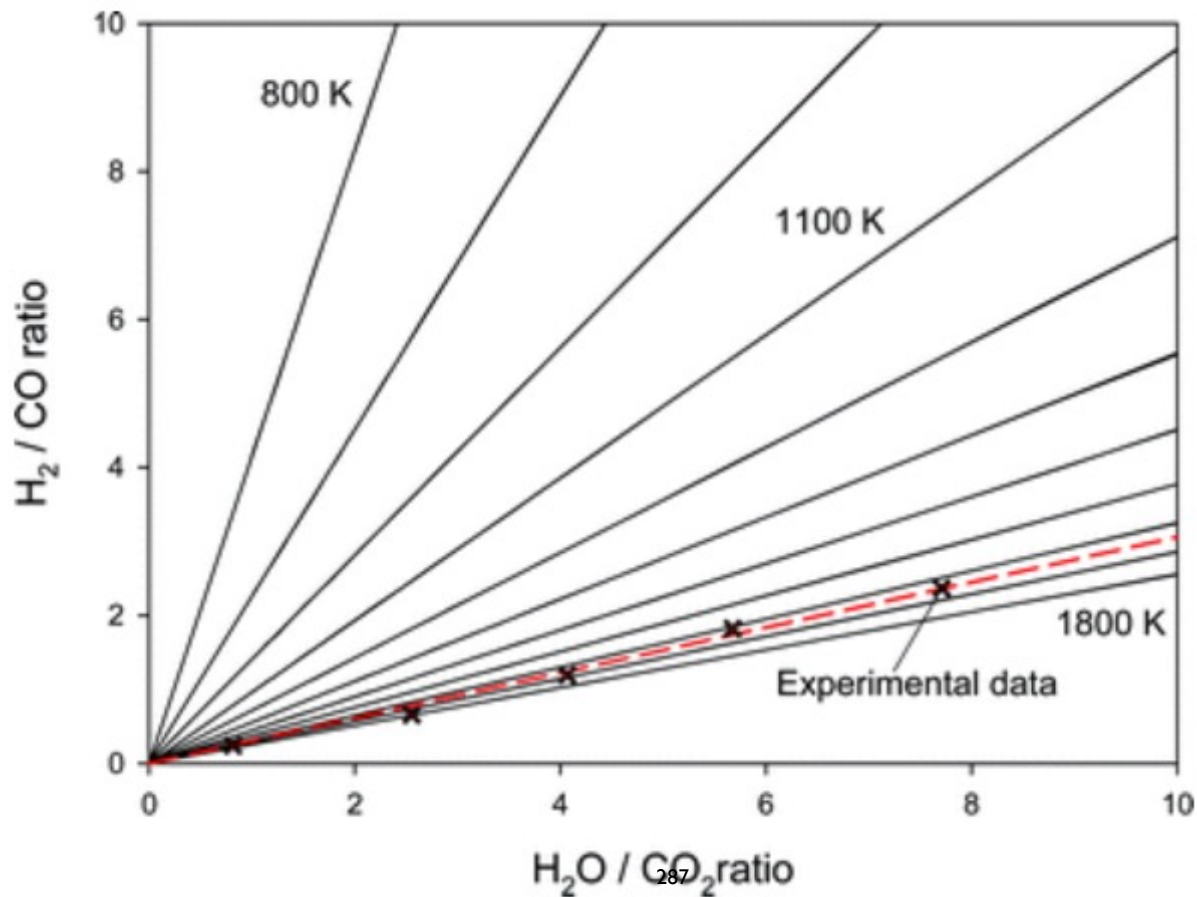
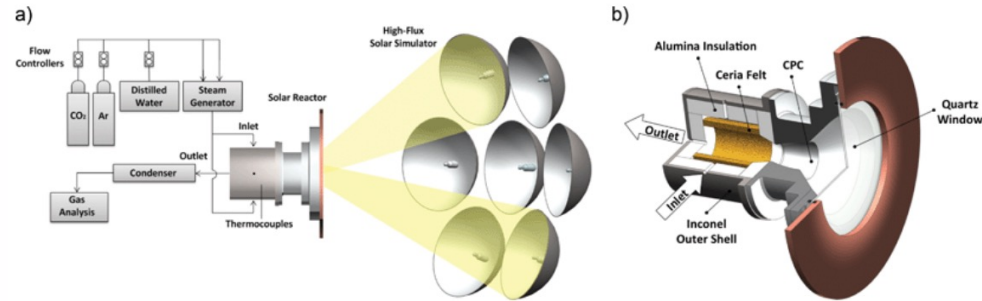
Fig. 1 (a) Experimental setup of ETH's High-Flux Solar Simulator and (b) schematic of the solar reactor configuration.



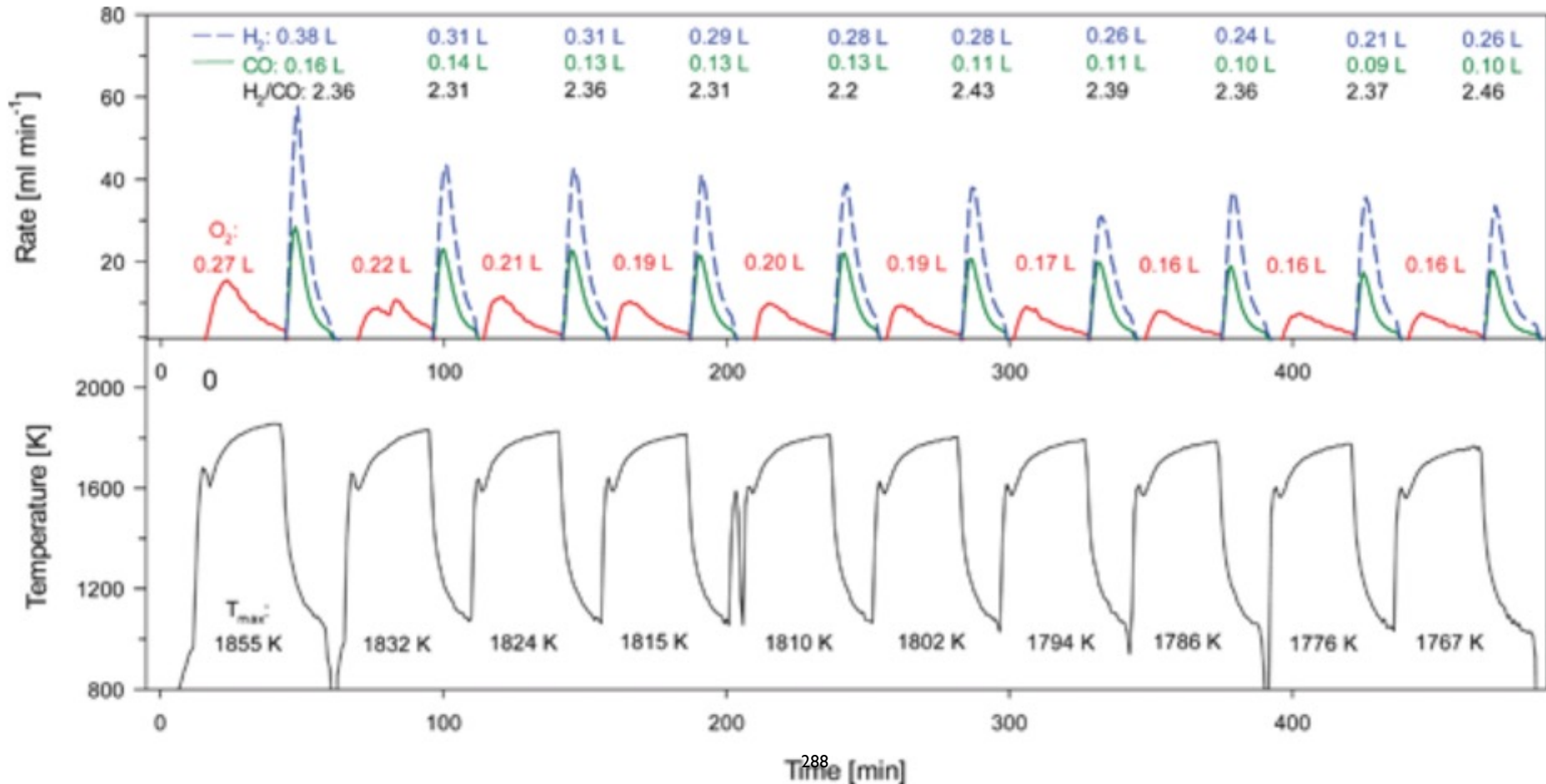
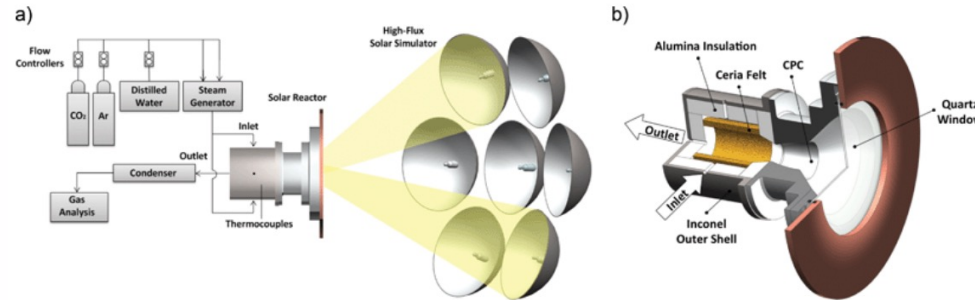
Solar Reduction/Oxidation Reactions



Solar Reduction/Oxidation Reactions



Solar Reduction/Oxidation Reactions



Solar Reduction/Oxidation Reactions

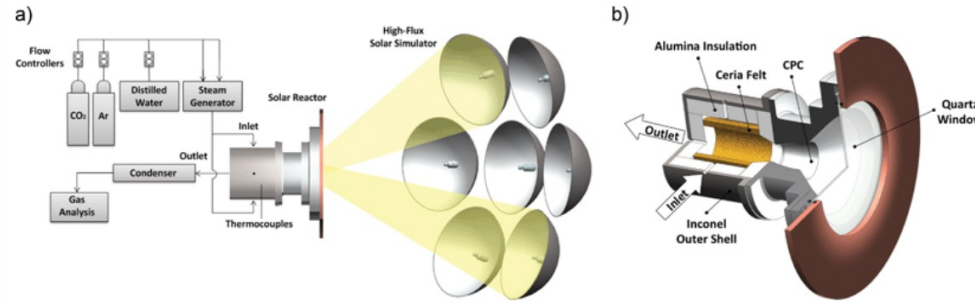


Fig. 1 (a) Experimental setup of ETH's High-Flux Solar Simulator and (b) schematic of the solar reactor configuration.

Calculation of Efficiency

$$\eta_{\text{average}} = \frac{\Delta H_{\text{fuel}} \int r_{\text{fuel}} dt}{\int P_{\text{solar}} dt + E_{\text{inert}} \int r_{\text{inert}} dt}$$

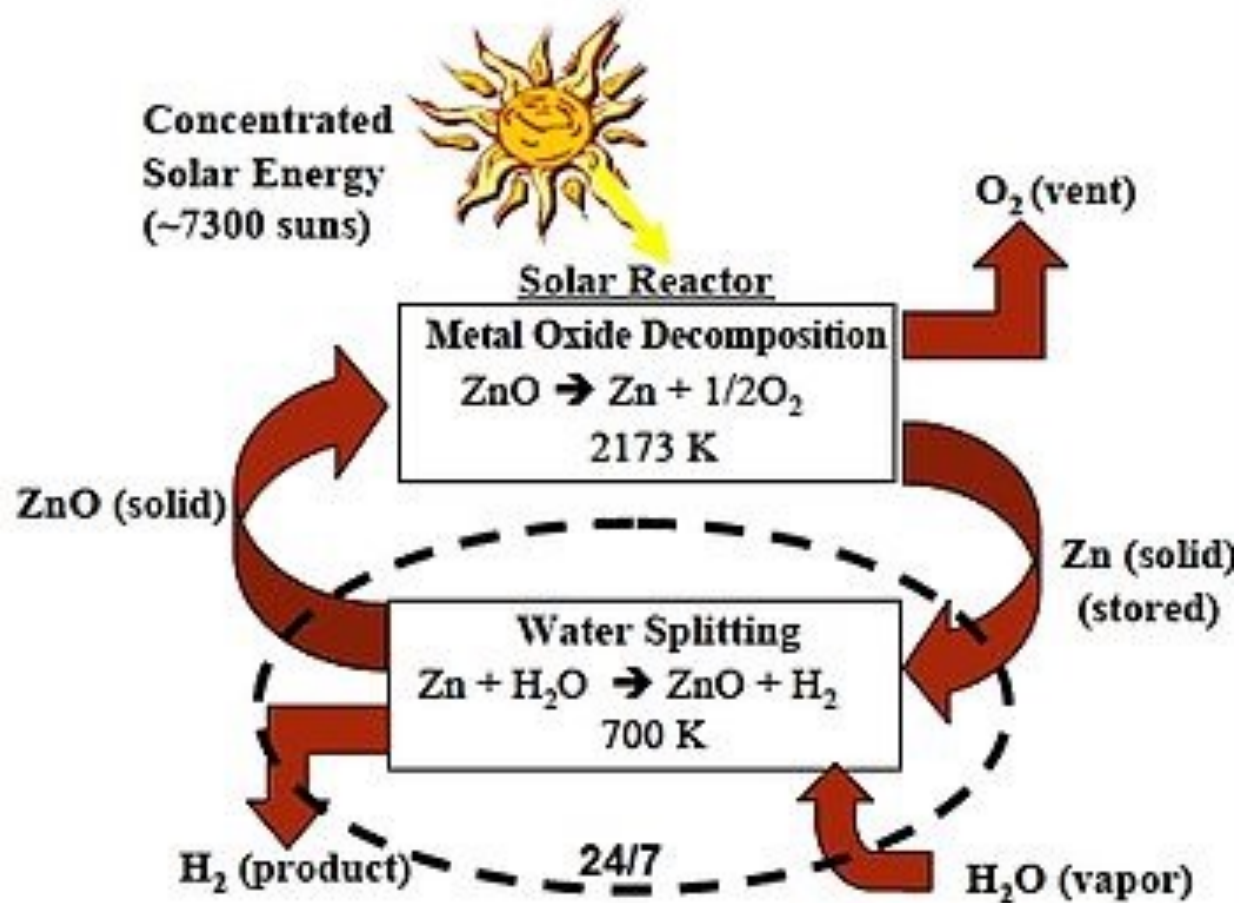
$$\eta_{\text{peak}} = \frac{2r_{\text{oxygen}} \Delta H_{\text{fuel}}}{P_{\text{solar}} + r_{\text{inert}} E_{\text{inert}}}$$

One and Ten Cycles

	η_{average}	η_{peak}
One Cycle	15%	31%
Ten Cycles	9%	16%

20% is the target for commercial use

[Zn => ZnO Cycle](http://en.wikipedia.org/wiki/Zinc%E2%80%93zinc_oxide_cycle) (http://en.wikipedia.org/wiki/Zinc%E2%80%93zinc_oxide_cycle)



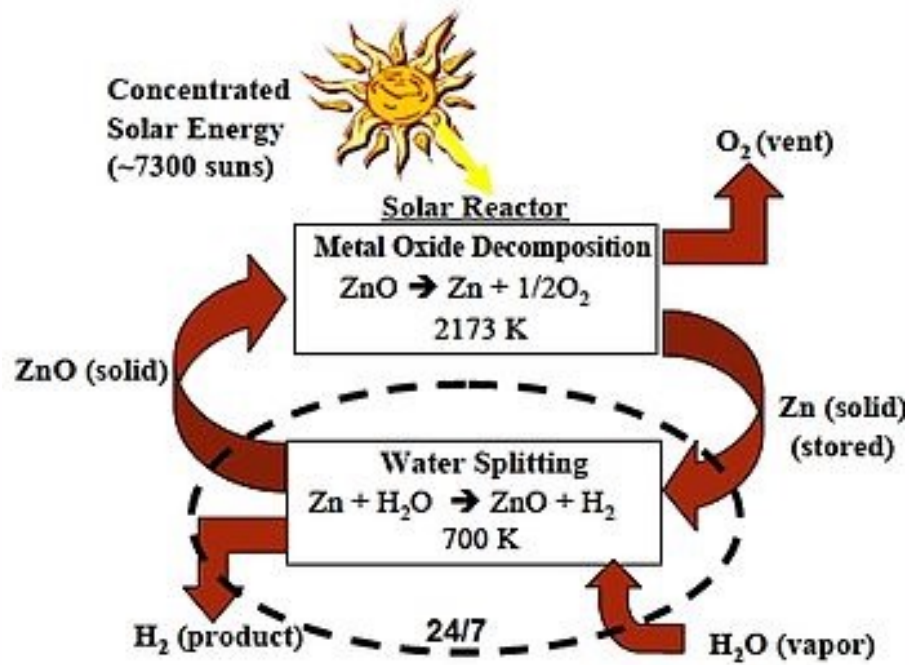
Overview of different redox reactions

[UNLV](http://www.hydrogen.energy.gov/pdfs/review06/pd_10_weimer.pdf) (http://www.hydrogen.energy.gov/pdfs/review06/pd_10_weimer.pdf)

[PSI/ETHZ](https://www.psi.ch/media/producing-pure-recycling-zinc-with-concentrated-solar-energy) (<https://www.psi.ch/media/producing-pure-recycling-zinc-with-concentrated-solar-energy>)

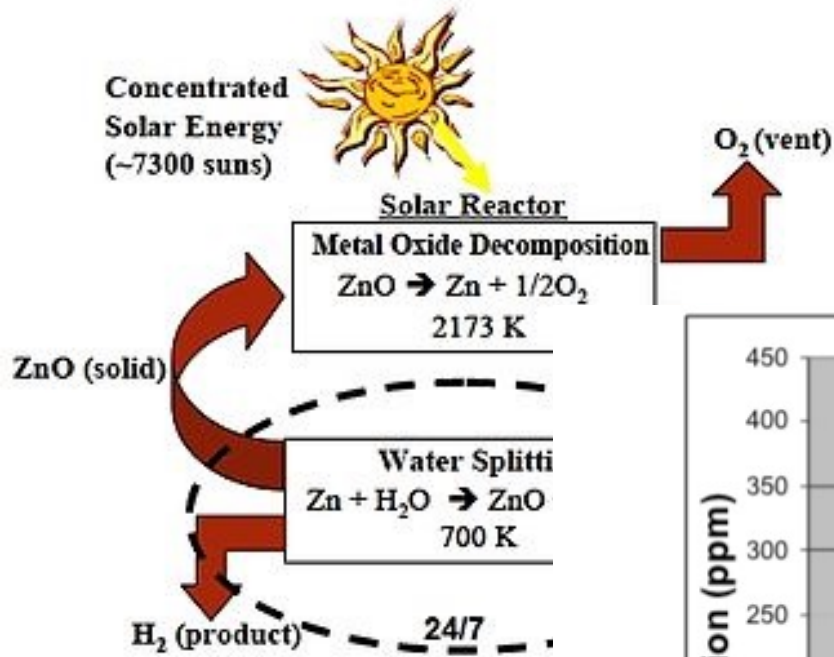
[France Solar Furnace Talk](http://sfera.sollab.eu/downloads/Conferences/SolarPACES_2012_SFERA_Meier.pdf) (http://sfera.sollab.eu/downloads/Conferences/SolarPACES_2012_SFERA_Meier.pdf)

Zn => ZnO Cycle (http://en.wikipedia.org/wiki/Zinc%E2%80%93zinc_oxide_cycle)

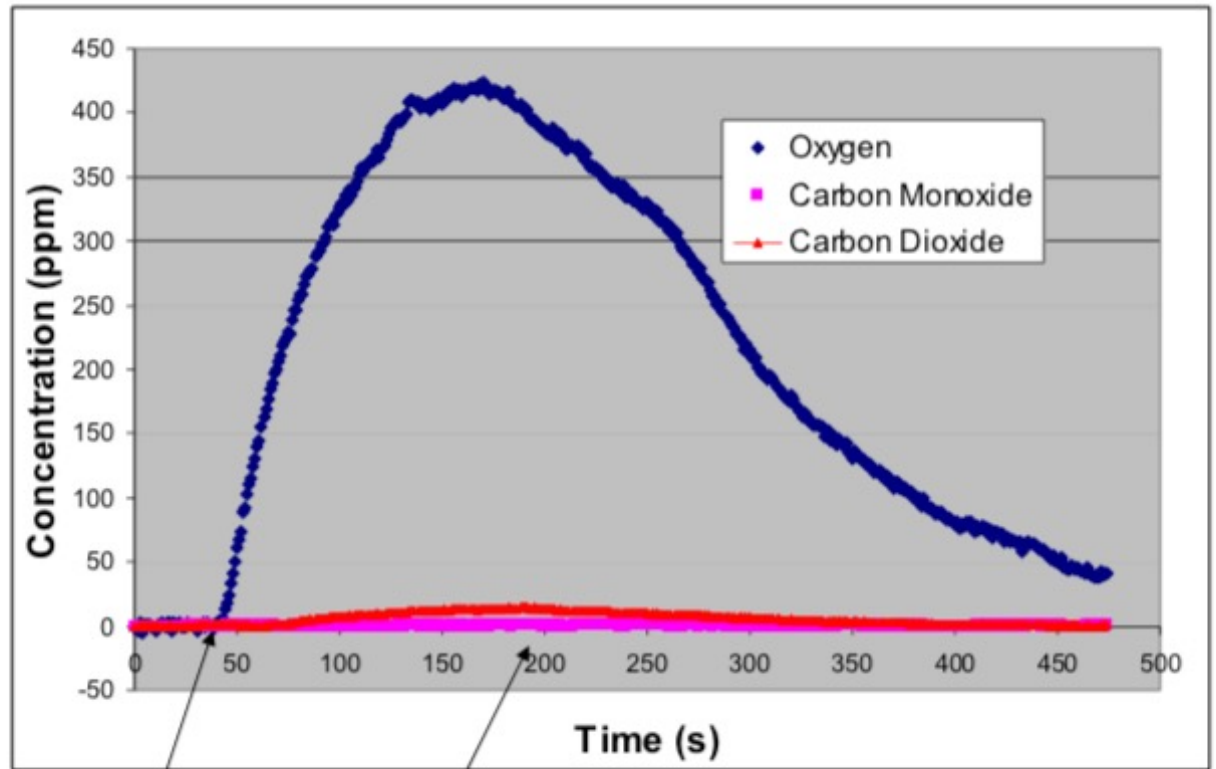


Aerosol Reactor





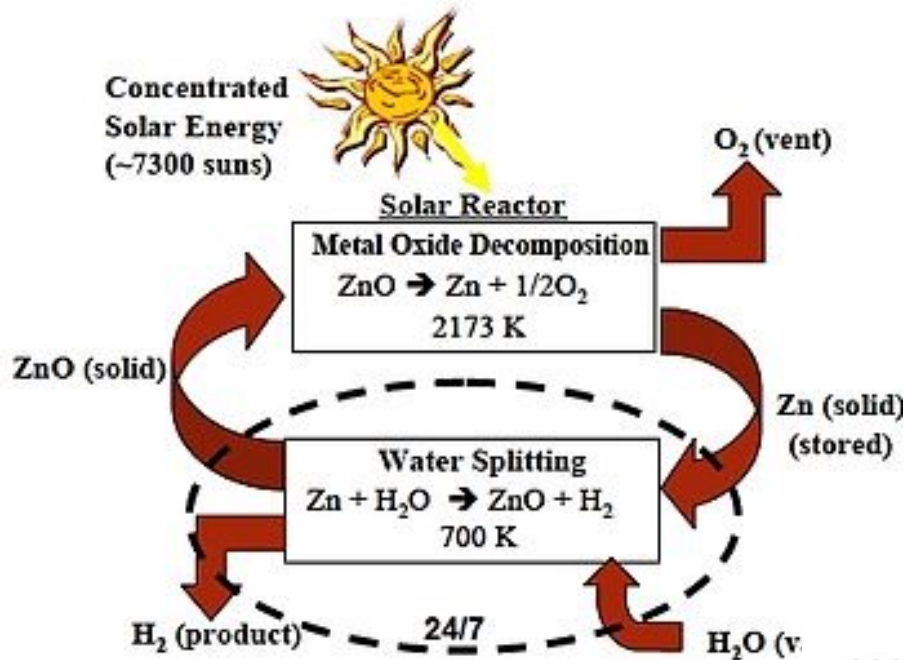
Reduction



Feeding initiated Feeding stopped

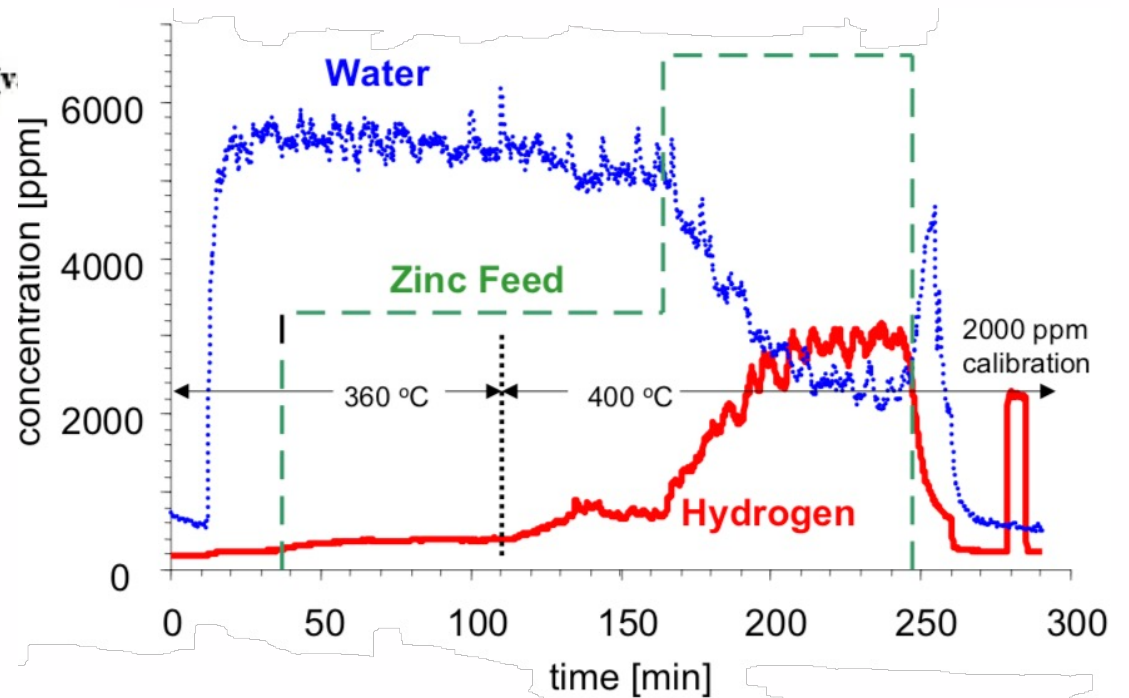
- Demonstration of rapid (< 1s) ZnO dissociation for Zn/ZnO cycle
- Highest conversion ever (>40%) for thermal dissociation of ZnO
- Conversion consistent with kinetic model

[Zn => ZnO Cycle](http://en.wikipedia.org/wiki/Zinc%E2%80%93zinc_oxide_cycle) (http://en.wikipedia.org/wiki/Zinc%E2%80%93zinc_oxide_cycle)



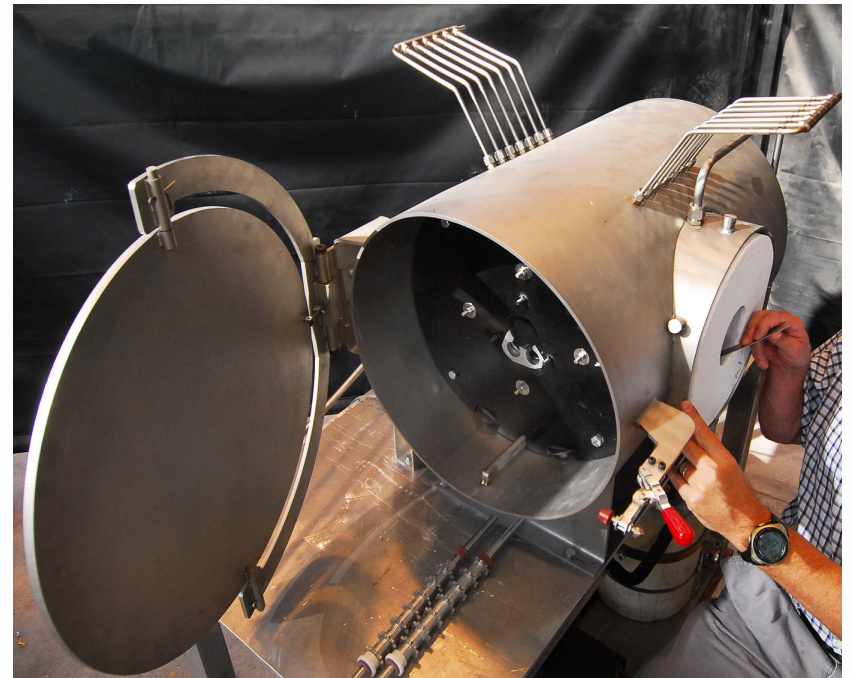
57 to 68 % Efficiency

Oxidation





Sandia Solar Furnace

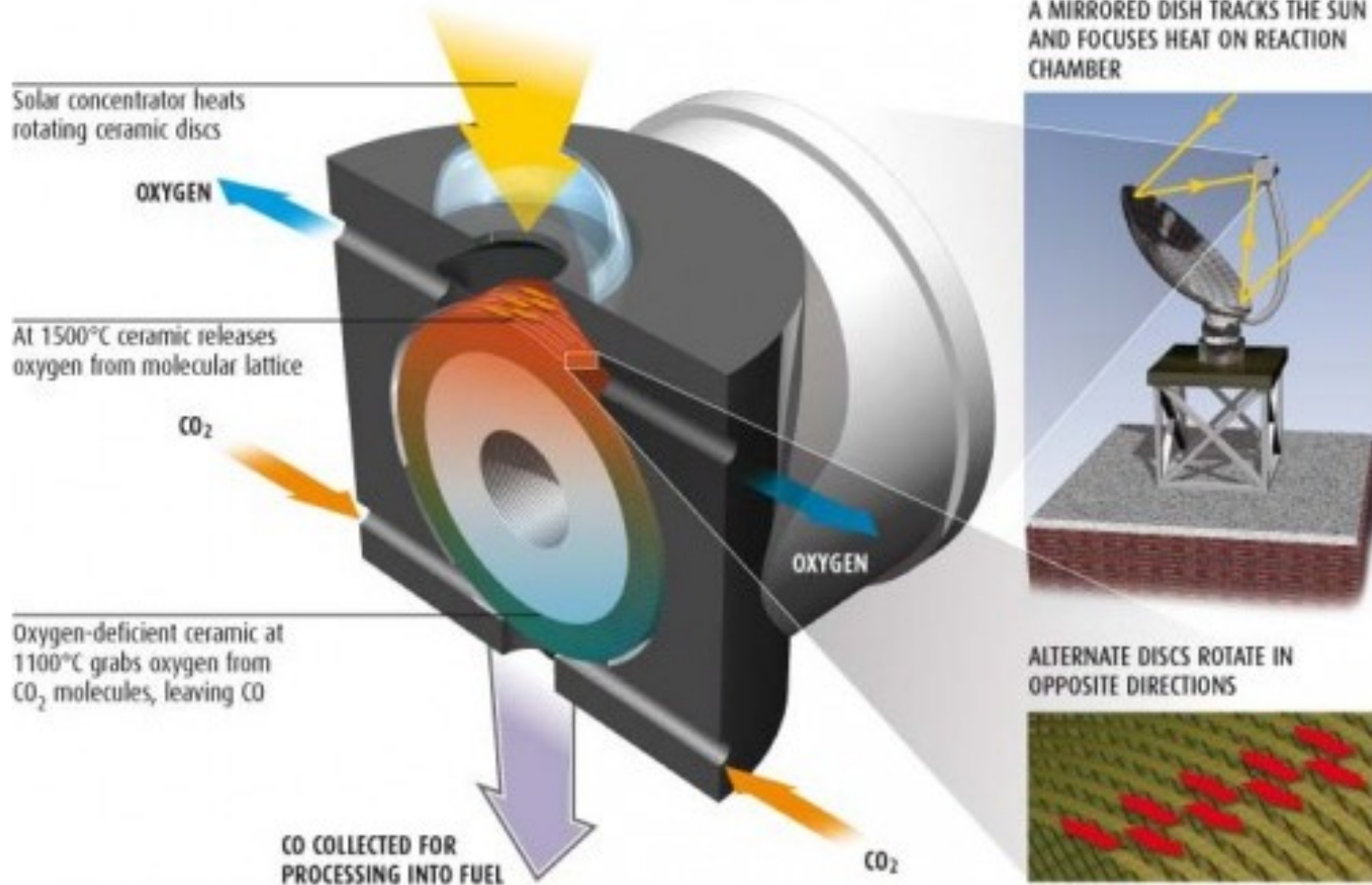


**Counter Rotating Ring Reactor
(Recovers Heat)**

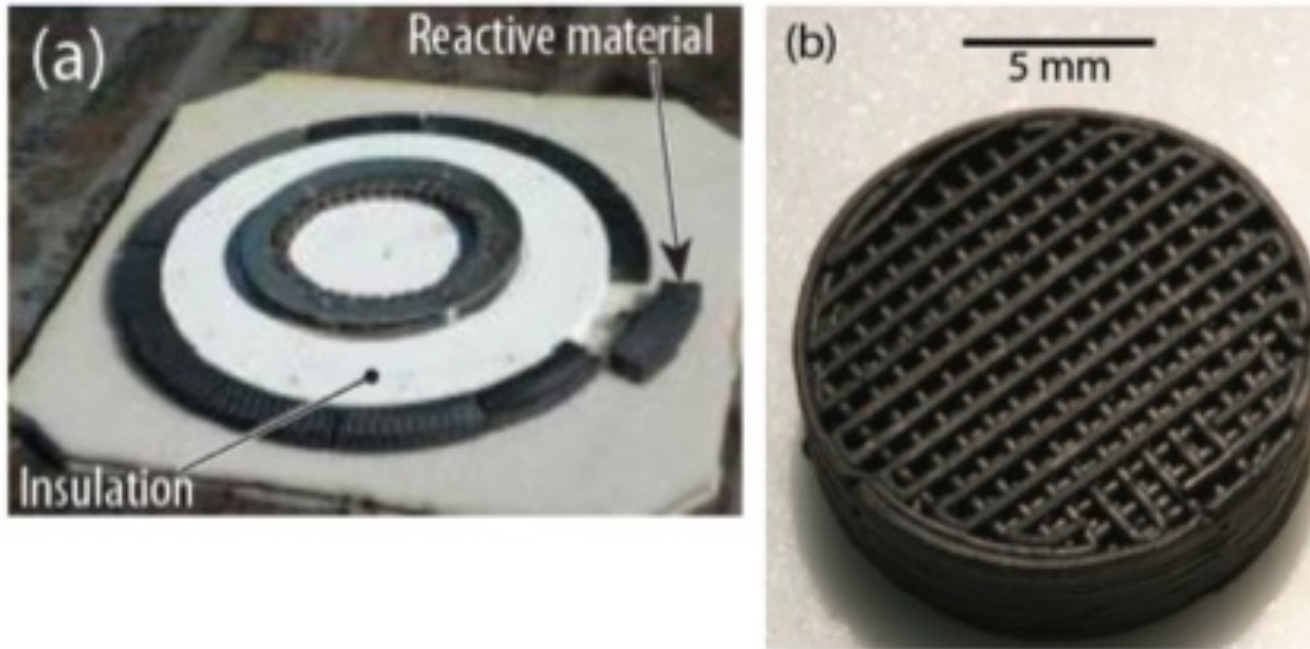
Counter Rotating Ring Reactor (Recovers Heat)

CO₂ SPLITTER

Heat from the sun provides energy to break down CO₂, releasing CO which can then be used to produce synthetic fuels

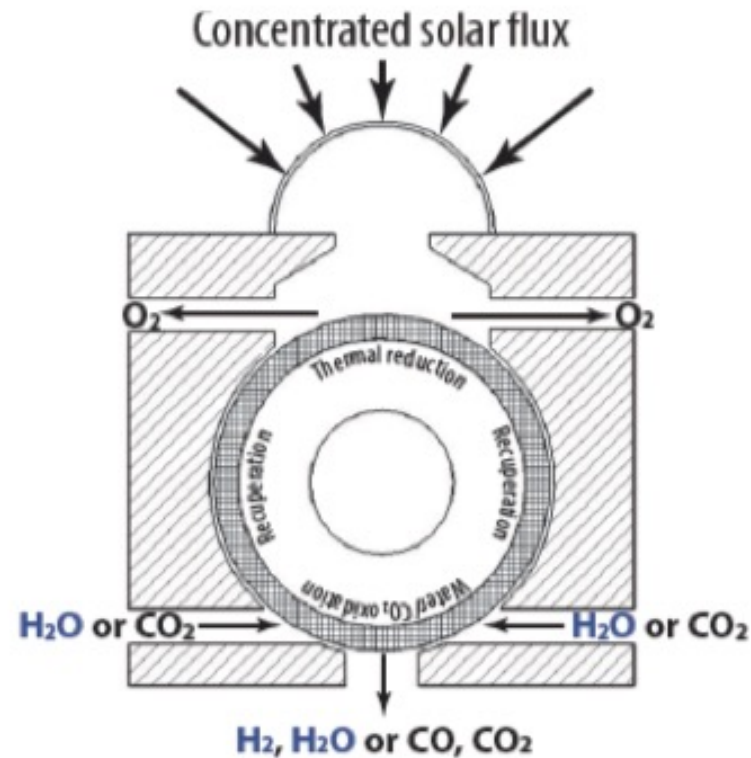


Counter Rotating Ring Reactor (Recovers Heat)



(a) The CR5 device employs a mixed valent metal oxide, arranged around the perimeter of a rotating ring. Shown here are iron oxides supported in a yttria stabilized zirconia (YSZ) matrix that exploit the "ferrite" thermochemical cycle in which Fe^{+3} reduces to Fe^{+2} and reoxidizes back to Fe^{+3} . (b) A monolithic test sample fabricated from a cobalt ferrite/YSZ composite. Its lattice structure provides high geometric surface area.

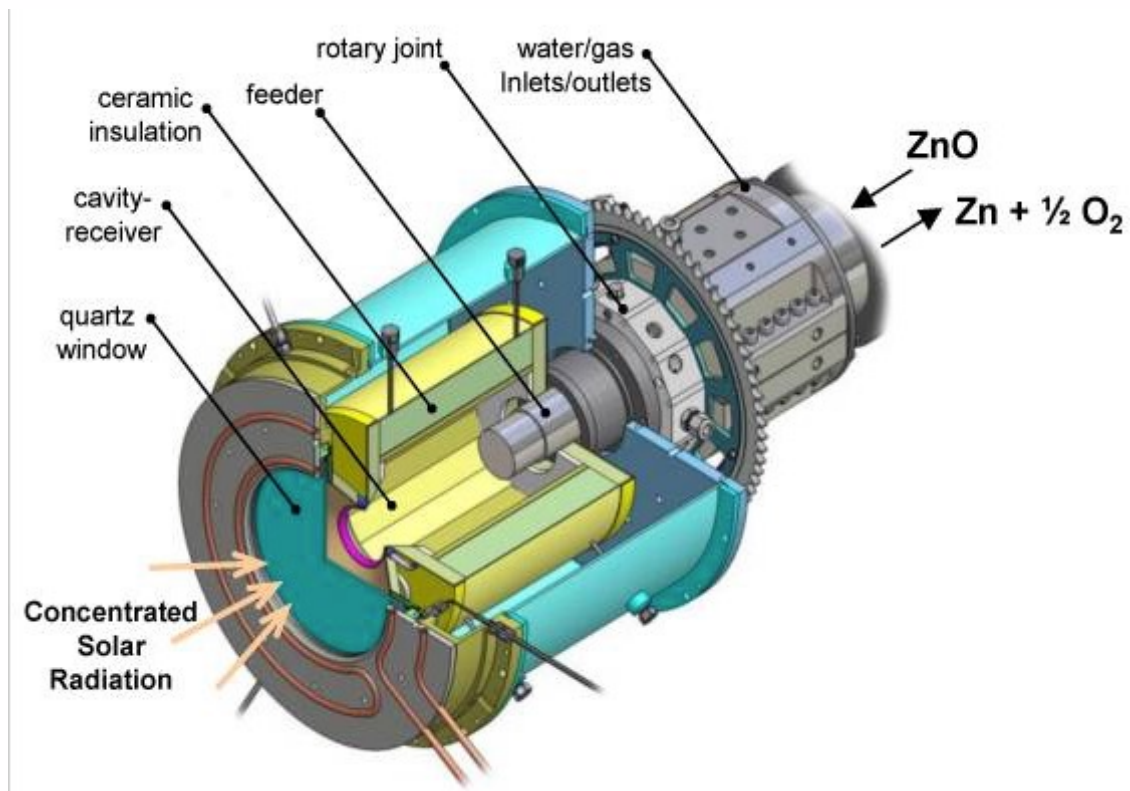
Counter Rotating Ring Reactor (Recovers Heat)



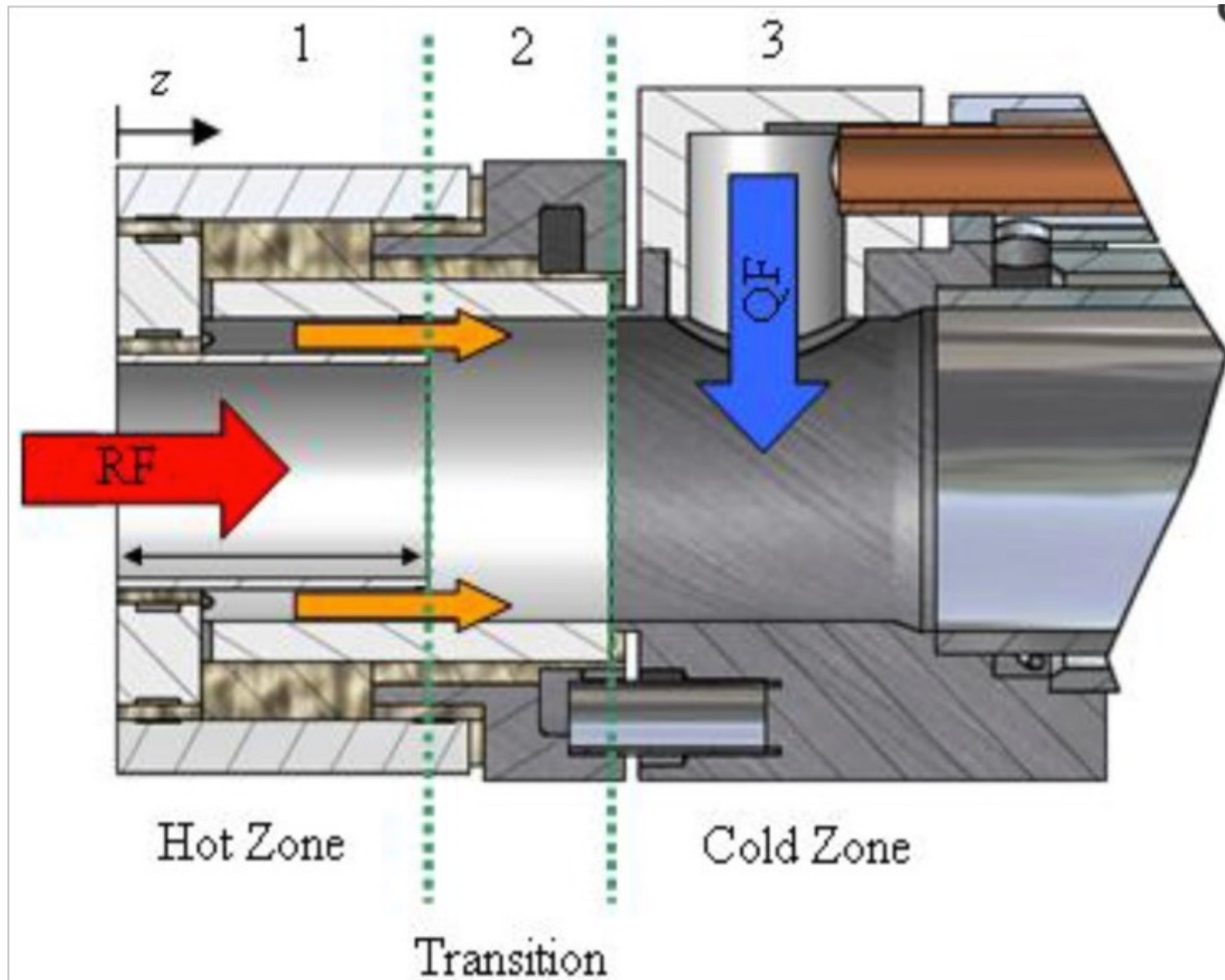
Side view of the CR5 showing a single ring. In the top chamber, concentrated solar irradiation heats the ferrite to ~1500 °C and thermally reduces the iron, driving off some oxygen. In the opposite chamber, the oxygen-deficient reduced ferrite is exposed to either water vapor or carbon dioxide at a lower temperature to produce either hydrogen or carbon monoxide. Heat is recuperated between the ceramic oxide materials as they leave the two reactant chambers by counter rotating the reactive rings relative to one another.

Swiss Aerosol Reactor ETHZ/PSI

Zn => ZnO Cycle
(Solar Driven Redox Reactions)



Need to rapidly quench and dilute Zn + O₂ mixture



http://sfera.sollab.eu/downloads/Conferences/SolarPACES_2012_SFERA_Meier.pdf

Outline

100 kW Pilot Plant at MWSF

- Installation
- Commissioning

Scientific Background

- Solar ZnO dissociation at 2000 K
- Solar reactor technology

Experimental Results

- Solar reactor experiments
- Flux measurements

Outlook / Acknowledgements



CNRS 1 MW Solar Furnace
Odeillo, France



Table 1. Major assumptions and findings for cost and efficiency of the Zn/ZnO cycle from Steinfeld [5] and Charvin et al. [22].

	Steinfeld (792 kg/hr)[5]	Charvin et al., (250 kg/hr)[22]	Charvin et al., (50 kg/hr)[22]
<i>Plant size, energy and mass flows</i>			
Concentration ratio, C	5,000 suns	5,000 suns	5,000 suns
Solar plant size (power input to solar reactor) [MW_{th}]	90	55	11
Beam irradiation [$kWh_{th}/m^2 \cdot yr$]	2300	2000	2000
Heliostat area [m^2]	155,172	54,800	10,960
<i>Efficiencies</i>			
Optical efficiency of solar concentration system, η_{optics}	58%	68.4%	not included
Cycle efficiency, η_{cycle}	29%	30.4%	not included
Global efficiency, η_{global}	17%	20.8%	not included
<i>Assumptions</i>			
Pump or work input	none	none	none
Solar step temperature [K]	2300	2000	2000
Reactor re-radiation losses	accounted for	accounted for	accounted for
Endothermic reaction losses	accounted for	accounted for	accounted for
Heat recovery from quenching after first step	no heat recovery	heat recovery	heat recovery
Recovery of heat of exothermic reaction	no heat recovery	complete heat recovery	complete heat recovery
Efficiency of separation of Zn & O_2	no recombination	20% recombination	20% recombination
Efficiency of hydrolysis step	complete hydrolysis	complete hydrolysis	complete hydrolysis
Hydrogen energy content [kJ/mol]	241(LHV)	286 (HHV)	286 (HHV)
<i>Costs</i>			
Heliostat field [MS , assuming $\$150/m^2$]	23.28	8.22	1.65
Land [MS , assuming $\$1/m^2$]	not included	0.28	0.06
Tower [MS]	3.60	1.50	1.00
Tower reflector and CPCs [MS]	5.30	not included	not included
Solar receiver-reactor + periphery [MS]	7.00	2.00	1.00
Quencher [MS]	3.00	not included	not included
Hydrolyzer [MS]	4.00	1.00	0.50
Balance of plant, indirects, contingency [MS]	8.90	2.00	1.00
H_2 storage [MS]	not included	1.00	0.50
Total capital cost for solar H_2 [MS]	55.08	16.00	5.70
<i>Annual Cost</i>			
Annual fixed charge rate [MS]	15%	not included	not included
Capital cost for solar H_2 [MS]	8.26	not included	not included
O&M cost for solar H_2 [MS]	1.10	1.01	0.42
Total annual cost for solar H_2 [MS]	9.36	1.01	0.42
<i>Hydrogen production rate [kg/hr]</i>			
	792	250	50
<i>Hydrogen cost [$\\$/kg$]</i>			
	5.02	7.98	14.75

ES2010- 0

RENEWABLE HYDROGEN FROM THE Zn/ZnO SOLAR THERMOCHEMICAL CYCLE: A COST AND POLICY ANALYSIS

Julia F. Haltiwanger*
Mechanical Engineering
University of Minnesota
Minneapolis, Minnesota 55407

Jane H. Davidson
Mechanical Engineering
University of Minnesota
Minneapolis, Minnesota 55407

Elizabeth J. Wilson
Humphrey Institute of Public Affairs
University of Minnesota
Minneapolis, Minnesota 55407

steam methane reforming (SMR).

Prior work projects that hydrogen produced by the zinc/zinc-oxide cycle will cost between $\$5.02$ and $\$14.75/kg$, compared to $\$2.40$ to $\$3.60/kg$ for steam methane reforming. Overcoming this cost difference would require a carbon tax of $\$119$ to $\$987/tCO_2$, which is significantly higher than is likely to be implemented in most countries. For the technology to become cost competitive, incentive policies that lead to early implementation of solar hydrogen plants will be necessary to allow the experience effect to draw down the price. Under such policies, a

Zn => ZnO Cycle (Solar Driven Redox Reactions)

Julia Haltiwanger Nicodemus
Engineering Studies
Lafayette College
Easton, PA
Email: nicodemj@lafayette.edu

Morgan McGuinness
Physics and Math
Lafayette College
Easton, PA

To put these costs in perspective, comparison to the cost of natural gas is appropriate. The industrial cost of natural gas is \$0.246/kg, or, on an energy basis, \$0.0046/MJ¹. Because the heating value of natural gas is about twice that of syngas, costs are better compared on an energy basis. Table 2 lists the costs of solar syngas for 100MW_{th} and 500MW_{th} plants, for low cost water (\$0.01/L) and high cost water (\$0.1/L) for all six carbon pricing scenarios. Assuming low cost water and CO₂ captured from a power plant with no additional costs, the cost of solar syngas is 4 and 5 times the cost of natural gas for the 100MW_{th} and 500MW_{th} plants, respectively.

In this analysis, we will consider six possible scenarios for pricing CO₂: carbon capture from a power plant (CC), carbon capture plus the social cost of carbon (CC+SCC), carbon capture plus a carbon tax (CC+tax), CO₂ supplied by a chemical supplier (Chem), CO₂ from a chemical supplier plus the social cost of carbon (Chem+SCC), and CO₂ from a chemical supplier plus a carbon tax (Chem+tax).

TABLE 2: SYNGAS COST PER MEGAJOULE (MJ)

	100MW _{th}		500MW _{th}	
	low H ₂ O cost	high H ₂ O cost	low H ₂ O cost	high H ₂ O cost
CC	\$0.0246	\$0.0282	\$0.0190	\$0.0226
CC + SCC	\$0.0252	\$0.0288	\$0.0196	\$0.0232
CC + tax	\$0.0354	\$0.0390	\$0.0299	\$0.0334
Chem	\$0.0257	\$0.0293	\$0.0201	\$0.0237
Chem + SCC	\$0.0263	\$0.0299	\$0.0207	\$0.0243
Chem + tax	\$0.0365	\$0.0401	\$0.0310	\$0.0345

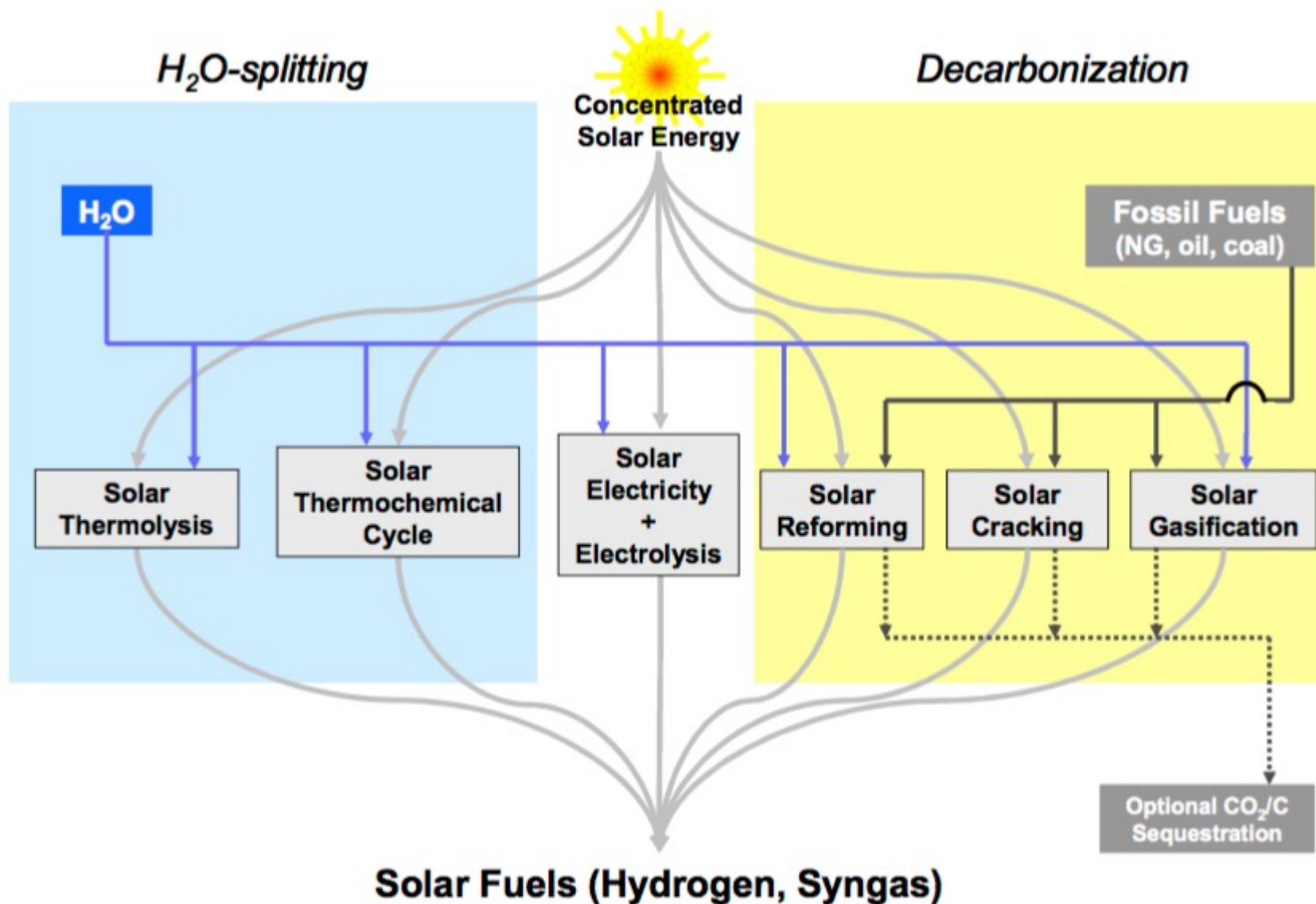


Fig. 2: Thermochemical routes for solar hydrogen production – Indicated is the chemical source of H_2 : H_2O for the solar thermolysis and the solar thermochemical cycles; fossil fuels for the solar cracking, and a combination of fossil fuels and H_2O for the solar reforming and gasification. For the solar decarbonization processes, optional CO_2/C sequestration is considered. All of those routes involve energy consuming (endothermic) reactions that make use of concentrated solar radiation as the energy source of high-temperature process heat. Adapted from [1,2].³⁰³

Cite this: *Energy Environ. Sci.*, 2011, **4**, 73

www.rsc.org/ees

REVIEW

Solar-driven gasification of carbonaceous feedstock—a review

Nicolas Piatkowski,^a Christian Wieckert,^b Alan W. Weimer^c and Aldo Steinfeld^{*ab}

Received 28th July 2010, Accepted 28th September 2010

DOI: 10.1039/c0ee00312c

Given the future importance of solid carbonaceous feedstocks such as coal, coke, biomass, bitumen, and carbon-containing wastes for the power and chemical industries, gasification technologies for their thermochemical conversion into fluid fuels are developing rapidly. Solar-driven gasification, in which concentrated solar radiation is supplied as the energy source of high-temperature process heat to the endothermic reactions, offers an attractive alternative to conventional autothermal processes. It has the potential to produce high-quality synthesis gas with higher output per unit of feedstock and lower specific CO₂ emissions, as the calorific value of the feedstock is upgraded through the solar energy input by an amount equal to the enthalpy change of the reaction. The elimination of an air separation unit further facilitates economic competitiveness. Ultimately, solar-driven gasification is an efficient means of storing intermittent solar energy in a transportable and dispatchable chemical form. This review article develops some of the underlying science, examines the thermodynamics and kinetics of the pertinent reactions, and describes the latest advances in solar thermochemical reactor technology.

Alan W. Weimer

Sears Professor • C2B2 Executive Director

✉ alan.weimer@colorado.edu

☎ (303) 492-3759

- 📄 [Curriculum Vitae](#)
- 📄 [Google Scholar Profile](#)
- 📄 [Weimer Research Group](#)

JSCBB C224

Education

B.S., University of Cincinnati (1976)

M.S., Ph.D., University of Colorado (1978, 1980)

Dow Chemical Company(1980-1996)



Solar Thermochemical Production of Fuels

Anton Meier^{1, a} and Aldo Steinfeld^{1, 2, b}

¹Solar Technology Laboratory, Paul Scherrer Institute, 5232 Villigen PSI, Switzerland

²Department of Mechanical and Process Engineering, ETH Zurich, 8092 Zurich, Switzerland

^aanton.meier@psi.ch, ^baldo.steinfeld@ethz.ch

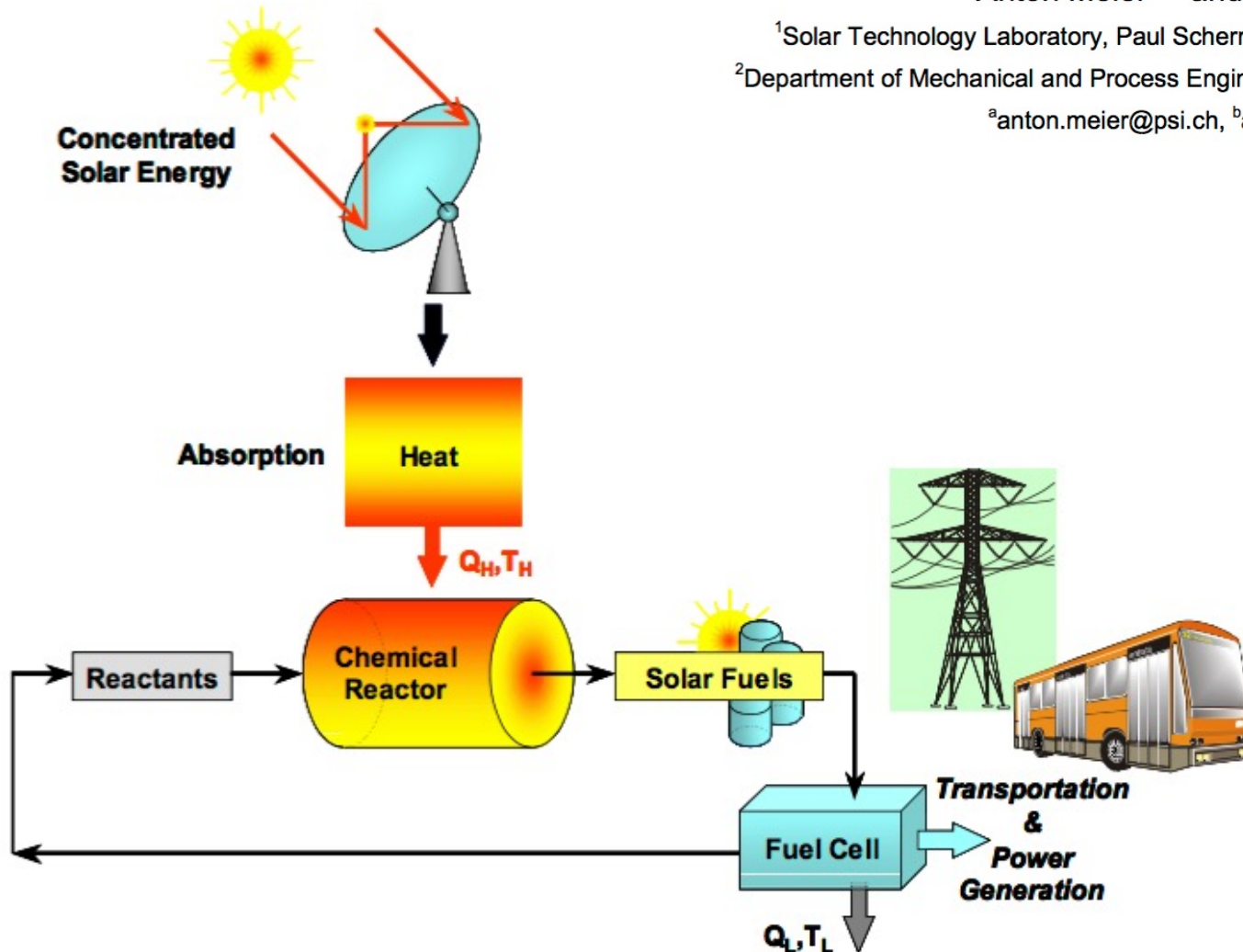


Fig. 1: Energy conversion into solar fuels for transportation and power generation – Concentrated solar radiation is used as the energy source of high-temperature process heat for driving thermochemical reactions towards the production of storable and transportable fuels. Adapted from [1].



Fig. 8: 1 MW_{th} solar plant in Broomfield, Colorado – The plant uses an array of 2700 mirrors to concentrate sunlight on a 20-meter-tall solar tower to produce heat needed to drive the chemical reactor. From [43].



California Mojave Desert

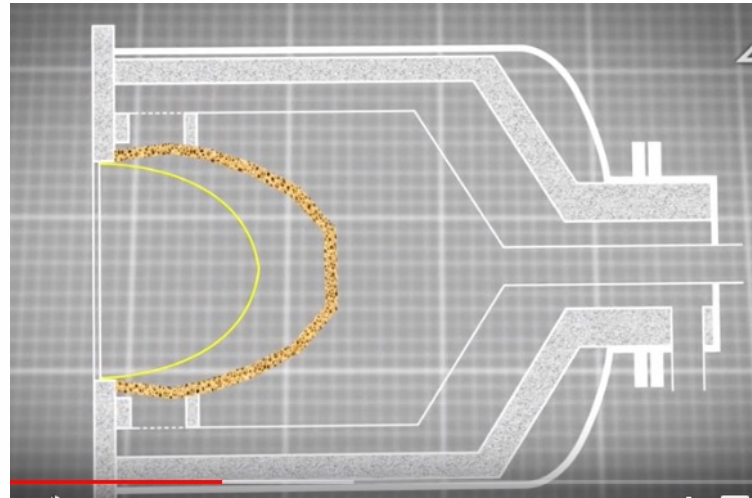


Elevation view of the Odeillo MWSF facility

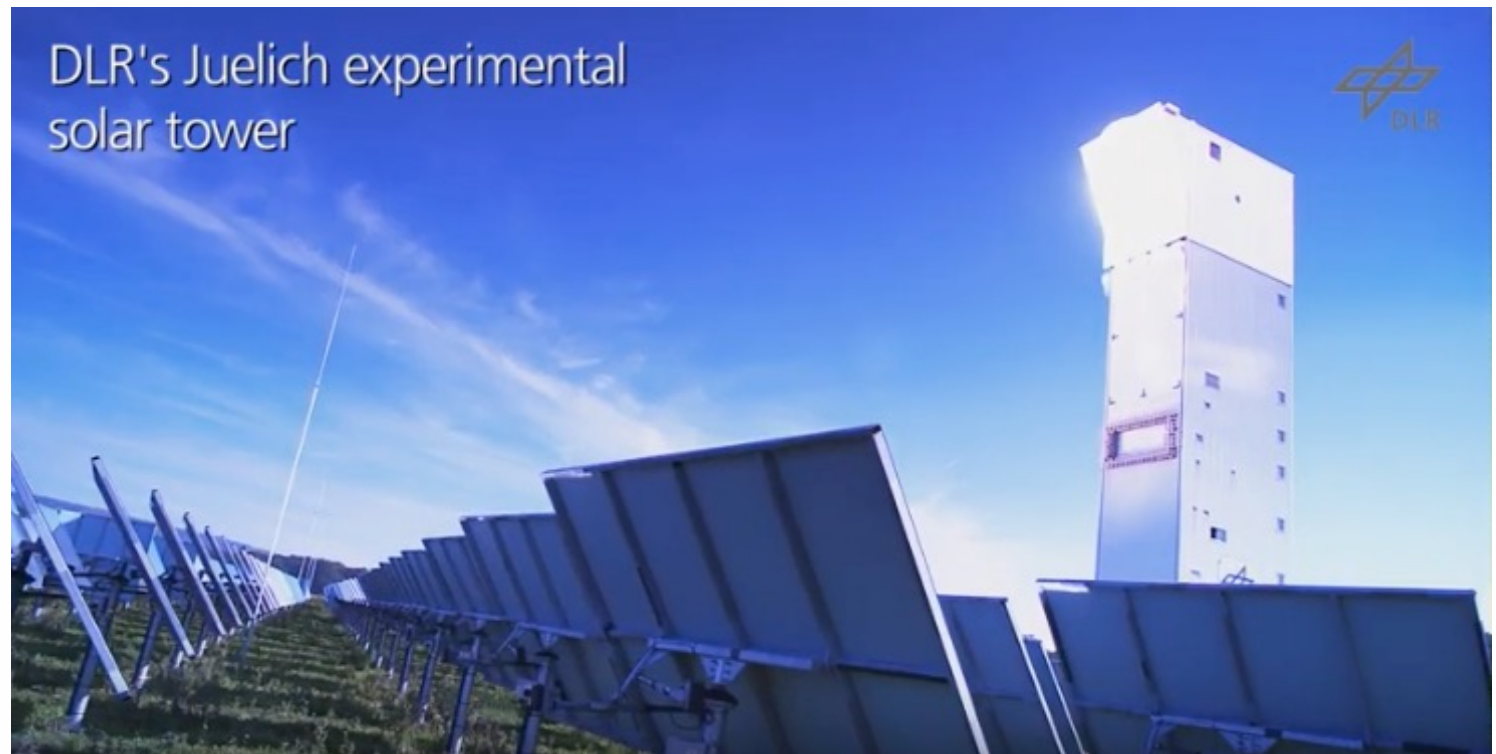
Odeillo, France



Hydrogen Production in Spain



DLR Institute

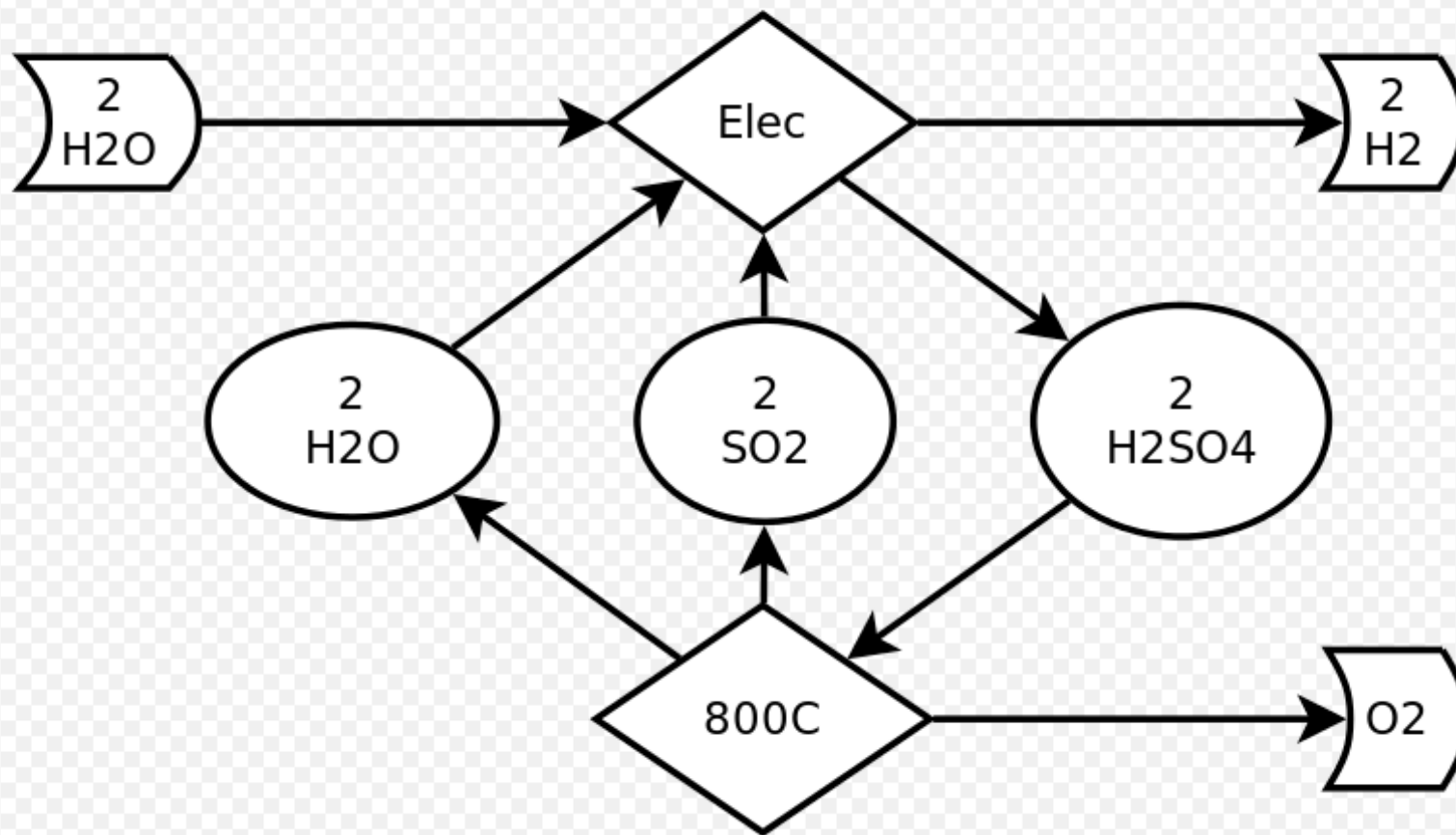




Crescent Dunes Nevada

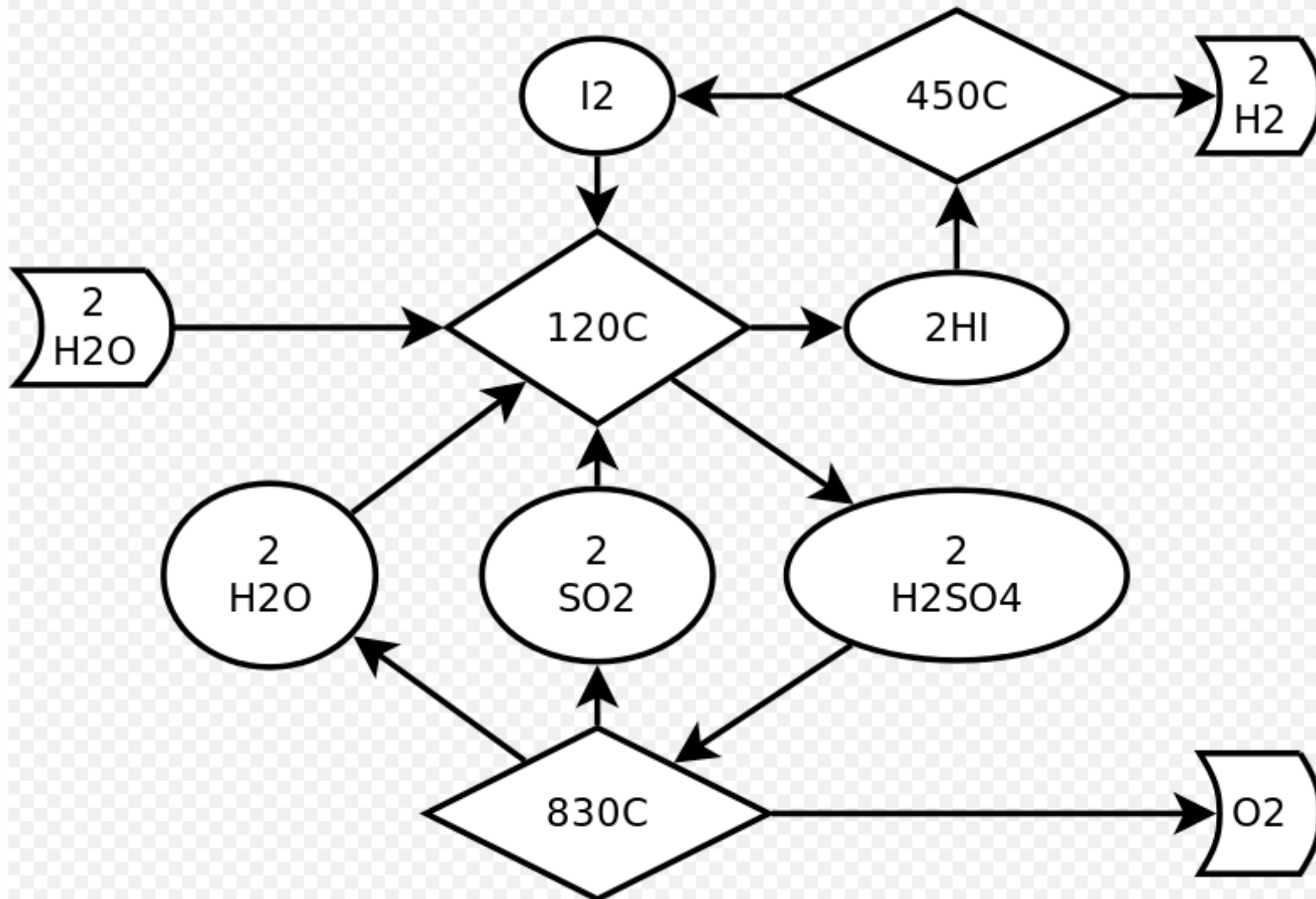


Hybrid Sulfur Cycle



Electricity Needed (about 1/2 of electrolysis)

Sulfur-Iodine Cycle



[Sandia Study \(no electricity needed\)](#)

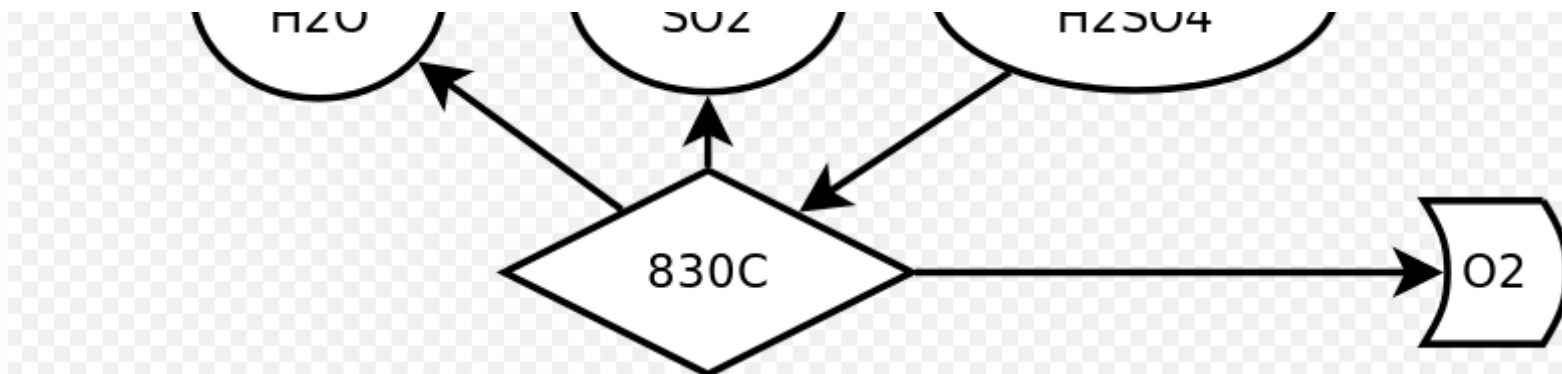
Sulfur-Iodine Cycle



Advantages and disadvantages [\[edit \]](#)

The characteristics of the S-I process can be described as follows:

- All fluid (liquids, gases) process, therefore well suited for continuous operation;
- High utilization of heat predicted (about 50%), but very high temperatures required (at least 850 °C);
- Completely closed system without byproducts or effluents (besides hydrogen and oxygen);
- Corrosive reagents used as intermediaries (iodine, sulfur dioxide, hydriodic acid, sulfuric acid); therefore, advanced materials needed for construction of process apparatus;
- Suitable for application with solar, nuclear, and hybrid (e.g., solar-fossil) sources of heat;
- More developed than competitive thermochemical processes (but still requiring significant development to be feasible on large scale).



Hydrogen Production by the Solar-powered Hybrid Sulfur Process: Analysis of the Integration of the CSP and Chemical Plants in Selected Scenarios

Raffaele Liberatore¹, Michela Lanchi¹ and Luca Turchetti^{1, a)}

¹ENEA - Italian National Agency for New Technologies, Energy and Sustainable Economic Development, via Anguillarese 301 - 00123 Rome, Italy.

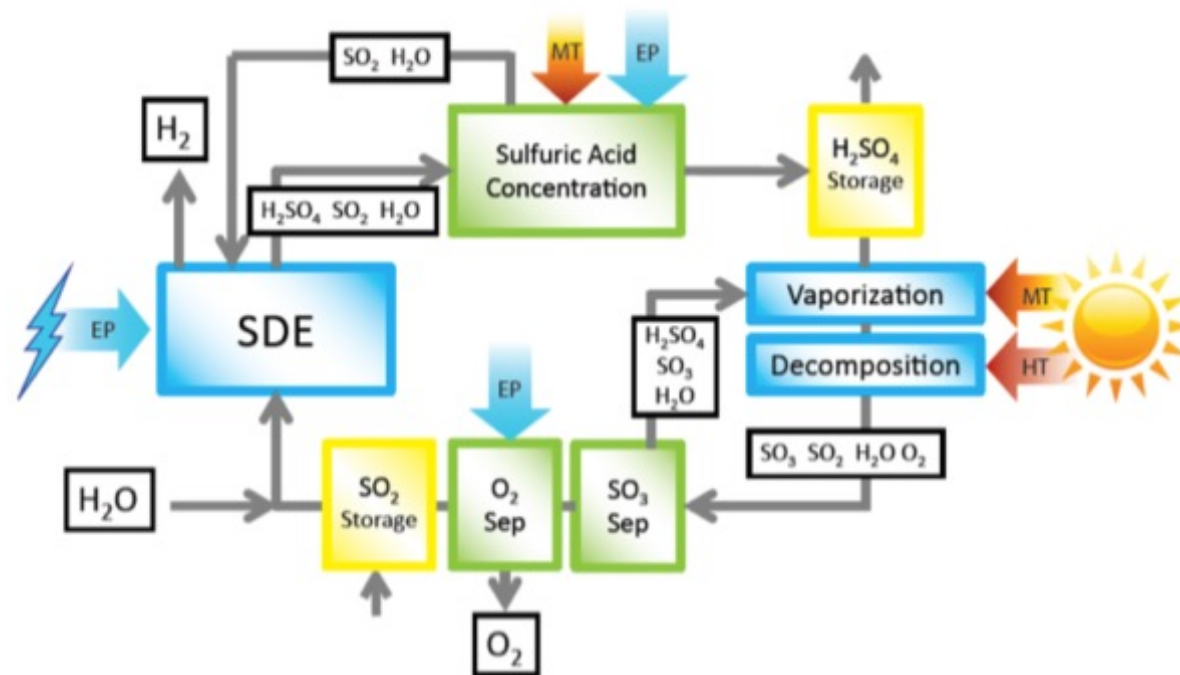


FIGURE 1. Simplified block diagram of the HyS process considered here. The main energy input type required by the different process blocks is highlighted (MT: medium temperature heat; HT: high temperature heat; EP: electric power; SDE: sulfur depolarized electrolyzer).

Hydrogen Production by the Solar-powered Hybrid Sulfur Process: Analysis of the Integration of the CSP and Chemical Plants in Selected Scenarios

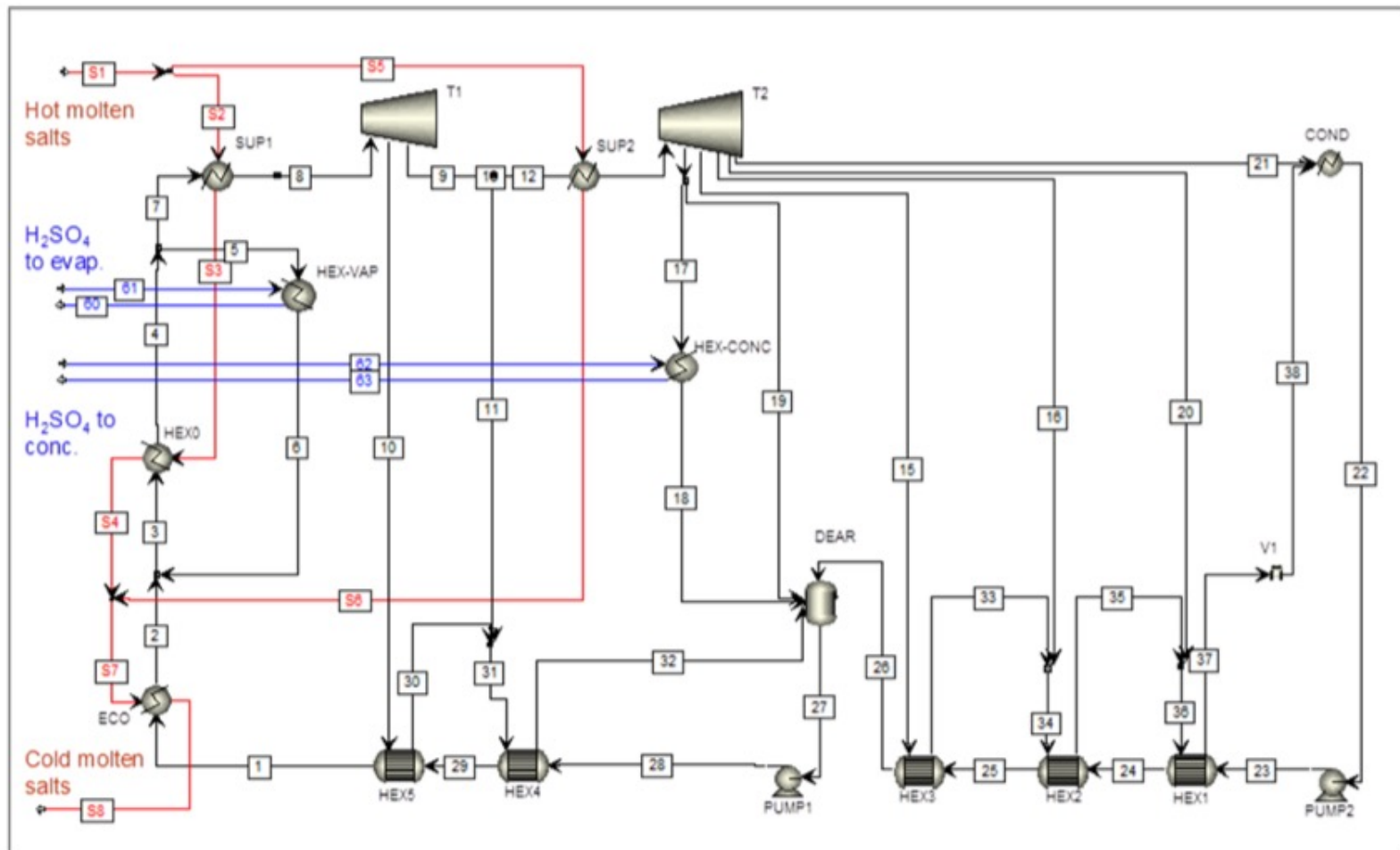


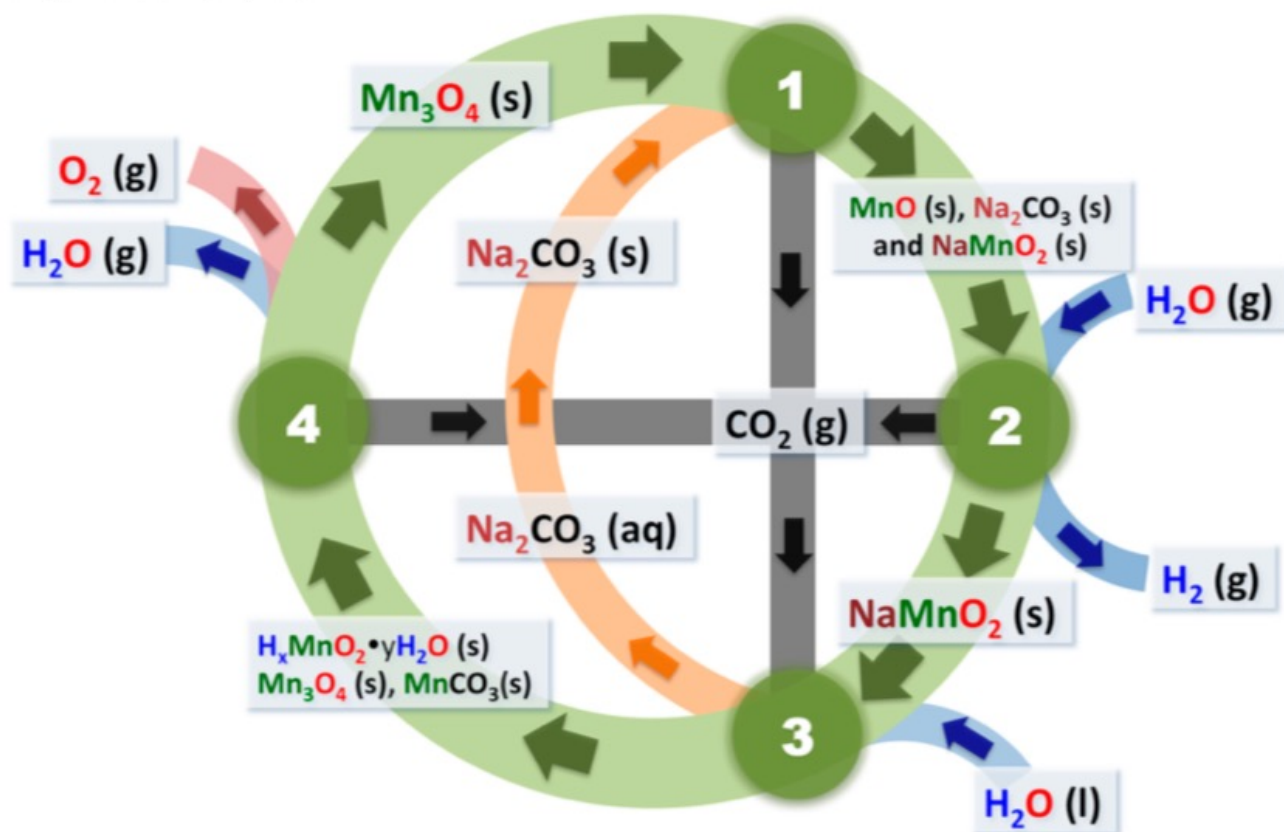
FIGURE 2. Process scheme of the Rankine cycle powered by molten salts sensible heat. In Case 1a (8 hours solar operation) both the heat exchangers HEX-VAP and HEX-CONC work, while in Case 1b (16 hours operation) only the HEX-CONC is in operation. In Case 2 the heat exchangers HEX-VAP and HEX-CONC are not present. HEX: exchangers; HEX-VAP: evaporator for the H₂SO₄ evaporation in the discontinuous step of the cycle; HEX-CONC: evaporator for the H₂SO₄ concentration in the continuous step; DEAR: degasifier; COND: condenser; T1, T2: steam turbines; ECO: economizer; SUP: super-heater; V: valve.

Low-temperature, manganese oxide-based, thermochemical water splitting cycle

Bingjun Xu, Yashodhan Bhawe, and Mark E. Davis¹

Chemical Engineering, California Institute of Technology, Pasadena, CA 91125

Contributed by Mark E. Davis, April 17, 2012 (sent for review April 5, 2012)



Step	Reaction	Temp (°C)
1	$3\text{Na}_2\text{CO}_3(\text{s}) + 2\text{Mn}_3\text{O}_4(\text{s}) \rightarrow 4\text{NaMnO}_2(\text{s}) + 2\text{CO}_2(\text{g}) + 2\text{MnO}(\text{s}) + \text{Na}_2\text{CO}_3$	850
2	$2\text{MnO}(\text{s}) + \text{Na}_2\text{CO}_3(\text{s}) + \text{H}_2\text{O}(\text{g}) \rightarrow \text{H}_2(\text{g}) + \text{CO}_2(\text{g}) + 2\text{NaMnO}_2(\text{s})$	850
3	$6\text{NaMnO}_2(\text{s}) + ay\text{H}_2\text{O}(\text{l}) + (3 + b)\text{CO}_2(\text{g}) \rightarrow$ $3\text{Na}_2\text{CO}_3(\text{aq}) + a\text{H}_x\text{MnO}_2 \cdot y\text{H}_2\text{O}(\text{s}) + b\text{MnCO}_3(\text{s}) + c\text{Mn}_3\text{O}_4(\text{s})$	80
4	$a\text{H}_x\text{MnO}_2 \cdot y\text{H}_2\text{O}(\text{s}) + b\text{MnCO}_3 + \rightarrow$ $(2-c)\text{Mn}_3\text{O}_4(\text{s}) + ay\text{H}_2\text{O}(\text{g}) + b\text{CO}_2(\text{g}) + 0.5\text{O}_2(\text{g})$	850
Net	$\text{H}_2\text{O}(\text{g}) \rightarrow \text{H}_2(\text{g}) + 0.5\text{O}_2(\text{g})$	

a , b and c satisfy following relations: $a + b + 3c = 6$ and $(4-x)a + 2b + 8c = 18$

Fig. 2. Schematic representation of the low-temperature, Mn-based thermochemical cycle.

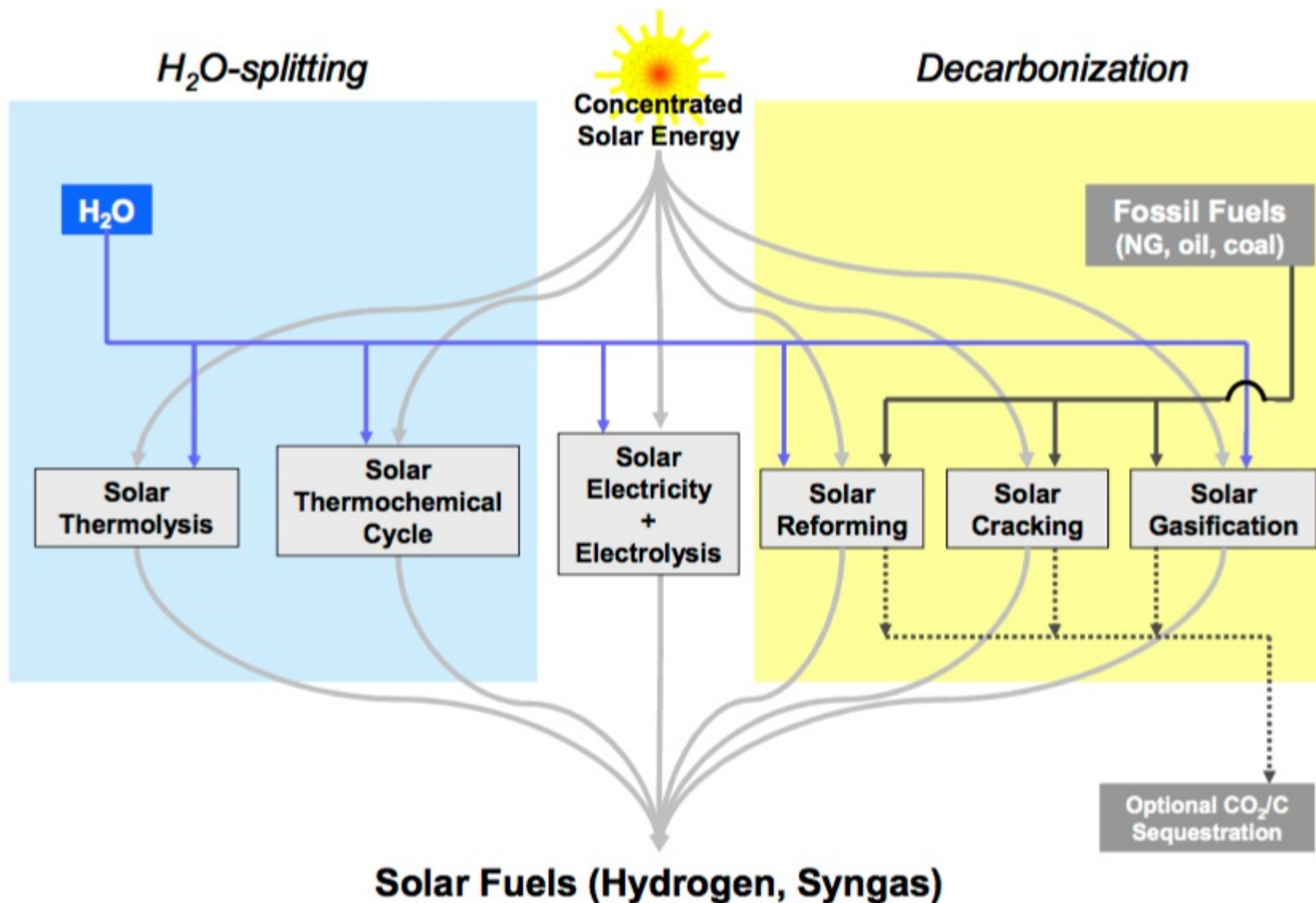


Fig. 2: Thermochemical routes for solar hydrogen production – Indicated is the chemical source of H_2 : H_2O for the solar thermolysis and the solar thermochemical cycles; fossil fuels for the solar cracking, and a combination of fossil fuels and H_2O for the solar reforming and gasification. For the solar decarbonization processes, optional CO_2/C sequestration is considered. All of those routes involve energy consuming (endothermic) reactions that make use of concentrated solar radiation as the energy source of high-temperature process heat. Adapted from [1,2].³²⁰

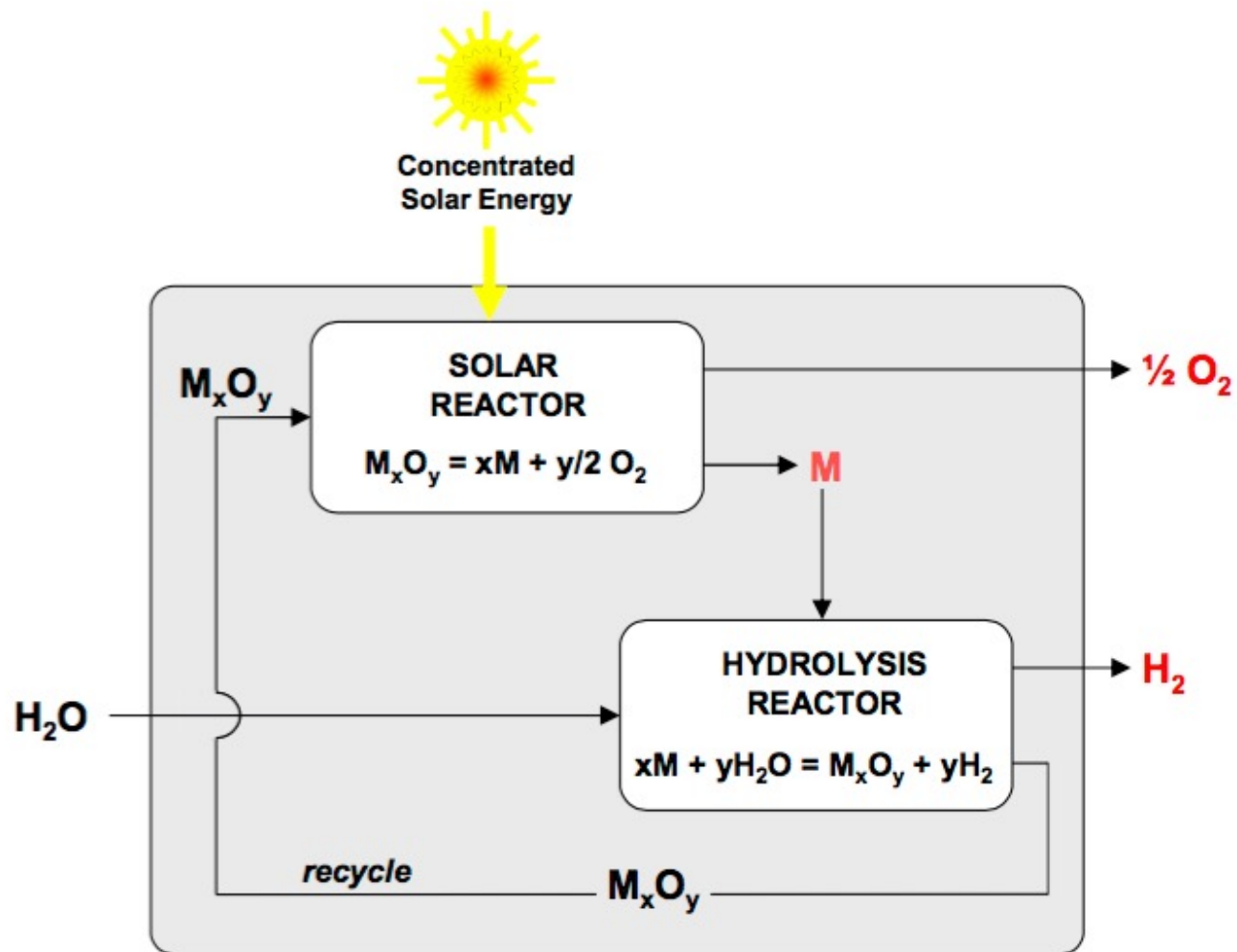


Fig. 3: Thermochemical route based on metal oxide redox reactions – The first step of the cycle is the solar thermal release of O_2 from the metal oxide (M_xO_y). This step requires very high temperatures. The second step is the reaction of the metal (M) with H_2O to form H_2 and the corresponding M_xO_y . This step proceeds at lower temperatures and does not require additional heating in some cases. Since H_2 and O_2 are formed in different steps, the need for high-temperature gas separation is thereby eliminated. This cycle was originally proposed for an iron oxide FeO/Fe_3O_4 redox system. Adapted from [1].

Mixed Iron Oxide Cycle. Other metal oxides such as manganese oxide or cobalt oxide, as well as mixed oxides redox pairs – mainly based on iron – have also been considered [17-20]. For example, a mixed iron oxide cycle was demonstrated within the European P&D project *HYDROSOL-2* [21]. Figure 5 depicts the monolithic dual chamber solar reactor. A quasi-continuous H_2 flow is produced by cyclic operation of the two reaction chambers through sequential oxidation and reduction steps at 800°C and 1200°C , respectively.

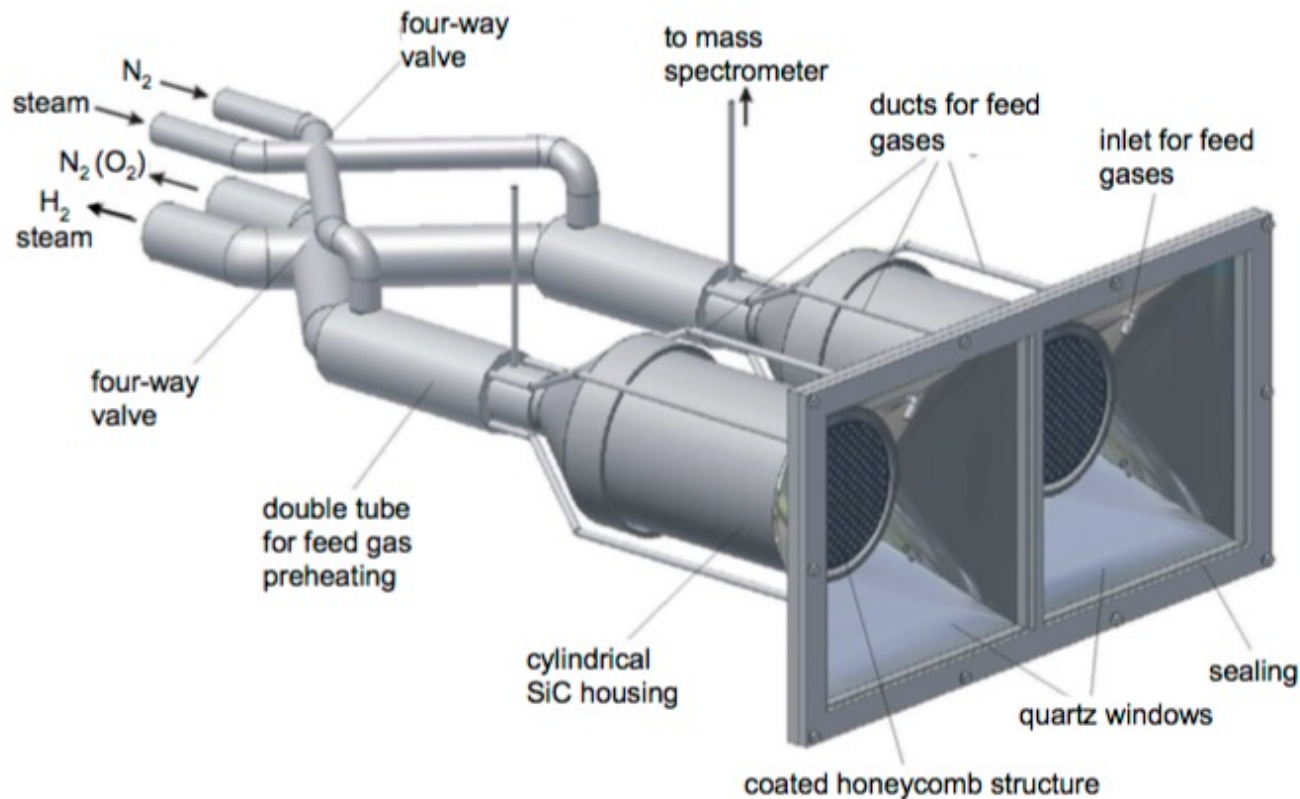


Fig. 5: Monolithic dual chamber solar receiver-reactor for continuous H_2 production – The concept features a closed receiver-reactor constructed from ceramic multi-channeled monoliths. Cyclic operation of the water-splitting and regeneration steps is established in two reaction chambers. Their individual temperature levels are controlled by focusing and defocusing heliostats. Adapted from [21].

Semi-continuous production of H_2 with dual reactors.

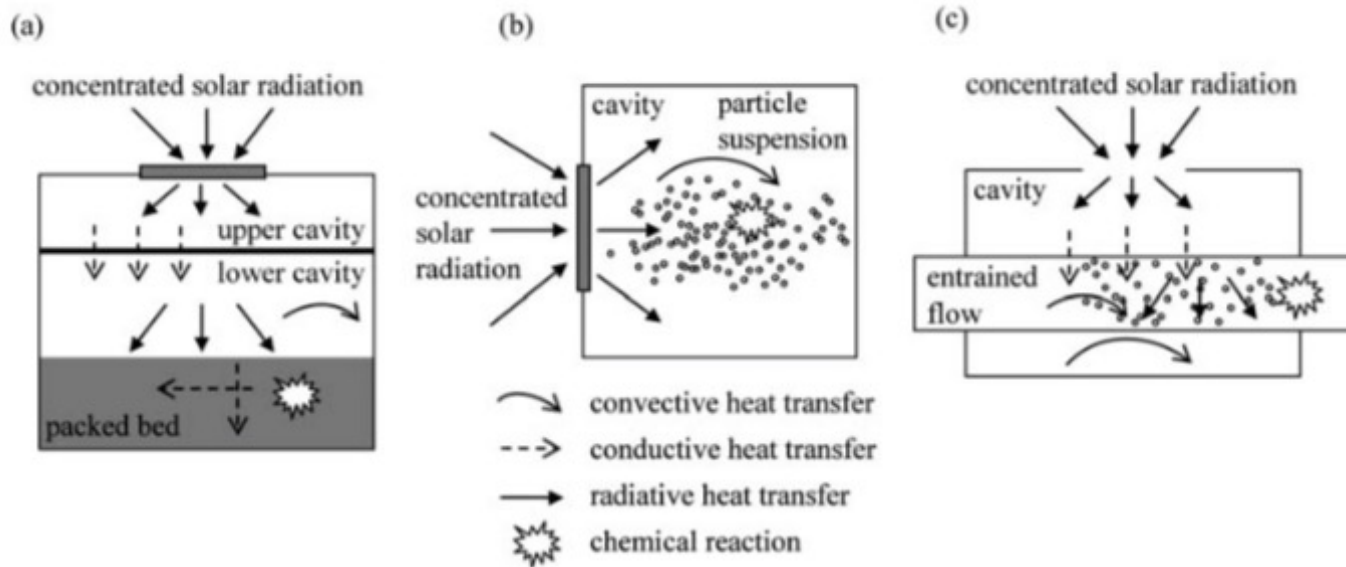


Fig. 10 Modeling schematics for the three solar reactor concepts: (a) indirectly irradiated packed-bed; (b) directly irradiated vortex-flow, and (c) indirectly irradiated entrained flow.

Directly irradiated vortex-flow reactor

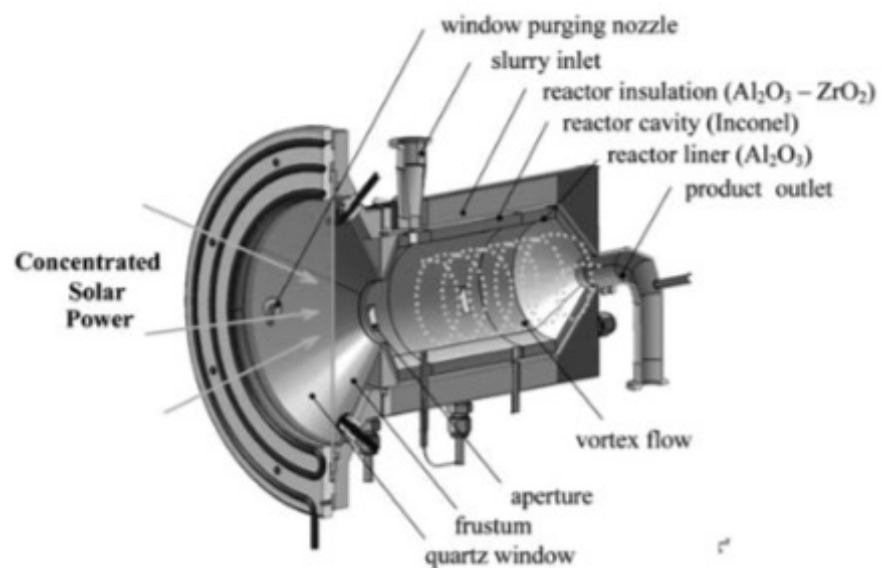


Fig. 6 Scheme of the directly irradiated vortex-flow solar reactor configuration, featuring a helical flow of carbonaceous particles and steam confined to a cavity-receiver and directly exposed to concentrated solar radiation.

Indirectly irradiated packed-bed reactor

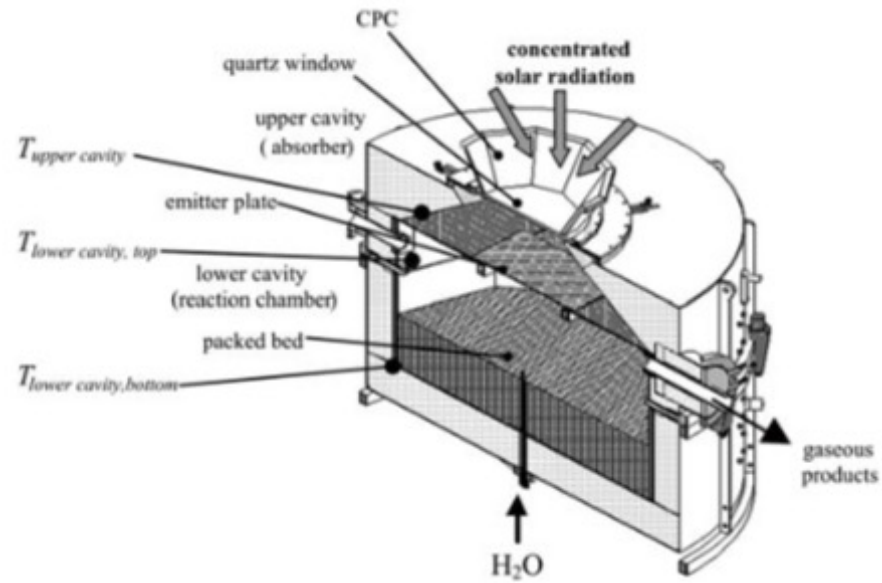


Fig. 4 Scheme of the indirectly irradiated packed-bed solar reactor configuration, featuring two cavities separated by an emitter plate, with the upper one serving as the radiative absorber and the lower one containing the reacting packed bed that shrinks as the reaction progresses.

Indirectly irradiated entrained-flow reactor

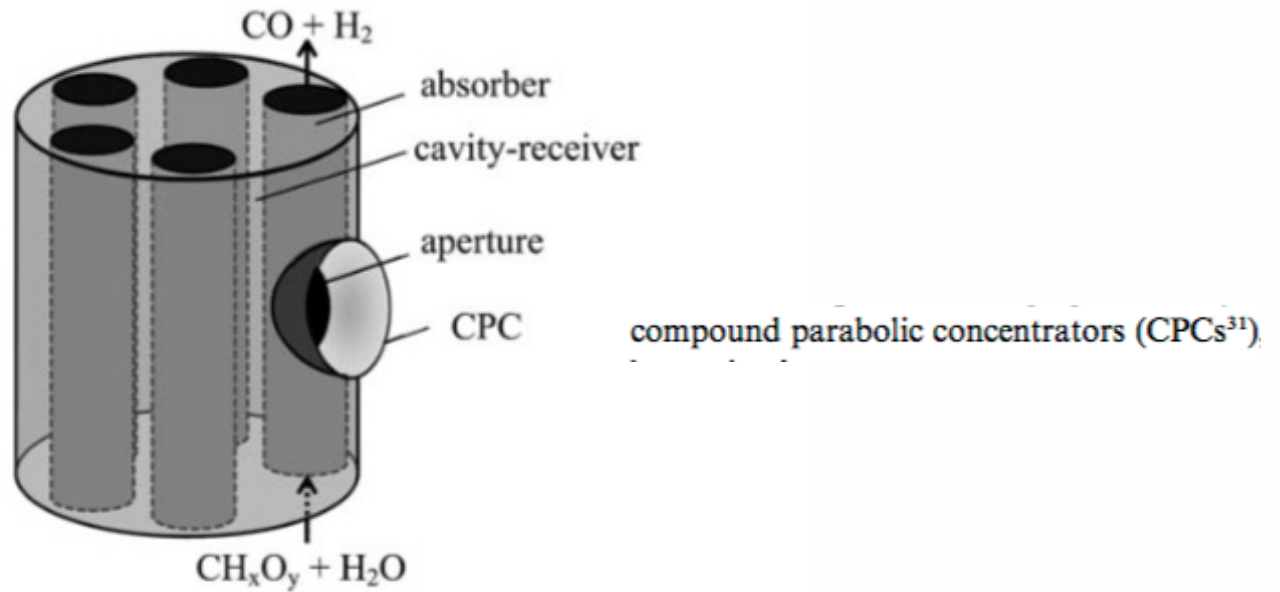


Fig. 8 Scheme of the indirectly irradiated entrained-flow solar reactor configuration, featuring a cylindrical cavity-receiver containing an array of tubular absorbers through which a continuous flow of water vapor laden with carbonaceous particles reacts to form syngas.

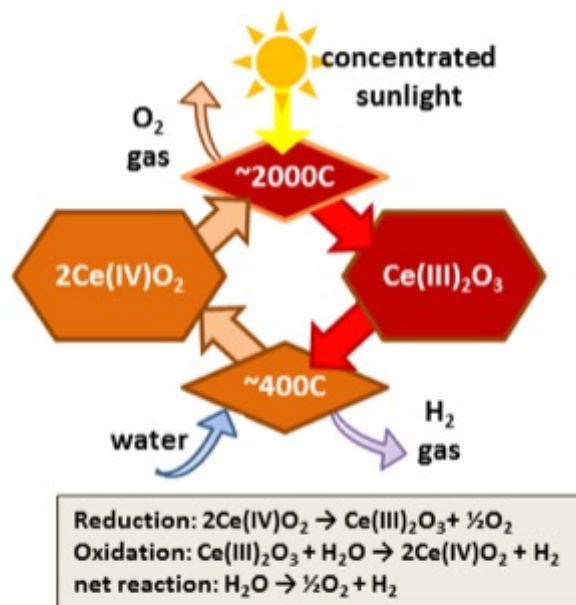
Need to rapidly quench and dilute Zn + O₂ mixture

Zn => ZnO Cycle
(Solar Driven Redox Reactions)

fossil-based fuels in sustainable future transportation systems. Economic analyses have been carried out to determine the long-term potential of the Zn/ZnO-cycle realized in a solar tower system. The cost of H₂ ranged between 0.10 and 0.15 \$/kWh (based on its LHV and a heliostat field cost at 100 to 150 \$/m²), and thus might become competitive *vis-à-vis* other paths for producing solar H₂ from H₂O [15,72,73,74]. Credit for pollution abatement and CO₂ mitigation can accelerate the deployment of the solar thermochemical technology. A comparison of H₂ produced via steam methane reforming and the Zn/ZnO cycle concluded that a significantly higher carbon tax is required to make the Zn/ZnO competitive than is likely to be implemented [75]. Therefore, the economic viability of the Zn/ZnO cycle must also include competitive, incentive policies that lead to early implementation of solar H₂ plants. On the other hand, the Zn/ZnO cycle can be applied to split both H₂O and CO₂ and produce both H₂ and CO, thereby laying the path to the solar production of synthetic liquid hydrocarbons for fueling the transportation sector and the existing massive global infrastructure.

Two Other Redox Systems (<http://energy.gov/eere/fuelcells/hydrogen-production-thermochemical-water-splitting>)

cerium oxide two step cycle



copper chloride hybrid cycle

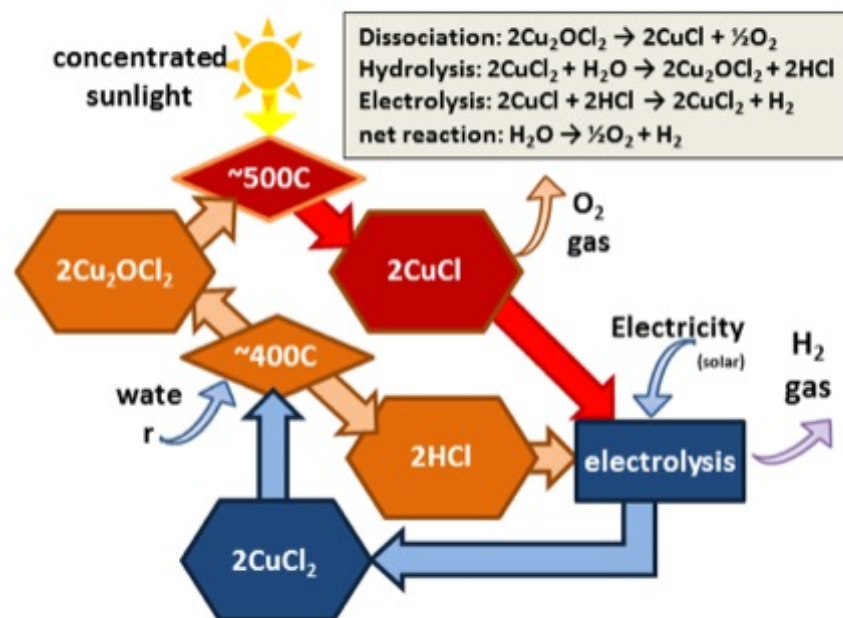


Figure 2. This illustration shows two example water-splitting cycles: (left) a two-step "direct" thermochemical cycle based on oxidation and reduction of cerium oxide particles; and (right) a multi-step "hybrid" thermochemical cycle based on copper chloride thermochemistry, which includes an electrolysis step that needs some electricity input.

Solar Thermochemical Hydrogen Production
Research (STCH)
Thermochemical Cycle Selection and Investment
Priority
Robert Perret

Volatile Metal Oxide:		
CdO(s)	→ Cd(g) + ½ O ₂ (g)	(1450°C)
Cd(l,s) + H ₂ O	→ CdO(s) + H ₂ (g)	(25-450°C)
Non-Volatile Metal Oxide:		
Ferrite:		
NiMnFe ₄ O ₈ (s)	→ NiMnFe ₄ O ₆ (s) + O ₂ (g)	(~1800°C)
NiMnFe ₄ O ₆ (s) + H ₂ O(g)	→ NiMnFe ₄ O ₈ (s) + H ₂ (g)	(~800°C)
Multi-step cycle:		
2a-NaMnO ₂ (s) + H ₂ O(l)	→ Mn ₂ O ₃ (s) + 2NaOH(a)	(~100°C)
2Mn ₂ O ₃ (s)	→ 4MnO(s) + O ₂ (g)	(~1560°C)
2MnO(s) + 2NaOH	→ 2a-NaMnO ₂ (s) + H ₂ (g)	(~630°C)
Sulfuric Acid:		
2H ₂ SO ₄ (g)	→ 2SO ₂ (g) + 2H ₂ O(g) + O ₂ (g)	(~850°C)
I ₂ + SO ₂ (a) + 2H ₂ O	→ 2HI(a) + H ₂ SO ₄ (a)	(~100°C)
2HI	→ I ₂ (g) + H ₂ (g)	(~300°C)
Hybrid Copper Chloride:		
2CuCl ₂ + H ₂ O	→ Cu ₂ OCl ₂ + 2HCl	(~400°C)
2Cu ₂ OCl ₂	→ O ₂ + 4CuCl	(~500°C)
2CuCl + 2HCl ^{e-}	→ 2CuCl ₂ + H ₂	(~100°C)

Figure 1.1. Thermochemical cycle class examples.

Solar Thermochemical Hydrogen Production
Research (STCH)
Thermochemical Cycle Selection and Investment
Priority
Robert Perret

2 Cycle Inventory Development and Initial Selection

Many hydrogen producing thermochemical cycles have been proposed over the last 40 years. A literature search was performed to identify all published cycles¹⁻⁵⁸. These were added to an

Table 2.4. Listing of non-zero efficiencies for top-scoring cycles.

PID	Cycle Name	Eff. (LHV)	PID	Cycle Name	Eff. (LHV)
110	Sodium-Mn-3	50.0	184	Hybrid Antimony-Br	30.6
106	High T Electrolysis	49.1	134	Cobalt Sulfate	29.9
147	Cadmium Sulfate	46.5	56	Cu Chloride	29.2
5	Hybrid Cd	45.1	114	Hybrid N-I	28.2
6	Zinc Oxide	45.0	62	Iron Bromide	27.7
182	Cadmium Carbonate	44.3	23	Mn-Chloride-1	26.6
2	Ni-Mn Ferrite	44.0	51	K-Peroxide	23.5
194	Zn-Mn Ferrite	44.0	61	Sodium-Iron	22.8
67	Hybrid Sulfur	43.1	185	Hybrid Cobalt Br-2	21.7
7	Iron Oxide	42.3	53	Hybrid Chlorine	21.6
191	Hybrid Copper Chloride	41.6	160	Arsenic-Iodine	21.2
149	Ba-Mo-Sulfate	39.5	152	Iron-Zinc	19.9
1	Sulfur-Iodine	38.1	103	Cerium Chloride	18.0
193	Multivalent Sulfur-3	35.5	26	Cu-Mg Chloride	17.4
131	Mn Sulfate	35.4	199	Iron Chloride-11	16.9
72	Ca-Fe-Br-2	33.8	200	Iron Chloride-12	16.9
70	Hybrid S-Br	33.4	104	Mg-Ce-Chloride	15.1
24	Hybrid Li-NO ₃	32.8	132	Ferrous Sulfate-3	14.4
201	Carbon Oxides	31.4	68	As-Ammonium-I	6.7
22	Fe-Chloride-4	31.0	129	Mg Sulfate	5.1

Table 2.5. Cycles that could move to Phase 3 detailed theoretical and experimental study.

Cycle	PID	Efficiency %	Estimated Max T
Sulfuric Acid Cycles			
Hybrid Sulfur	67	43	900
Sulfur Iodine	1	45	900
Multivalent Sulfur	193	42	1570
Metal Sulfate Cycles			
Cadmium Sulfate	147	55	1200
Barium Sulfate	149	47	1200
Manganese Sulfate	131	42	1200
Volatile Metal Oxides			
Zinc Oxide	6	53	2200
Cadmium Carbonate: Cadmium Oxide	182: 213	52: 59	1600: 1450
Hybrid-Cadmium	5	53	1600
Non-volatile Metal Oxides			
Iron Oxide	7	50	2200
Mixed Metal Sodium Manganese; Sodium Manganese	110	59	1560
Nickel Manganese Ferrite	2	52	1800
Zinc Manganese Ferrite	194	52	1800
Hybrid Cycles			
Hybrid Copper Chloride	191	49	550

Table 3.1. Cycles considered in the formal evaluation process.

Class	Cycle	Lead Organization
Sulfuric Acid Cycles	Sulfur Iodine	General Atomics, Sandia National Labs, CEA
	Hybrid Sulfur	Savannah River National Laboratory
Volatile Metal Oxide Cycles	Zinc Oxide	University of Colorado
	Cadmium Oxide	General Atomics
Non-volatile Metal Oxide Cycles	Sodium Manganese and Sodium Manganate	University of Colorado
	Reactive Ferrite	Sandia National Laboratories
	ALD Ferrite	University of Colorado
Hybrid Cycles	Hybrid Copper Chloride	Argonne National Laboratory
	Photolytic Sulfur Ammonia	SAIC

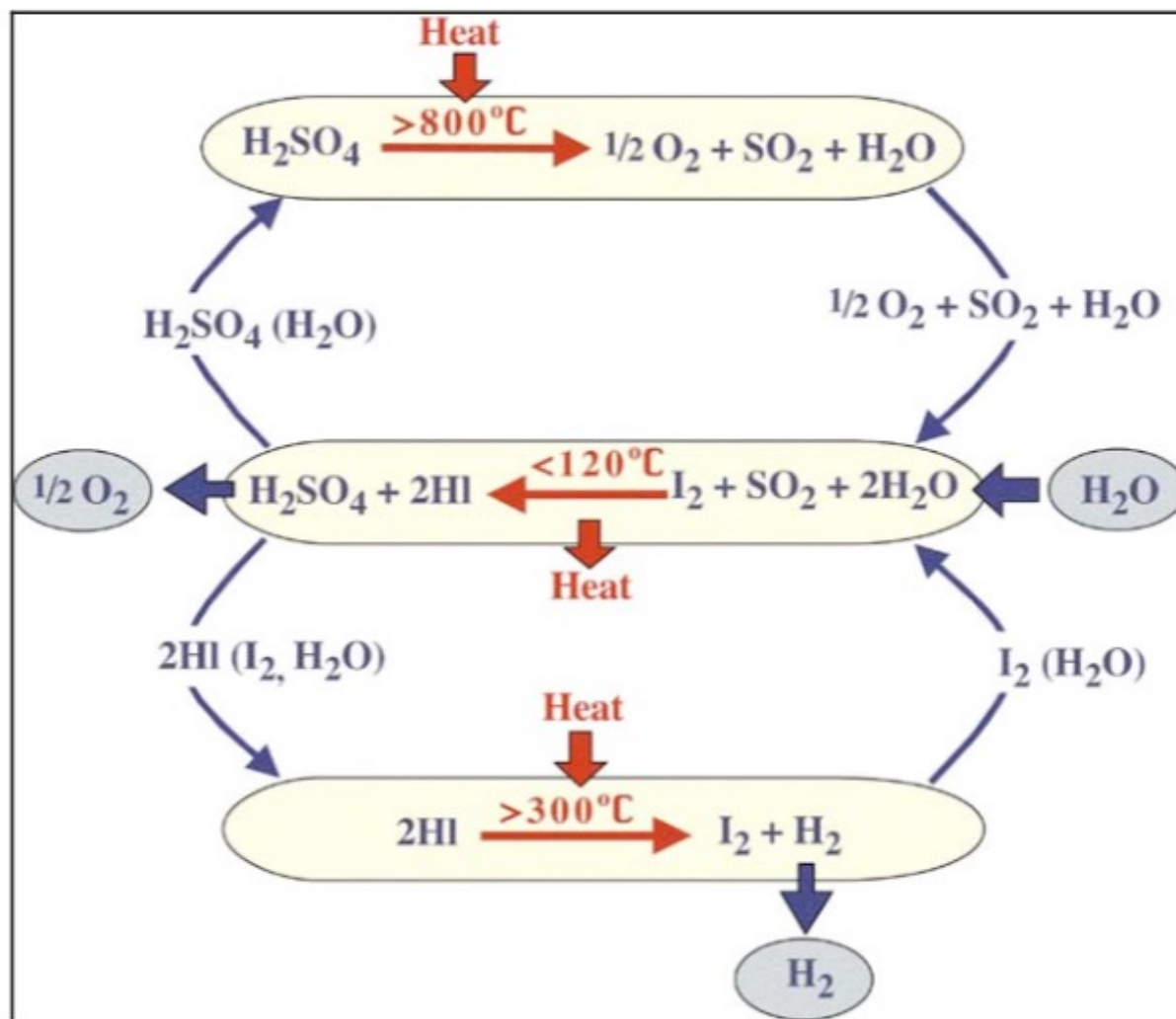


Figure 4.1.1. Sulfur iodine three-step cycle.

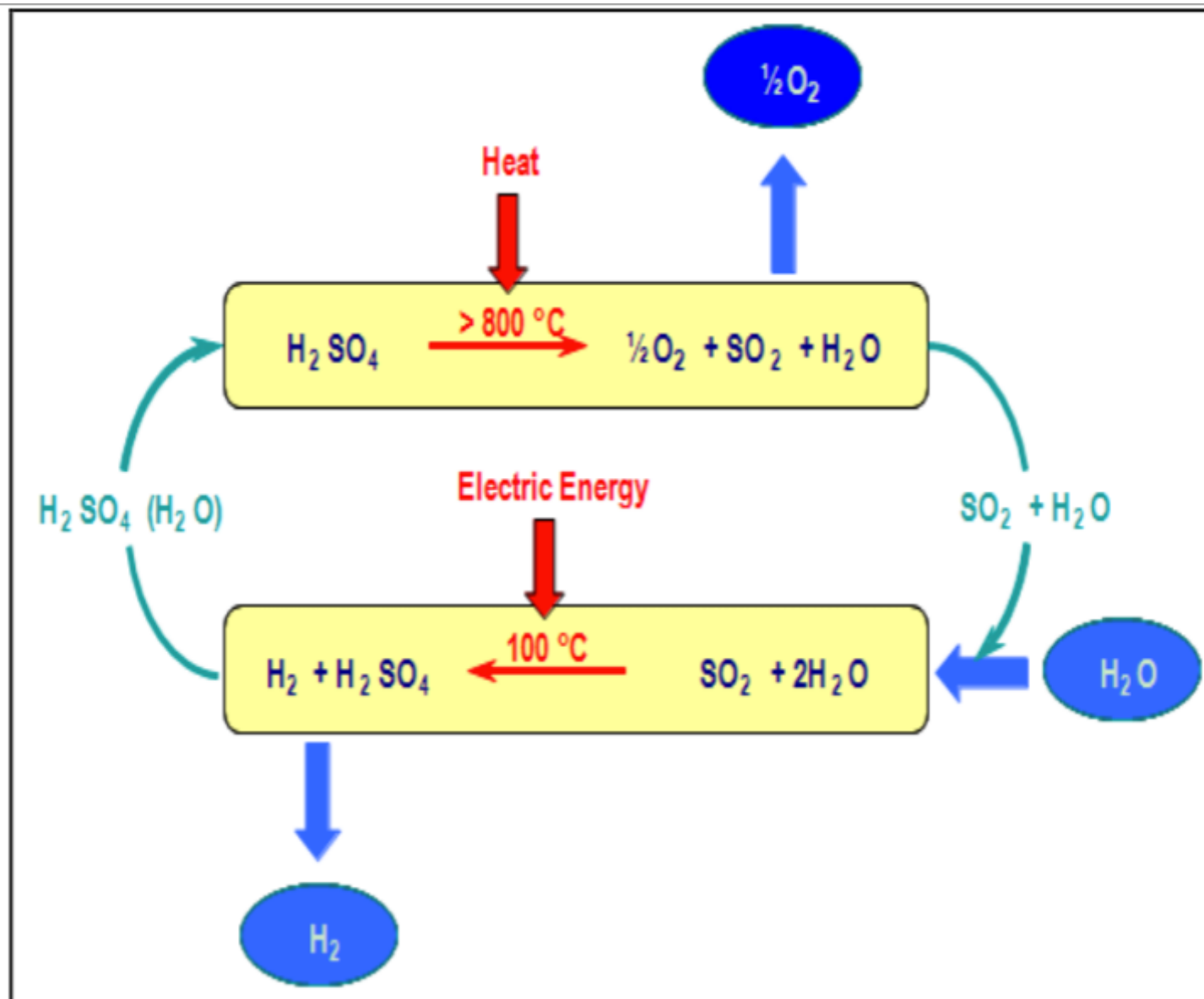


Figure 4.2.1. The Hybrid Sulfur cycle.

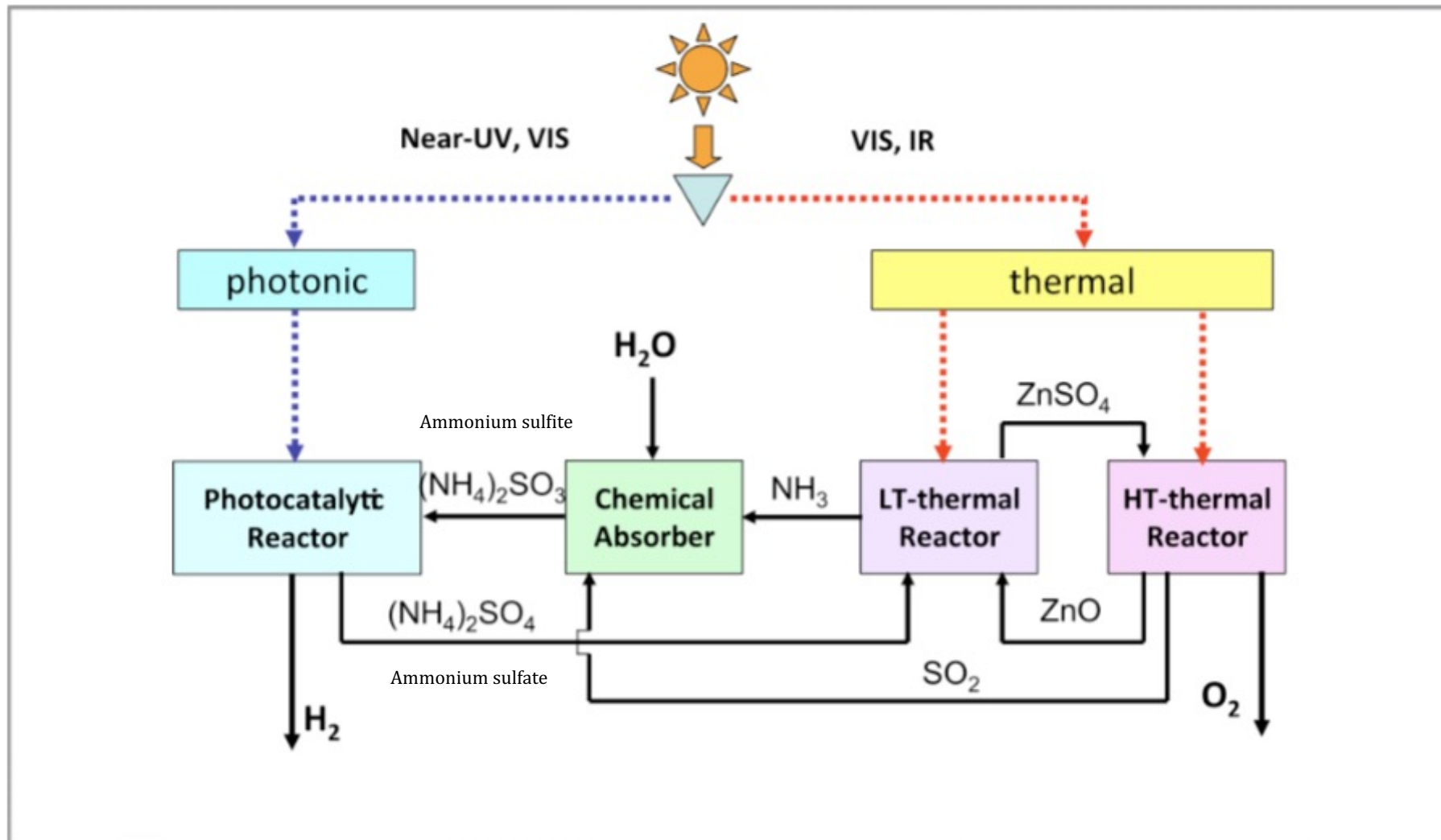


Figure 4.3.1. Photolytic Sulfur Ammonia schematic process.

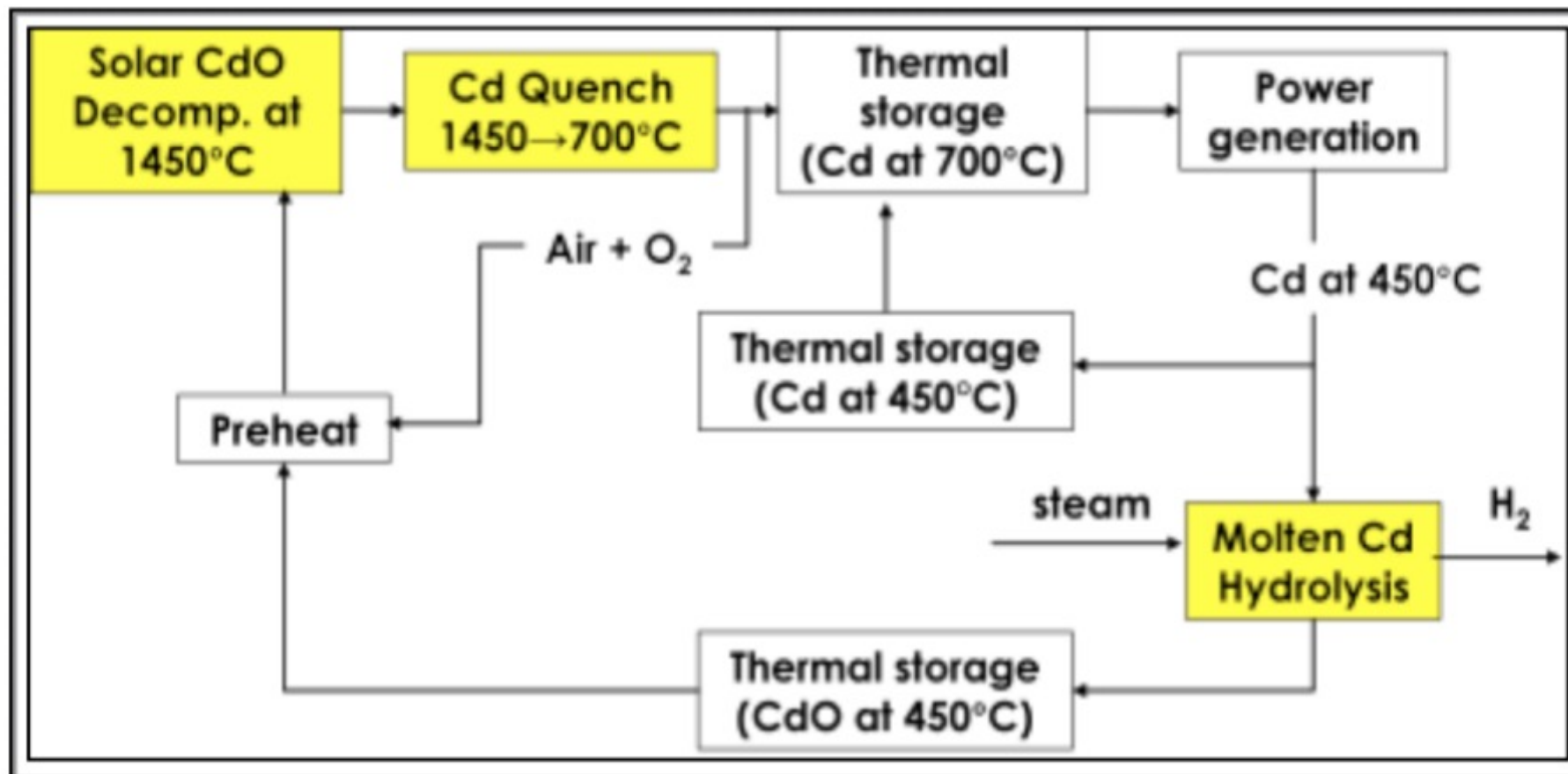


Figure 4.5.2. Process flow for a diurnal solar cadmium oxide hydrogen cycle.

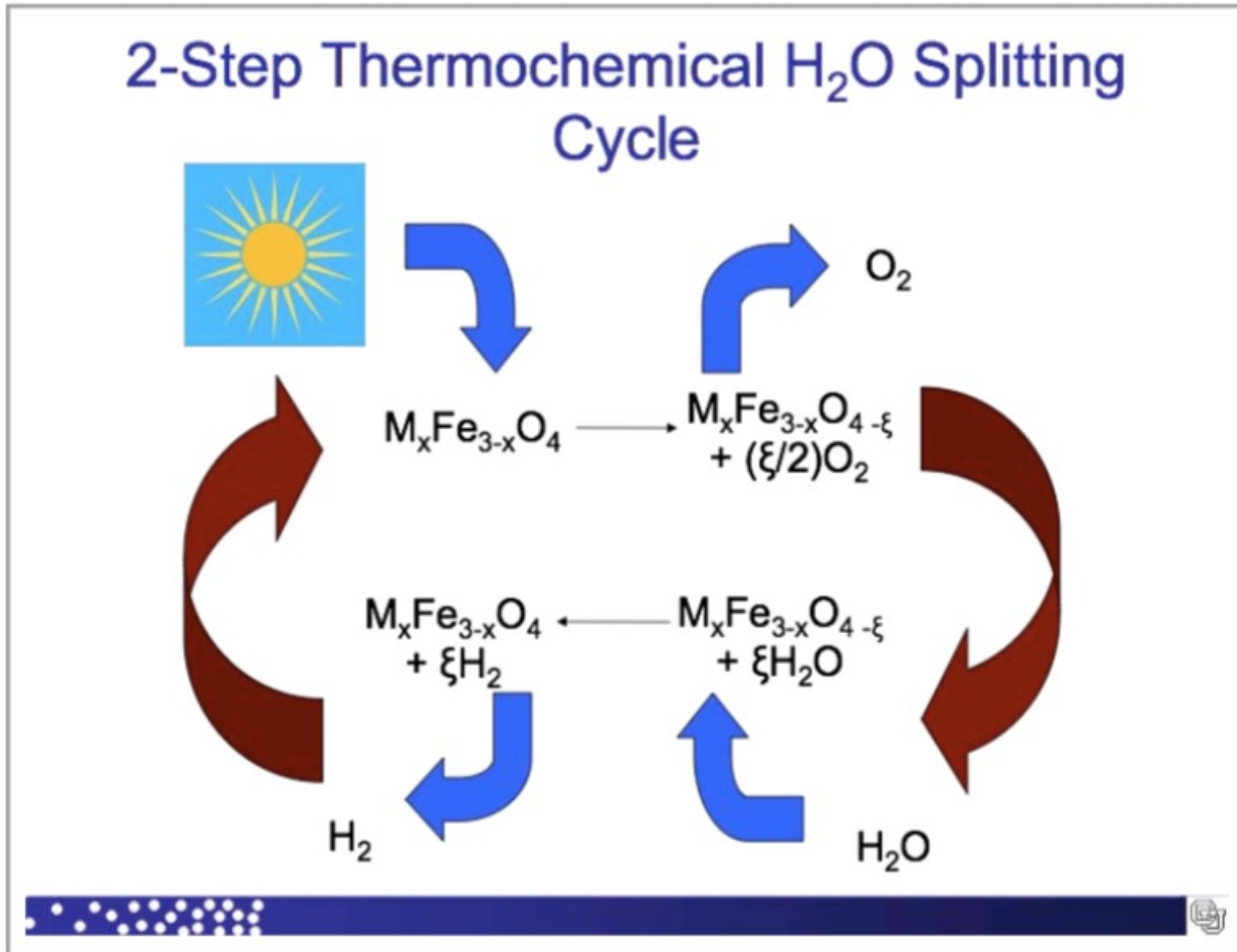


Figure 4.8.1. Schematic chemistry of a water-splitting ferrite cycle.

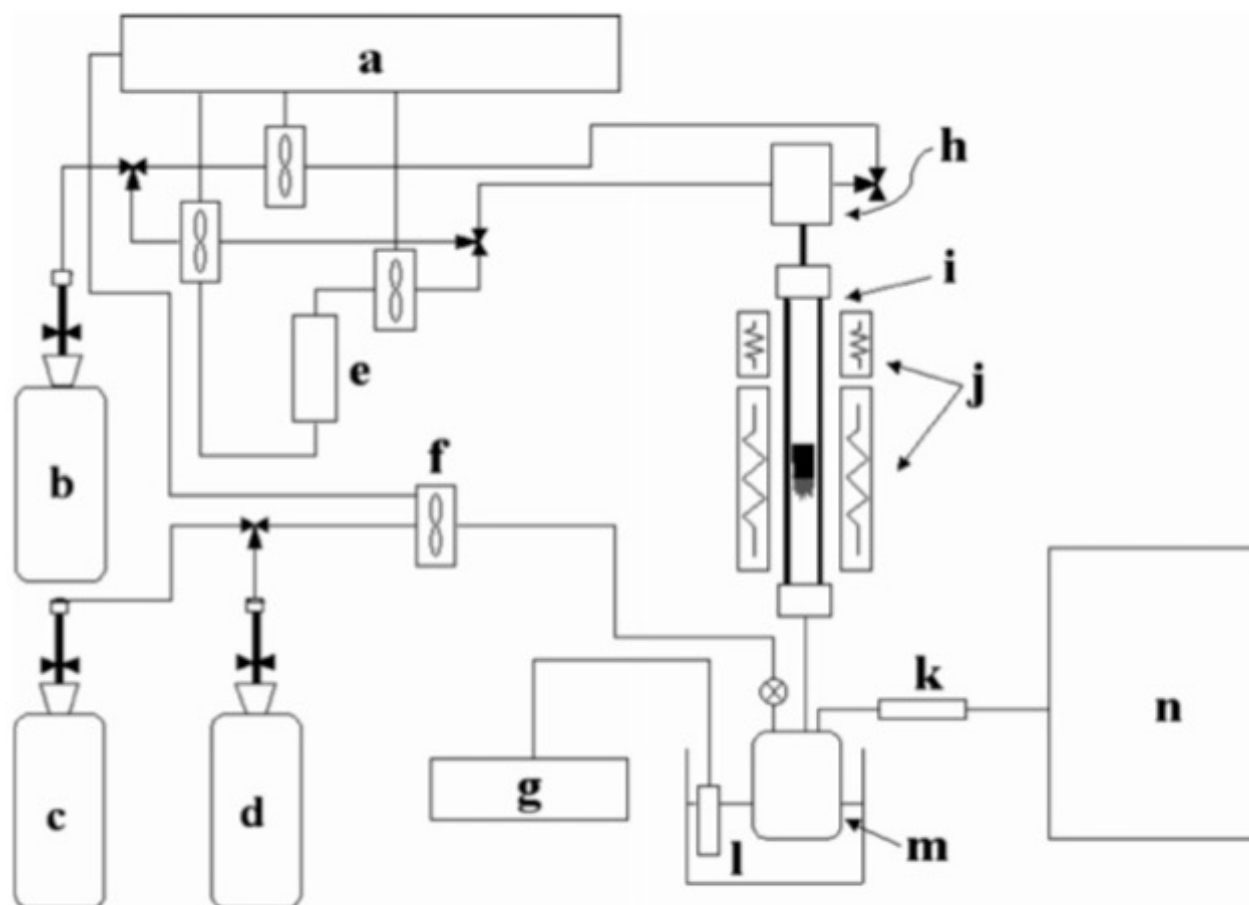


Fig. 1. Experimental apparatus for H₂O decomposition: (a) MFC & Temperature controller, (b) He, (c) H₂, (d) O₂, (e) water, (f) MFC, (g) Condenser, (h) Controlled evaporator mixer, (i) Reactor, (j) Furnace, (k) Silica-gel, (l) Ethanol, (m) Water trap, and (n) Mass.

S.B. Han et al. / Solar Energy 81 (2007) 623–628



Hydrogen generation through cuprous chloride-hydrochloric acid electrolysis

**Natarajan Sathaiyan^{1,*}, Venkataraman Nandakumar¹, Ganapathy Sozhan²,
Jegan Gandhibha Packiaraj¹, Elumalai Thambuswamy Devakumar¹, Damaraju Parvatalu³,
Anil Bhardwaj³, Bantwal Narayana Prabhu³**

¹Electro Hydro Metallurgy Division, CSIR-Central Electro-Chemical Research Institute, Karaikudi, India

²Electro Inorganic Chemicals Division, CSIR-Central Electro-Chemical Research Institute, Karaikudi, India

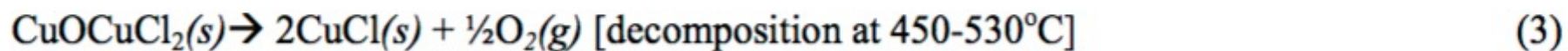
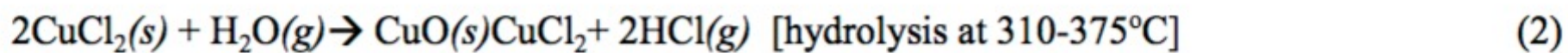
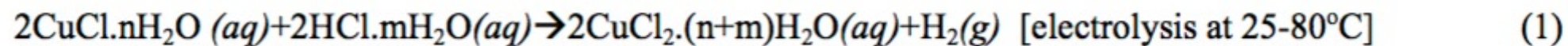
³ONGC Energy Centre, IEOT, Panvel, Navi Mumbai, India

Email address:

enes@rediffmail.com (N. Sathaiyan)

To cite this article:

Natarajan Sathaiyan, Venkataraman Nandakumar, Ganapathy Sozhan, Jegan Gandhibha Packiaraj, Elumalai Thambuswamy Devakumar, Damaraju Parvatalu, Anil Bhardwaj, Bantwal Narayana Prabhu. Hydrogen Generation through Cuprous Chloride-Hydrochloric Acid Electrolysis. *International Journal of Energy and Power Engineering*. Vol. 4, No. 1, 2015, pp. 15-22. doi: 10.11648/j.ijepe.20150401.13



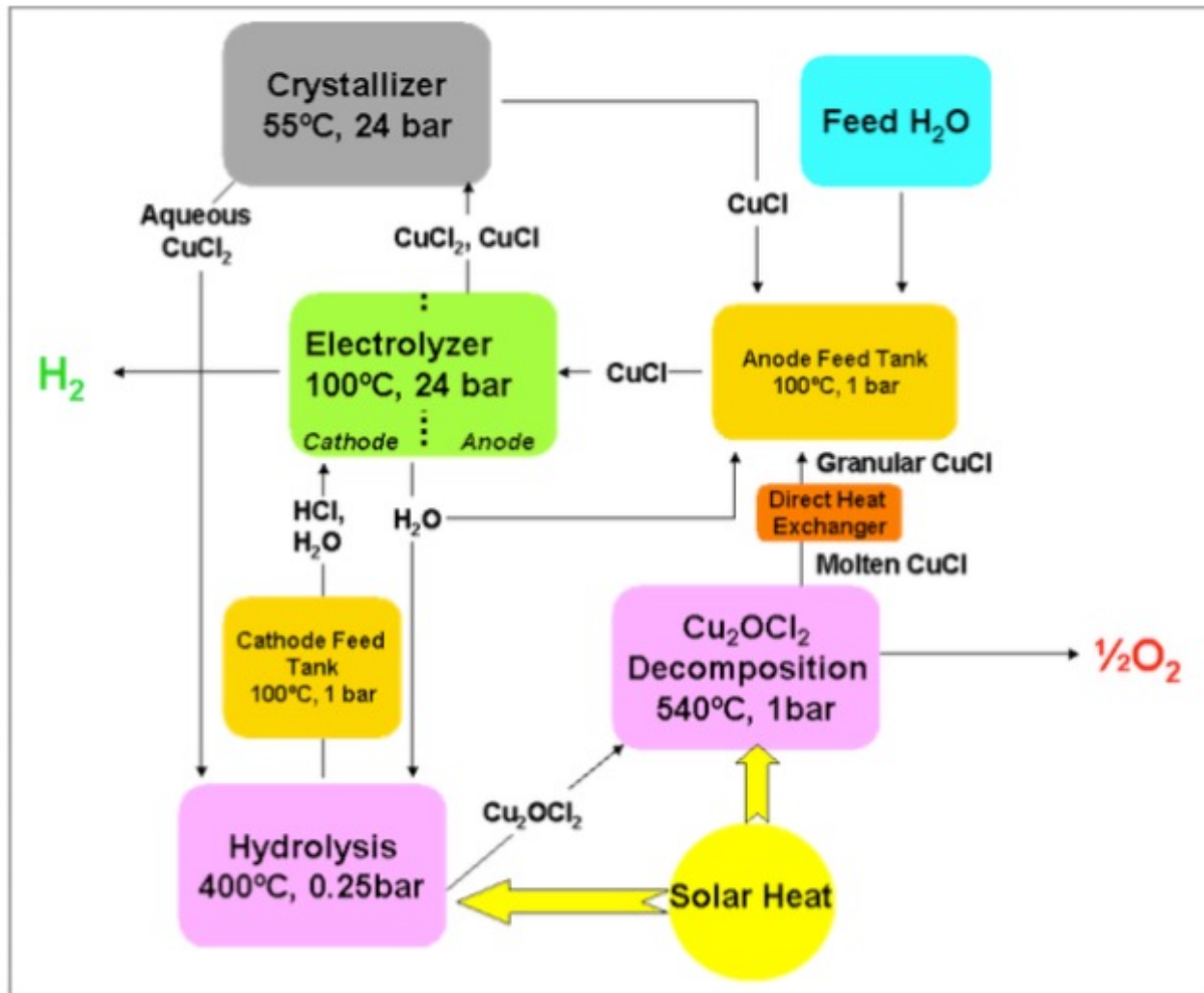


Figure 4.9.2. Hy-CuCl conceptual block flow chart.

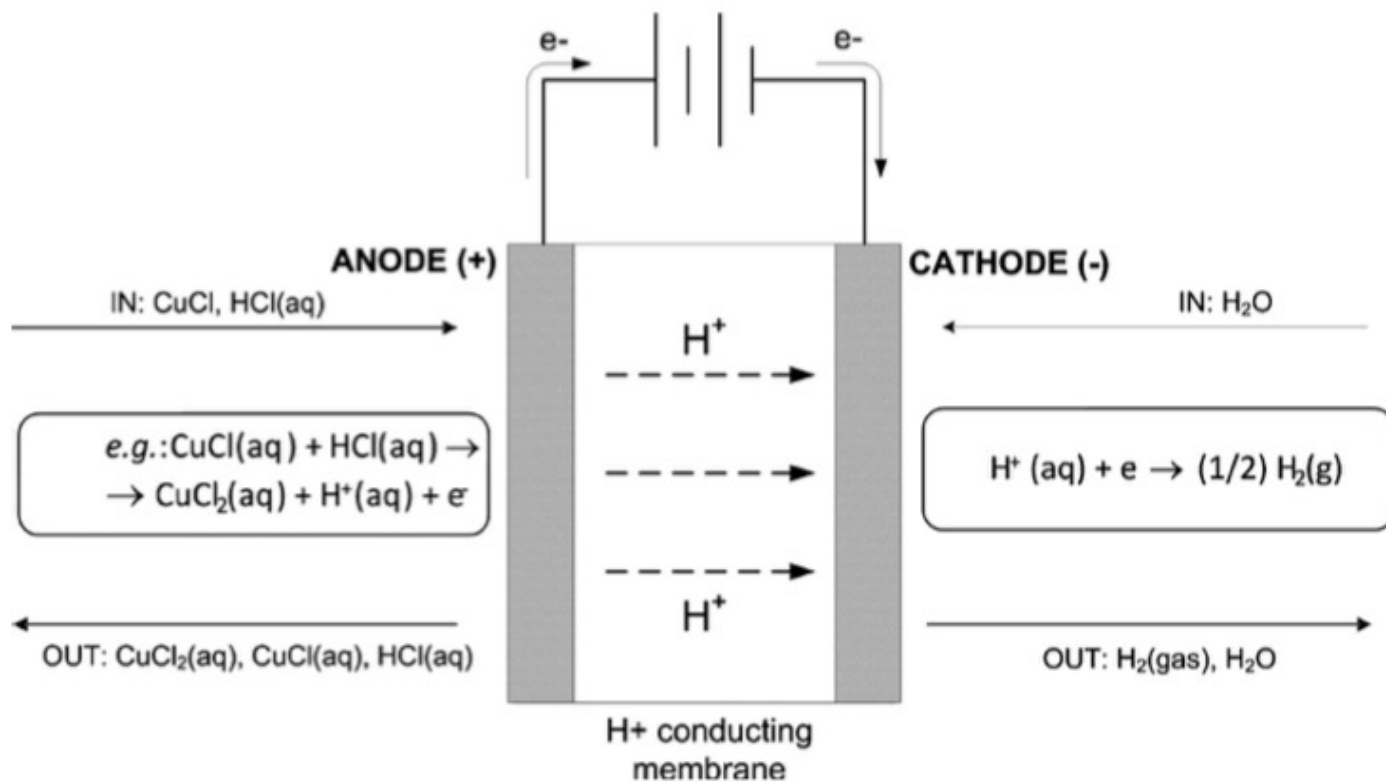


Figure 1. Conceptual scheme of the CuCl electrolysis in a cell with a proton-conducting membrane.

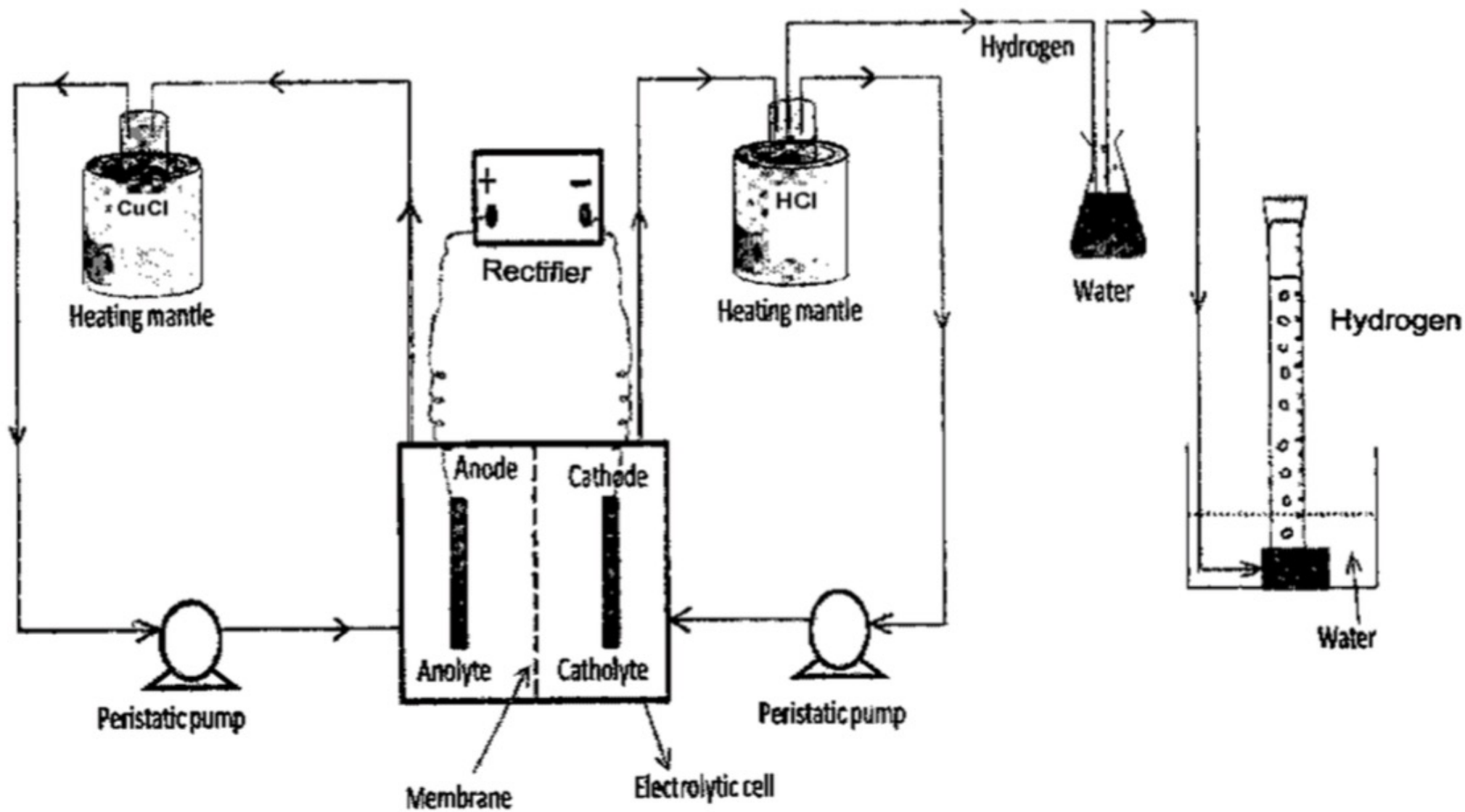
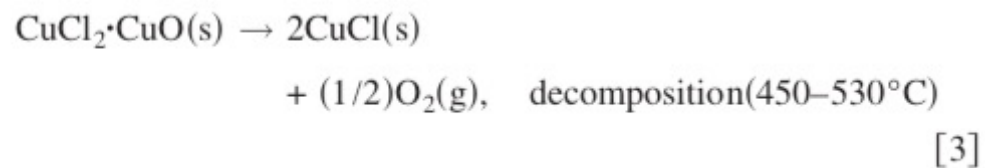
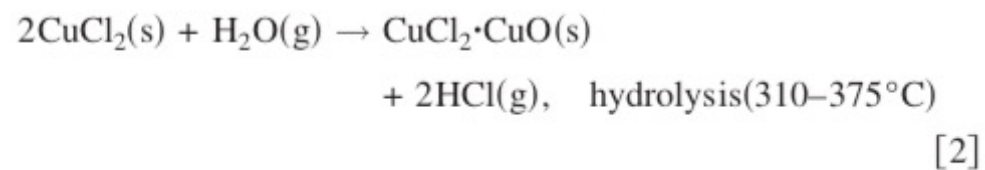
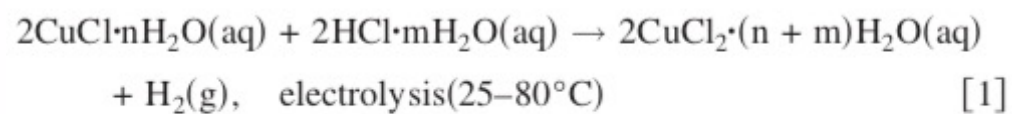


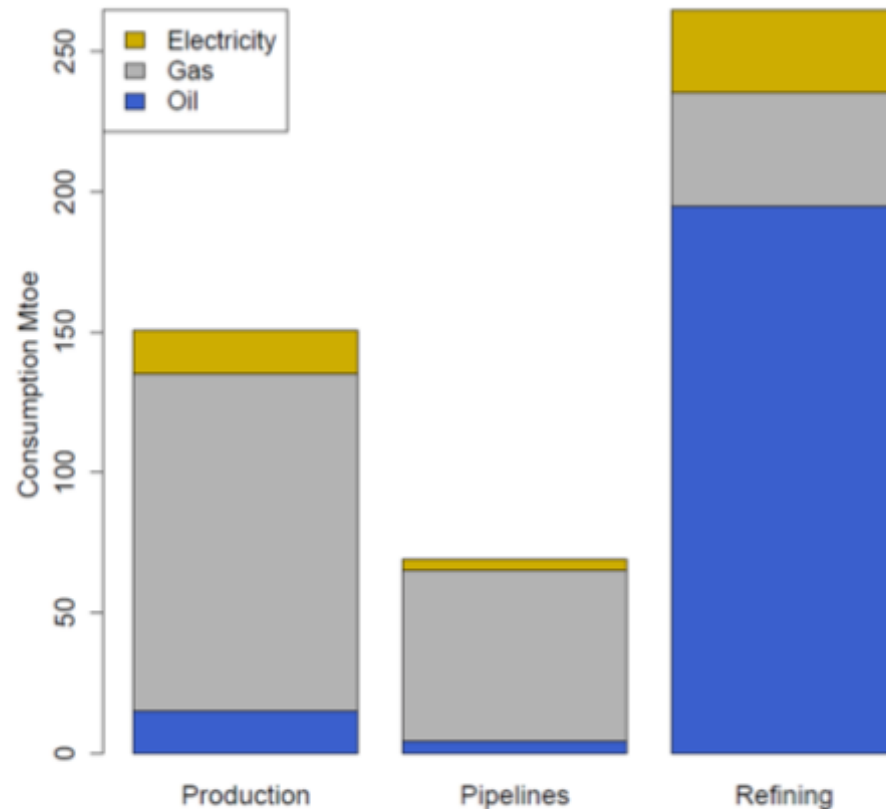
Fig 1. Cell Set-Up for the hydrogen generation through CuCl-HCl electrolysis



Direct Use of Solar in the Petrochemical Industry

Energy use in the petrochemical industry

Megaton oil equivalent
Mtoe



Blue is similar to the charcoal problem you burn a lot of oil to make gasoline

21 million barrels/day
7.33 barrel/ton
2.86 Mtoe/day
About 1000 Mtoe/year
About 1/3 to 1/2 is used to power refining, transport, and production

Figure 6. Energy consumption in oil and gas industry. Adapted from (Halabi, Al-Qattan and Al-Otaibi 2015)

How to cut US energy use in half: Power refining using solar

- Oil is first heated to 200–300° F (90–150° C) and washed with water to remove salt and other suspended solids (Worrell, Corsten and Galisky 2015).
- Distillation then separates products based on their boiling point in the crude distillation unit (CDU), where crude oil is heated to temperatures around 750° F (390° C) (Worrell, Corsten and Galisky 2015).
- Heavy fuel oils are further treated in the vacuum distillation unit (VDU) at temperatures between 730 and 850° F (390 and 450° C) (Worrell, Corsten and Galisky 2015).
- Additional processing occurs in the fluid catalytic cracker (FCC), the hydrocracker, and coking unit. Each of these processes separate heavier oil products into lighter and more valuable products.

Trillion 10^{12}

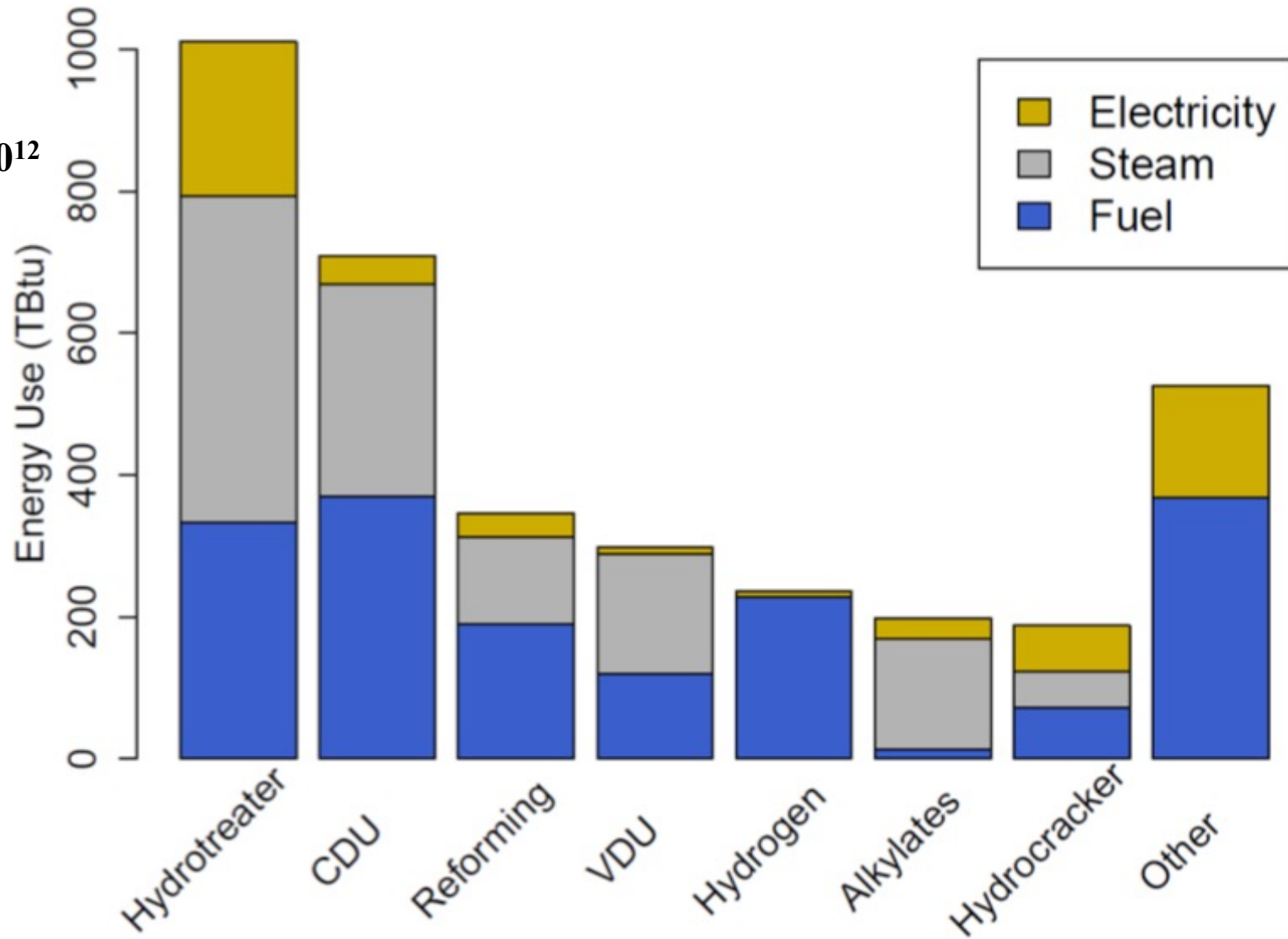


Figure 7. Energy use by refinery process. *Figure adapted from (Worrell, Corsten and Galisky 2015)*

Hydrotreating mixes hydrogen with the feedstream at temperatures between 500 and 800 ° F (260 and 460 ° C) to remove sulfur (Worrell, Corsten and Galisky 2015). A catalytic reformer uses a catalytic reactor to produce high octane gasoline and hydrogen. Additional processes, such as alkylation, which uses steam, power, and various acids to produce alkylates, are also common. Figure 7 displays yearly estimated energy use by refining process for U.S. refineries in 2012. Hydrotreatment and the crude distillation unit (CDU) account for nearly 50% of total energy requirements.

-Hydrogen is used in the hydrotreatment process to lower the sulfur content of diesel fuel. Refinery demand for hydrogen has increased as demand for diesel fuel has risen and sulfur-content regulations have become more stringent (Hicks and Gross 2016).

-Hydrogen is produced as a co-product of the catalytic reformation of gasoline, demand for hydrogen exceeds supply produced from the refining process itself (Philibert, Cédric 2017).

-Hydrogen is produced primarily through steam-reforming natural gas (Likkasit, et al. 2016).

-Costs of hydrogen production from renewables is currently higher than conventional production methods (Likkasit, et al. 2016).

Electrification of Drilling

Drilling rig uses 1MW of power

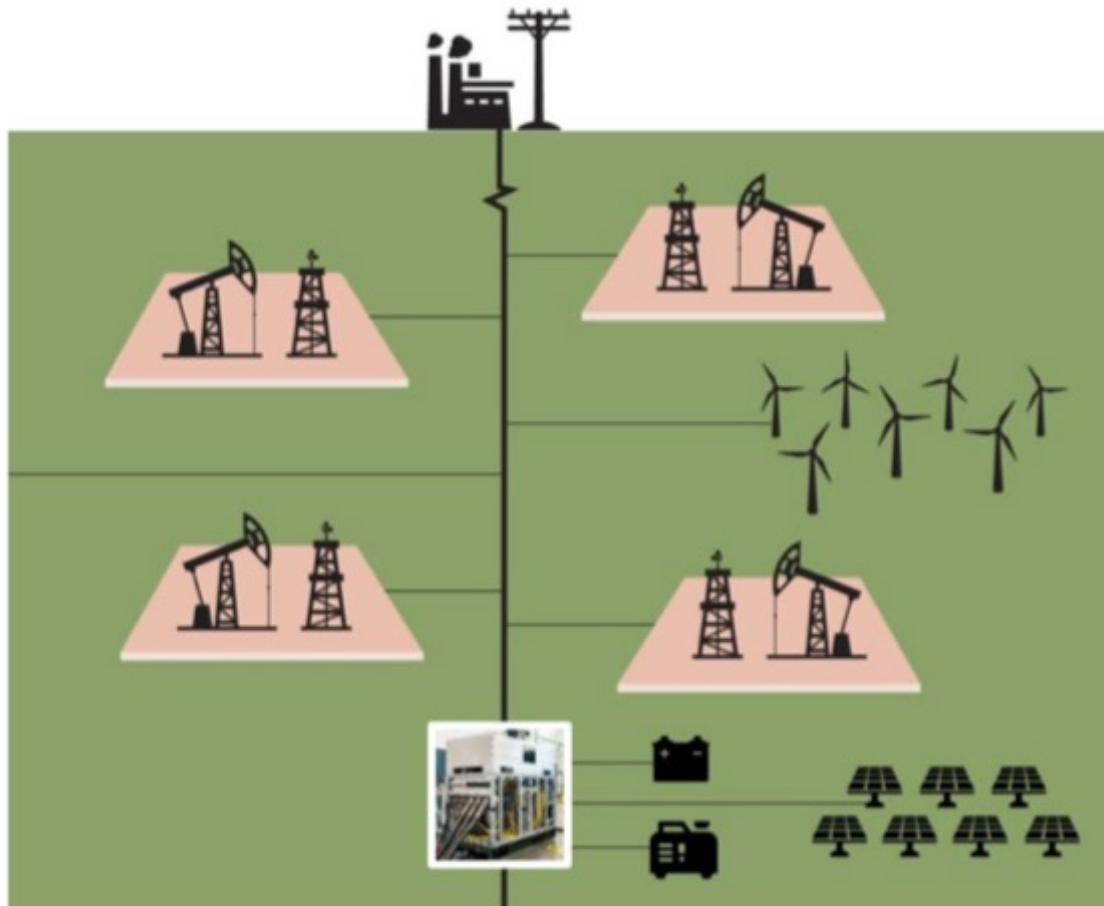


Figure 4. Schematic for a comprehensive approach to electrification of the wellpad and platform via microgrids

Rod Beam Artificial Lift Pump

- When there is not enough well pressure for oil to flow to the surface, a rod beam artificial lift pump—often referred to as a “sucker rod pump” or a “Jack pump”—is used to assist extraction.
- 80% of oil production wells operating in the western United States are installed with a rod beam pump (Endurthy, Kialashaki and Gupta 2016).
- Solar power, combined with a capacitor to store regenerative power during the rod down-stroke, can be used to power a rod beam pump. Test cases have shown significant potential energy savings (Endurthy, Kialashaki and Gupta 2016), and solar powered oil pumps are now beginning to see commercial operation (Healing 2015).
- Combined with battery storage, solar power pumps could be applicable to off-grid locations with sufficient sunlight.

Secondary Oil Recovery

- Use offshore wind power to power water injection pumps.
- By one analysis, offshore wind was found in 2012 to be an economic and environmentally sound option for supplying electricity to offshore oil and gas platforms in some cases (Korpas, et al. 2012).
- Substitute power from diesel and gas generators with power from wind platforms.
- Wind-powered water injection can provide water injection far from the platform, which reduces the need for lengthy water injection lines and can eliminate the need for costly modifications for oil platforms not initially designed for water injection.
- The Wind Powered Water Injection project recently completed an initial testing phase in which it was shown that wind power can provide water injection at competitive prices (Feller 2017).

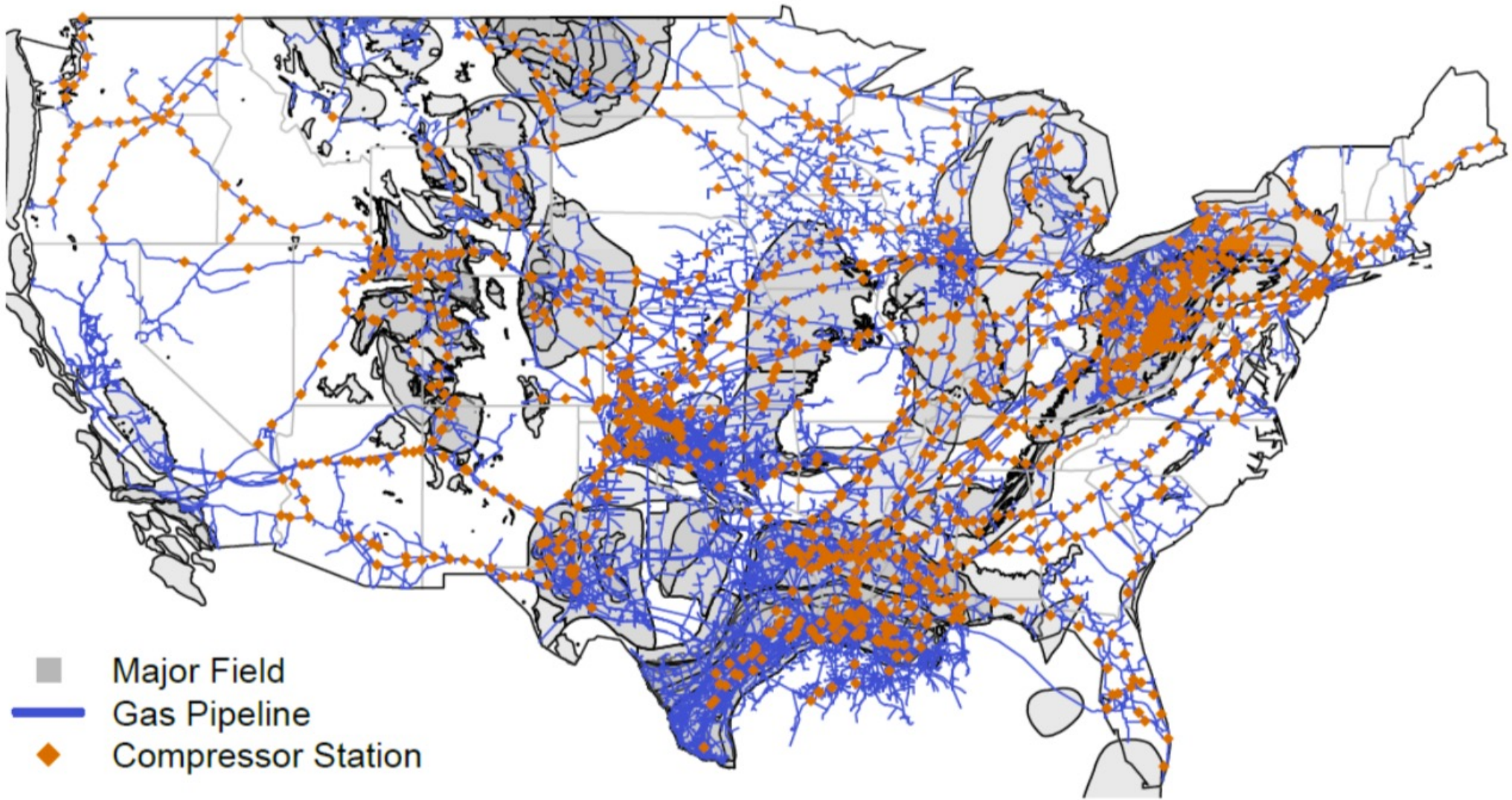


Figure 5. Natural gas transportation system. *Figure produced using data from (EIA 2018)*

Solar Thermal Carbon Black Production

[New Link](#)

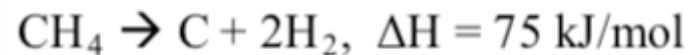
Current method of Carbon Black production by industry

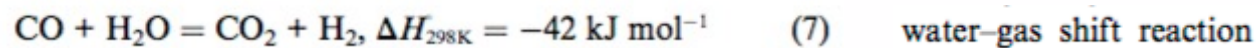
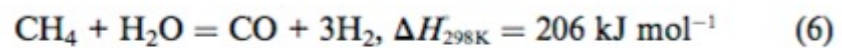
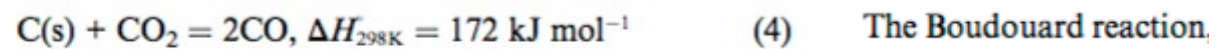


Carbon Black production via solar thermal cracking

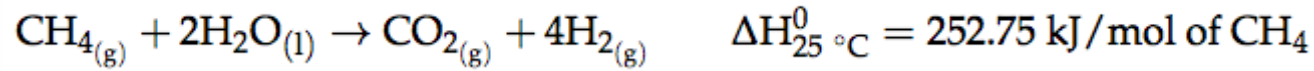


Figure 1 Carbon black production by industry vs. via solar cracking

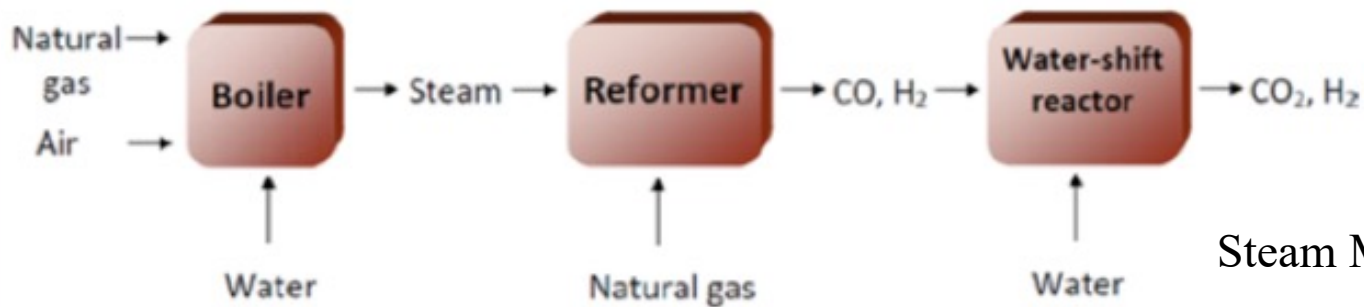




Solar Thermal Cracking for H₂



Current method of Hydrogen production by industry

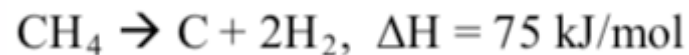


Steam Methane Reforming

Hydrogen production via solar thermal cracking



Figure 2 Hydrogen production by industry vs. via solar cracking



Review

Methane Cracking for Hydrogen Production: A Review of Catalytic and Molten Media Pyrolysis

Malek Msheik, Sylvain Rodat  and Stéphane Abanades * 

Processes, Materials and Solar Energy Laboratory, PROMES-CNRS, 7 Rue du Four Solaire,
66120 Font Romeu, France; malek.msheik@promes.cnrs.fr (M.M.); sylvain.rodats@promes.cnrs.fr (S.R.)

* Correspondence: stephane.abanades@promes.cnrs.fr; Tel.: +33-(0)4-68-30-77-30

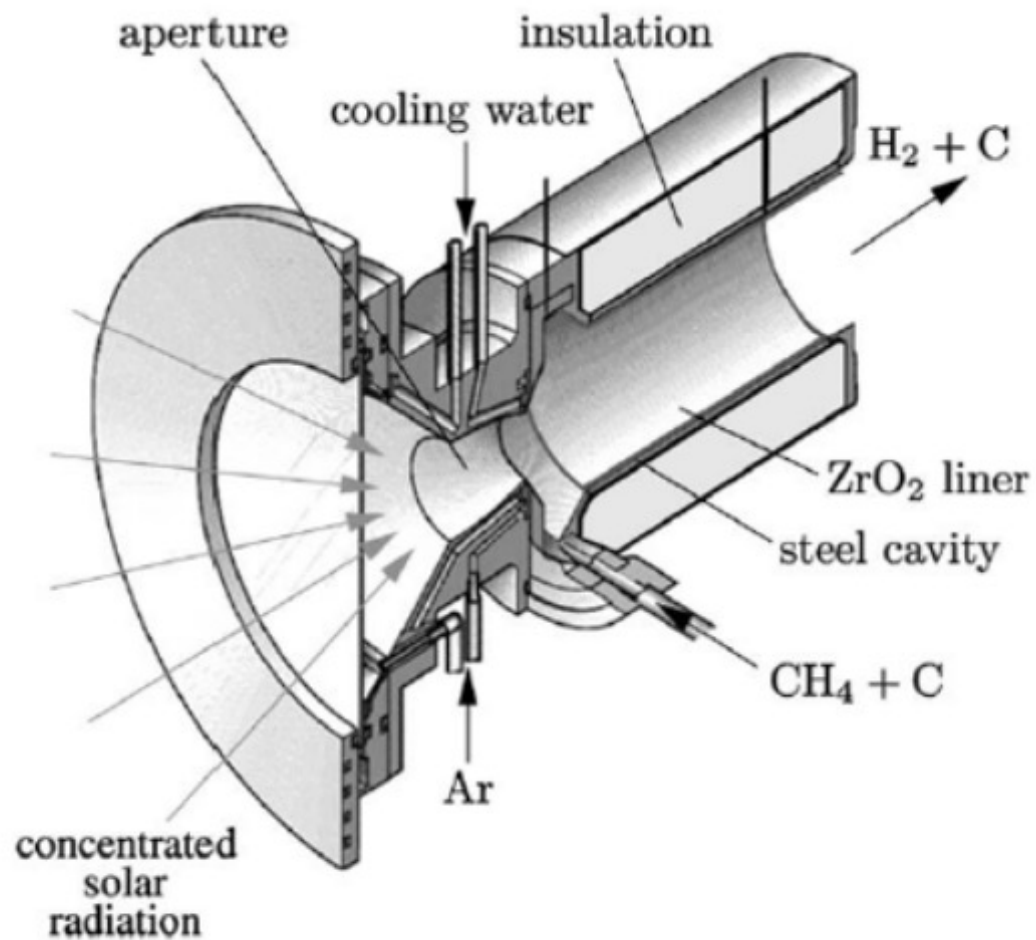
Citation: Msheik, M.; Rodat, S.;
Abanades, S. Methane Cracking for
Hydrogen Production: A Review of
Catalytic and Molten Media Pyrolysis.
Energies **2021**, *14*, 3107. [https://
doi.org/10.3390/en14113107](https://doi.org/10.3390/en14113107)

Academic Editor: Abdul-Ghani Olabi

Received: 16 April 2021

Accepted: 22 May 2021

Published: 26 May 2021



(a)

Figure 1. Directly- vs. indirectly-irradiated solar reactors used for methane pyrolysis: (a) 5 kW directly-irradiated reactor (Copied from Ref. [108] with Elsevier permission), (b) 50 kW indirectly-irradiated reactor (Copied from Ref. [102] with Elsevier permission).

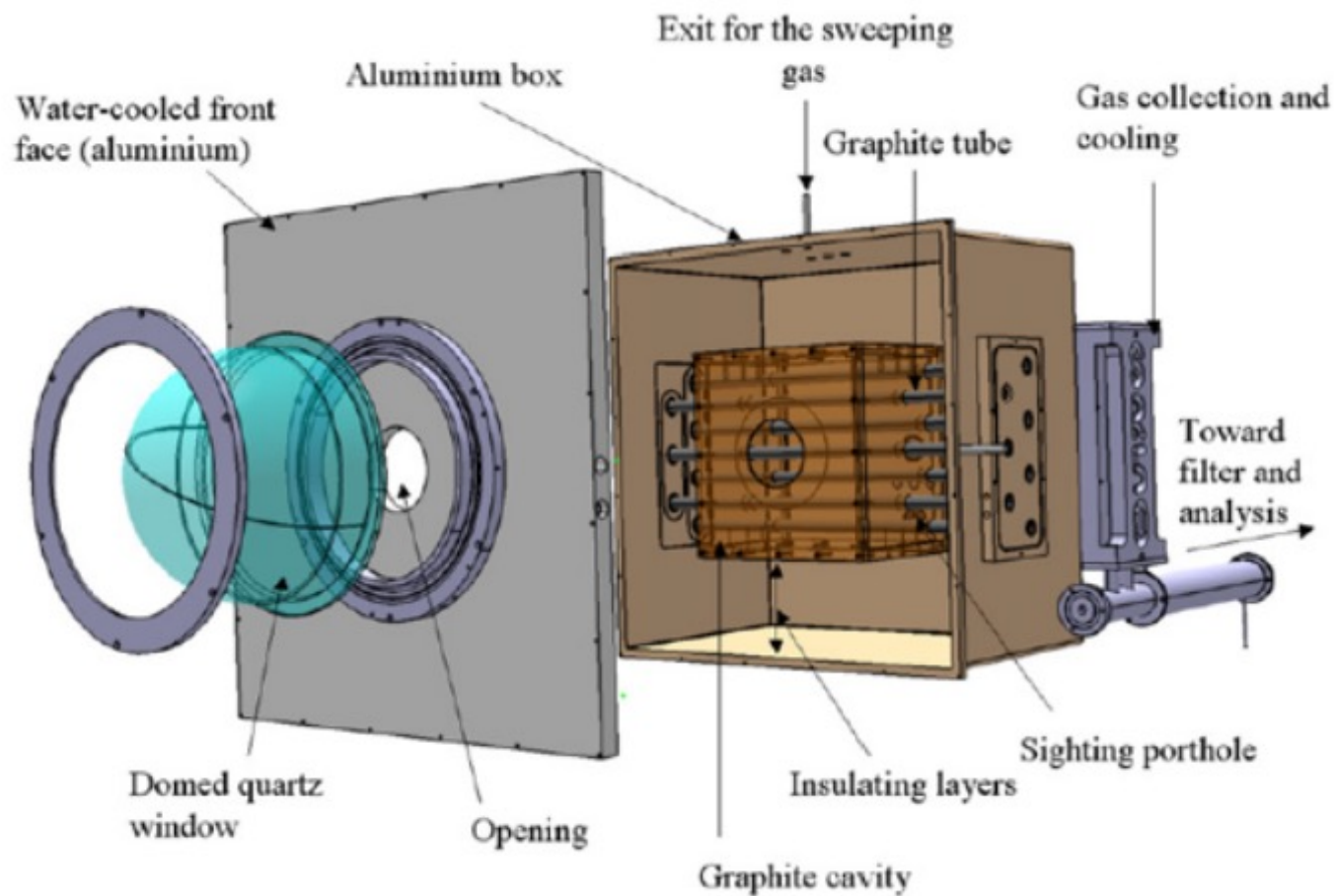


Figure 1. Directly- vs. indirectly-irradiated solar reactors used for methane pyrolysis: (a) 5 kW directly-irradiated reactor (Copied from Ref. [108] with Elsevier permission), (b) 50 kW indirectly-irradiated reactor (Copied from Ref. [102] with Elsevier permission).

Table 1. Main studies concerning solar methane cracking in gas phase (NA: not available).

Reference	Year	Heating Mode	Catalyst	Carbon Co-Feed	T (°C)	τ_r (s)	X_{CH_4} (%)
Kogan and Kogan [107]	2003	Indirect irradiation	No catalyst	None	1047	NA	27.3
Dahl et al. [95]	2004	Indirect irradiation	No catalyst	CB	1860	0.01	90
Abanades and Flamant [14]	2007	Direct irradiation	No catalyst	None	1385	0.1	97
Abanades and Flamant [112]	2008	Direct irradiation	No catalyst	None	1400	0.25	99
Abanades et al. [98]	2008	Indirect irradiation	No catalyst	None	1580	0.018	99
Rodat et al. [103]	2009	Indirect irradiation	No catalyst	None	1550	0.011	78
						0.032	100
					1700	0.011	93
					1800	0.011	100
Rodat et al. [104]	2009	Indirect irradiation	No catalyst	None	1500	0.032	98
					1470	0.012	62
						0.035	98
Maag et al. [108]	2009	Direct irradiation	No catalyst	CB	1043	<2	98.8
Rodat et al. [102]	2010	Indirect heating	No catalyst	None	1520	0.061	99
Rodat et al. [96]	2011	Indirect irradiation	No catalyst	None	1700	0.011	93
					1800		100
Yeheskel and Epstein [106]	2011	Direct irradiation	No catalyst	None	1450	NA	100
			Fe(CO) ₅		1200		50
			Fe(C ₅ H ₅) ₂		800		15–20
Abanades et al. [113]	2014	Indirect irradiation	CB	None	1200	0.12	≈100
Paxman et al. [109]	2014	Indirect irradiation	No catalyst	None	1100	NA	69
Abanades et al. [110]	2015	Indirect irradiation	CB (co-feed considered as catalyst)	CB	1250	0.113	50
						0.038	15

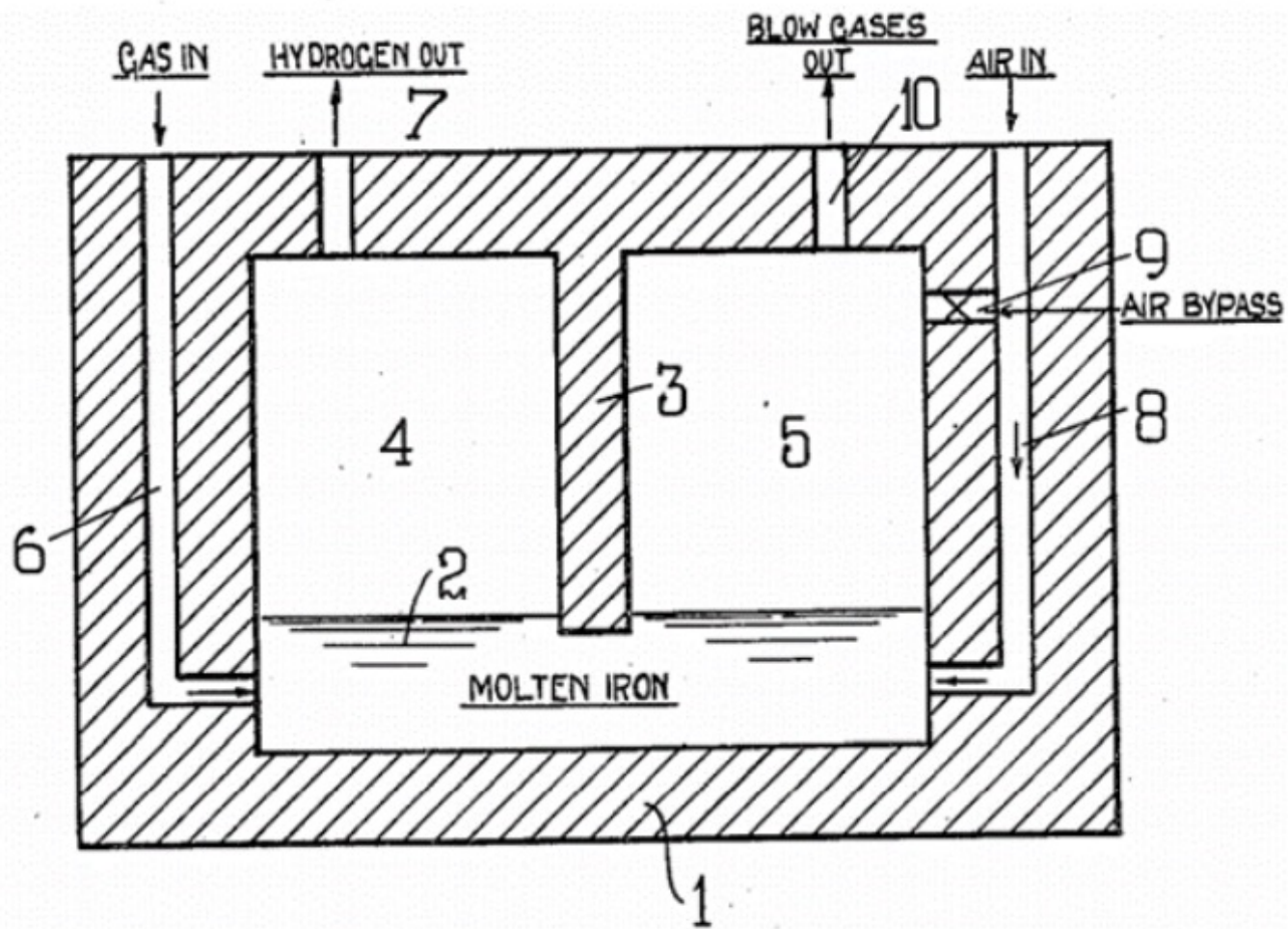


Figure 2. Two-chamber reactor design for pyrolysis in molten media from US patent of Tyrer (Copied from Ref. [29]).

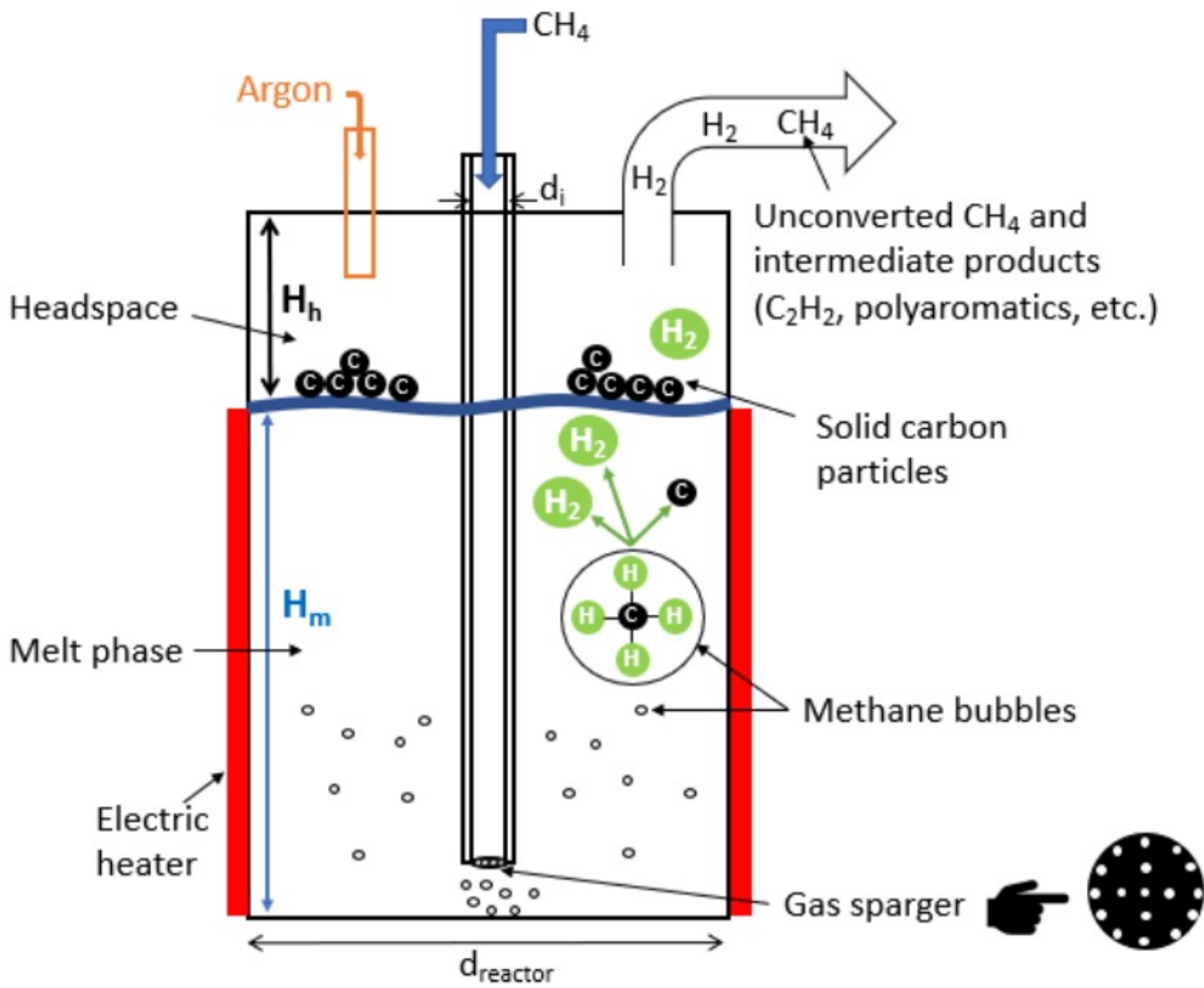


Figure 3. Representative scheme of a molten media reactor for methane pyrolysis.

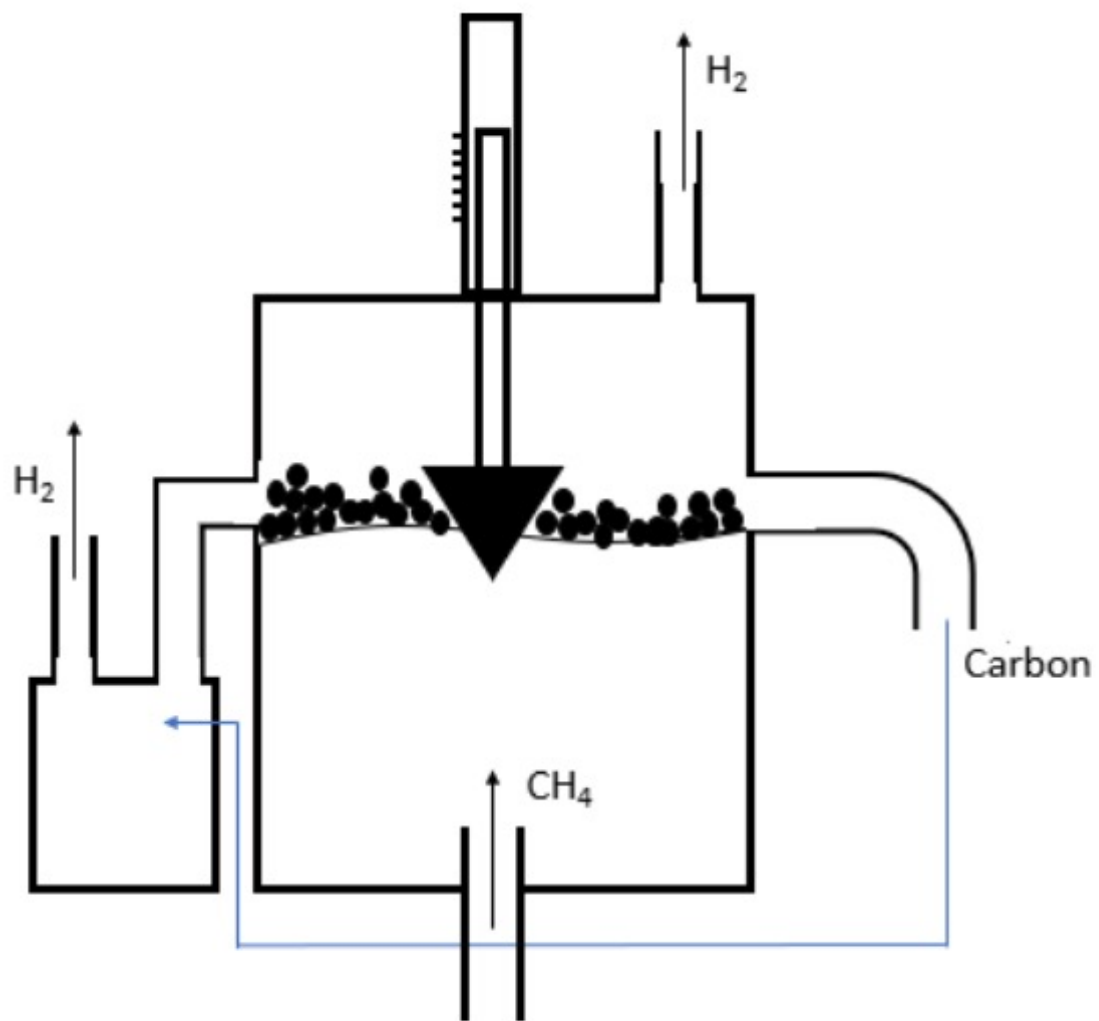


Figure 4. Reactor design for periodic carbon separation in a continuous molten media methane cracking process (adapted from Ref. [32] with Elsevier permission).

Table 2. Results of methane cracking main studies in molten media (gray: molten metals, white: molten salts, pink: two-phase molten media, green: metals suspended in molten salts).

Source	Year	Reactor Material	D (mm)	L(mm)	Filled Height (mm)	Methane Flow Rate (ml/min)	Bubble Generator Diameter	Molten Medium	Residence Time (s)	Temp (°C)	X _{CH₄} (%)	X _{CH₄} (%) Theoretical
Plevan et al. [3]	2015	SS	35.9	1190	600-1000	5	1 mm orifice	Tin	1.7-2.7	900	18	98
Geissler et al. [133]	2015	Quartz	40.6	1268	250 + (tin-packed bed combination (Quartz Glass, space porosity 76 vol.%, 850 mm long)	50	0.5 mm orifice	Tin	3.2-4.9	1000	32	99
Serban et al. [134]	2003	SS	25.4	355.6	101.6	15	Mott 0.5 μm porous distributor	Tin	0.3-0.5	750	51	93
Upham et al. [122]	2017	SS	30	1200	1200 (all)	10 (10% Ar)	3 mm orifice	NiBi (27:73)	≈7 s (calculated)	1065	95	99
Zeng et al. [130]	2020	Quartz	NA	70	NA	10 (43% Ar)	12 mm orifice	Te	0.5	977	22	98
Leal Pérez B] et al. [129]	2020	NA	NA	NA	NA	450 (50% Ar)	Duran 0.2 mm porous distributor	Gallium	0.2-0.3 0.5-0.8	960-995 936-1119	69-74 61-91	98-99 98-99
Wang et al. [123]	2008	SS	16	200	15 (calculated)	5	NA	Mg NaCl	NA	700 1000	30 5.46	89 99
Parkinson et al. [135]	2021	Quartz	16	250	190	15	2 mm orifice	KCl	0.69-0.76	1000	4.36	99
								NaBr				
								KBr				
								NaBr:KBr (48.7:51.3 mol%)				
Kang et al. [136]	2019	Quartz	25	250	125 (half)	20 (50% Ar)	2 mm orifice	MnCl ₂ /KCl (67:33)	0.6	1050	55 (starts at 45)	99
Kang et al. [131]	2020	Quartz	25	250	125 (half)	20 (50% Ar)	2 mm orifice	Fe (3 wt.%)/NaKCl	0.5	1000	9	99
Rahimi et al. [121]	2019	Quartz	22	300-430-1000	L-80	10 (43% Ar)	2 mm orifice	NiBi (27:73)/NaBr	4.2/1.1	1000	37.5	99
Patzschke et al. [137]	2021	Quartz	16	250	190	45 (67% Ar)	2 mm orifice	Co-Mn (molar ratio = 2) dispersed in NaBr:KBr (48.7:51.3 mol%)	NA	850-1000	10.52	98-99

Table 3. Main metal properties with calculated volumetric heat capacity (LME: London metal exchange) [138,139].

Metal	Symbol	Melting Point (°C)	Boiling Point (°C)	Density (g/cm ³) Solid vs. Liquid		LME Price (EUR/ton)	Specific Heat (J/g.°C)	$\rho \cdot C_p$ (J/cm ³ .°C)
Tin (2 types: gray and white)	Sn	232	2602	5.77 (gray)	6.99	25,891	0.21	1.46
				7.27 (white)				
Nickel	Ni	1455	2730	8.91	7.81	14,223	0.50	3.92
Cobalt	Co	1495	2900	8.90	7.75	36,957	0.42	3.24
Iron	Fe	1538	2861	7.87	6.98	422 (scrap)	0.46	3.21
Manganese	Mn	1246	2061	7.47	5.95	NA	0.48	2.84
Bismuth	Bi	271	1564	9.78	10.05	NA	0.13	1.26
Tellurium	Te	450	988	6.24	5.70	NA	0.20	1.15
Copper	Cu	1085	2562	8.96	8.02	8489	0.38	3.02
Aluminum	Al	660	2519	2.70	2.38	2006	0.92	2.19
Gallium	Ga	30	2204	5.90	6.10	NA	0.37	2.26

Table 4. Apparent activation energies for different catalysts used in methane pyrolysis reaction.

Medium	Catalyst	Apparent Activation Energy (kJ/mol)
Gas phase	Gas phase (uncatalyzed) [14–17]	356–452
	Carbon-based catalysts [14]	205–236
	Solid Ni [140]	65
	Solid Ni/SiO ₂ [141]	96.1
Molten phase	Molten Fe(3 wt.%)-NaKCl: (Fe (III) introduced as FeCl ₃ ·6H ₂ O) [131]	171
	Molten MnCl ₂ (67%)-KCl(33%) [136]	161
	Molten Te [130]	166
	Molten Ni(67%)-Bi(33%) [122]	208
	Molten Cu(45%)-Bi(55%) [33]	222
	Molten Bi [122]	310
	Molten Tin	NA
	NaCl-KCl-NaBr-KBr [135]	231–236–278–224
	NaBr(48.7):KBr(51.3) [135]	246.7
	NaBr(48.7):KBr(51.3) [137]	236.3
	(Co-Mn)/NaBr:KBr (48.7:51.3) [137]	175.5

Table 5. Comparison of liquid catalyst activity for methane pyrolysis at 1000 °C when CH₄ is flowed over 38.5 mm² of molten metal in a differential reactor. (*) indicates that alloy is at the solubility limit of the dissolved active metal at 950 °C.

Liquid Catalyst	Rate of Hydrogen Production (mol H ₂ Produced. cm ⁻² s ⁻¹)
In	8.2×10^{-11}
Bi	8.2×10^{-11}
Sn	8.5×10^{-10}
Ga	3.2×10^{-9}
Pb	3.3×10^{-9}
Ag	4.3×10^{-9}
Pb vapor	2.1×10^{-9}
17% Cu-Sn *	3.1×10^{-9}
17% Pt-Sn	1.6×10^{-9}
17% Pt-Bi	4.2×10^{-9}
62% Pt-Bi *	6.5×10^{-9}
17% Ni-In	4.7×10^{-9}
17% Ni-Sn	5.6×10^{-9}
73% Ni-In *	6.4×10^{-9}
17% Ni-Ga	7.9×10^{-9}
17% Ni-Pb	8.3×10^{-9}
17% Ni-Bi	9.0×10^{-8}
27% Ni-Au *	1.2×10^{-8}
27% Ni-Bi *	1.7×10^{-8}

Turn Over Frequency

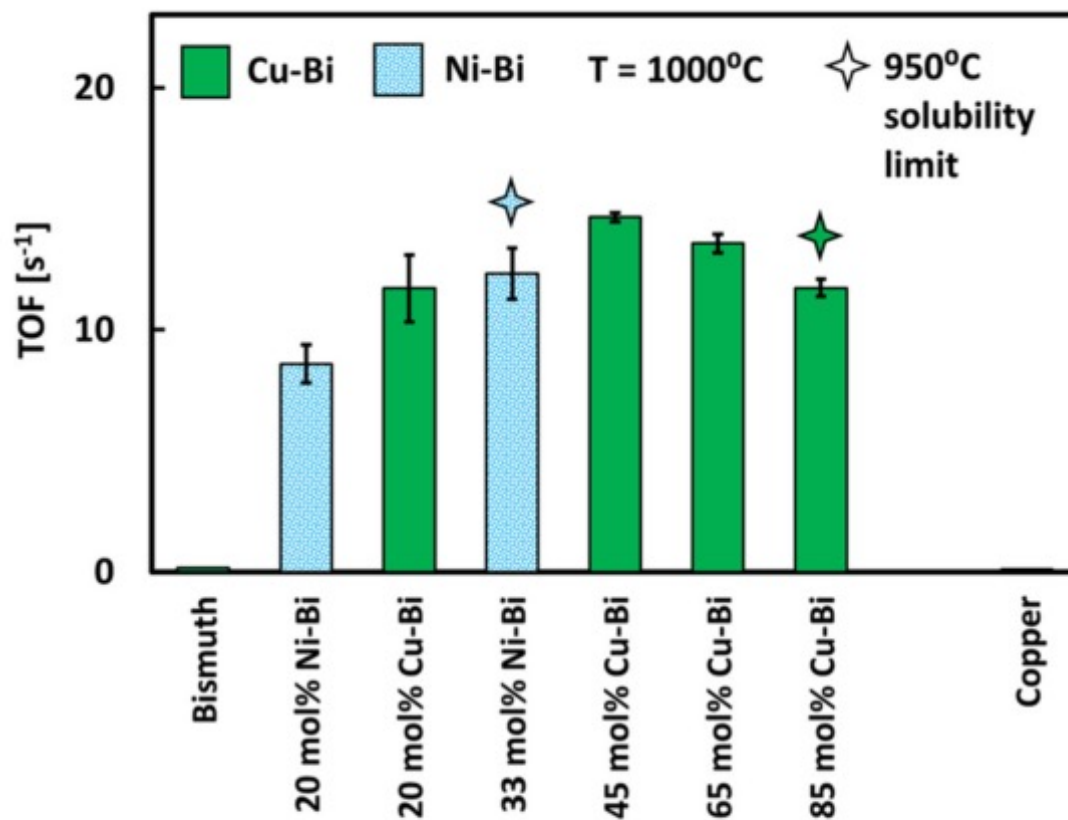


Figure 5. TOF for methane cracking over Cu-Bi, Ni-Bi alloys and pure Bi at 1000 °C. Pure copper is tested at 1100 °C (Copied from Ref. [33] with American Chemical Society permission).

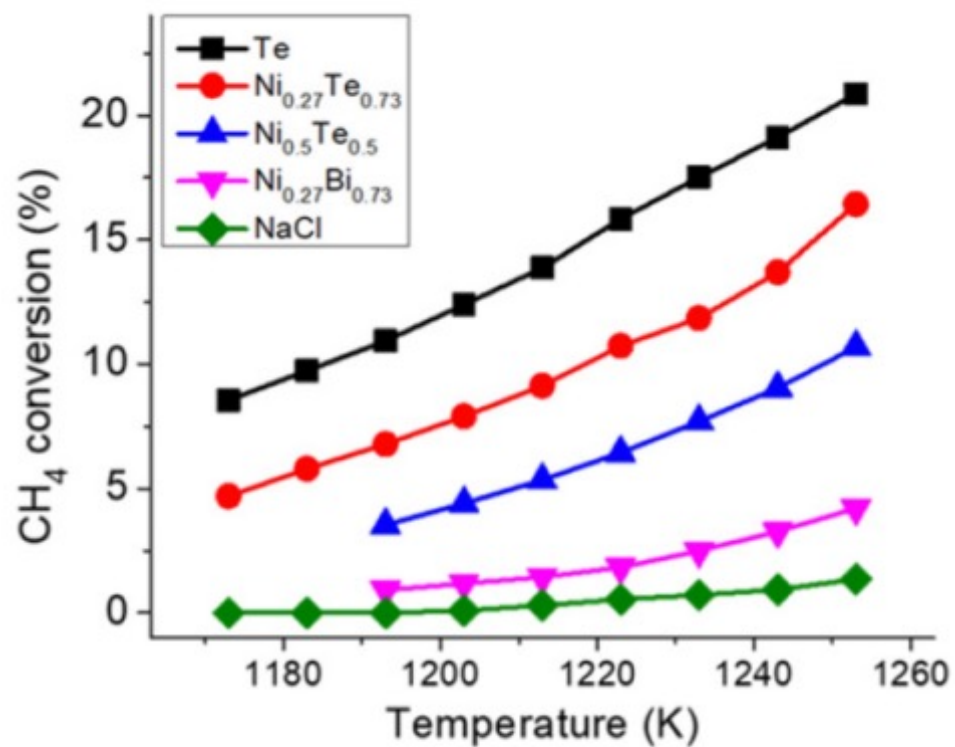
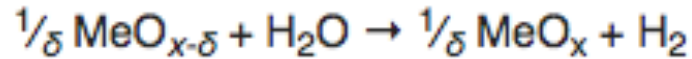
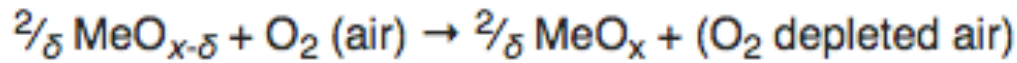
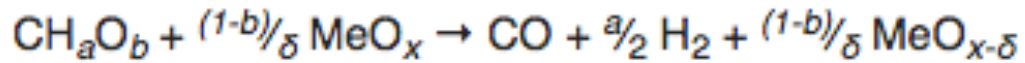


Figure 6. Methane conversion of pure Te compared with Ni–Bi and Ni–Te alloys, as well as with molten NaCl (Copied from Ref. [130] with American Chemical Society permission).

Table 7. Comparison between the features of molten metals and molten salts used in methane cracking.

	Cost	Catalytic Activity	Carbon Purification	Vapor Pressure	Melting Points
Metals	High	High	Complex	High	High
Salts	Low	Moderate or low	Easy	Low	Low



Reduce Metal Oxide
High Temp

Oxidize Metal Oxide
Low Temp

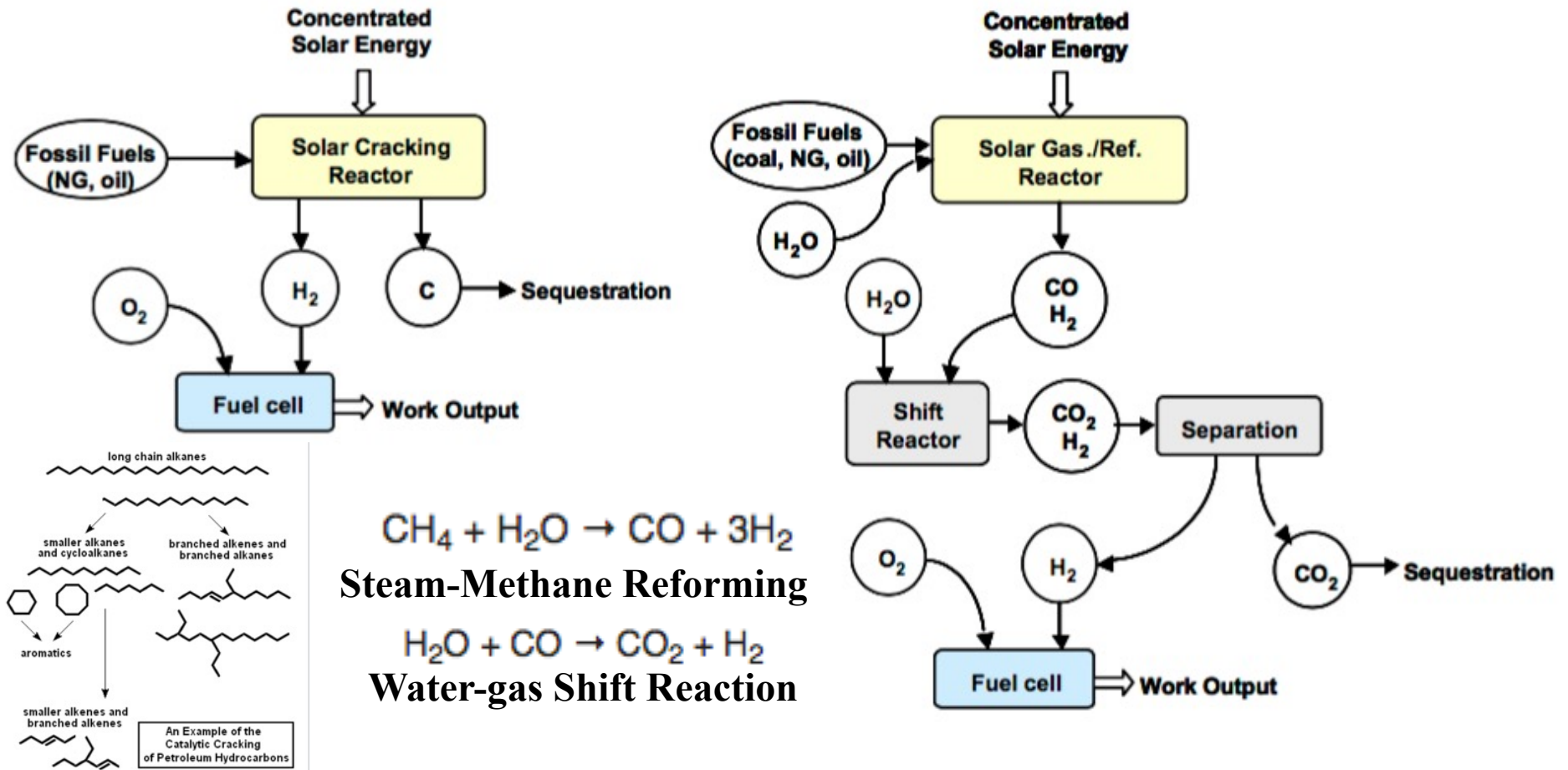


Fig. 7: Solar thermochemical routes for H_2 production using fossil fuels and H_2O as the chemical source – Solar cracking (left), and solar reforming and gasification (right). From [1].

Round-the-clock power supply and a sustainable economy via synergistic integration of solar thermal power and hydrogen processes

Emre Gençer^a, Dharik S. Mallapragada^a, François Maréchal^b, Mohit Tawarmalani^c, and Rakesh Agrawal^{a,1}

^aSchool of Chemical Engineering, Purdue University, West Lafayette, IN 47907; ^bIndustrial Process and Energy Systems Engineering Group, École Polytechnique Fédérale de Lausanne, CH-1951 Sion, Switzerland; and ^cKrannert School of Management, Purdue University, West Lafayette, IN 47907

Edited by Hans Joachim Schellnhuber, Potsdam Institute for Climate Impact Research (PIK), Potsdam, Germany, and approved November 17, 2015 (received for review July 12, 2015)

We introduce a paradigm—“hydricity”—that involves the coproduction of hydrogen and electricity from solar thermal energy and their judicious use to enable a sustainable economy. We identify and implement synergistic integrations while improving each of the two individual processes. When the proposed integrated process is operated in a standalone, solely power production mode, the resulting solar water power cycle can generate electricity with unprecedented efficiencies of 40–46%. Similarly, in standalone hydrogen mode, pressurized hydrogen is produced at efficiencies approaching ~50%. In the coproduction mode, the coproduced hydrogen is stored for uninterrupted solar power production. When sunlight is unavailable, we envision that the stored hydrogen is used in a “turbine”-based hydrogen water power (H₂WP) cycle with the calculated hydrogen-to-electricity efficiency of 65–70%, which is comparable to the fuel cell efficiencies. The H₂WP cycle uses much of the same equipment as the solar water power cycle, reducing capital outlays. The overall sun-to-electricity efficiency of the hydricity process, averaged over a 24-h cycle, is shown to approach ~35%, which is nearly the efficiency attained by using the best multijunction photovoltaic cells along with batteries. In comparison, our proposed process has the following advantages: (i) It stores energy thermochemically with a two- to three-fold higher density, (ii) coproduced hydrogen has alternate uses in transportation/chemical/petrochemical industries, and (iii) unlike batteries, the stored energy does not discharge over time and the storage medium does not degrade with repeated uses.

solar | electricity | hydrogen | solar thermal power | process synthesis

metrics of interest. The STE efficiency refers to the fraction of incident solar energy that is recovered as the net electricity output and accounts for the losses in the solar concentrators and blackbody collection system. Heat-to-electricity efficiency refers to the fraction of process heat input that is recovered as the net electricity output and is a true measure of the efficiency of the power cycle. The third metric, OSTE efficiency (*SI Appendix, Eq. S4*), is the net STE efficiency for a constant power delivery round-the-clock—that is, over the average 24-h production accounting for energy storage and delivery of the stored energy. Hydrogen production cycles are evaluated based on sun-to-hydrogen efficiency, which refers to the fraction of incident solar energy that is recovered as the net hydrogen output based on its lower heating value (*SI Appendix, Eq. S10*).

Solar photovoltaic (PV) and solar thermal are the two main methods of solar power generation. Solar PV systems generate electricity using only a portion of the solar spectrum (7). However, PV systems are suitable for both diffuse and direct sunlight applications (8). To date, the maximum reported STE efficiencies for silicon-crystalline PV is 27.6%, single-junction gallium arsenide PV is 29.1%, and concentrator four-junction PV is 44.7% (9). Solar thermal systems use concentrators to absorb photons of all wavelengths in the incident spectrum as high-temperature heat (10, 11). Due to the use of optical concentrators, these systems can only be operated under direct sunlight, which imposes geographical limitations (12). Further, these systems are anticipated to be cost-effective only as large-scale power plants, owing to the capital costs of installing solar concentrators (12, 13). However, the highest STE

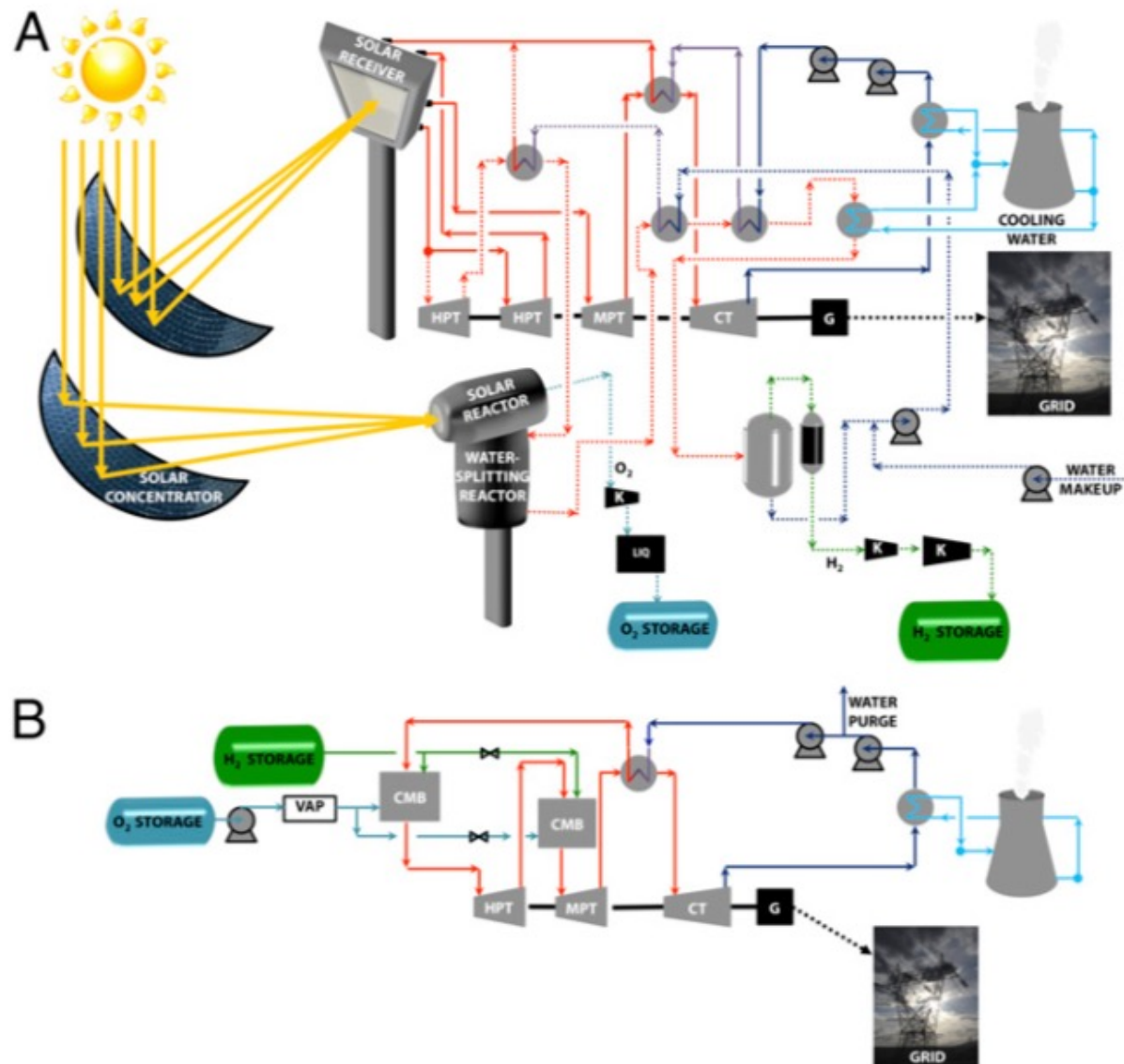


Fig. 1. (A) An example hydricity process: SWH₂P cycle with two-step hydrogen production using the FeO/Fe₃O₄ cycle. Solid lines represent streams that are solely involved in the electricity production (i.e., SWP-1). Dotted lines represent streams that are related to hydrogen production as well as electricity production. CT, condensing turbine; G, generator; HPT, high-pressure turbine; K, compressor; LIQ, liquefaction process; MPT, medium-pressure turbine. (B) H₂WP cycle, hydrogen oxy-combustion in water environment. CMB, hydrogen combustor.

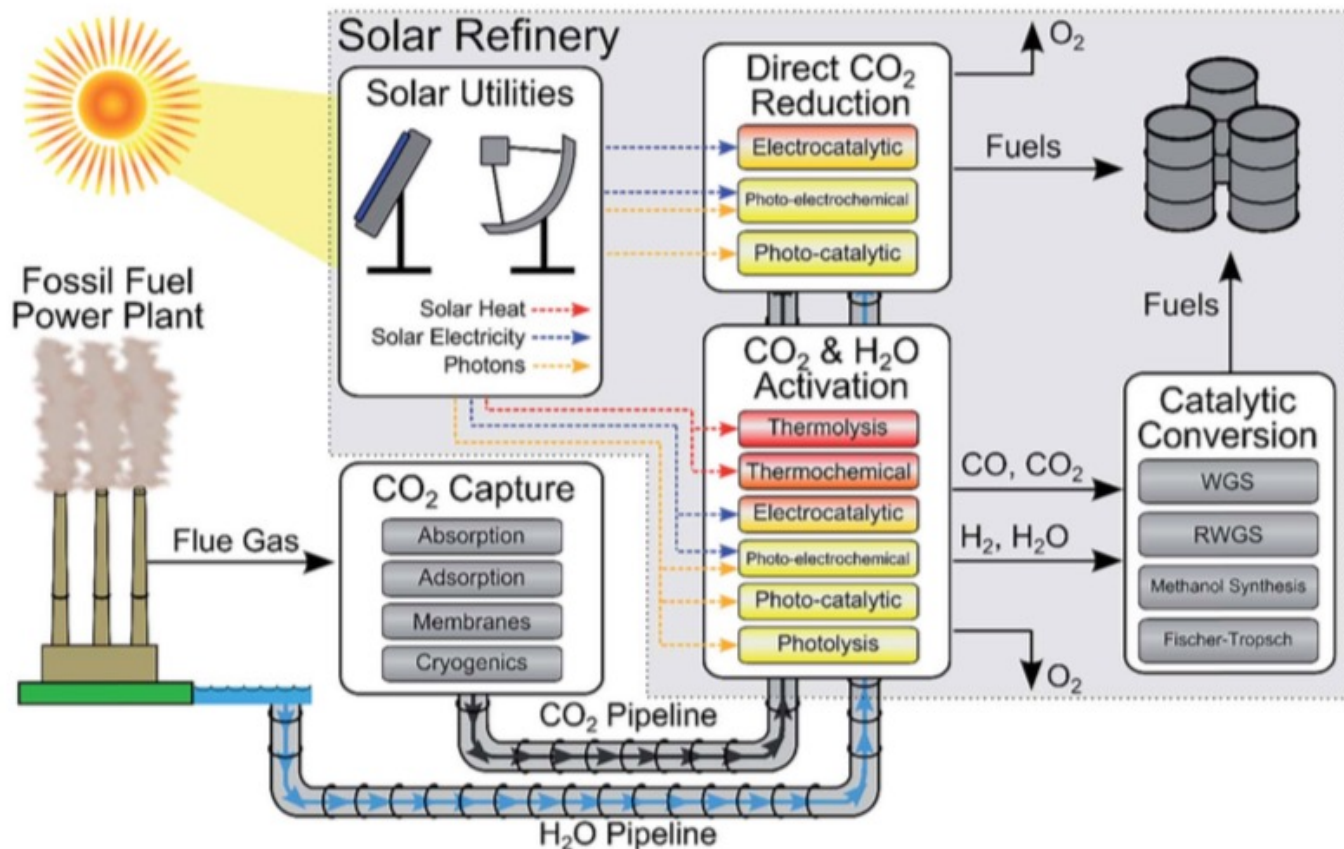


Fig. 1 Schematic for solar fuels production. Solar fuel feedstocks (CO₂, H₂O, and solar energy) are captured on-site and/or transported to the solar refinery. Solar energy provides solar utilities in the form of heating, electricity, and photons which are used in the solar refinery to convert CO₂ and H₂O into fuels. CO₂ and H₂O are converted to fuels through two principal routes: (1) direct solar-driven CO₂ reduction by H₂O to fuels or (2) solar activation of CO₂/H₂O to CO/H₂, respectively, and subsequent catalytic conversion to fuels *via* traditional processing (*i.e.* methanol synthesis or Fischer-Tropsch). The approximate temperature requirements for the solar-driven conversion processes are color-coded (red = high temperature, yellow = ambient temperature).



Cite this: *Energy Environ. Sci.*, 2015, 8, 126

A general framework for the assessment of solar fuel technologies†

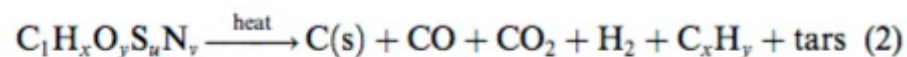
Jeffrey A. Herron, Jiyong Kim,[‡] Aniruddha A. Upadhye, George W. Huber and Christos T. Maravelias*

The conversion of carbon dioxide and water into fuels in a solar refinery presents a potential solution for reducing greenhouse gas emissions, while providing a sustainable source of fuels and chemicals. Towards realizing such a solar refinery, there are many technological advances that must be met in terms of capturing and sourcing the feedstocks (namely CO₂, H₂O, and solar energy) and in catalytically converting CO₂ and H₂O. In the first part of this paper, we review the state-of-the-art in solar energy collection and conversion to solar utilities (heat, electricity, and as a photon source for photo-chemical reactions), CO₂ capture and separation technology, and non-biological methods for converting CO₂ and H₂O to fuels. The two principal methods for CO₂ conversion include (1) catalytic conversion using solar-derived hydrogen and (2) direct reduction of CO₂ using H₂O and solar energy. Both hydrogen production and direct CO₂ reduction can be performed electro-catalytically, photo-electrochemically, photo-catalytically, and thermochemically. All four of these methods are discussed. In the second part of this paper, we utilize process modeling to assess the energy efficiency and economic feasibility of a generic solar refinery. The analysis demonstrates that the realization of a solar refinery is contingent upon significant technological improvements in all areas described above (solar energy capture and conversion, CO₂ capture, and catalytic conversion processes).

Received 25th June 2014
Accepted 1st October 2014

DOI: 10.1039/c4ee01958j

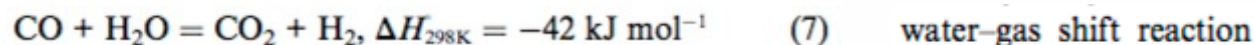
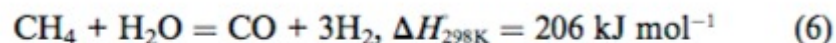
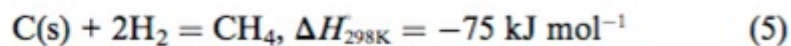
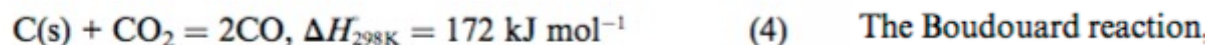
www.rsc.org/ees



Pyrolysis has been extensively studied empirically for various coal ranks ranging from anthracite (~10 wt% volatile matter) to peat (>65 wt% volatile matter), as well as for scrap tires, plastics, biomass, and refuse derived fuels.¹³⁻¹⁷ Solar-driven pyrolysis was investigated in early studies on biomass and coal.¹⁸⁻²¹ Subsequent to pyrolysis, char serves as the reactant for the highly endothermic carbon-steam gasification reaction,

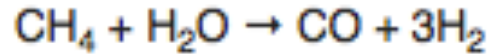


Favorable conditions for this reaction are temperatures above 1100 K, where the reaction kinetics is fast and equilibrium is entirely on the side of the products. Eqn (3) summarizes the overall reaction, but a number of intermediate competing reactions need to be considered:



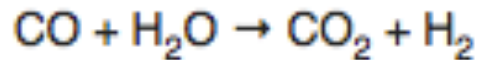
Biomass/Syngas

Steam Reforming Reaction: CH₄ to H₂ and CO



At high temperatures (700 – 1100 °C) and in the presence of a metal-based catalyst (nickel), **steam** reacts with methane to yield carbon monoxide and hydrogen. ...

Water Shift Gas Reaction: CO to H₂



The shift reaction will operate with a variety of catalysts between 400°F and 900

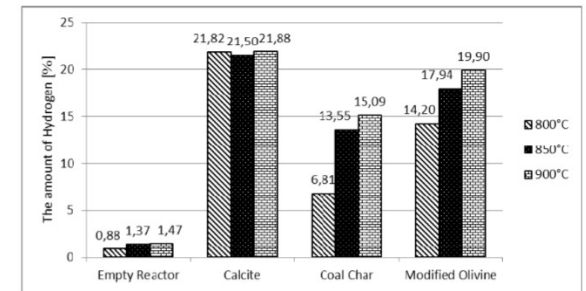
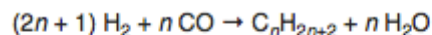


Fig. 3. Average percentage representation of hydrogen for the studied catalysts at t=800, 850 and 900°C

Fischer-Tropsch Reaction: H₂ and CO to Liquid Fuel

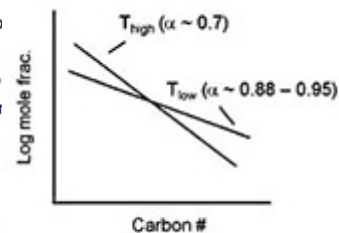
Reaction mechanism [\[edit \]](#)

The Fischer–Tropsch process involves a series of chemical reactions that produce a variety of hydrocarbons, ideally having the formula (C_nH_{2n+2}). The more useful reactions produce **alkanes** as follows:



where *n* is typically 10–20. The formation of methane (*n* = 1) is unwanted. Most of the alkanes produced tend to be straight-chain, suitable as **diesel fuel**. In addition to alkane formation, competing reactions give small amounts of **alkenes**, as well as **alcohols** and other oxygenated hydrocarbons.^[4]

- Nickel (Ni) tends to promote methane formation, as in a [methanation process](#); thus generally it is not desirable
- Iron (Fe) is relatively low cost and has a higher water-gas-shift activity, and is therefore more suitable for a lower hydrogen/carbon monoxide ratio (H₂/CO) syngas such as those derived from coal gasification
- Cobalt (Co) is more active, and generally preferred over ruthenium (Ru) because of the prohibitively high cost of Ru
- In comparison to iron, Co has much less water-gas-shift activity, and is much more costly.



Low T	Sasol Arge	High T	Sasol Synthol
• low C ₁ – C ₄	13.3	• higher C ₁ – C ₄	43.0
• low C ₅ – C ₁₁	17.9	• higher C ₅ – C ₁₁	40.0
• low C ₁₂ –C ₁₉	13.9	• less C ₁₂ –C ₁₉	7.0
• 50-70% wax	51.7	• low wax	4.0
• 220-270°C		• 325 – 350°C	
• α: 0.87+		• α: ~0.7	
• gasoline/diesel: 1:2		• gasoline/diesel: 2:1	
• 80° Cetane #		• 50-60 Cetane #	
• 0-20 Octane #		• 0-60 Octane #	

Biomass/Syngas

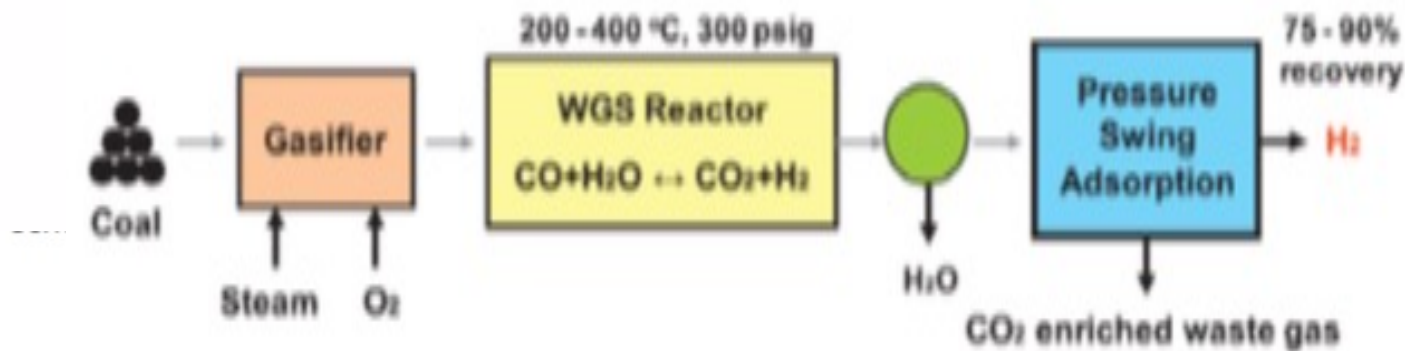


Figure1: Conventional process flow sheet for the production of hydrogen from coal gasification (Bell et al., 2011)

Carbon Dioxide Capture and Hydrogen Purification from Synthesis Gas by Pressure Swing Adsorption

Cheng-tung Chou ^{a*}, Fei-hong Chen ^a, Yu-Jie Huang ^a, Hong-sung Yang ^b

^a Department of Chemical and Materials Engineering, National Central University, Jhong-Li, Taiwan

^b Center for General Education, Hwa-Hsia Institute of Technology, Chung-Ho District, New Taipei City, Taiwan
t310030@ncu.edu.tw

More Polar Molecules will Adsorb



More Polar Molecules will Adsorb

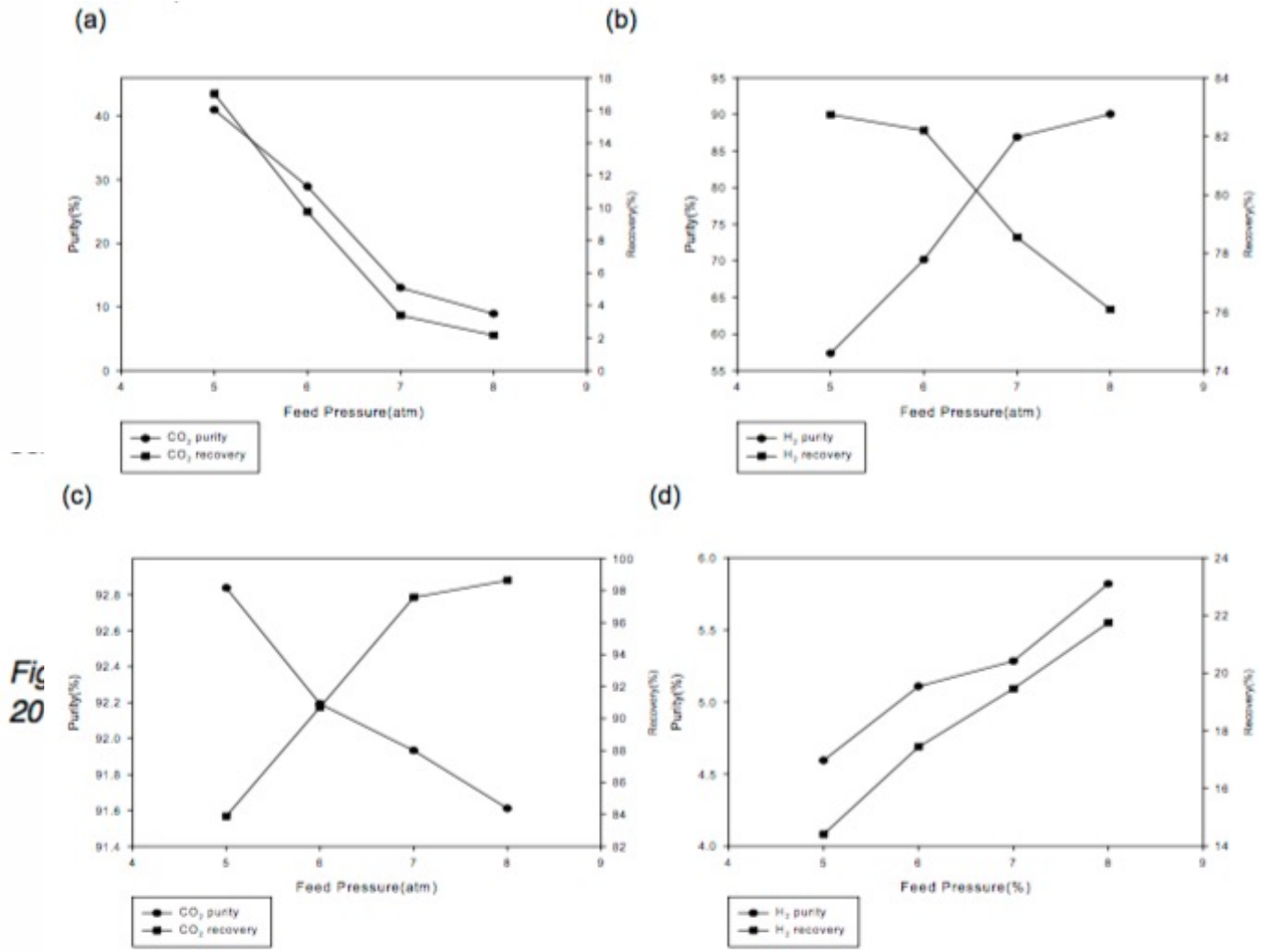


Fig 20

Bell et al.,

Figure 4: Effect of feed pressure at CO₂-PSA on (a) CO₂ in top product (b) H₂ in top product (c) CO₂ in bottom product (d) H₂ in bottom product

Biological Digestion

India Biogas Reactor (<https://www.youtube.com/watch?v=9kKRdIAFuZw>)



[Biogas Reactor for the Developing World](https://www.youtube.com/watch?v=Cwm5Rm8ulsk) (<https://www.youtube.com/watch?v=Cwm5Rm8ulsk>)




Biomass/Syngas

[Single House Biogas](http://www.youtube.com/watch?v=3th2bcqHbsk) (<http://www.youtube.com/watch?v=3th2bcqHbsk>)



Biomass/Syngas

[Biogas in Kenya](http://www.youtube.com/watch?v=qh3mmgiybTw) (<http://www.youtube.com/watch?v=qh3mmgiybTw>)

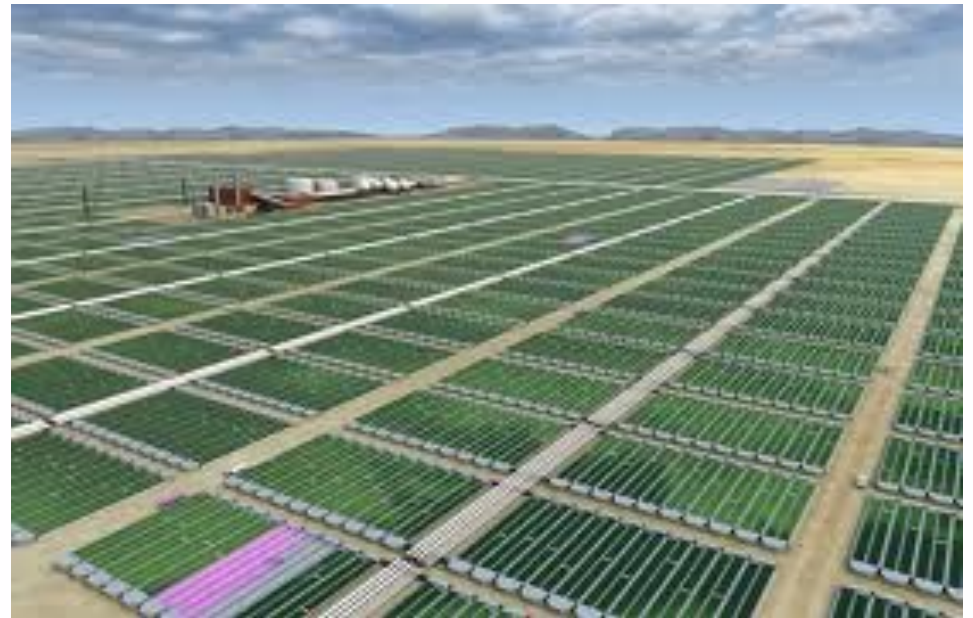


Dominic Wanjihia
CEO, Biogas International

Algae

Algae:

**Food
Diesel Fuel
Hydrogen**



[Spirulina Summary](#)

<http://wellnessmama.com/4738/spirulina-benefits/>

Algae:

Food



Spirulina Summary

<http://wellnessmama.com/4738/spirulina-benefits/>

It also contains (per Tablespoon):

Wellness Mama

SPIRULINA

Only 20 Calories – 4 grams of Protein
11% of the RDA of Vitamin B1 (Thiamin)
15% of the RDA of Vitamin B2 (Riboflavin)
4% of the RDA of Vitamin B3 (Niacin):
Copper- 21% and Iron-11% of the RDA

1 TABLESPOON
(15.0 ML)

Algae in Lake Chad



<https://www.youtube.com/watch?v=d7VXoFSDHJM>

<https://www.youtube.com/watch?v=9rbrXgEqfFc>

[Spirulina Algae in West Africa](https://www.youtube.com/watch?v=CxSA5iiGgiY) (<https://www.youtube.com/watch?v=CxSA5iiGgiY>)



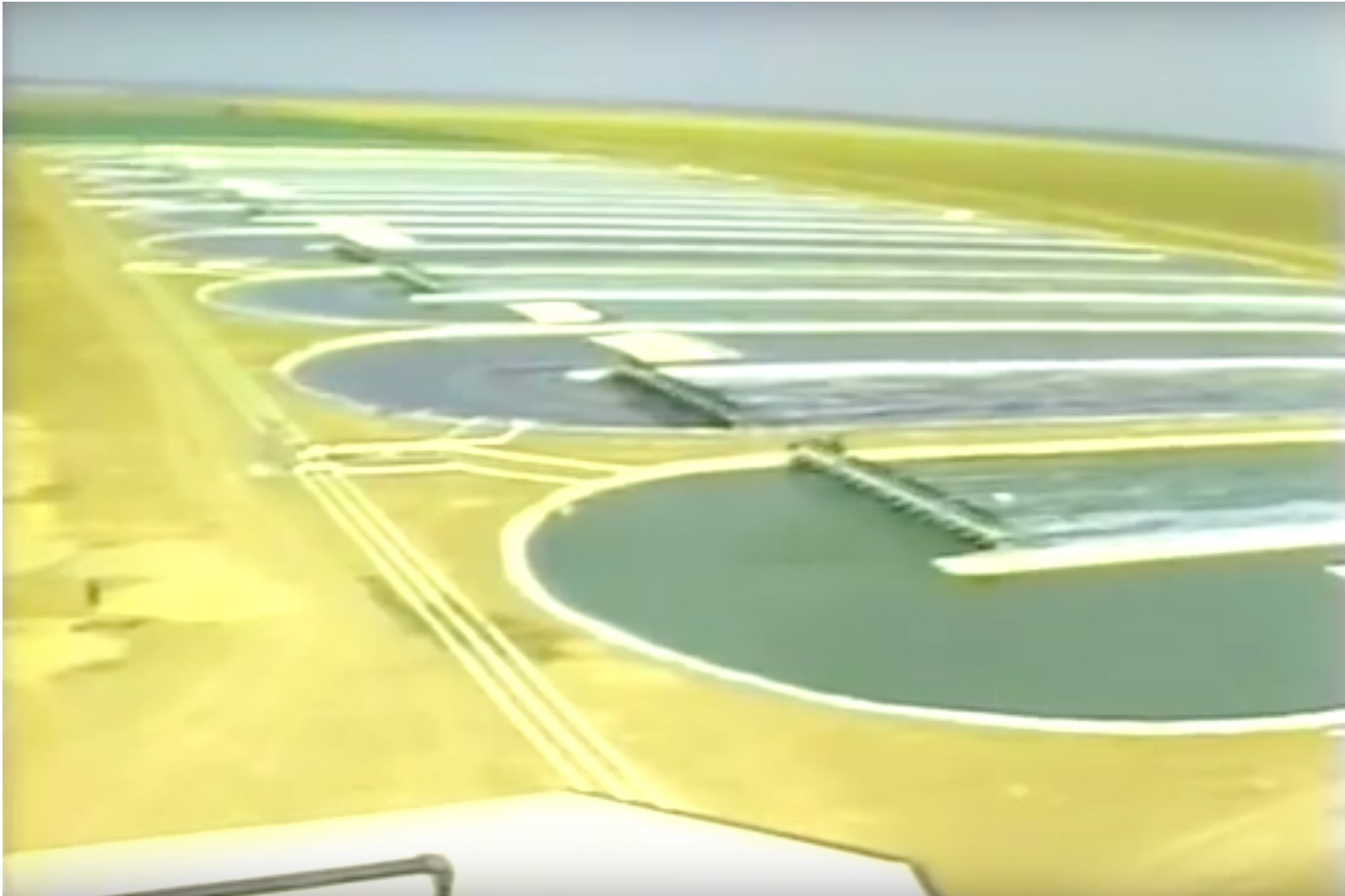
Grow Spirulina in Northern California

<https://www.youtube.com/watch?v=f6Kff2WauO8>



[Spirulina in France](https://www.youtube.com/watch?v=qfCBDyPiTS4) (<https://www.youtube.com/watch?v=qfCBDyPiTS4>)





[Cooking with Spirulina](https://www.youtube.com/watch?v=_UVWLMjk6Vw) (https://www.youtube.com/watch?v=_UVWLMjk6Vw)



Hydrogen from Algae

Simple schematic for biological hydrogen production

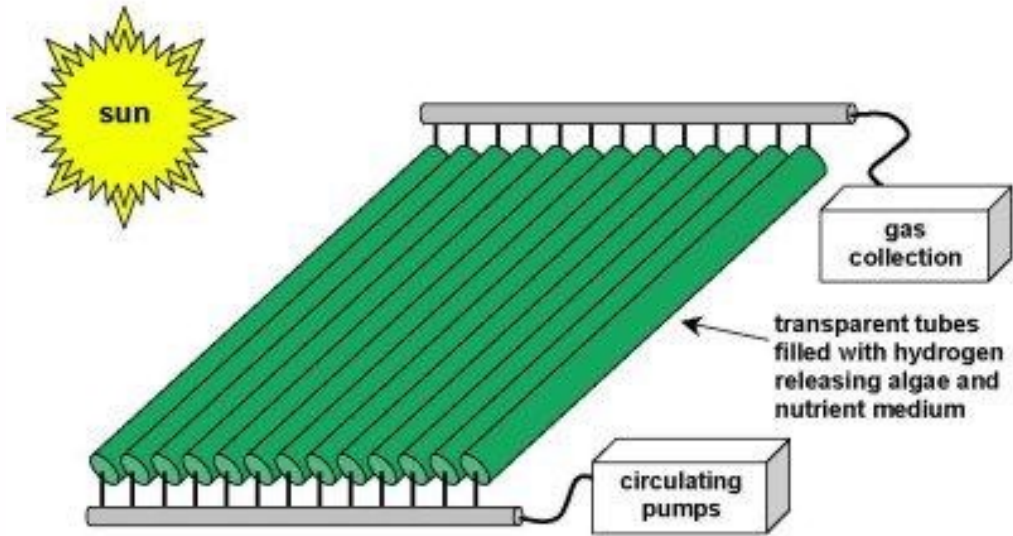


Table 1

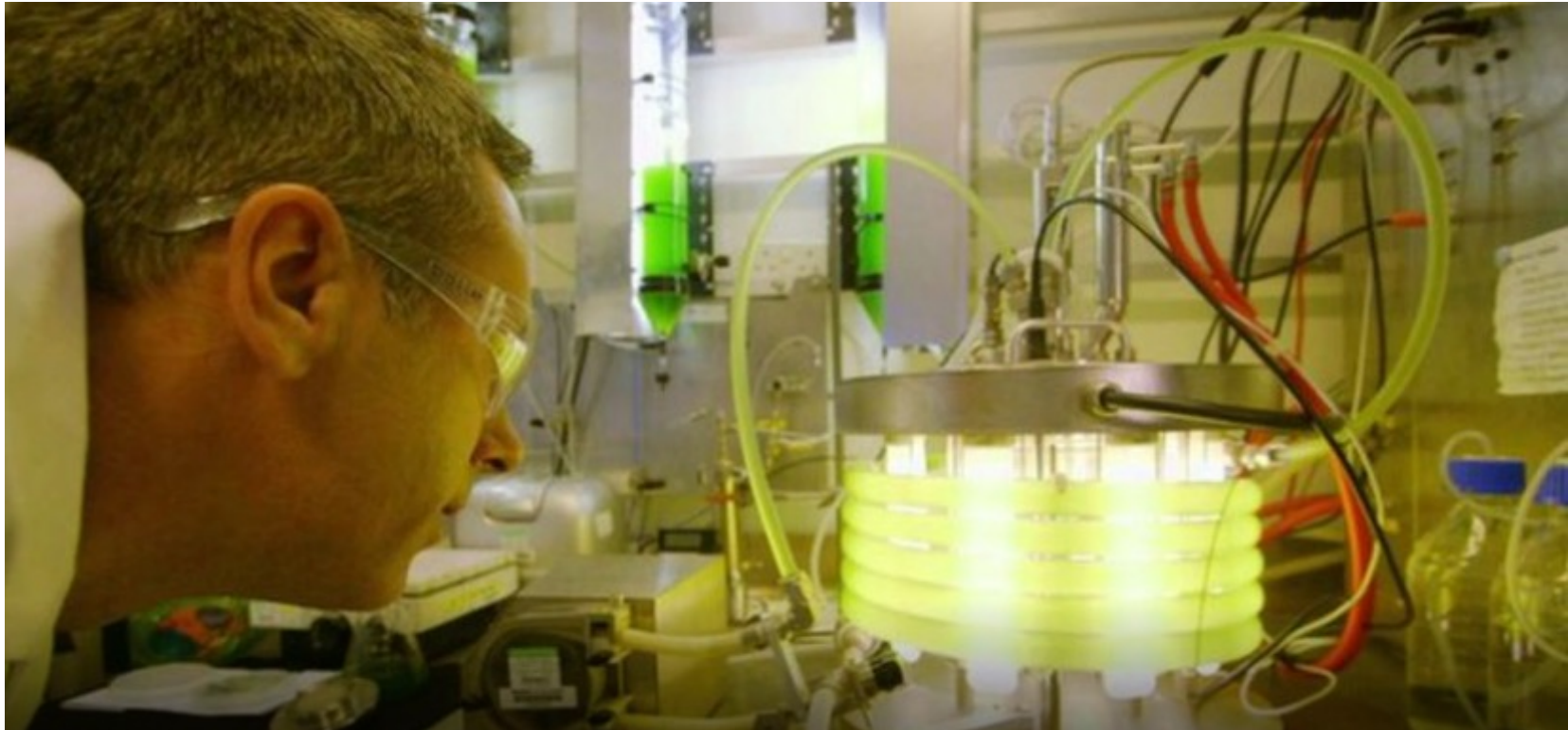
Microorganisms used in hydrogen production.

Microorganism	Mode of Operation	References
<i>C. reinhardtii</i> <i>Phaeodactylum tricornutum</i>	Genetic engineering using expressed sequence tags (ESTs)	[30]
<i>Thalassiosira pseudonana</i>		
<i>Cyanidioschyzon merolae</i>		
<i>Ostreococcus lucimarinus</i>		
<i>Ostreococcus tauri</i>		
<i>Micromonas pusilla</i>		
<i>Fragilariopsis cylindrus</i>		
<i>Pseudo-nitzschia</i>		
<i>Thalassiosira rotula</i>		
<i>Chlorella vulgaris</i>		
<i>Dunaliella salina</i>		
<i>Micromonas pusilla</i>		
<i>Galdieria sulphuraria</i>		
<i>Porphyra purpurea</i>		
<i>Volvox carteri</i>		
<i>Aureococcus anophagefferens</i>		
<i>Chlorella pyrenoidosa</i>	Lipid Biosynthesis	[31]
<i>Chlamydomonas moewusii</i>	Anaerobic Fermentation	[32]
<i>Scenedesmus oblique</i>	Anaerobic Fermentation	[33]
<i>Anabaena variabilis</i>	Photo-Fermentation	[34]
<i>Rhodobactersphaeroides</i>	Transcriptional analysis	[29]
<i>Enterobacter aerogenes</i>	Batch Fermentation	[35]
<i>Clostridium butyricum</i>	Anaerobic Fermentation	[36]
<i>Bacillus coagulans</i>	Anaerobic Fermentation	[10]
<i>Clostridium acetobutylicum</i> ATCC 824	Anaerobic Fermentation	[37]
<i>Laminaria japonica</i>	Anaerobic Fermentation	[38]
<i>Gelidium amansii</i>	Dark Fermentation	[39]

Silicon Clusters to Produce H₂



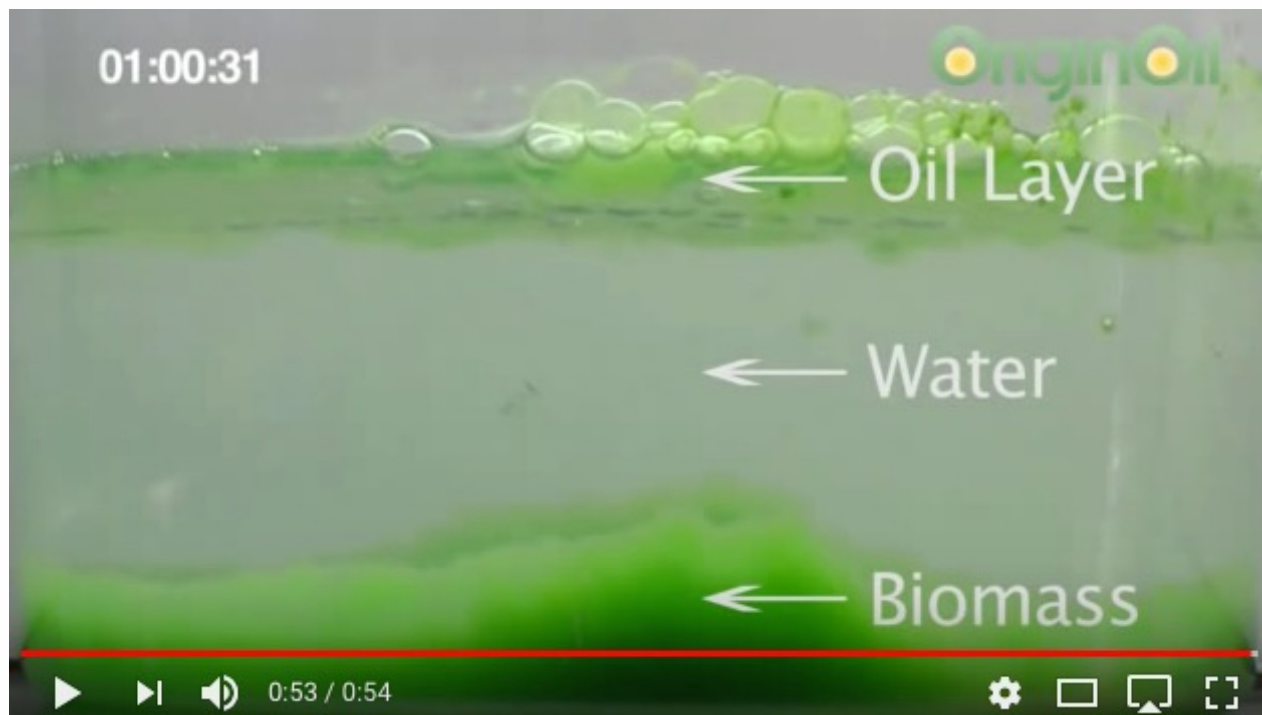
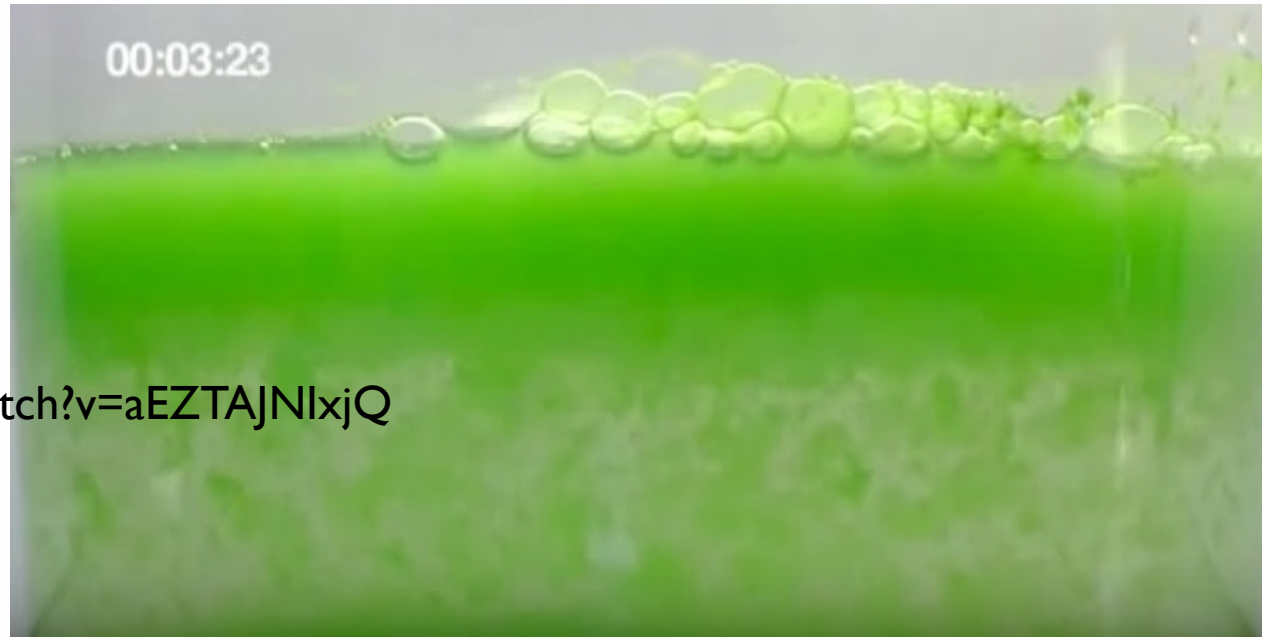
Two stage algae reactor for hydrogen production



Oil from Algae

Algae oil extraction

<https://www.youtube.com/watch?v=aEZTAJNlxjQ>



Cellana's Kona Demonstration Facility



Oil from Algae in lab



<https://www.youtube.com/watch?v=oQqlsk3cuWY>

Biofuel from Algae in Vermont



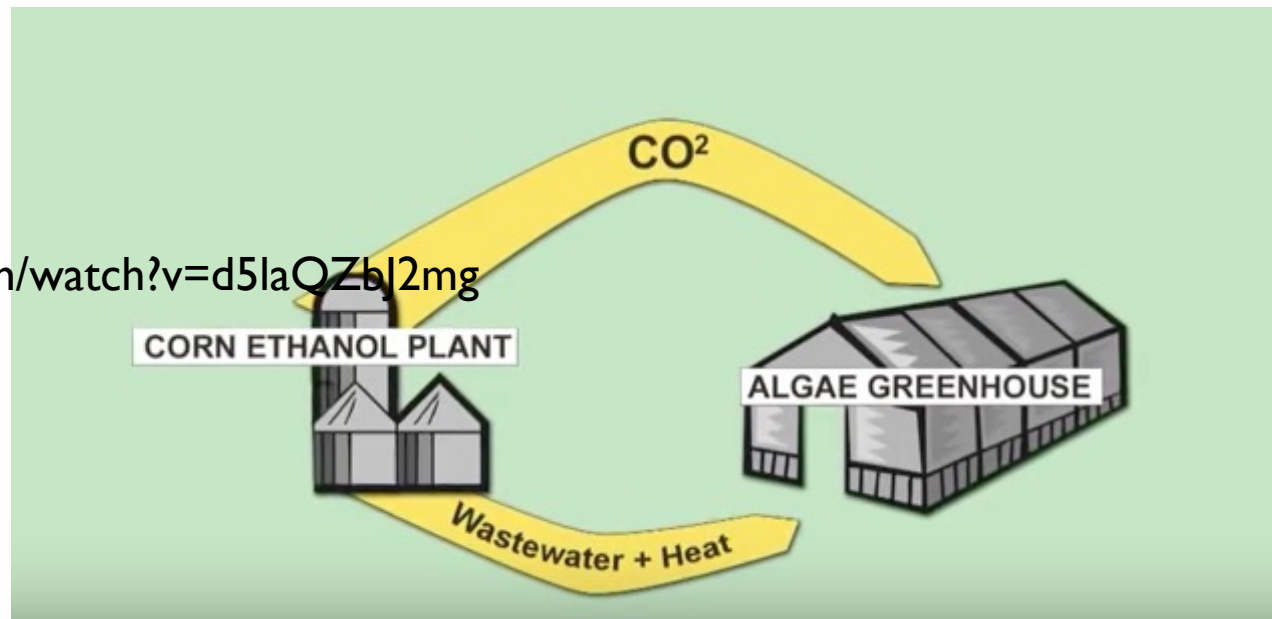
[US DOE Algae to Fuel Promo Video](#)

<https://www.youtube.com/watch?v=IxyvVkeW7Nk>



[Iowa Algae farm](#)

<https://www.youtube.com/watch?v=d5laQZbJ2mg>

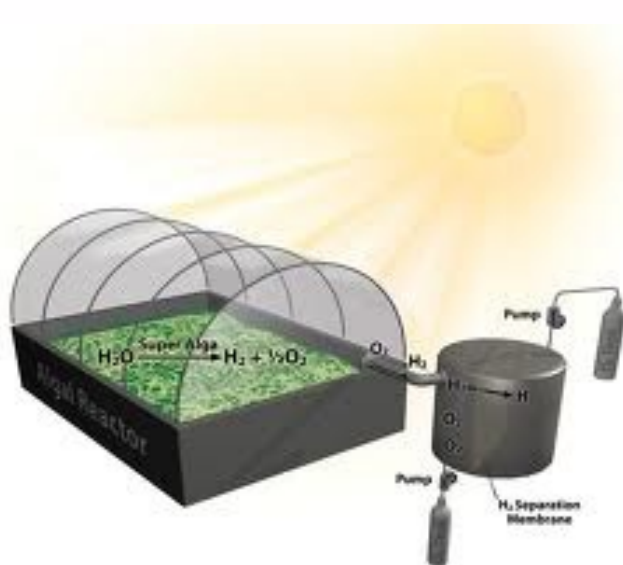


Algae Tower

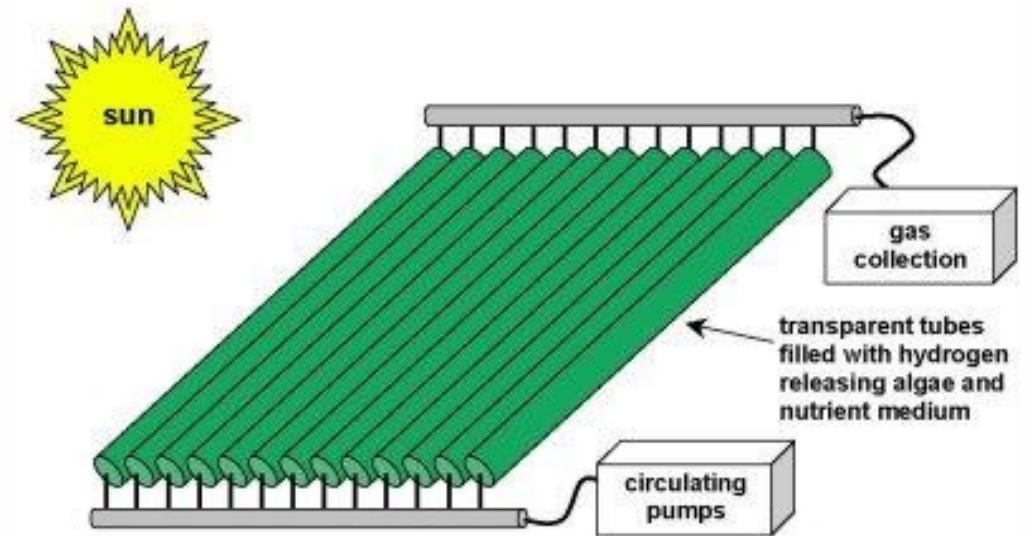
Algae Building in Germany

NASA Floating Algae Farm Project

(<http://www.youtube.com/watch?v=c7Goyg12Reg>)



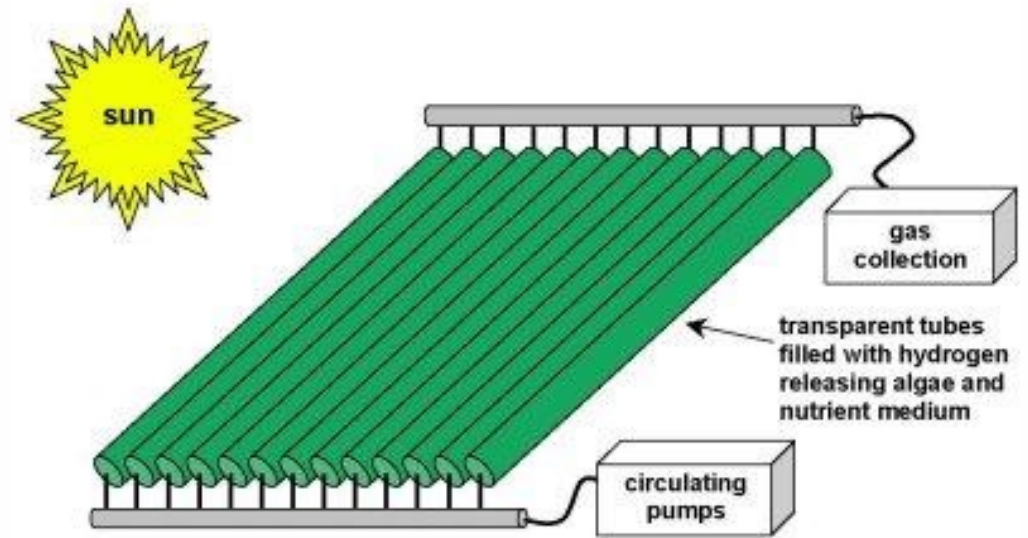
Simple schematic for biological hydrogen production



Algae Tower



Simple schematic for biological hydrogen production



Hydrogen from Algae

(http://www.youtube.com/watch?v=Or_F6qC0sK4) Comic look at H₂ from Algae

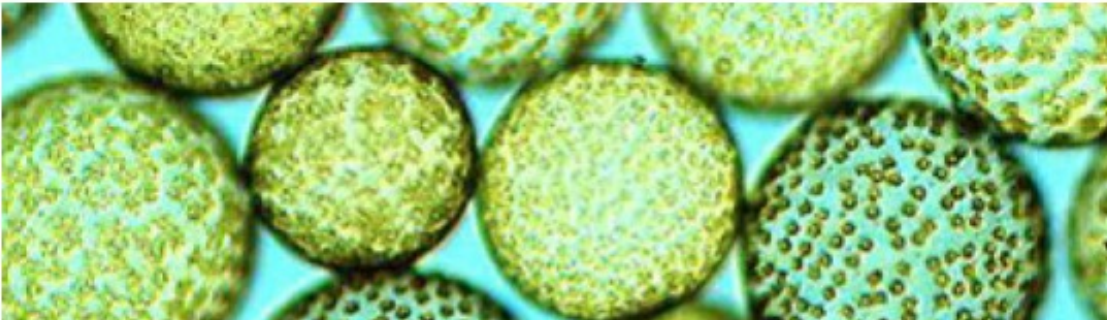
Hydrogen from Algae Imperial College

(<https://www.youtube.com/watch?v=OFByDMRbucs>)

<https://www.greentechmedia.com/articles/read/lessons-from-the-great-algae-biofuel-bubble#gs.PjrIF3k>

Entrepreneurs can have tunnel vision. VC herd mentality doesn't produce results. Physics and thermodynamics are fairly important in energy applications.

ERIC WESOFF | APRIL 19, 2017



According to some sources, an acre of algae could yield 5,000 to 10,000 gallons of oil a year, making algae far more productive than soy (50 gallons per acre), rapeseed (110 to 145 gallons), jatropha (175 gallons), palm (650 gallons), or cellulosic ethanol from poplars (2,700 gallons).

Jim Lane of *Biofuels Digest* authored what was possibly history's least accurate market forecast, projecting that algal biofuel capacity would reach 1 billion gallons by 2014. In 2009, Solazyme promised competitively priced fuel from algae by 2012. Algenol planned to make 100 million gallons of ethanol annually in Mexico's Sonoran Desert by the end of 2009 and 1 billion gallons by the end of 2012 at a production rate of 10,000 gallons per acre. PetroSun looked to develop an algae farm network of 1,100 acres of saltwater ponds that could produce 4.4 million gallons of algal oil and 110 million pounds of biomass per year.

Nothing close to 1 billion (or even 1 million) gallons has yet been achieved -- nor has competitive pricing.

Today, the few surviving algae companies have had no choice but to adopt new business plans that focus on the more expensive algae byproducts such as cosmetic supplements, nutraceuticals, pet food additives, animal feed, pigments and specialty oils. The rest have gone bankrupt or moved on to other markets.

- **Algae Floating Systems** is "temporarily shifting its focus away from fuel to nutraceutical and animal feed markets."
- **Algenol** intended to use nitrogen-fixing blue-green algae (cyanobacteria) in photobioreactors to produce ethanol directly. With tens of millions of dollars in public money and hundreds of millions in private-sector investment, **Algenol** once claimed its technology "enables the production of the four most important fuels (ethanol, gasoline, jet, and diesel fuel) for around \$1.30 per gallon each using proprietary algae, sunlight, carbon dioxide and saltwater at production levels of 8,000 total gallons of liquid fuel per acre per year." In 2015, the firm fired its CEO and shifted its focus to carbon capture and nutraceuticals.
- **Algae Tec**: An Australian PBR penny stock company with algae oil and algae byproduct dreams.
- **Algix** develops fish farms and algae harvest equipment.
- **AlgaeLink** was a sketchy retailer of photobioreactors and commercial algae cultivation equipment.
- **Alga Technologies** grows algae in closed bioreactors to harvest astaxanthin in Israel's Arava desert.
- **Aquaflow Biomimics** once intended to produce biofuel from wild algae harvested from open-air environments. The company is now a biofuel site developer called **NXT Fuels**.
- **Aurora Biofuels**: Aurora moved from fuel to food with its genetically modified algae in 2011. The firm went **bankrupt** in 2015 after winning more than \$23 million from Oak, Noventi Ventures and Gabriel Venture Partners.
- **Cellana** and its Hawaii-based algae feedstock production system received DOE funding to boost algae productivity as a way to reduce cost. The firm produces DHA and omega-3 EPA and DHA oils, animal feed/food, and biofuel feedstocks.
- **Global Algae Innovations** is exploring algal biofuels at a 3.2-acre algae farm co-located with a power plant in **Hawaii**. The firm has received \$11 million from the U.S. DOE.
- **GreenFuel Technologies**, long bankrupt, was backed with more than \$27 million in funding from Polaris Ventures, Draper Fisher Jurvetson and Access Private Equity.
- **Heliae** raised \$80 million from two \$20 billion food conglomerates in 2016, and has spent years developing a "platform technology" to produce nutraceuticals, personal care products and perhaps fuel through a mixture of phototrophic and fermentation processes.
- **LiveFuels** received \$10 million in funding from The Quercus Trust in 2007. Lissa Morgentahler-Jones and David Jones are still listed as officers of the firm on LinkedIn.
- **OriginOil** is now **OriginClear** and has shifted to water decontamination.
- **PetroAlgae** changed its name to **Parabel** as it shifted from fuel to foods in 2012.

- **Phycal** received significant DOE funding to design a high-yield algae farm and biorefinery in Hawaii.
- **Pond Technologies** is cultivating algae for carbon capture and nutraceuticals.
- **Renewable Algal Energy** is a microalgae products company that received DOE funding to prove out its algal oil harvesting and extraction technologies.
- **Sapphire Energy** produces omega-3 oils and animal feed ingredients. Sapphire raised more than \$100 million from Bill Gates' Cascade Investments and ARCH Venture Partners.
- **Seambiotic** uses raceway/paddle-wheel open pond algae cultivation. According to Israel 21C, Seambiotic "recently launched a commercial algae farm in China" to produce a "valuable nutraceutical food additive."
- **Solix**, once a well-funded algae fuel aspirant, repositioned itself as an astaxanthin, DHA, and omega-3 supplier.
- **Synthetic Genomics**, founded by Craig Venter and ExxonMobil, announced earlier this year that it has extended its agreement on joint research into advanced algae biofuels "after making significant progress in understanding algae genetics, growth characteristics and increasing oil production."
- **TerraVia** (formerly Solazyme) shifted from supplying fuels to oils, algal flour and proteins with a heterotrophic process that ferments genetically modified algae fed sugars.
- **XL Renewables** developed algal production systems using dairy waste streams, then changed its name to Phyco Biosciences and went out of business.

Considering the immense technical risks and daunting capital costs of building an algae fuel company, it doesn't seem like a reasonable venture capital play. And most -- if not all -- of the VCs I've spoken with categorize these investments as the longer-term, long-shot bets in their portfolio. But given the size of the liquid fuels market, measured in trillions of dollars, not the customary billions of dollars, it makes some sense to occasionally take the low-percentage shot.

Select History of Vertical Farming



1999 Dickson Despommier, Columbia University

[Video 1](#); [Video 2](#)

2009 Pilot production system was installed at Paignton Zoo Environmental Park in the United Kingdom

2010 Green Zionist Alliance, Israel

2012 Singapore Sky Greens Farms 3 story farm

2012 [The Plant, Chicago](#)

2013 Association for Vertical Farming Munich

2015 Growing Underground, London

2016 TerraFarm in Shipping containers

2017 Mirai, Japan

2018 Largest indoor farm in Europe Lincolnshire Jones Food Company

2019 Freight Farms Greenery farm-to-table system

Plantagon



[Bowery NJ](#)



Singapore

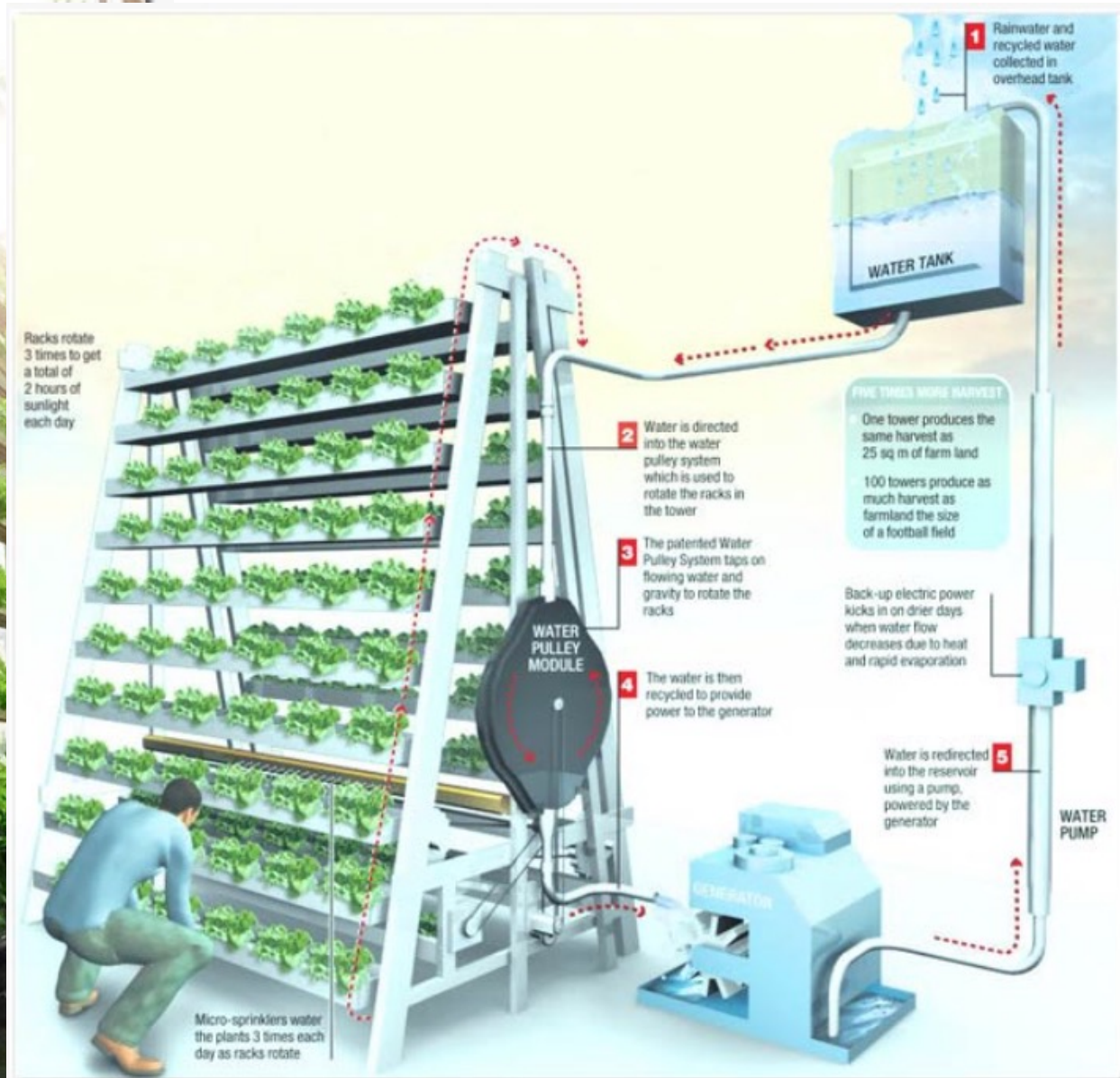




Image Courtesy MNDSingapore

Sky Greens Singapore

MND Singapore



Advantages:

Efficiency

Resistance to Weather

Environmental Conservation

No Pesticides

Almost Total Control

Location, Location, Location

Disadvantages:

Startup Costs

Aspects of Vertical Farming

Hydroponics, plant growth with no soil

Aquaponics, plant/fish coupled growth/production

Aeroponics (not yet applied except by NASA)

CEA: Controlled-Environment Agriculture

Types of Vertical Farming

Building-based

Shipping-container based

Deep Farms

Advantages

- It offers a plan to handle future food demands
- It allows crops to grow year-round
- It uses significantly less water
- Weather doesn't affect the crops
- More organic crops can be grown
- There is less exposure to chemicals and disease

Disadvantages

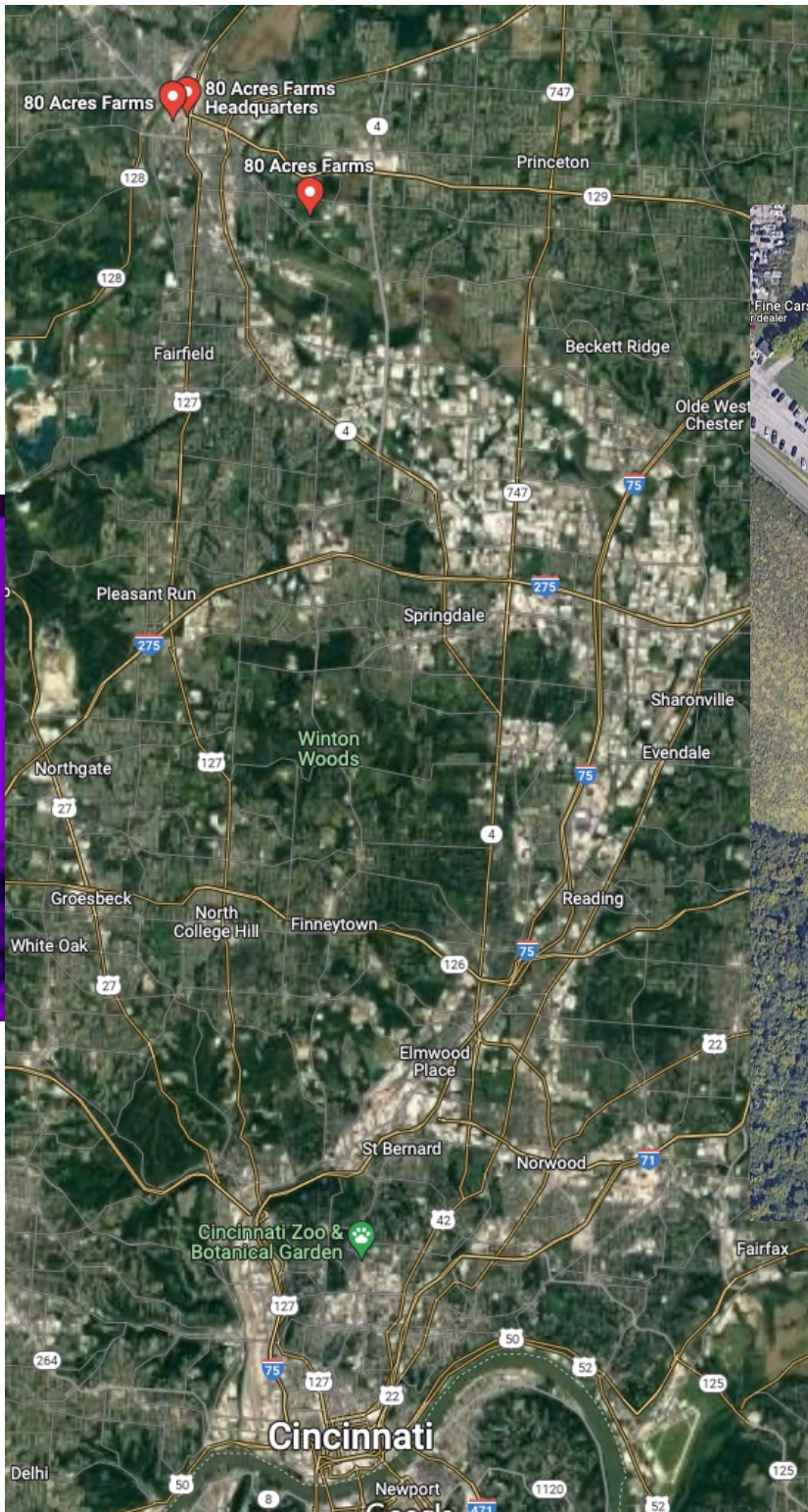
- It could be very costly to build and economic feasibility studies haven't yet been completed
- Pollination would be very difficult and costly
- It would involve higher labor costs
- It relies too much on technology and one day of power loss would be devastating



Vertical Farming in Cincinnati



BETTER THAN ORGANIC, ALWAYS PESTICIDE FREE



Vertical Farming Colorado

VERTICAL HARVEST JACKSON HOLE



Plenty



Aerofarms

AEROFARMS™

[OUR GREENS](#) [ABOUT US](#) [RECIPES](#) [OUR FLAVORSPECTRUM™](#) [NEWS](#)



Bright Farms

OUR MISSION

HOW WE GROW

OUR FARMS

OUR PRODUCTS

WHERE TO BUY

FAQ

SELINGROVE, PENNSYLVANIA

WILMINGTON, OHIO

ROCHELLE, ILLINOIS

CULPEPER, VIRGINIA

HENDERSONVILLE, NORTH CAROLINA

LOUDON, NEW HAMPSHIRE

VIRTUAL TOUR

INTRODUCING CRUNCH

Our easy-to-make crunch kit takes Sunny Crunch® lettuce and combines it with tasty toppings and dressing for a simple, great-tasting salad in a snap!

TRY ONE TODAY!

JUST TOSS,
SERVE,
& SAVOR



InFarm



Freight Farms



Science Barge

🌐 Add languages ▾

Article [Talk](#)

[Read](#) [Edit](#) [View history](#) [Tools](#) ▾

From Wikipedia, the free encyclopedia

The **Science Barge** is a floating urban farm and environmental education center that has been docked in [Yonkers, New York, USA](#) since late 2008.^[1] The Barge grows crops using a [hydroponic](#) greenhouse powered by [solar panels](#), [wind turbines](#), and [biofuels](#). The crops in the greenhouse are irrigated by captured rainwater and desalinated river water. Food is grown without carbon emissions, no agricultural waste is discharged into the watershed and no pesticides are used. The Science Barge is also a public education tool and hosts school groups from [Westchester, New York City](#) and the greater New York area visiting during the week, and the general public on weekends. From 2006–2008, the Science Barge docked for periods of two months at each of six stops along the Manhattan waterfront with the goal of educating the public on urban [sustainable agriculture](#).

In 2015, Nathalie Manzano-Smith and [Ted Caplow](#) won the Knight Cities Challenge grant competition from the [John S. and James L. Knight Foundation](#) with a proposal to build a [Miami Science Barge](#) and moor it in [Museum Park](#) in downtown [Miami, FL](#). The Miami Science Barge opened on Earth Day, April 22, 2016. The following April, the Barge was gifted to [Frost Science Museum](#). Compared with the original Science Barge, the Miami Science Barge places more emphasis on marine science, conservation, and sustainable aquaculture, while also updating many of the urban agricultural systems featured on the original.



Docked at [North River Pier 84](#) in 2007



Closer view of the wind turbines in 2008

TerraFarm



Growing Underground



Persona O2 Tokyo



Jonathan Webb

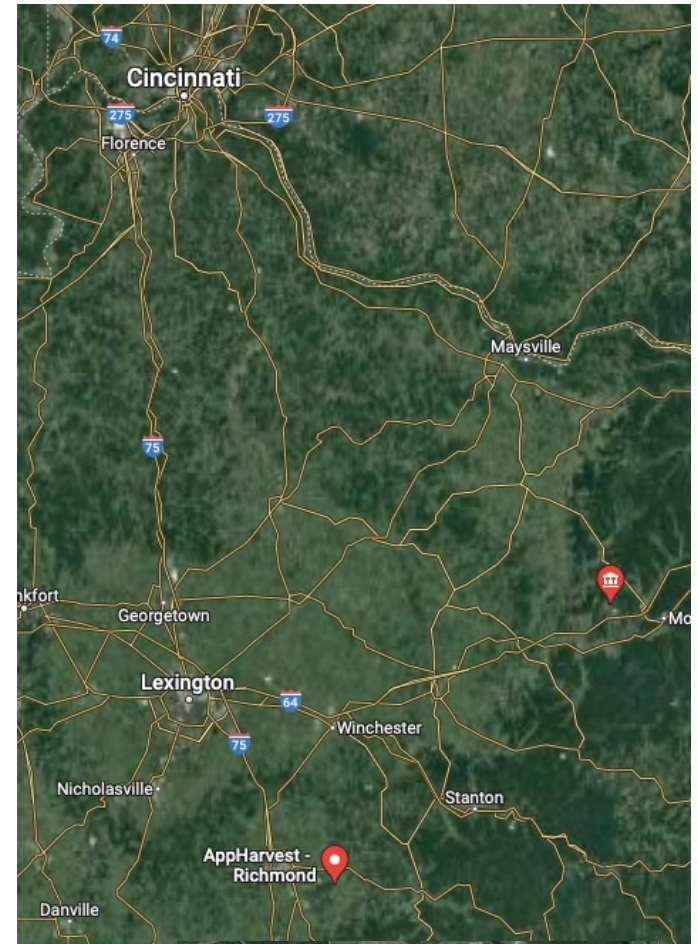


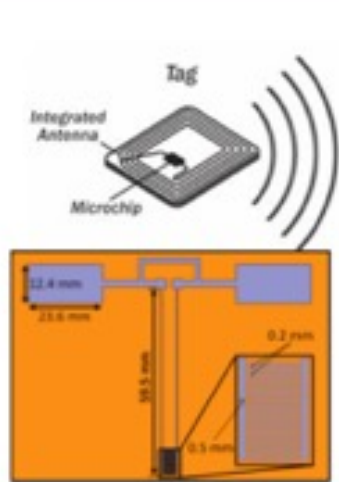
LEARN ▾ ENGAGE ▾ EAT ▾



PROCESS

Technology that empowers nature





Sensor, inkjet printed on paper
 Sensor & RFID Tag <\$ 0.50 each
 6 month lifetime in soil
 Manufactured in Ethiopia
 Place at 10, 20, 50 cm depths
 In an array on a field



RFID Reader ~ \$5
 Assembled in Ethiopia



Manually read soil moisture
 content and adjust drip irrigation.

Drip Irrigation

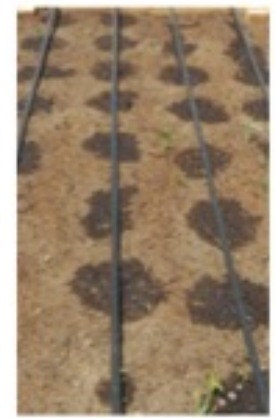


Figure 1. Sketch of printed soil moisture sensor concept. The sensor and RFID tag can be screen or inkjet printed on paper in Ethiopia. These would be buried at variable depths through a field to monitor soil moisture with a hand held RFID reader, assembled in Ethiopia. The system could be automated or manually read to control a drip irrigation system. The Hararghe Catholic Secretariat near Dire Dawa already installs drip irrigation systems in the Oromo/Somali Region. (Sensor drawing from Kim S, Le T, Tentzeris MM, Harrabi A, Collado A, Georgiadis A (2014).)

Printed Soil Moisture Sensors for Drip Irrigation

- Uses printable conductive ink
- Doped titania nanoparticles
- RFID interrogation
- Moisture affects impedance
- Can be used for chemical detection (CO)

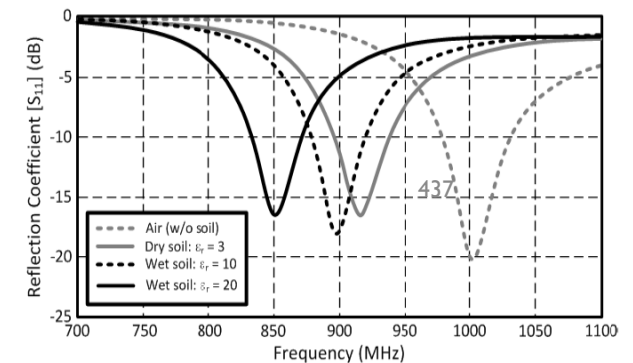
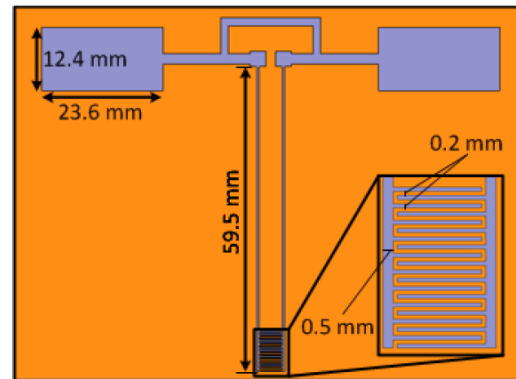
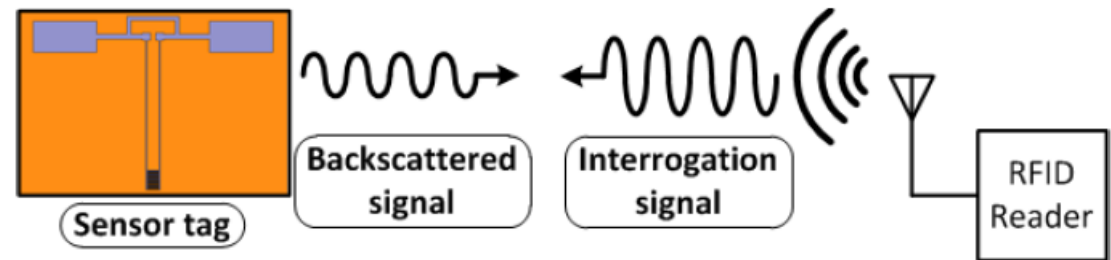
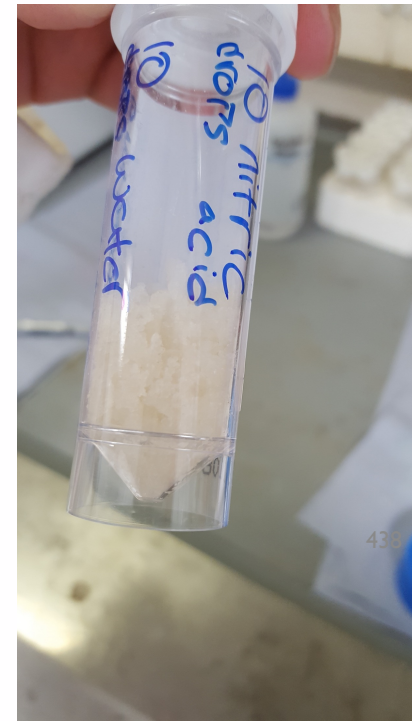


Fig. 3. Simulated reflection coefficients (S_{11}) of the proposed soil moisture sensor in air, dry soil and wet soil.

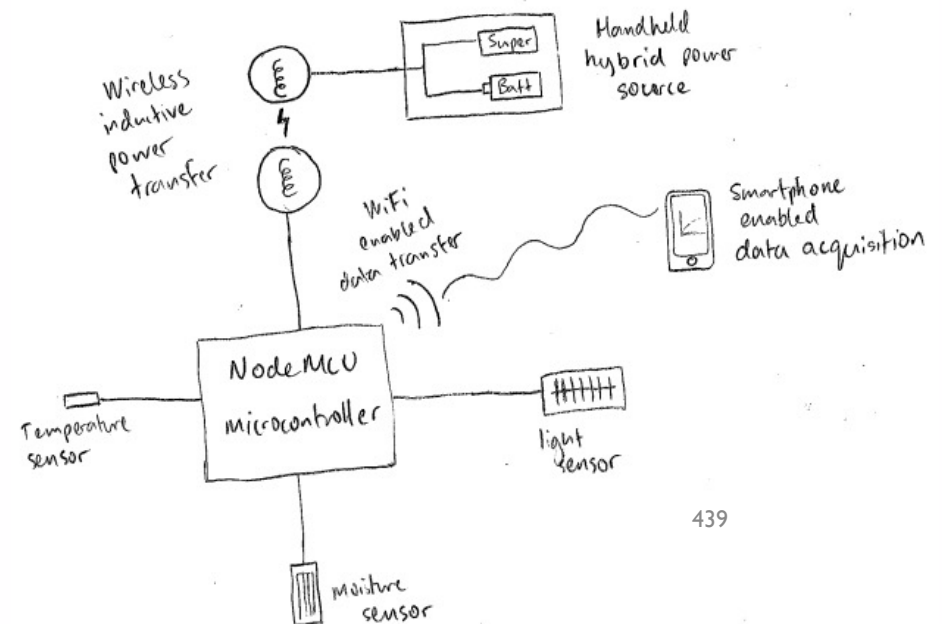
Niobium-doped titania nanoparticles

- Chemical synthesis
- Reagents:
 - Titanium chloride
 - Niobium ethoxide
 - Tert-butyl alcohol
- Challenging to produce printable consistency
- Requires screen printer
- Alternative to titania is silver nanoparticles



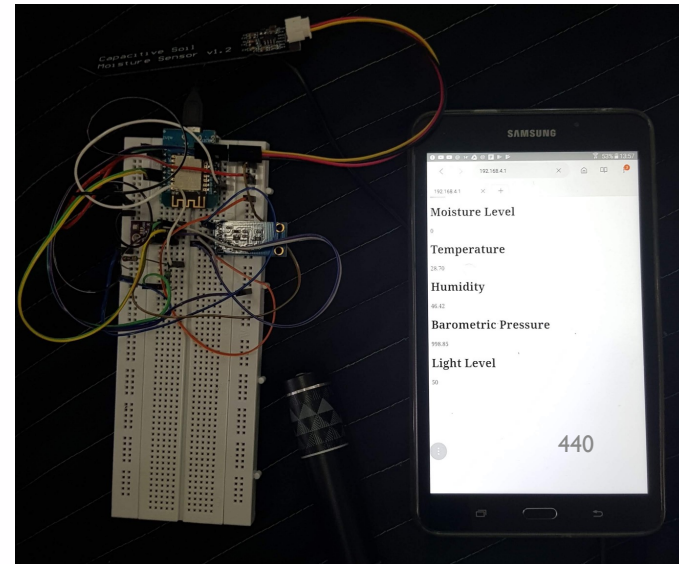
Electronic sensor

- Electronic sensor platform system
- 5V system
- Controlled by microcontroller
- Inductive power transfer
- Data sent wirelessly to smartphone
- Can charge using solar panel
- Can be modified to accept power from supercapacitors
- Costs roughly \$5
- (cost does not include smartphone)



Electronic sensor

- Capacitive sensor
- Additional Sensors included, but not necessary
 - Temperature
 - Humidity
 - Light
- Expandable (NodeMCU microcontroller has many digital I/O pins)
- Soil conductivity measurement?







- Tested in field
- Initial reading taken
- Reading increased when water added
- Reading decreased as soil dried (10 mins)

Field test









Vodacom Lesotho 3G 12:50 PM 36%

±19.69ft

10085.49^{ft}

Coordinates ±16.40ft

29.0651 ^S	28.4063 ^E
-29° 3' 54"	28° 24' 22"

Barometric Pressure (Device Barometric Sensor)

10.25 psi	70653.50 Pa
Pounds per Square Inch	Pascals
20.8640 inHg	529.94 mmHg
Inches of Mercury	Millimeters of Mercury
70.65 kPa	706.53 hPa
Kilopascals	Hectopascals

Water Boiling Point

90.16°C	194.28°F
---------	----------

Device Sensor Data Files



ETHIOPIA SENSORS ELECTRONICS COMPANY

BUSINESS PLAN

ESEC has three goals:

- 1) Manufacture of moisture sensors targeting initially foreign development funding for drip irrigation systems and later the larger Ethiopian agricultural market.
- 2) Training of a new generation of entrepreneurial technologists and businessmen who will expand the market for sensors and battery technology in Ethiopia, as well as support indigenously manufactured and locally installed equipment. Market expansion will take advantage of expertise and centers at *TUoS* and *UC*.
- 3) Enhance the economic situation for faculty and administrators at Ethiopian universities through an Ethiopian adaptation of the US/UK university-based start-up incubator model.

Strengths

- **The proposed sensor design is efficient, sustainable, cheap and easily constructible**
- **Availability of trained human power with technical expertise**
- **Associated Universities management have a strong commitment and initiation to the implementation of the project and are pioneers in irrigation regulation**

Weaknesses

- **Need for full characterisation and scale up production of sensors**
- **Need for RFID devices for measurement read**

Opportunities

- **Promising market in the rural area of the region**
- **Development of the sensor technology to suit other applications**
- **Possibility of sensor being produced from locally sourced starting materials in the near future**
- **Provision of taxes relief by the government to import inputs to the solar panel production plant**

Threats

- **Delay at maritime transit and shortage of foreign currencies**
- **Lack of basic knowledge and trust of the customers in purchasing the product manufactured locally**

Program Title: *Ethiopian Manufacture of Drip Irrigation Control Systems*
US Embassy Addis Ababa Cultural Affairs Project

Proposed Start Date: October 1, 2021

Proposed End Date: September 30, 2022

Purpose of Program: The funds will be used to initiate a business in Addis to manufacture drip irrigation control systems that were previously designed and field tested during a Fulbright Fellowship by Prof. Greg Beaucage (University of Cincinnati, Addis Ababa University, Dire Dawa University, University of Sheffield, UK). In the first year, with US Embassy funding, we plan to develop a manufacturing protocol for drip irrigation (DI) control systems and to install the systems in two agricultural test sites including in East Hararghe/Dire Dawa with the Fair Planet NGO and at Bishoftu near Addis at the AAU agricultural test facility. At the end of the first year we hope to have a business plan for a marketable DI control system, manufacturing protocol and capital investment to initiate commercial activity in Ethiopia to manufacture DI control systems for Ethiopian farms. The program chiefly involves the Stem Synergy International NGO which has recent experience with Ethiopian startups and has manufacturing facilities and an office in Addis, 22 STEM centers across Ethiopia and offices in the Washington DC area. The one-year funding will result in the initial manufacture of soil moisture sensors, solar irradiance, temperature and humidity detectors, electronic valves and a control app for control of the system using a cell phone. In the first year these initial systems will be field tested in collaboration with Fair Planet, an Israeli NGO operating at Dire Dawa and in the East Hararghe region, as well as in collaboration with Addis Ababa University at their Bishoftu agricultural test facilities near Addis. This seed funding will be coupled with further investment developed during the first year so that a functional startup business will result that employs Ethiopian trained engineers and scientists towards the manufacture of DI control systems for Ethiopian farms run by a cell-phone app and including solar powered electronic valves, solar-powered soil moisture/temperature/humidity/irradiance detectors and a new app that can take the humidity/temperature/irradiance/soil moisture readings and calculate and implement the needed irrigation and fertilizer addition based on existing algorithms available in textbooks on drip irrigation.

Applicants:

Yisehak Shata, MEng, PE, ENV SP

Chairman and Board of Directors STEM Synergy International

Mobile: 540-355-5250

Email: yshata@stemsynergy.org Website: <https://stemsynergy.org/>

Tsegaye Legesse MBA/CPA

President and Executive Director STEM Synergy International

Cell Phone: 202-203-8240

Email: tlegesse11@stemsynergy.org

Abiyot Lakew, Manager of STEM Synergy's Addis Ababa facility.

Prof. Gregory Beaucage,

Department of Chemical and Materials Engineering

University of Cincinnati

513 373 3454 (Cell)

beaucag@uc.edu

Berhanu Assefa (Dr.- Ing) Associate Professor, Chemical Engineering

Addis Ababa Institute of Technology, Addis Ababa University

Addis Ababa, Ethiopia Tel: +251 (0) 911 40 54 91

humberhanu@yahoo.com



Figure 1. Field testing and assembly of soil moisture sensors. Top: Drip irrigation; sensor field tested in Dire Dawa (two images); Field test in a green house. Bottom: Field tests in Dire Dawa; AAU Bishoftu agricultural station near Addis; assembly of sensors at AAIT/AAU.

The project will be conducted over one year with:

- 1) Initiation of technology and manufacturing practice in Addis at Stem Synergies' manufacturing facility;
- 2) Manufacture of two initial control systems for implementation in Fair Planet's drip irrigation system and at a drip irrigation research farm operated by AAU in Bishoftu near Addis;
- 3) Development of a business plan and solicitation of capital investment including market development in Ethiopia;
- 4) Initiation of commercial production of control systems initially for cash-crop farmers near Addis taking advantage of Stem Synergies' 22 STEM centers across Ethiopia.

At the end of one year the business is expected to employ about 5 engineers and technicians in Addis who will be responsible for design, manufacture, installation, and maintenance of the control systems. The Embassy grant will initially support two PhD engineers and one staff manager at Stem Synergy.

In 2012 the Embassy funded \$2,000 citizen diplomacy grant for expenses related to University of Cincinnati undergraduate student exchange with Haramaya University. That project involved undergraduates from HU and UC who designed and installed solar power in a medical clinic in a small village in the East Hararghe region. The same group planned for a solar well for an elementary school which was implemented the following year, Figure 2.



Figure 2. Summary of Beaucage activity in Ethiopia partially funded by the US Embassy. Top: installation of solar lighting in class rooms in East Hararghe. Middle: Electrification of a clinic and installation of a solar well for the school shown at the top. Bottom: Solar well for high-school near Haramaya University and solar street light company showing initial manufacture at DDIT.

In 2014 a \$10,000 seed grant was funded to initiate interactions between DDU, MU, and UC. A memorandum of understanding was signed between UC and DDU and faculty exchange between the campuses occurred. A faculty member from DDU and Mekelle visited Cincinnati and Argonne National Laboratory in Chicago. Two faculty from Cincinnati visited DDU and MU and gave seminars on their research. A plan for interaction was developed. The Vice President for International Affairs from UC visited DDU and MU in a later trip. The main outcome from this grant and the MOU was a series of startup business development projects including manufacture of solar street lights at DDU which is still being pursued after several technical improvements over the initial design. 200 street lights have been installed in Somali villages near DDU. We have held annual undergraduate and graduate student exchanges and faculty visits with DDU up until the pandemic curtailed international travel.

In 2018 to 2019 Beaucage was awarded a Fulbright Global Scholar award that included one month in Ethiopia as well as six months at University of Sheffield UK, and one month in South Africa and Lesotho. In Sheffield Beaucage collaborated with a graduate student, Max Yan, six undergraduates and a technical expert, Horace McFarlane, in the development of solar powered soil moisture sensors that can be operated from a cell phone. Using British funding, the Sheffield collaborators traveled to Ethiopia in December 2019 to join Beaucage in successful manufacturing of the device at DDU and AAU as well as field testing of the soil moisture sensors in a test farm in Dire Dawa operated by the Fair Planet NGO and in the AAU Bishoftu drip irrigation test fields near Addis.

Max Yan and Horace McFarlane: Max Yan and Horace McFarlane are collaborators from Sheffield. They have agreed to participate in the development of the drip irrigation control system manufacturing startup in Addis. This is a continuation of the collaboration in the development of the existing field-tested device.

Fair Planet: Fair Planet is an Israeli NGO that targets agricultural development in Ethiopia through providing more productive seed varieties, training farmers, providing agricultural experts to interact with local farmers with extended visits, and by demonstration of improved farming practices such as crop rotation, trellising, fertilization, and drip irrigation. Fair Planet has test farms in Dire Dawa and in the Eastern Hararghe area affiliated with DDU and HU. Fair Planet has agreed to participate in the project by providing test plots for the drip irrigation control systems.

Berhanu Assefa: Dr. Assefa is a Professor of Chemical Engineering at AAU/AAIT who has worked with Beaucage, Yan and McFarlane in the manufacture of soil moisture sensors and the field testing of the sensors. Assefa has links with the drip irrigation test facilities at AAIT where field testing of the drip irrigation control system will be carried out.

Program Goals and Objectives:

The goal of the project is to develop a viable business plan for the manufacture of drip irrigation control systems in Ethiopia and to attract startup funding from Ethiopian, US, and other foreign investors. The control systems will contribute to employment of recent technical graduates of Ethiopian Universities in work that contributes to domestic food security and export through increased crop yields and lowers water and fertilizer usage as well as slows the degradation of irrigated land through salt buildup, and reduction in weeds.

- 1) *1-6 months*: Design of a complete drip irrigation control system that can be run from a cell phone based on our existing soil moisture sensor which currently simultaneously detects soil moisture, temperature, atmospheric humidity, and solar irradiance. We hope to add pH sensing. The new phone app will also control solar powered valves and possibly solar pumps for irrigation. This work will be done in collaboration with the University of Sheffield, AAU/AAIT, and Fair Planet.
- 2) *4-12 months*: The design will be field tested in Dire Dawa on about a 1-hectare field at the Fair Planet research farm preferably with vegetables during the dry season. The timing may be somewhat difficult if the project is initiated in October 2021. The Fair Planet test site is typical of the Somali Region with arid conditions and sandy soil. Parallel to the Fair Planet test site we will test the system in Addis at a test agricultural fields outside of the city. The soil at this test site is rich loam with moderate climate conditions. We previously used both the Fair Planet and the AAIT facilities to test the cell phone-controlled soil moisture sensors⁴⁵⁸ which were assembled at AAIT and at DDIT.
- 3) *6-12 months*: Preparation of a business plan to solicit commercial investment based on the field tests and consultation with agricultural experts. We plan to solicit capital from contacts in Addis, the US, and possibly other locations such as Turkey and Israel. We are looking for an initial market value of about \$1.5M.
- 4) *12 month and onward*: Further growth of the business after this one-year grant will rely on long term interaction with Fair Planet, AAIT, and the Ethiopian Agricultural Transformation Agency (ATA) and will involve more significant funding.

Table 1. Timeline for project.

Time Span	1-3 Months	3-6 Months	6-9 Months	9-12 Months	12 Months and Beyond
1) Design of a complete drip irrigation control system	x				
2) Fair Planet Field Testing		x	x	x	
2) AAU Bishoftu Field Testing		x	x	x	
3) Preparation of Business Plan			x	x	
4) Solicitation of Capital Investment and Expansion				x	x

**Grants / Contracts
1 Year Budget**

Sponsoring Agency : US Embassy Addis Ababa Ethiopia
 Principal Investigator : Stem Synergy
 Period : 10/01/21 thru 09/29/22

Titled : Ethiopian Manufacture of Drip Irrigation Control Systems

					Year 1			CUMULATIVE
					Sal	FB	Total	
A. AAUP Faculty								
	App'l Type	% Effort	PM	Salary				
PI	ACAD	0.00%	0.00	\$ -	-	\$0	-	-
PI	SUMR	0.00%	0.00	\$ -	-	\$0	-	-
Co		0.00%	0.00		-	\$0	-	-
		0.00%	0.00		-	\$0	-	-
Co		0.00%	0.00		-	\$0	-	-
Co	CAL	0.00%	0.00	\$ -	-	\$0	-	-
Co	CAL	0.00%	0.00	\$ -	-	\$0	-	-
<i>AAUP Faculty Subtotal :</i>					-	0	0	-
B Dual Compensation Faculty								
PI	CAL	0.00%	0.00	\$ -	-	\$0	-	-
Co	CAL	0.00%	0.00	\$ -	-	\$0	-	-
Co	CAL	0.00%	0.00	\$ -	-	\$0	-	-
Co	CAL	0.00%	0.00	\$ -	-	\$0	-	-
<i>Dual Comp Faculty Subtotal :</i>					-	0	0	-
C. Other Personnel								
Exempt Staff (Monthly)	Name							
Supervisor Stem Synergy		35.00%	4.20	\$ 10,000	3,570	1,176	4,746	4,746
PhD Engineer		100.00%	12.00	\$ 6,000	6,120	2,016	8,136	8,136
PhD Engineer		100.00%	12.00	\$ 6,000	6,120	2,016	8,136	8,136
		0.00%	0.00	\$ -	-	0	0	-
<i>Total Exempt Staff</i>					15,810	5,208	21,018	21,018
Post Doctoral Support		0.00%	0.00	\$ -	-	0	0	-
Graduate Students		0.00%	0.00	\$ -	-	0	0	-
Undergrad Students		0.00%	0.00	\$ -	-	0	0	-
Part-time Faculty/Staff		0.00%	0.00	\$ -	-	0	0	-
Non-Exempt Staff (Bi-Weekly)		0.00%	0.00	\$ -	-	0	0	-
<i>Sub Totals</i>					15,810	5,208	0	-
Total Salaries and Fringe Benefits :					21,018			21,018
D. Equipment								
(list)					-		-	-
(list)					-		-	-
<i>Total Equipment :</i>					-		-	-
E. Travel								
Domestic	(list)				7,000		7,000	
International	(list)				10,000		10,000	
<i>Total Travel :</i>					17,000			17,000
G. Supplies and Other Direct Costs								
Materials & Supplies					28,939		28,939	
LAM					-		-	
Fair Planet					10,000		10,000	
AIT Agricultural Field					10,000		10,000	
<i>1% Tuition rates (Not Subject to Interest)</i>								
Lab Expenses					-		-	
Other (Analytical Services/Instrument Use)					-		-	
Subcontracts 1)					-		-	
2)					-		-	
3)					-		-	
4)					-		-	
Total Supplies and Other Direct Costs :					48,939			48,939
TOTAL DIRECT COSTS:					86,957			86,957
<i>Facilities and Administrative Cost Base:</i>					86,957			86,957
Facilities and Administrative Costs Calculation:								
F&A Cost (on MTDC):		15.00%			13,044		13,044	
Total F&A Cost :					13,044			13,044
Total Cost					100,001			100,001

Facilities and Administrative Data

Purpose of Grant / Contract : P (R = Research, I = Instruction, P = Public Service, S = Special Rate on Total Costs)
 Special F&A Rate : 10.00%
 Campus Status : O (C = On Campus, O = Off Campus)

Ethiopia News:



FIGURE 10.2 Photograph of a SEGS plant (source: www.energylan.sandia.gov/sunlab/Snapshot/TROUGHS.HTM).

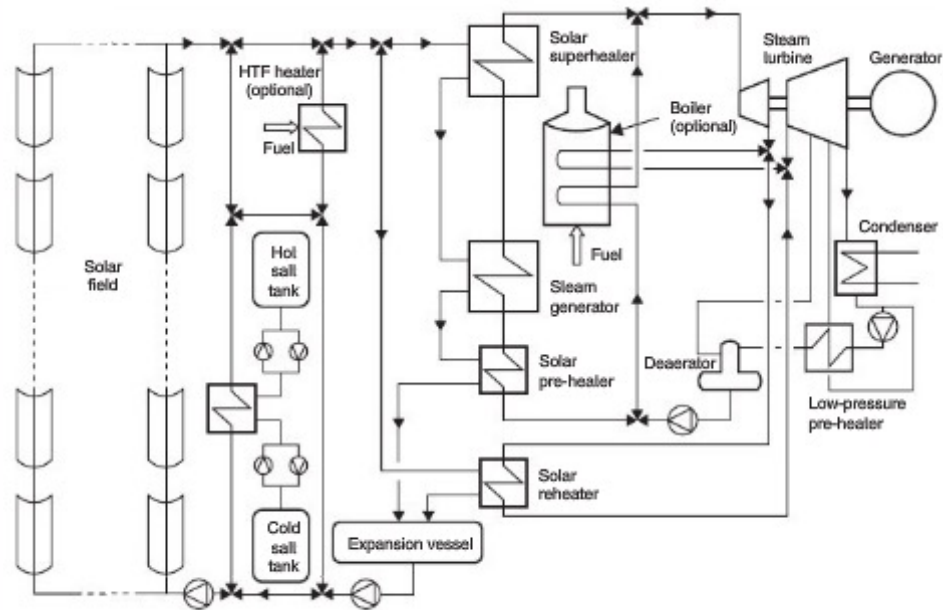


FIGURE 10.3 Schematic diagram of a solar Rankine parabolic trough system.

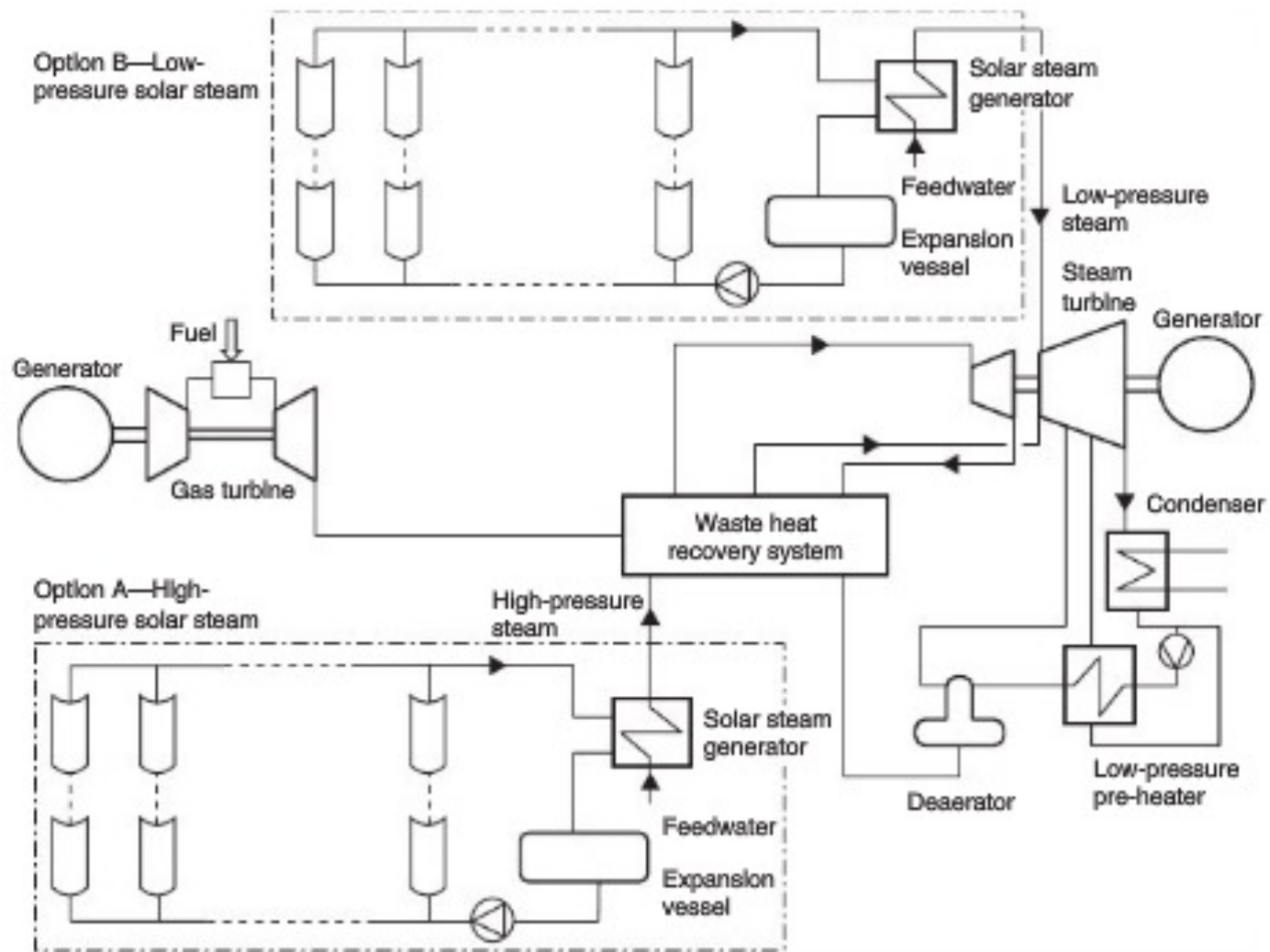
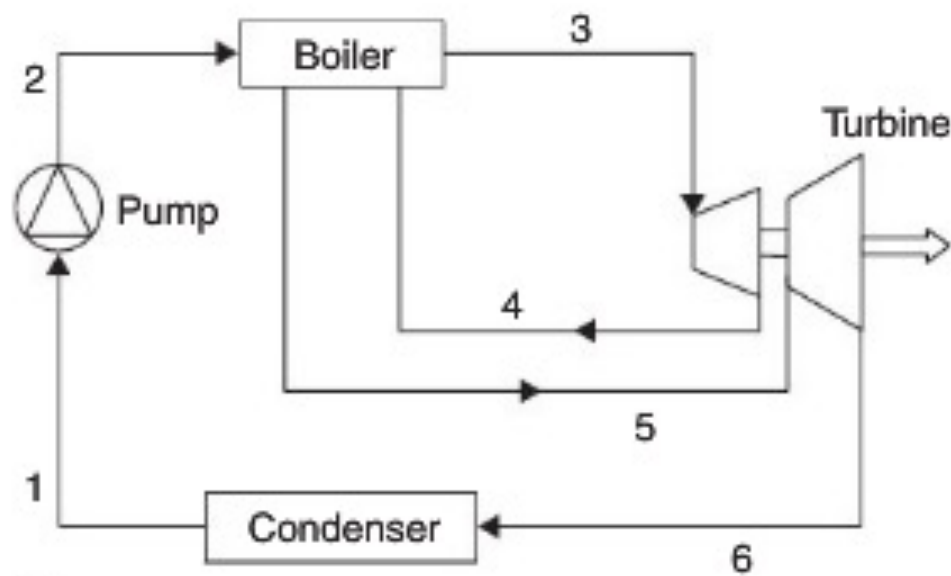
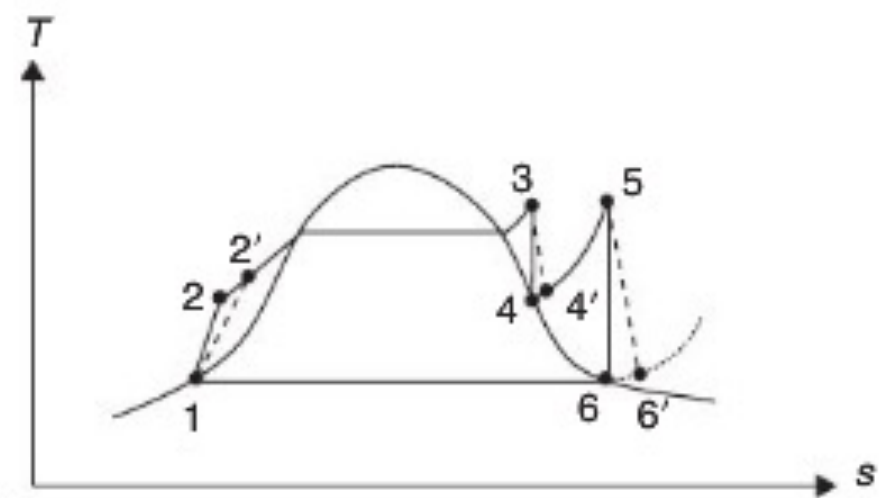


FIGURE 10.4 Schematic diagram of the integrated solar combined-cycle plant.



(a)



(b)

FIGURE 10.10 Reheat Rankine power plant cycle. (a) Reheat Rankine cycle schematic.